

NASA CR 54-855
Aerojet 3184

TOPICAL REPORT

PARAMETRIC STUDY OF GLASS-FILAMENT-REINFORCED
METAL PRESSURE VESSELS

by

E. E. Morris, F. J. Darms, R. E. Landes, and
J. W. Campbell

prepared for

NATIONAL AERONAUTICS AND SPACE ADMINISTRATION

April 1966

Contract NAS 3-6292

Technical Management
NASA Lewis Research Center
Cleveland, Ohio
Liquid Rocket Technology Branch
James R. Barber

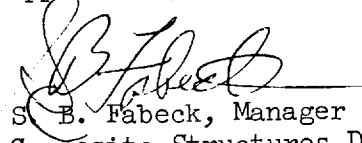
AEROJET-GENERAL CORPORATION
Von Karman Center
Azusa, California

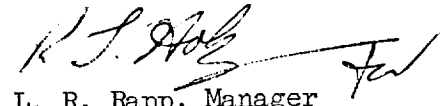
FOREWORD

This report was prepared by the Chemical and Structural Products Division of the Aerojet-General Corporation under National Aeronautics and Space Administration Contract NAS 3-6292 ("Glass-Fiber-Reinforced Metallic Tanks for Cryogenic Service"). It covers the first phase of work, conducted from 16 June 1965 to 28 February 1966; glass-fiber-reinforced metal tanks will be fabricated and tested during the remainder of the contract. The work is under the direction of the NASA, Lewis Research Center, Liquid Rocket Technology Branch, James R. Barber, Project Manager.

The program is being conducted by personnel of the Composite Structures Department. E. E. Morris is the Project Manager and principal investigator. F. J. Darms and Dr. J. W. Lambert developed the structural analysis for glass-fiber-reinforced metal tanks and formulated the computer-program logic sequences. Mr. Darms made additional valuable contributions in the parametric study. R. E. Landes conducted the parametric study, and assisted in the preparation of the structural analysis and the computer program. J. W. Campbell, metallurgist for this program, analyzed the candidate metal-shell materials. Dr. Lambert and R. McCowan were responsible for computer programming.

Approved by:


S. B. Fabeck, Manager
Composite Structures Department
Chemical and Structural Products Division


L. R. Rapp, Manager
Chemical and Structural Products Division

PARAMETRIC STUDY OF GLASS-FILAMENT-REINFORCED
METAL PRESSURE VESSELS

by

E. E. Morris, F. J. Darms, R. E. Landes, and
J. W. Campbell

ABSTRACT

27740

Advantages of and design requirements for a load-bearing metal shell with an overwrapped glass-filament shell for high-pressure-fluid storage at +75 to -423°F were investigated. The work covered characterization of metal-shell materials, definition of design-allowable strengths for S-HTS glass-filament-wound composites, analytical procedures for design and evaluation of glass-fiber-reinforced metal tanks, parametric study, and comparative rating. Proper design permits (1) utilization of the maximum load-bearing capabilities of both shells, and (2) operating pressures from 1000 to 4000 psi and above with significantly higher performance than the best cylindrical and spherical homogeneous metal tanks.

CONTENTS

	<u>Page</u>
Summary _____	xv
Symbols _____	xviii
I. INTRODUCTION _____	1
II. STUDY CONSIDERATIONS _____	2
A. Background _____	2
B. Metal-Liner Concepts _____	3
C. Design Concept and Criteria for Parametric Study _____	5
III. DESIGN APPROACH _____	9
A. General Considerations _____	9
B. Load and Strain Compatibility _____	10
C. Optimum Shape and Head Contours _____	12
D. Buckling Strength of Metal Shell _____	13
E. Creep _____	16
F. Cyclic Loads and Fatigue Strength _____	17
G. Temperature Effects _____	17
H. Fabrication Considerations _____	18
I. Specific Design Criteria _____	20
IV. ANALYSIS OF MATERIAL PROPERTIES _____	22
A. Glass-Filament Shell _____	22
B. Metal Shell _____	22
C. Design Allowables _____	26
V. STRUCTURAL ANALYSIS _____	27
A. Analytical Approach _____	27
B. Computer Program _____	29
VI. PARAMETRIC STUDY _____	31
A. Performance Factor _____	31
B. Comments on Spherical and Circumferentially Wrapped, Closed-End Vessels _____	31
C. Design of Completely Wrapped GFR Metal Tanks _____	32
1. Fixed and Variable Parameters _____	32
2. Head Contours _____	34
3. Relationship Between Geometric Parameters and Internal Volume _____	36

CONTENTS (cont.)

	<u>Page</u>
4. Design Relationships and Optimum Configurations _____	37
5. Detailed Analysis of Stress-Strain Relationships _____	43
6. Design Variations _____	45
7. Use of Design Curves _____	46
D. Performance of Homogeneous Metal and Glass-Filament-Wound Tanks _____	47
1. Homogeneous Metal Pressure Vessels _____	47
2. Glass-Filament-Wound Pressure Vessels _____	48
VII. CONCLUSIONS AND COMPARATIVE RATING OF DESIGNS _____	50
References _____	54
	<u>Table</u>
Elements of Glass-Filament-Reinforced Metal Shells _____	1
Preferential Rating of Candidate Metal-Shell Materials _____	2
Material Properties Used in Parametric Study _____	3
Metal-Pressure-Vessel Strength Levels _____	4
Operating-Pressure Performance Factors, Homogeneous Metal Tanks _____	5
	<u>Figure</u>
Pressure-Vessel Performance Levels _____	1
Modulus of Elasticity vs Temperature for Plastics and Rubbers _____	2
Stress-Strain Characteristics of Component Materials (75°F) _____	3
Liner-Design Concepts _____	4
Stress-Strain Diagram for GFR Metal Shell _____	5
Concave-Convex Form _____	6
Buckled Form _____	7
Constrictive-Wrap Buckling Strengths for Cylinders _____	8
D/t Ratio vs Allowable Elastic Compressive Stress at 75°F _____	9
D/t Ratio vs Allowable Elastic Compressive Stress at -320°F _____	10
D/t Ratio vs Allowable Elastic Compressive Stress at -423°F _____	11
D/t Ratio vs Allowable-Elastic-Compressive-Stress-to-Density Ratio at 75°F _____	12
D/t Ratio vs Allowable-Elastic-Compressive-Stress-to-Density Ratio at -320°F _____	13

CONTENTS (cont.)

	<u>Figure</u>
D/t Ratio vs Allowable-Elastic-Compressive-Stress-to-Density Ratio at -423°F _____	14
Stress-Strain Diagram, Glass-Filament-Overwrapped Metal Shell _____	15
Volume-Diameter Relationship for Pressure Vessels (0 to 35,000 in. ³) _____	16
Volume-Diameter Relationship for Pressure Vessels (0 to 6000 in. ³) _____	17
Balanced-in-Plane Contours (Back-to-Back Heads) _____	18
Balanced-in-Plane Contours ($L/D = 1.0$) _____	19
Balanced-in-Plane Contours ($L/D = 2.0$) _____	20
Balanced-in-Plane Contours ($L/D = 3.0$) _____	21
Stresses at Operating Pressures in GFR Inconel X-750 (STA) Vessel _____	22
Stresses at Operating Pressures in GFR Ti-5Al-2.5Sn Vessel _____	23
Stresses at Zero Pressure in GFR Inconel X-750 (STA) Vessel _____	24
Stresses at Zero Pressure in GFR Ti-5Al-2.5Sn Vessel _____	25
GFR Metal Pressure Vessel _____	26
GFR Metal Vessel, Relationship Between L/D and V/D^3 Ratios _____	27
GFR Metal Vessel, Relationship Between Volume, Diameter, and Load Fraction Taken by Liner _____	28
Relationship of Room-Temperature Proof Pressure to Operating Pressures at 75, -320 , and -423°F _____	29
GFR, Titanium, Oblate Spheroids - D/T_L vs Maximum Metal-Shell Compressive Stress _____	30
GFR, Titanium, Cylindrical Vessels - D/T_L vs Maximum Metal-Shell Compressive Stress _____	31
GFR Titanium Vessels, Optimum D/T_L Ratio _____	32
GFR, Titanium, Oblate Spheroids - D/T_L vs T_L/T_0 Ratios _____	33
GFR, Titanium, Cylindrical Vessels - D/T_L vs T_L/T_0 Ratios for $L/D = 1.0$ _____	34
GFR, Titanium, Cylindrical Vessels - D/T_L vs T_L/T_0 Ratios for $L/D \geq 2.0$ _____	35
GFR Titanium Vessels, Optimum T_L/T_0 Ratio _____	36
GFR Titanium Vessels, $p_0 V/W$ at 75°F _____	37
GFR Titanium Vessels, $p_0 V/W$ at -320 and -423°F _____	38
Factors of Safety for GFR Titanium Vessels _____	39

CONTENTS (cont.)

	<u>Figure</u>
GFR Inconel X-750 Vessels, Optimum D/T_L Ratio _____	40
GFR Inconel X-750 Vessels, Optimum T_L/T_0 Ratio _____	41
GFR Inconel X-750 Vessel, p_0V/W at 75°F _____	42
GFR Inconel X-750 Vessel, p_0V/W at -320 and -423°F _____	43
Factors of Safety for GFR Inconel X-750 Vessels _____	44
GFR 2219-T62 Aluminum Vessels, Optimum D/T_L Ratio _____	45
GFR 2219-T62 Aluminum Vessels, Optimum T_L/T_0 Ratio _____	46
GFR 2219-T62 Aluminum Vessels, p_0V/W at 75°F _____	47
GFR 2219-T62 Aluminum Vessel, p_0V/W at -320 and -423°F _____	48
Factors of Safety for GFR 2219-T62 Aluminum Vessels _____	49
GFR 301 Stainless Steel Vessels, Optimum D/T_L and T_L/T_0 Ratios _____	50
GFR 301 SS Vessels, p_0V/W at 75°F _____	51
GFR 301 SS Vessels, p_0V/W at -320 and -423°F _____	52
Factors of Safety for GFR 301 SS Vessels _____	53
Room-Temperature Stress-Strain Relationship, Optimum GFR Inconel X-750 Vessel _____	54
-320°F Stress-Strain Relationship, Optimum GFR Inconel X-750 Vessel _____	55
-423°F Stress-Strain Relationship, Optimum GFR Inconel X-750 Vessel _____	56
Room-Temperature Stress-Strain Relationship, Optimum GFR Ti-5Al-2.5Sn Vessel _____	57
-320°F Stress-Strain Relationship, Optimum GFR Ti-5Al-2.5Sn Vessel _____	58
-423°F Stress-Strain Relationship, Optimum GFR Ti-5Al-2.5Sn Vessel _____	59
Metal-Pressure-Vessel Performance Levels _____	60
Operating-Pressure Performance for Metal-Lined Filament-Wound Tankage _____	61
Glass-Filament-Wound Pressure-Vessel Performance _____	62

CONTENTS (cont.)

APPENDIX A - CHARACTERIZATION OF GLASS-FILAMENT-SHELL PROPERTIES

Table

Design-Allowable Strength Levels for S-HTS Glass Filaments in GFR Metal Tanks _____	A-1
Strength and Modulus of 19-S Glass Single Fibers at Room Temperature and -320°F _____	A-2

Figure

Single-Pressure-Cycle, Design-Allowable, Hoop-Filament Stress at 75°F for S-HTS Roving _____	A-1
Single-Pressure-Cycle, Design-Allowable, Longitudinal- Filament Stress at 75°F for S-HTS Roving _____	A-2
Cyclic-Pressurization Effects on Strength of Filament- Wound Pressure Vessels _____	A-3
Typical Stress-Strain Diagrams for 19-S Glass Fibers at Room Temperature and -320°F _____	A-4
Thermal Contraction of S-HTS Glass-Filament Composites _____	A-5
Steady-State Temperature Effects on Strength of Filament- Wound Pressure Vessels _____	A-6
Projected Cryogenic-Temperature Stress-Strain Characteristics of S-HTS Glass Filaments _____	A-7

APPENDIX B - CHARACTERIZATION OF METAL-SHELL MATERIALS

Table

Uniaxial and Biaxial Properties of Materials at 75°F _____	B-1
Uniaxial and Biaxial Properties of Materials at Various Temperatures _____	B-2
Properties Used in Evaluation of Candidate Metal-Shell Materials ____	B-3
Typical Room-Temperature Strengths of Type 301 SS _____	B-4
Effect of Stress Relief on Properties of Cold-Worked Tempers of Type 301 SS _____	B-5
Type 301 SS (1/2 Hard), Typical Properties _____	B-6
Ti-5Al-2.5Sn (ELI Grade), Typical Properties _____	B-7
2219-T62 Aluminum, Typical Properties _____	B-8
Inconel X-750 (Solution-Treated and Aged), Typical Properties _____	B-9

Figure

Biaxial-to-Uniaxial Ductility Ratios for Ti-5Al-2.5Sn _____	B-1
Biaxial-to-Uniaxial Ductility Ratios for Type 310 SS (3/4 Hard) ____	B-2

CONTENTS (cont.)

	<u>Figure</u>
Biaxial-to-Uniaxial Ductility Ratios for 2219-T81 Aluminum _____	B-3
Effect of Biaxial-Stress State on Tensile-Yield Strength _____	B-4
Effect of Biaxial-Stress State on Tensile Strength _____	B-5
Effect of Biaxial-Stress State on Modulus of Elasticity _____	B-6
Bauschinger Effect _____	B-7
Poisson's Ratio as a Function of Temperature _____	B-8
Type 301 SS - Typical Yield Strength, Longitudinal _____	B-9
Type 301 SS - Typical Tensile Strength and Elongation, Longitudinal _____	B-10
Type 301 SS (3/4 Hard), Tensile Properties _____	B-11
Type 301 SS (3/4 Hard), Notch-to-Unnotch Strength Ratio _____	B-12
Type 301 SS (3/4 Hard), Notch-Strength to Unnotch-Yield- Strength Ratio _____	B-13
Type 301 SS (1/4 and 1/2 Hard), Notch-to-Unnotch Strength Ratios _____	B-14
Type 301 SS (3/4 Hard), Weld-Joint Properties _____	B-15
Ti-6Al-4V (Annealed) - Ultimate Tensile Strength and Elongation, Longitudinal _____	B-16
Ti-6Al-4V (Annealed) - Ultimate Tensile Strength and Elongation, Transverse _____	B-17
Ti-6Al-4V (Annealed) - Yield Strength, Longitudinal _____	B-18
Ti-6Al-4V (Annealed) - Yield Strength, Transverse _____	B-19
Ti-6Al-4V (Annealed) - Notch-to-Unnotch Strength Ratio _____	B-20
Ti-6Al-4V (Annealed, ELI Grade) - Tensile Strength and Elongation, Longitudinal _____	B-21
Ti-6Al-4V (Annealed, ELI Grade) - Tensile Strength and Elongation, Transverse _____	B-22
Ti-6Al-4V (Annealed, ELI Grade) - Yield Strength, Longitudinal _____	B-23
Ti-6Al-4V (Annealed, ELI Grade) - Yield Strength, Transverse _____	B-24
Ti-6Al-4V (Annealed, ELI Grade) - Notch-to-Unnotch Strength Ratio _____	B-25
Ti-6Al-4V (Annealed), Weld Properties _____	B-26
Ti-6Al-4V (Annealed, ELI Grade) - Ultimate Tensile Strength and Joint Efficiency, As Welded _____	B-27
Ti-5Al-2.5Sn (Annealed) - Yield Strength, Longitudinal _____	B-28

CONTENTS (cont.)

	<u>Figure</u>
Ti-5Al-2.5Sn (Annealed) - Yield Strength, Transverse _____	B-29
Ti-5Al-2.5Sn (Annealed) - Tensile Strength and Elongation, Longitudinal _____	B-30
Ti-5Al-2.5Sn (Annealed) - Tensile Strength and Elongation, Transverse _____	B-31
Ti-5Al-2.5Sn (Annealed), Notch-to-Unnotch Strength Ratio _____	B-32
Ti-5Al-2.5Sn (Annealed, ELI Grade) - Tensile Properties, Longitudinal _____	B-33
Ti-5Al-2.5Sn (Annealed, ELI Grade) - Tensile Properties, Transverse _____	B-34
Ti-5Al-2.5Sn (Annealed, ELI Grade), Notch-to-Unnotch Strength Ratio _____	B-35
Ti-5Al-2.5Sn (Annealed), Welded Tensile Strength and Weld-Joint Efficiency _____	B-36
Ti-5Al-2.5Sn (Annealed), As-Welded Elongation _____	B-37
Ti-5Al-2.5Sn (Annealed, ELI Grade), Welded Tensile Strength and Weld-Joint Efficiency _____	B-38
Ti-5Al-2.5Sn (Annealed, ELI Grade), As-Welded Elongation _____	B-39
2219-T87 Aluminum - Tensile Properties, Longitudinal _____	B-40
2219-T87 Aluminum - Tensile Properties, Transverse _____	B-41
2219-T87 Aluminum, Notch-to-Unnotch Strength Ratio _____	B-42
2219-T62 Aluminum - Tensile Properties, Longitudinal _____	B-43
2219-T62 Aluminum - Tensile Properties, Transverse _____	B-44
2219-T62 Aluminum, Notch-to-Unnotch Strength Ratio _____	B-45
2219-T87 Aluminum, Welded Tensile Strength and Weld-Joint Efficiency _____	B-46
2219 Aluminum, Welded Tensile Strength and Joint Efficiency _____	B-47
2219 Aluminum, Comparison of Parent-Metal and Welded Properties _____	B-48
2219 Aluminum, Effect of Thickness on Average Tensile Strength of Welds _____	B-49
7039-T6 Aluminum, As-Welded Properties _____	B-50
Inconel X-750 (Solution-Treated and Aged) - Tensile Properties of Sheet, Longitudinal _____	B-51
Inconel X-750 (Solution-Treated and Aged) - Tensile Properties of Sheet, Transverse _____	B-52

CONTENTS (cont.)

	<u>Figure</u>
Inconel X-750 (Solution-Treated and Aged) - Notch-to-Unnotch Strength Ratio of Sheet _____	B-53
Inconel X-750, As-Welded Properties _____	B-54
Haynes 25, Tensile Properties _____	B-55
Haynes 25, Notch-to-Unnotch Strength Ratio _____	B-56
Haynes 25, Tensile Properties as Welded _____	B-57
Type 301 SS (1/2 Hard) - Typical Stress-Strain Curves, Longitudinal _____	B-58
Type 301 SS (1/2 Hard) - Typical Stress-Strain Curves, Transverse _____	B-59
Type 301 SS, Modulus of Elasticity _____	B-60
Type 302 SS, Thermal Contraction _____	B-61
Ti-5Al-2.5Sn (ELI Grade), Typical Stress-Strain Curves for Longitudinal and Transverse Tension _____	B-62
Ti-5Al-2.5Sn (Annealed), Modulus of Elasticity _____	B-63
Ti-5Al-2.5Sn (Annealed), Thermal Contraction _____	B-64
2219-T62 Aluminum - Typical Stress-Strain Curves, Longitudinal and Transverse Tension _____	B-65
2219-T87 Aluminum, Modulus of Elasticity _____	B-66
2219-T87 Aluminum, Thermal Contraction _____	B-67
Inconel X-750 (Solution-Treated and Aged) - Typical Stress-Strain Curves, Tension _____	B-68
Inconel X-750 (Annealed and Aged) - Typical Stress-Strain Curve, Compression _____	B-69
Inconel X-750, Modulus of Elasticity _____	B-70
Inconel X-750 (Solution-Treated and Aged), Thermal Contraction _____	B-71
APPENDIX C - LOW-CYCLE, HIGH-STRAIN FATIGUE RESISTANCE OF CANDIDATE MATERIALS	
	<u>Table</u>
Estimated Maximum Operational-Pressure-Cycling Strain Range _____	C-1
Predicted Elastic-Strain Ranges, Cycles to Failure, and Factors of Safety on Strain Cycling for Candidate Metals _____	C-2
	<u>Figure</u>
Stress-Strain Diagram for GFR Metal Shell _____	C-1
Maximum Operational-Pressure-Cycling Strain Range for GFR Metal Shell _____	C-2

CONTENTS (cont.)

	<u>Figure</u>
Stress-Strain Relationships for Uniaxial Cyclic Loading, and Hysteresis Loop for Strain-Cycle Fatigue Specimen _____	C-3
Variation of Stress Range with Number of Cycles for Strain Cycling About Zero Mean Strain _____	C-4
Cyclic and Virgin Tensile Stress-Strain Curves _____	C-5
Effect of Diametral Strain Range on Fatigue Life _____	C-6
Resistance of Ductile, Strong, and Tough Metals to Cyclic Strains _____	C-7
Comparison of the Methods of Manson and Coffin _____	C-8
Relationship of Plastic, Elastic, and Total Strain Ranges to Cycles to Failure _____	C-9
Elastic, Plastic, and Total Strain-Range Variations with Cyclic Life at 75°F _____	C-10
Predicted Elastic-Strain Range vs Cycles to Failure for Ti-6Al-4V (Annealed) _____	C-11
Predicted Elastic-Strain Range vs Cycles to Failure for Ti-5Al-2.5Sn _____	C-12
Predicted Elastic-Strain Range vs Cycles to Failure for 301 SS (1/2 Hard) _____	C-13
Predicted Elastic-Strain Range vs Cycles to Failure for 301 SS (3/4 Hard) _____	C-14
Predicted Elastic-Strain Range vs Cycles to Failure for Inconel X-750 _____	C-15
Predicted Elastic-Strain Range vs Cycles to Failure for 2219-T62 Aluminum _____	C-16
Uniaxial and Biaxial S-N Curves for 301 SS (As Rolled), R = 0.10 _____	C-17
Uniaxial and Biaxial S-N Curves for 301 SS (As Rolled), R = 0.50 _____	C-18
S-N Curves for 301 SS from 2-to-1 Biaxial Specimens (As Rolled) and Cylindrical Pressure Vessels (Shear-Spun) _____	C-19
Uniaxial and Biaxial S-N Curves for Ti-6Al-4V (As Rolled), R = 0.10 _____	C-20
Uniaxial and Biaxial S-N Curves for Ti-6Al-4V (As Rolled), R = 0.50 _____	C-21
Uniaxial S-N Curves for Ti-6Al-4V with Different Material Conditions _____	C-22
Fatigue Life of 301 SS for Various States of Stress _____	C-23
Fatigue Life of Ti-6Al-4V for Various States of Stress _____	C-24

CONTENTS (cont.)

APPENDIX D - ANALYSIS OF FILAMENT-WOUND-COMPOSITE PRESSURE
VESSELS WITH LOAD-CARRYING LINERS

	<u>Table</u>
Unknowns at Equator of Head _____	D-1
	<u>Figure</u>
Geometry of General Winding Pattern _____	D-1
Geometry of In-Plane Winding Pattern _____	D-2

APPENDIX E - FACTOR OF SAFETY FOR GFR METAL TANKS

	<u>Figure</u>
Overlapping Strength and Load Distributions _____	E-1
Reliability vs Factor of Safety for Various Strength Degradaions _____	E-2
	<u>Page</u>
Distribution List _____	F-1

PARAMETRIC STUDY OF GLASS-FILAMENT-REINFORCED METAL PRESSURE VESSELS

by E. E. Morris, F. J. Darms, R. E. Landes, and
J. W. Campbell

SUMMARY

The advantages of combining a load-bearing metal shell with an over-wrapped glass-filament shell for high-pressure-fluid storage in the +75 to -423°F range were investigated, as were the design requirements. The research was concentrated on the characterization of candidate metal-shell materials, definition of design-allowable strength levels for S-HTS glass-filament-wound composites, development of analytical procedures for the design and evaluation of glass-fiber-reinforced (GFR) metal tanks, parametric study of the tanks, and comparative rating of GFR-metal-tank performance with homogeneous metal tankage made from Ti-6Al-4V, Type 301 stainless steel, Inconel 718 (a nickel-base alloy), and the 2219-T87 aluminum alloy.

Proper design of GFR metal tanks permits the utilization of the maximum load-bearing capabilities of both the metal shell and the filament-wound composite. It makes possible GFR metal tanks with operating pressures in the range from 1000 to 4000 psi and above having performances significantly greater than those of the highest-performance, cylindrical and spherical, homogeneous metal tanks.

The design criteria used in the study included a requirement that the compressive buckling and yield strengths of the metal shell were not to be exceeded at zero internal pressure, when the metal shell is in maximum compression due to the external forces produced by the overwrapped filaments. The designs that were developed consequently do not require an adhesive bond between the glass-fiber and metal shells to keep the latter from buckling. The service-cycle requirement for the tanks included sustained loading and 100 pressure cycles to the operating pressure. To minimize hysteresis effects in the metal shell during cyclic applications of the operating pressure, the tanks were designed so that, after the application of an initial prestress pressure load (which plastically deforms the metal shell beyond its biaxial-yield stress), the stress range in the metal shell between zero pressure and the operating pressure was within the offset biaxial compressive and tensile elastic limits. In the parametric study, the metal-shell stress at the operating pressure was required not to exceed 90% of the biaxial yield stress.

Designing to assure that the metal-shell operating-strain range is elastic distinguishes GFR metal tanks from glass-filament-wound pressure vessels with very thin, smooth, metal liners. In vessels with the thin and smooth liner, the liner must work in a hysteresis loop during cyclic application of the operating pressure. Thicker liners are required to meet the design criteria of GFR metal tanks, making the tanks heavier than thin metal-lined, filament-wound, pressure vessels. Elimination of the metal-liner hysteresis loop, however, will improve the cyclic-fatigue resistance of GFR metal tanks. In addition, GFR metal tanks do not require a bond between the liner and the glass-filament overwrap to prevent buckling (as do the thin, smooth, metal-lined tanks). Consequently, adhesive-bond integrity during service is not an area of concern.

Analyses of material properties revealed that several available alloys will provide sufficient ductility and strength to meet the design requirements for the metal shell. The alloys selected for study in the parametric evaluation were Ti-5Al-2.5Sn [annealed, extra-low-interstitial (ELI) grade], Type 301 stainless steel (1/2-hard temper), the 2219-T62 aluminum alloy, and the Inconel X-750 [solution-treated and aged (STA)] nickel-base alloy. Because of cyclic-pressurization effects on the strength of filament-wound composites, the filament-stress level at the operating pressure had to be maintained at 60% or less of the single-pressure-cycle burst stress to sustain the 100-pressure-cycle requirement for the tanks. An operating-pressure design-allowable filament-stress level of 200,000 psi at 75°F, compared with a tankage-burst-pressure filament-stress level of 330,000 psi, was necessary to sustain the service-cycle requirements. At -320 and -423°F, these allowable-stress levels are expected to increase by 50%.

A structural analysis and computer program were developed for use in designing and analyzing complete tanks, wound with either geodesic or in-plane patterns along the cylinder and over the end domes, and complemented by circumferential windings in the cylinder. Optimum head contours were developed, and the following were computed for more than 1000 different configurations of GFR metal tanks: filament and metal-shell stresses and strains at zero pressure and the design pressure; thickness of hoop wrap required for the cylindrical portion of the vessel; and weight, volume, and filament-path lengths for the components and complete vessel. For these designs, the computer program also determined the stresses and strains in the filament and metal shells during the service-cycle history of the vessel from a series of input pressures, composite temperatures, and metal-vessel temperatures.

The head contours for filament-wound pressure vessels combined with load-carrying liners are intermediate between the filament-wound pressure-vessel head contour and the spherical shape optimum for homogeneous metal heads. In GFR-metal-pressure-vessel heads with the optimum contour, stresses are constant in the filaments up the contour and a 1-to-1 stress field is produced in the metal shell at the design pressure and temperature, thus satisfying the requirements for optimum closure design. Completely wrapped GFR metal pressure vessels with optimum head contours have higher performance than spherical GFR

metal tanks or circumferentially reinforced, cylindrical, metal pressure vessels with hemispherical end closures. Completely wrapped oblate spheroids had a performance level comparable to that of completely wrapped, cylindrical, pressure vessels.

The parametric study of GFR metal tanks indicated their performance advantages over homogeneous metal tanks. Optimum room-temperature designs were found to be optimum designs for cryogenic temperatures if the tank is warmed at some time during its service life. At cryogenic temperatures, the optimum room-temperature designs can work at an increased operating pressure to improve performance if use is made of the change in metal-shell tensile-yield strength produced by the change in temperature.

The maximum efficiency over the 75 to -423°F range is provided by GFR Ti-5Al-2.5Sn pressure vessels, which have performances considerably greater than those of the other GFR metal tanks and 35 to 70% greater than homogeneous Ti-6Al-4V pressure vessels. The performance improvement (when compared with the highest-strength homogeneous metal pressure vessels made from 301 stainless steel, Inconel 718, and 2219-T87 aluminum) ranges from 40 to 130%, depending on the shape and material used for the homogeneous metal tanks. The second highest performance is provided by GFR 2219-T62 aluminum tanks, followed by GFR 301 stainless steel (1/2 hard) and Inconel X-750 (STA) tanks.

The performance of GFR Inconel X-750 tanks may be increased because of the high-strain capability of the Inconel. The metal shell of GFR Inconel X-750 tanks has sufficient ductility to strain to the ultimate strength of the filaments over the complete 75 to -423°F range, thereby achieving the maximum performance obtainable with this material combination and the design requirements imposed on GFR metal tanks. Because of the good performance of the Inconel X-750 metal shell (large biaxial-strain capability and 100% weld-joint efficiency), it appears feasible to operate this type of GFR tank at pressures that produce liner stresses equal to the liner's offset yield stress (rather than the 90% level assumed for the parametric study) to improve efficiency of the vessels. If this is done, the GFR Inconel X-750 tank performance at 75 to -423°F is equivalent to that of GFR aluminum and stainless steel tanks. The GFR Inconel tanks are superior to all configurations of homogeneous metal tanks made from stainless steel and the representative titanium, aluminum, and nickel base alloys at 75°F . When cryogenic-temperature properties are used to increase the operating-pressure performance, however, homogeneous titanium spheres and cylinders, and homogeneous stainless steel spheres, have higher performances than GFR Inconel X-750 tanks.

SYMBOLS

	<u>Definition</u>	<u>Units</u>
a	Vessel radius	in.
D	Diameter	in.
D _b	Diameter of boss on pressure-vessel head	in.
E	Modulus of elasticity	lb/in. ²
E _{ga}	Modulus of elasticity of filament-wound cylinder composite in longitudinal direction	lb/in. ²
E _{gh}	Modulus of elasticity of filament-wound cylinder composite in hoop direction	lb/in. ²
E _s	Metal-shell elastic or secant modulus	lb/in. ²
K	Load fraction carried by metal-shell component of GFR metal tank in meridional direction of head	--
L	Length	in.
N _H	Number of layers of hoop windings	--
N _L	Number of layers of longitudinal windings	--
N _{S_H}	Number of turns of tape per layer per inch of hoop winding	--
N _{S_L}	Number of turns of tape per layer per inch of longitudinal winding	--
N _θ	Pressure-vessel membrane force in hoop direction	lb/in.
N _φ	Pressure-vessel membrane force in longitudinal direction	lb/in.
N _{φL}	Metal-shell membrane force in longitudinal direction	lb/in.
P _D	Design operating pressure	lb/in. ²
p	Pressure	lb/in. ²
P _b	Burst pressure	lb/in. ²
P _O	Operating pressure	lb/in. ²
P _P	Prestress, proof, or initial pressure	lb/in. ²
R	Radius	in.
T	Tension	lb
T _D	Design operating temperature	°F
T _H	Winding tension in hoop tape	lb
T _L	Winding tension in longitudinal tape (or metal-shell thickness)	lb (or in.)

SYMBOLS (cont.)

	Definition	Units
T_0	Longitudinal filament-wound-composite thickness at equator	in.
t	Thickness	in.
t_g	Equivalent glass-filament thickness or filament-wound-composite thickness	in.
t_ℓ	Metal-shell thickness	in.
t_o	Longitudinal filament-wound-composite thickness at equator	in.
t_s	Metal-shell thickness	in.
V	Internal volume	in. ³
v_g	Volume fraction of filaments in composite	--
W	Pressure-vessel weight	lb
x	Radial dimension of point on head contour	in.
z	Normalized radial distance (x/a)	--
α	Winding angle between filament path and meridional direction	degrees
α_o	Longitudinal-filament-winding angle	degrees
ν_s	Poisson's ratio of metal shell	--
σ	Stress	lb/in. ²
σ_c	Critical buckling stress	lb/in. ²
σ_{fd}	Filament stress at design pressure	lb/in. ²
σ_g	Stress in glass filaments	lb/in. ²
σ_{ga}	Longitudinal stress in filament-wound cylinder composite	lb/in. ²
σ_{gh}	Hoop stress in filament-wound cylinder composite	lb/in. ²
σ_ℓ	Stress in metal shell	lb/in. ²
σ_o	Maximum metal-shell tensile stress at operating pressure	lb/in. ²
σ_p	Metal-shell tensile stress at prestress pressure	lb/in. ²
σ_{sa}	Longitudinal stress in metal shell	lb/in. ²
σ_{sh}	Hoop stress in metal shell	lb/in. ²

SYMBOL SUBSCRIPTS

A,A'	Points on a stress-strain curve	--
B,B'		

I. INTRODUCTION

The use of glass-filament-wound tank structures for cryogenic pressure vessels should result in considerable weight savings because the filament-wound-composite material has a much higher strength for its weight than do metal-tankage materials. Although the filament-wound material is light in weight, it has a serious limitation when used for cryogenic pressure vessels. The filament/resin composite is permeable to pressurized fluids, and a sealant liner is needed inside the tank wall.

Suitable liner materials are available for room-temperature service. Liners that can be used at cryogenic temperatures, however, have presented difficult developmental problems (described in Refs. 1 to 6a) because the liner must respond a number of times to very large biaxial strains without failure in order to be compatible with the filament-wound composite at its operating-stress level.

Metals appear to have the properties necessary for a liner that must operate at cryogenic temperatures. However, the high strength and low modulus of glass fibers currently used for filament-wound pressure vessels produce elastic strains 3 to 10 times the biaxial elastic strain of metals. Considerable effort is being devoted to the development of strain-compatible metal liners that increase the strain range by rotation of geometric surfaces or by working relatively thin liners in their plastic region for a limited number of cycles. Attempts to use high-elongation foil materials and to strain-cycle the liners in their plastic range have had only moderate success because of (a) liner buckling on depressurization of the vessel when the bond between the liner and composite failed, and (b) subsequent fatigue failure of the liner in the buckled area.

Combining a glass-filament-wound composite with a load-bearing metal shell provides the necessary sealant liner and permits the strength potential of the glass fibers to be exploited. For high-pressure-fluid storage containers, a metal shell can be combined with a glass-fiber overwrap to achieve a vessel of less total weight for a given operating pressure and volume than is possible with an all-metal vessel. In order for inner and outer shells to operate at their optimum efficiencies, however, a proper preload or strain relationship must be achieved when the vessel is unpressurized.

The parametric study described in this report was conducted as the first phase of the work under Contract NAS 3-6292 to determine analytically the advantages and design requirements of combining a load-bearing metal shell with an overwrapped glass-filament shell for high-pressure gas or liquid storage in the temperature range from 75 to -423°F . Glass-fiber-reinforced metal tanks will be fabricated and tested later in the program, and the results will be used to verify or modify the structural-performance capabilities of glass-fiber-reinforced metal tanks predicted in this report and depicted in Figure 1.

II. STUDY CONSIDERATIONS

A. BACKGROUND

Interest in filament-wound tankage has increased because of the need for maximum weight saving. The successful use of glass-filament-wound structures in many pressure-vessel and rocket-motor-case applications has demonstrated that the reliability level needed in specific systems can be attained with filament winding. The state-of-the-art advancements typified by these applications have resulted from improvements in the properties of the fibers and resin forming the basic structure, and improvements in tooling and fabrication techniques. Another very important factor has been the use of effective composite-structure designs.

The property of glass-filament-wound composites of most significance for pressure vessels is the high composite-wall strength-to-density ratio attainable - of the order of 2.0×10^6 in. for the pressure-vessel cylinder and 3.20×10^6 in. for the pressure-vessel heads at 75°F. This high performance, with accompanying high operating fiber stresses and strains, creates extremely difficult design problems when the requirement for a sealant liner to contain cryogenic fluids is introduced.

1. Filament-Wound-Composite Material

A filament-wound reinforced-plastic structure contains a large number of continuous, small-diameter, high-strength fibers imbedded in a matrix of organic or inorganic material such as epoxy resin. The fibers, which in most applications have been glass, constitute the primary load-carrying element of the composite because of their relatively high modulus of elasticity. The maximum structural efficiency is obtained by the orientation of these fibers to provide the strength components to meet the applied loads. In pressure vessels and other structures, where the direction and relative magnitudes of forces are fixed, the resin is relegated to a secondary role of controlling fiber efficiency by transferring loads from broken fibers, hardening the structure in terms of shape and fiber orientation, and protecting fibers from each other and from degrading environments.

2. Sealant-Liner Requirements for Filament-Wound Pressure Vessels

A limitation of filament-wound composites is permeability to gases and liquids under pressure. Furthermore, the filament and/or resin components of the composite may be subject to chemical corrosion by certain contained fluids, such as propellants. These limitations are overcome by using a thin liner inside the filament-wound structure to prevent or minimize fluid contact or transmission through the composite wall. Because the performance of a pressure vessel is based on its total weight, operating pressure, and volume, a minimum liner weight is desired.

The functional requirements for sealant liners of filament-wound pressure vessels include

- a. Impermeability to gases and liquids under pressure
- b. Resistance to corrosion by contained fluids
- c. Strain compatibility with the composite structure up to its failure stress
- d. Resistance to fatigue when subjected to the large, cyclic strains associated with repetitive loading of the composite structure to the operating-stress level.

3. Liner Materials

Materials such as molded rubber, polymeric films, metal coatings, metal foil, and thin metal sheet have been used for liners. The polymeric materials have been suitable when the pressure-vessel service life has been short, and/or when some permeation through the structure has been tolerable. To date, the use of polymer liners has been restricted to temperatures greater than -65°F , due to the loss of extensibility that occurs as the glass-transition temperature of the polymer is approached. Examples are shown in Figure 2 for several plastics and rubbers (derived from Ref. 6b).

When a polymer liner is functionally adequate for a specific application, the designing of the liner and filament-wound vessel is relatively straightforward. When stringent limitations are imposed on the leakage of fluids and/or the operational temperatures are below -65°F , metallic liners must be used because of the present inability of polymeric materials to provide the necessary properties. However, the high operating strains repetitively applied to glass-filament-wound-composite pressure vessels during service have presented extremely difficult problems in the design of compatible metal liners.

B. METAL-LINER CONCEPTS

The high strength and low modulus of glass filaments create a requirement for large strains in the liner, and are the most significant factors influencing metal-liner design. Utilization of the filament strength potential in a metal-lined, filament-wound, pressure vessel requires that the metal liner strain biaxially to (1) an efficient operating-stress level in the filaments, and (2) the ultimate strength of the filaments at the burst pressure.

Unlike metals, which usually have both elastic and plastic components in their stress-strain curves, glass filaments are elastic throughout the entire stress-strain range (except at elevated temperatures). At 75°F , S-HTS glass filaments have an elastic modulus of 12.4×10^6 psi and a representative ultimate filament strength in pressure vessels of 330,000 psi, yielding a failure strain of about 2.7%. For a pressure-vessel safety factor of 1.5, currently associated with high-pressure aerospace tankage, the 75°F glass-filament and metal-liner strain at the operating pressure is of the order of 1.6 to 2.0% for efficient design. For lower factors of safety, the strains are even larger. Over the 75 to -423°F range, the mechanical properties of glass filaments undergo significant change, with the -423°F tensile strength increased about 50% and the -423°F tensile modulus increased 10% over the

75°F values. The net effect is to increase the ultimate strain of the filaments by about 30 to 40%.

Comparative stress-strain relationships for S-HTS glass filaments and four possible metal-liner materials at 75°F are shown in Figure 3. As indicated there, the filament strains at the operating stress will cause the metal liner to exceed its yield point and plastically deform. In general, plastic deformation will occur even if the liner is designed to make use of its complete compression-to-tension elastic-strain range.

Aerojet has evaluated two basic approaches for the design of metal-lined, glass-filament-wound, pressure vessels: (1) The metal liner must always work within its compressive and tensile proportional limits during application of the zero-to-maximum use or limit pressures, or (2) the metal liner is permitted to work beyond the proportional limit or limits into its plastic zone or zones upon application of the zero-to-maximum use or limit pressures.

Metal-liner design concepts arising from these criteria have been categorized into four groups (described below), based on their zero-to-operating-to-zero-pressure strain characteristics. Figure 4 presents schematic stress-strain curves for these concepts; for simplicity, these plots assume no liner compressive prestress during fabrication and a common origin for the liner and filament-wound-composite stress-strain curves.

1. Elastic Liner

This is a very thin, smooth, metal liner that is strained only in the tensile elastic zone or the compressive and tensile elastic zones. It may or may not require a bond to the tank wall to prevent buckling under compression loading.

2. Smooth, Bonded Liner

This is a very thin, smooth, metal liner that is strained in the tensile and compressive elastic and plastic zones, and requires a bond to the tank wall to prevent buckling under compressive stress.

3. Corrugated Liner

This very thin, corrugated-metal liner is designed so that pleats give it considerably increased elastic-strain capability as compared with the smooth parent material from which it is fabricated. The liner is strained only in its elastic zone.

4. Plastic-Elastic Load-Bearing Liner

This is a thicker, smooth, load-bearing, metal liner that is strained only in the tensile and compressive elastic zones after an initial prestress into the plastic zone.

In this report, the first three liner concepts will be referred to as metal-lined glass-filament-wound pressure vessels, and the fourth as the glass-fiber-reinforced (GFR) metal pressure-vessel concept.

Considerable work is being done to evaluate these design concepts using metal coatings, foils, and welded sheet (patterned and unpatterned) to provide liners compatible with glass-filament-wound pressure vessels. Each has advantages and disadvantages.

The elastic liner is limited in the relative magnitude of its operating-strain range, and yields a light tank only if the required safety factor for the design operating pressure is high (e.g., 3 or 4), resulting in low-operating-pressure filament stresses and strains. This concept has been evaluated successfully by Aerojet in an Independent Research and Development (IR&D) program. For aerospace tankage with lower factor-of-safety requirements (1.5 to 2.2), the compressive-to-tensile elastic-strain range of the metal liner will not generally produce sufficient glass-filament strain to attain an efficient operating-stress level, and thus make use of the potential of the filament winding. With an allowable filament stress based on the magnitude of the liner's elastic-strain capability, this concept results in a heavy tank for glass-filament-wound construction in low-factor-of-safety applications.

The smooth, bonded liner has been evaluated successfully by Aerojet for the Air Force under Contract AF 33(615)-1671 (an exploratory evaluation of filament-wound composites for tankage of rocket oxidizers and fuels, reported in Ref. 7). Douglas Aircraft Company is studying this concept for application to cryogenic pressure vessels under a NASA contract.

The corrugated liner was evaluated by Aerojet under NASA Contract NAS 3-4189 (on design improvements in liners for glass-fiber filament-wound tanks to contain cryogenic fluids, reported in Ref. 6). In this program, corrugated-liner patterns were analytically developed that would allow expansion to the required filament operating-strain level without exceeding the elastic limit of the liner materials. Two sizes (8- and 18-in.-dia tanks) were fabricated for testing. Fabrication difficulties were encountered, and limited testing did not provide adequate substantiation of the designs, although concept feasibility was demonstrated by tests of the 8-in.-dia chambers.

Plastic-elastic load-bearing liners are being studied analytically and experimentally by Aerojet in the present NASA program. The design concept is discussed in detail below.

C. DESIGN CONCEPT AND CRITERIA FOR PARAMETRIC STUDY

When design requirements dictate the use of a metal liner inside filament-wound pressure vessels to meet performance specifications, the use of thick metal liners, which share loads with the filament-wound-composite shell, offers an excellent approach to the attainment of workable, minimum-weight, high-pressure-fluid, storage vessels. This concept provides a pressure vessel formed by combining a load-bearing metal shell with an overwrapped glass-filament shell. Metal-pressure-vessel fabrication procedures are used in

constructing the liner. The glass-filament shell is fabricated by winding a specifically oriented pattern of pretensioned, resin-impregnated, continuous filaments over the metal shell.

A schematic stress-strain diagram for a pressure vessel constructed by combining a glass-filament-wound shell over a load-bearing metal liner is presented in Figure 5. A "load-bearing metal shell" is defined as one capable of resisting buckling at the compressive-stress level (E) shown in Figure 5 (produced by external pressure from the overwrapped shell), when no bond exists between the metal and glass-fiber shells. The metal shell and overwrapped glass filaments are designed to minimize the metal-shell hysteresis loop in the operational pressure-cycle stress range (E) to (J) to (E) [i.e., (E) to (J)] is an elastic stress-strain curve.

The stress-strain relationship that must be achieved between the metal liner and the glass-fiber shell in order for both to operate at their maximum load-carrying potentials is controlled by the many factors enumerated in Table 1.

In GFR metal-shell pressure vessels, efficient utilization of filament strength requires that the liner have sufficient ductility in the parent metal and weldments to permit biaxial straining to (1) the maximum design-allowable filament stress at the operating pressure, (2) the ultimate elongation of the glass filaments at the burst pressure, and (3) the strain associated with cyclic loading between zero pressure and the operating pressure. Metallic shells without the required strain capability [due to cryogenic-temperature effects, heat-treatment level, low joint efficiency, presence of propagating defects in the welds (cracks, incomplete fusion, lack of penetration, excessive porosity, excessive inclusions, etc.)] will fail prematurely by local fracture of weldments or the parent metal and subsequent leakage. Candidate metal-shell materials must therefore have suitable elongation capability to be strain-compatible with the glass filaments.

1. Stress-Strain Conditions in Metal Shell

Significantly different stress-strain conditions are imposed on GFR metal tanks during application of the internal pressures associated with tank fabrication, proof testing, burst testing, and operation. Figure 5 depicts these stress-strain states for the metal and glass-fiber components during fabrication, after mandrel removal, at proof-pressure prestress, at zero pressure, at operating pressure, and at burst pressure. It provides a basis for the ensuing discussion, which makes repeated references to points depicted there. As indicated in the figure, the metal may be held in a stress-free (strain-free) state by a rigid mandrel while being overwrapped with tensioned filaments [point (M)]. Upon removal of the mandrel, however, the metal shell will spring back into a compressive state, due to the filament-overwrapping pressure [point (O)]. The magnitude of compression in the metal shell at zero internal-pressure equilibrium depends on the relative thicknesses and moduli of the overwrapped filaments and metal shell, as well as the biaxial stress-strain characteristics of the metal liner and the filament-winding tension used during fabrication.

When the first pressure load, p_p , is applied to the GFR metal tank, the structure is strained to point (A), which is fixed by the component-material properties and thicknesses, and by the pressure load. For factors of safety associated with aerospace-tankage and with the glass-filament and metallic materials being considered in this study, point (A) will be beyond the metal-shell yield point and considerable plastic deformation will occur. In general it can be said that the biaxial tensile strain produced in the metal shell by the initial prestress pressure load will exceed 1% and may be greater than 2.5%.

When the initial prestress pressure load is removed, the metal liner will spring back along the offset, biaxial, elastic, stress-strain curve (A)-(E) and will be pushed into high compression by external pressure from the overwrapped glass filament until load equilibrium is reached at point (E) [strain (G)]. The GFR metal tanks are to be designed so that point (E) does not exceed the critical buckling-stress level of the metal shell in the absence of a bond between the metal and glass-filament shells, or the compressive elastic limit of the metal shell.

The operating-pressure level, p_o , will always be less than or equal to p_p . During application of cyclic operating-pressure loads to the GFR metal tank, therefore, the metal-liner strain range is between points (G) and (K), and the value of (K) may be as large as (B).

Specific stress and strain values fixing the range between (G) and (K) depend on details of tank design, but maximum values for the stress and strain ranges between (G) and (K) can be estimated from the candidate-material properties by assuming that the minimum value of (G) occurs at the biaxial compressive-yield stress of the metal shell and that the maximum value of (K) occurs when $p_o = p_p$ and is equal to the strain (B). Associated with the minimum value of strain (G) is the stress σ_E and with the maximum value of strain (K) the stress σ_j . As an approximation, and in the absence of the Bauschinger effect,* it may be assumed that $-\sigma_E = \sigma_j =$ material tensile-yield point, in accordance with the foregoing assumptions. This strain range between σ_E and σ_j is the maximum-permissible operating-strain range for GFR metal tanks.

2. Design Criteria

Designs of GFR metal pressure vessels must be based on both internal-pressure requirements and zero-pressure stress states in the metal liner. In addition to the usual internal-pressure design requirements, the following conditions are imposed on the metal-shell design:

a. An adhesive bond between the glass-fiber and metal shells is not required to keep the metal shell from buckling when it is loaded in compression. The unbonded metal liner must be designed to have sufficient

* Reduced deformation resistance in one loading direction following initial prestraining in the opposite direction.

buckling strength and load-carrying capability to sustain external forces from the overwrapped glass filament.

b. The compressive-stress level in the liner will not exceed the compressive elastic limit, to minimize hysteresis effects and thereby improve the cyclic-fatigue endurance.

c. The stress level in the liner at the operating pressure will not exceed the tensile elastic limit, to minimize hysteresis effects during cyclic applications of the operating pressure.

III. DESIGN APPROACH

A. GENERAL CONSIDERATIONS

Considerations involved in the design of GFR metal pressure vessels are introduced below in a review of pertinent, basic questions about the design concept. The comments are based on Aerojet work on GFR metal tanks.

1. Can the complete shell be strained to point (B) of Figure 5 on the first cycle without damage to the component parts? In past studies, Aerojet has strained the metal shells of both circumferentially reinforced and completely overwrapped GFR cylindrical pressure vessels to point (B) without damaging component parts. The magnitude of this strain has been 1 to 1-1/2% beyond the yield point of the metal-shell materials employed.

2. Can the metal shell be loaded to point (E) without failure? Aerojet has loaded both circumferentially reinforced cylinders and completely overwrapped cylindrical pressure-vessel metal shells to the relatively high compressive stress represented by point (E) without failure. This was accomplished by straining the complete shell to point (A), using internal pressure, and then unloading the pressure vessel.

3. By what means can the metal shell be loaded in compression? Loading to specific values can be accomplished by the use of filament-winding tension during fabrication. The degree of compression loading in the metal shell depends on the metal-shell thickness, roving tension, number of rovings per inch per layer, and number of layers applied. Aerojet has successfully applied compressive loads in 18-in.-dia metal shells during fabrication up to the compressive proportional limit of the shell. The shell can also be loaded in compression to specific values after fabrication by applying internal pressures that force it to strain past its proportional limit. Aerojet has used such a process to compress metal shells beyond their compressive-yield strengths.

4. Can the complete shell operate over the strain range from point (G) to point (K)? Yes, but the structural integrity of GFR metal pressure vessels subjected to repetitive loadings in this strain range is undoubtedly dependent on the number of loading cycles as well as the properties of the structural materials employed and the stress levels corresponding to strains (G) and (K). Each design will require test evaluation to establish fatigue-resistance characteristics.

5. What is the upper limit for (B)? This has not been defined in past experimental work. In Aerojet programs, (B) has been limited to the minimum value consistent with the required filament-strain level to obtain an optimum performance level for the complete shell. Values of (B) as great as 2-1/2% have been attained at Aerojet for steel shells reinforced in the cylinder with glass-filament winding. Both theoretical and practical factors control the magnitude of (B). The required value to obtain minimum weight can be determined on the basis of the required factor of safety, the material

properties, the winding-precompression stress in the metal shell, and thermal-contraction effects. From a practical standpoint, it is desirable to minimize (B) because of the inevitable fabrication defects in the metal shell and the tendency for them to propagate once the shell is forced from its elastic zone into the plastic region.

6. What variable controls the upper limit for (B)? This limit is controlled by specific properties of the materials of construction (desired operating-stress level in the filaments, fatigue resistance of the metal shell, etc.), and by fabrication quality.

7. At what limiting value of (E) (corresponding to minimum compression in the metal shell) can a weight saving no longer be achieved by the relationships established above? A weight saving can no longer be achieved when no filament reinforcements are applied to the metal shell, or when thermal contraction causes the liner to separate from the glass-filament shell. Even when hoop reinforcements are wound onto a cylindrical vessel using no tension (minimum compression in metal shell), the added strength makes it possible to reduce the metal-cylinder thickness to save weight.

B. LOAD AND STRAIN COMPATIBILITY

As with all pressure vessels, maximum performance is the primary objective of the design of a load-carrying metal shell that is to be compatible with a glass-filament-wound shell. Optimum performance is obtained when equal margins of safety exist in all directions at all points on the surface of the shell, whether the vessel is fabricated from isotropic material, anisotropic material, or a combination of the two. Because tank performance is based on weight, operating pressure, and internal volume, and the filament-wound material has a higher strength-to-weight ratio than all-metal-shell materials, it is extremely desirable to minimize the metal-shell thickness while maintaining equal margins of safety.

The achievement of equal margins of safety in a filament-wound vessel that is combined with an isotropic load-carrying metal shell requires that tensile strains in the metal at the design pressure be equal in all directions. At the design pressure, therefore, the metal shell must be in a 1-to-1 stress field at all points, including the cylindrical section. Likewise, if the hoop-filament strength equals the longitudinal-filament strength, tensile strains in the hoop and longitudinal filaments must be at the same level at the design pressure throughout the glass-filament shell, as is common in standard filament-wound pressure-vessel design.

For an optimum design, the filament-wound composite should develop its ultimate design stress at the same internal pressure (design pressure) at which the metal shell develops its ultimate design stress in the principal stress directions. This requirement may be expected to be compromised in practice by several factors; however, if the metal is worked to its yield point or beyond, most of its strength is utilized and the effect on performance produced by the deviation is expected to be slight.

If boundary conditions are not imposed on the allowable metal-shell strain, the applied pressure load can be sustained by many combinations of metal and filament-wound-composite thicknesses.

For this condition, the load-compatibility equation is

$$N = \sigma_l t_l + \sigma_g t_g$$

where

N = pressure-vessel membrane force, lb/in.

σ_l = stress in metal shell, psi

t_l = thickness of metal shell, in.

σ_g = stress in glass filaments, psi

t_g = thickness of glass filaments, in.

As boundary conditions are imposed on allowable metal-shell strain at the design pressure, specific thicknesses of metal and filament-wound composite required to sustain the pressure load within these boundaries are greatly influenced and controlled by the strength and modulus of the metal shell as well as the degree of precompression produced in it by glass-filament overwrapping. Theoretically, the proper application of filament-winding tension during fabrication may be used to shift the relative positions of the glass-filament and metal-shell stress-strain curves so that (1) the strains at which the design-ultimate-strength levels of the metal shell and filament winding occur are closer together or equal (the condition for optimum design), and/or (2) maximum use is made of the strength capabilities of the metal shell and filament winding within the imposed strain limits.

As previously mentioned, the initial application of prestress or operating pressure will generally load the structure past the proportional limit of the metal shell, causing permanent set in it and a shift in the relative position of the stress-strain diagrams for the two component materials. This prestress into the plastic zone decreases the amount of deformation that occurs on subsequent pressure loadings and proves the structure (especially welded joints) because the metal shell is forced to work, in a controlled manner, past its yield point into the plastic zone.

A review of the design alternatives available for GFR metal shells reveals that (in addition to technical problems related to analytical determination of optimum designs based on load compatibility, allowable metal-strain-boundary conditions at operating, proof, and/or prestress pressures, and material properties) the influence of the following parameters must be fully understood:

Optimum head contour (for spheroidal and completely wrapped, cylindrical, pressure vessels)

Buckling strength of metal shell

Effects of cyclic and sustained pressure loading

Differential thermal contraction on exposure to temperature variations

Winding-tension variables

Metal-shell and filament-wound-composite fabrication-process limitations.

These parameters are reviewed in the paragraphs that follow.

C. OPTIMUM SHAPE AND HEAD CONTOURS

1. Shape

To attain the theoretical optimum performance, the pressure vessel must meet all loads within the structure and provide equal margins of safety in all directions. The criterion of equal margins of safety for isotropic metal pressure vessels results in the selection of a sphere as the optimum shape. The sphere also represents the optimum design for heads of cylindrical vessels; however, the cylindrical section of a metal pressure vessel with hemispherical heads will be less efficient than the heads because the 2-to-1 stress field of the cylinder produces unequal safety margins in the metal shell.

The optimum shell can assume a multitude of shapes because equal margins of safety can be obtained for numerous stress relationships, including the 2-to-1 stress field of a cylinder. This theoretical number of optimum shapes is reduced in practice by the difference in efficiencies of circumferential, helical, and longitudinal fibers; bending stress created by the juncture of head to cylinder; and physical factors (composite thickness, vessel diameter, filament continuity, fabrication limitations, etc.). In practice, the back-to-back head configuration produces the most efficient designs. If it is necessary to have a cylindrical section, however, the longer ones are the more efficient. The head contours for a vessel with a non-load-carrying liner approach an ellipse with a ratio of minor-to-major axes of 0.62, which is modified to some extent by the size of the axially located port, the wrap angle, and other geometric factors.

2. Head Contour

The optimum head contours for filament-wound shells combined with load-carrying metal shells will fall between those of the complete filament-composite configuration and the spherical shape. The exact curvature of

any specific design depends on the load fractions carried by the filament and metal shells, which are a function of the relative moduli, strengths, thermal coefficients of contraction, and thicknesses of the metal and filament-shell components. To determine the head contour, the loads in the metal shell must first be defined. Next, the optimum head contour is established from the combined strength of the metal shell and filament-wound-composite structure in order to produce a balance between membrane forces and strength. Strains in the liner are computed from bidirectional-stress-strain data or from unidirectional data and the physical properties of the materials, because the 1-to-1 stress-field stress-strain curve can be predicted from uniaxial properties.

3. Other Geometric Considerations

It is desirable to keep the diameter of the axial ports to a minimum in order to reduce vessel weight. However, the minimum axial-port dimension is regulated by the efficiency of the filament-wound-composite structure around the ports, which is reduced as the stacking (buildup) of the composite is increased. Aerojet studies, conducted on vessels for room-temperature service, have indicated that a tape-width to chamber-diameter ratio of 0.015 limits the axial port to a minimum diameter of about 20% of the chamber diameter for maximum efficiency. For a greater ratio, the axial-port diameter could be reduced; e.g., a port diameter approximately 10% of the chamber diameter could be used with a tape-width to chamber-diameter ratio greater than 0.025.

D. BUCKLING STRENGTH OF METAL SHELL

The most apparent design innovation associated with GFR metal tanks is extension of the elastic range of the metal by operating from compression to tension rather than in just the tension range. This is accomplished by imposing on the glass-filament composite at zero chamber pressure a positive tension load that is reacted by a compressive load in the metal shell. Compressive liner stress at zero chamber pressure can be set up by a number of techniques: using filament-winding tension during metal-shell overwrapping, subjecting the fabricated GFR metal tank to a prestress pressure that produces plastic yielding of the metal liner, or combinations of these two techniques. Some support of the metal shell under compressive loads (and increase of the critical buckling stress) is provided by the bond of this shell to the glass-filament shell. However, the integrity of the adhesive bond after tank fabrication and at any time during service life may be questioned. Additionally, the destruction of this bond by fracture of the adhesive (e.g., because of embrittlement at subzero temperatures) could reduce the support. In view of these unreliable features of a bond between the metal and glass-filament shells, it was decided in this study to ignore any beneficial effect on metal-liner compressive-buckling strength produced by the bond.

1. Cylindrical Section

The amount of pressure induced on the metal shell depends on the filament tension and the curvature of the part: $p = T/R$, where T is tension (lb/in. of width) and R is radius (in.). This pressure, therefore, does not act in a manner similar to hydrostatic pressure. The buckling of cylindrical

sections of the metal shell from hoop wraps (other than the cusp buckling mentioned below) will theoretically not occur, because buckling requires a reversal of the radius of curvature of the metal shell and a reduction to zero of the radial driving force as the radius approaches infinity. The compressive hoop force in the liner remains constant, however, and resists the passing of the curvature through the inflection point.

It has been found experimentally that a cylindrical metal shell overwrapped circumferentially with filaments will collapse violently if the windings are too tight. This phenomenon apparently can occur only if the windings are unbonded and free to separate from the shell when buckling occurs, as explained in the following terms by H. Langhaar, A. Boresi, L. Marcus, and G. Love in Ref. 8:

If the fibers are imbedded in resin or are otherwise bonded to the shell, the stress resultants . . . for the composite shell are zero, and according to shell theory, only these quantities effect stability if the layers act together as a unit. However, the situation is different if the fibers can separate from the shell. Then, conceivably, buckling of the type shown in [Figure 6] might occur, since the strain energy of the buckled system is less than that of the unbuckled shell because of relief of stress in the windings caused by buckling. Buckling in the infinitesimal sense of Euler is not possible, however, if the cross section remains a smooth curve, since separation of the fibers cannot occur unless the cross section assumes a concave-convex form, as indicated in [Figure 6]. Since the cross section is initially circular, the shell cannot arrive at such a form without passing through oval forms, for a change of curvature greater than the reciprocal of the original radius is required to produce a concavity. For an oval form, the fibers everywhere maintain contact with the shell; therefore, there is no relief of fiber stress. However, the shell is bent; accordingly, the strain energy of bending is increased; hence, the total strain energy is greater for an oval form than for the original circular form. Since intervening oval forms always separate a concavo-convex form from the circular form, there is always a potential-energy hill that the shell must pass over before it gets into a buckled form.

This argument breaks down, however, if a cusp occurs in the buckled cross section. Experiments have shown that a fiber-wound shell may buckle into the form shown in [Figure 7]. Naturally strain energy of the plastic hinge represented by the cusp must be considered. The hinge tends to form where the maximum plastic bending moment is reduced by small holes or other imperfections such as mismatch of the parts, flat spots on parts, and externally applied non-symmetrical loads.

Buckling of the overwrapped cylinder is expected to occur at a lower level when longitudinal forces are present, because the longitudinal radius is at infinity initially and the prestresses in the liner may be as high in the longitudinal direction as in the hoop direction.

To design the load-bearing metal-shell component of GFR metal tanks, it is necessary to know the metal-shell compressive-stress level at which (a) liner buckling occurs, or (b) the liner's elastic limit is exceeded. Present methods of analysis do not permit the calculation of metal-shell compressive-buckling-stress design limits; however, this design information has been established by experimental evaluation.

R. H. Johns and A. Kaufman of the NASA Lewis Research Center tested the buckling of metal cylinders due to overwrapping in the circumferential direction with layers of tensioned filaments. Twenty-nine tests were conducted on mild steel, stainless steel, nickel, titanium, and aluminum with diameter-to-thickness (D/t) ratios ranging from 175 to 3000. Another five data points, with D/t ratios in the range from 320 to 600, were obtained from the literature. The results are summarized in Ref. 9 and are illustrated in Figure 8. They indicate that a straight-line correlation exists in logarithmic coordinates between D/t for the metal-shell cylinder and the parameter σ_c/E_s , where σ_c is the critical stress from overwrapping at buckling failure and E_s is the metal-cylinder secant modulus at failure taken from the stress-strain curve.

E_s is always equal to the elastic modulus, E, because of the GFR-metal-tank design criterion that the springback stress in the metal shell after initial prestress in the plastic region of the metal stress-strain curve should not exceed (a) the compressive proportional limit of the metal shell, or (b) the compressive-buckling stress of the metal shell. The hoop compressive stress in the metal shell at buckling, σ_c , is given by

$$\sigma_c = \frac{pR}{t} = \frac{p}{2} \frac{D}{t}$$

The empirical relationship of D/t vs p/E_s shown in Figure 8 was converted to D/t vs σ_c for several candidate metal-shell materials (see Section IV,B) - Ti-5Al-2.5Sn, 2219-T62 aluminum, 301 SS, and Inconel X-750 - using the foregoing equation and appropriate values for E_s . Figure 9 presents the resulting plot of metal-shell D/t ratio vs 75°F allowable-elastic-hoop-compressive stresses. Predicted allowable-elastic-hoop-compressive stresses at -320 and -423°F, based on the use of low-temperature values for E_s , are shown in Figures 10 and 11. The relationships between D/t and allowable compressive stress shown in Figures 9, 10, and 11 were used in the parametric study to determine optimum metal-shell D/t values for minimum-weight GFR-metal-tank designs.

2. Heads

Data are not available on the buckling strength of metal-shell heads that have been overwrapped with tensioned filaments. Because of their two-dimensional radii of curvature, however, the heads are expected to be more stable than hoop-wound cylinders with the same D/t ratio. The primary compressive loads in the metal-shell heads are in the meridional direction. At the equator of the head, the meridional radius of curvature of typical GFR metal tanks is smaller than the cylinder radius, and along the head the meridional

radius of curvature remains less than the radius of the cylinder. Hence, the head has a lower D/t ratio than the cylinder (e.g., the meridional radius of curvature at the equator of a filament-wound pressure vessel with a very thin metal liner is about one-half of the cylinder radius. For a relatively thick load-carrying metal liner, the meridional radius of curvature approaches the radius of the cylinder, but the overwrap thickness is low, as are the compressive stresses produced by it.

To be safe in the design of the equator of the heads for GFR metal tanks, cylinder buckling stress vs cylinder D/t was used to give conservative results. Acceptable designs for the equator of the head based on this criterion will be assumed not to be based on buckling at any other point up the contour (until experimental data are developed that show otherwise).

3. Comparison of Metals

For comparisons of materials, it is desirable to know the relationship of the metal-shell D/t ratio to the allowable ratio of elastic hoop compressive stress to density. The relationships of Figures 9, 10, and 11 were replotted on Figures 12, 13, and 14 as D/t vs allowable ratio of elastic hoop compressive stress to density. The result is very nearly a single line for steel, nickel, aluminum, and titanium, due to the closeness of their modulus-to-density ratios. The significance of Figures 12, 13, and 14 is that for a given design and a required value of the product σ_{tg} at springback, steel, nickel, titanium, and aluminum are capable of providing the required load-carrying capabilities at the same weight, within the limits of their strength-to-density range. However, the rating of these materials on the basis of maximum strength-to-density ratios shows the titanium alloy to be superior, followed by the aluminum, stainless steel, and Inconel alloys. From the standpoint of compressive properties, metal-shell materials in each class with high ratios of proportional limit to density and of buckling stress to density are the most desirable for GFR metal tanks.

E. CREEP

All metals creep to some extent under loading, but in general this factor is not expected to be a primary consideration in the study of GFR metal pressure vessels, except for titanium-alloy shells, because

1. Under tension loads, creep should not occur in the overwrapped metal shell, because of the restraint imposed by the glass filaments.
2. Under compression loads, the measured creep in glass-overwrapped metal cylinders has been shown to be negligible in prior Aerojet studies.

Room-temperature creep has been reported for various titanium alloys and appears to be particularly serious in the ELI grades of Ti-6Al-4V and Ti-4Al-2.5Sn. The latter has been shown to be susceptible to considerable creep at room temperature for applied stresses amounting to 60% of the ultimate. As a result, a precautionary note has been incorporated in MIL-HDBK-5 as part of Change Notice 5. While not a problem under tension loads in most GFR-metal-tank designs because of restraint imposed by the glass filaments, creep could become serious during compression loading of the metal shell (at zero internal pressure in the GFR metal tank).

F. CYCLIC LOADS AND FATIGUE STRENGTH

Cyclic loads constitute one of the most important factors regulating the performance of the filament-wound-composite structure. Aerojet has conducted many evaluations to establish the effect. The data from these studies show that the loss in strength from 10 pressure cycles to 80% of the single-cycle burst pressure will result in a strength reduction of 5 to 10%. This reduction approaches a logarithmic rate, so that 100 cycles to 80% of the original strength will result in a strength reduction of 10 to 20%.

The high-strength performance of the filament-wound composite, with its accompanying high operating fiber stresses and strains, induces extremely large biaxial-strain requirements on the metal shell, and cyclic application of these large strains results in reduction of the metal-shell fatigue life. Past studies have shown that complex welded joints generally have a much shorter fatigue life than does the parent metal. These factors make the attainment of highest-quality metal-shell weldments the most important consideration in the fabrication of GFR metal tanks.

For this study, it is necessary to use as realistic a number of cycles for the tankage as possible. Based on past applications, it appears that the number of cycles (proof, checkout, and operating) to which the high-pressure gas bottles will be subjected is from 3 to 5, with a possible maximum of 10. However, because of the inconsistent response of filament-wound bottles to cyclic loads and the severe deformation requirements imposed on the metal shell, the number of cycles used for design purposes in the present study was set at 100.

G. TEMPERATURE EFFECTS

In establishing GFR metal-shell pressure-vessel designs suitable for cryogenic service, provision must be made in the analysis for thermal-expansion/contraction effects on the stress-strain relationship produced by glass-filament overwrapping a metal shell at ambient temperatures, curing the resin at ambient or elevated temperatures, and then operating the pressure vessel at cryogenic temperatures.

The effect of operating at temperatures considerably lower than that used during fabrication is a shift in the amount of compressive preload on the liner because of the difference in the thermal coefficients of contraction of the materials. The +75 to -423°F thermal coefficient of contraction

for filament-wound composite (in the range from 2.00 to 3.00×10^{-6} in./in.-°F, depending on the winding pattern) is less than the values for the metal-shell materials under consideration:

<u>Material</u>	<u>Coefficient, 10^{-6} in./in.-°F</u>
Inconel X-750	4.99
2219 aluminum	8.915
Ti-5Al-2.5Sn	3.910
301 SS	6.760

The effect of this difference will be to reduce preloads in the liner, which is undesirable because the strength of the metal is increasing (the preload should be increased for optimum performance and minimum tank weight at cryogenic temperatures). As an example, a drop of 500°F in a 2219 aluminum metal shell could result in a contraction of approximately 0.34% at the maximum thermal-coefficient difference of about 7×10^{-6} in./in.-°F; for low metal-to-composite-thickness ratios, this could eliminate the total preload. With regard to values for thermal coefficient of contraction, it is of specific interest that the coefficient for filament-wound composite will not be the same in all directions because of differences in resin and glass volume ratios and fiber orientation, and that titanium has the coefficient closest to that of the filament-wound composite.

H. FABRICATION CONSIDERATIONS

1. Winding Mandrel

Tension in filaments deposited on a curved surface generates high radial and/or longitudinal compressive forces on the already deposited layers and in the metal shell. Winding tensions as high as 5 to 10% of the ultimate glass-roving strength have been shown to be important in achieving the best glass-strength levels in filament-wound composites; higher tensions may be desirable in some designs to help obtain the required degree of precompression in the metal shell.

During overwrapping, the metal shell can either be supported or unsupported. Because the design criteria for GFR metal tanks include a requirement that the unbonded metal shell sustain the compressive forces of the overwrapped filaments without buckling when no mandrel is in the metal shell, it is not necessary to provide metal-shell support during overwinding for this purpose. However, unsupported-metal-shell deflection during winding will produce a loss of tension in the inner layers of filaments; for optimum structural performance it may be necessary to program the filament-tension level during the winding of successive layers to gain essentially constant residual stress in the filaments of the finished pressure vessel. If rigid mandrel support is provided to the metal shell, nearly constant winding tension can be used unless the filament-wound composite is extremely thick.

2. Winding Tension

Filament-winding tension can be used to place the metal shell in initial compression and thereby increase the pressure-vessel elastic strain by an amount, ϵ , which is defined in Figure 15.

The cylindrical-section load equilibrium between the winding and the metal shell in the hoop direction after mandrel removal can be stated as follows (see Figure 15):

$$N_{\theta} = \sigma_{sh_B} t_s + \sigma_{gh_B} t_g = pR$$

$$p = 0$$

$$\sigma_{gh_B} = - \frac{\sigma_{sh_B} t_s}{t_g}$$

$$\epsilon = - \frac{\sigma_{sh_B} - \nu_s \sigma_{sa_B}}{E_s} = \frac{\sigma_{gh_A} - \sigma_{gh_B}}{E_{gh}}$$

$$\begin{aligned} \sigma_{gh_A} &= - \frac{E_{gh}}{E_s} \left[\sigma_{sh_B} - \nu_s \sigma_{sa_B} \right] + \sigma_{gh_B} \\ &= - \frac{E_{gh}}{E_s} \left[\sigma_{sh_B} - \nu_s \sigma_{sa_B} \right] - \frac{\sigma_{sh_B} t_s}{t_g} \end{aligned}$$

The relationship of σ_{sh_B} to σ_{sa_B} is established from the biaxial-stress ratio determined from the load and strain compatibility analysis. Before removal of the mandrel,

$$N_{\theta} = \sigma_{sh_A} t_s + \sigma_{gh_A} t_g$$

$$N_{\theta} = T_H N_{s_H} N_H$$

Therefore,

$$T_H = \frac{\sigma_{sh_A} t_s + \sigma_{gh_A} t_g}{N_{s_H} N_H}$$

However, if the mandrel is rigid during winding,

$$\sigma_{sh_A} = 0 \quad \text{and} \quad T_H = \frac{\sigma_{gh_A} t_g}{N_{s_H} N_H}$$

where σ_{gh_A} is defined as above. For the longitudinal direction,

$$\sigma_{ga_A} = - \frac{E_{ga}}{E_s} \left[\sigma_{sa_B} - \nu_s \sigma_{sh_B} \right] - \frac{\sigma_{sa_B} t_s}{t_g}$$

and

$$T_L = \frac{\sigma_{ga_A} t_g}{N_{s_L} N_L}$$

The hoop and longitudinal filament-winding tensions required for compression of magnitudes σ_{sh_B} and σ_{sa_B} in the metal shell can be computed from the above equations, using the applicable values for the other design parameters.

I. SPECIFIC DESIGN CRITERIA

The parametric study of GFR metal pressure vessels was undertaken to define the stress-strain relationship that must exist between the metal shell and the glass-filament shell to give optimum performance. The ranges of pressure-vessel shapes, diameters, lengths, and internal volumes of NASA interest in the parametric study are shown in the shaded areas of Figures 16 and 17. The specific ranges of parameters for the study are summarized below.

The shapes include (1) spheres; (2) oblate spheroids; (3) circumferentially wrapped, cylindrical, closed-end vessels; and (4) completely wrapped, cylindrical, closed-end vessels. Optimum head contours for GFR metal tanks were analytically developed and used in the parametric study.

The sizes include (1) spheres, 12 to 40 in. in diameter; (2) oblate spheroids, 12 to 40 in. in major diameter; and (3) cylinders, 12 to 40 in. in diameter, with a maximum volume of 34,000 in.³ for any diameter.

The pressure-vessel volumes range from 500 to 34,000 in.³

The operating pressures range from 1000 to 4000 psig.

The operating temperatures include +75, -320, and -423°F.

The overwrap material consists of S-HTS glass-filament roving and an epoxy-resin matrix.

Candidate metal-shell material for use in GFR metal tanks include Type 301 SS, Ti-6Al-4V, Ti-5Al-2.5Sn, 2219 aluminum alloy, 7039 aluminum alloy, and the Inconel X-750 nickel-base alloy.

The tankage service-life requirement includes a minimum fatigue life of 100 pressure cycles and 72 hours of sustained loading at the operating-pressure level.

The factor of safety is as follows:

$$\text{Factor of safety} = \frac{\text{failure pressure after service cycle}}{\text{service-cycle pressure load}} = 1.00$$

To minimize the magnitude of the hysteresis loop in the metal shell during pressure cycling, the maximum metal-shell operating-stress level is maintained at a fixed ratio below its initial proof-pressure prestress level. This is accomplished by implementation of the design condition that

$$\sigma_o = 0.90 \sigma_p$$

where

σ_o = maximum metal-shell tensile stress at the operating pressure

σ_p = metal-shell tensile stress at the prestress pressure

The springback stress in the metal shell at zero pressure does not exceed (1) the compressive proportional limit of the metal shell, and (2) the compressive-buckling stress of the unbonded metal shell.

IV. ANALYSIS OF MATERIAL PROPERTIES

A. GLASS-FILAMENT SHELL

An analysis was made to determine the minimum, maximum, and typical values of room-temperature, single-pressure-cycle, allowable, S-HTS glass-filament, strength levels in pressure vessels having operating pressures from 1000 to 4000 psi, diameters in the 12- to 40-in. range, and length-to-diameter (L/D) ratios ranging from 0.62 to 5. This analysis is covered in detail in Appendix A. It showed that representative filament-strength values ranged from 314,000 to 368,000 psi for hoop filaments and from 272,000 to 370,000 psi for longitudinal filaments; a typical value suitable for use in calculations was found to be 330,000 psi.

Adjustments were made in the single-pressure-cycle design allowables to account for the effects of cyclic and sustained tank-loading requirements (assumed to be 100 pressure cycles and 72 hours of sustained loading at the operating-stress level). The typical single-pressure-cycle strength level of 330,000 psi had to be reduced by a factor of 0.60 to 200,000 psi to provide for the service-life requirement.

Data on the properties of glass fibers and filament-wound composites at cryogenic temperatures were compiled and developed. Based on them, the following estimates were made for S-HTS glass filaments with a design-temperature decrease from 75°F to -320 or -423°F: a design-allowable filament-strength increase of 50%, and a tensile-modulus increase of 10%. Using these values, pressure-vessel filament strengths increase from the typical value of 330,000 psi at 75°F to 495,000 psi at -320 and -423°F, the tensile modulus increases from 12.4×10^6 psi at 75°F to 13.6×10^6 psi, and the ultimate filament tensile strain increases from about 2.68% at 75°F to about 3.64% at -320 and -423°F.

For the S-HTS filament/epoxy-resin composite (67/33 volume ratio), with a 2-to-1 transverse-to-longitudinal filament ratio, the thermal coefficient of contraction at 75 to -423°F is estimated as 2.01×10^{-6} in./in.-°F in the transverse direction and 2.81×10^{-6} in./in.-°F in the longitudinal.

B. METAL SHELL

Candidate materials were selected from the classes of alloys that apparently have suitable ductility and strength at 75 to -423°F for use as load-bearing shells of GFR metal tanks. The materials evaluated included titanium alloys, stainless steels, aluminum alloys, nickel-base alloys, and cobalt alloys. The complete analysis is presented in Appendix B, and is summarized below.

Each prospective candidate material was subjected to a characterization analysis. This work involved an extensive literature survey, regarding each material in the unwelded and welded conditions for all the available properties in tension and compression at 75, -320, and -423°F.

A complete compilation of properties was not required to adequately rate a material; ductility, weld-joint efficiency, and fracture toughness were the main criteria in determination of the most suitable material in each alloy class. Materials thus identified were subjected to a more comprehensive evaluation, which served as the basis for a preliminary rating (in order of preference) of each material in its alloy class for use as the metal-shell component of GFR metal tanks for cryogenic service.

Design-allowable properties and stress-strain curves were obtained for 75, -320, and -423°F service for each alloy determined to be a possible candidate (best in its alloy class). These data were used in the parametric study (covered in Section VI), which resulted in the final ranking of the candidate materials for 75 to -423°F applications of GFR metal-shell pressure vessels.

The basic metal-shell design requirements to attain optimum performance of GFR metal tanks were established before the characterization of candidate materials. It was determined that the two primary liner properties needed to provide maximum pressure-vessel performance were (1) high-tensile-strain capability to match the elongation of the glass filaments, at the operating and burst pressures, and (2) a high ratio of compressive proportional limit to density to permit the use of high elastic-springback stresses in designing the metal shell. Because the ductility and proportional limit of a given metal have an inverse relationship (as ductility increases, yield strength decreases), the materials were evaluated first on the basis of meeting a minimum ductility requirement and second on proportional-limit-to-density-ratio characteristics.

To provide a tank capable of being burst-tested at a high filament-stress level, the minimum metal-shell tensile-strain capabilities required in a 1-to-1 biaxial-stress field for optimum burst performance of the filament-wound composite were established as 2.0 to 2.7% at 75°F and 2.7 to 3.8% at -320 and -423°F.

Under 1-to-1 biaxial-stress-field conditions, metals have a significantly reduced strain capability as compared with their uniaxial (1-to-0) ductility. Test data (presented in Appendix B) showed that the allowable elongation under 1-to-1 stress-field conditions was less than 50% of the uniaxial ductility, and closer to 25% of the uniaxial ductility. This value is lower than the ductility that would theoretically be expected from a material. Based on the data, an allowable biaxial elongation of 25% of the uniaxial value was selected for the design of GFR metal tanks.

With a design allowable for biaxial elongation under 1-to-1 stress conditions equal to 25% of the uniaxial elongation, metal-shell materials must have an 8.0 to 10.8% uniaxial elongation at 75°F and a 10.8 to 15.2% uniaxial elongation at -320 and -423°F to achieve the full strength potential of the glass-filament-wound shell.

If the GFR metal tank is not required to demonstrate high-burst-strength performance at the operating temperature, but only a satisfactory

strain-cycling capability between zero pressure and the operating pressure, the minimum metal-shell tensile-strain capabilities required in a 1-to-1 biaxial-stress field for optimum performance include (1) an initial prestress past yield to a plastic-strain value dictated by design considerations (this prestress will generally be conducted at room temperatures), and (2) 100 strain cycles between the compressive proportional limit and the offset tensile proportional limit.

For successful application, the following properties were also considered essential to pressure-vessel performance: notched-to-unnotched strength ratio, notched-strength to unnotched-yield-strength ratio, weld-joint tensile strain at fracture, weld-joint efficiency, and the number of cycles to failure at the maximum operating-strain range. Using this group of properties, the following materials were determined to be the best in their respective alloy classes for metal-shell fabrication:

Stainless steel	Type 301 (1/2-hard temper)
Titanium alloy	Ti-5Al-2.5Sn (annealed, ELI* grade)
Aluminum alloy	2219 heat-treated to the T62 temper after fabrication (2219-T62 aluminum)
Nickel-base alloy	Inconel X-750, solution-treated and aged (STA) after fabrication

For performance at both the operating and burst pressures, Inconel X-750 was found to be the only alloy that meets all basic requirements of the metal shell over the entire 75 to -423°F range. It appears to be the only material for which the optimum -320 and -423°F burst-strength performance of GFR metal tanks can be expected at this time. Candidate materials from the other alloy classes (stainless steel, titanium, and aluminum) were found to have low weld-joint efficiencies, and/or inadequate weld-joint tensile-strain capabilities at cryogenic temperatures. For these latter materials, therefore, development programs aimed at improving the pertinent properties are required before improved-performance GFR metal tanks can be attained by the use of lighter, more-ductile, and higher-strength metal shells than provided by Inconel X-750.

For operating-pressure performance (i.e., no specific burst-pressure requirement), all these candidates show good promise of meeting the 100-strain-cycle requirement between the compressive-to-tensile proportional limits, for operation at 75 to -423°F (see Appendix C), if the metal shell is prestressed into the plastic region at room temperatures. If prestressing is to be accomplished at cryogenic temperatures, Inconel X-750 is the only material that can be recommended at this time.

Table 2 summarizes essential properties for the four candidate materials and gives their preferential rating for each property. Analysis of these ratings led to conclusions that the four candidates are considered suitable for GFR-tank metal-shell fabrication in preferential orders discussed below.

* ELI represents extra-low-interstitial content.

1. Tankage Required for High Performance at Operating and Burst Pressures

The first choice for service at 75 to -423°F is Inconel X-750 (STA). Although rated third on the basis of ratios between compressive proportional limit and density and of notch-to-unnotch strength, a high rating with respect to the other essential properties makes this alloy superior to the others. Inconel X-750 (STA) appears to be the only candidate capable of performing as required over the entire temperature range.

The second choice for service at 75 to -320°F is 2219-T62 aluminum. It was determined primarily on the basis of good notch-strength to unnotch-yield-strength ratio, good weld-joint efficiency, and high-strain-range fatigue life as compared with Ti-5Al-2.5Sn. This material is not recommended for -423°F service in GFR metal tanks that are to be burst-tested, because of its extremely poor weld-joint tensile-strain properties and low weld-joint efficiency.

The third choice for service at 75 to -320°F is Ti-5Al-2.5Sn (annealed, ELI grade). A superior ratio of compressive proportional limit to density and acceptable notch-to-unnotch strength ratios are obtainable, but this material is rated third for its low tensile-strain properties and fourth ranking with regard to its estimated low-cycle, high-strain-range fatigue life. Additional factors were (a) the possibility that cryogenic-temperature creep may occur in compression, and (b) the fact that extremely poor weld-joint tensile-strain properties at -423°F make the performance of GFR metal tanks at that temperature questionable.

The fourth choice for service at 75 to -320°F is Type 301 SS (1/2 hard). Because of the directionality effect resulting from cold-rolling operations required to produce the 1/2-hard temper, this material provides the lowest ratios of compressive proportional limit to density and of notch strength to unnotch yield strength, and in general offers poor weld-joint efficiency in the as-rolled condition. The stress-relieved material could not be properly rated because insufficient data were available for evaluation. The compressive-yield strength, modulus of elasticity, and density are similar to those of Inconel X-750, indicating that GFR metal tanks of these materials might be expected to display about the same level of performance. However, the performance with 1/2-hard 301 SS may be somewhat lower because of the following factors:

a. At the same parent-metal yield-strength levels, the weld-joint efficiency and ductility of 301 SS are well below those of Inconel X-750. The sheet thickness will therefore have to be increased in the weld area to provide adequate strength and control of strain in the joint.

b. Cold working results in a large directionality effect and reduction of properties in compression.

2. Tankage Required for High-Operating-Pressure Performance Only

For service at 75 to -423°F , the first choice is Ti-5Al-2.5Sn (annealed, ELI grade); second, 2219-T62 aluminum; third, Inconel X-750 (STA); and fourth, 301 SS (1/2 hard).

C. DESIGN ALLOWABLES

Table 3 summarizes the properties of the S/HTS glass-filament-wound-composite and candidate-metal-shell materials [Inconel X-750 (STA), 2219-T62 aluminum, Ti-5Al-2.5Sn (annealed, ELI grade), and 301 SS (1/2 hard)] used in the computerized parametric study.

V. STRUCTURAL ANALYSIS

The parametric study required the development of a structural-analysis approach for GFR metal tanks, and a computer program using the analysis to solve specific design problems. They are discussed below.

The analysis assumes the metal shell to be isotropic, load-bearing, smooth, and of constant thickness. Load and strain compatibility relationships were written for the glass-fiber and metal-shell end-closure and cylindrical sections of the tank. They were related to design criteria for GFR metal tanks with regard to residual stresses in the filament-wound and metal shells, overwrap pressures, rigid or pressurized mandrel support of the metal shell during overwrapping, and operating-pressure and operating-temperature cycles. The complete analysis was written in FORTRAN IV computer language and was programed into an IBM 7094 digital computer for use in pressure-vessel-design and service-cycle-history analyses.

The program designs and analyzes complete GFR metal tanks, wound with either geodesic (helical) or in-plane patterns along the cylinder and over the end domes and complemented by circumferential windings in the cylinder. It establishes the optimum head contours at both ends of the pressure vessel, computes the filament and metal-shell stresses and strains at zero pressure and design pressures, establishes the hoop-wrap thickness required for the cylindrical portion, and computes the weight, volume, and filament-path length of the components and complete vessel. It also determines the stresses and strains in the filament and metal shells throughout service cycling on the basis of a series of pressure, composite-temperature, and metal-shell-temperature inputs.

A. ANALYTICAL APPROACH

The analysis was based on assumptions that

1. The filament stresses are constant along their length.
2. The metal-liner stresses are constant in the meridional direction.
3. Equal strains are produced in the hoop and meridional directions at the equator of the head and in the cylinder as pressure is increased from the winding pressure to the design pressure.
4. The liner thickness is constant to permit ease of fabrication.
5. The effect of the resin matrix is negligible (a netting analysis can be used).
6. The rotation of filaments is negligible as pressure is increased or decreased from the winding pressure.

7. The radii of curvature of the head contour have negligible differences between the unpressurized and pressurized conditions.
8. The stress-strain relationship of the metal liner can be represented by two straight lines (i.e., primary and secondary moduli).
9. The stress-strain relationship of filaments can be represented by a straight line.
10. Poisson's effect in a filament-wound composite is negligible.
11. Poisson's ratio = $1/2$ in the plastic range of the metal-liner stress-strain curve.
12. The metal-liner biaxial-yield stress equals the uniaxial-yield stress in a 1-to-1 stress field.

The portion of the analysis dealing with governing equations and optimizing conditions, as well as defining computer-program calculation sequences, is presented in detail in Appendix D. A brief discussion follows.

The filament shell is analyzed by a netting analysis that assumes stresses are constant along the length of the filament; both geodesic and planar filament-winding paths are analyzed. In the filament-wound shell, the structural contribution of the resin matrix is ignored. That shell and the metal shell are combined in the analysis by equating strains in the meridional and hoop directions and adjusting the radii of curvature of the shells to match the combined strengths of the materials at the design pressure. The pressure-vessel heads are designed first, and the cylinder is designed to complement the heads. Once the pressure-vessel design is fixed, another analysis is used to determine vessel stresses and strains at any condition of temperature and pressure. Effects of temperature variation are accounted for by the input of thermal coefficients of contraction and the changes in various physical properties of the filament-wound and metal shells with respect to temperature. For this analysis, it has been assumed that the physical-property changes are directly proportional to the temperature, because the end conditions caused by temperature change are the primary concern.

In general, the metal-shell compressive hoop force imposed on the head at zero internal pressure by the composite cannot approach the liner's meridional compressive stress because of filament-shell strength components. The difference in relative rigidities in the hoop and meridional directions is most noticeable at the equator of the head at zero vessel pressure. At this point the hoop force applied by the glass-fiber shell is extremely small in comparison with the force in the meridional direction, because the wrap angle, α , is small and the hoop force is equal to the meridional force times $\tan^2 \alpha$. Because the forces within the composite structure have to balance the forces within the metal shell, it is impossible to induce equal compressive stresses in the liner in all directions, except for the specific condition when $\alpha = 45^\circ$, or when the wrapping tension and pressures are zero. Therefore, the analysis does not require that the head stresses be equal in the hoop and meridional

directions. The analysis does require that the strain changes be equal in the hoop and meridional directions at the equator of the head as the pressure is increased from the winding to the design pressure. For the special case in which rigid mandrel support is given to the liner during overwrapping, equal strains (and hence equal stresses) are produced in the hoop and meridional directions at the equator of the head, up the meridian of the head, and in the hoop and longitudinal directions of the cylinder.

B. COMPUTER PROGRAM

The computer program includes four functional parts for use in pressure-vessel-design and service-cycle-history analyses.

Input data for material properties, geometric configurations, and design pressures are analyzed to identify fixed parameters and variable or optional parameters.

Head contours are optimized and contour coordinates of the neutral axis, inside surface, and outside surface are computed from given design conditions and input data. Optimum metal-shell and filament-wound-shell head thicknesses are computed. Stresses and strains in the metal and filaments of the head are computed at the winding and relaxed conditions and at the design pressure and operating-temperature conditions.

The overall vessel is optimized by designing the cylinder section to complement the head design. Weights of the metal shell, glass-filament shell, and total vessel are calculated, as are the surface area and contained volume. The pressure-vessel performance factor, pV/W ,^{*} is calculated.

Stresses and strains in the metal and filaments are computed for a given history of pressure- and/or temperature-cycle applications, such as values at a given pressure level and values after removal of the pressure load.

1. Vessel Design

The first three parts of the computer program analyze and design complete pressure vessels, wound with either geodesic (helical) or in-plane patterns along the cylinder and over the end domes and complemented by circumferential windings in the cylinder.

The computer-program input includes pressure-vessel geometric parameters, metal-shell-material properties, filament-shell-material properties, filament and longitudinal metal-shell stresses at the winding condition, and design conditions of temperature. The program also has seven optional variables, of which four must be input: (a) the tensile hoop strain in the metal shell at the design pressure, (b) the tensile longitudinal strain in the metal shell at the design pressure, (c) the filament stress at the design pressure, (d) the design pressure, (e) the thickness of the metal shell, (f) the

*Where p = design pressure, psi (e.g., operating pressure, p_o , or burst pressure, p_b); V = internal volume, in.³; and W = pressure-vessel weight, lb (not including fittings).

thickness of the filament shell at the equator, and (g) the metal-shell hoop stress at the winding condition.

The program establishes the optimum head contours at both ends of the pressure vessel, computes the filament- and metal-shell stresses and strains at zero pressure and design pressures, establishes the hoop-wrap thickness required for the cylindrical portion of the vessel, and computes the weight, volume, and filament-path length for the components and complete vessel. The vessel may be designed to a specific condition of pressure and of metal-shell and composite temperatures, and stress and strain calculations for the design condition will be as established by these conditions. All information at zero internal pressure assumes room-temperature conditions; should information be required for zero pressure at other temperatures, the pressurization-history analysis summarized below may be used.

2. Service-Cycle History

The fourth part of the program permits analysis of the stresses and strains in the filament and metal shells during the sequential operational history of the vessel through the input of a series of pressures, composite temperatures, and metal-shell temperatures. It permits the analysis of pressure and temperature cycles on the vessel, taking into account previous strains and loads.

VI. PARAMETRIC STUDY

A. PERFORMANCE FACTOR

Exact weight comparisons are often made for different pressure-vessel configurations to determine the best design for specific hardware requirements. This detailed approach is not convenient, however, for use in obtaining a broad comparative view of the relative weight efficiencies of various shape and material combinations.

Several methods of rating homogeneous metal pressure vessels, including use of the strength-to-density ratio and burst pressure, were reviewed. The study revealed that the most satisfactory method of judging the efficiency of metal, filament-wound, and GFR metal pressure vessels is one that incorporates all the basic parameters of the pressure vessel by means of the performance factor, pV/W , where p is the design pressure, psi (and may be the operating pressure, p_o , or the burst pressure, p_b); V the internal volume, in.³; and W the pressure-vessel weight, lb.

This factor has an advantage over other design-rating methods in that complete vessels (heads, cylinder, bosses, reinforcements, etc.) may be rated by a single term, and a variety of designs can be compared directly. Optimum designs are noted when the performance factor of the complete vessel, as measured by pV/W , has a maximum value.

B. COMMENTS ON SPHERICAL AND CIRCUMFERENTIALLY WRAPPED, CLOSED-END VESSELS

Experience has shown that filament-wound spheres have an efficiency below that of several other configurations because of certain practical considerations. The effectiveness of the multiple-wrap patterns required by a filament-wound sphere is considerably lower than that of other standard winding patterns. The composite-wall-strength levels obtainable in spheres constructed from S-HTS glass filaments is only about 80,000 psi, which is equivalent to a strength-to-weight ratio of about 1.10×10^6 in. This low performance for the filament-wound composite, when combined with a heavier load-carrying metal liner, results in a total vessel efficiency below that obtainable with some homogeneous metal materials and an efficiency considerably below the performance of optimum GFR metal tanks. Consequently, spherical GFR metal tanks do not warrant study.

Optimum, constant-thickness, isotropic, metal, pressure vessels circumferentially reinforced with filaments in the cylindrical section are designed so that the metal shell carries the entire longitudinal load and one-half the hoop load. Some design and performance features of hoop-wound filament-reinforced cylindrical vessels are described in Refs. 9 and 10. This configuration for GFR metal tanks was considered in the study, and the range of use was defined (see following section). For the metal-shell materials considered and compressive-stress design criteria used for GFR metal tanks, the range of application of hoop-filament-reinforced cylindrical vessels was generally below the pressure range of interest. Because GFR metal tanks of higher performance could be obtained with

completely wrapped oblate-spheroid and cylindrical pressure vessels, primary emphasis was placed on extensive study of the completely wrapped configuration.

C. DESIGN OF COMPLETELY WRAPPED GFR METAL TANKS

1. Fixed and Variable Parameters

Complete designs of GFR metal tanks are obtained with the computerized analysis described in Section V. Selected tank-design parameters were held constant for most of the configurations evaluated. This was done primarily because past experience had indicated optimum values for some parameters or because of practical, manufacturing considerations. The fixed parameters were axial-port-to-diameter ratio, type of filament-winding pattern, filament-winding tension, type of metal-shell support mandrel, maximum filament- and metal-shell stresses at the operating pressure, and other material properties. Values selected for these parameters are reviewed briefly below. Unless otherwise stated, it can be assumed that the values given in paragraphs VI,C,1, a through f, below, were used in the parametric study.

a. Axial-Port-to-Diameter Ratio

The maximum efficiency of filament-wound pressure vessels is obtained when the axially located ports are small. As previously noted, however, the axial-boss dimension should not normally be reduced much below 20% of the vessel diameter for maximum efficiency. A boss-to-vessel diameter ratio (D_b/D) of 0.20 is used, and port sizes on each head are assumed to be equal. The weight calculations used in determining the pressure-vessel performance factor, $p_0 V/W$, do not include the weight of the bosses located at the axis of the vessel.

b. Type of Filament-Winding Pattern

Contours in two major categories are used in the filament-winding industry. Structures employing helical winding patterns incorporate some form of geodesic-isotensoid closure contour, and those based on longitudinal (planar) and circumferential wrapping patterns use a balanced-in-plane closure contour. The two types have been subjected to extensive analysis and experimental study (see Ref. 11). The computer program for GFR-metal-tank design analyzes both. It was shown in Ref. 11, however, that a longitudinal-in-plane winding pattern along the cylinder and over the end domes, complemented by circumferential windings in the cylinder, produces the highest-efficiency filament-wound pressure vessels with an axial-port to vessel-diameter ratio of 0.20. This type of pattern was therefore selected for the design and analysis of GFR metal tanks, and a limited evaluation of the geodesic-isotensoid winding pattern was planned, to establish its effect on GFR-metal-tank performance.

c. Filament-Winding Tension

The proper choice and careful control of filament tension constitute an important aspect of the winding operation. Winding tension

as high as 5 to 10% of the glass-roving strength has been shown to be significant in achieving the best glass-strength levels in filament-wound composites (Ref. 12). Filament-winding tension compresses the metal shell and reduces the amount of metal-shell plastic deformation required to attain the design operating-pressure filament-stress level. In general, the reduction of metal-shell deformation is highly desirable; high winding tension is therefore assumed in the design.

At Aerojet, glass-filament-wound structures are usually fabricated with a tension level in the range from 19,000 to 38,000 psi (0.4 to 0.8 lb per end) and an upper limit of about 47,000 psi (1 lb per end) for current production equipment. A constant longitudinal filament-winding-tension stress of 47,000 psi was therefore chosen for the parametric study, and a limited evaluation of lower tension levels was scheduled to establish the effect on GFR-metal-tank performance.

d. Metal-Shell Support Mandrel

A rigid mandrel (e.g., a soluble plaster or salt shell) is assumed to support the metal shell during overwrapping with filaments. The effect of using internal fluid pressure to give mandrel support to the metal shell during winding was evaluated.

e. Maximum Filament and Metal-Shell Stresses
at Operating Pressures

The allowable operating-pressure stresses were established after a review of factors of safety for GFR metal tanks (see Appendix E). This review resulted in the decision to design the tanks to have a safety factor of 1.00 after completion of their cyclic and sustained pressure-loading, service-life requirement. Using this value, it was determined that the filament-stress level at the operating pressure should not exceed 200,000 psi at 75°F and 300,000 psi at -320 and -423°F. The maximum metal-shell stress at the operating pressure will be 90% of the offset yield stress at the operating temperature. The effect on GFR-metal-tank performance of operation at the offset yield stress at the design temperature, rather than 90% of this stress level, was scheduled for evaluation.

f. Material Properties

Properties of the metal-shell materials and the glass-filament overwrap used for the parametric study are shown in Table 3.

g. Variable Parameters

Parameters varied during the study were vessel-diameter to metal-shell-thickness ratio (D/T_L), vessel length-to-diameter ratio (L/D), metal-shell material, proof (prestress) pressure (p_p), operating pressure (p_D or p_O), and design operating temperature (T_D). It was assumed that winding was accomplished at 75°F.

2. Head Contours

The principal forces on all types of closures are in the meridional and circumferential directions. The head contours for filament-wound pressure vessels with a non-load-carrying metal shell approach an ellipse with a ratio of minor-to-major axes of 0.62, as described in detail in Ref. 11. The head contours for filament-wound pressure vessels combined with load-carrying liners fall between the shape optimum for the complete filament-composite configuration and the spherical shape optimum for homogeneous isotropic metal heads.

Optimum head contours for GFR metal tanks were determined using the analysis described in Section V and Appendix D. For the parametric study, it was assumed that an in-plane winding pattern was used for the head. With this pattern, the filament path is described by the intersection of the plane and the head, and filament stresses are required to remain essentially constant. The in-plane winding pattern therefore combines the desirable qualities of both the geodesic-isotensoid contour and the in-plane wrapping method by providing a head contour designed to meet the filament-orientation requirement while incorporating simple wrapping patterns.

The head contour becomes primarily a function of the load fractions carried by the filament and metal shells, because the filament-wound and metal shells are combined in the analysis by (a) requiring that the constant-thickness metal-liner load stresses are constant in the meridional direction, (b) requiring that the filament stresses are constant along their length, (c) equating strains in the meridional and hoop directions, and (d) adjusting the radii of curvature of the shells to match the combined strengths of the materials at the design pressure.

The load fraction, K , carried by the metal shell in the meridional direction of the head at the equator at the design pressure is given by

$$K = \frac{N_{\phi L}}{N_{\phi}}$$

where

$N_{\phi L}$ = meridional force per unit of width in liner

N_{ϕ} = meridional force per unit of width

The metal-shell load fraction is also equal to the total internal-pressure load minus the load fraction carried by the filaments:

$$K = 1 - \frac{\sigma_{fd} v_g T_0 \cos^2 \alpha_o}{p_d a/2}$$

where

σ_{fd} = filament stress at design pressure, psi

v_g = volume fraction of filaments in composite

T_0 = longitudinal composite thickness at equator, in.

α_0 = longitudinal-filament-winding angle, degrees

p_d = design pressure, psi

a = vessel radius, in.

Because the longitudinal-wrap-plane angle, α_0 , is a function of the vessel length as well as of the boss size, D_b , the head contour is also a function of these two parameters. Figures 18 to 21 show the balanced-in-plane head contours for GFR metal tanks for a range of K values [from $K = 0.0$ (filament-wound pressure vessel) to $K = 1.00$ (homogeneous metal pressure vessel)] and vessel length-to-diameter ratios, L/D , for a fixed center-boss size of $D_b/D = 0.20$. The contours are for the neutral axis of the filament-wound composite.

When K is very small, the contours approach the balanced-in-plane head shape for filament-wound pressure vessels. For increasing values of K , the head contours assume intermediate shapes between the filament-wound pressure-vessel head contour and the spherical head contour optimum for homogeneous metal pressure vessels. The effect of L/D on head contour is slight.

The stress conditions in the metal and glass-filament shells along the contour of the heads and in the cylinder of two specific optimum designs of GFR metal pressure vessels with $L/D = 1$ are shown in Figures 22 to 25. Figure 22 shows stresses at the operating pressures for 75, -320, and -423°F in an optimum GFR Inconel X-750 (STA) pressure vessel with a 2220-psi proof pressure and 2000-psi operating pressure at 75°F (the cryogenic operating pressure, at both -320 and -423°F, is 2300 psi). Figure 23 shows the conditions in a GFR Ti-5Al-2.5Sn (annealed, ELI grade) pressure vessel with operating pressures of 3000 psi at 75°F, 4246 psi at -320°F, and 4497 psi at -423°F. In these figures, stresses are plotted as a function of the normalized radial distance, Z ($Z = x/a$). Stresses in the filaments and metal shell at the 75°F design temperature are constant up the contour at the design-pressure condition, thus satisfying the requirement for optimum closure design. For the GFR Inconel tank, stresses also remain essentially constant along the contour for the pressurized conditions at -320 and -423°F. For the GFR titanium tank, however, the filament stresses remain essentially constant up the contour at -320 and -423°F and the corresponding operating pressures, while the metal-shell stresses increase as the normalized radial distance decreases.

Stresses in these same tanks at zero pressure after proof pressure are shown in Figures 24 and 25 for 75, -320, and -423°F exposure temperatures. In both the GFR Inconel and titanium tanks, the compressive stresses at

zero pressure increase significantly up the head contour. Because the tanks have cylindrical sections, however, the compressive stress in the hoop direction of the cylinder controls the tank design. An exposure-temperature decrease from 75°F to -320 and -423°F produced only slight changes in the compressive stresses in the tanks in the unpressurized condition. The stress-strain relationships of the GFR Inconel and titanium tanks are described further in Section VI,C,5, below.

As expected, the compressive stresses in the metal-shell heads at zero pressure after the proof pressure controlled the design of oblate-spheroid GFR metal tanks. The stresses increase from relatively low values at the equator of the head ($Z = 1.00$) to very large values near the axial-port-opening diameter at $Z = 0.20$. In review, the design criteria of the tank regarding compressive stresses in the head are (a) the critical-buckling stress must not be exceeded at the equator of the head, and (b) the stresses in the head must not exceed the compressive-yield stress. In many cases, stresses in the metal shell did not exceed the buckling stress allowable at the equator, but did exceed the compressive-yield stress at $Z \leq 0.40$. Therefore, either the metal-shell thickness or the composite thickness at $Z \leq 0.40$ had to be increased to reduce the metal-shell stresses to acceptable values at zero pressure after proof pressure.

In practice, for a tank with a port-to-diameter ratio of 0.20, the thicker axial-port boss will be welded to the metal shell at about $Z = 0.30$. A glass-filament reinforcement may be added locally at $0.20 \leq Z \leq 0.40$, as shown in Figure 26, to reduce the metal-shell compressive stresses at zero pressure to acceptable levels. The local reinforcement will also reduce the radial deflection of the composite adjacent to the rigid center boss, and thereby reduce abrupt increases in metal-shell strain adjacent to the center boss.

For designs in which the compressive stress exceeded the allowable values at $0.20 \leq Z \leq 0.40$, it was always assumed that the metal-boss flange and/or use of a local reinforcement pattern would move the point of maximum compressive stress to $Z \geq 0.40$; the magnitude of this stress was kept within acceptable limits.

3. Relationship Between Geometric Parameters and Internal Volume

Preliminary design criteria for pressure vessels generally include the envelope dimensions of diameter and length, or diameter and internal-volume requirements. Two figures are presented that define the relationship between GFR-metal-tank geometry and volume. Figure 27 shows the relationship between vessel L/D ratio and tank V/D^3 ratio (volume to diameter-cubed). The narrow band describing this relationship is due to the effect of K in controlling the exact head contour, and hence the internal volume for a given L/D . A value of $K = 0.00$ corresponds to a unlined filament-wound tank, while $K = 1.00$ represents the homogeneous metal tank. Figure 28 shows in detail the effect of K in controlling the internal volume of the heads and the volume of vessels with various L/D ratios. It relates V/D^3 to K for a range of L/D values.

4. Design Relationships and Optimum Configurations

With material properties and design temperatures held constant, each set of values for vessel shape, design pressure, and vessel-diameter to metal-liner-thickness ratio (D/T_L) resulted in characteristic stress-strain relationships, hoop- and longitudinal-filament thicknesses, and pressure-vessel performance factors (p_0V/W). When all the design requirements except shape were held constant, there was a significant difference between the stress-strain relationship and the performance of vessels with and without cylindrical sections. However, the effect of cylinder length on the stress-strain relationships of cylindrical vessels was small.

Tanks for service at 75°F were designed in accordance with the criteria listed in Section VI,C,1, above. Optimum room-temperature designs were identified on the basis of these criteria. These designs had the maximum permissible compressive stress in the metal shell at zero pressure after the proof test, as determined from the compressive-buckling or compressive-yield criteria of the specific metal-shell material. Because additional plastic deformation of the metal shell at any temperature would result in too high compressive stresses in the shell at 75°F, and because it can be assumed that tanks will be warmed during their service life, the optimum room-temperature designs are also optimum cryogenic-temperature designs. At cryogenic temperatures, the optimum room-temperature designs can work at an increased operating pressure, if use is made of the change in the metal-shell tensile-yield strength produced by the change in temperature. However, the optimum room-temperature designs must not be worked past the metal-shell offset yield stress at the pressurization temperature, unless it can be assured that the tanks will not warm up, or that the internal pressure will not be reduced below the level that holds the metal-shell compressive stress above the critical value.

In establishing optimum room-temperature designs, the use of a 210,000-psi proof-pressure stress in the longitudinal filaments, and the requirement that the metal-shell stress at operating pressure equal 90% of the proof-pressure stress, resulted in an operating-pressure filament stress of 200,000 to 208,000 psi. This stress level is close to the 75°F design-allowable filament stress of 200,000 psi at the operating pressure required to sustain the GFR-metal-tank service-cycle requirement.

The tanks were designed to sustain specified proof- and operating-pressure levels. The compressive-stress conditions in these tanks at zero pressure after proof-pressure application were evaluated in accordance with the following requirements:

The compressive-yield stress is not exceeded at any point on the head (from the equator to a normalized radial distance, Z , equal to 40% of the vessel radius) or in the cylinder.

The critical-buckling-stress level for cylinders overwrapped in the circumferential direction with tensioned filaments is not exceeded in the cylinder or at the equator of the head.

The stresses in the metal shell at various internal pressure levels and temperatures were analyzed in detail to establish the relationship between the room-temperature proof pressure and the maximum operating pressures at 75, -320, and -423°F that would not cause the metal-shell stresses to exceed 90% of the offset yield stress at the pressurization temperature. The relationships between proof pressure and operating pressures are given in Figure 29 for Ti-5Al-2.5Sn (annealed, ELI grade), 2219-T62 aluminum, Inconel X-750 (STA), and 301 SS (1/2 hard) GFR tanks.

At room temperatures, it was found that the equatorial hoop stress in the metal-shell head always reached 90% of the proof-pressure offset yield stress before the other metal-shell stresses, as the tank pressure was increased from zero to the operating pressure. The pressure required to reach 90% of the offset yield stress was 90% of the proof pressure.

At cryogenic temperatures, the stress distribution in the heads of oblate spheroids was such that the metal-shell meridional stress at $Z = 0.40$ always reached 90% of the offset yield stress at the pressurization temperature before the other metal-shell stresses. For cylindrical pressure vessels, the stress distribution was such that the hoop stress in the cylinder always reached the 90% level first.

The design relationships and optimum configurations for GFR metal tanks are presented below. Titanium tanks are discussed in detail, and briefer comments are provided for Inconel, aluminum, and stainless steel GFR tanks.

a. Ti-5Al-2.5Sn (Annealed, ELI Grade)

Optimum GFR titanium pressure-vessel designs at 75°F were determined for various proof-pressure levels, p_p , and D/T_L ratios. The maximum springback stresses in the metal shell for these designs, occurring at zero pressure after proof-pressure application, were plotted as a function of D/T_L ratio with p_p as a parameter. Where the resulting isobars intersected the compressive-buckling-stress or compressive-yield-stress envelope, an optimum design for that p_p value was identified, because that design had a maximum D/T_L value and consequently a minimum weight.

The relationships between the proof pressure, D/T_L , and maximum compressive stress are shown in Figure 30 for oblate spheroids, and in Figure 31 for cylindrical pressure vessels. Figure 30 indicates that, for oblate spheroids with proof pressures ranging from 1000 to about 2600 psi, the maximum permissible compressive stress is controlled by compressive-buckling criteria at the equator of the head (at $Z = 1.00$). For proof pressures ranging from 2600 to 4500 psi and above, the design is controlled by compressive-yield criteria on the head at $Z = 0.40$.

With regard to completely wrapped cylindrical pressure vessels, the maximum compressive stress was always in the hoop direction of

the cylinder. As shown in Figure 32, the D/T_L value was sufficiently small for proof pressures below 1360 psi to assure that no windings were required in the head to take the pressure load. For proof pressures below 1360 psi, therefore, pressure vessels with all-metal heads reinforced with hoop-wound filaments in the cylindrical section should be used. Actually, because of certain considerations given subsequently, the minimum proof pressure for completely wrapped cylindrical pressure vessels should be greater than 1360 psi. For proof pressures in the range from 1360 to 2350 psi, completely wrapped cylindrical-pressure-vessel designs are controlled by the critical-buckling-stress criteria. When the proof pressure is in the range from 2350 to 4500 psi and above, the design is controlled by the metal-shell D/T_L ratio needed to keep the hoop direction of the cylinder from exceeding the compressive-yield stress.

For both oblate spheroids and completely wrapped cylindrical pressure vessels, the maximum (optimum) D/T_L values within the yield-stress and buckling-stress design envelope were identified for proof pressures in the range from 1000 to 4500 psi, as shown in Figure 32. The abrupt change in the relationship at $p_p = 2600$ psi for oblate spheroids is caused by the change in the controlling design criteria of the tank from critical-buckling stress at the equator of the head for $1000 \leq p_p \leq 2600$ psi to compressive-yield stress at $Z = 0.40$ for $2600 \leq p_p \leq 4500$ psi and above. The change in relationship for cylindrical vessels at $p_p = 2350$ psi is due to a change in the controlling design criteria from critical-buckling stress in the hoop direction of the cylinder for $1360 \leq p_p \leq 2350$ psi to compressive-yield stress for $2350 \leq p_p \leq 4500$ psi and greater.

Next, plots were made of the metal-shell to longitudinal-composite thickness* ratio (T_L/T_0) as a function of D/T_L for different proof-pressure levels (shown in Figure 33 for oblate spheroids and in Figures 34 and 35 for cylindrical vessels). The optimum T_L/T_0 values as a function of proof-pressure level were identified with the aid of the optimum values for D/T_L for each proof-pressure level in Figures 33 to 35. Optimum T_L/T_0 values vs p_p are given in Figure 36. As was the case for D/T_L , T_L/T_0 vs p_p changes at $p_p = 2600$ psi for oblate spheroids and at 2350 psi for cylindrical vessels, because of the change in tank compressive-stress design criteria. It is important to note from Figure 36 that $T_0 = 0.0$ for cylindrical vessels with a proof pressure of 1360 psi ($D/T_L = 3.40$); the T_L/T_0 value decreases from a very large one (unfavorable) as the proof pressure increases above 1360 psi until a constant value of about 2.30 is reached at 2350 psi. For oblate spheroids, T_L/T_0 decreases until it reaches a constant value of 1.20 at a proof-pressure level of 2600 psi.

With regard to the T_L/T_0 ratio, the metal shell is at a biaxial tensile strain considerably beyond its yield point at the proof-pressure condition (the strain is approximately equal to the glass-filament

*The longitudinal composite thickness, T_0 , is the thickness of filaments and resin at the equator of the pressure-vessel head.

strain at a stress of 210,000 psi minus the strain at a filament-winding stress of 47,000 psi, or about 1.3%). Some winding over the metal shell is clearly necessary to restrain the head from local yielding, creep, or plastic instability under the proof-pressure load. The minimum amount of overwrap needed for this purpose is a subject for conjecture, however, and is not discussed further. From a practical standpoint, a minimum winding thickness must be applied during fabrication, and is about 0.007 in. for current glass-roving products used in filament winding. Some tank configurations requiring specific values for D , and the D/T_L and T_L/T_0 ratios to meet design requirements at lowest weight, may not be practical because of the minimum-obtainable value of T_0 .

Operating-pressure performance factors, $p_0 V/W$, were determined for optimum designs. Figure 37 shows the 75°F factors vs operating pressures for oblate-spheroid vessels and for cylinders with $L/D = 1, 2, 3$, and 10. Extremely high operating-pressure performance factors, in the range from 450,000 to 490,000 in., were obtained for the GFR titanium tanks at 75°F. Oblate spheroids were more efficient than cylindrical vessels with $L/D = 1$, and less efficient than vessels with $L/D = 2$. The effect of changes in compressive-stress design criteria on pressure-vessel performance is clearly indicated in Figure 37.

Operating-pressure performance factors for -320 and -423°F were determined on the basis of assumptions that the cryogenic properties of the metal shell could be used and that the metal-shell operating stress could equal 90% of the offset yield stress at the operating temperature. The operating-pressure performance factors for -320 and -423°F service are shown in Figure 38. The $p_0 V/W$ range at -320°F was from 650,000 to 690,000 in. and at -423°F, from 690,000 to 760,000 in.

The safety factors for the various designs were determined with the single-cycle burst pressure and the maximum operating pressure that could be used in the tanks without metal-shell stresses exceeding 90% of the proof-pressure stress at 75°F, or 90% of the offset yield stress at -320 or -423°F. If required, these minimum factor-of-safety values may be increased by reducing the operating pressure from the "90% value" that was used, with a consequent reduction in the pressure-vessel performance factor.

Safety factors for GFR titanium tanks are shown in Figure 39 as a function of proof pressure, operating temperature, and vessel shape. For 75°F service, oblate spheroids have factors ranging from 1.40 to 1.57, and cylindrical vessels from 1.31 to 1.42. When the operating temperature is reduced from 75°F to -320 and -423°F, all safety factors decrease. At -320°F, the minimum factors range from 1.21 to 1.30 for oblate spheroids and from 1.16 to 1.22 for cylinders. At -423°F, all vessels have a fixed minimum of 1.08. For use at -320 and -423°F, an operating pressure that will produce a stress in the metal shell equal to 90% of the offset yield stress results in a factor of safety that is too low for most applications. The operating pressure should therefore be reduced to the value that results in the required value.

It was found that the burst pressures were controlled by three criteria, as described below.

(1) At 75°F, the metal shell could strain to the ultimate filament-stress level of 330,000 psi without exceeding the maximum 3.0% biaxial-strain design allowable for Ti-5Al-2.5Sn (annealed, ELI grade) weldments. At this temperature, GFR titanium tanks should fail in the filaments.

(2) At -320°F, the metal shell reached the maximum biaxial-strain design allowable for the weldments of 2.0% before the design-allowable filament-stress level of 495,000 psi was attained. At this temperature, GFR titanium tanks should fail in the weldments before the ultimate filament strength is developed.

(3) At -423°F, the metal shell reached the maximum biaxial-strain design allowable established for the weldments of 1.0% (measured from the original origin of the stress-strain curve) before the metal was stressed to its -423°F offset yield stress. It was assumed that the metal shell could be strained past the 1.0% value to the -423°F offset yield stress before its actual biaxial-strain limit was exceeded. At -423°F, GFR titanium tanks should fail in the weldments well before the ultimate filament strength is attained.

b. Inconel X-750 (STA)

The curves for optimum designs of GFR Inconel X-750 pressure vessels had characteristics similar to those for the GFR titanium tanks. Optimum D/T_L ratios as a function of proof pressure are shown in Figure 40, optimum T_L/T_0 ratios as a function of proof pressure in Figure 41, 75°F pressure-vessel performance factors as a function of operating pressure in Figure 42, and -320 and -423°F performance factors as a function of operating pressure in Figure 43. As was noted for the GFR titanium tanks, changes in the controlling compressive-stress design criteria produced abrupt changes in the characteristic relationships between D/T_L , T_L/T_0 , p_p , p_0 , and p_0V/W . They were noted at a proof pressure of 1850 psi for cylindrical vessels and one of 2000 psi for oblate spheroids.

As for GFR titanium tanks, the required thickness of longitudinal composite, T_0 , is zero when the proof pressure and D/T_L are reduced below a minimum value. This occurs at a proof pressure of 1400 psi and D/T_L of 378 for GFR Inconel tanks. The use of constant-thickness metal pressure vessels reinforced with windings in the hoop direction of the cylinder is therefore indicated when the proof pressure is less than 1400 psi. The T_L/T_0 ratio decreased from a very unfavorable value for cylinders to about 6.30 at a proof pressure of 1850 psi and above. The T_L/T_0 ratio for oblate spheroids decreased to a constant value of 1.66 for proof pressures of 2000 psi and above.

The p_0V/W factor ranged from about 290,000 to 343,000 in. for oblate-spheroid and cylindrical vessels operated at 75°F. Oblate

spheroids had higher performance than cylinders with L/D ratios less than 2. At -320 and -423°F, the performance factors ranged from 310,000 to 395,000 in.

Minimum safety-factor values were determined by comparison of the single-cycle burst strength with the operating pressure that would produce metal-shell stresses equal to 90% of the offset yield stress. The factors of safety are presented in Figure 44. At 75°F, oblate spheroids have factors ranging from 1.40 to 1.51, while cylinders have minimum values in the range from 1.25 to 1.30. At -320 and -423°F, all safety factors increase. Oblate spheroids have values of 1.60 to 1.86 and cylinders have values in the range from 1.37 to 1.48.

It is highly significant that Inconel shells in GFR tanks appear to be capable of straining biaxially to ultimate-filament-stress levels of 330,000 psi at 75°F and 495,000 psi at -320 and -423°F. Such tanks should fail in the filaments over the entire 75 to -423°F range. Because of the high-strain capability of Inconel X-750, the possibility of operating the tanks at a pressure that produces metal-shell stresses equal to the offset yield stress should be considered. The use of the higher operating pressure would increase $p_0 V/W$ about 10%, to 319,000 to 377,000 in. at 75°F, and 341,000 to 435,000 in. at -320 and -423°F.

c. 2219-T62 Aluminum

For $1000 \leq p_0 \leq 4000$ psi, the design of GFR aluminum pressure vessels was based on compressive-yield criteria. Optimum D/T_L values vs proof pressure are given in Figure 45, and optimum T_L/T_0 ratios vs proof pressure in Figure 46. The 75°F pressure-vessel performance factors are presented in Figure 47, and the -320 and -423°F factors in Figure 48. Factors of safety are given in Figure 49 for 75, -320, and -423°F operating temperatures.

For all proof pressures from 1000 to 4000 psi, T_L/T_0 is constant at 4.35 for oblate spheroids and at about 16.50 for cylindrical vessels. The T_L/T_0 ratio for cylindrical vessels is probably too high for the overwrapped filaments to be able to restrain the metal head from creep, local instability, and/or failure produced by normal pressure fluctuations, when it is stressed beyond the yield point during proof-pressure application. If 2219-T62 aluminum is to be used in cylindrical tanks, the metal shells should be designed to be circumferentially wrapped with a constant thickness of glass filament rather than completely wrapped.

The performance factors at 75°F ranged from 355,000 to 405,000 in., and at -320 and -423°F increased somewhat to a range from 390,000 to 445,000 in.

The factors of safety at 75°F were 1.57 for oblate spheroids and 1.43 for cylindrical vessels. At -320°F, the minimum factors decreased to 1.43 for oblate spheroids and ranged from 1.25 to 1.40 for cylinders. The minimum value was 1.08 for all vessels at -423°F.

At 75°F, the metal shell could strain biaxially to the ultimate filament stress without exceeding the design-allowable strain in the weldments. At -320 and -423°F, however, the burst pressure was based on the maximum design-allowable metal-shell biaxial strain.

d. Type 301 SS (1/2 Hard)

Type 301 SS in the 1/2-hard temper had a 75°F compressive-yield stress of only 80,000 psi. The metal shell had to be thickened considerably to keep the springback stress in the hoop direction of the cylinder from exceeding the 80,000-psi maximum-allowable compressive stress. It was determined that for cylinders with a proof-pressure filament stress of 210,000 psi, the metal shell had to be thickened sufficiently to assure that no longitudinal windings were required on the heads to take the pressure load. The operating-pressure filament stress had to be reduced to 185,000 psi before workable designs of completely wrapped cylindrical vessels were obtained. The 185,000-psi filament stress, in combination with the metal-shell weight, produced performance-factor values below those of the other tank designs. Type 301 SS, GFR, cylindrical, pressure vessels were therefore not subjected to detailed study. For cylindrical 301 SS tanks, a constant-thickness metal shell with circumferential filament reinforcements in the cylindrical section should be used.

Optimum D/T_L and T_L/T_0 ratios from the design analysis of oblate spheroids are presented in Figure 50, performance factors in Figures 51 and 52, and factors of safety in Figure 53. The pressure-vessel performance factors at 75°F ranged from 310,000 to 333,000 in.; at -320°F the range was 380,000 to 405,000 in., and at -423°F was 410,000 to 420,000 in. The factors of safety ranged from 1.35 to 1.47 at 75°F, 1.50 to 1.77 at -320°F, and 1.08 to 1.10 at -423°F. The ultimate-filament-strength design allowable could be developed at 75 and -320°F, but the tank performance at -423°F was controlled by the maximum design-allowable biaxial strain of the weldments.

5. Detailed Analysis of Stress-Strain Relationships

Selected for a detailed analysis of the stress-strain relationships for typical optimum GFR-metal-tank designs were an Inconel X-750 (STA) tank (2220 psi proof pressure and 2000 psi operating pressure at 75°F) and a Ti-5Al-2.5Sn (annealed, ELI grade) tank (3335 psi proof pressure and 3000 psi operating pressure at 75°F). Both were designed to have $L/D = 1$ so that the stress-strain relationships of the heads and the cylindrical section could be shown. They are considered individually below.

a. Optimum Inconel X-750 (STA) Tank

The design parameters of the GFR metal tank were as follows:

<u>Parameter</u>	<u>Temp, °F</u>	<u>Value</u>
P_o	75	2000 psi
P_p	75	2220 psi
P_o	-320	2300 psi
P_o	-423	2300 psi
D/T_L	--	283
T_L/T_o	--	6.06
L/D	--	1.0

Figure 54 presents the 75°F stress-strain relationships for the hoop and longitudinal directions of the cylinder and at the equator of the heads. Figures 55 and 56 show the -320 and -423°F stress-strain relationships, respectively. The stress-strain conditions in the component materials are shown in Figure 54 at winding, after mandrel removal, at the 2220-psi proof pressure, at zero pressure after the proof pressure, at the 2000-psi operating pressure, and at the burst pressure. It is of specific interest that (1) the maximum compressive stress after the proof pressure occurs in the hoop direction of the cylinder and equals 108,000 psi (the design-allowable compressive-yield stress for Inconel X-750); (2) the maximum metal-shell tensile stress at the operating pressure occurs in the hoop direction of the head at the equator and equals 90% of the metal-shell stress at the proof pressure; and (3) the maximum-allowable filament stress of 330,000 psi is developed in the longitudinal direction of the cylinder at a pressure of 2597 psi.

Figures 55 and 56 show the -320 and -423°F stress-strain conditions in the GFR metal tank; the shifts in stress-strain curves due to the temperature changes are indicated. The maximum metal-shell tensile stress at the operating pressure occurs in the hoop direction of the cylinder and equals 90% of the metal-shell offset yield stress at the operating temperature. The filament stress reaches a maximum of 495,000 psi in the longitudinal direction of the cylinder at a pressure of 3394 psi at -320 and of 3459 psi at -423°F.

Stresses in the GFR metal tank heads and cylinder at 75, -320, and -423°F at the operating pressures are given in Figure 22. Of primary interest is the evidence given that the head contours developed for GFR metal tanks are optimum: Stresses are constant in the filaments up the head contour and a 1-to-1 stress field is produced in the metal shell at the design pressure and temperature.

Stresses in the heads and cylinder at zero pressure after the 2220-psi proof pressure at 75, -320, and -423°F are shown in Figure 24. At 75°F, the maximum compressive stress occurs in the hoop direction of the cylinder, and is equal to the 75°F compressive-yield stress of the metal shell.

b. Optimum Ti-5Al-2.5Sn Tank

The design parameters of the GFR metal tank were as follows:

<u>Parameter</u>	<u>Temp, °F</u>	<u>Value</u>
P_o	75	3000 psi
P_p	75	3335 psi
P_o	-320	4250 psi
P_o	-423	4500 psi
D/T_L	--	206
T_L/T_o	--	2.28
L/D	--	1.0

Figure 57 shows the 75°F stress-strain relationships for the hoop and longitudinal directions of the cylinder and at the equator of the heads. Figures 58 and 59 give the -320 and -423°F relationships. As for Inconel X-750, the maximum compressive stress after proof pressure is in the hoop direction of the cylinder, and equals the design-allowable compressive stress for the D/T_L ratio. At 75°F, the maximum-allowable filament stress at 330,000 psi is developed at a burst pressure of 4244 psi. At -320 and -423°F, the burst performance of the tank is controlled by the strain limits established for the metal shell. Figure 25 shows the stresses in the heads and cylinder at zero pressure after the 3335-psi proof pressure at 75, -320, and -423°F.

6. Design Variations

Three of the fixed parameters used for tank design were varied in the computer program to evaluate the effect of each on tank performance.

a. Geodesic-Isotensoid Winding Pattern

The performance of GFR metal tanks employing the geodesic-isotensoid contour was found to be 0.1% less than that of tanks with balanced-in-plane contours. Axial-port to vessel-diameter ratios other than 0.20 were not investigated and may be expected to exhibit larger performance deviations as the ratio is increased. One significant result of the different closures was a 0.005% stress variation over the geodesic-isotensoid contour for both filaments and metal shell, as compared with a 3% variation in filament stress and a 0.4% variation in metal-shell stress for the balanced-in-plane contour at the design temperature and pressure. Although the latter wrapping pattern does not exhibit a completely isotensoid stress distribution, fabrication considerations make it a highly desirable choice.

b. Winding Tension

A 2% increase in performance was obtained by decreasing the filament-winding tension from the upper limit of 47,000 psi to zero. The total load carried by the metal shell at the proof pressure was increased 3 to 4% (depending on the metal-shell material), resulting in smaller composite-thickness requirements and a corresponding decrease in total tankage weight. Because the internal volume remained constant, the decreased weight completely accounted for the increase in tankage performance. With zero winding tension, it was noted that the total metal-shell strain at the proof pressure increased 29% in order to allow the filaments to work at their required stress level. In strain-limited designs, this increase may be undesirable in view of the small increase in tank performance.

c. Pressure Mandrel

The substitution of a fluid-pressurized mandrel for a rigid mandrel had no effect on the performance or design of GFR metal tanks. Either technique should produce the same optimum tank, and manufacturing considerations can be used as a basis for the choice of a metal-shell support mandrel.

7. Use of Design Curves

The design curves presented in this report are used here to illustrate the procedure for preliminary design of GFR metal tanks. The following design criteria are assumed:

Operating pressure at -423°F	2220 psi
Required volume	6570 in. ³
Maximum diameter	25 in.
Factor of safety at operating conditions	1.50
Metal-shell material	Inconel X-750 (STA)
Overwrap material	S-HTS glass filaments

If it is further assumed that $D_0/D = 0.20$ and that an in-plane winding pattern, rigid mandrel, and filament-winding stress of 47,000 psi are used, a preliminary design can be developed with the aid of the design curves. From the relationship given in Figure 29 for operating pressure vs room-temperature proof pressure, it is found that for a 2220-psi operating pressure at -423°F in a GFR Inconel X-750 (STA) tank, the room-temperature proof pressure is 2220 psi. The use of a higher proof pressure will result in too high a compressive stress in the metal shell at zero pressure and room temperature.

The V/D^3 ratio for the vessel is $6570/25^3 = 0.42$. Reference to Figure 27, which gives the relationship between L/D and V/D^3 , shows that the volume and diameter requirement can probably be met with a back-to-back head-configuration pressure vessel.

With the above information, the GFR Inconel X-750 (STA) design curves (Figures 40 to 44) can be used to establish the design parameters of the tank. From Figure 40 it is found that a D/T_L ratio of 385 is required when the proof pressure is 2220 psi and the shape is an oblate spheroid. For $D = 25$ in. and $D/T_L = 385$, $T_L = 0.065$ in. The optimum T_L/T_0 ratio is found (from Figure 41) to be 1.67 for the given proof-pressure level. Thus, with $T_L = 0.065$ in. and $T_L/T_0 = 1.67$, the longitudinal filament-wound-composite thickness at the equator of the head, T_0 , is 0.039 in. From Figure 42, p_0V/W for the design at 75°F is 327,000 in. From Figure 43, p_0V/W at -423°F is 365,000 in. if the operating pressure develops 90% of the metal-shell offset yield stress at that temperature.

In practice, the p_0V/W of GFR Inconel tanks may be increased about 10% by operating the tanks at the metal-shell proof-stress level at room temperature and/or at the metal-shell offset yield stress at the use temperature. This procedure will increase p_0V/W at 75°F to 360,000 in. and at -423°F to 402,000 in.

The factor of safety for the design (given in Figure 44) is 1.85 at -423°F. This is higher than the specified (assumed) value of 1.50, but cannot be reduced if the tank's operating pressure is maintained at 2220 psi at -423°F. The reason is that the tank design is based on structural requirements for both the metal and glass-filament shells at the operating pressure and the resultant burst pressure is uniquely controlled by these requirements.

D. PERFORMANCE OF HOMOGENEOUS METAL AND GLASS-FILAMENT-WOUND TANKS

1. Homogeneous Metal Pressure Vessels

The state-of-the-art performance of homogeneous, metal, spherical and cylindrical, pressure vessels was determined for comparison with that of GFR metal tanks. The following representative high-performance metals used or considered for use in pressure vessels to operate at 75 to -423°F were evaluated for the comparison: Ti-6Al-4V (STA), presently considered unsuitable for service at -320 and -423°F; Ti-6Al-4V (annealed, ELI grade); 2219-T87 aluminum; Type 301 SS (extra-full-hard temper); and Inconel 718 (STA). Design values for their uniaxial yield and ultimate strengths at 75, -320, and -423°F are given in Table 4.

In accordance with current design practice, the metal-pressure-vessel performance was determined with an operating stress amounting to 67% of the ultimate tensile strength (a factor of safety of 1.50 on ultimate) or 77% of the yield strength (a factor of safety of 1.30 on yield), whichever gave the lower operating-stress level. The resultant design operating-stress levels for 75, -320, and -423°F are presented in Table 4. Although in general it may not be good practice to use the low-temperature properties of metals for the design of cryogenic pressure vessels (because of the possibility of vessel warming during service life, temperature gradients, or other factors), calculations were made on the basis of cryogenic properties to show maximum performance. For the welded-joint strength of the metals covered in the analysis, manufacturing procedures will

make necessary the use of thicker stock adjacent to the joints. The thickness of the lands will depend on the specific material (greater for aluminum than for titanium), and the vessel-weight effect of lands at the weld joint will depend on both the material and the vessel configuration. The weight calculations, however, do not include the extra weight due to the lands or flanges in order to show maximum performance.

Figure 60 shows the relative performance of metal pressure vessels based on the operating-pressure performance factor, $p_o V/W$. The titanium alloy (followed by 301 SS, Inconel 718, and 2219-T87 aluminum) was the highest-performance material by a significant margin, as indicated by the summary of performance levels given in Table 5.

With regard to the performance of titanium pressure vessels, room-temperature creep has been reported for various titanium alloys. Although present in standard alloys, it appears to be particularly serious in the ELI grades of Ti6Al-4V and Ti-5Al-2.5Sn. As a result, the following precautionary note was incorporated in MIL-HDBK-5, Change Notice 5, issued June 1965:

"Below about 300°F, as well as above about 700°F, creep deformation of titanium alloys can be expected at stresses below the yield strength. Available data indicate that room-temperature creep of unalloyed titanium may be significant (exceed 0.2 percent creep strain in 1000 hours) at stresses that exceed approximately 50 percent F_{ty} ; room-temperature creep of Ti-5Al-2.5Sn ELI may be significant at stresses above approximately 60 percent F_{ty} ; and room-temperature creep of the standard grades of titanium alloys may be significant at stresses above approximately 75 percent F_{ty} ."

There is also concern about creep of Ti-5Al-2.5Sn at cryogenic temperatures, because test results have shown that appreciable creep will occur at -320°F.

2. Glass-Filament-Wound Pressure Vessels

The performance of filament-wound pressure vessels, assumed to be made from S-HTS glass filaments, was determined for comparison with that of GFR metal tanks. The operating filament-stress levels assumed were the same as those being used for GFR metal tanks: 200,000 psi at 75°F and 300,000 psi at -320 and -423°F.

Performance factors were determined for pressure vessels without liners, and for vessels with 0.060-in.-thick elastomeric liners (density of 0.045 lb/in.³), 0.006-in.-thick stainless steel liners, and 0.006-in.-thick aluminum liners. The liners are essentially non-load-bearing. The performance of a filament-wound vessel with a thin liner is directly proportional to the relative thicknesses of the filament winding and liner. In turn, for a fixed liner thickness, the relative thickness of the liner and filament winding is proportional to the design pressure of the tank and the tank diameter; tanks with higher pressures and large diameters will have higher performance than tanks with lower pressure requirements and small diameters. This effect is shown in Figure 61, where the operating pressure of the tank is held constant and the tank diameter is varied

from 5 in. to 100 in. Thin metal-lined filament-wound tanks were compared with GFR metal tanks on the basis of a specific high-pressure metal-lined filament-wound tank of 20-in. diameter and a 4000-psi operating pressure.

Figure 62 shows the relative performance of glass-filament-wound pressure vessels, based on the operating-pressure performance factor. The unlined filament-wound-tank operating-pressure performance, $p_o V/W$, ranged from 570,000 to 605,000 in. at 75°F and from 860,000 to 905,000 in. at -320 and -423°F. For lined tanks, vessels with the 0.006-in. aluminum liner had 96 to 98% of the performance of unlined tanks. The 0.006-in. nickel liner gave 91 to 95% of the unlined-tank performance, and the 0.060-in. elastomeric liner resulted in 87 to 93% of the performance of the unlined tanks.

VII. CONCLUSIONS AND COMPARATIVE RATING OF DESIGNS

The head contours for filament-wound pressure vessels combined with load-carrying liners are intermediate between the filament-wound pressure-vessel head contour and the spherical shape that is optimum for homogeneous metal heads. In GFR metal pressure-vessel heads with the optimum contour, stresses are constant in the filaments up the contour and a 1-to-1 stress field is produced in the metal shell at the design pressure and temperature, thus satisfying the requirements for optimum closure design. Completely wrapped GFR metal pressure vessels with optimum head contours yield higher performance than spherical GFR metal tanks or circumferentially reinforced cylindrical metal pressure vessels with hemispherical end closures. Completely wrapped oblate spheroids have a performance level comparable to that of completely wrapped cylindrical pressure vessels.

Tanks were designed for room-temperature service so that the compressive-yield stress is not exceeded at any point on the head and in the cylinder, and so that the critical buckling-stress level for cylinders is not exceeded in the cylinder or at the equator of the head, when the metal shell is in maximum compression due to the external forces produced by the overwrapped filaments. Thus, the metal-shell designs developed in this study do not require an adhesive bond between the glass-fiber and metal shells to keep the metal shell from buckling.

Optimum room-temperature designs of GFR metal tanks were found to be optimum designs for cryogenic temperatures if the tank is warmed up at some time during its service life. The reason is that optimum room-temperature designs have the maximum-permissible compressive stress in the metal shell at zero pressure after the proof test, and additional plastic deformation of the metal shell at any temperature results in too high compressive stresses in the metal shell at room temperature. At cryogenic temperatures, the optimum room-temperature designs can work at an increased operating pressure to improve the performance if use is made of the change in metal-shell tensile-yield strength produced by the change in temperature.

For tanks with axial bosses equal to 20% of the vessel diameter, balanced-in-plane contours for in-plane winding patterns yielded performances equivalent to those of the geodesic-isotenoid contour required for helical winding patterns. The vessel-performance effect of glass-filament winding-tension variation from 0 to 47,000 psi was found to be slight; however, the higher winding tensions reduced the metal-shell biaxial strain required for the overwrapped filaments to work at their operating-stress level. The substitution of a fluid-pressurized mandrel for a rigid mandrel had no effect on the performance or the design of GFR metal tanks.

Figure 1 presents a summary comparison of operating-pressure performance factors, $p_0 V/W$, for completely wrapped GFR metal tanks, homogeneous metal pressure vessels, and high-pressure glass-filament-wound pressure vessels with very thin metal liners. Their relative performances are shown for 75°F and for cryogenic operating temperatures. The design stress of the homogeneous metal

tanks was 67% of the ultimate tensile strength or 77% of the yield strength, whichever gave the lower operating-stress level. The GFR metal tanks and filament-wound pressure vessels were assumed to operate at a filament-stress level of 200,000 psi at 75°F and of 300,000 psi at -320 and -423°F. The low-temperature performances are maximum values based on the full use of the material properties at the temperature. The GFR metal tanks are designed, however, so that after they are worked at their operating pressure at cryogenic temperatures, they may be warmed to room temperature without exceeding the maximum-permissible compressive stress in the metal shell. If the vessel warms during use or there are other reasons for not employing the properties of the structural material at the operating temperature, the performance factors given for each type of vessel as a function of temperature must be adjusted to provide for this change in design criteria.

Maximum-performance vessels for cryogenic service will be high-pressure filament-wound pressure vessels with very thin metal liners, providing that a reliable liner design can be developed. For this reason, the comments that follow pertain only to the comparison of GFR metal tanks and homogeneous metal pressure vessels.

Maximum efficiency over the 75 to -423°F range is provided by GFR Ti-5Al-2.5Sn pressure vessels. Their performance is considerably greater than that of the other GFR metal tanks and all candidate homogeneous metal pressure vessels. At room temperatures, their performance is 35% higher than that of Ti-6Al-4V (annealed) spheres and 70% better than that of Ti-6Al-4V (annealed) cylindrical vessels. When compared with the performance of the highest-strength homogeneous metal pressure vessels made from 301 SS, Inconel 718, and 2219-T87 aluminum (see Figure 1), the improvement ranges from 40 to 130%, depending on the shape and material used for the homogeneous metal tanks. The GFR titanium tanks have a minimum safety factor of 1.40 to 1.57 at 75°F, which is comparable to that of the homogeneous metal tanks. At -320 and -423°F, the burst-strength performance of the pressure vessels is limited by the biaxial-strain capability of the metal-shell weldments, and the full strength potential of the glass filaments cannot be realized. When the cryogenic properties are used to maximize $p_0 V/W$, the safety factors are 1.16 to 1.30 at -320°F and 1.08 at -423°F. However, if the cryogenic strength properties of the metal and glass-filament shells are not utilized to increase the operating-pressure level, the safety factor of the GFR titanium tanks increases to about 1.70 to 1.80 at -320°F and 1.60 to 1.70 at -423°F. In designing GFR titanium tanks for cryogenic service, a compromise must therefore be reached between the factor of safety and the resulting value for $p_0 V/W$.

The second highest performance of pressure vessels at 75°F is provided by GFR 2219-T62 aluminum tanks. Compared with Ti-6Al-4V (annealed) spheres and cylindrical vessels, the performance is as much as 15% better than that of spheres and 25 to 45% higher than that of cylinders. The GFR aluminum tanks have safety factors of 1.43 to 1.57 at 75°F, depending on the shape and pressure. At -320°F, the safety factors are close to 1.40 at the maximum operating-pressure level. When the temperature is reduced to -423°F, however, the low weldment ductility decreases the factor to only 1.08 when the maximum operating pressure is used. As was the case for titanium, safe operation of GFR aluminum tanks at

-423°F therefore requires that a compromise be reached between adequate safety factor and a high p_0V/W value. As an example, if the 75°F p_0V/W of 355,000 to 405,000 in. for GFR aluminum tanks is acceptable at -320 and -423°F, the operating pressure could be held at the 75°F value when the tanks are used at the low temperatures. If this is done, the 75°F safety factor of 1.43 to 1.57 changes to about 1.50 at -320°F but drops to 1.20 at -423°F.

The performance of GFR 301 SS (1/2 hard) pressure vessels of the oblate-spheroid configuration is slightly below that of GFR aluminum tanks and of Ti-6Al-4V (annealed) spheres, but is above that of all the other homogeneous metal pressure vessels. The factors of safety at the maximum operating pressure are about 1.5 at 75°F and 1.70 at -320°F; at -423°F, the value is reduced to only 1.08, due to the low strain capability of the metal-shell weldments.

The GFR Inconel X-750 (STA) tanks have a number of unique features. In the 75 to -423°F range, the metal shell has sufficient ductility to strain to the ultimate strength of the filaments, thereby achieving the maximum performance obtainable with this combination of materials and the design requirements imposed on GFR metal tanks. The factors of safety based on the maximum-permissible operating pressure increase as the operating temperature decreases; except for cylindrical vessels at 75°F, the tanks have safety factors ranging from 1.50 to 1.85 at 75 to -423°F. Because of the good performance of the metal shell (large biaxial-strain capability and 100% weld-joint efficiency), it appears feasible (and is recommended, if optimum performance is to be attained) to operate the tank at pressures that produce metal-shell stresses equal to the proof-pressure stress at 75°F or at the offset yield stress as the temperature is reduced from 75 to -423°F. This operating-pressure increase results in an improvement of about 10% in p_0V/W .

If GFR Inconel tanks are operated at 90% of the offset yield stress, the 75°F vessel performance is about 20% greater than that for homogeneous metal cylinders made from Ti-6Al-4V (annealed), and about 30% greater than for 301 SS (extra-full-hard temper) cylindrical vessels. The performance advantage is maintained at these and higher values when the tanks are compared with spherical and cylindrical homogeneous metal tanks fabricated from Inconel 718 (STA) and 2219-T87 aluminum. The GFR Inconel X-750 (STA) tanks can have equivalent or slightly greater performance factors than Ti-6Al-4V and 301 SS spheres. If use is made of the low-temperature mechanical properties, the rate of performance increase for GFR Inconel X-750 tanks at cryogenic temperatures is less than that for homogeneous titanium and stainless steel vessels, which develop superior performance factors at low temperatures.

If the GFR Inconel tanks are operated at 100% of the offset yield stress, the 75 to -423°F vessel performance is equivalent to that of GFR aluminum and stainless steel tanks, as shown in Figure 1. At 75°F, the tanks are superior to all configurations of homogeneous metal tanks made from the representative stainless steel and titanium-, aluminum-, and nickel-base alloys. When cryogenic-temperature properties are used to increase the operating-pressure performance, homogeneous titanium spheres and cylinders and homogeneous stainless steel spheres

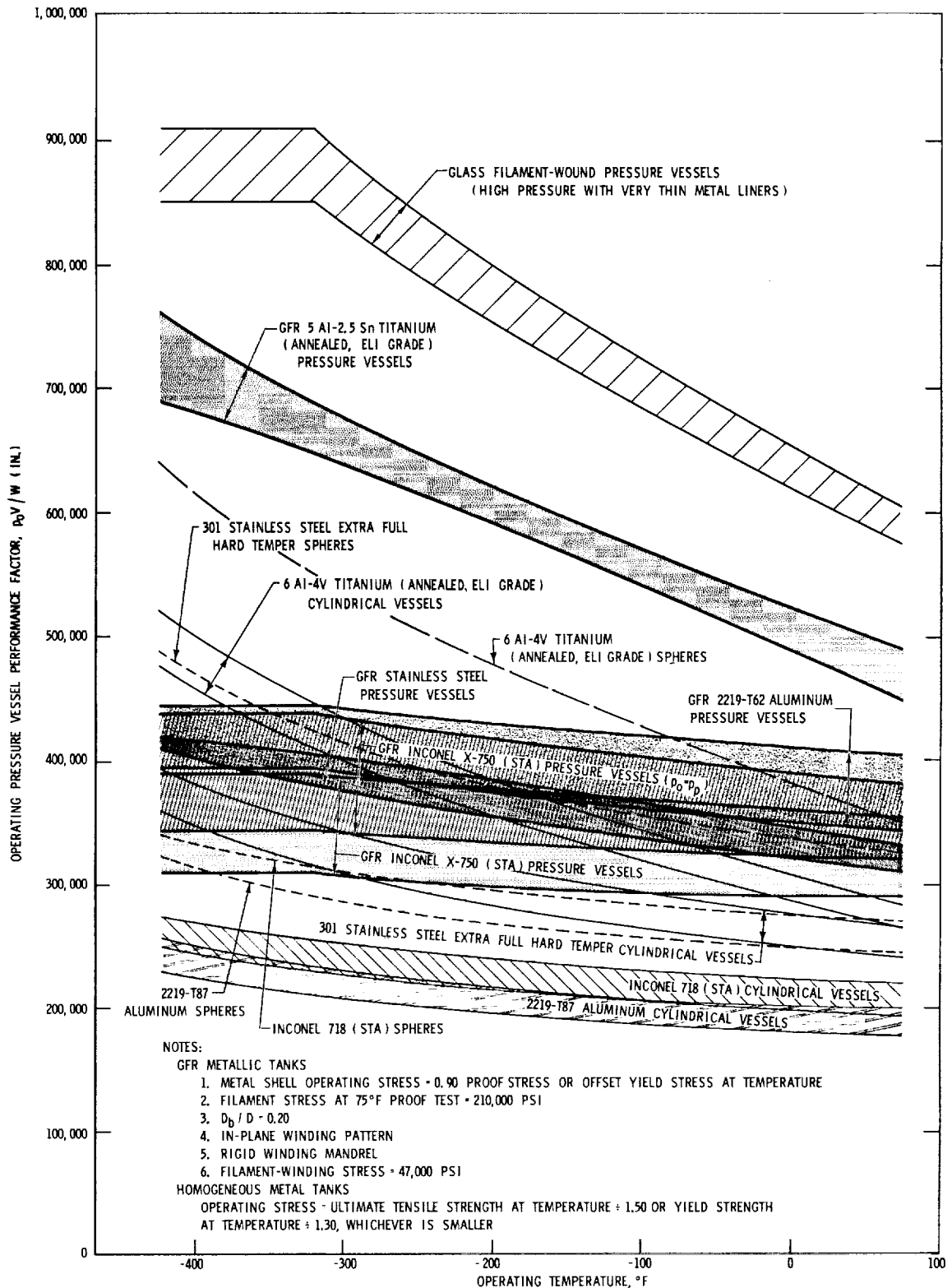
have higher performance than GFR Inconel tanks. Creep of homogeneous titanium-alloy pressure vessels, when subjected to the pressure-vessel operating-stress levels assumed in this analysis, may create a problem in the 75 to -423°F range. If the problem is shown to be serious, the performance advantages offered by GFR Inconel tanks will be greatly amplified.

REFERENCES

1. M. P. Hanson, H. T. Richards, and R. O. Hickel, Preliminary Investigation of Filament-Wound Glass-Reinforced Plastics and Liners for Cryogenic Pressure Vessels, NASA TND-2741, Lewis Research Center, National Aeronautics and Space Administration, Cleveland, Ohio, March 1965.
2. J. M. Toth, Jr., W. C. Sherman, and D. J. Soltysiak, Investigation of Structural Properties of Fiber-Glass Filament-Wound Pressure Vessels at Cryogenic Temperatures, NASA CR-54393 (Douglas Aircraft Company Report SM-48845, prepared under Contract NAS 3-2562), September 1965.
3. R. W. Frischmuth, Jr., Investigation of Thin Films as Floating Liners for Fiber-Glass Cryogenic Propellant Tanks, NASA TND-3205, Lewis Research Center, January 1966.
4. R. W. Frischmuth, Jr. and P. T. Hacker, Investigation of Bonded Plastic Tape for Lining Filament-Wound Fiber-Glass Cryogenic Propellant Tanks, NASA TND-3206, Lewis Research Center, January 1966.
5. R. W. Frischmuth, Jr., Experimental Investigation of Glass Flakes as a Liner for Fiber-Glass Cryogenic Propellant Tanks, NASA TMX-1193, Lewis Research Center, January 1966.
- 6a. R. W. Buxton and R. N. Hanson, Design Improvements in Liners for Glass-Fiber Filament-Wound Tanks to Contain Cryogenic Fluids, NASA CR 54-854, Aerojet-General Report 3141 (prepared under Contract NAS 3-4189), January 1966.
- 6b. Henry Lee, "New Polymers for Structural Adhesives, Honeycombs, and Reinforced Composites," presented at the Aviation and Space Conference, American Society of Mechanical Engineers, Los Angeles, 14-18 March 1965.
7. M. J. Sanger, R. Molho, and W. W. Howard, Exploratory Evaluation of Filament-Wound Composites for Tankage of Rocket Oxidizers and Fuels, Air Force Materials Laboratory Report AFML-TR-65-381 (prepared by Aerojet-General Corporation under Contract AF 33(615)-1671), January 1966.
8. H. Langhaar, A. Boresi, L. Marcus, and G. Love, "Buckling of a Long Fiber-Wound Cylindrical Shell Due to Stresses Caused by Windings," Journal of Applied Mechanics, pp. 81-86, March 1965.
9. R. H. Johns and A. Kaufman, Filament-Overwrapped Metallic Cylindrical Pressure Vessels, NASA TMX-52171, Lewis Research Center, 1966.
10. C. N. Odell and W. E. Albert, "The Filament-Reinforced Motor Case," Aerospace Engineering Magazine, April 1962.
11. F. J. Darms, R. Molho, and B. E. Chester, Improved Filament-Wound Construction for Cylindrical Pressure Vessels, Air Force Materials Laboratory Report ML-TDR-64-43 (prepared by Aerojet-General Corporation), 1964.

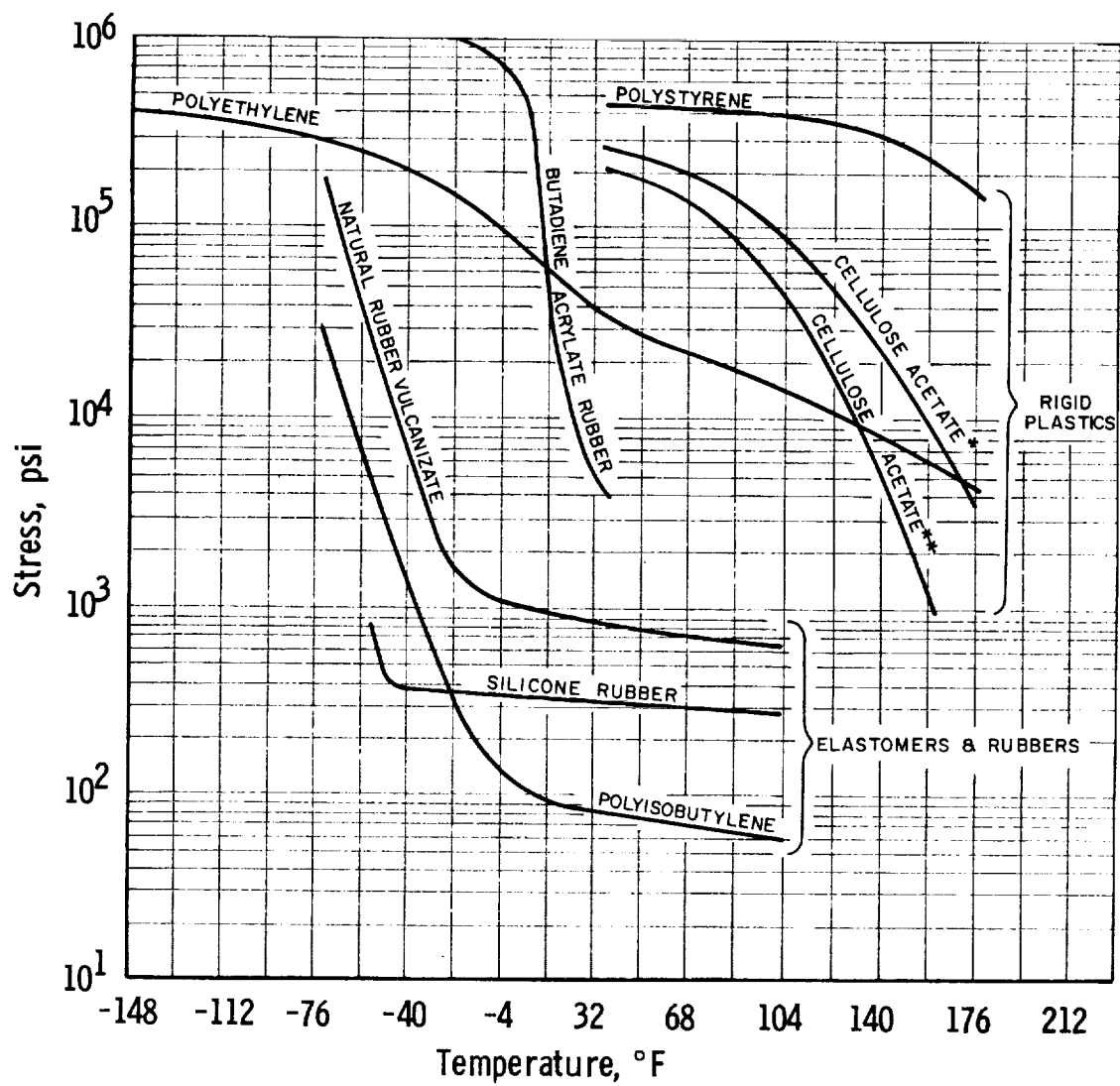
REFERENCES (cont.)

12. R. W. Buxton and O. Weingart, Development of Improved Processes for Filament-Wound Reinforced Plastic Structures, Air Force Materials Laboratory Report AFML-TR-65-80 (prepared under Contract AF33(657)-9726 by Aerojet-General Corporation), March 1965.



SUMMARY COMPARISON OF GFR METAL AND HOMOGENEOUS METAL
PRESSURE VESSEL PERFORMANCE LEVELS

Figure 1

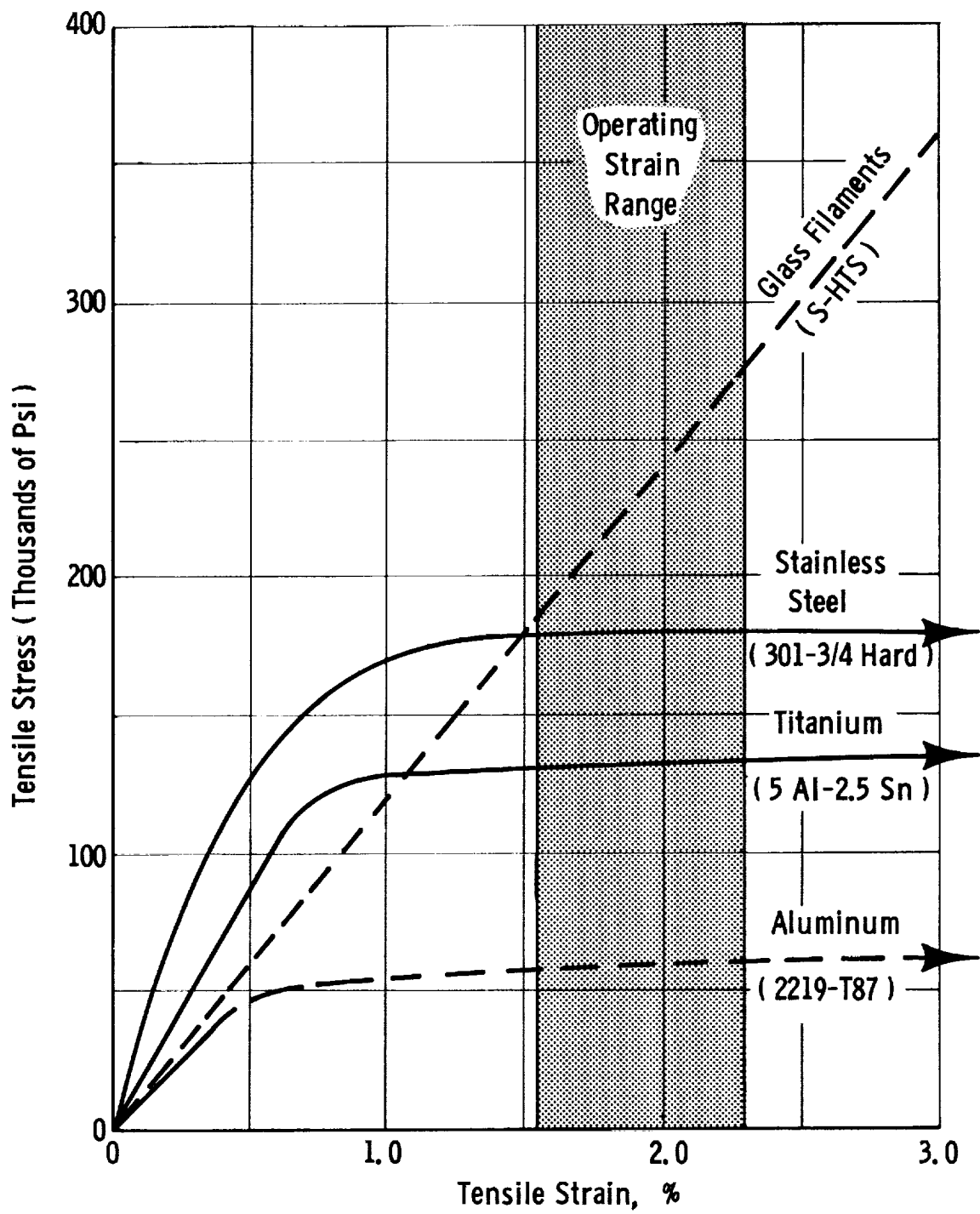


* 20% Methyl phthalyl ethyl glycollate

** 50% Methyl phthalyl ethyl glycollate

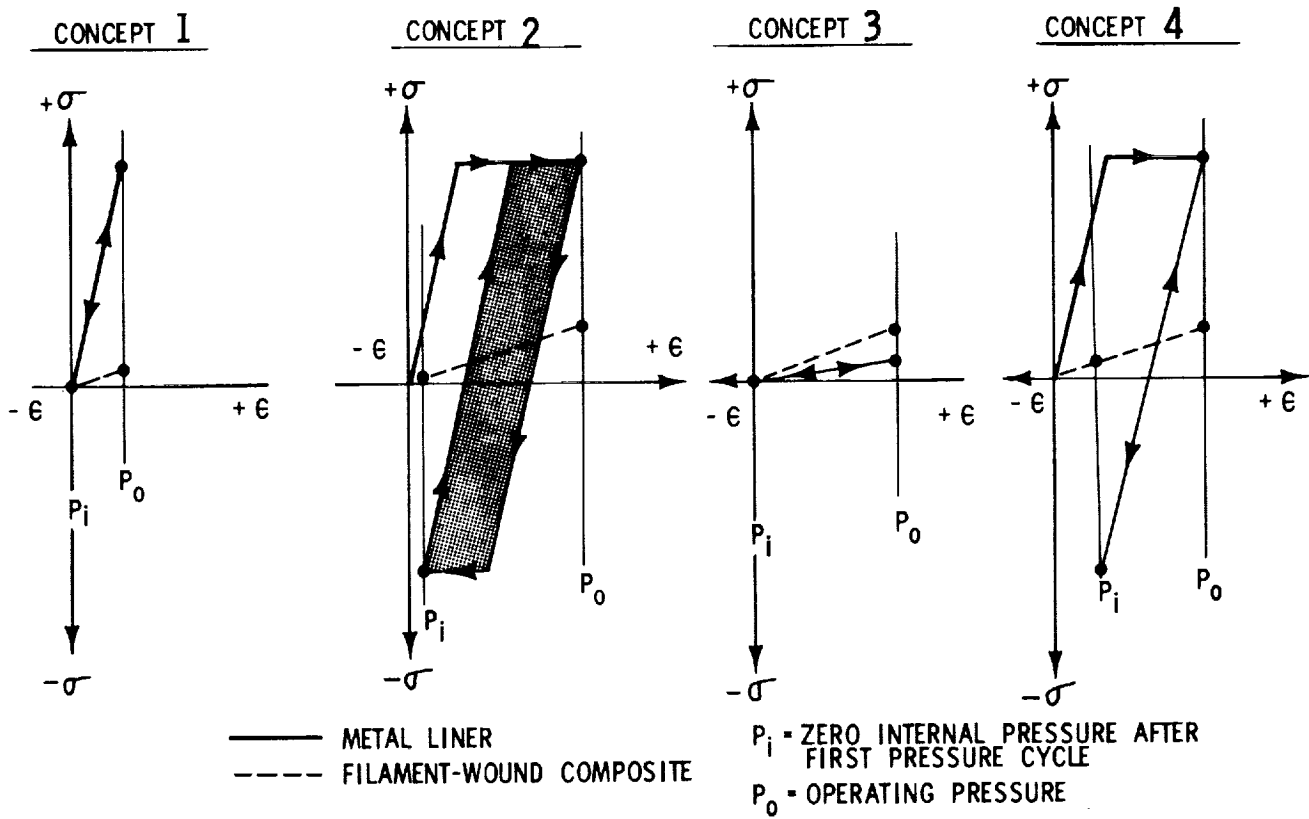
MODULUS OF ELASTICITY VS TEMPERATURE FOR
SEVERAL PLASTICS AND RUBBERS (REF. 6b)

Figure 2



STRESS-STRAIN CHARACTERISTICS OF COMPONENT MATERIALS (75°F)

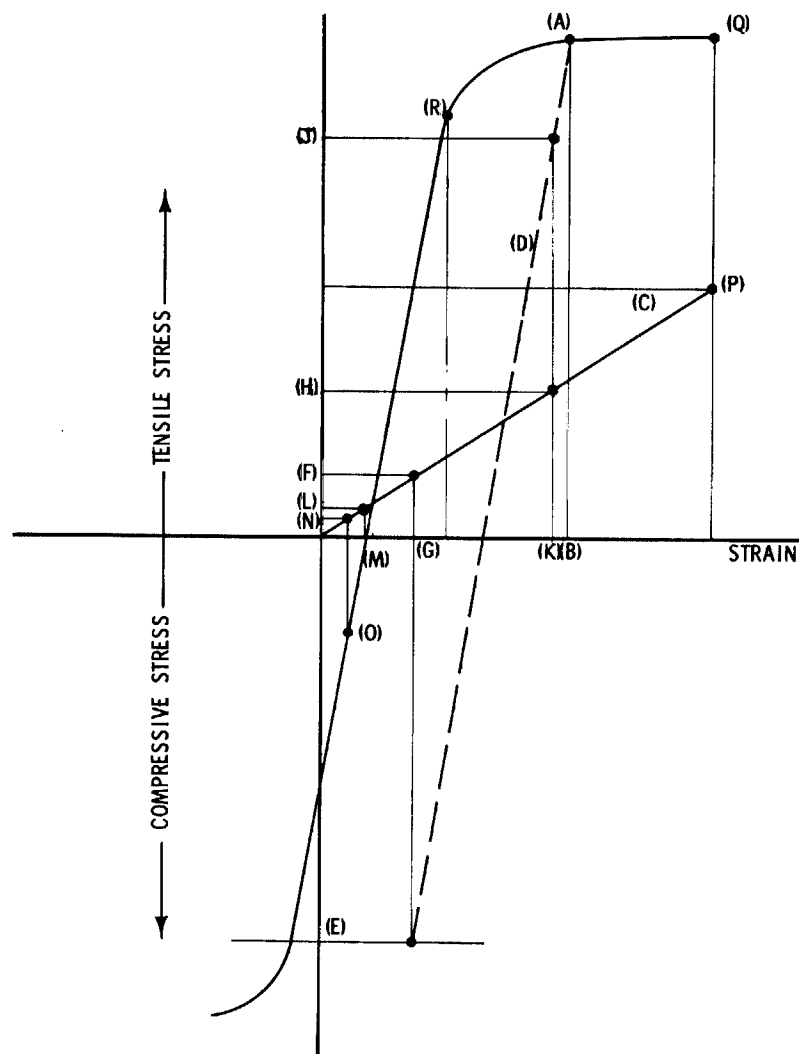
Figure 3



LINER DESIGN CONCEPTS

Figure 4

Figure 5



STRESS-STRAIN DIAGRAM FOR GLASS FILAMENT REINFORCED METALLIC SHELL

- (A) STRESS-STRAIN CURVE FOR METAL SHELL - FIRST CYCLE
- (B) MAXIMUM STRAIN REQUIRED OF COMPLETE SHELL - FIRST CYCLE
- (C) STRESS-STRAIN CURVE FOR GLASS-FIBER SHELL - ALL CYCLES
- (D) STRESS-STRAIN CURVE FOR METAL SHELL-UNLOADING FROM FIRST CYCLE
- (E) COMPRESSIVE STRESS ACHIEVED IN METAL SHELL WHEN VESSEL PRESSURE IS ZERO AFTER STRAIN TO (A)
- (F) TENSION STRESS IN GLASS FIBER SHELL THAT BALANCES COMPRESSION STRESS (E) IN METAL SHELL
- (G) RESIDUAL STRAIN IN GLASS FIBER AND METAL SHELLS WHEN VESSEL PRESSURE IS ZERO AFTER STRAIN TO (A)
- (H) OPERATING STRESS IN GLASS FIBER SHELL - ALL CYCLES SUBSEQUENT TO THE FIRST
- (I) OPERATING STRESS IN METAL SHELL - ALL CYCLES SUBSEQUENT TO FIRST
- (J) OPERATING STRAIN IN GLASS-FIBER AND METAL SHELLS - ALL CYCLES SUBSEQUENT TO FIRST
- (K) STRESS IN GLASS FIBER SHELL FROM WINDING ON RIGID MANDREL
- (L) STRAIN IN GLASS FIBER SHELL FROM WINDING ON A RIGID MANDREL;
- (M) ZERO STRAIN POINT OF METAL SHELL BEFORE WINDING
- (N) STRESS IN GLASS FIBER SHELL AFTER MANDREL REMOVAL WHEN VESSEL PRESSURE IS ZERO
- (O) STRAIN IN METAL AND GLASS FIBER SHELLS AFTER MANDREL REMOVAL WHEN VESSEL PRESSURE IS ZERO
- (P) ULTIMATE STRESS OR STRAIN OF GLASS FIBER SHELL
- (Q) ULTIMATE STRESS OR STRAIN OF METAL SHELL WHEN FILAMENTS FRACTURE
- (R) ARBITRARY STRAIN POINT IN METAL SHELL AND GLASS FIBER SHELL BELOW METAL SHELL PROPORTIONAL LIMIT

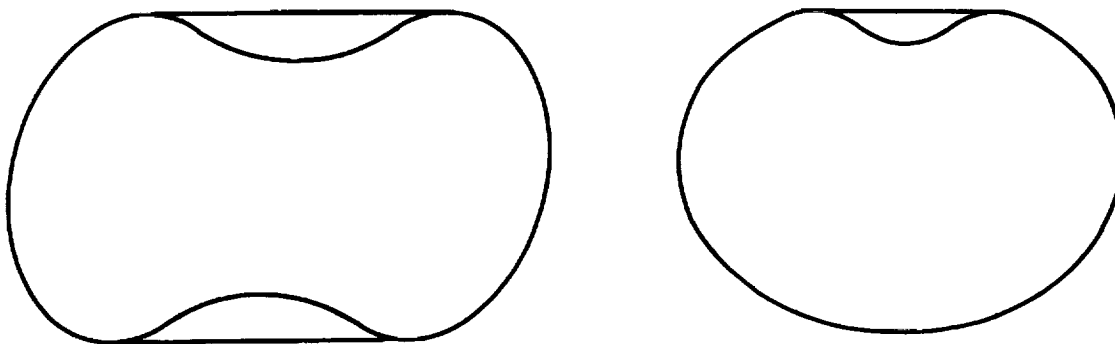


FIGURE 6. CONCAVE-CONVEX FORM

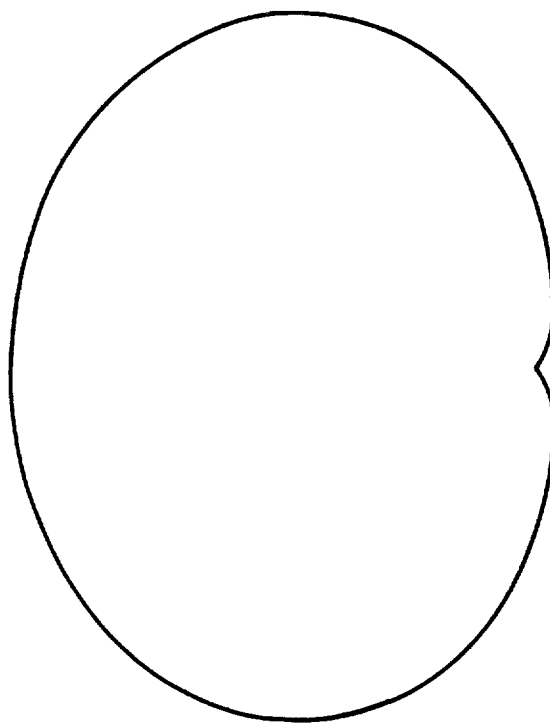
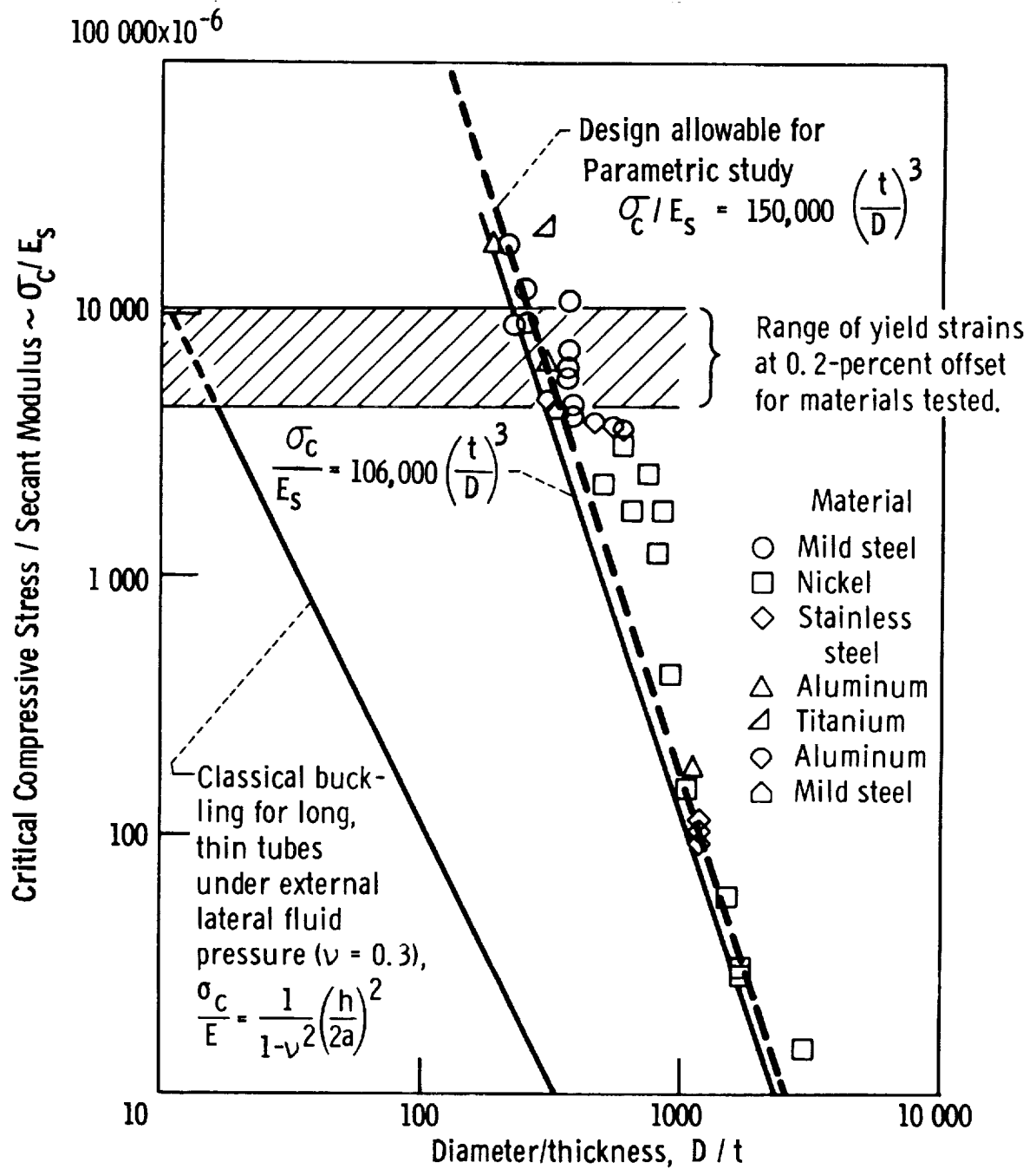


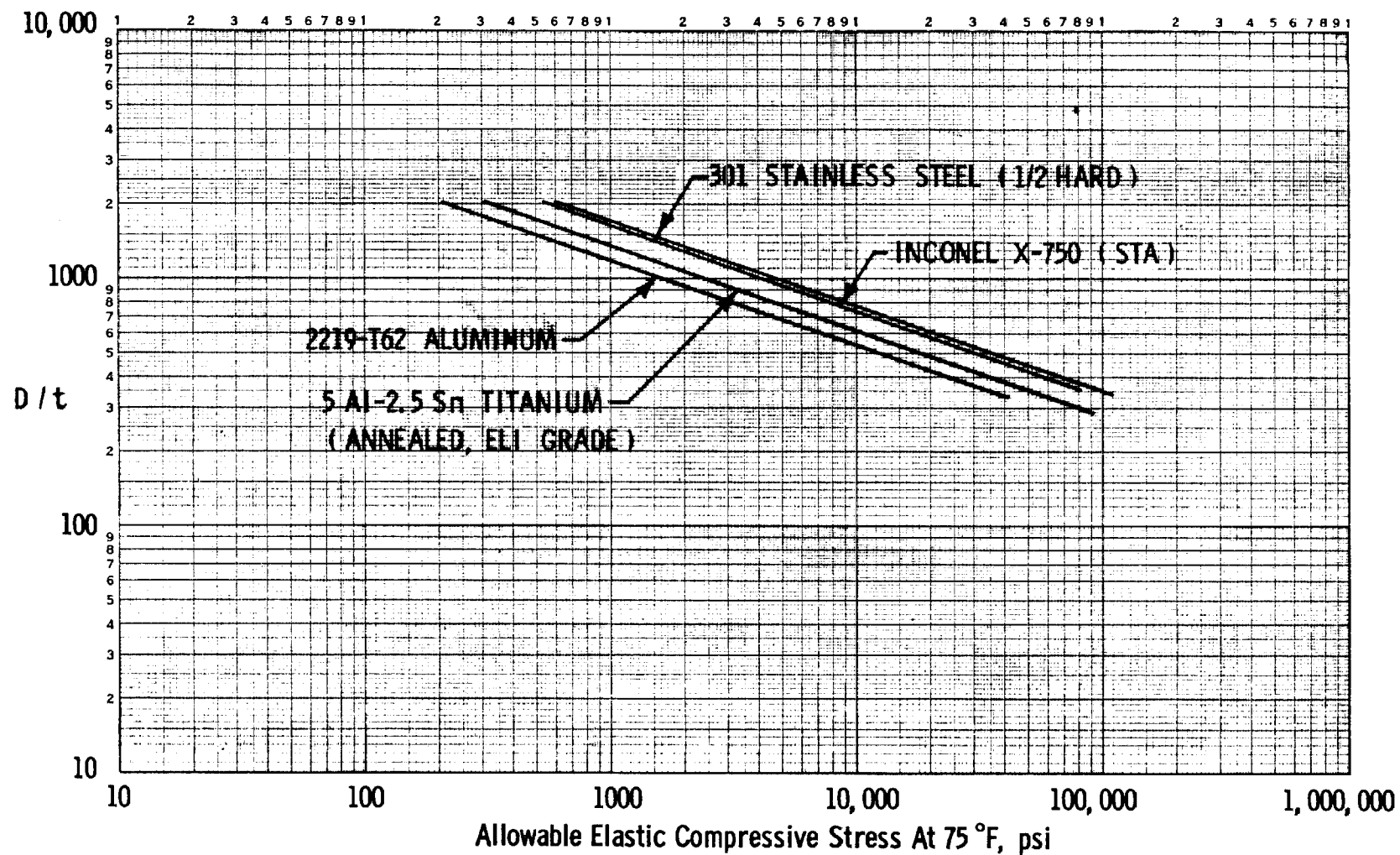
FIGURE 7. BUCKLED FORM



COMPARISON OF CONSTRICTIVE-WRAP BUCKLING STRENGTHS FOR CYLINDRICAL TUBES (REF. 9) WITH DESIGN ALLOWABLE USED FOR PARAMETRIC STUDY

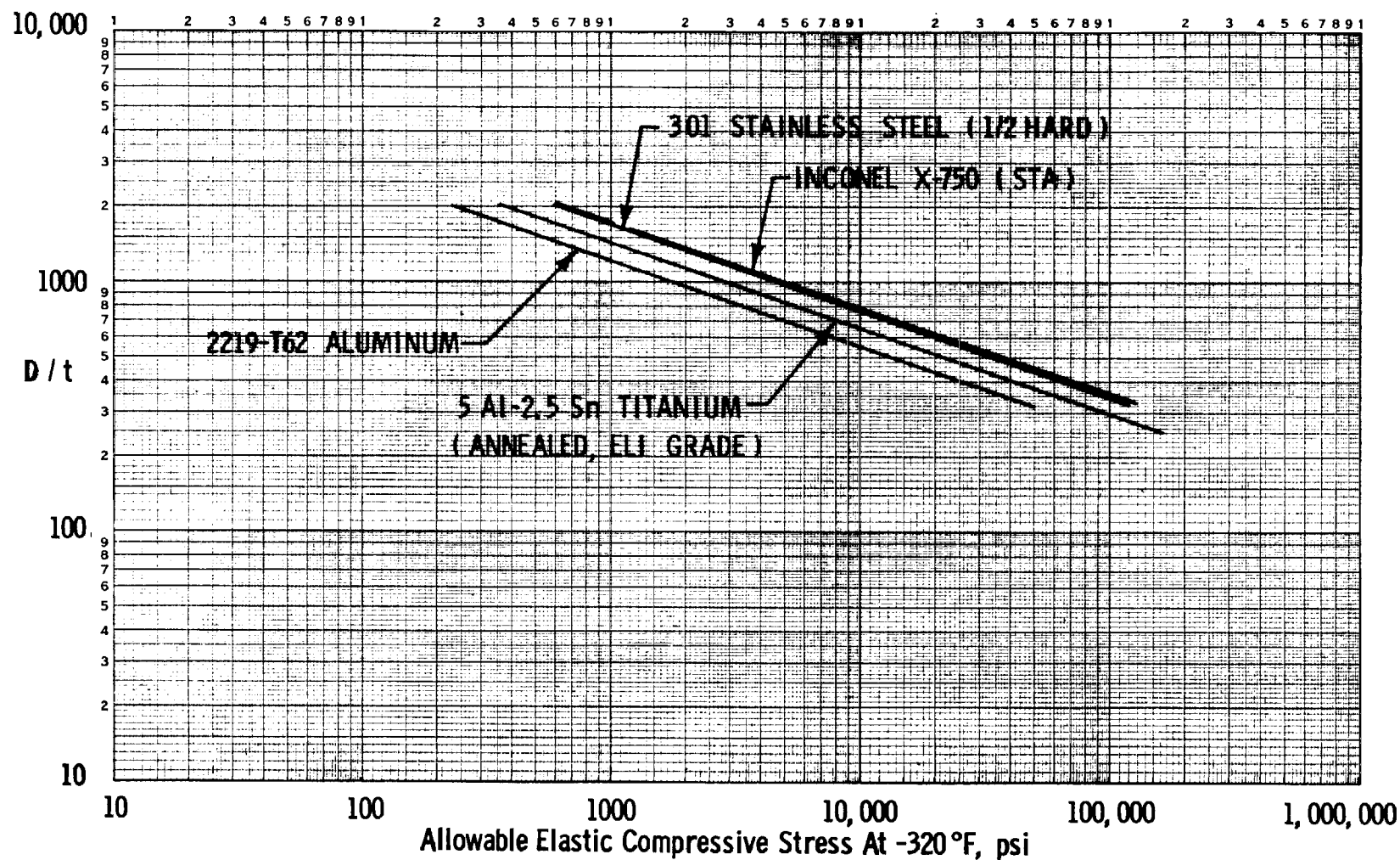
Figure 8

Figure 9

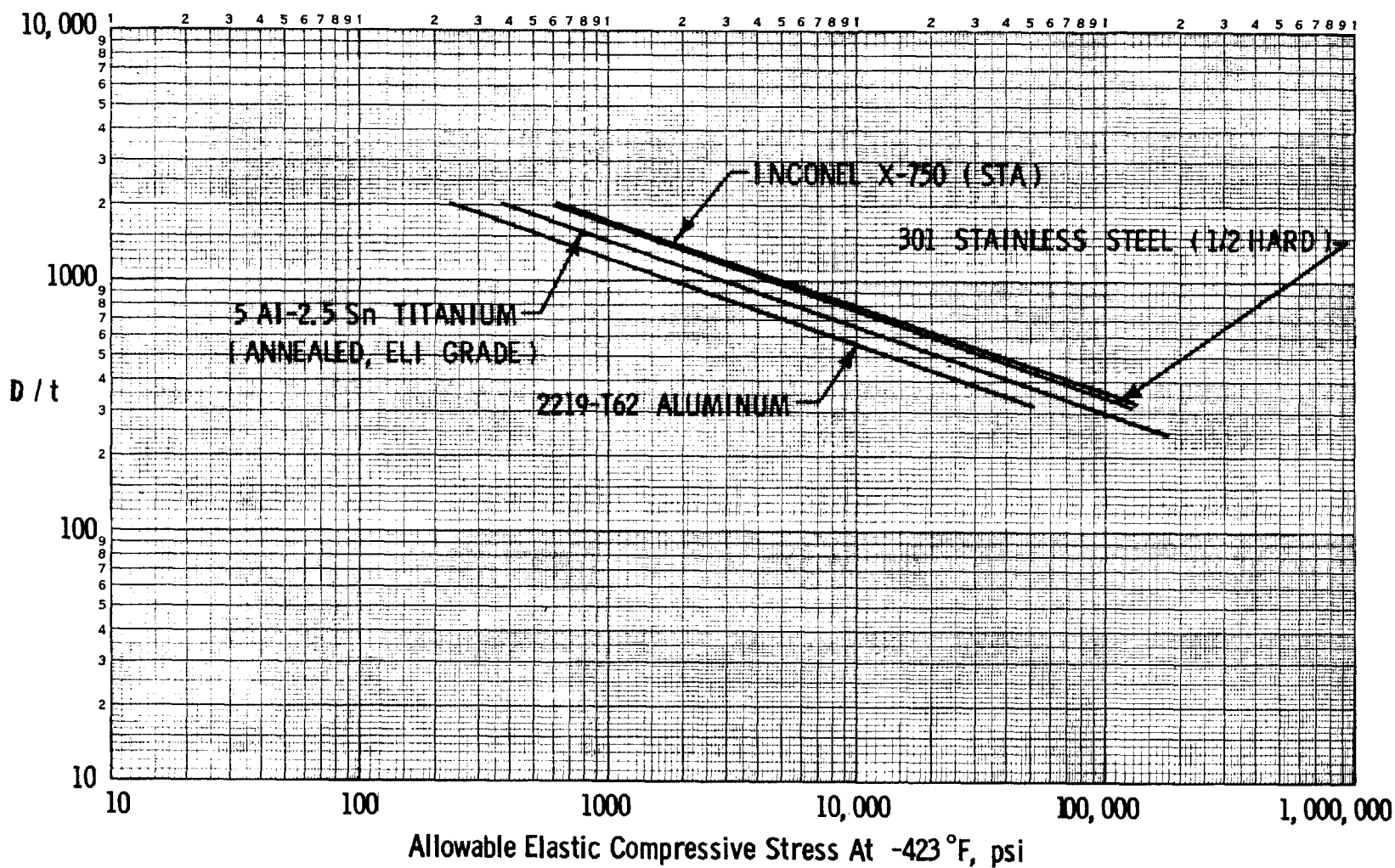


D/t RATIO VS ALLOWABLE ELASTIC COMPRESSIVE STRESS AT 75 °F

Figure 10



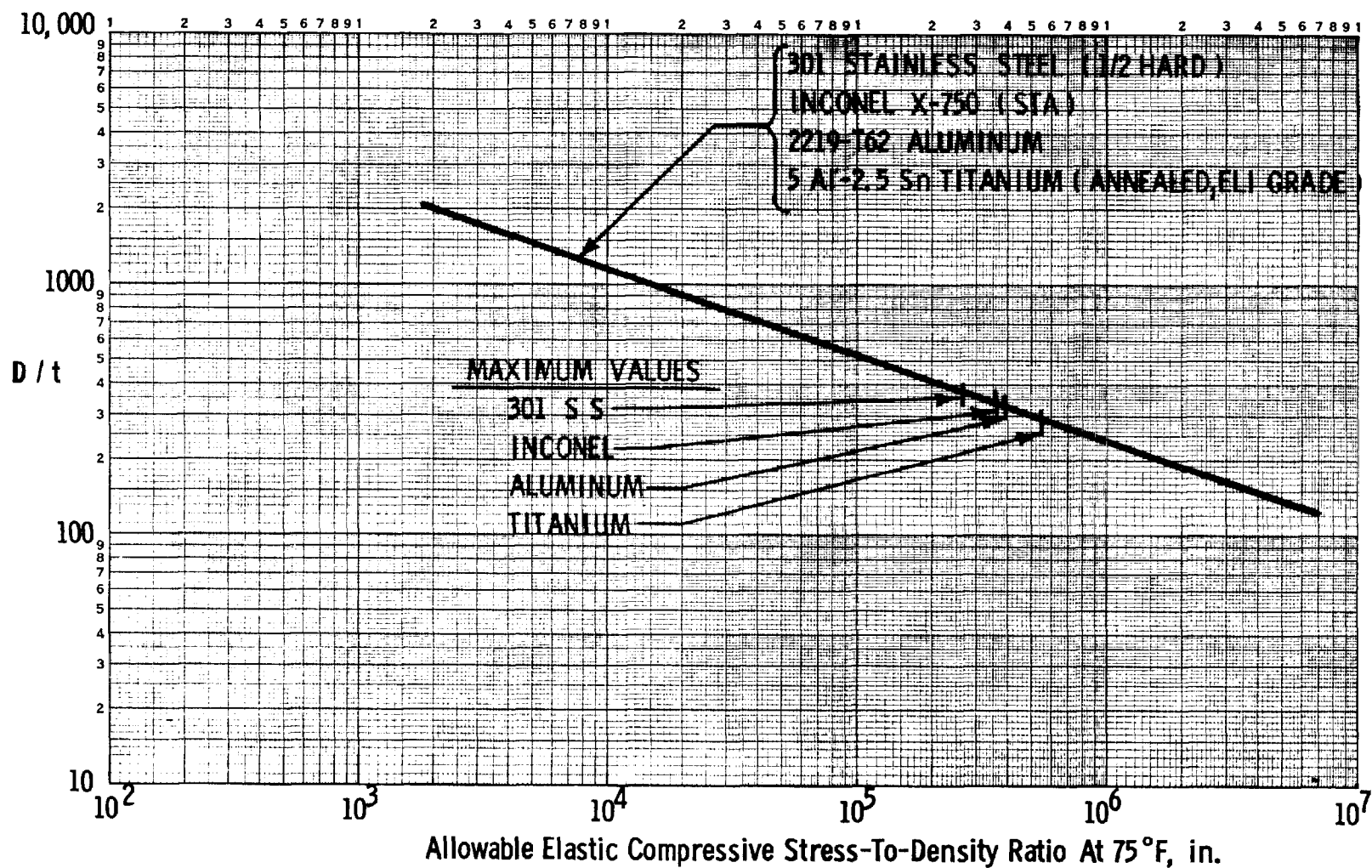
D/t RATIO VS ALLOWABLE ELASTIC COMPRESSIVE STRESS AT -320 °F



D/t RATIO VS ALLOWABLE ELASTIC COMPRESSIVE STRESS AT -423 °F

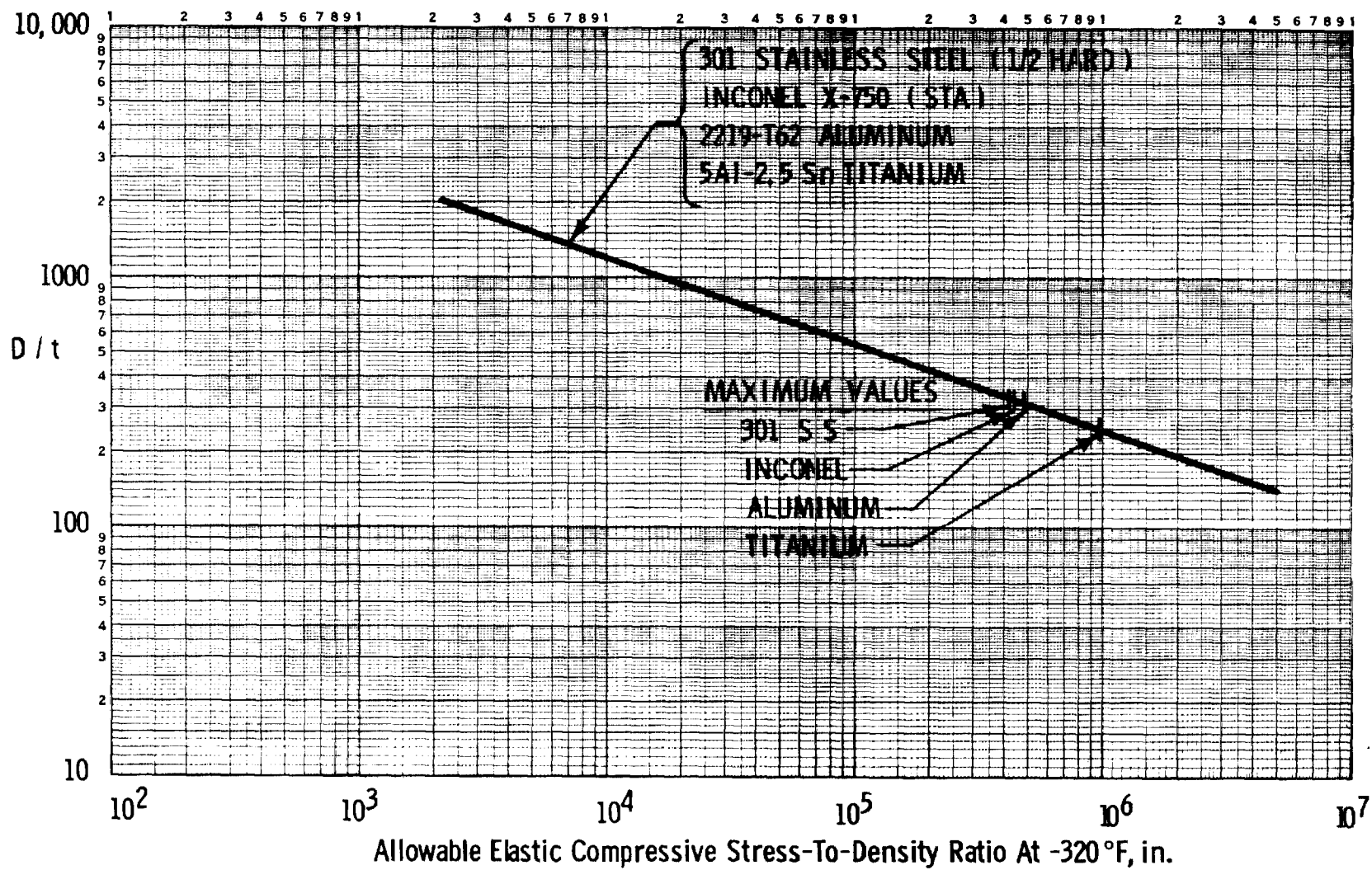
Figure 11

Figure 12



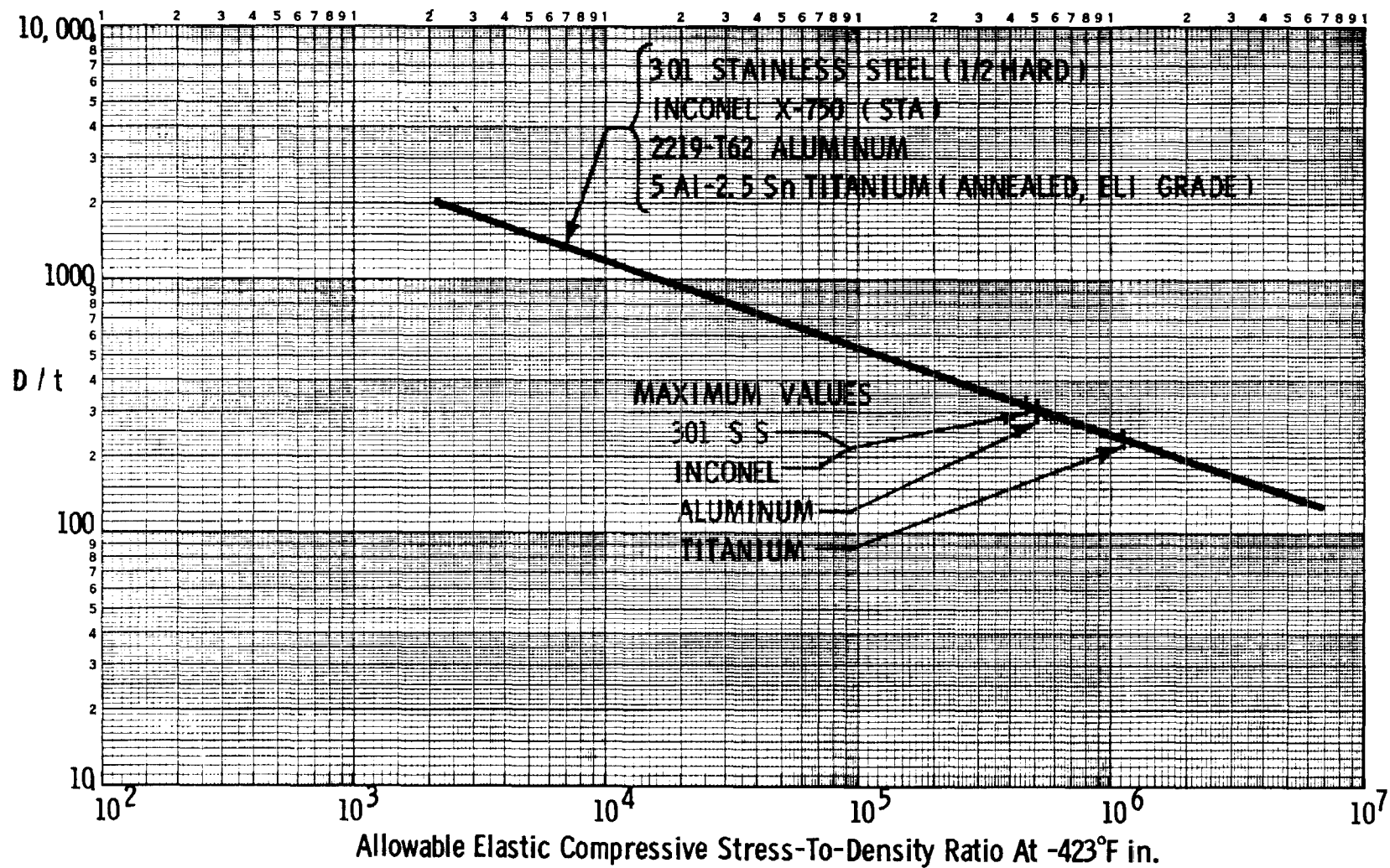
D / t RATIO VS ALLOWABLE ELASTIC COMPRESSIVE STRESS-TO-DENSITY RATIO AT 75°F

Figure 13

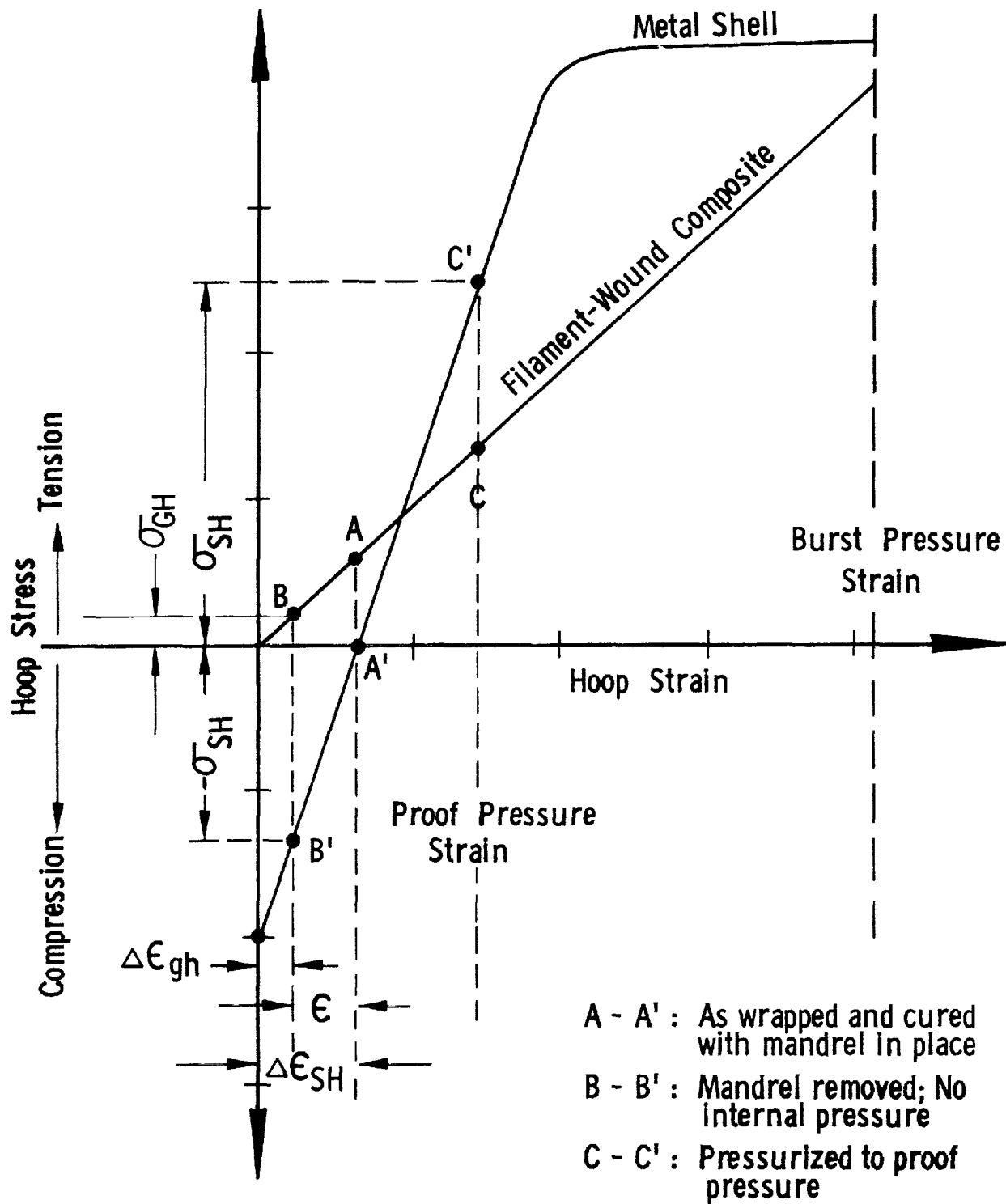


D/t RATIO VS ALLOWABLE ELASTIC COMPRESSIVE STRESS-TO-DENSITY RATIO AT -320°F

Figure 14



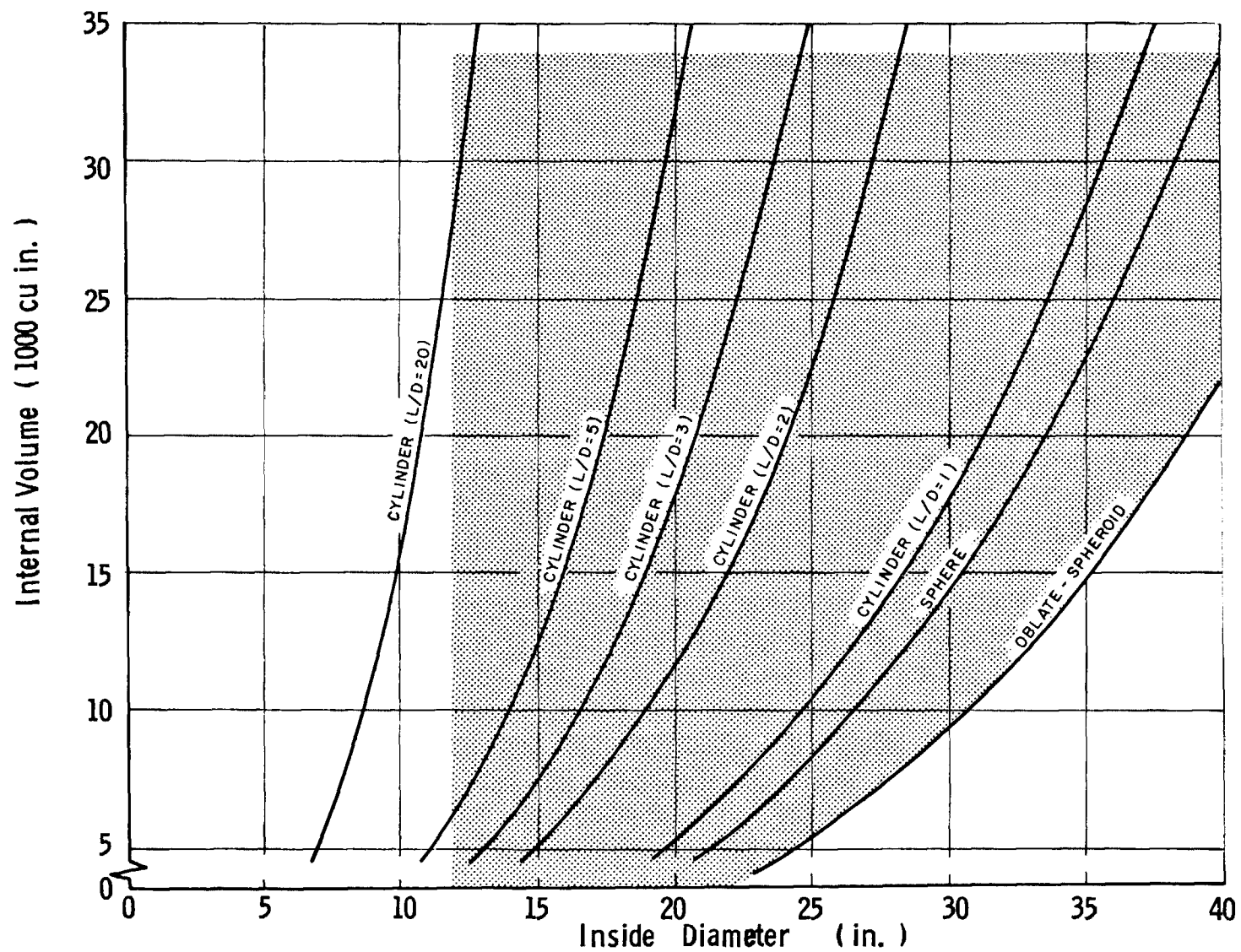
D / t RATIO VS ALLOWABLE ELASTIC COMPRESSIVE STRESS-TO-DENSITY RATIO AT -423°F



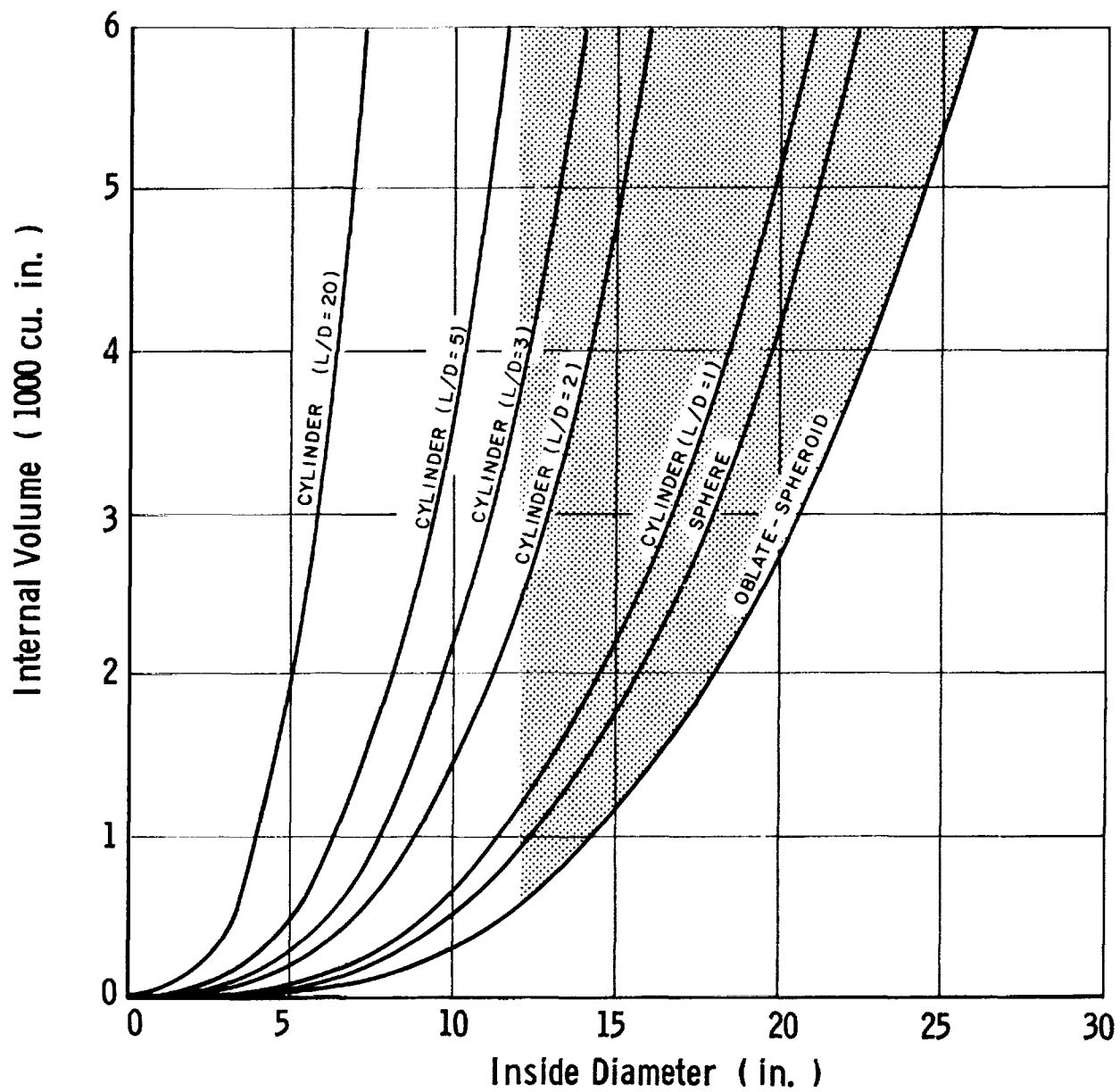
STRESS-STRAIN DIAGRAM OF GLASS-FILAMENT-OVERWRAPPED METAL SHELL

Figure 15

Figure 16



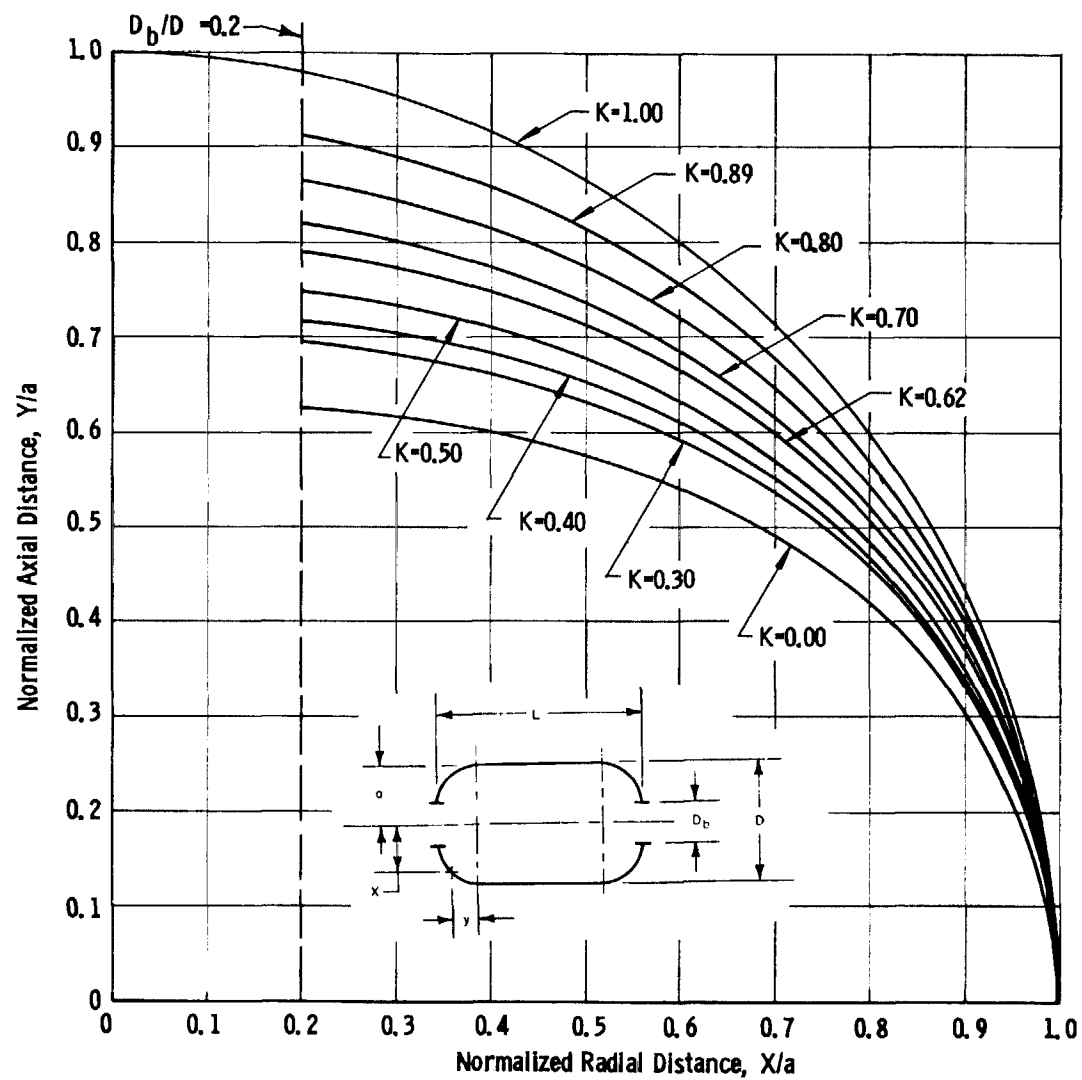
VOLUME-DIAMETER RELATIONSHIP FOR PRESSURE VESSEL CONFIGURATIONS (5000-35,000 CU IN. RANGE)



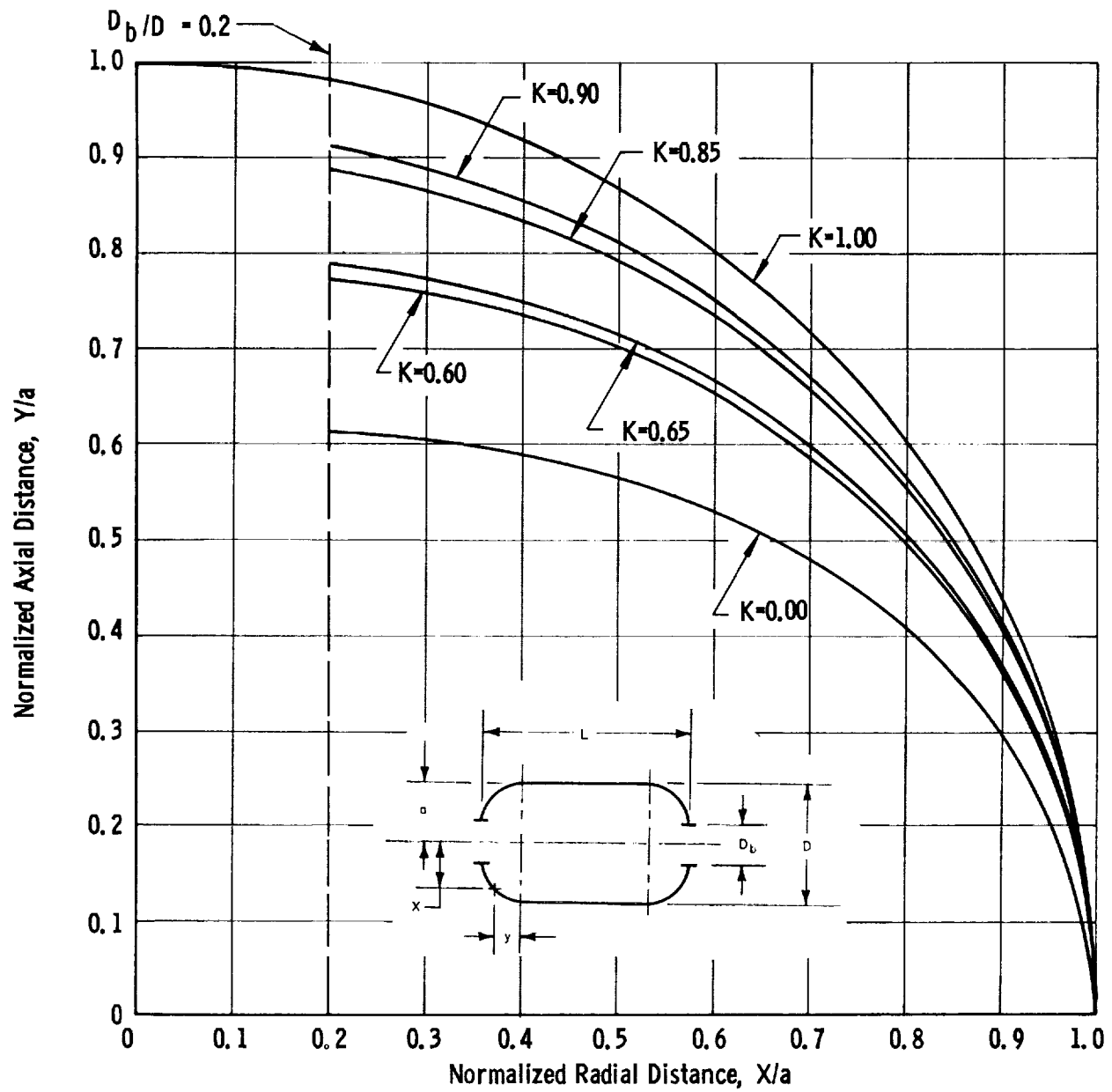
VOLUME-DIAMETER RELATIONSHIP FOR PRESSURE VESSEL CONFIGURATIONS
(0-6000 CU. IN. RANGE)

Figure 17

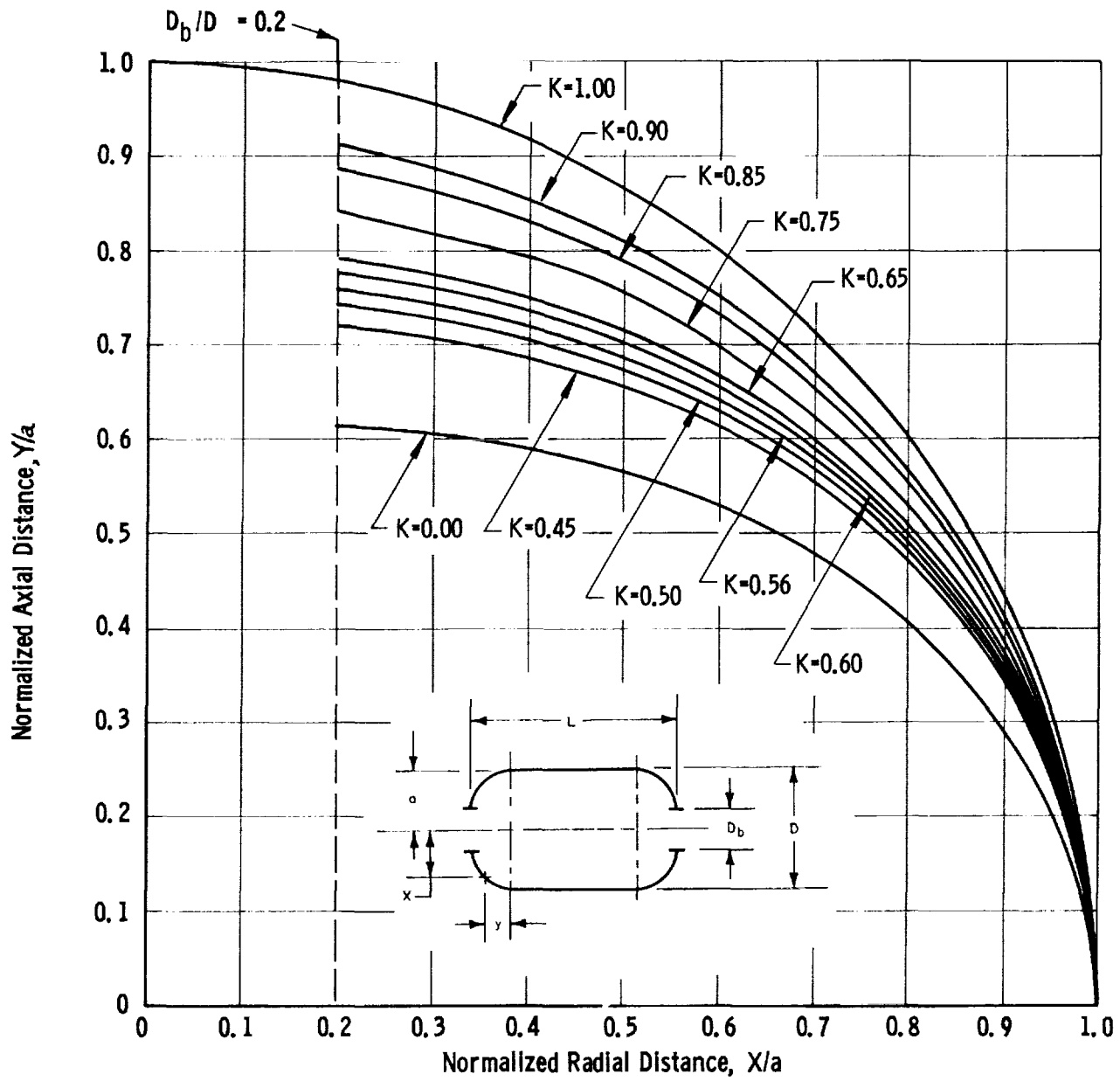
Figure 18



BALANCED-IN-PLANE-WRAP HEAD CONTOURS FOR GFR METAL PRESSURE VESSELS (BACK-TO-BACK HEADS)

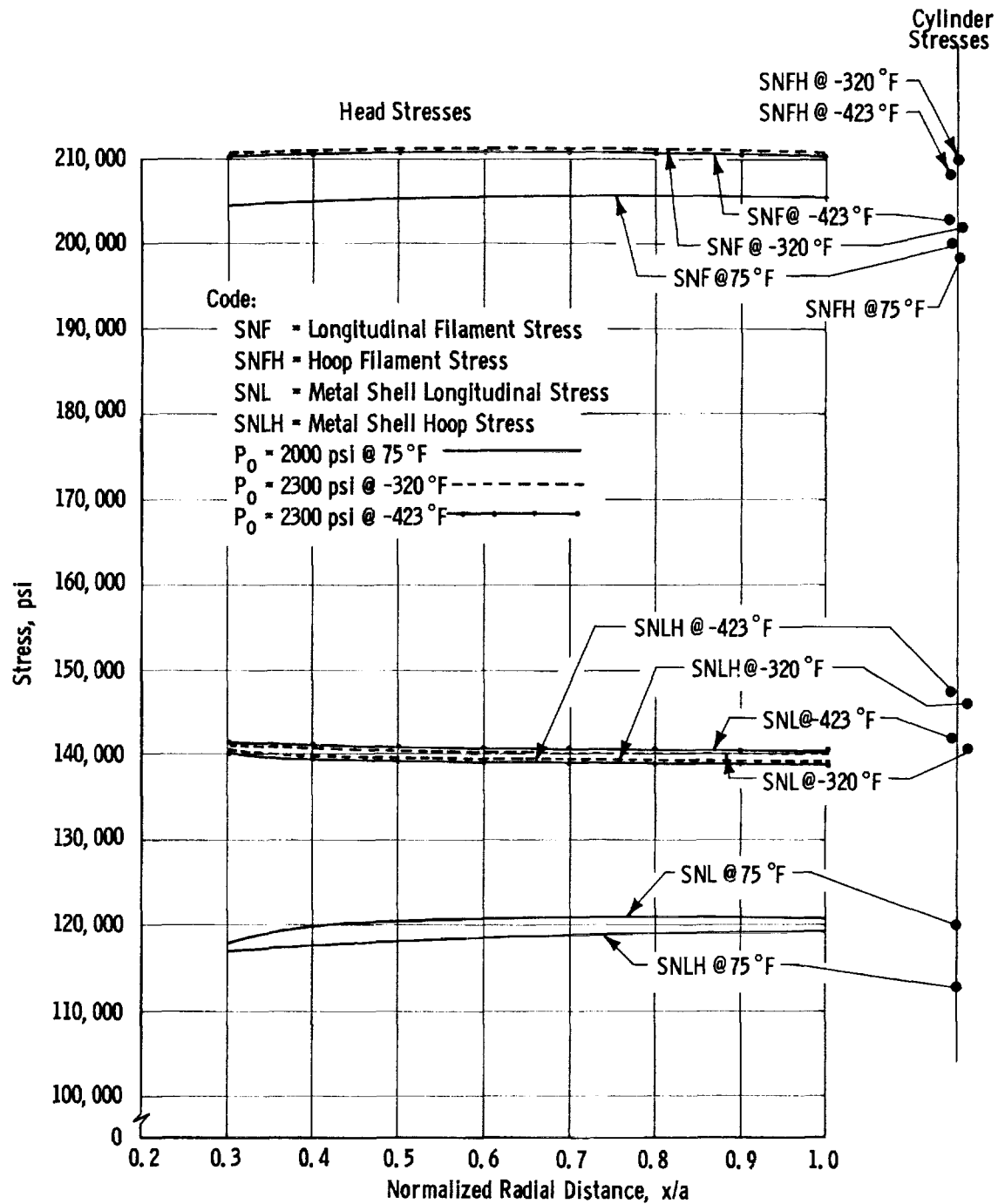


BALANCED-IN-PLANE-WRAP HEAD CONTOURS FOR GFR METAL PRESSURE VESSELS ($L/D = 2.0$)

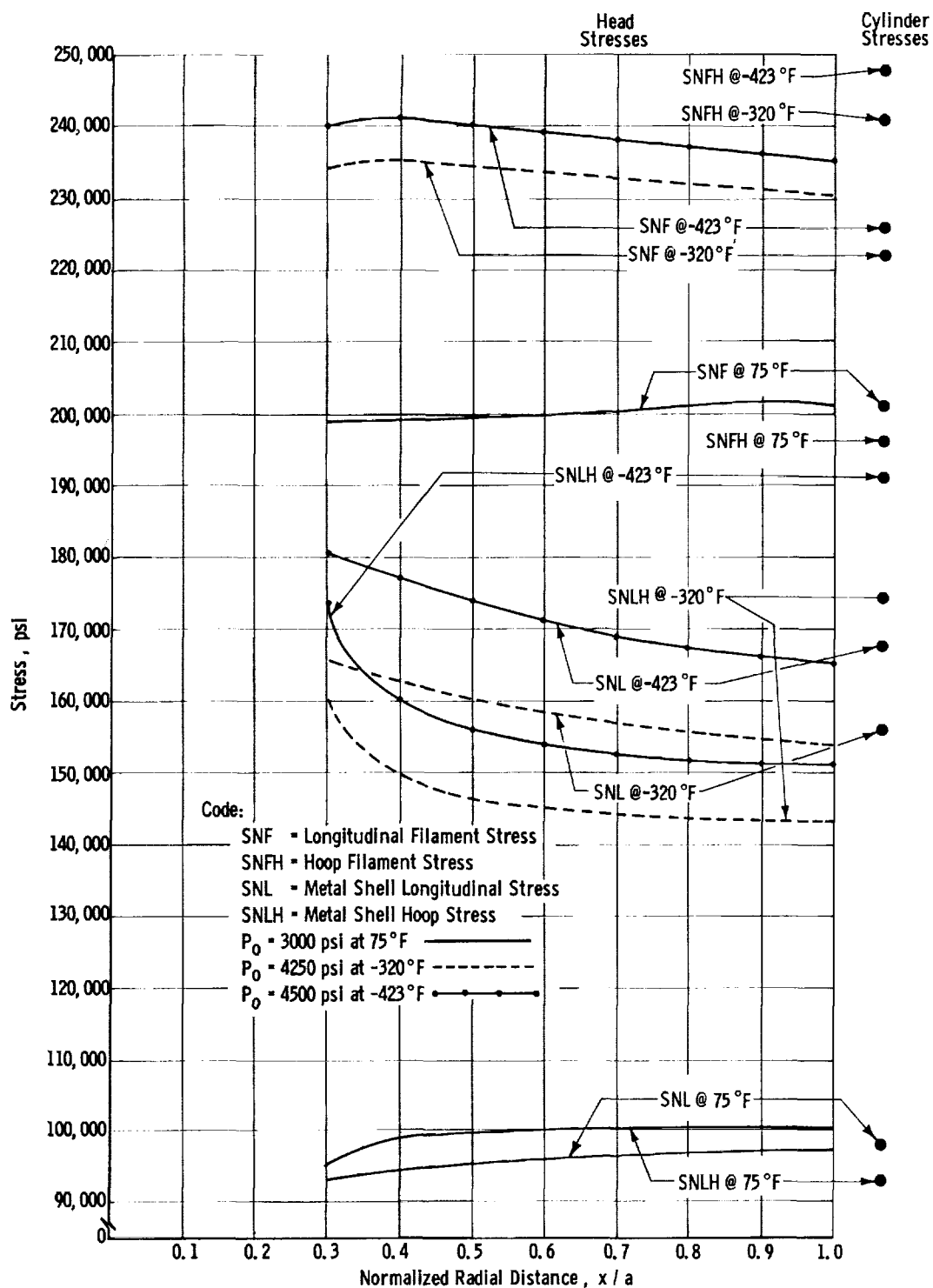


BALANCED-IN-PLANE-WRAP CONTOURS FOR GFR METAL PRESSURE VESSELS ($L/D=3.0$)

Figure 21

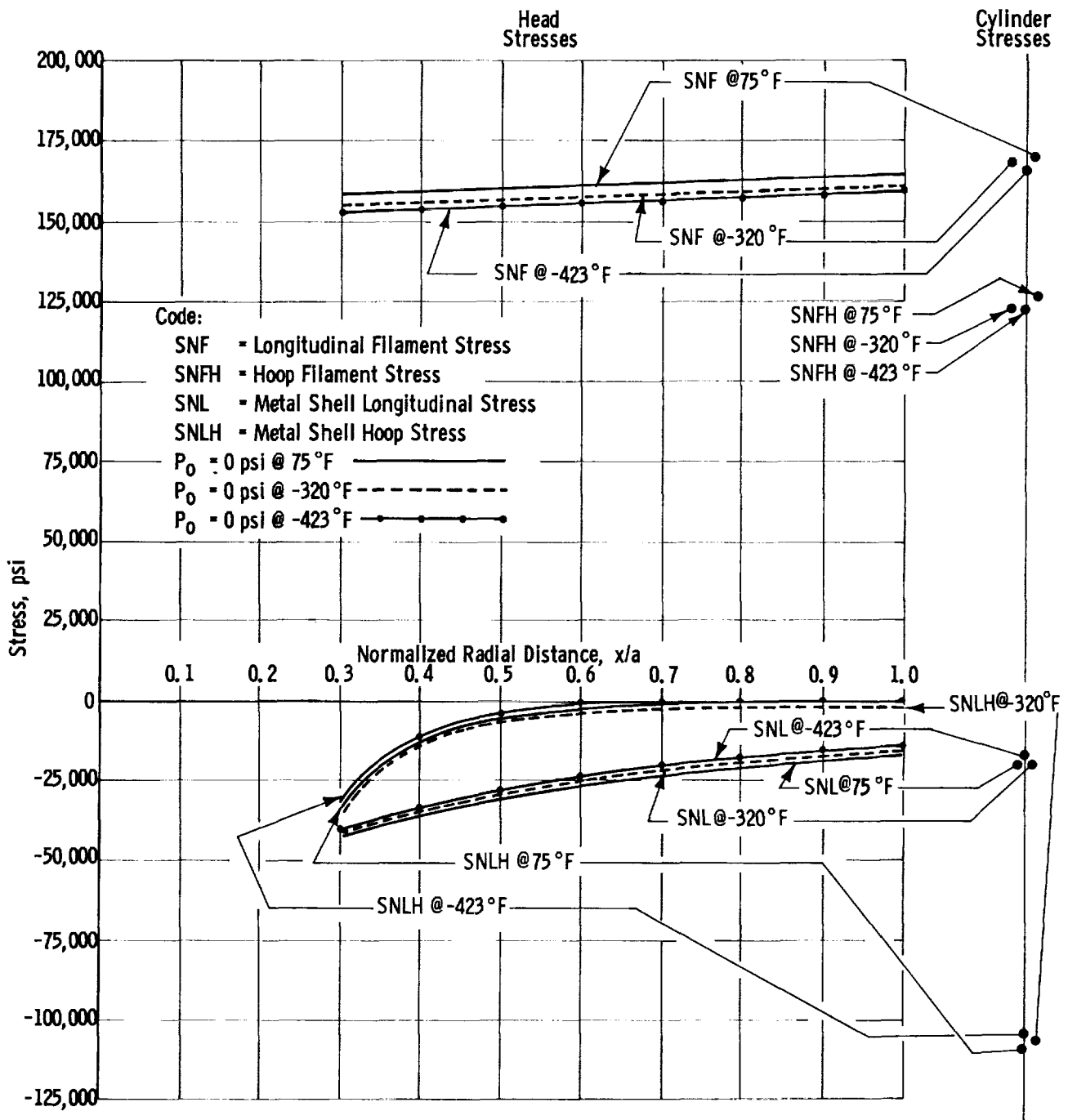


STRESSES AT OPERATING PRESSURES IN OPTIMUM GFR INCONEL X-750 (STA) PRESSURE VESSEL
WITH 2220 PSI PROOF PRESSURE AND 2000 PSI OPERATING PRESSURE AT 75°F ($L/D=1$)



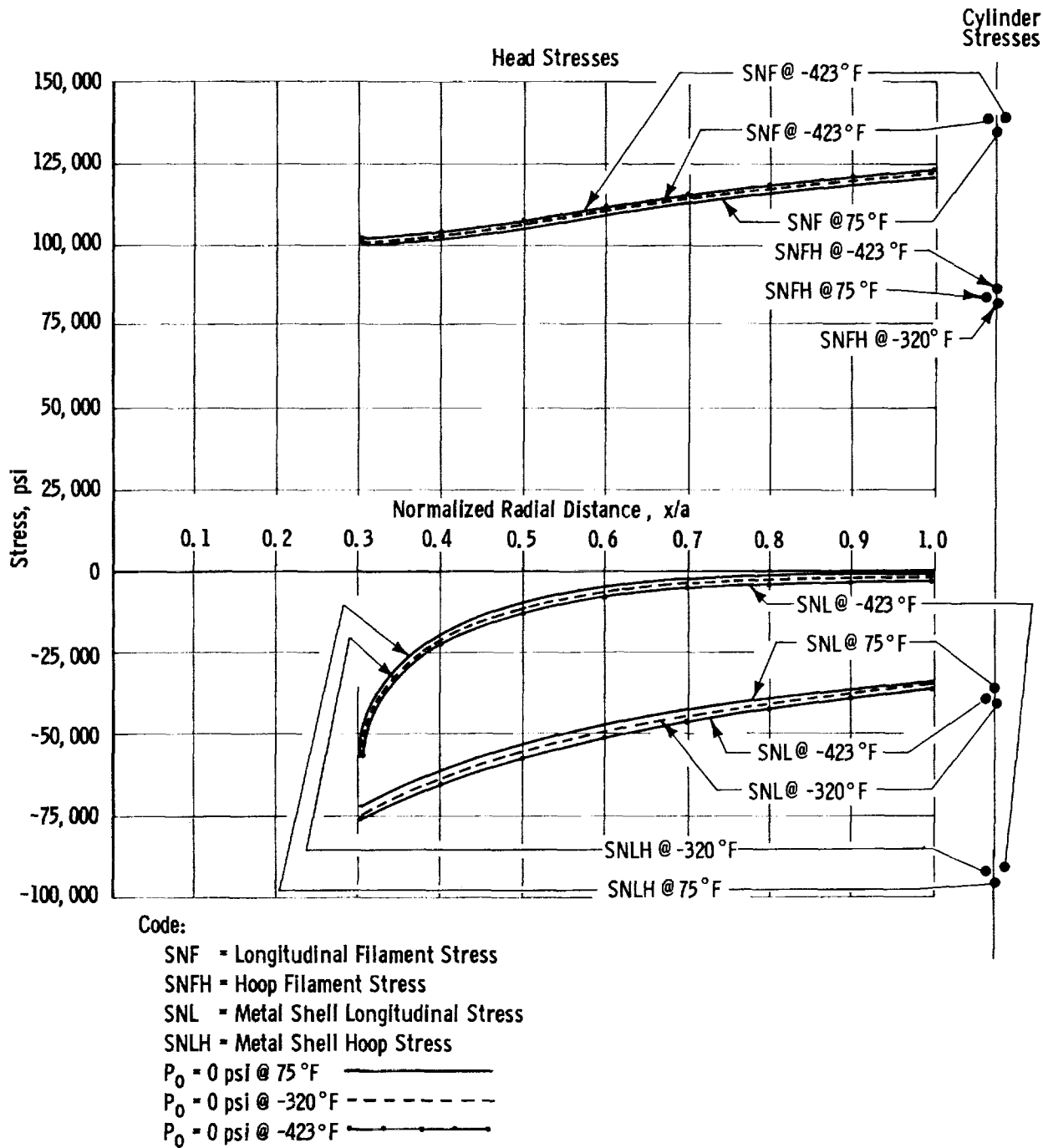
STRESSES AT OPERATING PRESSURES IN OPTIMUM GFR 5 Al-2.5 Sn TITANIUM (ANNEALED, ELI GRADE)
PRESSURE VESSEL WITH 3335 PSI PROOF PRESSURE AND 3000 PSI OPERATING PRESSURE AT 75°F (L/D=1)

Figure 23



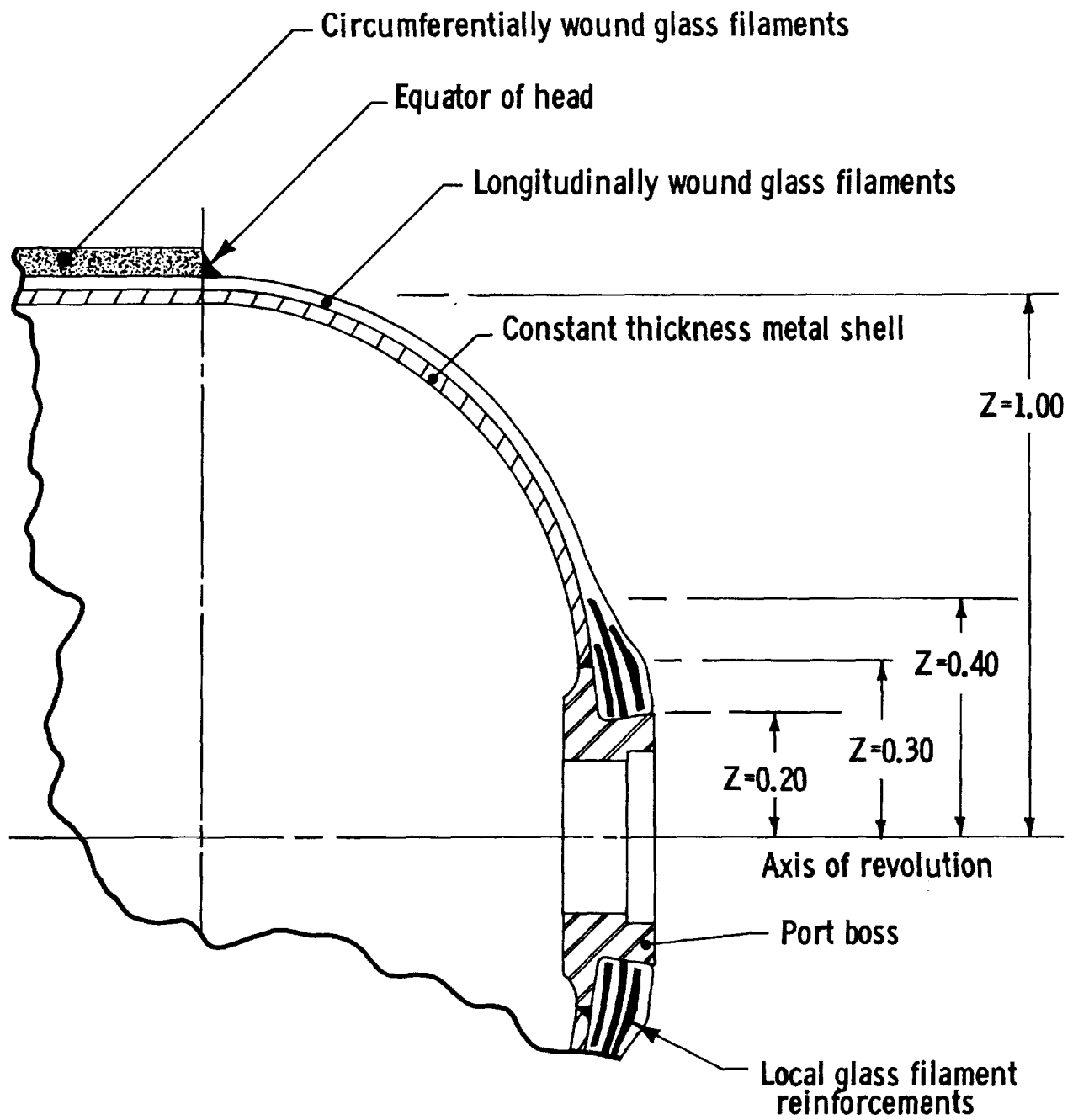
STRESSES AT ZERO PRESSURE AFTER PROOF PRESSURE IN OPTIMUM GFR INCONEL X-750
(STA) PRESSURE VESSEL WITH 2220 PSI PROOF PRESSURE AND 2000 PSI
OPERATING PRESSURE AT 75°F (L/D =1)

Figure 24



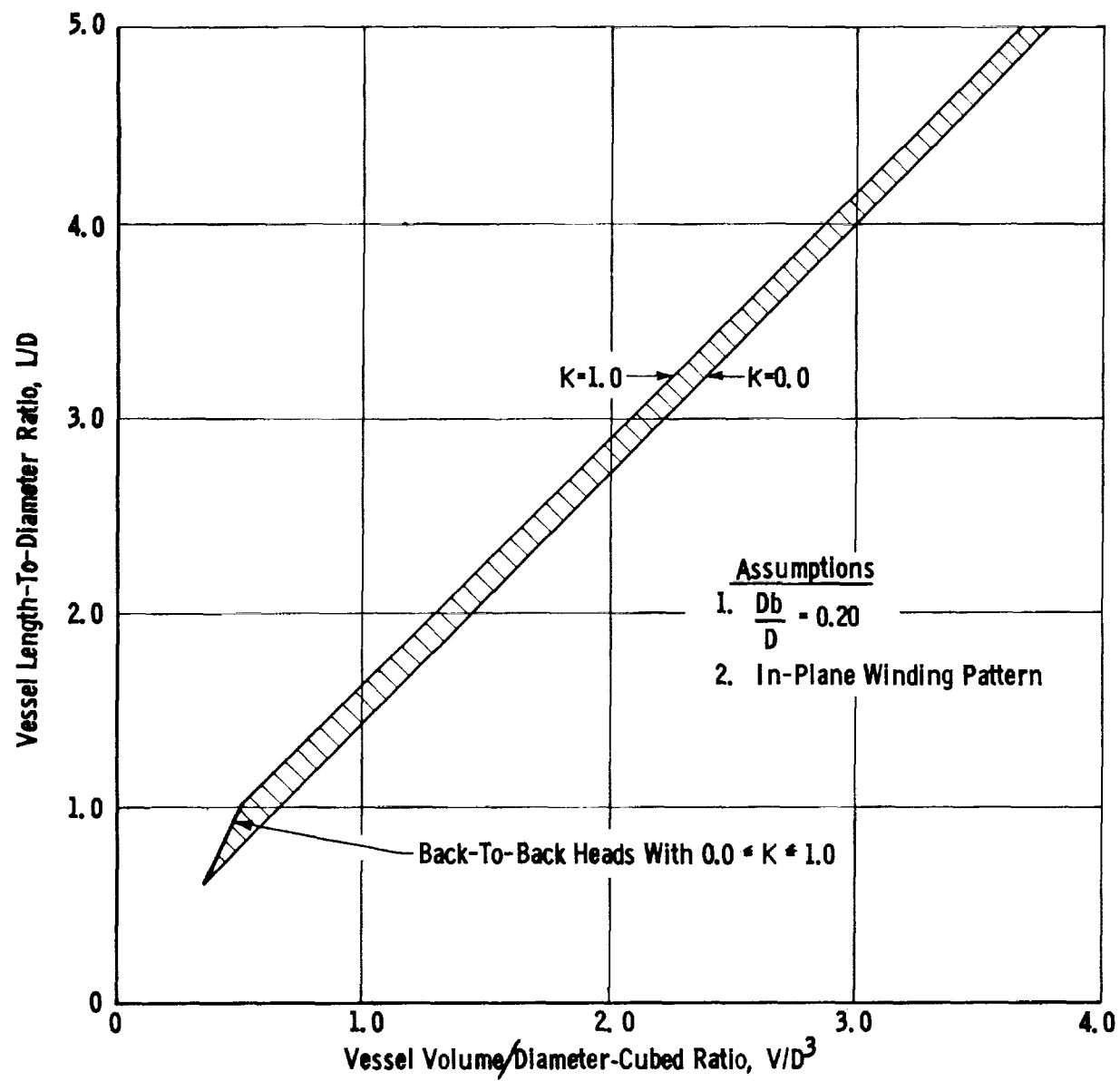
STRESSES AT ZERO PRESSURE AFTER PROOF PRESSURE IN OPTIMUM GFR 5Al - 2.5 Sn TITANIUM
(ANNEALED, ELI GRADE) PRESSURE VESSEL WITH 3335 PSI PROOF PRESSURE AND
3000 PSI OPERATING PRESSURE AT 75°F (L/D=1)

Figure 25



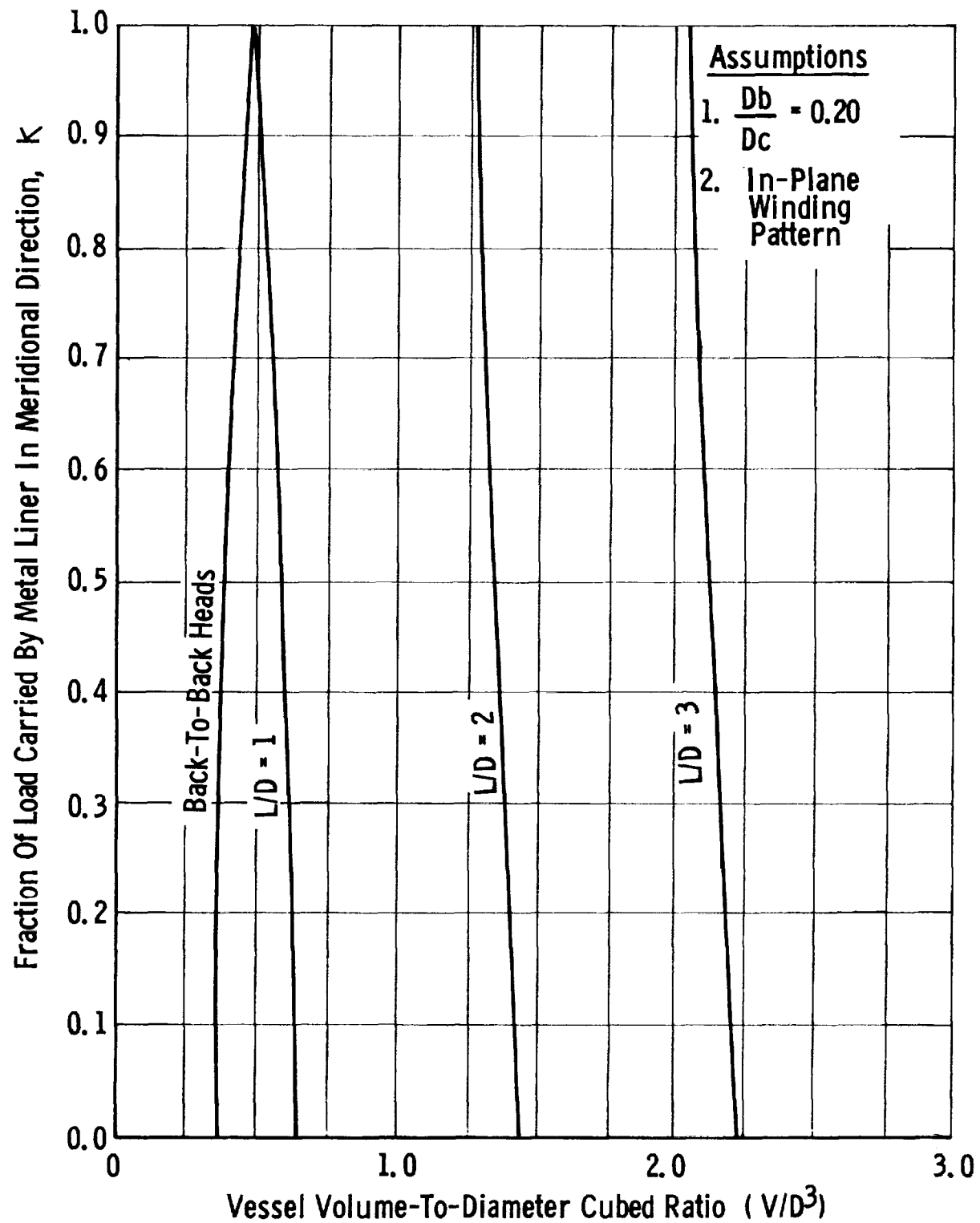
GLASS FIBER REINFORCED METAL PRESSURE VESSEL

Figure 26



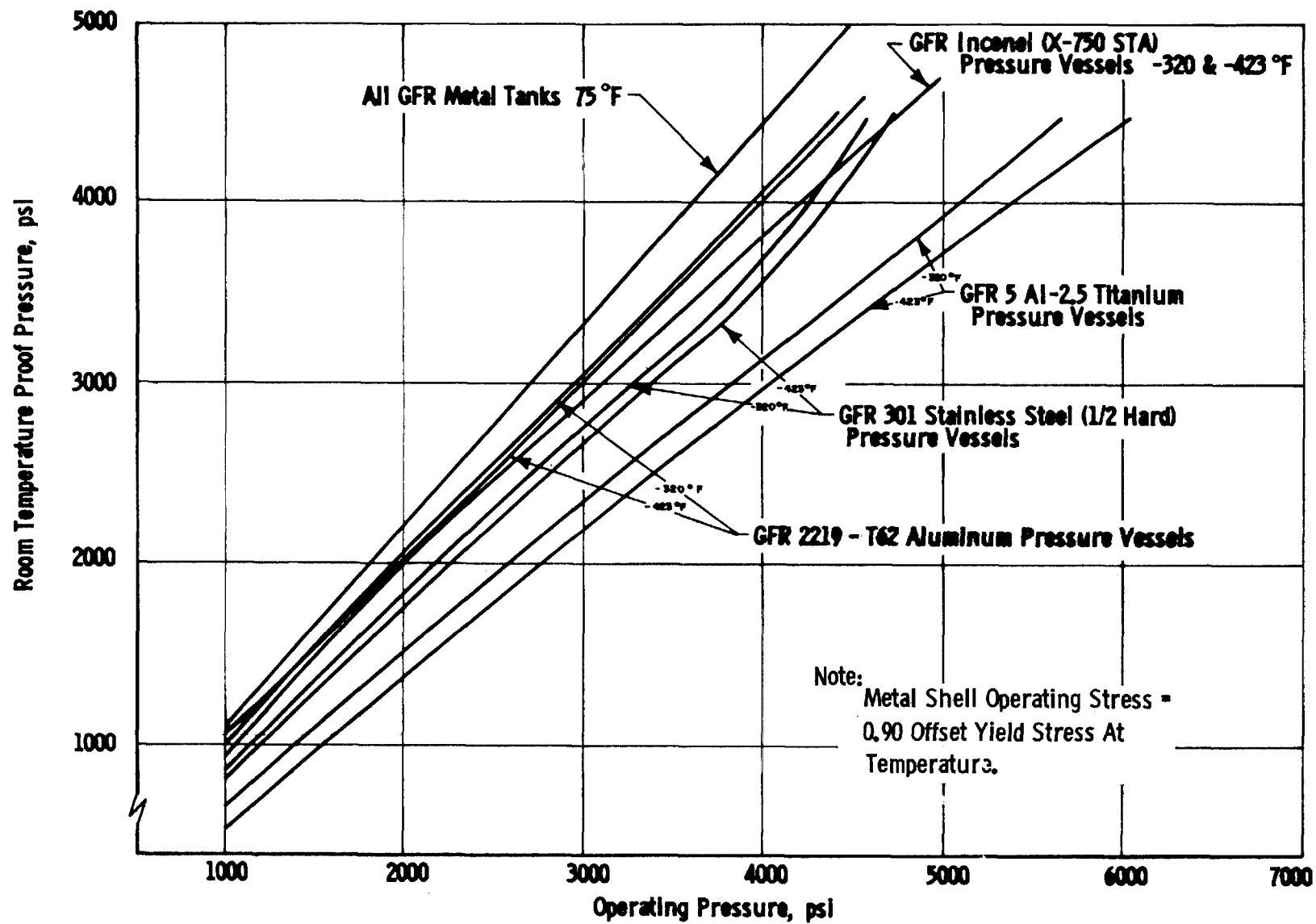
GFR METAL PRESSURE VESSELS—RELATIONSHIP BETWEEN VESSEL L/D RATIO AND V/D^3 RATIO

Figure 27



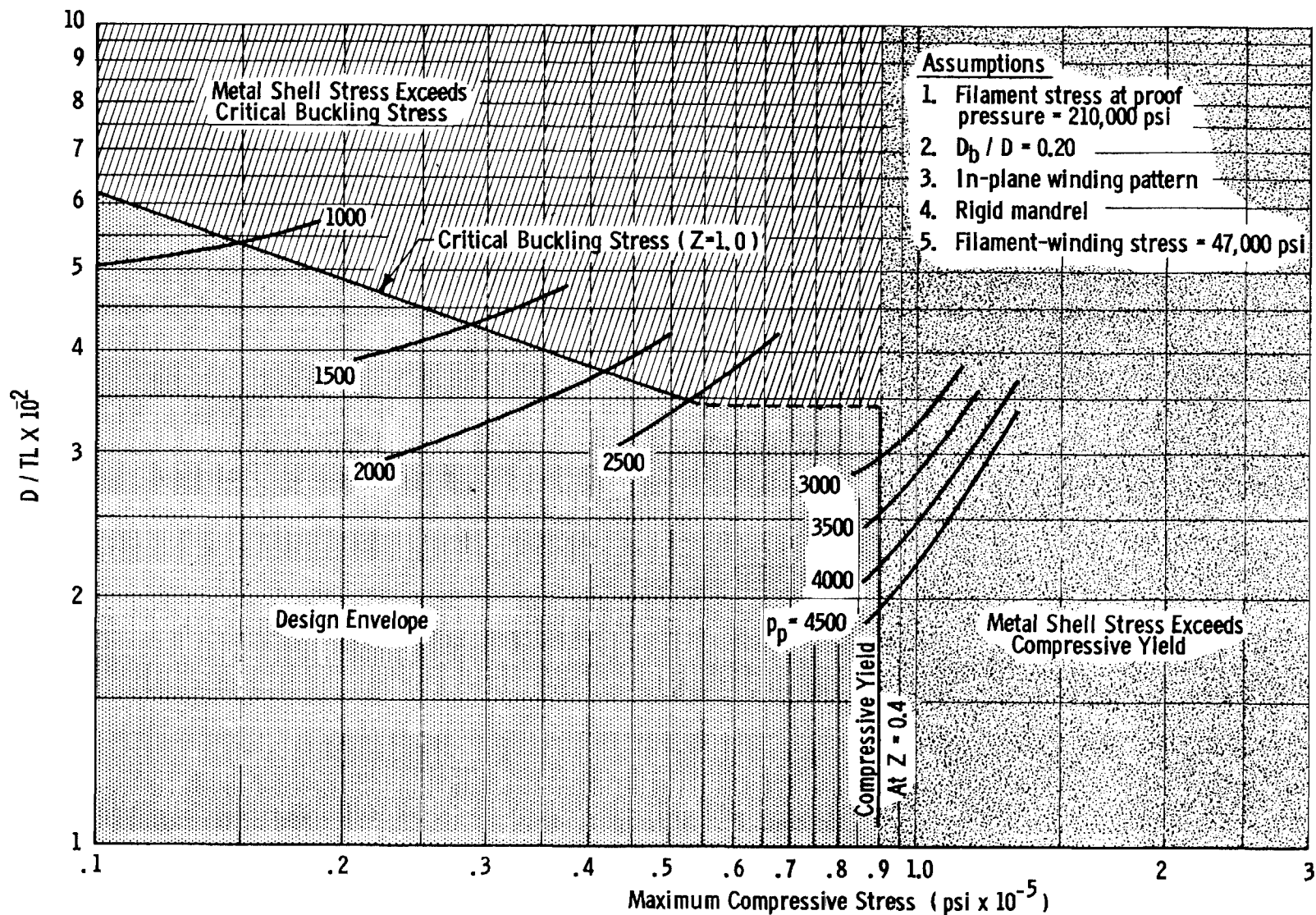
GFR METAL PRESSURE VESSEL — RELATIONSHIP BETWEEN VOLUME, DIAMETER, AND LOAD FRACTION TAKEN BY LINER

Figure 29



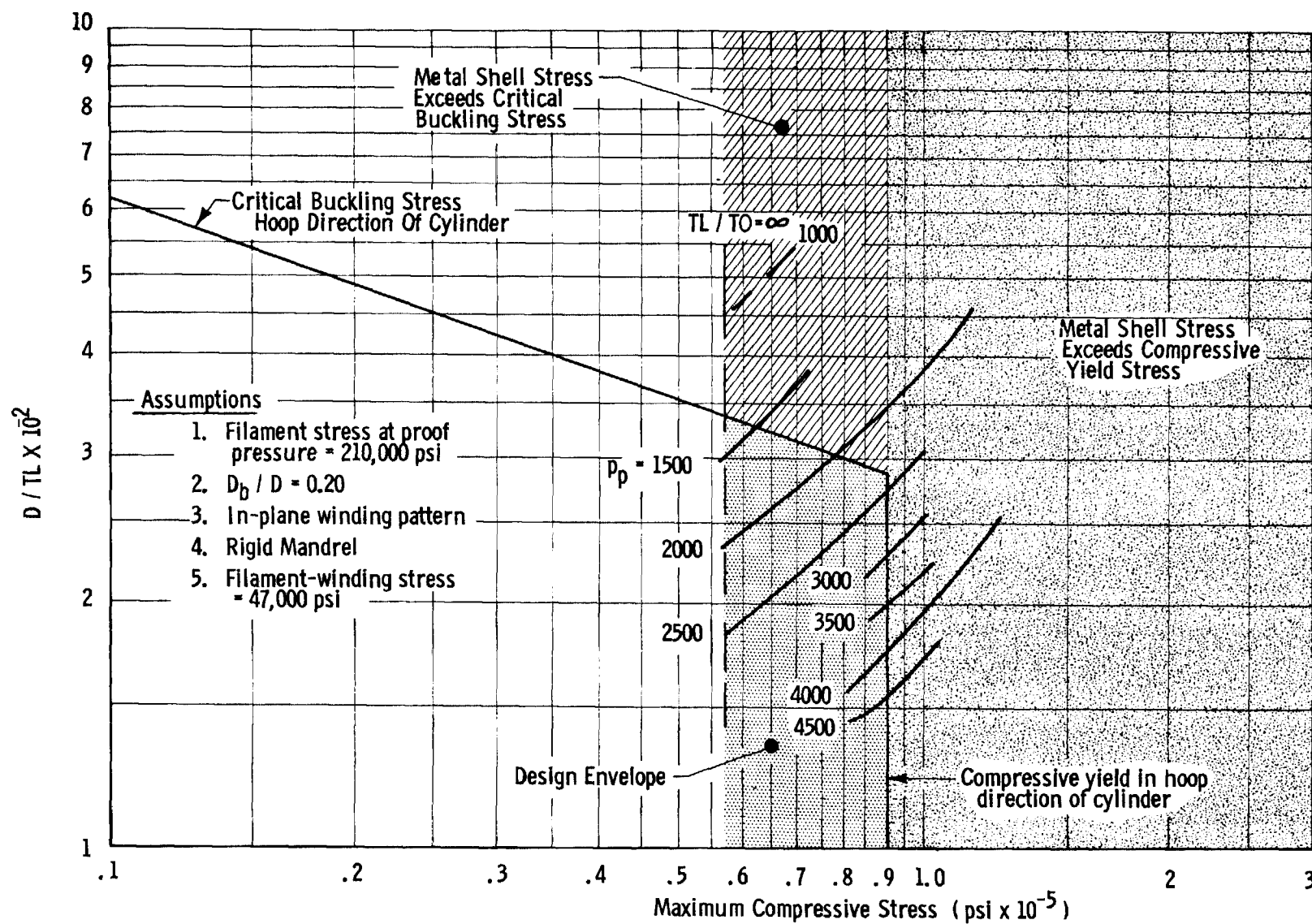
RELATIONSHIP OF ROOM TEMPERATURE PROOF PRESSURE TO OPERATING PRESSURES AT 75, -320, AND -423 °F

Figure 30

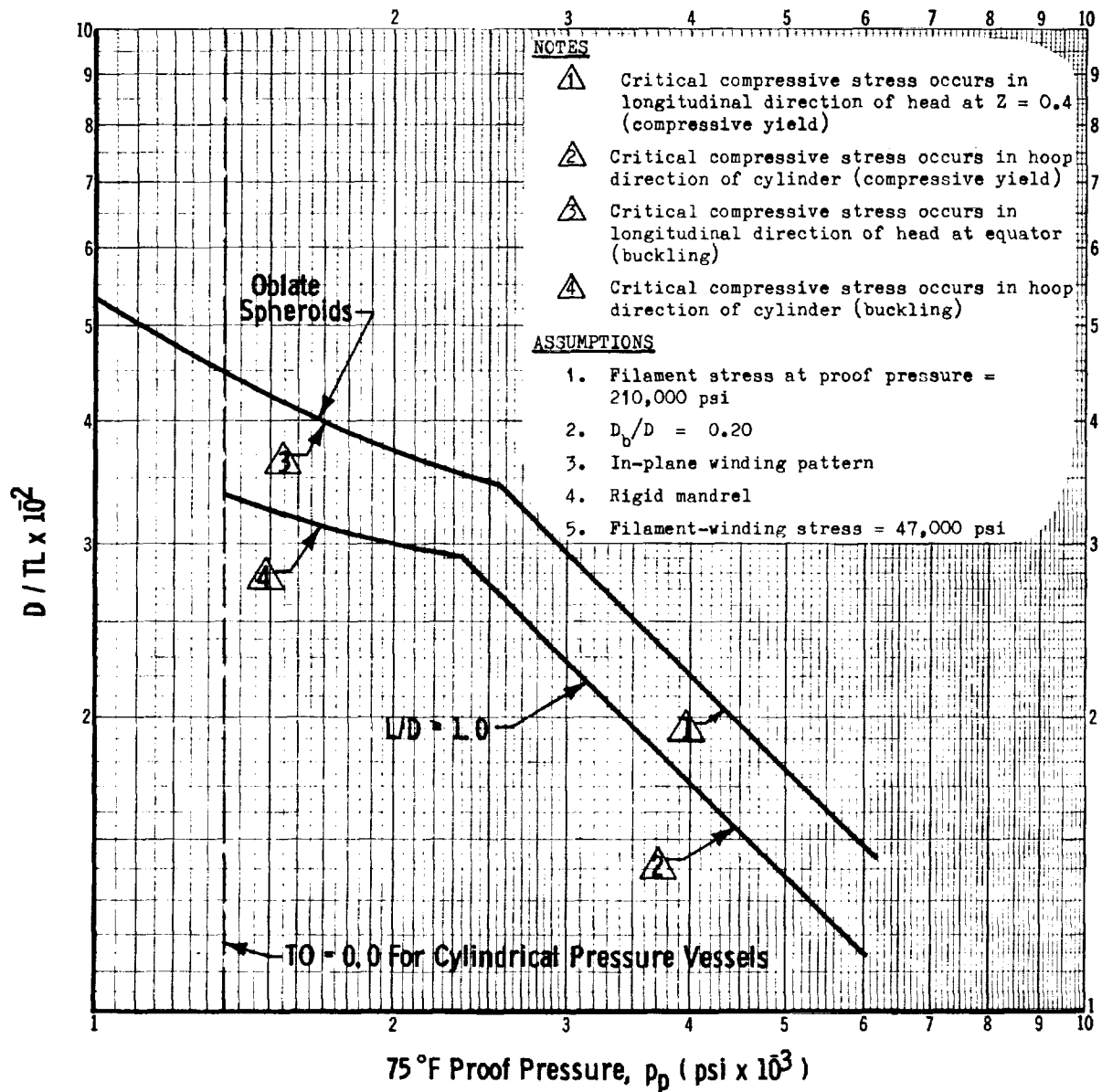


GFR 5 Al-2.5 Sn TITANIUM OBLATE SPHEROID PRESSURE VESSELS
DIAMETER-TO-LINER THICKNESS RATIO VS MAXIMUM METAL SHELL COMPRESSIVE STRESS
FOR VARIOUS PROOF PRESSURE LEVELS ($T_D = 75^\circ\text{F}$)

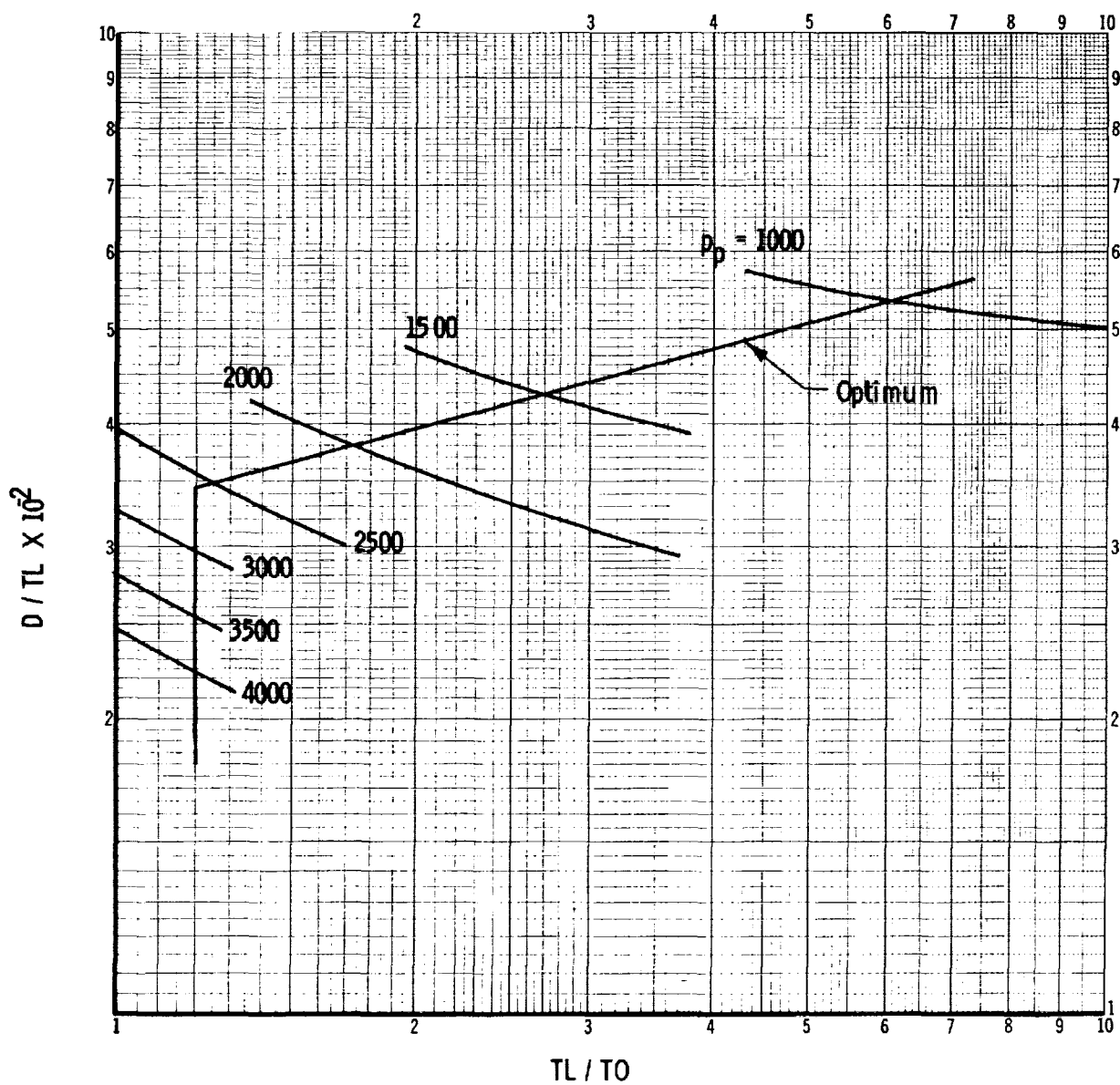
Figure 31



GFR 5 Al-2.5 Sn TITANIUM CYLINDRICAL PRESSURE VESSELS (L/D = 1)
DIAMETER-TO-LINER THICKNESS RATIO VS MAXIMUM METAL SHELL COMPRESSIVE
STRESS FOR VARIOUS PROOF PRESSURE LEVELS (TD = 75°F)

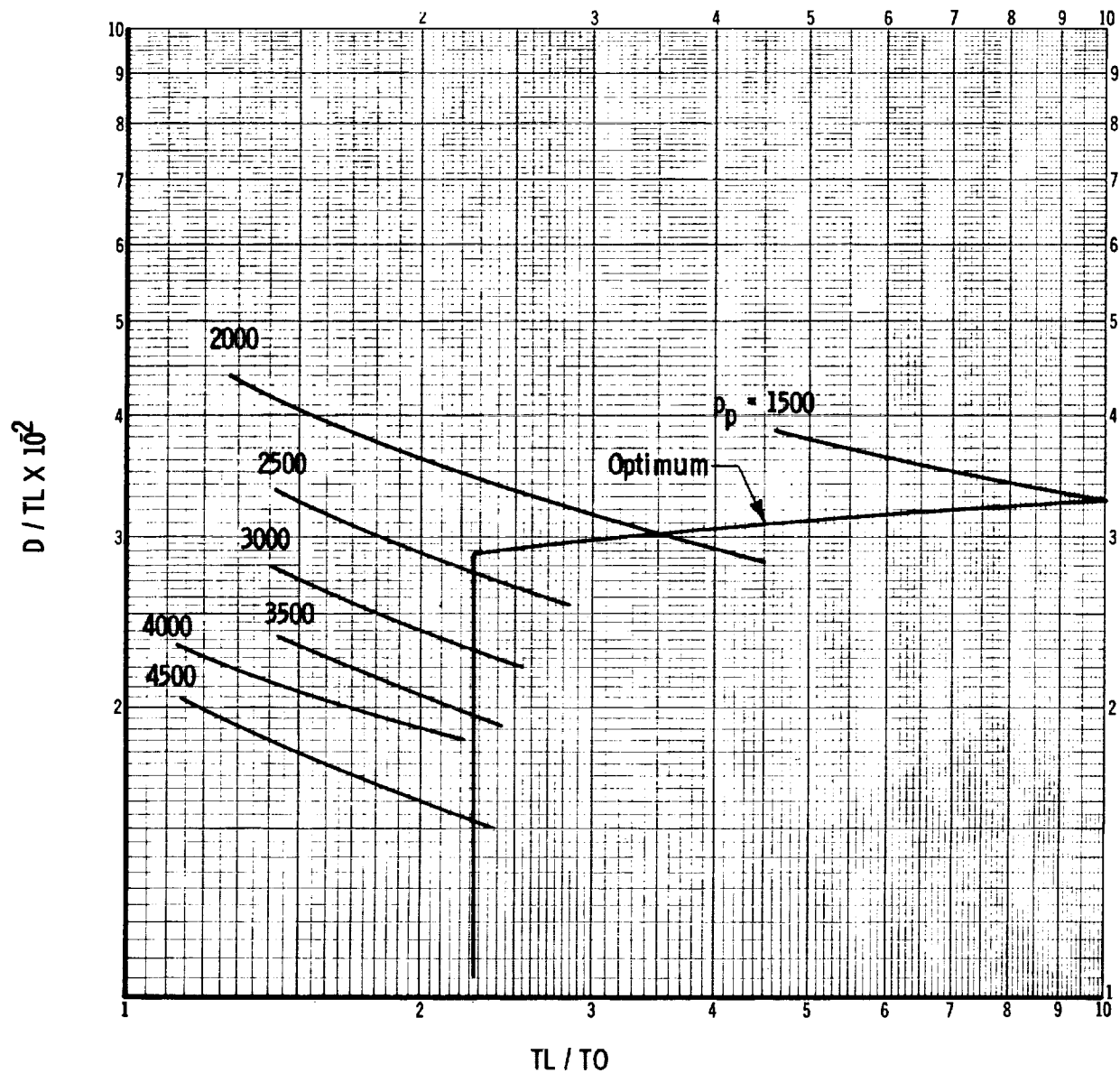


GFR TITANIUM (5 Al-2.5 Sn, ELI GRADE) PRESSURE VESSELS
OPTIMUM DIAMETER-TO-LINER THICKNESS RATIO ($T_D = 75^\circ\text{F}$)



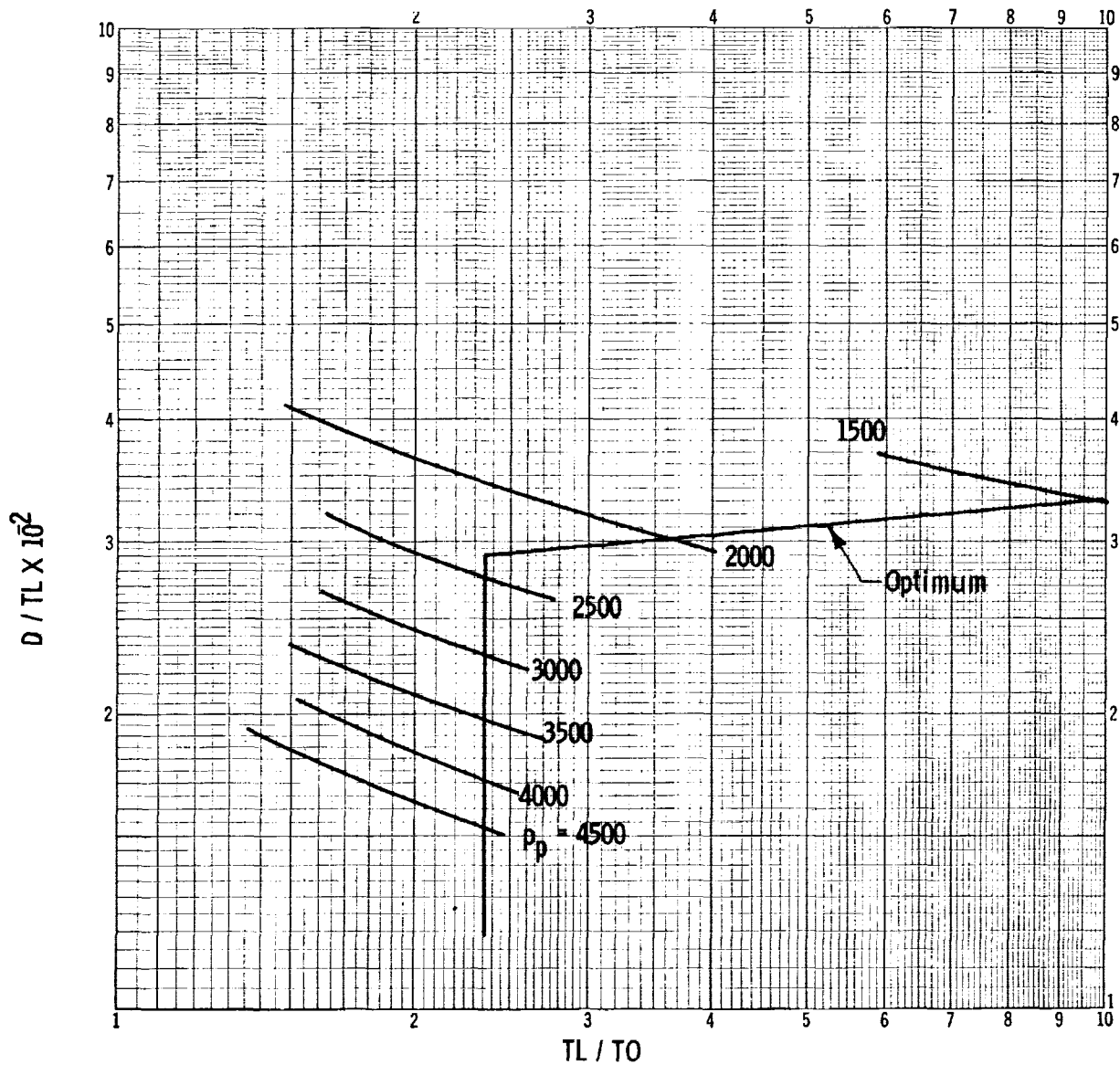
GFR 5 Al-2.5 Sn TITANIUM OBLATE SPHEROID PRESSURE VESSELS
 DIAMETER-TO-LINER THICKNESS RATIO VS LINER-TO-LONGITUDINAL
 COMPOSITE THICKNESS RATIO FOR VARIOUS PROOF PRESSURE LEVELS ($T_D = 75^\circ\text{F}$)

Figure 33



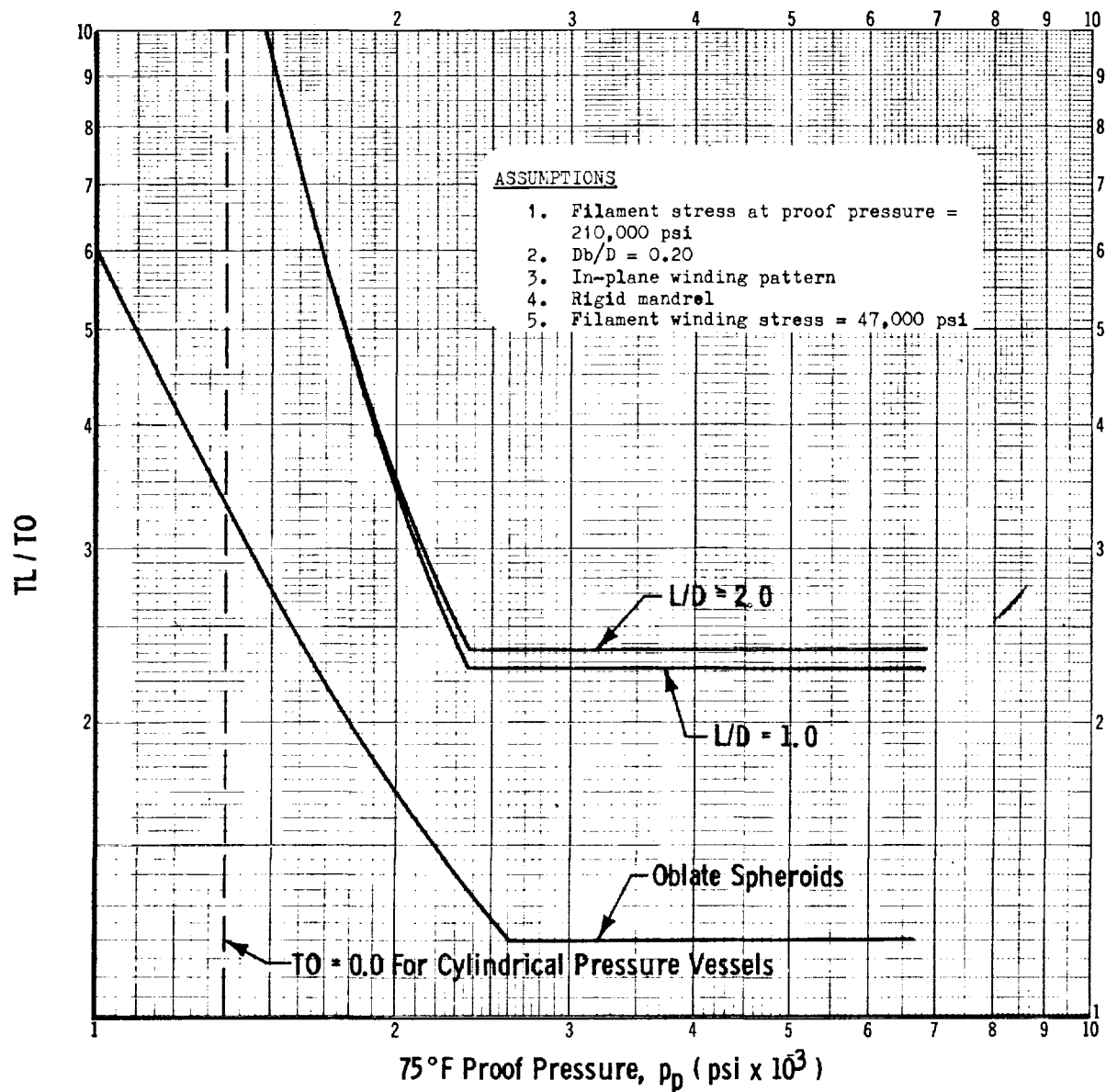
GFR 5 Al-2.5 Sn TITANIUM CYLINDRICAL PRESSURE VESSELS (L/D=1)
 DIAMETER-TO-LINER THICKNESS RATIO VS LINER-TO-LONGITUDINAL COMPOSITE
 THICKNESS RATIO FOR VARIOUS PROOF PRESSURE LEVELS (TD = 75°F)

Figure 34



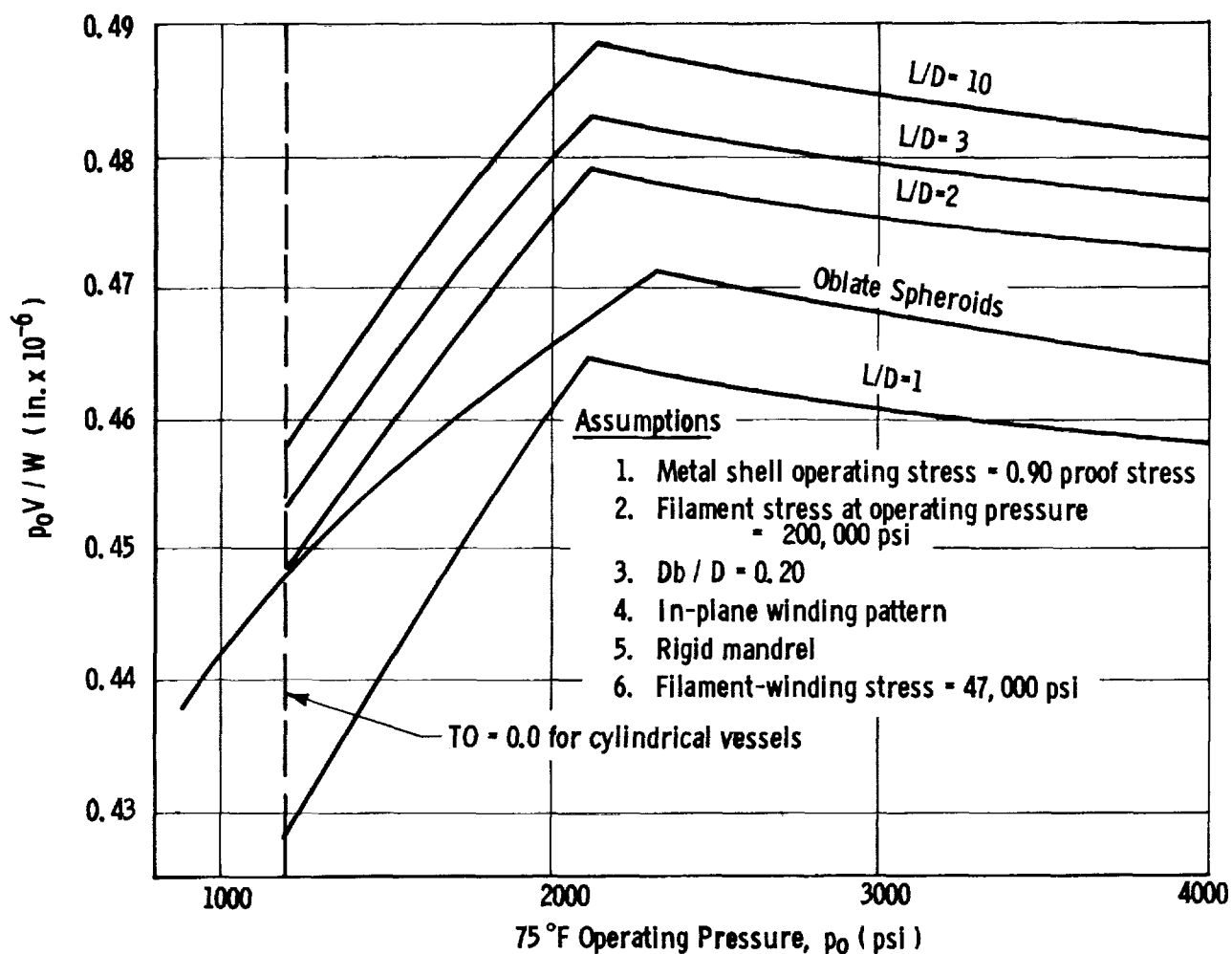
GFR 5 Al-2.5 Sn TITANIUM CYLINDRICAL PRESSURE VESSELS ($L/D \approx 2$)
 DIAMETER-TO-THICKNESS RATIO VS LINER-TO-LONGITUDINAL COMPOSITE THICKNESS
 RATIO FOR VARIOUS PROOF PRESSURE LEVELS ($T_D = 75^\circ F$)

Figure 35



GFR TITANIUM (5 Al-2.5 Sn, ELI GRADE) PRESSURE VESSELS
OPTIMUM LINER-TO-LONGITUDINAL COMPOSITE THICKNESS RATIO (TD = 75°F)

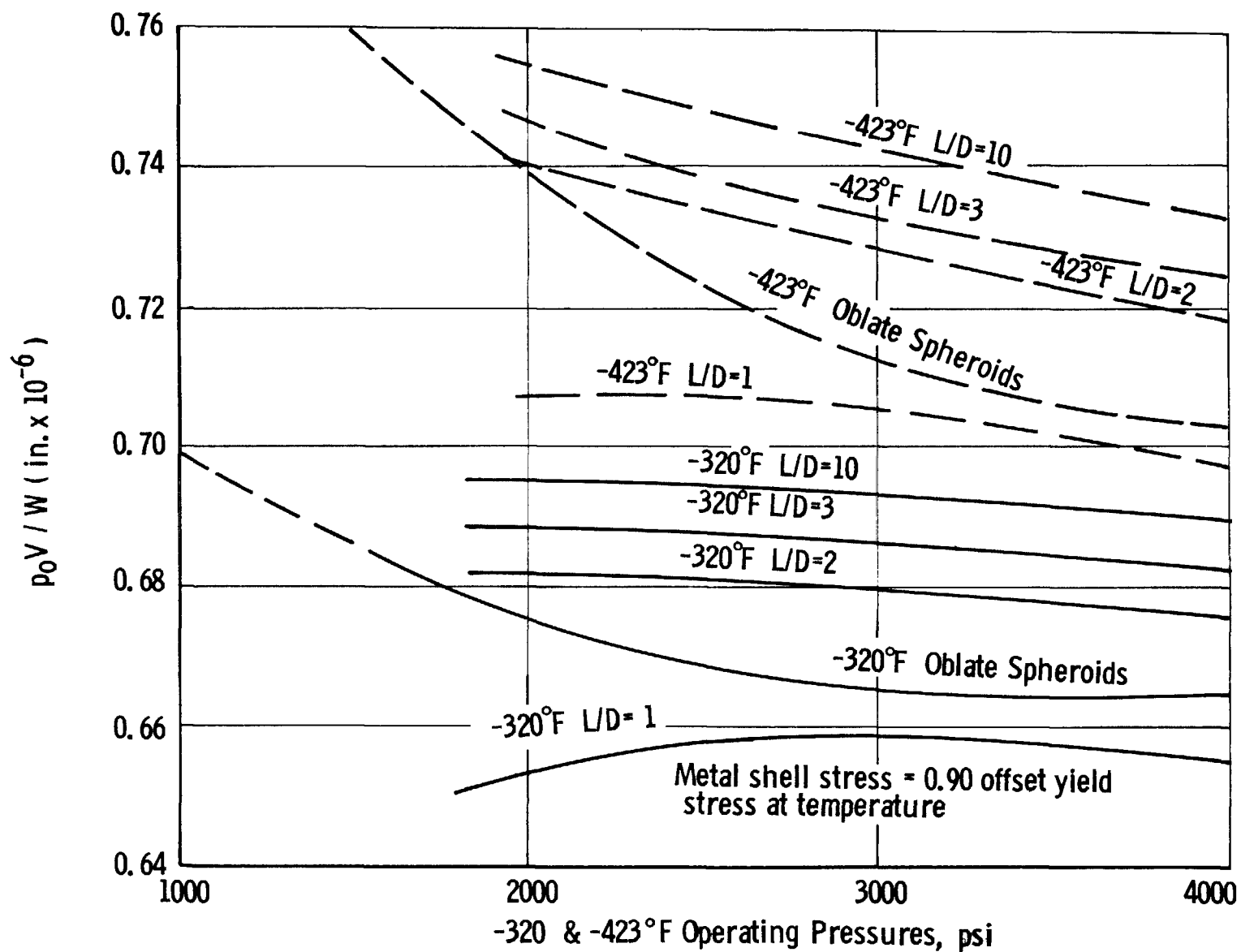
Figure 36



OPTIMUM EFFICIENCY
 GFR TITANIUM (5 Al-2.5 Sn, ELI GRADE) PRESSURE VESSELS ($T_D = 75^\circ\text{F}$)

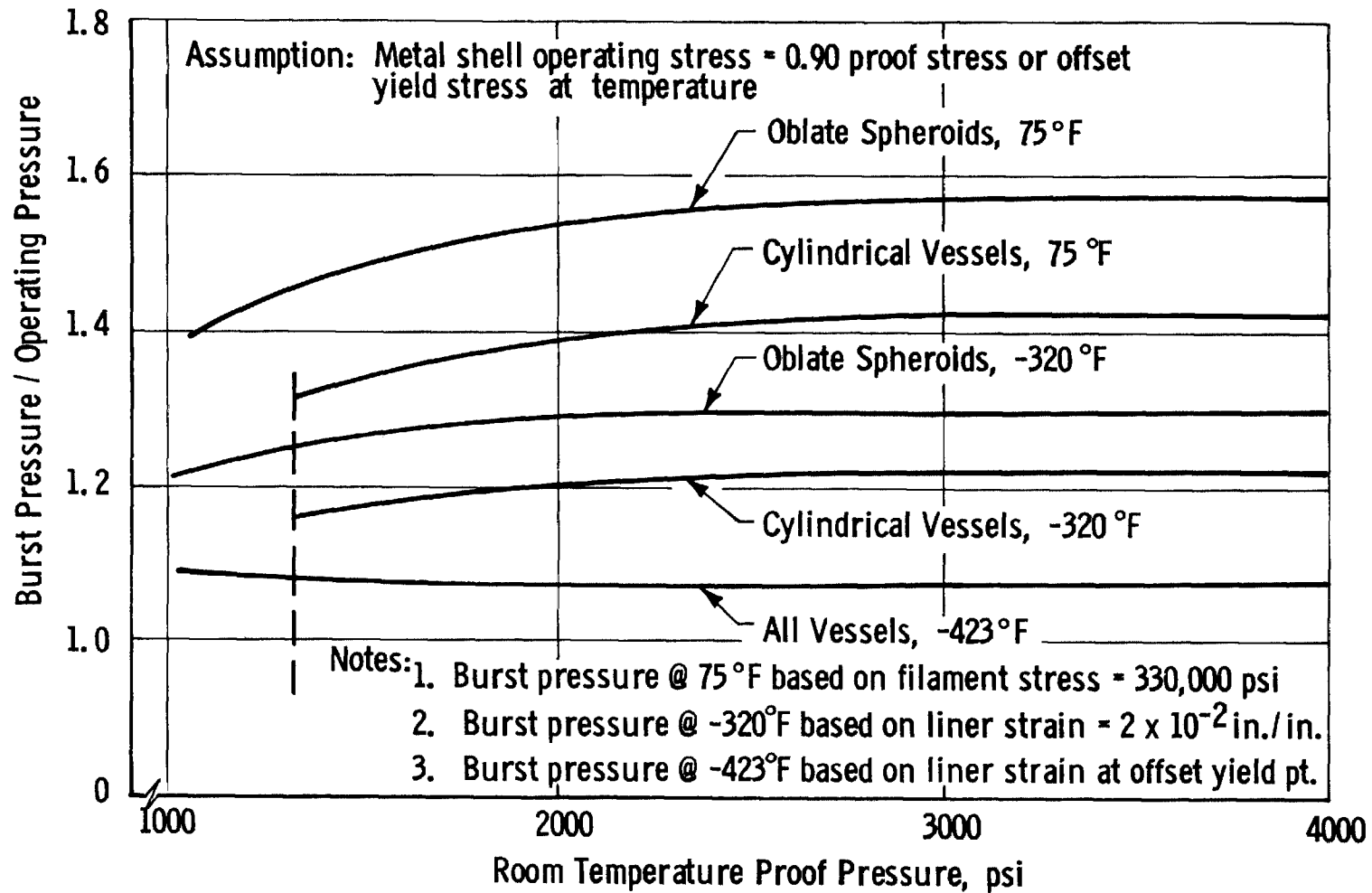
Figure 37

Figure 38

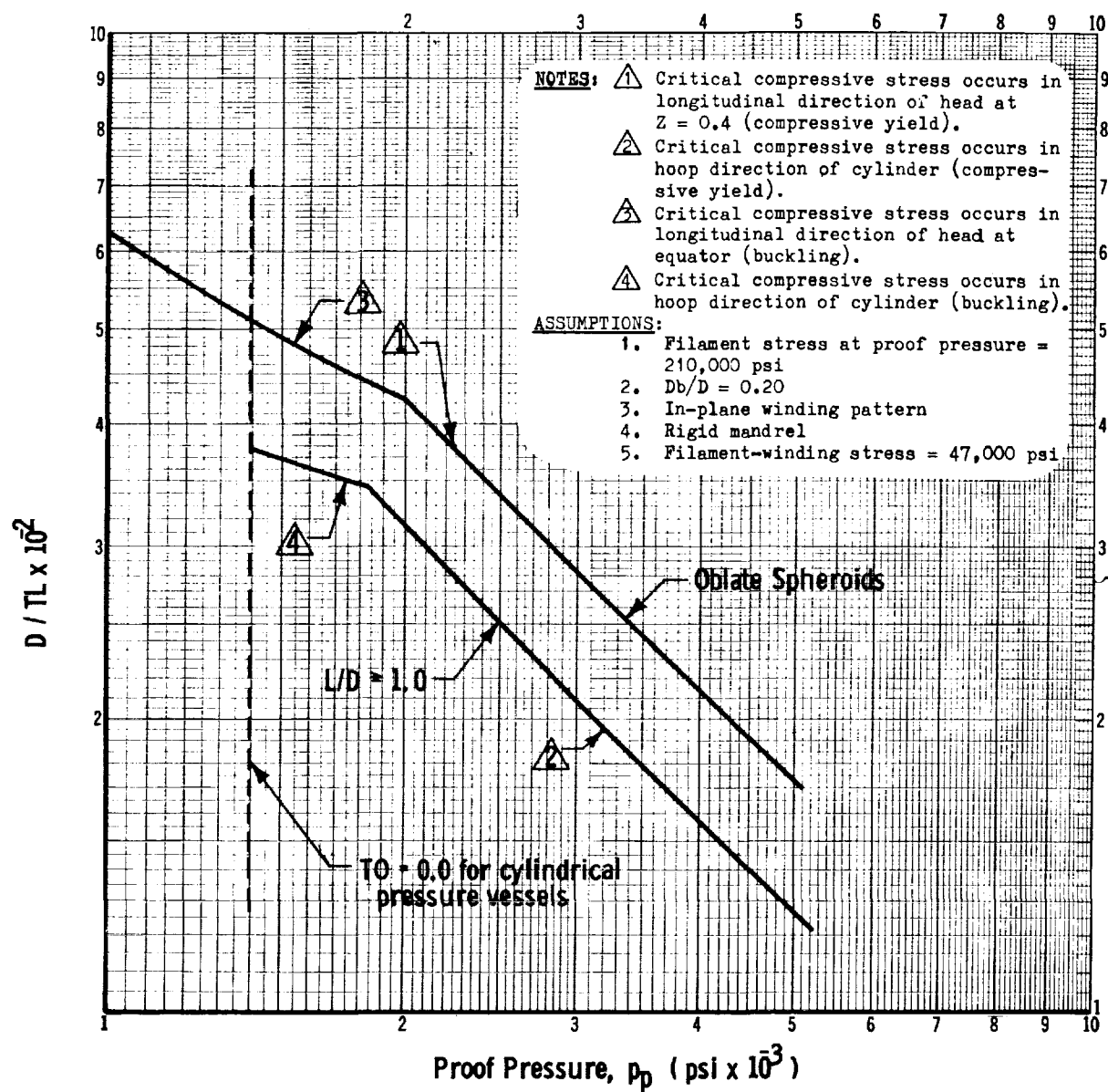


OPTIMUM EFFICIENCY
 GFR TITANIUM (5Al-2.5 Sn, ELI GRADE) PRESSURE VESSELS
 OPTIMUM ROOM TEMPERATURE DESIGNS OPERATED AT -320 AND -423 °F

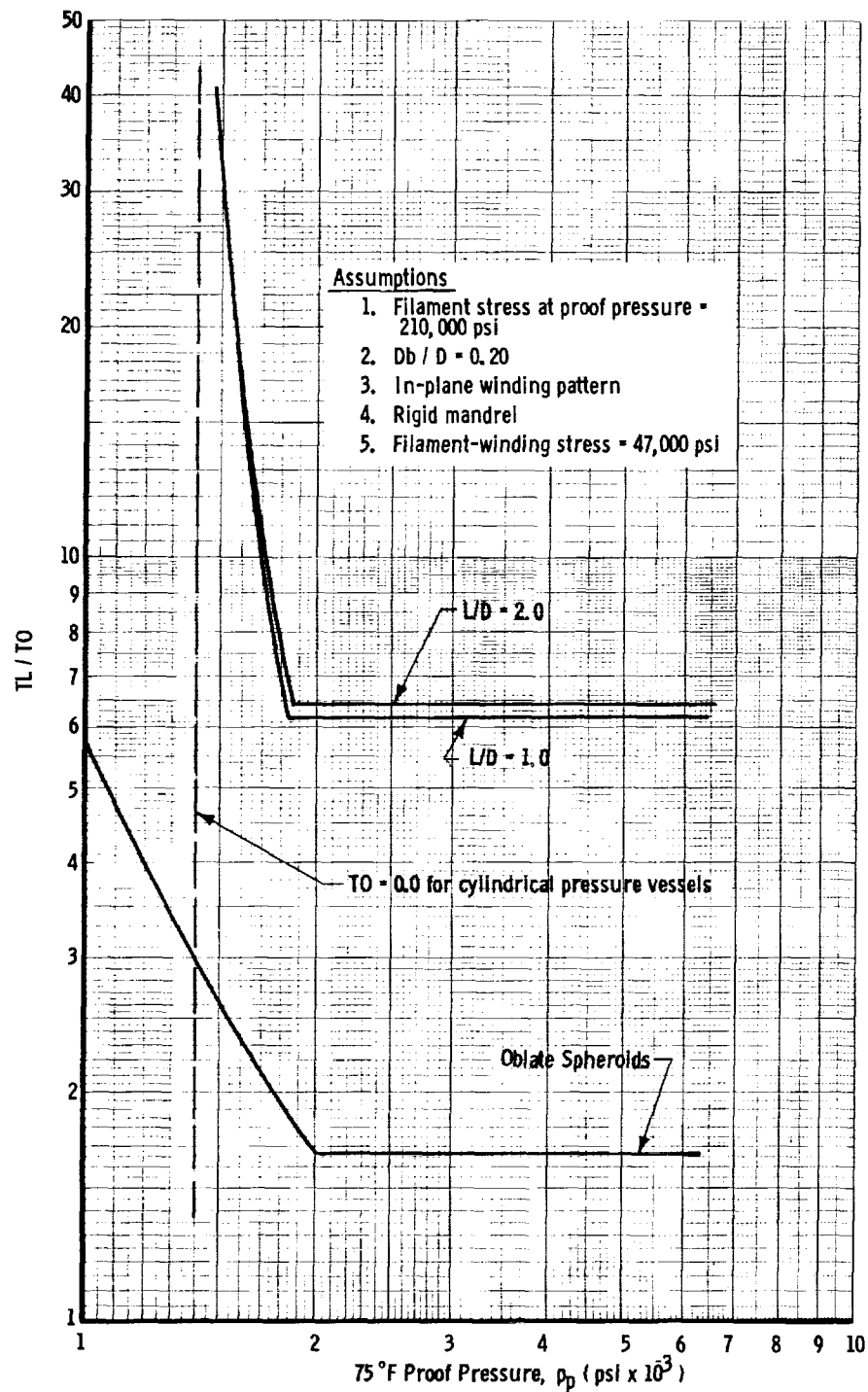
Figure 39



FACTORS OF SAFETY FOR GFR 5 Al-2.5 Sn TITANIUM (ANNEALED, ELI GRADE) PRESSURE VESSELS

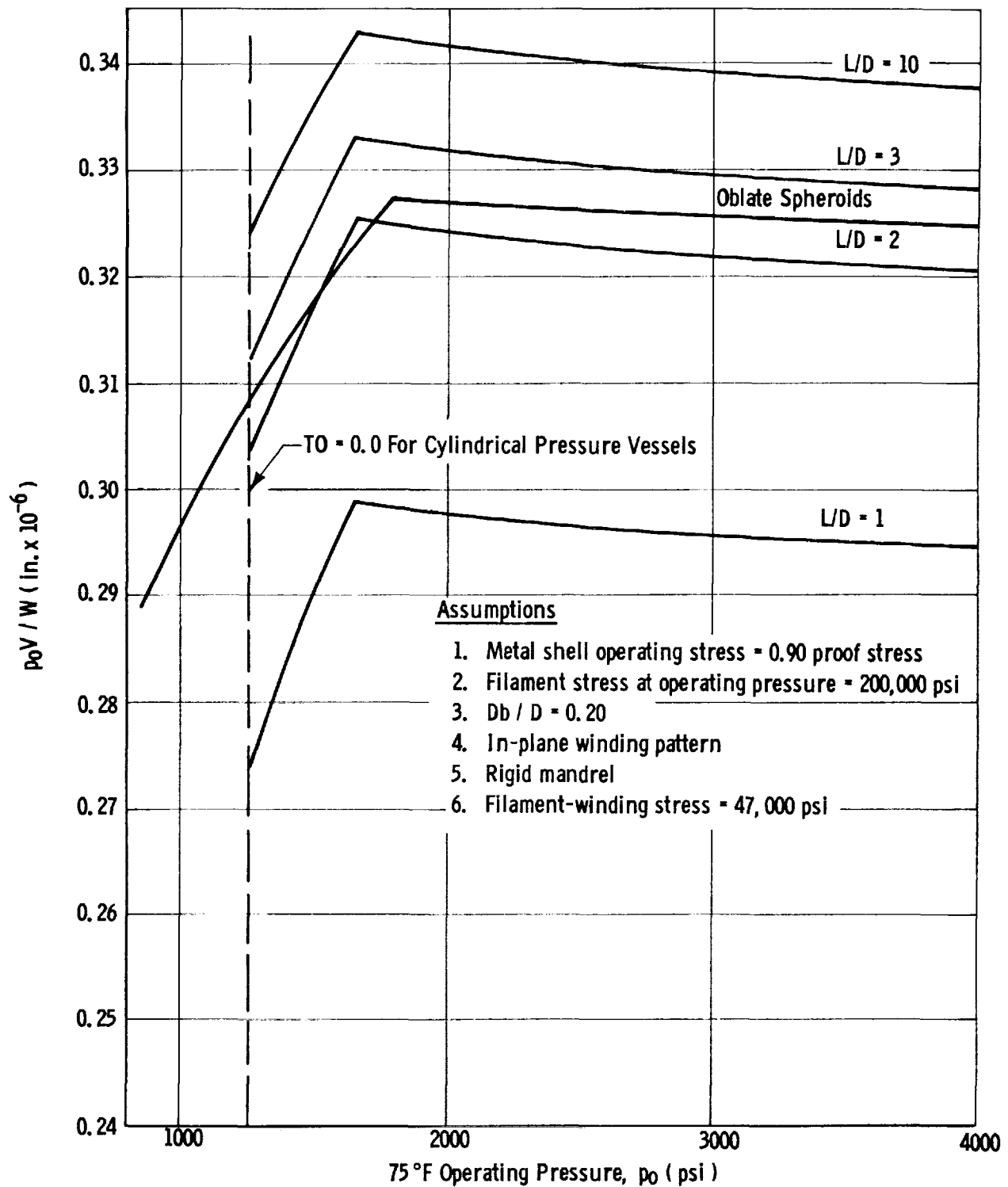


GFR INCONEL X-750 (STA) PRESSURE VESSELS
OPTIMUM DIAMETER-TO-LINER THICKNESS RATIO ($T_D = 75^\circ F$)



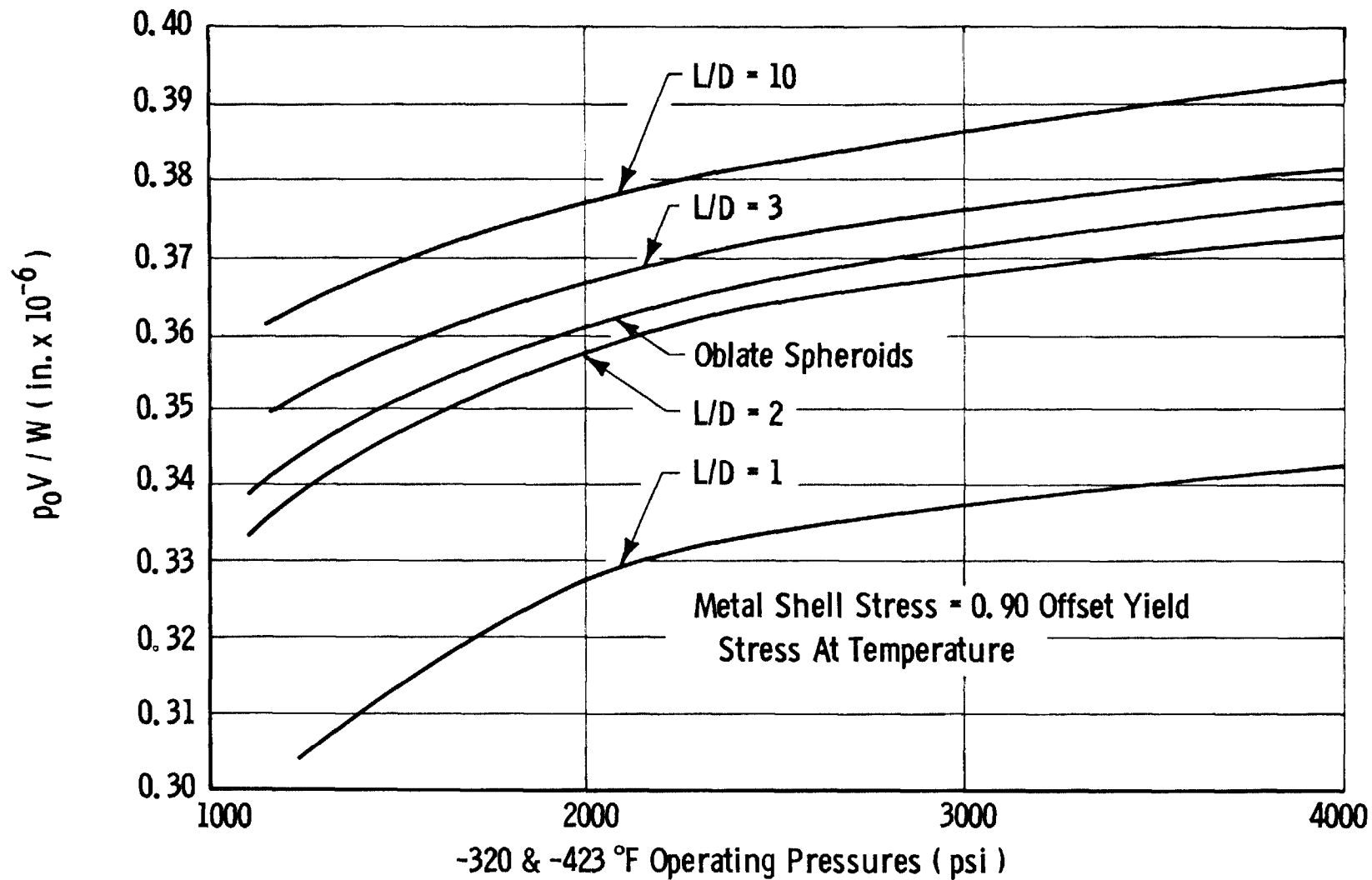
GFR INCONEL X-750 (STA) PRESSURE VESSELS—OPTIMUM
LINER-TO-LONGITUDINAL COMPOSITE THICKNESS RATIO (TD = 75 °F)

Figure 41

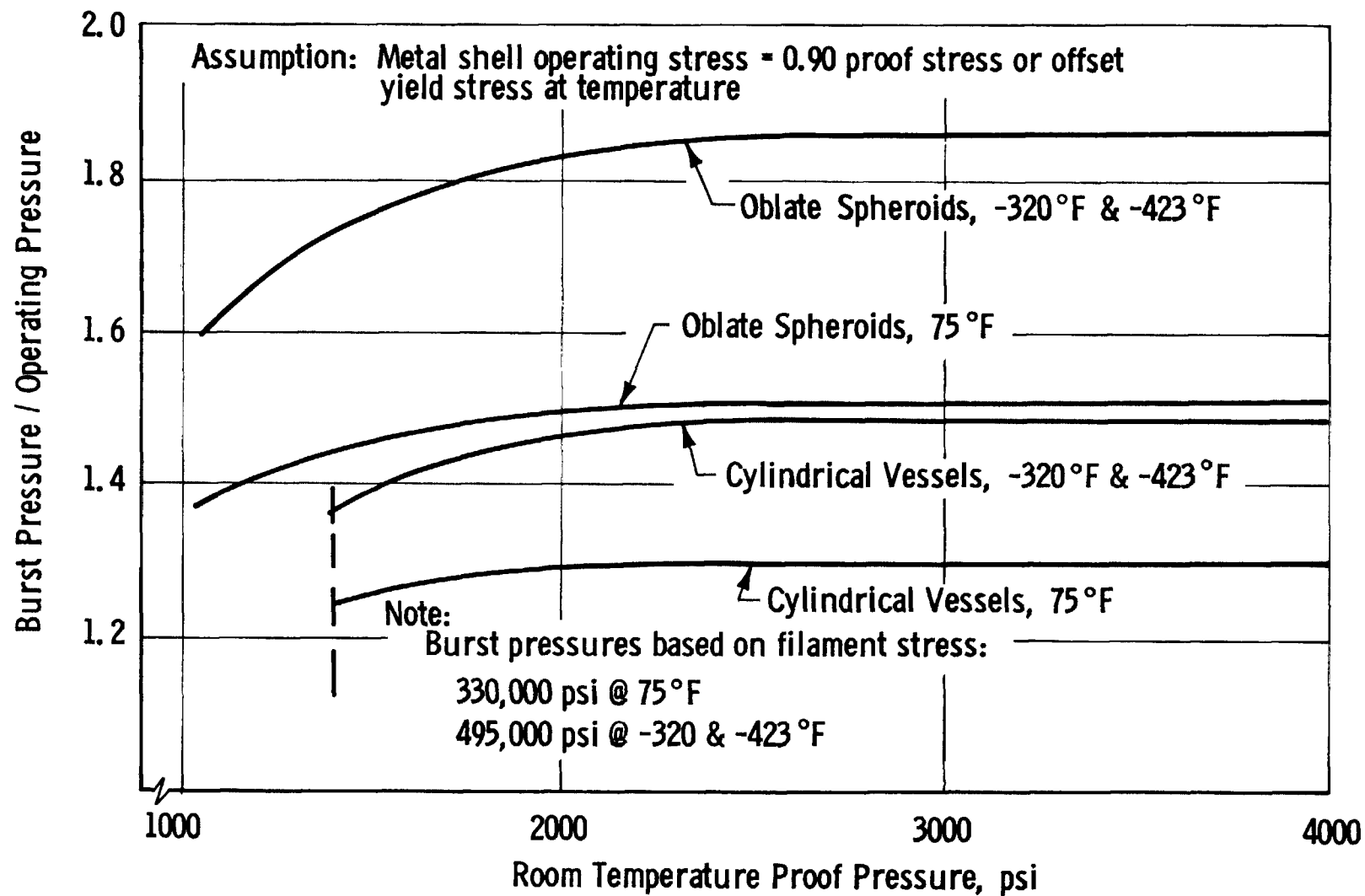


OPTIMUM EFFICIENCY
GFR INCONEL X-750 (STA) PRESSURE VESSELS (TD = 75°F)

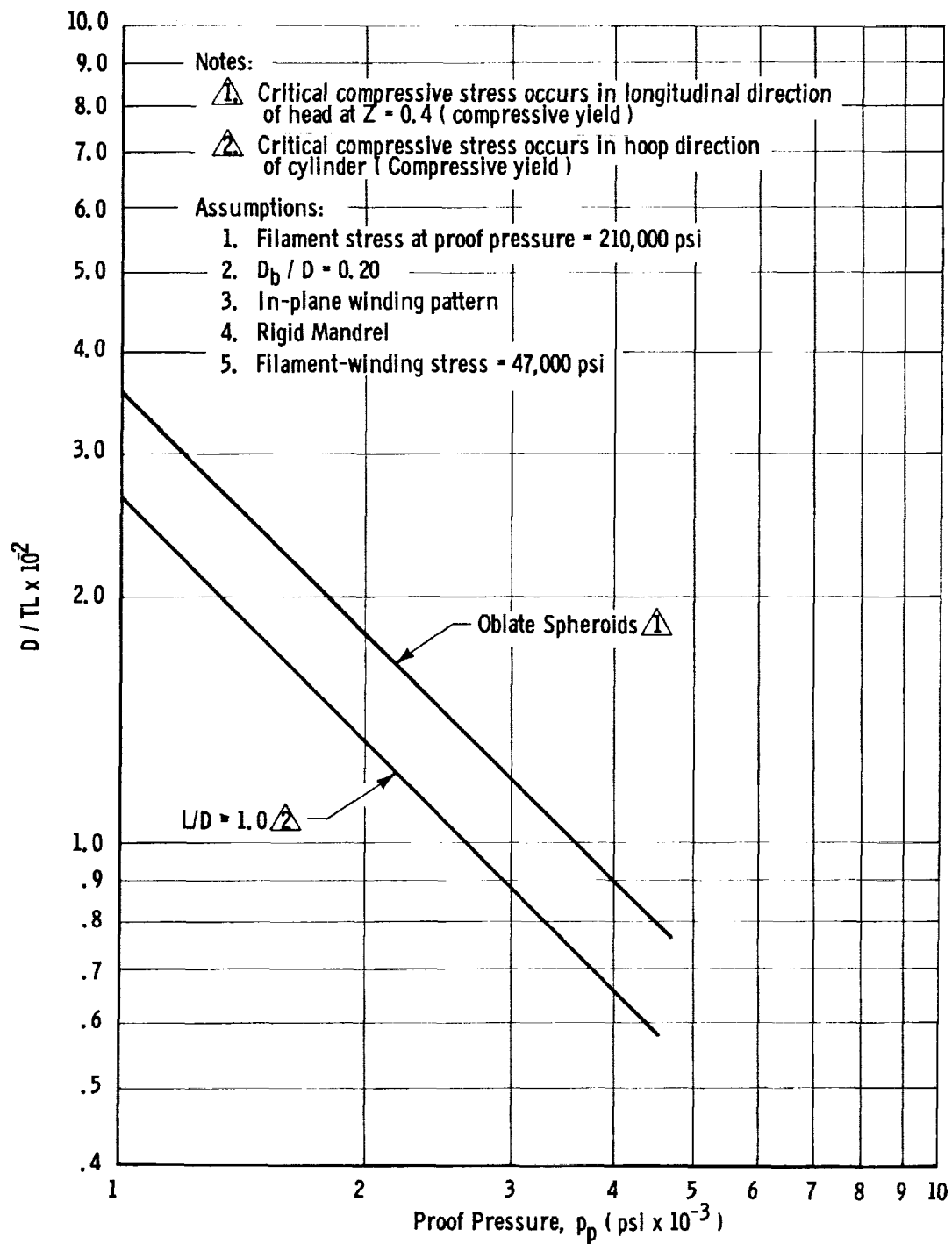
Figure 43



OPTIMUM EFFICIENCY
GFR INCONEL X-750 (STA) PRESSURE VESSELS—OPTIMUM ROOM TEMPERATURE
DESIGNS OPERATED AT -320 AND -423 °F

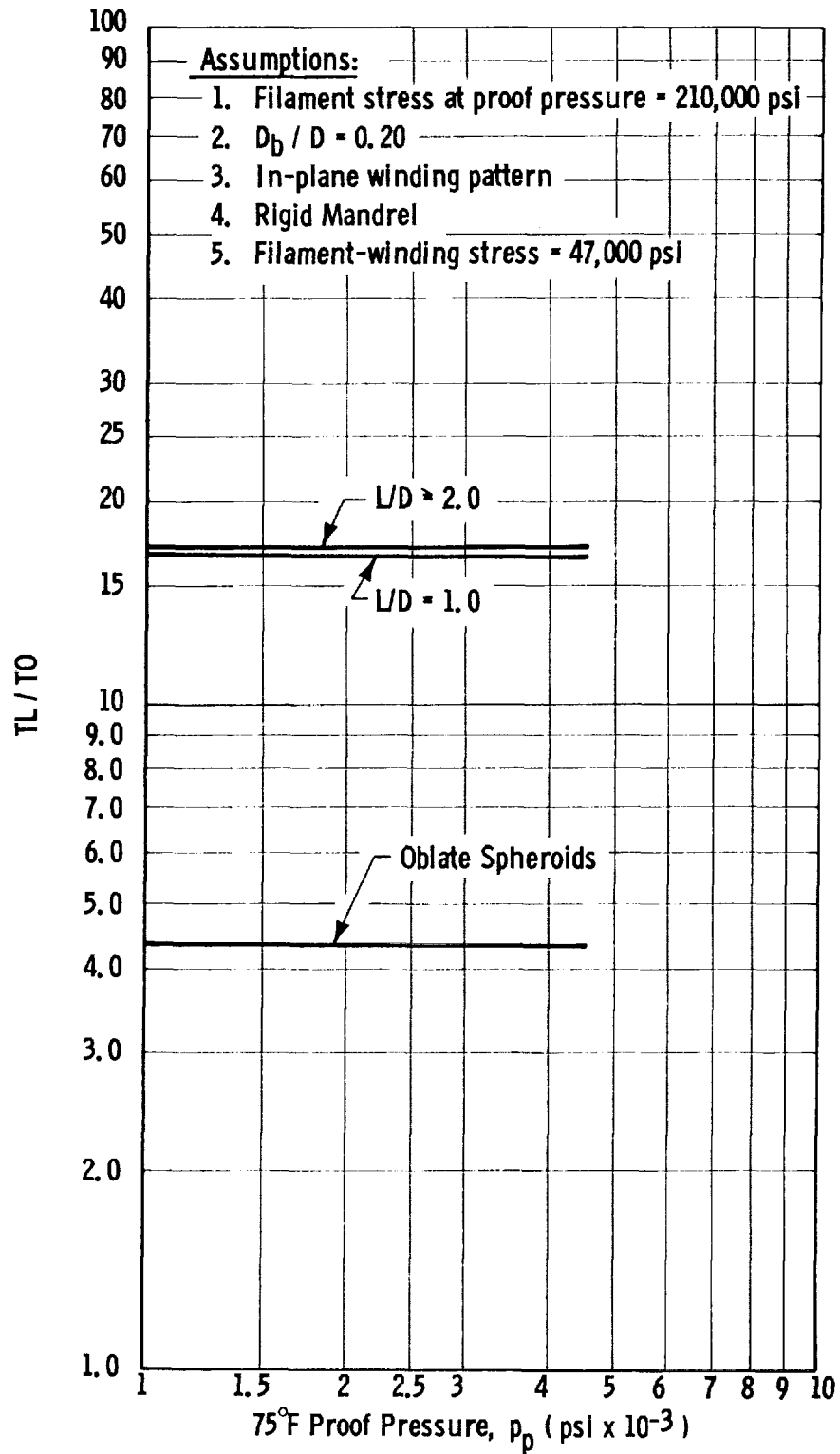


FACTORS OF SAFETY FOR GFR INCONEL X-750 (STA) PRESSURE VESSELS



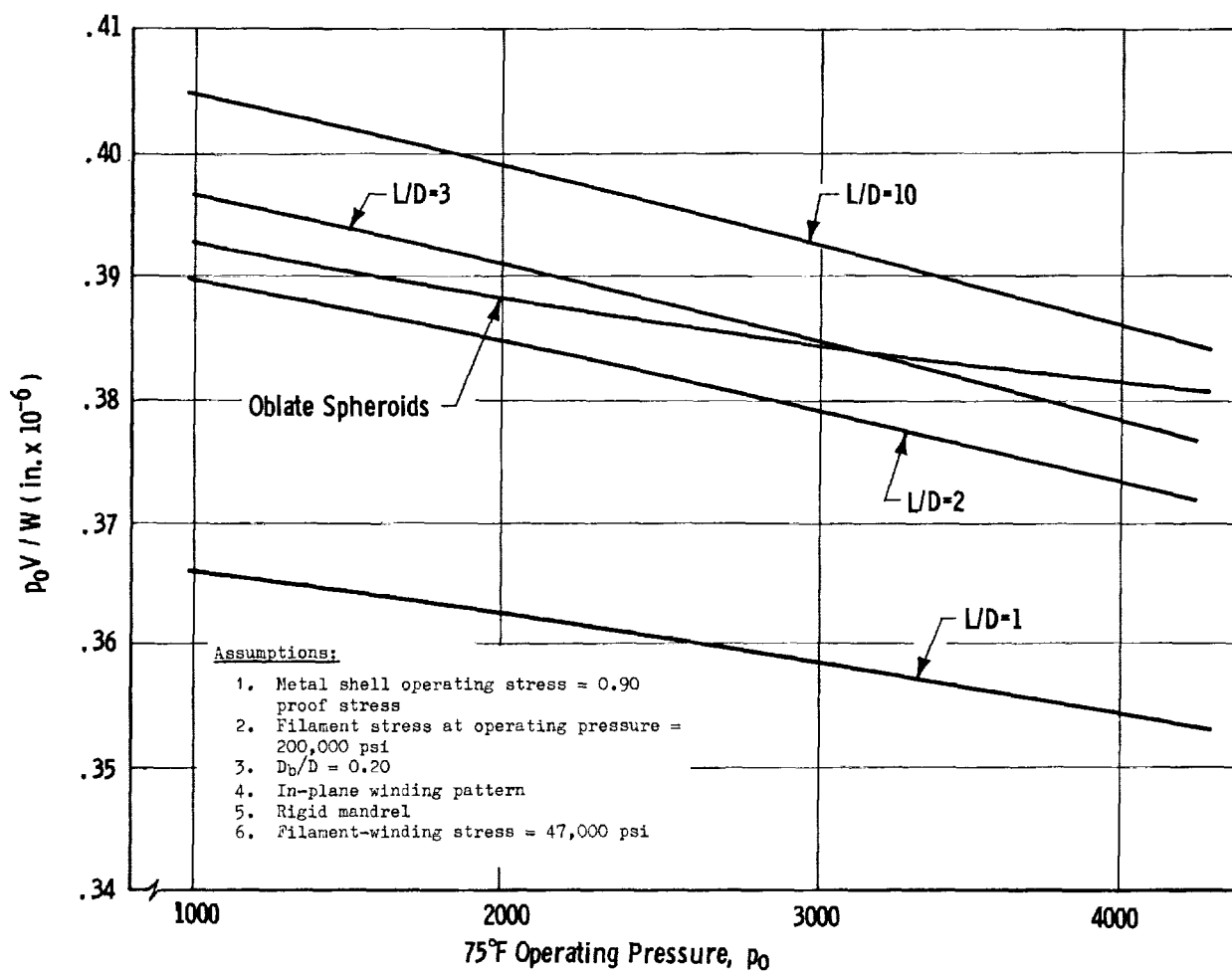
GFR 2219-T62 ALUMINUM PRESSURE VESSELS
OPTIMUM DIAMETER-TO-LINER THICKNESS RATIO ($T_D = 75^\circ\text{F}$)

Figure 45



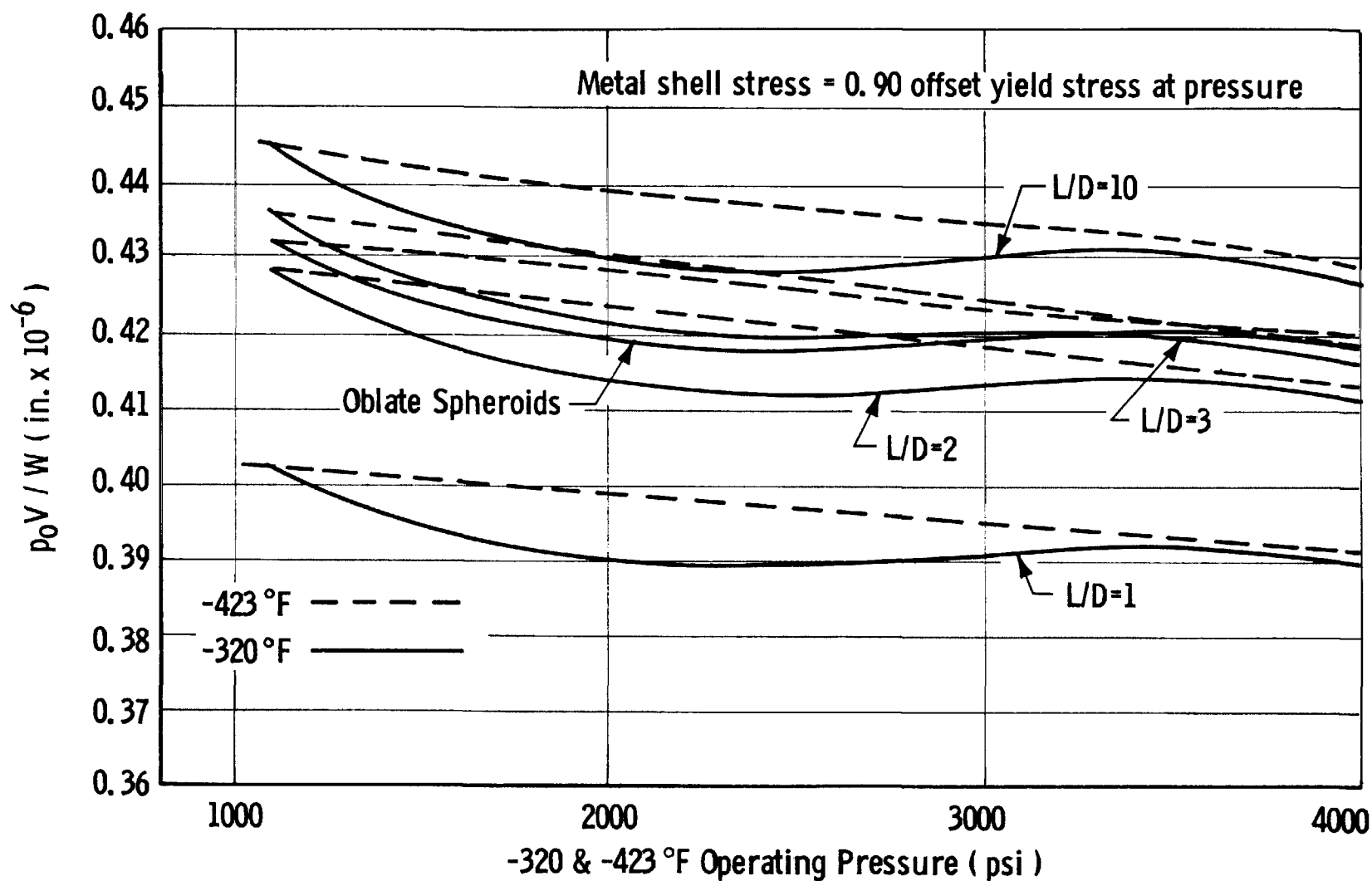
GFR 2219-T62 ALUMINUM PRESSURE VESSELS—OPTIMUM
LINER-TO-LONGITUDINAL COMPOSITE THICKNESS RATIO ($T_D = 75^\circ\text{F}$)

Figure 46



OPTIMUM EFFICIENCY
GFR 2219-T62 ALUMINUM PRESSURE VESSELS ($T_D = 75^\circ\text{F}$)

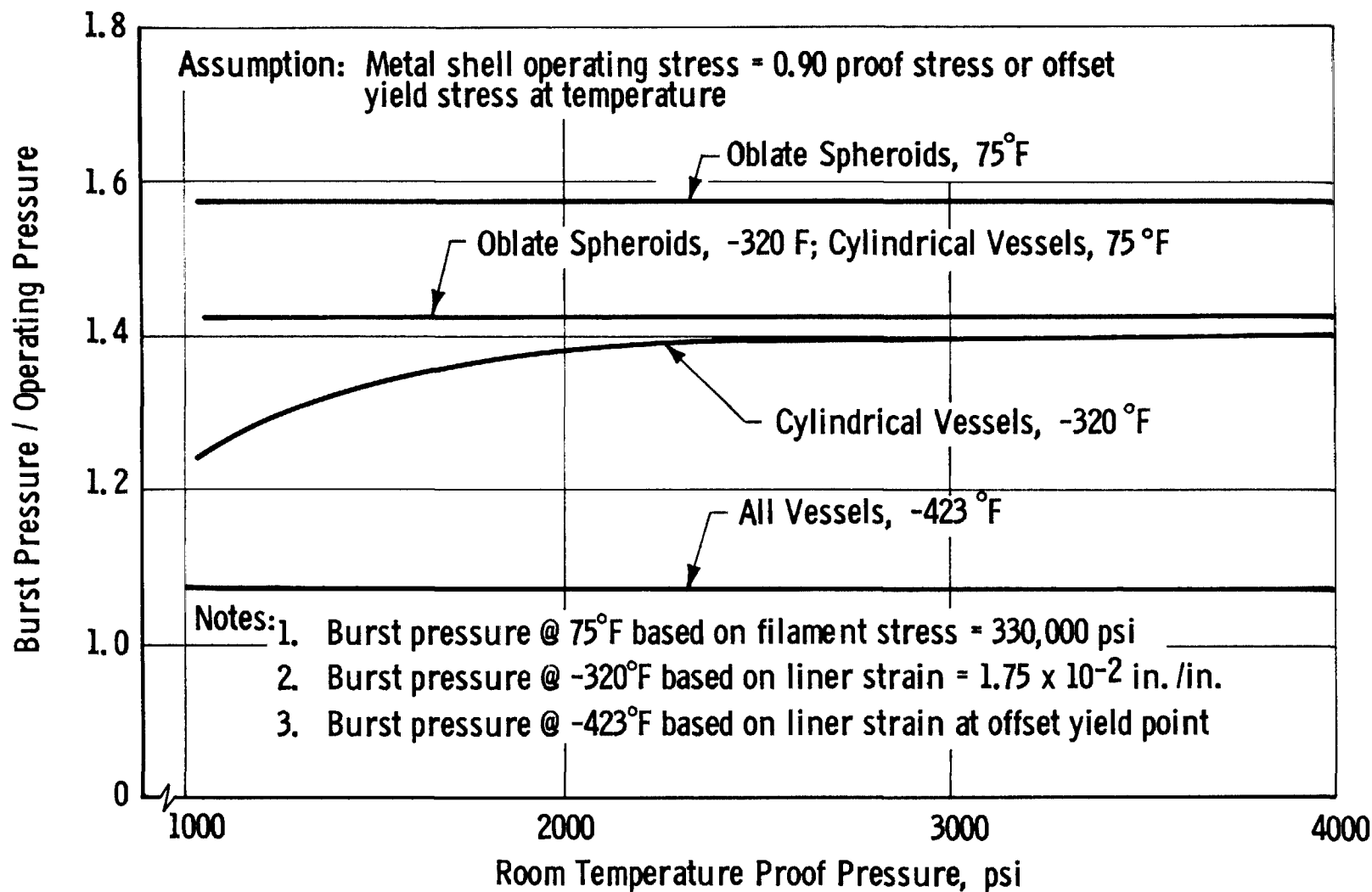
Figure 47



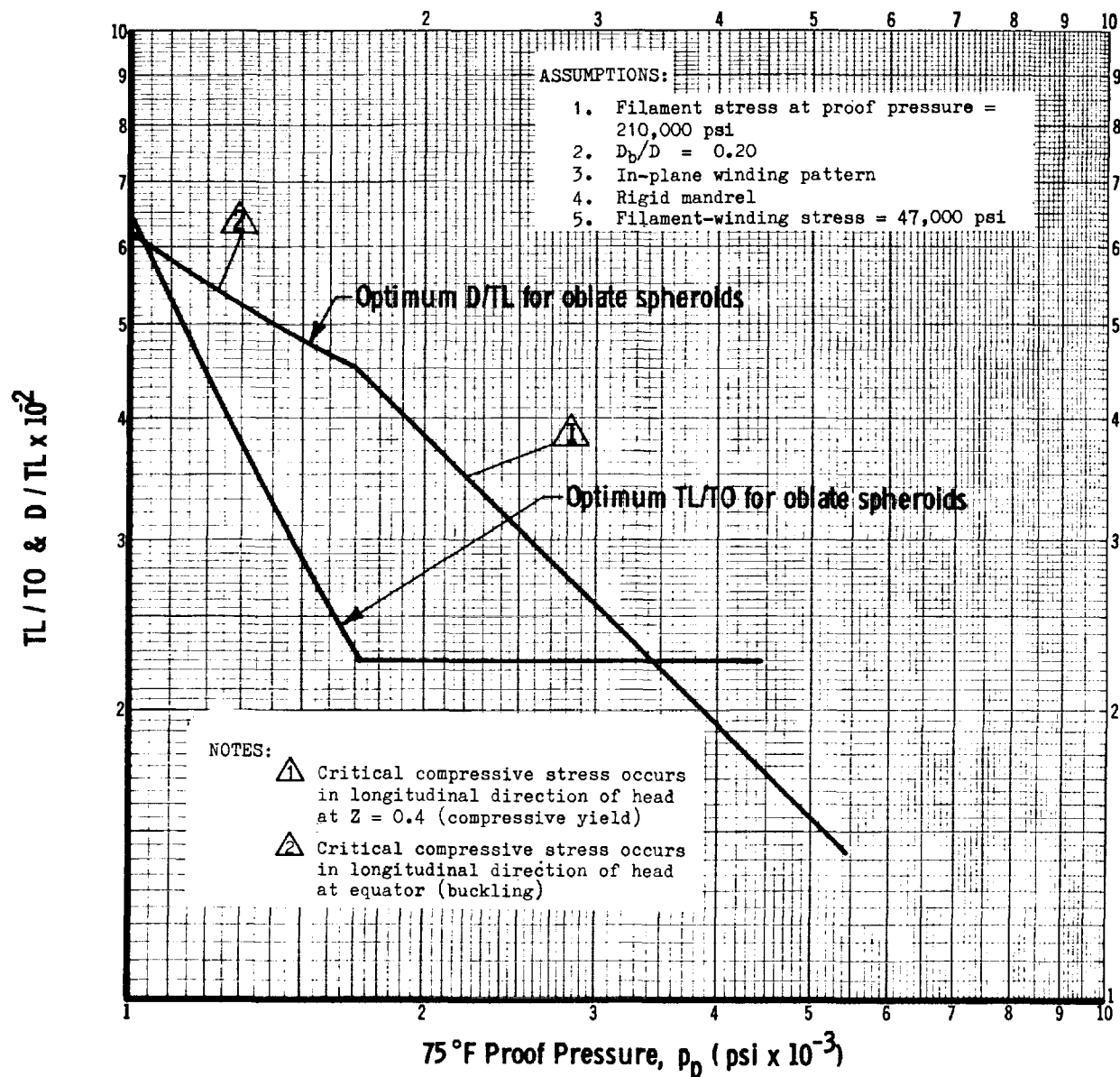
OPTIMUM EFFICIENCY

GFR 2219-T62 ALUMINUM PRESSURE VESSEL—OPTIMUM ROOM
TEMPERATURE DESIGNS OPERATED AT -320 AND -423 °F

Figure 49



FACTORS OF SAFETY FOR GFR 2219-T62 ALUMINUM PRESSURE VESSELS



GFR 301 STAINLESS STEEL (1/2 HARD) PRESSURE VESSELS—OPTIMUM DIAMETER-TO-LINER THICKNESS RATIO AND OPTIMUM LINER-TO-LONGITUDINAL COMPOSITE THICKNESS RATIO (TD = 75°F)

Figure 51

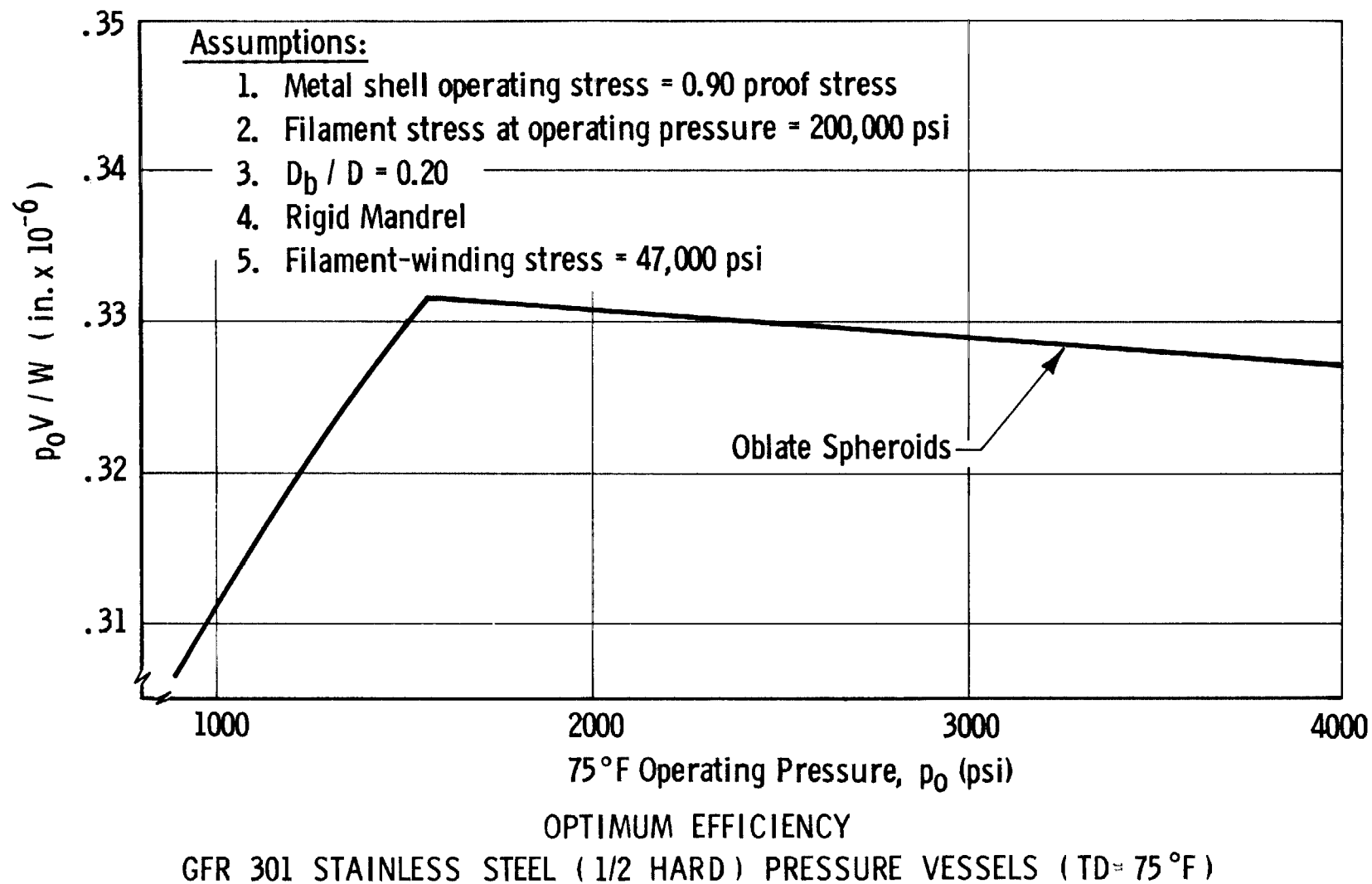
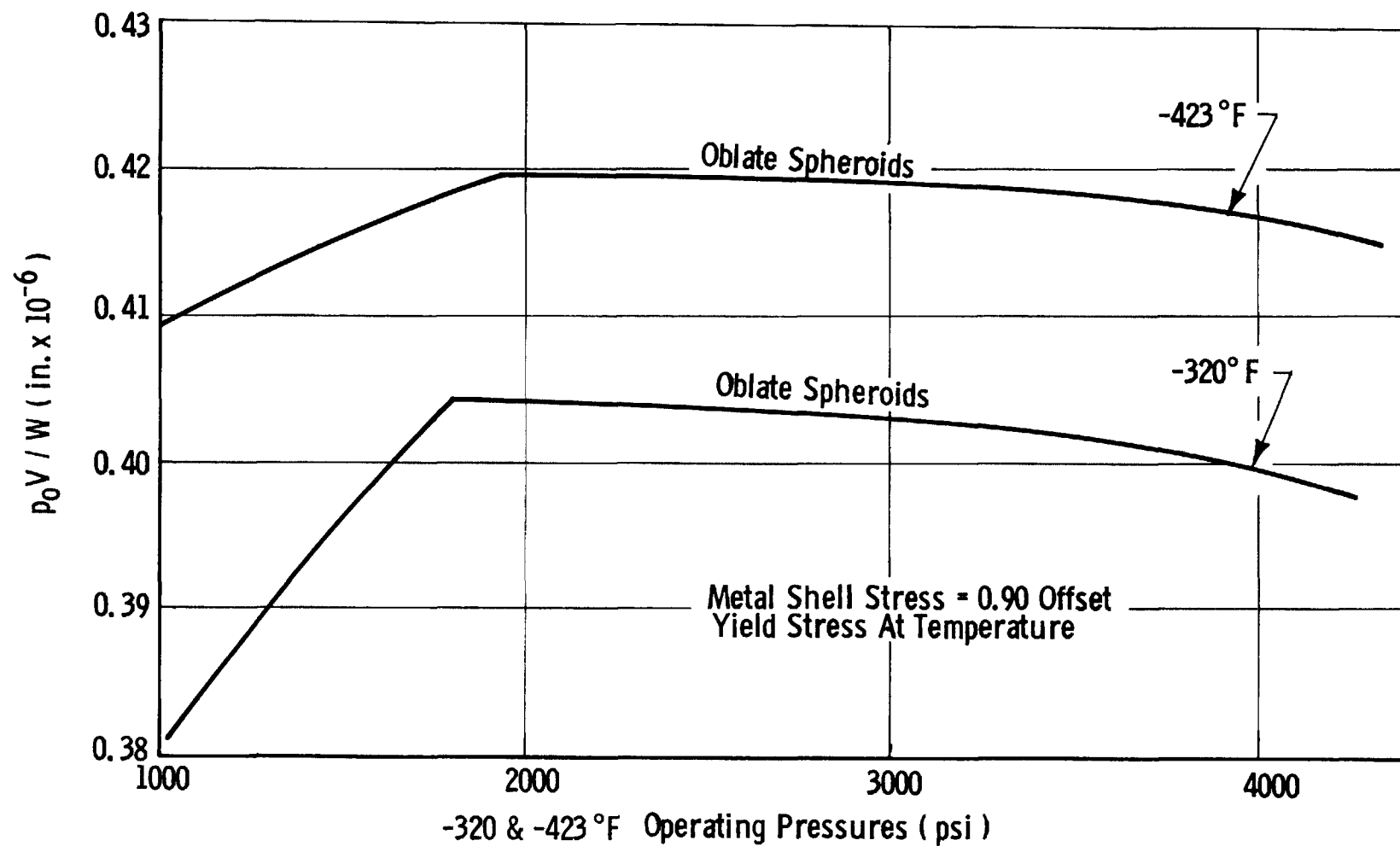
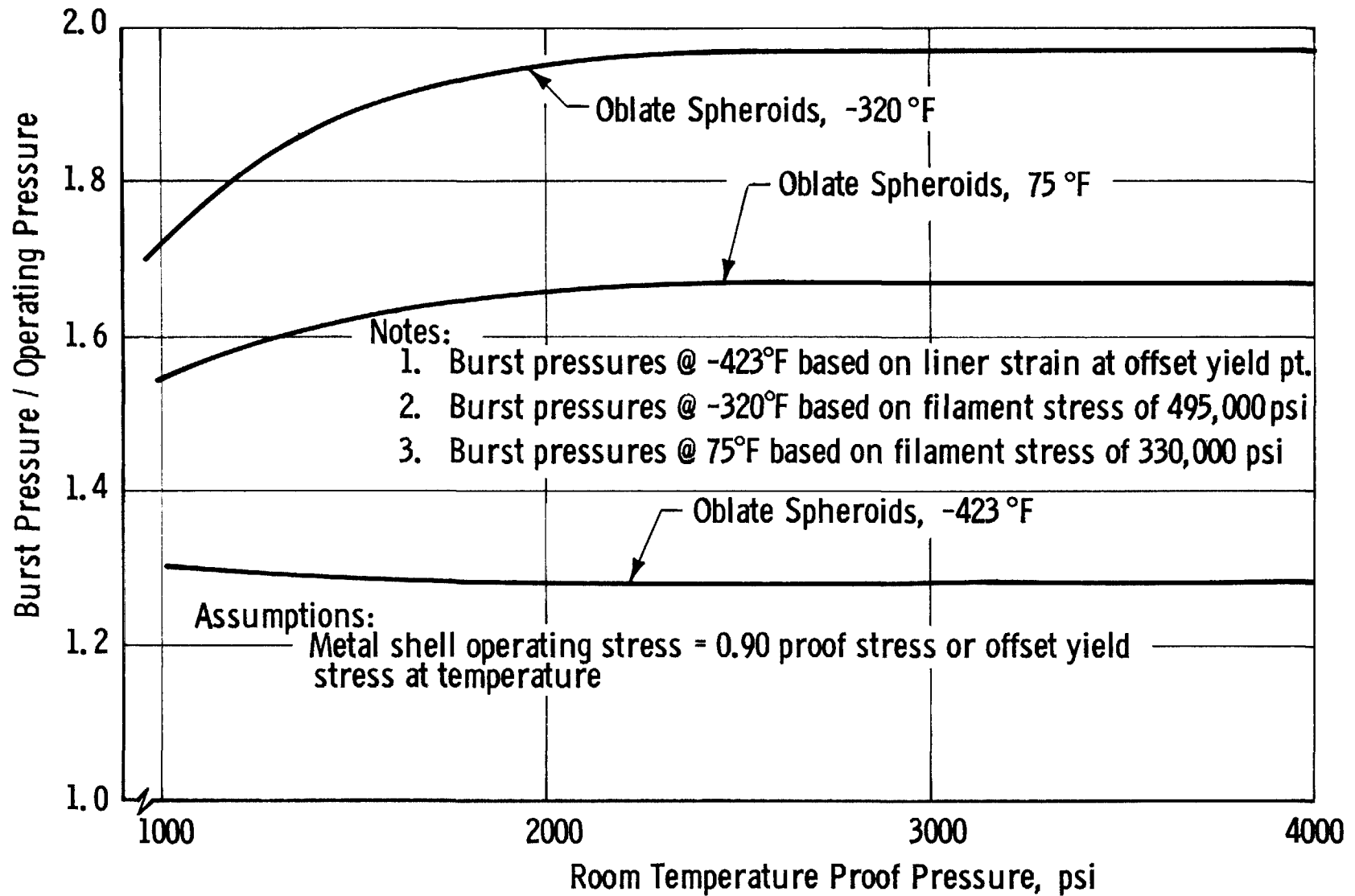


Figure 52



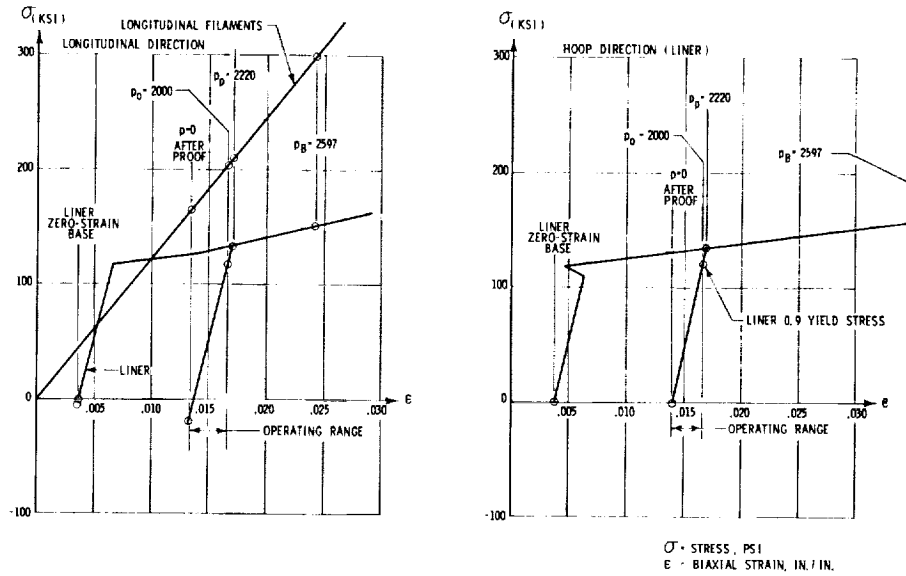
OPTIMUM EFFICIENCY
 GFR STAINLESS STEEL (1/2 HARD) PRESSURE VESSELS
 OPTIMUM ROOM TEMPERATURE DESIGNS OPERATED AT -320 AND -423°F

Figure 53

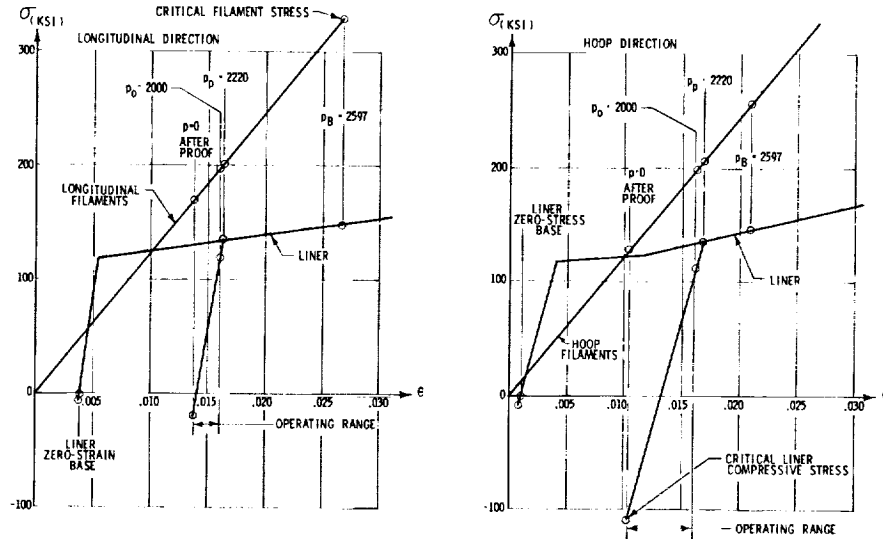


FACTORS OF SAFETY FOR GFR 301 STAINLESS STEEL (1/2 HARD) PRESSURE VESSELS

EQUATOR OF HEADS (Z=1.0)

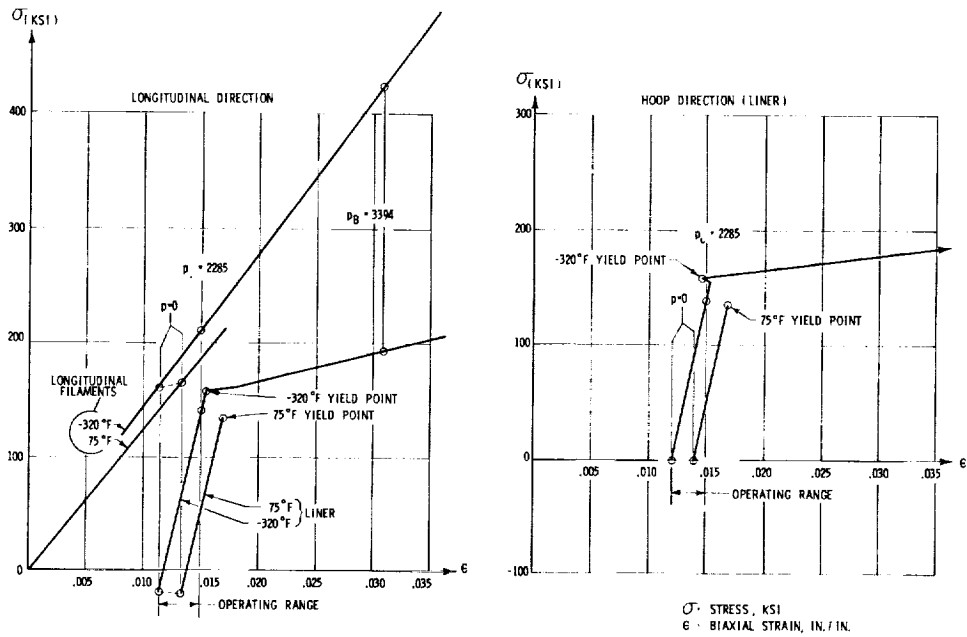


CYLINDRICAL SECTION

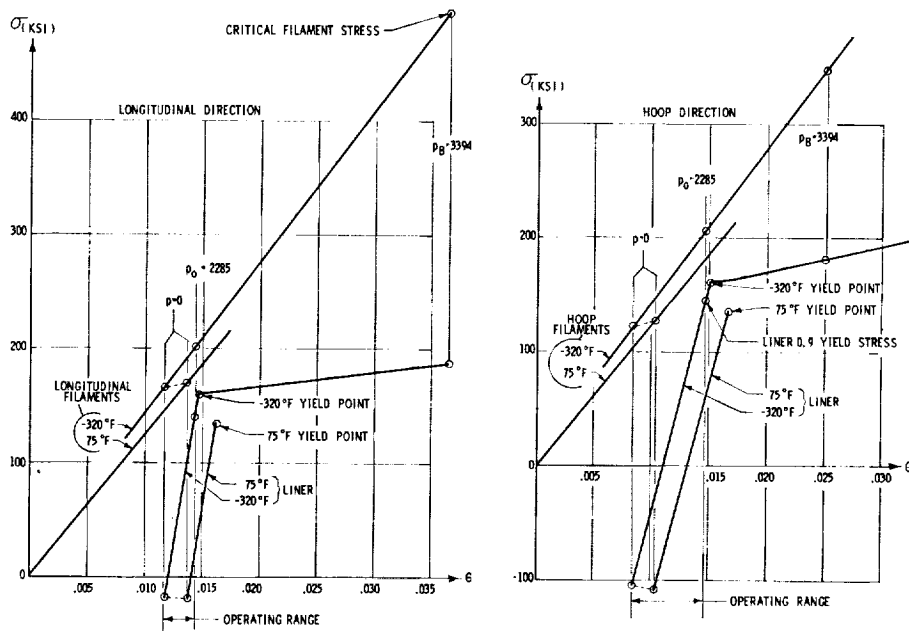


ROOM TEMPERATURE STRESS-STRAIN RELATIONSHIP OF OPTIMUM GFR INCONEL X-750 (STA) PRESSURE VESSEL WITH 2220 PROOF PRESSURE AND 2000 PSI OPERATING PRESSURE (L/D=1.0)

EQUATOR OF HEADS (Z=1.0)

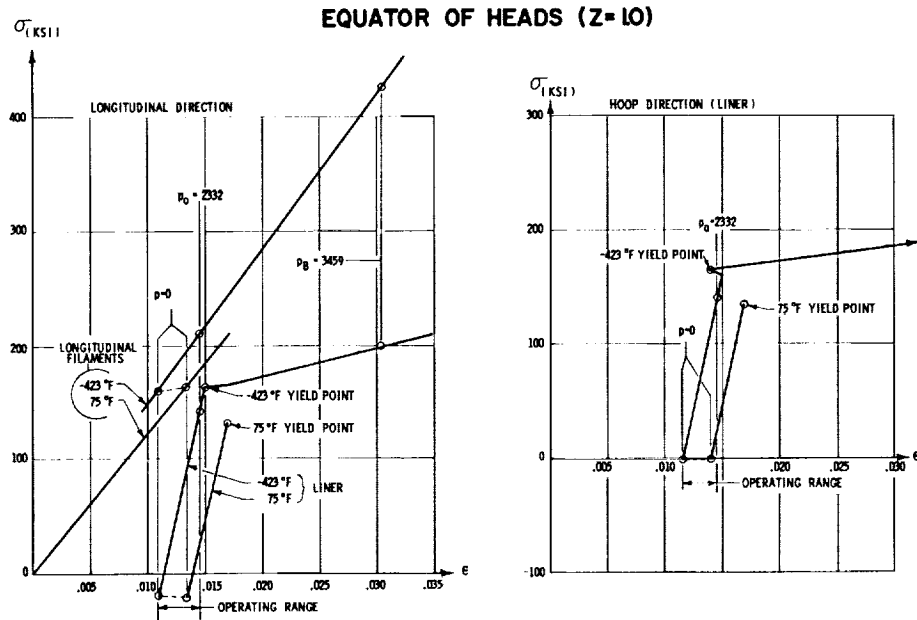


CYLINDRICAL SECTION

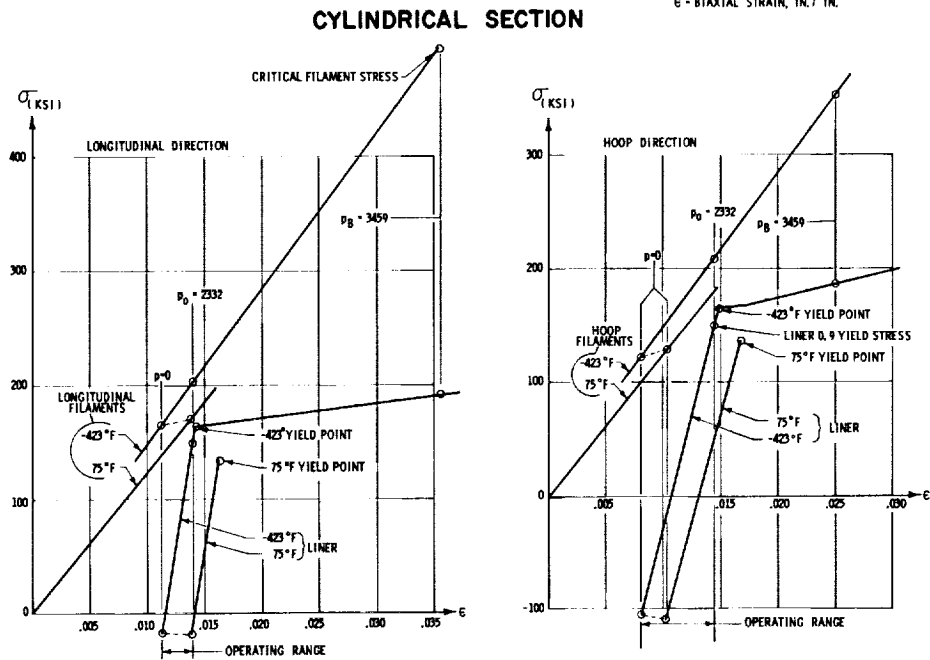


-320°F STRESS-STRAIN RELATIONSHIP OF OPTIMUM ROOM TEMPERATURE DESIGN GFR INCONEL X-750 (STA) PRESSURE VESSEL WITH 2220 PSI PROOF PRESSURE AT 75°F AND 2285 PSI OPERATING PRESSURE AT -320°F (L/D=1)

Figure 55



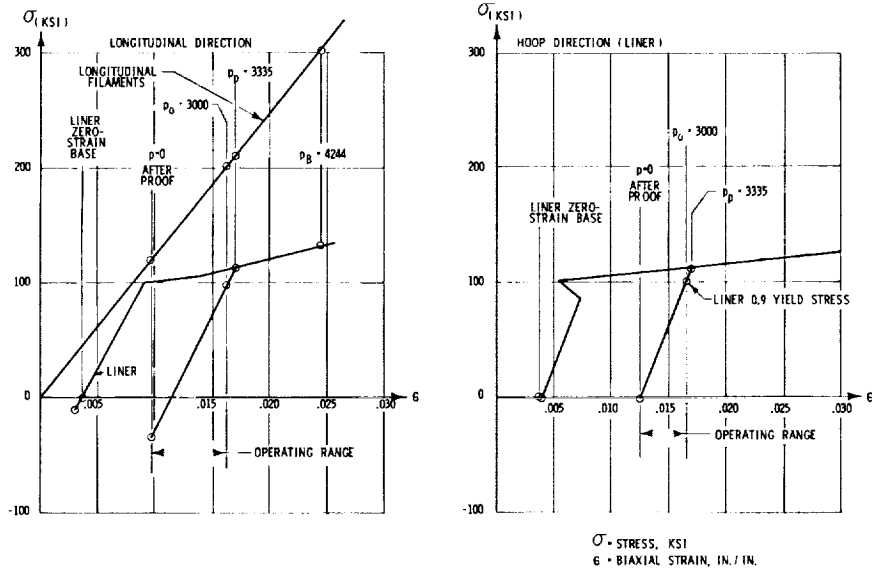
σ - STRESS, KSI
 ϵ - BIAxIAL STRAIN, IN. / IN.



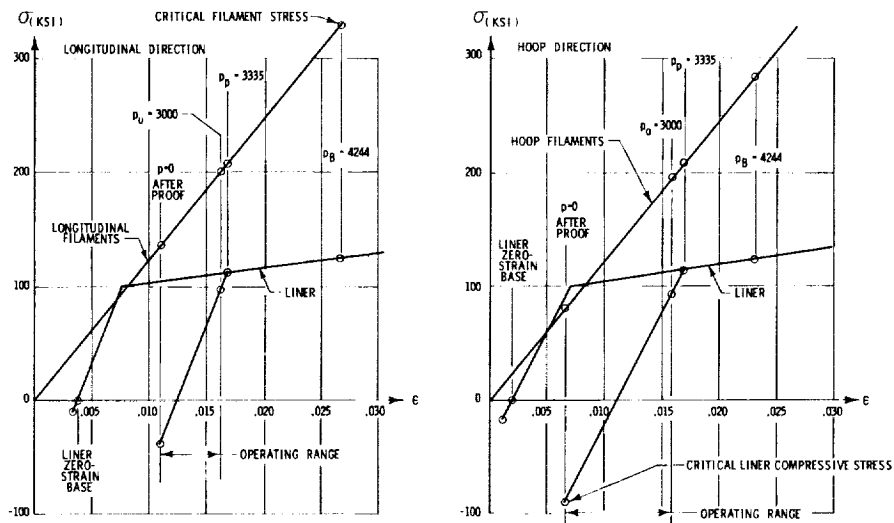
**-423°F STRESS-STRAIN RELATIONSHIP OF OPTIMUM ROOM TEMPERATURE
 DESIGN GFR INCONEL X-750 (STA) PRESSURE VESSEL WITH 2220 PSI PROOF
 PRESSURE AT 75°F AND 2332 PSI OPERATING PRESSURE AT -423°F (L/D=1)**

Figure 56

EQUATOR OF HEADS (Z=1.0)



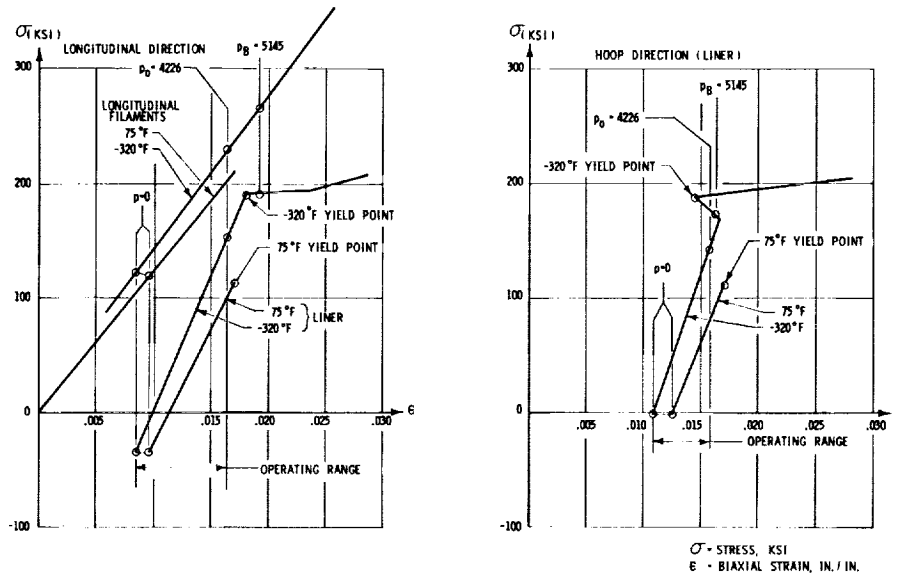
CYLINDRICAL SECTION



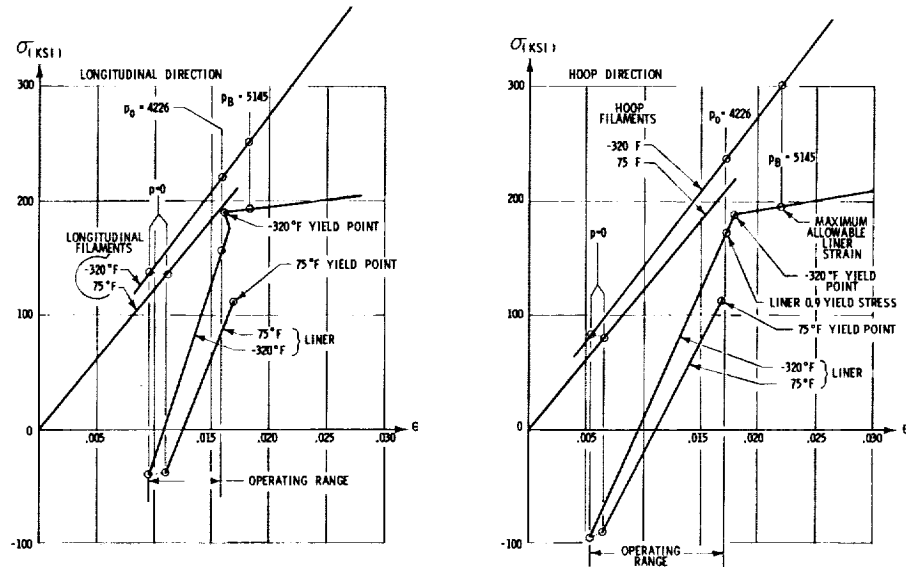
ROOM TEMPERATURE STRESS-STRAIN RELATIONSHIP OF OPTIMUM GFR
 5 Al-2.5 Sn TITANIUM (ANNEALED, ELI GRADE) PRESSURE VESSEL WITH
 3335 PSI PROOF PRESSURE AND 3000 PSI OPERATING PRESSURE (L/D=1)

Figure 57

EQUATOR OF HEADS (Z=1.0)



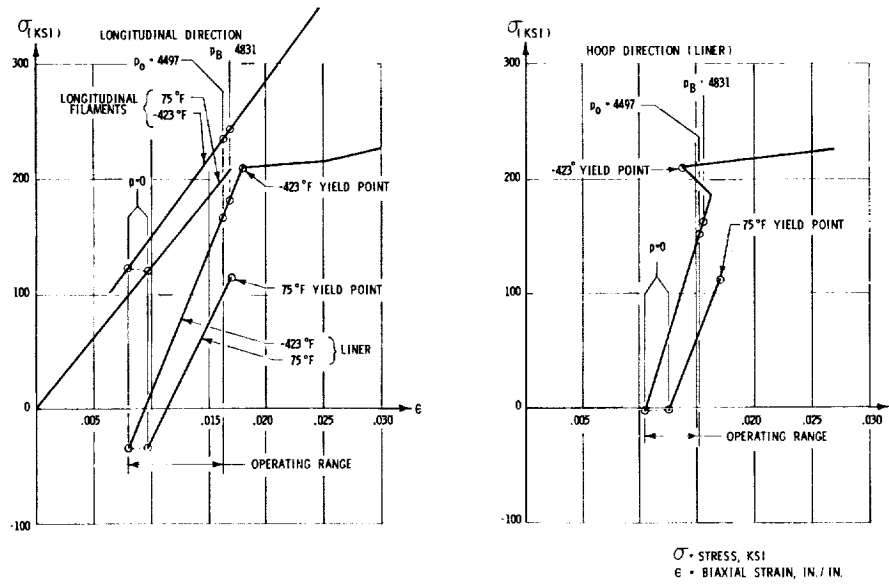
CYLINDRICAL SECTION



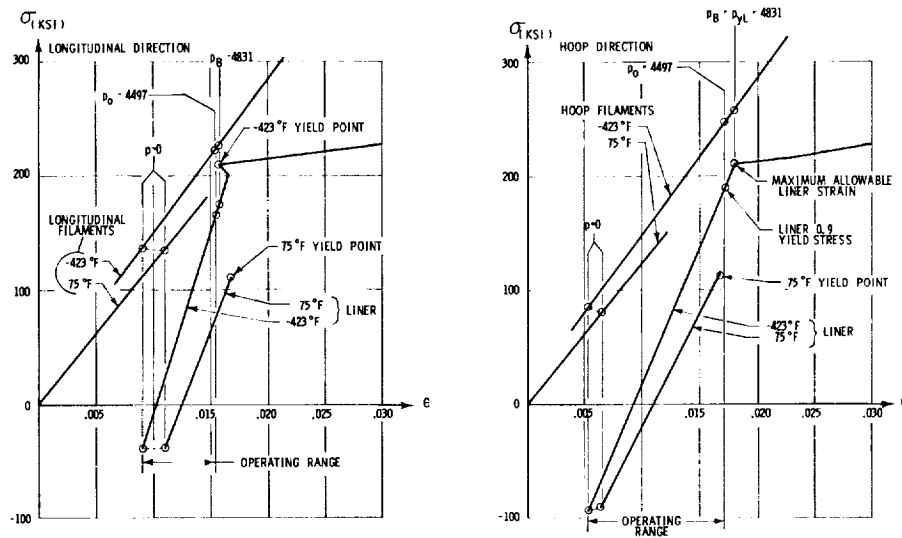
-320°F STRESS-STRAIN RELATIONSHIP OF OPTIMUM ROOM TEMPERATURE DESIGN GFR 5 Al-2.5 Sn TITANIUM (ANNEALED, ELI GRADE) PRESSURE VESSEL WITH 3335 PSI PROOF PRESSURE AT 75°F AND 4226 PSI OPERATING PRESSURE AT -320°F (L/D=1)

Figure 58

EQUATOR OF HEADS (Z=1.0)



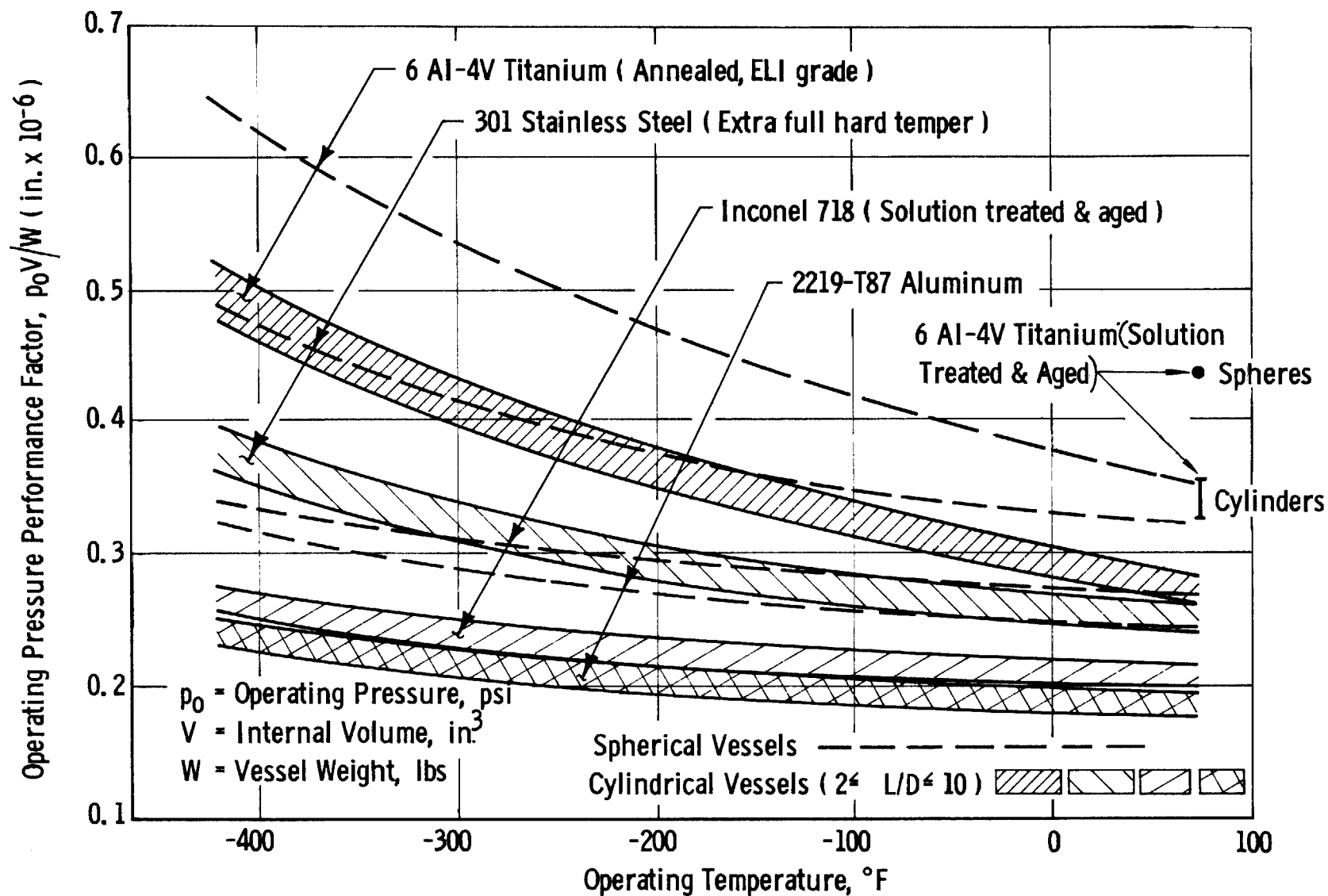
CYLINDRICAL SECTION



**-423°F STRESS-STRAIN RELATIONSHIP OF OPTIMUM ROOM TEMPERATURE
 DESIGN GFR 5Al-2.5 Sn TITANIUM (ANNEALED, ELI GRADE) PRESSURE
 VESSEL WITH 3335 PSI PROOF PRESSURE AT 75°F AND 4497 PSI
 OPERATING PRESSURE AT -423 (L/D=1)**

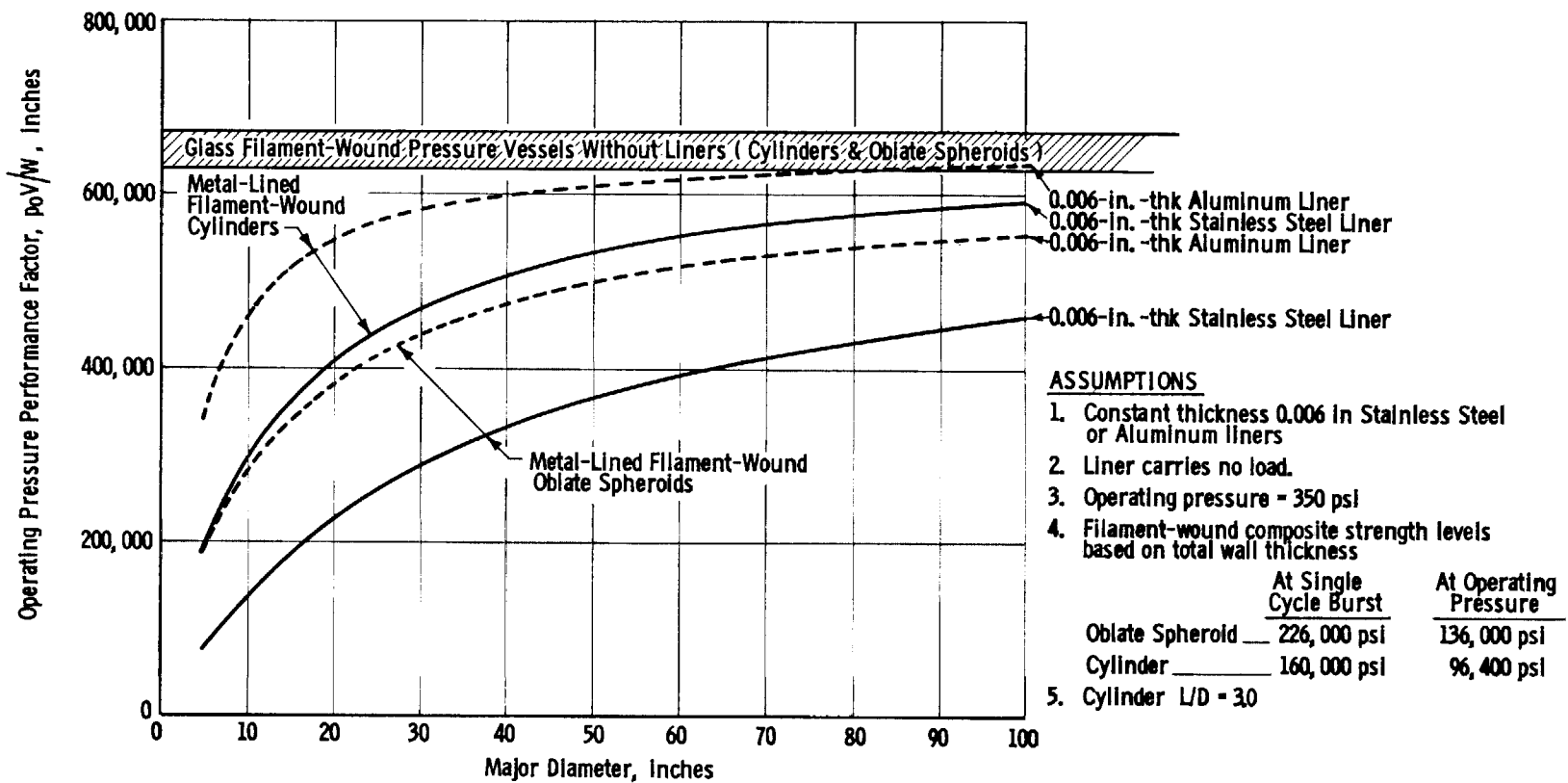
Figure 59

Figure 60



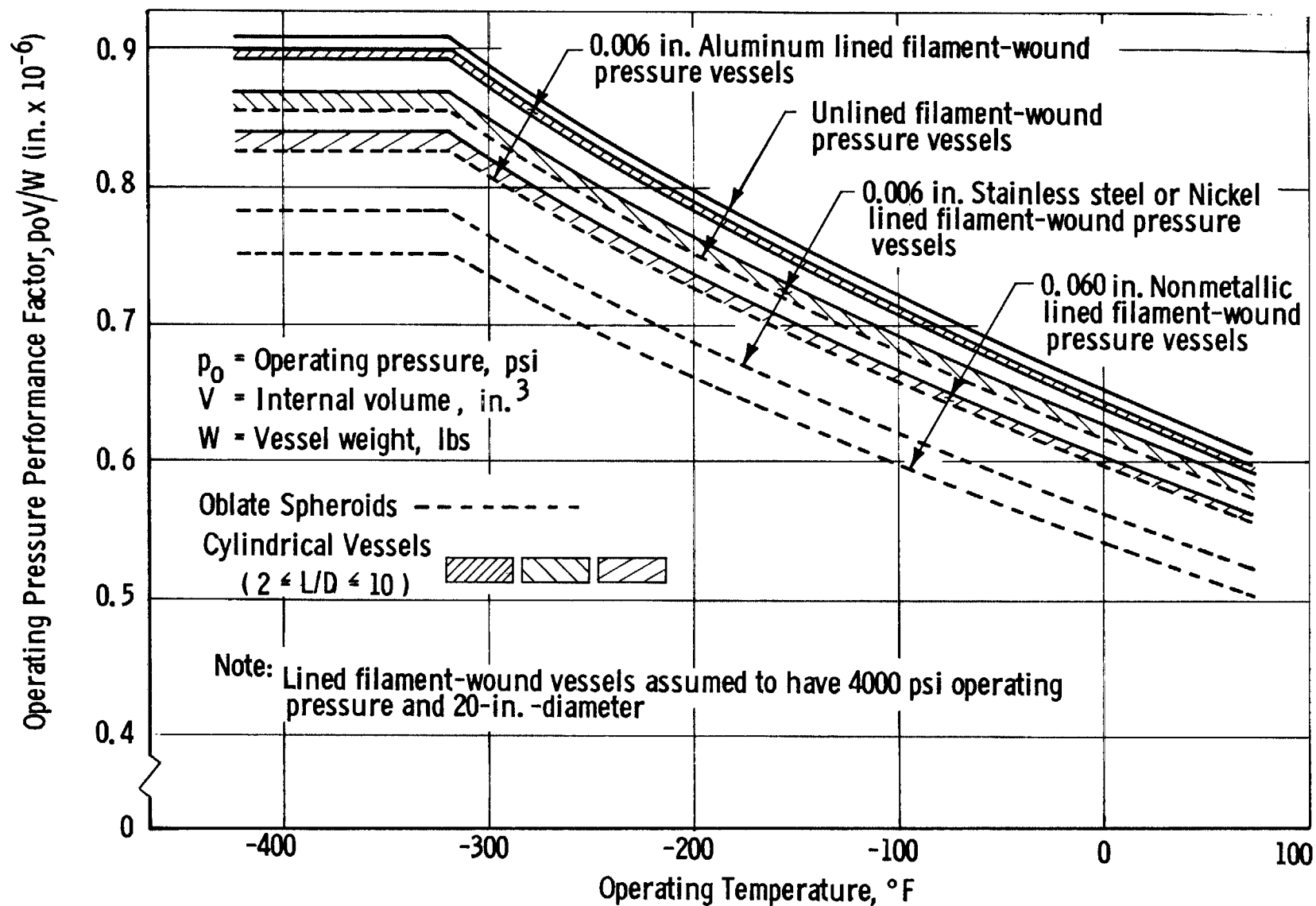
METAL PRESSURE VESSEL PERFORMANCE LEVELS

Figure 61



OPERATING PRESSURE PERFORMANCE FOR METAL-LINED GLASS FILAMENT-WOUND TANKAGE

Figure 62



GLASS-FILAMENT-WOUND PRESSURE VESSEL PERFORMANCE

TABLE 1

ELEMENTS OF GLASS-FILAMENT-REINFORCED METAL SHELLS

	<u>Variables</u>
Material	Glass-filament-wound composite shell
	Stress-strain relationship in tension
	Ultimate tensile strength
	Ultimate tensile elongation
	Composite modulus of elasticity
	Metallic shell
	Stress-strain relationship in tension and compression (proportional limit, yield strength, and ultimate strength in tension and compression)
	Elongation in parent metal and welded joints
	Modulus of elasticity in tension and compression
	Yield to ultimate strength margin
	Welded-joint efficiencies
	Poisson's ratio
	Strength of bond between metallic shell and filament- wound composite
Design (for constant-PV requirement)	Factor of safety
	Strain boundary conditions imposed on metal shell
	Relative thicknesses of filament-wound composite and metallic shells
	Shape (sphere, oblate spheroid, cylinder)
	Closure contours
	Thermal-contraction effects
	Winding-tension precompression force on metallic shell
Fabrication	Winding-tension parameter
	Integrity of welded joints in metal shell
	Winding-mandrel rigidity

Table 1

TABLE 2

PREFERENTIAL RATING OF CANDIDATE METAL-SHELL MATERIALS

Temp °F	Values for Properties (Ratings)				
	301 SS, Half-Hard As Rolled *	Stress- Relieved	Ti-5Al-2.5Sn ELI Grade Annealed	Aluminum Alloy 2219 T62 Temper	Inconel X-750 Solution- Treated & Aged
Ratio, Compressive Proportional Limit to Density - $\times 10^3$					
+75	87 (5)	175 (4)	556 (1)	379 (2)	360 (3)
-320	245 (5)	332 (4)	975 (1)	490 (2)	407 (3)
-423	290 (5)	378 (4)	1111 (1)	510 (2)	420 (3)
Uniaxial Tensile Strain at Fracture - % Elongation in 2 in.					
+75	23 (3)	29 (1)	14 (4)	10 (5)	25 (2)
-320	29 (2)	**	11 (4)	12 (3)	30 (1)
-423	20 (2)	**	11 (4)	14 (3)	30 (1)
Ratio, Notch-to-Unnotch Ultimate Strength ***					
+75	1.19 (2)	**	1.33 (1)	0.93 (4)	0.99 (3)
-320	1.15 (1)	**	1.11 (2)	0.86 (4)	0.88 (3)
-423	0.91 (1)	**	0.85 (2)	0.77 (4)	0.80 (3)
Ratio, Notch-to-Unnotch Yield Strength ***					
+75	0.85 (4)	**	1.43 (2)	1.28 (3)	1.44 (1)
-320	0.48 (4)	**	1.19 (3)	1.22 (2)	1.42 (1)
-423	0.33 (4)	**	0.91 (3)	1.24 (2)	1.50 (1)
Weld Joint, Uniaxial Tensile Strain at Fracture - % Elongation in 2 in.					
+75	21 (2)	**	12 (3)	9 (4)	20.5 (1)
-320	14 (2)	**	8 (4)	7 (3)	21 (1)
-423	3 (3)	**	4 (2)	4 (2)	24 (1)
Weld-Joint Efficiency - %					
+75	70 (4)	**	93 (3)	100 (2)	105 (1)
-320	96 (3)	**	94 (4)	99 (2)	119 (1)
-423	89 (3)	**	92 (2)	87.5 (4)	116 (1)
Low-Cycle, High-Strain Fatigue - No. of Cycles to Failure at Maximum-Operating-Strain Cycling Range					
+75	900 (3)	**	400 (4)	1500 (2)	3500 (1)
-320	9000 (1)	**	180 (4)	1500 (3)	7000 (2)
-423	3000 (3)	**	130 (4)	3500 (2)	10,000 (1)
Fabrication Characteristics - Forming					
-	Poor (3)	-	Requires heating } (2)	Good (1)	Good (1)
Fabrication Characteristics - Welding					
-	Good (1)	-	Requires maximum atmosphere protection } (3)	Good if Clean (2)	Good (1)

* The direction of rolling providing the lowest value was generally used.

** Values not available.

*** At $K_T = 7.2$ for 301 SS, Ti-5Al-2.5Sn, and Inconel X-750. At $K_T = 8.0$ for 2219-T62 aluminum.

Table 2

TABLE 3

MATERIAL PROPERTIES USED IN PARAMETRIC STUDY

Property	Inconel X-750 Solution- Treated & Aged	Aluminum 2219-T62	Ti-5Al-2.5Sn ELI Grade Annealed	Type 301 SS Half-Hard	Glass-Filament- Wound Composite
Density, lb/in. ³	0.300	0.102	0.162	0.286	0.072
Coefficient of thermal expansion, in./in.-°F at +75 to -423°F	4.990×10^{-6}	8.915×10^{-6}	3.910×10^{-6}	6.760×10^{-6}	2.010×10^{-6}
Tensile yield strength, psi	118,000	42,500	100,000	120,000	-
Derivative of yield strength with respect to temperature, psi/°F	-60.1	-29.1	-197.5	-116.0	-
Proportional limit, psi	108,000	39,600	90,000	80,000	-
Derivative of proportional limit with respect to temperature, psi/°F	-54.2	-25.3	-180.5	-104.0	-
Elastic modulus, psi	31.0×10^6	10.5×10^6	15.5×10^6	27.0×10^6	12.4×10^6
Derivative of elastic modulus with respect to temperature, psi/°F	-2010	-2510	-6210	-8030	-2410
Plastic modulus, psi	796,000	750,000	703,000	800,000	-
Derivative of plastic modulus with respect to temperature, psi/°F	-0.1	94.3	-74.3	-0.1	-
Poisson's ratio	0.290	0.325	0.295	0.295	-
Derivative of Poisson's ratio with respect to temperature, 1/°F	0.0	-0.2005×10^{-4}	-0.2005×10^{-4}	0.0	-
Maximum metal-shell biaxial longitudinal strain at design condition, in./in.					
At +75°F	0.0625	0.0250	0.0350	0.1250	-
At -320°F	0.0750	0.0300	0.0275	0.0750	-
At -423°F	0.0700	0.0350	0.0275	0.0500	-
Volume fraction of filament in composite	-	-	-	-	0.673
Filament, design allowable stress, psi*					
At +75°F	-	-	-	-	330,000
At -320°F	-	-	-	-	495,000
At -423°F	-	-	-	-	495,000

* Single-pressure-cycle design allowable, which must be reduced to account for effects of cyclic and sustained loading.

TABLE 4
METAL PRESSURE VESSEL STRENGTH LEVELS*

Material	Condition	Use Temp**	Pounds per Square Inch								
			At +75°F			At -320°F			At -423°F		
			Yield Strength	Ultimate Tensile Strength	Operating Stress Level	Yield Strength	Ultimate Tensile Strength	Operating Stress Level	Yield Strength	Ultimate Tensile Strength	Operating Stress Level
Titanium Alloys											
6Al-4V	Annealed	RT	120,000	130,000	86,500	-	-	-	-	-	-
6Al-4V	Solution-treated and aged	RT	145,000	160,000	106,500	-	-	-	-	-	-
6Al-4V ELI	Annealed	CT	120,000	130,000	86,500	192,000	202,000	134,500	228,000	236,000	157,200
Aluminum Alloy											
No. 2219	T87 temper	RT & CT	50,000	62,000	38,500	59,500	77,000	45,800	66,000	93,000	50,700
Stainless Steel											
Type 301	Extra full hard or Ardeform process	RT & CT	180,000	222,000	138,500	235,000	320,000	181,000	270,000	330,000	208,000
Nickel-Base Alloy											
Inconel 718	Solution-treated and aged	RT & CT	155,000	188,000	119,000	180,000	238,000	138,500	195,000	262,000	150,000

* Based on design values from Metallic Materials and Elements for Flight Vehicle Structures, Military Handbook 5, August 1962, with Change Notices 1 through 4; Cryogenic Materials Data Handbook, ML-TDR-64-280, August 1964, with Supplements 1 and 2; and pertinent Aerospace Materials Specifications. Throughout table, operating stress level = ultimate strength/1.50, or yield strength/1.30, whichever is smaller.

** RT = room temperatures; CT = cryogenic temperatures.

TABLE 5

OPERATING-PRESSURE PERFORMANCE FACTORS, HOMOGENEOUS METAL TANKS

Material	Vessel Shape*	Performance Factor ($p_0 V/W$), in.		
		At +75°F	At -320°F	At -423°F
6Al-4V titanium (annealed, ELI grade)	Sphere	355,000	550,000	642,000
	Cylinder	263,000 to 287,000	407,000 to 445,000	475,000 to 520,000
Type 301 SS (extra-full-hard temper)	Sphere	325,000	425,000	487,000
	Cylinder	242,000 to 265,000	317,000 to 347,000	363,000 to 398,000
Inconel 718 (solution- treated and aged)	Sphere	270,000	313,000	340,000
	Cylinder	199,000 to 219,000	231,000 to 254,000	251,000 to 276,000
2219-T87 aluminum	Sphere	246,000	292,000	323,000
	Cylinder	178,000 to 197,000	212,000 to 234,000	233,000 to 258,000

*For cylinders, length-to-diameter ratios ranging from 2 to 10.

APPENDIX A

CHARACTERIZATION OF GLASS-FILAMENT-SHELL PROPERTIES

The characterization analysis reported in this appendix was undertaken to define design properties of S-HTS glass-filament and filament-wound composites at cryogenic temperatures for use in making detailed calculations for the parametric study of GFR metal tanks.

I. MATERIALS

A. GLASS FILAMENTS

S-glass filament roving with HTS finish was selected for the filament-wound-shell component of GFR metallic tanks on the basis of superior performance, experience in its use, and commercial availability. It should be noted that, under NASA Contract NAS 3-6297, Aerojet is engaged in the development of glass filaments and filament coatings having better properties at cryogenic temperatures than the best filament materials now available.

B. RESIN MATRIX

Current epoxy-resin formulations used in filament winding permit fiber strengths of approximately 80 to 95% of the laboratory-glass-strand strength to be achieved in pressure-vessel heads and cylinders. Test data indicate, however, that these values will vary with changes in the physical properties and formulations of resins. At cryogenic temperatures, it is believed, the resin will have a more important role in controlling composite performance than it did at room temperatures. Resin-matrix properties at cryogenic temperatures are affected to a much greater degree than glass properties. In general, the ductility greatly decreases and the tensile strength increases. Thermal-contraction stresses in the resin, greater extensibility of the filaments, and strain-magnification effects in the filament-wound-composite material combine to impose significantly increased strain requirements on the resin. Work is in progress to develop filament-winding resin systems specifically for cryogenic service that will have increased extensibility and improved shear transfer, as compared with presently available resins.*

C. RESIN CONTENT IN COMPOSITE STRUCTURE

The glass content of filament-wound pressure vessels is generally about 67 vol%, or 82 wt%. This ratio, with a density of 0.088 lb/in.³ for S-HTS glass and an epoxy-resin density of 0.042 lb/in.³, results in a composite density of 0.073 lb/in.³, which is about one-quarter the density of steel and less than one-half the density of titanium.

* NASA Lewis Research Center program (on improved cryogenic resins for glass-filament-wound structures) being conducted by Aerojet under Contract NAS 3-6287.

II. TECHNICAL DISCUSSION

A. GLASS-FILAMENT STRENGTH IN FILAMENT-WOUND COMPOSITES AT ROOM TEMPERATURE

The room-temperature properties of S-HTS glass filaments and filament-wound composites are well characterized (Ref. A-1). Using these properties, Aerojet has developed a systematic approach for the design of filament-wound pressure vessels (described in Refs. A-1, A-2, and A-3). The procedure is based on the use of design factors corresponding to a range of dimensional parameters to determine the allowable design strength for each pressure-vessel configuration. The factors are based on data obtained in Aerojet tests of several thousand filament-wound pressure vessels with significant variations in their design parameters. The factors used for the selection of design allowables include the strength of glass roving, standard deviation of glass-roving strength, resin content, envelope dimensions (length and diameter), internal pressure level, axial-port diameters, temperature, and rate of load application.

This analytical method was used to determine 75°F, S-HTS glass-filament-strength, design allowables for single-pressure-cycle burst tests at a 1%/min strain rate for the range of design parameters evaluated in the parametric study of GFR metallic tanks. The parameters of interest are

Tank diameter, in.	12 to 40
Tank length-to-diameter (L/D) ratio	0.6 to 25
Operational-pressure level, psi	1000 to 4000
Pressure cycles to operational pressure	100
Total duration at operational-pressure level, hours	72

The minimum, maximum, and typical values obtained for 75°F, single-pressure-cycle, allowable-strength levels are summarized in Table A-1 and presented graphically in Figures A-1 and A-2 as a function of pressure-vessel L/D ratios for hoop and longitudinal filaments. The analysis showed that the strengths ranged from 314,000 to 368,000 psi for hoop filaments, with an average of 341,000 psi. For the longitudinal filaments, representative strengths ranged from 272,000 to 370,000 psi, with an average of 321,000 psi. On the basis of these design-allowable strengths, 330,000 psi was selected as typical for use in detailed calculations. This value was adjusted to account for the effects of GFR-metal-tankage service-life requirements, which were assumed to consist of 100 cycles and 72 hours of sustained loading at the operational-pressure level. Data developed in an Aerojet Independent Research and Development (IR&D) program were used to establish the service-cycle design-filament-strength levels. (This program, completed in December 1965, evaluated the strength degradation produced in filament-wound pressure vessels by cyclic and sustained loading.) Preliminary review of the data indicates an interaction between the number of cycles and the time at load. This interaction, however, appears to be of such low magnitude that it may be assumed negligible until

proved otherwise. Current filament-wound pressure-vessel technology at Aero-jet is therefore based on selection of the maximum degradation caused by either of the two conditions, considered separately.

The 100-cycle condition was critical for the design criteria for the pressurized cryogenic tanks considered in the present study. Based on the IR&D test data presented in Figure A-3, the tanks can operate at 60% of the original strength for 100 cycles before failure. This resulted in a 100-cycle design allowable of 200,000 psi, as compared with the 330,000-psi single-cycle design allowable.

B. GLASS-FIBER PROPERTIES AT CRYOGENIC TEMPERATURES

The low-temperature properties (-320 and -423°F) of S-glass fibers needed for evaluation included fiber tensile strength, modulus, strain, and coefficient of contraction. These data were requested from the Owens-Corning Fiberglas Corporation and the U.S. Air Force Materials Laboratory. Owens-Corning replied that no known data exist on the properties of S-HTS glass fibers at cryogenic temperatures.* In the opinion of Owens-Corning, however, "... the increase in strength and modulus at cryogenic temperatures on S-glass would be approximately the same percentagewise as that which occurs for E-glass." The Air Force Materials Information Center also reported inability to find cryogenic data on single fibers of S-HTS glass.**

A literature survey produced only limited data on the properties of glass fibers at very low temperatures. The General Electric Company conducted tests of E-glass fibers at room temperature and -320°F (Ref. A-4); the average fiber tensile strength increased by 60% from 507,000 psi at room temperature to 814,000 psi at -320°F , and no values for tensile modulus were reported. Another source (Ref. A-5) presented data on the flexural strength and modulus of rods of optical glass (BSC-2, Corning 8370) tested between room temperature and liquid-hydrogen temperatures. The flexural strength of un-abraded specimens at -320°F increased by about 70% over the room-temperature values; the breaking stress at -423°F was nearly the same as at -320°F . The modulus of elasticity changed by less than 2% over the entire temperature range investigated. No information could be found on the coefficient of thermal contraction of single fibers or bulk glass in the range from $+75$ to -423°F .

* Private correspondence from E. M. Lindsay, Manager, Aerospace Research Laboratory, Owens-Corning Fiberglas Corporation, 20 August 1965.

** Private correspondence from G. C. Young, Materials Information Branch, Materials Applications Division, Air Force Materials Laboratory, Wright-Patterson Air Force Base, Ohio, 7 September 1965.

Aerojet therefore performed tests to obtain the necessary data on the strength and modulus of high-strength glass fibers. The testing of S-glass single fibers was not considered a satisfactory approach, because it was inadvisable to test S-fibers obtained by separation from a strand of roving or by drawing from a bushing at Aerojet. It was concluded, however, that meaningful results could be obtained from cryogenic-temperature tests of Aerojet's 19-S magnesium aluminum silicate glass composition* (the same glass type as S-glass), because these data could be used in predicting the characteristics of S-glass at cryogenic temperatures in the event that S-glass test results were not available.

A preliminary evaluation was performed under Contract NAS 3-6297 in which tensile tests were conducted at room temperature and at -320°F on 0.000361-in.-dia, freshly drawn, single fibers of 19-S glass. Monofilaments were captured between the bushing orifice and takeup drum and mounted onto cardboard tabs that provided a 1.00-in. fiber test span. Two specimens were obtained from each fiber capture. The fiber diameters were determined optically with an image-shearing measuring eyepiece at a 300X magnification. Specimens were mounted in an Instron testing machine and tested at a 20%/min strain rate. For the -320°F tests, the specimen and testing-machine grips were completely immersed in liquid nitrogen before and during load application. The tensile strength at failure was determined from the maximum load, and the modulus of elasticity was obtained from the stress-strain curve that was recorded automatically for each tensile test.

The test results for the 19-S glass fibers at ambient conditions and -320°F are summarized in Table A-2. The average room-temperature tensile strength of 732,000 psi increased by 50% to 1,097,000 psi at -320°F . The tensile modulus of the fibers increased by 10% from 13.40×10^6 psi at room temperature to 14.67×10^6 psi at -320°F . Typical stress-strain diagrams for the fibers at room temperature and -320°F are presented in Figure A-4.

C. GLASS-FILAMENT-WOUND-COMPOSITE PROPERTIES AT CRYOGENIC TEMPERATURES

The low-temperature properties (-320 and -423°F) of S-HTS glass-filament-wound composites needed for evaluation included the composite and filament tensile strength, modulus, strain, and coefficient of contraction.

A review of data on the strength of Naval Ordnance Laboratory (NOL) rings at -320 and -423°F (Refs. A-4 and A-6) shows that the increases over room-temperature strength have ranged from 25 to 60% for E-HTS glass; the increase noted for S-HTS glass is about 20 to 25% at both -320 and -423°F (Ref. A-6).

Limited data on the strength of filament-wound pressure vessels at cryogenic temperatures (Ref. A-6) indicate an increase of 50 to 60% in E-HTS

* This composition was selected for evaluation under Contract NAS 3-6297.

filament and composite strength when the test temperature is decreased from 75 to -320°F . This result correlates directly with the strength increase noted for single E and 19-S glass fibers at -320°F . The difference in strength noted between -320 and -423°F was very small. No cryogenic-test data were located for S-HTS glass in filament-wound pressure vessels.

Figure A-5 provides data* on the linear thermal contraction (between 75 and -423°F) of unidirectional and bidirectional S-HTS glass-filament-reinforced epoxy-resin composites.

III. DESIGN-ALLOWABLE PROPERTIES, S-HTS GLASS-FILAMENT-WOUND COMPOSITES FOR USE IN PARAMETRIC STUDY

The data given in the preceding section constitute the basis for the succeeding estimates of S-HTS filament-wound-composite properties for use in the parametric study of GFR metal tanks.

A. TENSILE STRENGTH

The -320 and -423°F strength of S-HTS glass filaments in pressure vessels is projected to be 50% greater than the 75°F strength. Strength-increase factors for steady-state low-temperature effects on filament-wound composites are given in Figure A-6; the effects of these factors on design-allowable single-pressure-cycle strength levels for S-HTS glass filaments in GFR metal tanks are summarized in Table A-1. On this basis, the 75°F , average, single-pressure-cycle, hoop-filament strength level of 341,000 psi and longitudinal-filament strength level of 321,000 psi (from Section II,A) will increase to 512,000 and 482,000 psi, respectively, at -320 and -423°F . The typical 75°F , GFR-metal-tank, single-pressure-cycle, design-filament-strength level of 330,000 psi will increase to 495,000 psi at -320 and -423°F .

The 75°F , operating-pressure, filament-stress level of 200,000 psi (maximum), required if the tankage is to withstand 100 pressure cycles and 72 hours of sustained loading at the operational pressure, will likewise increase by 50% to a value of 300,000 psi at -320 and -423°F .

B. TENSILE MODULUS

The -320 and -423°F tensile modulus of S-HTS glass filament will increase by 10% from 12.4×10^6 psi at 75°F to 13.6×10^6 psi at -320 and -423°F . The glass/resin-composite stress-strain curve is not expected to be perfectly elastic up to the point of failure (e.g., see Figure 8 of Ref. A-6 and Section VII of Ref. A-9), because of effects caused by resin-matrix crazing and high-load filament rupture at points of stress concentration.

C. TENSILE STRAIN

A projected stress-strain curve for S-HTS glass filaments in GFR metal pressure vessels at -320 and -423°F , based on the tensile-strength and

* From Refs. A-7 and A-8 and private communication with J. R. Barber of the NASA Lewis Research Center.

modulus values for S-HTS glass filament discussed above, is compared with the 75°F curve in Figure A-7. The ultimate tensile strain of the filament at 75°F ranges from 2.2 to 3.0%; it is estimated to range between 3.0 and 4.1% for the filaments at -320 and -423°F.

During tank fabrication, the winding-tension strain may be about 10% of the room-temperature ultimate glass-fiber strain. Using this value, an assumption that a rigid mandrel is employed to support the metal shell during overwrapping, and the data of the preceding paragraph, the following minimum metal-shell tensile-strain capabilities are required in a 1-to-1 biaxial-stress field for the optimum burst-strength performance of the filament-wound composite:

<u>Temp, °F</u>	<u>Metal-Shell Tensile Strain at Burst Pressure, %</u>
+75	2.0 to 2.7
-320 and -423	2.7 to 3.8

D. COEFFICIENT OF THERMAL CONTRACTION

The data presented in Section II,C, supplemented by calculation, indicate that the following values are reasonable for the +75 to -423°F coefficient of linear thermal contraction of S-HTS filament/epoxy-resin composite (67/33 volume ratio) with a 2-to-1 transverse-to-longitudinal filament ratio:

<u>Composite Direction</u>	<u>Coefficient of Linear Thermal Contraction (+75 to -423°F), in./in./°F</u>
Transverse	2.01×10^{-6}
Longitudinal	2.81×10^{-6}

REFERENCES

- A-1. Structural Materials Handbook, Chemical and Structural Products Division, Aerojet-General Corporation, February 1964.
- A-2. F. J. Darms, R. Molho, and B. E. Chester, Improved Filament-Wound Construction for Cylindrical Pressure Vessels, Technical Documentary Report ML-TDR-64-43, prepared by Aerojet-General under Contract AF 33(616)-8442, March 1964.
- A-3. F. J. Darms and E. E. Morris, "Design Concepts and Procedures for Filament-Wound Composite Pressure Vessels," paper presented at American Society of Mechanical Engineers Aviation and Space Conference, Los Angeles, March 1965.
- A-4. D. L. Hollinger, H. T. Plant, and R. F. Mulvey, High Strength Glass Fibers Development Program, Final Report under Contract NOW 61-0641-c (FBM), General Electric Company, Evendale, Ohio, May 1963.
- A-5. R. H. Kropschot and R. P. Mikesell, An Experimental Study of the Strength and Fatigue of Glass at Very Low Temperatures, National Bureau of Standards Report 3950, Technical Memorandum No. 37, Cryogenic Engineering Laboratory, Boulder, Colorado, June 1956.
- A-6. M. P. Hanson, H. T. Richards, and R. O. Hickel, Preliminary Investigation of Filament-Wound Glass-Reinforced Plastics and Liners for Cryogenic Pressure Vessels, NASA TND-2741, Lewis Research Center, Cleveland, Ohio, March 1965.
- A-7. J. M. Toth, Jr. and J. R. Barber, "Structural Properties of Glass-Fiber Filament-Wound Cryogenic Pressure Vessels," technical preprint prepared for Cryogenic Engineering Conference, Philadelphia, August 1964.
- A-8. M. D. Campbell, G. L. O'Barr, J. F. Haskins, and J. Hertz, Thermophysical Properties of Plastic Materials and Composites to Liquid Hydrogen Temperature (-423°F), Technical Documentary Report ML-TDR-64-33, Part II, prepared under Contract AF 33(657)-9160 by General Dynamics/Convair, San Diego, California, August 1963.
- A-9. Composite Properties of Filament-Wound Reinforced Plastics Determined by Analytical and Experimental Methods, Aerojet-General Corporation, Solid Rocket Operations, Sacramento Plant, July 1964.

TABLE A-1

DESIGN-ALLOWABLE SINGLE-PRESSURE-CYCLE STRENGTH LEVELS
FOR S-HTS GLASS FILAMENTS IN GFR METAL TANKS

Temperature °F	Range of Filament Strength Levels		Average Filament Strength Level		Typical
	Hoop	Longitudinal	Hoop	Longitudinal	
+75	314,000-368,000	272,000-370,000	341,000	321,000	330,000
-320 and -423	471,000-552,000	408,000-555,000	512,000	482,000	495,000

TABLE A-2

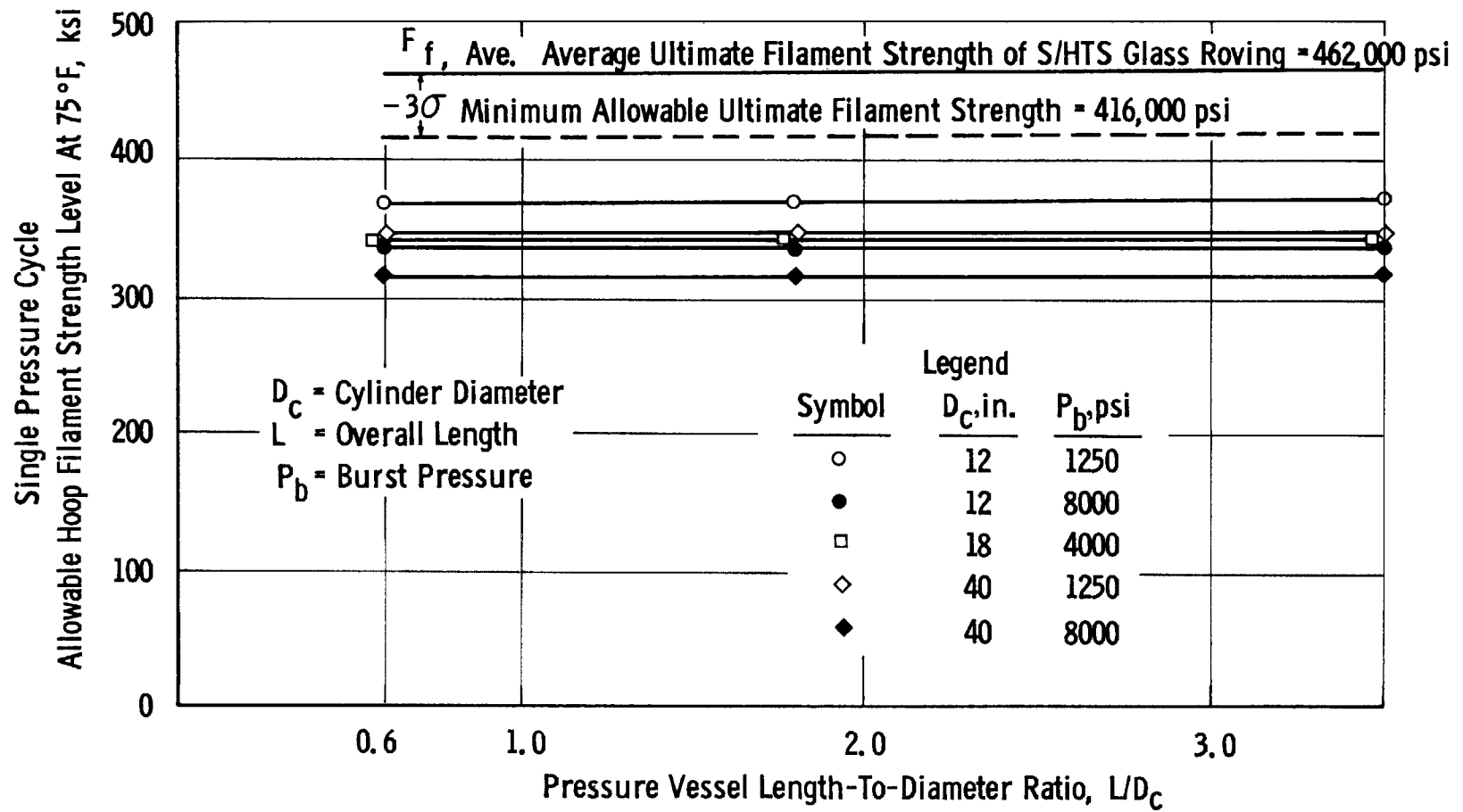
STRENGTH AND MODULUS OF 19-S MAGNESIUM SILICATE GLASS
SINGLE FIBERS AT ROOM TEMPERATURE AND -320°F*

Tensile Properties, psi							
Fiber No.	Fiber Dia, in.	A: Room-Temperature Tests		B: -320°F Tests		Ratio of A to B	
		Strength	Modulus	Strength	Modulus	Strength	Modulus
1	0.000361	594,000	13.05 x 10 ⁶	1,054,000	14.64 x 10 ⁶	1.77	1.12
2	0.000361	739,000	13.69	No test	No test	-	-
3	0.000361	767,000	13.58	1,261,000	14.37	1.71	1.06
4	0.000361	771,000**	14.15	1,318,000	15.57	1.71	1.10
5	0.000354	301,000	13.09	1,099,000**	14.46	-	1.10
6	0.000354	709,000	13.13	647,000	14.38	-	1.10
7	0.000355	688,000	13.10	826,000	14.62	1.20	1.12
8	0.000377	857,000	15.22	1,024,000	17.50	1.19	-
Av	0.000361	732,000	13.40 x 10 ⁶	1,097,000	14.67 x 10 ⁶	1.51	1.10

* Gage length = 1.00 in. Strain rate = 20%/min. Room-temp tests at 100°F and relative humidity of 60%.

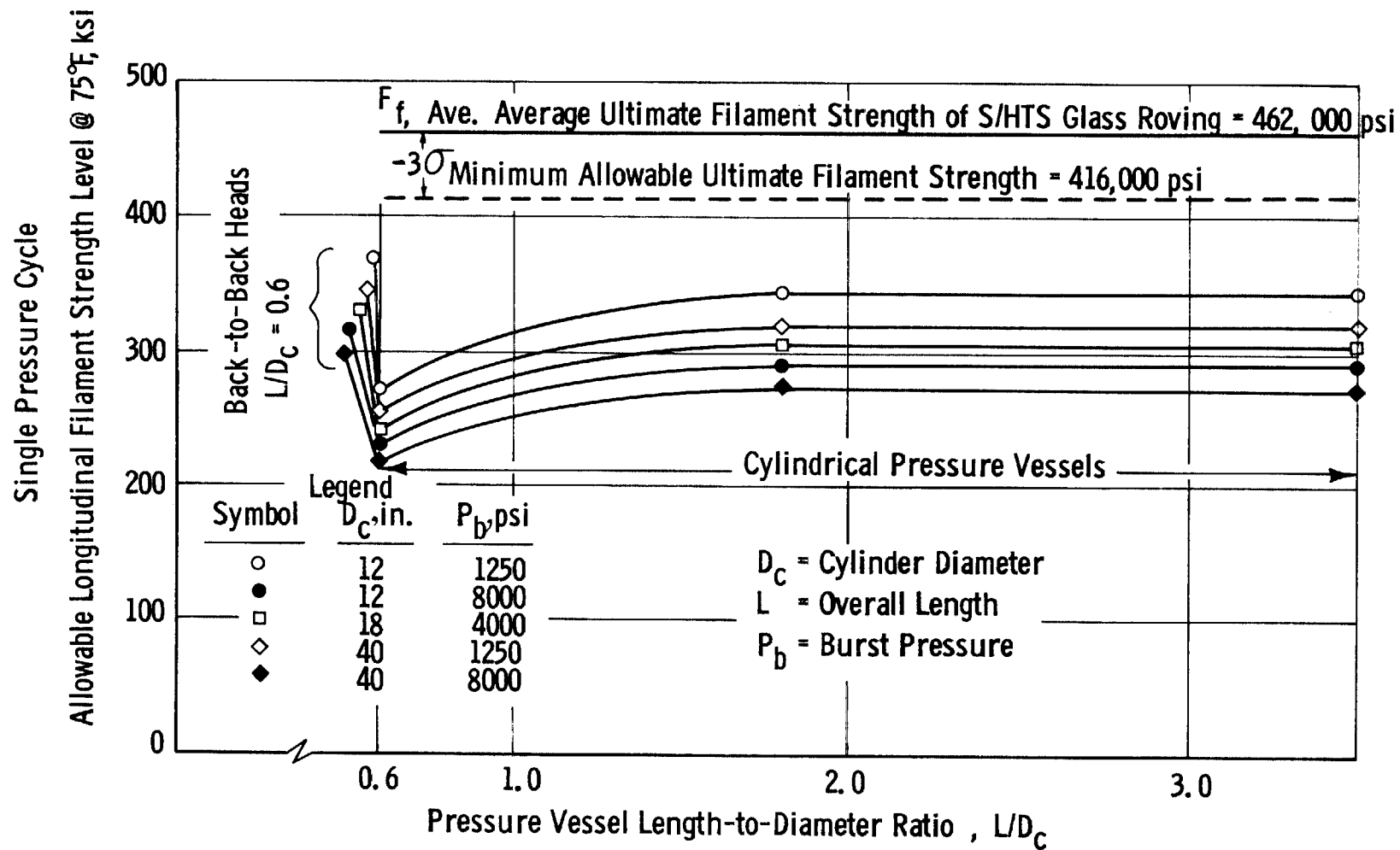
** Value considered not representative of batch and not included in averages or ratios.

Figure A-1

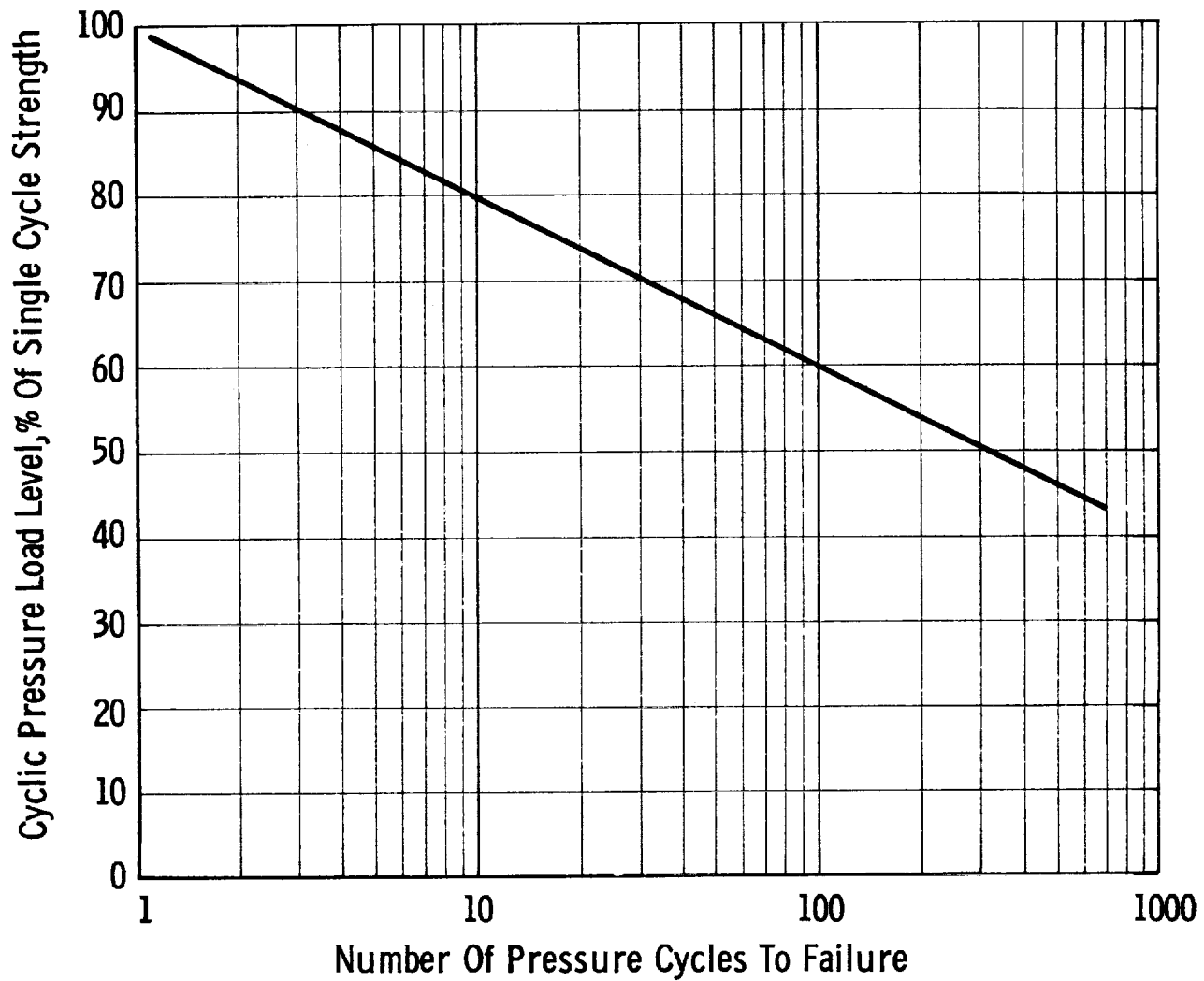


SINGLE PRESSURE CYCLE
 DESIGN ALLOWABLE HOOP FILAMENT STRESS AT 75°F FOR S/HTS ROVING IN GFR METALLIC TANKS

Figure A-2



SINGLE PRESSURE CYCLE
DESIGN ALLOWABLE LONGITUDINAL FILAMENT STRESS AT 75°F FOR S/HTS ROVING
IN GFR METALLIC TANKS

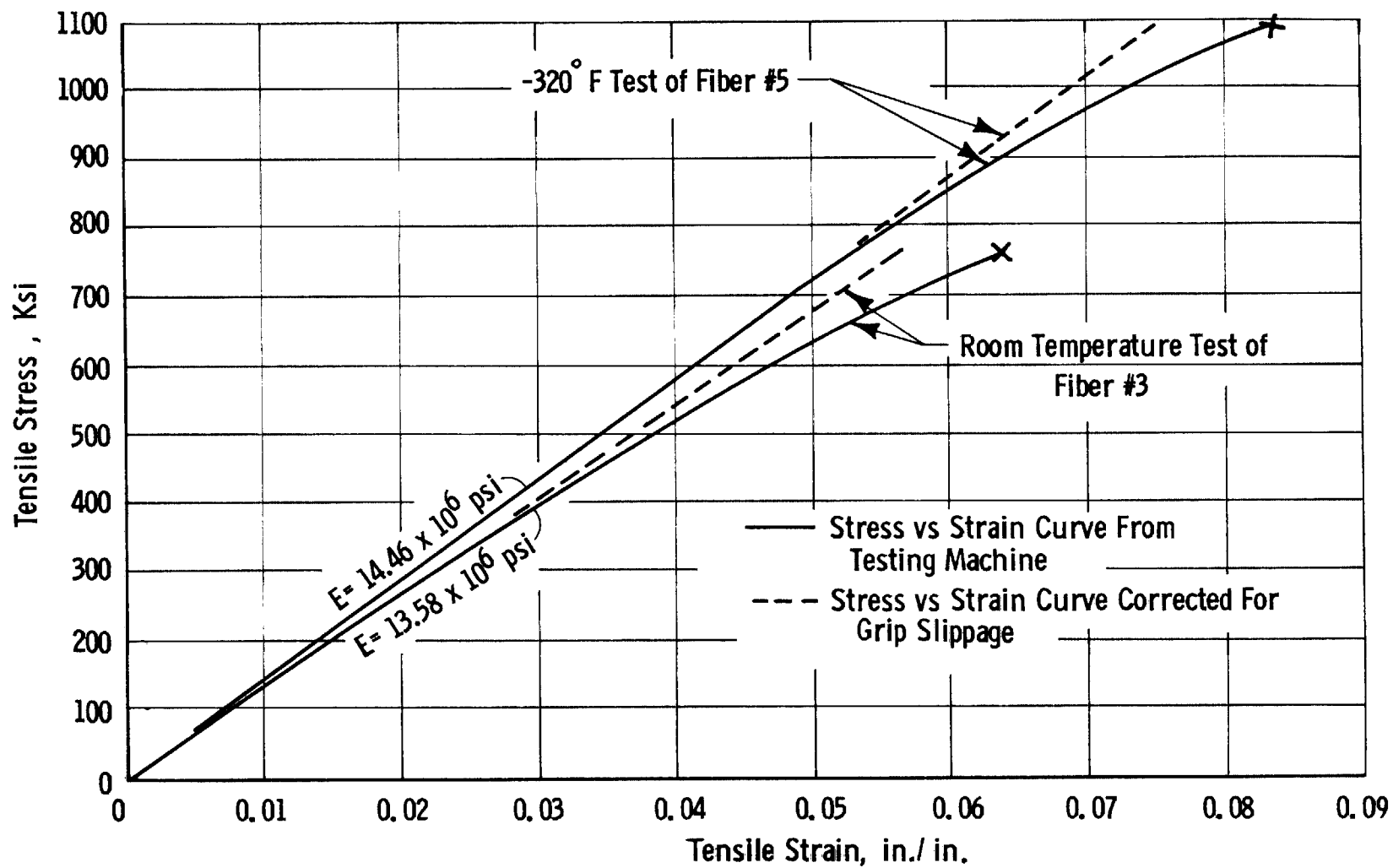


Note: Data from tests on 4-in. -dia cylindrical vessels made from S/HTS 20-end glass-filament roving.

CYCLIC PRESSURIZATION EFFECTS ON THE STRENGTH OF FILAMENT-WOUND PRESSURE VESSELS

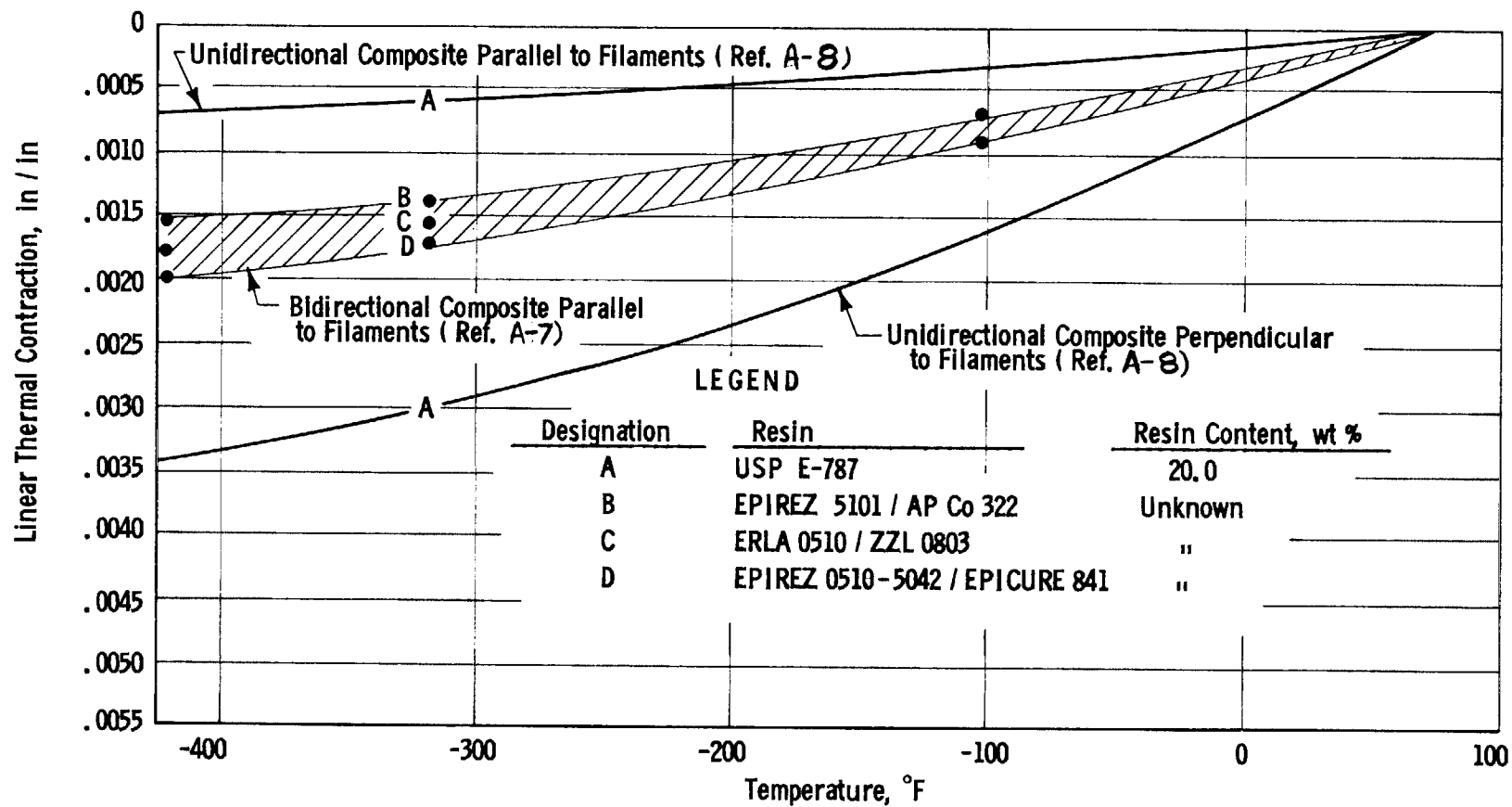
Figure A-3

Figure A-4

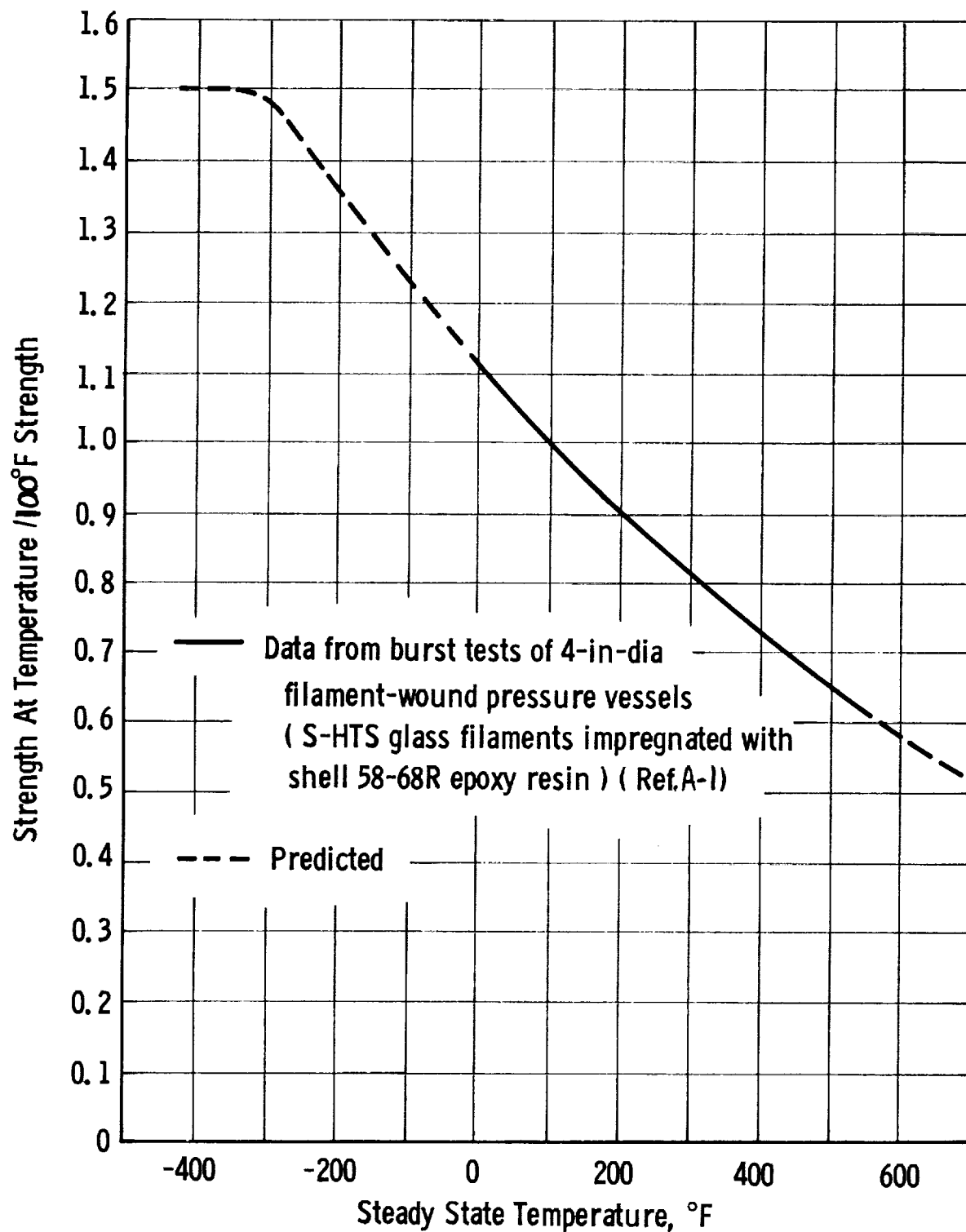


TYPICAL STRESS-STRAIN DIAGRAMS FOR 19-S GLASS SINGLE FIBERS TESTED AT ROOM TEMPERATURE AND -320°F

Figure A-5



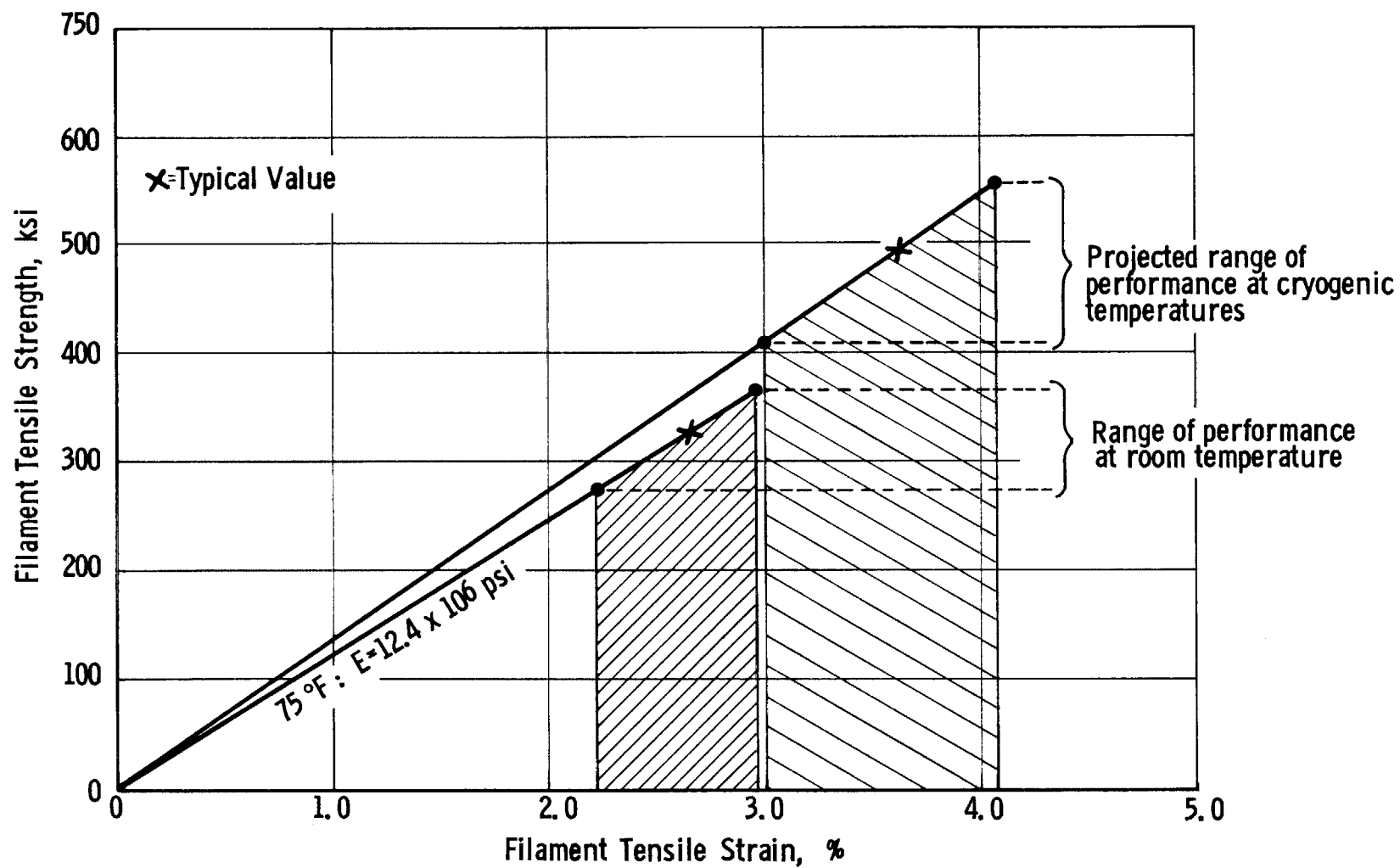
LINEAR THERMAL CONTRACTION OF S-HTS GLASS FILAMENT / EPOXY RESIN COMPOSITES



STEADY-STATE TEMPERATURE EFFECTS ON THE STRENGTH OF
FILAMENT-WOUND COMPOSITE PRESSURE VESSELS

Figure A-6

Figure A-7



PROJECTED CRYOGENIC TEMPERATURE STRESS-STRAIN CHARACTERISTICS OF S-HTS FILAMENTS IN GFR METALLIC PRESSURE VESSELS

APPENDIX B

CHARACTERIZATION OF METAL-SHELL MATERIALS

The objective of this analysis was to define design properties of materials considered candidates for load-bearing metal shells of GFR metal tanks for cryogenic service. The work included an extensive compilation of the 75 to -423°F properties of candidate materials, and evaluation of their applicability.

Before the analysis was performed, the basic requirements imposed on the metal shell for optimum GFR tank performance were defined, the properties for which design allowables had to be established were determined, and the scope of the analysis was defined. These are considered below.

I. REQUIREMENTS FOR OPTIMUM PERFORMANCE

A. IMPERMEABILITY

The metal shell must be impermeable to the passage of gases and liquids that may be contained in the vessel under pressure at the specified service-temperature range. This will require a metal shell with high-quality weld joints substantially free of porosity, with no cracks allowed during the service life of the pressure vessel.

B. TENSILE-STRAIN CAPABILITY IN BIAXIAL-STRESS FIELD

Efficient utilization of glass-filament strength in GFR metal tanks requires that the metal shell strain biaxially in a 1-to-1 stress field to elongation of the filaments at the burst pressure. For tankage that must have a fixed margin between the operating and burst pressures, it is necessary (to ensure optimum structural performance) that the liner material be capable of reliably attaining the ultimate strain of the glass-filament shell. This design condition requires considerable plastic deformation of the liner.

As described in Appendix A, the ultimate tensile strain of the S-HTS glass-filament shell at 75°F ranges from 2.2 to 3.0% in single-pressure-cycle burst testing, depending on specific GFR-metal-tank design parameters. At -320 and -423°F, the ultimate tensile strain of the filaments will probably range between 3.0 and 4.1%. During tank fabrication, the winding-tension strain may be as much as 0.34% (18 lb on a 20-end roving). With these values, the following metal-shell biaxial-tensile-strain capabilities are required in a 1-to-1 biaxial-stress field for optimum burst-strength performance of the filament-wound composite:

<u>Temp, °F</u>	<u>Requirement at Burst Pressure, %</u>
75	2.0 to 2.7
-320 and -423	2.7 to 3.8

From the standpoint of tensile properties, minimum-density materials displaying the required biaxial-tensile-strain capabilities are the most desirable for GFR metal tanks.

C. WELDED-JOINT PROPERTIES

Although a candidate material may show completely satisfactory parent-metal properties, welded joints necessary to fabricate the desired shape must satisfy the requirements considered below.

1. Adequate Ductility

The weld joint must have sufficient biaxial ductility to match or exceed the strain of the glass filament. Failing this, the weld joint will fracture prematurely unless additional glass-filament reinforcements or metal-shell thicknesses at the weld joint are utilized to locally control the filament-shell strain and compensate for the lack of weld-joint ductility. The minimum 1-to-1 stress-field biaxial-strain requirements desired in the weld material are the same as those established for the parent metal (2.0 to 2.7% at 75°F and 2.7 to 3.8% at -320 and -423°F to match the glass-filament strain).

2. Efficiency

A weld-joint efficiency of 100% of the parent-metal strength is desired. An efficiency in the range from 90 to 100% is acceptable, however, if sufficient ductility is obtained. A too low value will require metal-shell reinforcement at the weld-joint areas, with consequent sacrifice in the weight saving and increases in fabrication complexity and cost.

3. Fracture Toughness

Although the parent metal may have a high degree of fracture toughness over the range from 75 to -423°F, this property has more importance in a weld joint because of the cast structure of the weld-metal deposit. Fracture toughness was formerly indicated by high values obtained in the Charpy and Izod impact tests. Materials can be more accurately rated, however, through the use of notched tensile tests. By consistent use of the stress-concentration factor, K_T ,^{*} comparison of materials on the basis of their notched-to-unnotched tensile-strength ratios permits them to be rated with respect to toughness. A notched-to-unnotched strength ratio of 1.00 or greater with $K_T = 6.3$ to 7.2 is desired, but materials in the range from 0.85 to 1.00 may be considered as exhibiting acceptable toughness. Fracture toughness can also be expressed on the basis of ratios between notched tensile strength and unnotched yield strength. On this basis, for $K_T = 6.3$ to 7.2, when the notched-strength to unnotched-tensile-yield-strength ratio is 1.00 or greater, a material is considered as having adequate fracture toughness.

* The notch concentration factor, K_T , is an expression of the sharpness or acuity of the notch in test specimens. Its value increases as the notch radius decreases. For edge-notched flat specimens, K_T is determined as follows: $K_T = \sqrt{a/r}$, where a is one-half of the width between the notches and r is the notch radius.

More refined methods of evaluating fracture toughness utilize critical crack-extension-force values, G_C (in.-lb/in.²) or critical crack-toughness values, K_{IC} (ksi $\sqrt{\text{in.}}$). Because test methods are not standardized, however, G_C and K_{IC} values reported by various laboratories are not comparable, and it is practically impossible to adequately make comparisons and ratings with these parameters. Fracture toughness was consequently evaluated in this analysis primarily on the basis of the notched-strength to unnotched-tensile-strength ratio and the notched-strength to unnotched-yield-strength ratio.

4. Low-Cycle Fatigue

An important requirement for successful tank performance is the ability of the metal shell, particularly in its welded joints, to withstand 100 or more high-strain compression-tension cycles without failure. This property is designated as the low-cycle, high-strain fatigue capability of the material. A complete analysis of available data on low-cycle, high-strain fatigue resistance of candidate metal-shell materials is presented in Appendix C.

5. Weld Quality

The highest-quality weld joints commensurate with aerospace fabrication standards are required to obtain satisfactory joint properties. To meet these standards, a radiographic (X-ray) nondestructive-test quality level must be used that will provide joints with the following characteristics: (a) free of cracks in the weld metal, heat-affected zone, and adjacent parent metal; (b) no propagating defects, such as elongated porosity and inclusions; (c) minimum joint mismatch; (d) control of porosity and inclusions, with regard to size and frequency; and (e) control of weld-bead reinforcement and droptrough to minimize stress concentrations.

D. COMPRESSIVE PROPERTIES

For GFR metal tanks, it has been established that the springback stress in the metal shell due to the action of the overwrapped glass-filament shell should not exceed (1) the compressive-yield stress of the liner, or (2) the compressive-buckling stress of the liner.

Force equilibrium between the metal and glass-filament shells at the zero-internal-pressure springback condition is governed by

$$-\sigma_s t_s = \sigma_g t_g$$

where σ_s = compressive stress in metal shell at springback condition, psi
 t_s = thickness of metal shell, in.
 σ_g = tensile stress in glass-filament shell at springback condition, psi
 t_g = thickness of glass-filament shell, in.

The value of σ_g must not be greater than the metal-shell compressive-yield stress or compressive-buckling stress. For a given requirement for magnitude of springback force, $\sigma_g t_g$,* GFR-metal-tank weight is minimized by high values of σ_g and low values of t_g , because the liner weighs more than the glass-filament shell. From the standpoint of compressive properties, materials with high ratios of proportional limit to density and of buckling stress to density are the most desirable for GFR metal tanks.

E. FABRICATION CHARACTERISTICS

Suitable materials must

1. Show sufficient capability for cold or warm forming to permit small-diameter cylindrical sections for pressure vessels to be formed readily
2. Be formable into pressure-vessel head contours by means of cold or warm spinning or suitable cold-drawing fabrication techniques
3. Be readily weldable by means of the common welding techniques applicable to aerospace pressure vessels.

When cold-forming operations are performed, all permanent deformation occurs within the plastic range of a material (Ref. B-1). The lower limit of this range is the stress corresponding to the yield strength that must be exceeded to produce plastic movements. The upper limit is the stress corresponding to the ultimate strength that must be avoided to guard against rupture. A wide spread between yield strength and ultimate strength indicates that the material has high stretching ability. A narrow spread indicates that the applied stress required to produce plastic movement may closely approach the ultimate strength or rupturing point. As yield strength increases, stiffness correspondingly increases. The forces or stresses required to accomplish permanent deformation by means of cold-forming operations rise accordingly.

In the roll forming of cylindrical metal shells of 12-in. diameter and larger (such as will be required for GFR metal tanks), the bending characteristics are not of primary importance. The governing factor is the ability of the roll-forming equipment to apply sufficient pressure to exceed the yield strength and plastically form the cylindrical section desired. The required pressure will depend on the yield strength and thickness of the material used.

Materials with an initially low yield strength in the soft annealed condition and a low rate of strain hardening by cold working are

*For fixed design conditions of thickness, pressure, and diameter, the magnitude of $\sigma_g t_g$ is influenced by the relative moduli of the metal and glass-filament shells. The computerized analysis used for parametric study was used to establish the effect of metal-shell modulus on design.

better adapted to manual cold spinning than high-yield materials that cold-work-harden rapidly. Materials with a high rate of work hardening may be readily spun by mechanized means if it is possible to apply pressures sufficiently high to bring the work to intermediate shapes in one pass. Annealing to remove cold work is required between spinning operations in some materials displaying very rapid cold-working tendencies.

II. SPECIAL CONSIDERATIONS IN EVALUATION OF MATERIAL PROPERTIES

A. EFFECT OF BIAXIAL-STRESS FIELD ON TENSILE DUCTILITY

A primary area of concern in selection of metal-shell materials is the required strain capability under the 1-to-1 stress-field conditions encountered in GFR metal tanks. Available biaxial data were reviewed to establish an approximate relationship or "rule of thumb" useful in predicting the biaxial-strain capabilities of materials from their uniaxial ultimate elongation. The results of this investigation are discussed below.

The elongation or strain obtained under 1-to-1 biaxial-stress conditions depends on several factors: the work-hardening capability of the material, internal strains resulting from fabrication, and the magnitude of plastic-strain capability as compared with the elastic-strain component of the stress-strain curve. If a material exhibits considerable plastic-strain capability in uniaxial tests, the theoretical ratio of biaxial-to-uniaxial ductility of about 0.50 under 1-to-1 biaxial-stress conditions can prevail. Inherent stresses resulting from previous fabrication history, however, may lower this value.

Data were found in Refs. B-2 through B-6 for the biaxial properties of metallic materials, including Ti-6Al-4V at 75°F; Ti-5Al-2.5Sn, 300 series (Type 301 and 310) stainless steels, and 2219-T81 aluminum in the 75 to -423°F range, as well as a number of high-strength steels at 75°F. Refs. B-2 and B-4 provide data on uniaxial and biaxial elongation capabilities from 75 to -423°F. The biaxial data were obtained on cross-shaped specimens subjected to 1-to-1 and 2-to-1 stress fields. The elongation of uniaxial test specimens was measured with 1.0- and 2.0-in. gage-length extensometers; for the biaxial test specimens, 1/2-in. gage-length strain gages were used. (The difference between 1/2- and 1-in. gage lengths results in relatively larger apparent strains under biaxial-loading conditions than would be indicated if the lengths were identical for both uniaxial and biaxial specimens; this makes conclusions reached below tend to be optimistic rather than conservative.)

Data on uniaxial and biaxial ductility from Refs. B-3 and B-4 are summarized in Tables B-1 and B-2 for 301 SS (3/4 to full hard), Ti-6Al-4V (annealed), AM-355 SS (SCT), 300-series 18%-nickel maraging steel, 310 SS (3/4 hard), Ti-5Al-2.5Sn (annealed, ELI grade), and 2219-T81 aluminum. Representative 75°F uniaxial-strength properties are indicated there.

Figures B-1 to B-3 present biaxial-to-uniaxial ductility ratios at 75 to -423°F for Ti-5Al-2.5Sn, 310 SS (3/4 hard), and 2219-T81 aluminum (data given in Table B-2). Although in most instances there is a large scatter in the data, Figures B-1 to B-3 clearly indicate that the 1-to-1 stress state is the most severe or demanding condition from the standpoint of ductility, based on the reductions of elongation produced by that state as compared with the 1-to-1 or 2-to-1 states. In addition, the biaxial-to-uniaxial ductility ratios obtained from the cross specimens indicate that this ratio is less predictable than other mechanical properties. The following tabulation is based on data shown in Figures B-1 to B-3:

Temp, °F	Average Values for $\left(\frac{\text{Biaxial Elongation in 0.5 in.}}{\text{Uniaxial Elongation in 1 in.}} \right)$	
	1-to-1 Stress Field	2-to-1 Stress Field
75	0.59	0.47
-105	0.36	0.69
-320	0.38	0.81
-423	0.65	1.08

On the basis of the data, the following design criterion was adopted: The allowable material ductility in a 1-to-1 stress field is 25% of the uniaxial ductility over the entire 75 to -423°F range. Almost all data points in Figures B-1 to B-3 fall above this value. The rule is applicable to both unwelded and welded materials. Under this standard, materials must have the following uniaxial-elongation values to achieve the full strength potential of the glass-filament shell:

Temp, °F	Metal-Shell Tensile Strain in 1-to-1 Stress Field at Burst Pressure, %	Required Uniaxial Elongation to Meet Biaxial-Strain Requirement, %
75	2.0 to 2.7	8.0 to 10.8
-320 and -423	2.7 to 3.8	10.8 to 15.2

B. EFFECT OF BIAxIAL-STRESS STATE ON OTHER PROPERTIES

McClaren and Foreman (Ref. B-4) have reported the effects produced on tensile properties by multiaxial loading conditions. Comparative data for 2219-T81 aluminum, Ti-5Al-2.5Sn (ELI grade), and cold-rolled 301 SS for 1-to-0, 2-to-1, and 1-to-1 stress states are shown in Figures B-4 to B-6 for room-temperature, -320°F, and -423°F conditions. The most significant effect on the strength properties of all three alloys appears to occur with the 2-to-1 stress state at all exposure temperatures. For the 1-to-1 state, which is the condition prevalent in GFR metal tanks, the ultimate-tensile and tensile-yield strengths are nearly the same as the uniaxial values (1-to-0 stress state). However, the modulus of elasticity (Figure B-6) varies with change in stress state, showing maximum values with the 1-to-1 condition.

C. BAUSCHINGER EFFECT

For most metals free of residual stresses, the yield strength in tension is equal to the yield strength in compression. It has been observed, however, that when some materials are strain-hardened by initial stressing into the plastic range, the yield-strength increase is observable only in the direction of initial loading, and there may be a reduction from the original yield strength in the opposite direction. As illustrated by the tension-compression curves of Figure B-7, there is an unequal elevation of the flow limit or often an actual reduction when the flow stress is reversed. If the first load application is made in tension and the second in compression, the stress-strain curve would not be raised in the compression test but would tend to be lowered, resulting in a decrease in the compressive-yield strength. The original equality of behavior with respect to tension and compression is destroyed.

This phenomenon is the Bauschinger effect; it was named for its discoverer, who reported his observations in 1881. Bauschinger described it as a lowering of the elastic limit in compression after a stress in tension beyond the elastic limit. Conversely, the elastic limit in tension is reduced for a material strained beyond the elastic limit in compression.

The Bauschinger effect can be produced by a number of conditions imposed on a metal: e.g., cold stretching or cold forming resulting in residual stresses in titanium and its alloys (Ref. B-8). Other sources of residual stresses are processing operations or treatments involving differential heating and cooling rates, joining operations, machining, grinding, etc. The Bauschinger effect also appears in cold-rolled production metals when the high-strength properties are developed by strain hardening during rolling; in such cases (e.g., Type 301 SS) the tensile strength along the rolling direction is increased, but the compressive strength is reduced.

Data on the Bauschinger effect for several materials are presented in Refs. B-7 to B-11. The indication is that, for these materials, most of the effect is produced by prestrains smaller than about 1% and that very little increase is produced by prestrains greater than 1%. The magnitude of the Bauschinger effect, evaluated by the ratio σ_R/σ_T , where σ_T is the initial yield stress in tension and σ_R is the yield stress in the reversed direction of loading after application of the tensile load, is as low as 0.35 for Type 4330 steel. However, the magnitude seems to vary between the materials tested. No correlation has been found between Bauschinger effect and fatigue life or the manner in which yield stresses vary during fatigue testing.

Contrary to these observations, Ref. B-12 presents strain-cycling data for 16 materials, including the candidate materials Ti-6Al-4V and Inconel X-750. Type 304 ELC stainless steel (annealed and hard tempers) and 2014-T6 aluminum were also evaluated in the study, and are considered comparable with the candidate materials 301 SS and 2219-T62 aluminum, respectively. The following observation is made in Ref. B-12: ". . . during zero mean strain fatigue testing . . . the maximum compressive and tensile stresses during any one cycle remained approximately equal to one another throughout the test. In other words, cyclic strain hardening or softening affected the peak tensile

or compressive stresses equally, and the mean stress throughout a test was zero." This result provides a basis for ignoring the Bauschinger effect in analyzing the mechanical properties of candidate metal-shell materials.

D. CHANGE OF METAL PROPERTIES DURING STRAIN CYCLING

When metals are subjected to cycling between fixed strain limits near or above the proportional limits, the stress range generally changes during the test. If the stress range increases with the number of cycles, the material is called a cyclic-strain-hardening one; a decreasing stress range characterizes a cyclic-strain-softening material. The most significant stress-range changes for many materials occur within the first 20% of specimen life. During the remaining 80% or more, the stress range remains relatively constant; this range, $\Delta\sigma$, is considered as a characteristic value corresponding to the applied strain range. Because of the resultant effect on the GFR-metal-tank stress-strain relationship, the strain-hardening or strain-softening properties of candidate metals were considered to require identification in the characterization analysis. This subject is reviewed in Appendix C.

E. DUCTILE-BRITTLE TRANSITION TEMPERATURE

Candidate materials should not exhibit a transition from the ductile to the brittle type of failure in the range from 75 to -423°F . The ductile-to-brittle transition may be identified by a sharp decrease in notched tensile strength (or notched-to-unnotched tensile-strength ratio) as the test temperature is reduced; the transition is verified by an examination of the fracture surface. Materials should not be used in GFR metal tanks below their ductile-brittle transition temperatures.

F. POISSON'S RATIO

The designing of GFR metal tanks requires calculation of the metal-shell strains under multiaxial loading in each of the principal directions, taking into account each of the principal stresses and Poisson's ratio. Because the tanks will be used at 75 to -423°F , the effect of low temperatures on Poisson's ratio must be evaluated. Very few data are available on Poisson's ratio at subzero temperatures, particularly for specific alloys. Figure B-8 summarizes the available data (from Refs. B-4 and B-13) on Poisson's ratio as a function of temperature at 75 to -423°F for some metals and alloys in the classes under consideration. On the basis of the latest developed data (Ref. B-4), it may be assumed that Poisson's ratio is practically constant at 75 to -423°F .

III. BASIS OF CHARACTERIZATION ANALYSIS

A. SCOPE

All available properties in tension and compression at 75, -320 , and -423°F that could be located in an extensive literature survey were assembled for each candidate metal-shell material in the unwelded and welded

conditions. These data were analyzed to establish characteristics under the service conditions imposed. The properties examined included longitudinal and transverse, uniaxial and biaxial, stress-strain characteristics; weld-joint efficiency and ductility; fracture toughness; low-cycle, high-strain fatigue characteristics; Poisson's ratio; thermal contraction; and fabrication characteristics. Table B-3 provides a detailed summary of the characteristics used to evaluate the candidate materials.

B. SOURCES OF DATA

The data sources included the Air Force Materials Laboratory Cryogenic Materials Data Handbook (Ref. B-14), Metallic Materials and Elements for Flight Vehicle Structures (MIL-HDBK-5, Ref. B-15), U.S. Government agency technical reports, Defense Metals Information Center (DMIC) reports and memoranda, papers published in technical periodicals, and suppliers' literature. At Battelle Memorial Institute, DMIC specialists in each area of interest were consulted to obtain additional data needed for completion of the characterization analysis.

C. EVALUATION OF TECHNIQUE USED

A complete compilation of all the properties listed in Table B-3 was not required for the preliminary rating of candidate materials. Initially, the uniaxial characteristics of each candidate were summarized and its problem areas were identified. With this as a basis, the material or materials in each class of alloys most suitable for metal-shell use were identified. These were then completely evaluated on the basis of all characteristics listed in Table B-3 and were rated in preferential order for use in GFR metal tanks for cryogenic service.

IV. CHARACTERIZATION ANALYSIS

A. CLASSES OF ALLOYS

The alloy classes evaluated are reviewed briefly below, with an indication of the suitability of each for cryogenic-temperature service. The preliminary rating of the classes is based on ductility and fracture-toughness information presented in Ref. B-14.

1. Low-Alloy Steels, Medium and High Strength

This class of materials is unsatisfactory for service at cryogenic temperatures due to a transition from ductile to brittle behavior at about -100°F . The extremely low elongation values at -320°F and below eliminate all these alloys from consideration.

2. Precipitation-Hardening Stainless Steels

A rapid decrease in elongation below -320°F to practically 0% at -423°F and a sharp drop in the notched-to-unnotched strength ratio below -100°F (ductile-to-brittle transition) eliminate these materials from consideration.

3. Martensitic Stainless Steels

A ductile-to-brittle transition temperature of 0°F as indicated by impact tests and low elongation values at temperatures below -200°F make these materials unsatisfactory for this application.

4. Austenitic Stainless Steels

The austenitic stainless steels, in general, provide very satisfactory ductility properties for cryogenic service, particularly in the annealed condition. However, the initial room-temperature compressive-yield strength of the annealed material is too low to provide the optimum thickness for the metal shell of a GFR metal tank. These alloys can only be strengthened by cold working, and the increased compressive-yield strength with adequate tensile ductility required to minimize metal-shell thickness necessitates the use of a cold-rolled temper. Because such tempers are most readily available in Type 301 austenitic stainless steel, this type of material was considered suitable for evaluation and rating in tempers ranging from annealed through 1/4 hard, 1/2 hard, 3/4 hard, full hard, and extra full hard. Other types of austenitic stainless steels in cold-worked tempers may be superior to Type 301 in some property areas; because their cold-worked tempers are only available by means of special mill orders, they were eliminated from the characterization analysis.

5. Titanium-Base Alloys

High strength-to-density ratios make the titanium-base alloys very attractive when a marked degree of weight saving is desired. In GFR metal tanks, the high compressive-yield-strength-to-density ratios and low elastic modulus make titanium an attractive material if sufficient tensile ductility can be obtained. When both weldability and service at cryogenic temperatures are involved, the Ti-6Al-4V alpha-beta alloy and the Ti-5Al-2.5Sn all-alpha alloy appear to be those most generally used. The Ti-6Al-4V and Ti-5Al-2.5Sn alloys, normal interstitial grade, provide satisfactory properties down to -320°F. However, for service to -423°F, the extra-low-interstitial (ELI) grades are generally preferred because of the increased ductility and toughness obtainable below -320°F. Ti-5Al-2.5Sn (ELI grade) appears to be preferable for its superior weldability. Consequently, the characterization analysis concentrates primarily on the ELI grades.

6. Aluminum-Base Alloys

The aluminum-base alloys, on exposure to cryogenic temperatures, not only show increased strength as the temperature decreases but generally also improve in ductility, as evidenced by increasing elongation values. These factors, together with favorable compressive strength-to-density ratios, make them attractive for use in GFR metal tanks. Because weldability and weld-joint strength are key considerations in the evaluation of aluminum alloys, the newly developed, weldable, high-strength alloys in the 2219 and 7000 series are worthy of thorough analysis.

7. Nickel-Base Alloys

Originally developed for elevated-temperature applications, these alloys appear to provide very satisfactory performance at cryogenic temperatures. Most show improved ductility as the exposure temperature decreases from 75 to -423°F . In addition, strengths comparable to those of cold-worked stainless steels are obtainable by means of heat treatment without deleterious directionality effects. A review of readily available alloys indicates that the Inconel X-750 and Inconel 718 materials are the most promising candidates for metal-shell fabrication. The complete characterization analysis includes Inconel X-750, chosen as the most suitable of the two in a detailed review.

8. Cobalt-Base Alloys

The cobalt-base alloys, also originally developed for elevated-temperature applications, to date have undergone only very limited investigation for service at cryogenic temperatures. The Haynes 25 alloy, however, appears to have very satisfactory properties to -423°F , particularly high elongation and notched-to-unnotched strength ratios, and was considered worthy of inclusion in the complete characterization analysis.

B. ANALYSIS OF SELECTED, CANDIDATE, METAL-SHELL MATERIALS

1. Type 301 SS

This material is available in various strength levels ranging from the soft-annealed temper to the high-strength extra-full-hard temper. Because it is not hardenable by means of heat treatment, the various strengths are obtained by varying the amount of cold reduction applied. Typical room-temperature strengths for the various tempers are summarized in Table B-4. In tension, a slight directionality effect is apparent in the cold-worked grades. In compression, the effect in the rolling direction is very severe; a wide difference exists in the compressive-yield strength in the longitudinal direction as compared with the transverse. A stress relief at 750 to 1000°F may be used, however, to reduce these differences. The effect of stress relief is shown in Table B-5.

Figures B-9 and B-10 show the effect of exposure at 75 to -423°F on the tensile-yield strength, ultimate strength, and elongation for the different tempers of 301 SS as reported by various workers. No data were located for the effect of cryogenic-temperature exposure on the various cold-worked tempers that had been stress-relieved as indicated in Table B-5.

a. Extra-Full-Hard Temper

The extra-full-hard temper does not have enough elongation in the as-rolled or stress-relieved conditions to meet the minimum uniaxial-strain requirements, of 8.0 to 10.8% at 75°F and 10.8 to 15.2% at -320 and -423°F , that must be satisfied if the metal-shell biaxial strain is to match that of the glass-filament shell at the burst pressure. In addition,

the transverse notch toughness is poor from 75 to -423°F , as indicated by reported values of 0.40 to 0.50 for the notched-to-unnotched strength ratio at $K_T = 7.2$. These deficiencies, along with poor forming qualities at small diameters, results in a rating for the extra-full-hard temper of 301 SS as unsatisfactory for the present application.

b. Full-Hard Temper

The full-hard temper in the as-rolled condition has extreme differences in compressive-yield strength in the longitudinal and transverse directions and very low elongation at -423°F . When stress-relieved to minimize the directionality effect on compressive-yield strength, the ductility is adversely affected, resulting in values below the minimum required. These deficiencies, along with poor forming qualities at small diameters, make the full-hard temper of 301 SS unsatisfactory for this application.

c. 3/4-Hard Temper

As indicated in Figure B-10, this temper has satisfactory ductility at 75 to -423°F . The tensile-property effect of thicknesses in the range from 0.015 to 0.063 in. is shown in Figure B-11. For these thicknesses, the minimum elongation requirement is exceeded in the longitudinal direction over the entire temperature range; the transverse-elongation effect of exposure to cryogenic temperatures was not available. When this temper is stress-relieved to improve the compressive-yield strengths, a reduction in room-temperature elongation occurs (see Table B-5). This elongation, although slightly in excess of the minimum uniaxial-strain value required at 75°F , may not meet the values required at -320 and -423°F . This conclusion is based on assumption that the elongation of stress-relieved material will have the same trend as non-stress-relieved material as the service temperature is lowered from 75 to -423°F .

The notch toughness of as-rolled 3/4-hard Type 301 SS is shown in Figure B-12 on the basis of notched-to-unnotched strength ratio and in Figure B-13 on the basis of notched-strength to unnotched-yield-strength ratio. With a stress-concentration factor of $K_T = 7.2$, all thicknesses of the 3/4-hard temper have notched-to-unnotched ultimate-strength ratios of less than 1.00 at temperatures lower than about 0°F for 0.015- and 0.020-in. sheet and throughout the 75 to -423°F range for 0.063-in. sheet. A notched-strength to unnotched-yield-strength ratio in excess of 1.00 should therefore exist if the material is to be considered as having satisfactory notch toughness. As shown in Figure B-13, the 3/4-hard temper in general has a notched-strength to unnotched-yield-strength ratio of 0.90 to 1.00 at -423°F with $K_T = 7.2$ (this condition would be equivalent to a defect containing a sharp notch of approximately 0.005-in. radius). On the basis of notch toughness, 301 SS (3/4 hard) is unsatisfactory for service at -423°F .

d. 1/2-Hard, 1/4-Hard, and Annealed Tempers

The remaining tempers of 301 SS exhibit sufficient parent-metal ductility, throughout the 75 to -423°F range, to exceed the uniaxial-strain requirement of 8.0 to 10.8% at 75°F and 10.8 to 15.2% at -320 and -423°F (see elongation values in Figure B-10). After a stress relief of 2 hours at 1000°F , the compressive-yield strength of the 1/4- and 1/2-hard tempers is almost equalized in the longitudinal and transverse directions (Table B-5). This is accomplished with only a slight decrease in the ultimate tensile and yield strengths, but with a significant increase in elongation.

Very few data are available on the notch toughness of parent metal and on any properties of weldments at 75 to -423°F . The investigations have been confined entirely to the full-hard and extra-full-hard tempers (the strength levels desired for use in large-diameter vessels for which segments could be formed cold with the use of large bending radii).

With $K_T = 21$ representing a sharp notch defect of about 0.001-in. radius, the 1/2-hard temper would be satisfactory for service down to approximately -10°F . This observation is based on the notched-strength to unnotched-yield-strength ratio of 1.00 or greater from 75 to -10°F indicated in Figure B-14. It is a general opinion in the aerospace industry, however, that sharp notch defects, as represented by $K_T = 7.2$ to 10, are more representative of fabrication practices. For ultra-high-strength metals, the very sharp notch represented by $K_T = 21$ may be an important evaluation factor. Because the 1/4-hard and 1/2-hard tempers have a ductility considerably superior to that of the 3/4-hard temper, they should have notched-strength to unnotched-yield-strength ratios in excess of 1.00 from 75 to -320°F in the presence of notches with $K_T = 7.2$ to 10. This opinion is assumed correct in the characterization analysis, but test data are required to assure that satisfactory performance can be expected when these tempers are used for GFR metal tanks.

e. Comparison of Weldment Properties

The published data on weldment strengths and the resulting weld-joint efficiencies are primarily limited to the extra-full-hard temper. For 0.013- to 0.100-in. thicknesses this temper had weld-joint efficiencies of about 65 to 72% at 75°F . At -320°F , these values increased to the range from 85 to 93%. With a decrease to -423°F , however, evidence of weld-joint embrittlement was given by a decrease in efficiency values to those obtained at 75°F . Metal shells designed on the basis of the parent-metal properties would thus require considerable weld-joint reinforcement to compensate for the low efficiency at 75 and -423°F .

Limited information on weld-joint properties was found for a 0.016-in. thickness of 3/4-hard 301 SS (see Figure B-15). Although some improvement in weld-joint efficiency is indicated, reinforcement would be necessary, particularly at 75°F . Although weld-joint elongation at 75 and -320°F appears satisfactory, the extremely low value (3%)

at -423°F is far less than the minimum uniaxial value of 10.8 to 15.2% needed to match the biaxial strain of the glass-filament shell at the burst pressure. No weld-joint properties were located for the 1/4-hard and 1/2-hard tempers, and it is assumed that the performance will be the same as that of the 3/4-hard temper. The effect on welded-joint properties of stress relief after welding at 750 to 1000 $^{\circ}\text{F}$ is not known. Knowledge of properties in the as-welded and as-welded-and-stress-relieved conditions is therefore required for proper design and fabrication of the metal shell from 1/4-hard or 1/2-hard 301 SS.

f. Fabrication Characteristics

For 301 SS in the full-hard and extra-full-hard tempers, the pressures required to form cylindrical sections in diameters presently contemplated for GFR metal tanks may be beyond the capability of existing roll-forming equipment for the necessary thicknesses. On the basis of cold-bending characteristics, the 3/4-hard temper in thicknesses up to 0.050 in. may be satisfactorily formed if metal stresses below 175,000 psi but above 145,000 psi can be obtained. The 1/4-hard and 1/2-hard tempers in thicknesses up to 0.187 in. can be formed readily.

The high rate of work hardening inherently associated with 301 SS makes manual-spinning operations of severe character impractical. Annealed or possibly 1/4-hard 301 SS may be spun, however, by mechanized means if pressures sufficiently high to shape the work in one pass can be used. The higher-strength tempers are not adaptable to cold-spinning operations, due to the excessively high pressures required.

Type 301 stainless steels are readily weldable by all the common joining processes. For the metal-shell thicknesses required, the tungsten-inert-gas or metal-inert-gas methods are preferred. To reduce warpage and distortion, it is necessary to avoid excess heat buildup in the weld-joint area by means of copper backup strips to accelerate cooling.

As indicated in Table B-5, a stress-relief heat treatment at 800 to 1000 $^{\circ}\text{F}$ will improve the parent-metal compressive-yield strength of the cold-worked tempers of 301 SS with no major effect on the tensile properties. A new stress-aging treatment developed by Watervliet Arsenal (Refs. B-16 and B-17), when applied to cold-rolled austenitic stainless steels, results in a large increase in the proportional limit and elimination of the directionality effect on compressive properties. However, this approach requires the application of a stress to the component during the stress-relief heat treatment, and its use for metal-shell fabrication is not considered practical at present.

A fabrication technique that warrants future consideration is cryogenic stretch forming (Ardeform process) developed by Arde-Portland, Inc. of Paramus, New Jersey (Refs. B-18 and B-19). The metal shell could be fabricated, including all welding, from 301 SS in the annealed temper. After fabrication, the metal shell would be cryogenically stretched in a suitable die to the desired strength level and sized. Because the

parent metal and weld joints are strained simultaneously, practically 100% weld-joint efficiency is obtainable. A complete characterization analysis of 301 SS strengthened in this manner is necessary to determine the performance capabilities for the present application.

g. Preliminary Rating of Material

On the basis of superior fabrication characteristics, notch toughness, and ductility, the 1/2-hard temper of Type 301 SS appears to offer the maximum strength level usable in this alloy class for the fabrication of GFR metal tanks for use at 75 to -423°F. The low weld-joint efficiency and inferior compressive-yield strength in the longitudinal direction are the most unfavorable characteristics of this material. Because a stress relief of 4 to 8 hours at 800 to 1000°F results in improved room-temperature parent-metal properties, it is assumed that weld-joint and parent-metal properties at 75 to -423°F will not be detrimentally affected by such treatment. However, a complete analysis of material stress-relieved after welding should be performed to determine all significant properties over this range.

2. Titanium-Base Alloys

The titanium-base materials most frequently used to fabricate pressure vessels are the Ti-6Al-4V alpha-beta alloy and the Ti-5Al-2.5Sn all-alpha alloy, because of their welding characteristics. Although the latter exhibits slightly lower tensile properties, it is frequently preferred because of its superior weldability. Both are available in a normal-interstitial-content grade and an extra-low-interstitial grade. The interstitial content has a marked effect on the properties obtained at cryogenic temperatures, as noted below.

a. Ti-6Al-4V

(1) Normal-Interstitial Grade

The tensile properties of the annealed normal-interstitial grade of this alloy for sheet thicknesses ranging from 0.040 to 0.090 in. are shown in Figures B-16 through B-19 for the 75 to -423°F range. The effect of the rolling direction appears to be negligible. As indicated in the figures, the ultimate-tensile and tensile-yield strengths increase from typical values of 140,000 psi for the ultimate tensile strength and 130,000 psi for the yield strength at 75°F to around 260,000 and 250,000 psi, respectively, at -423°F. The ductility as represented by percentage of elongation is at an acceptable level of 10 to 15% at 75°F. When the temperature is lowered to -423°F, the elongation in general drops to less than 5%. At -320°F, some reported values are under the 10% minimum required for high-burst-strength performance. Susceptibility to sharp notch effects is indicated by the low notched-to-unnotched strength ratio of 0.60 to 0.70 at -423°F with the comparatively small notch-concentration factor, K_T , of 7.2, as shown in Figure B-20. When analyzed on the basis of notched-strength to

unnotched-yield-strength ratio, the normal-interstitial-grade alloy again exhibits poor notch toughness; the ratio at -423°F ranges from approximately 0.65 to 0.85.

Although the strength of the normal-interstitial grade can be increased 25 to 30% by a solution heat treatment plus aging, its ductility is drastically lowered. The heat-treated material shows only about 5% elongation at 75°F , as compared with 10 to 16% for the annealed condition. At -423°F , the solution-treated and aged (STA) material shows practically no ductility, its elongation being only 1%. The STA, normal-interstitial material can therefore be eliminated from further consideration.

(2) Extra-Low-Interstitial (ELI) Grade

By limiting the interstitial element oxygen to a maximum of 0.13% and placing a slightly lower maximum limit on iron and carbon, a low-interstitial grade of Ti-6Al-4V is obtained that reportedly provides better ductility and notch toughness at -423°F than obtainable with the normal-interstitial grade. The ultimate-tensile and tensile-yield strengths at 75 to -423°F obtainable with the ELI grade (Figures B-21 to B-24) are comparable to those indicated for the normal-interstitial grade. Although some ductility improvement at -423°F is evidenced by reported elongation values in the range from 6 to 12%, this improvement does not appear to be consistently obtainable in the ELI grade; some elongation values in the range from 1 to 5% were reported at -423°F . It is possible that with closer control of the harmful interstitial elements, improved ductility at -423°F can be consistently obtained. Notch toughness is shown in Figure B-25. With $K_T = 7.2$ to 8.0, the notched-to-unnotched strength ratio at -423°F ranges from about 0.75 to 1.00, a considerable improvement over the 0.60 to 0.70 reported for the normal-interstitial grade. On the basis of notched-strength to unnotched-yield-strength ratio, values of approximately 0.80 to 1.05 are indicated, with at least 50% of the reported values below the ratio of 1.0 required for satisfactory notch toughness. On the basis of a very sharp notch as represented by $K_T = 21$, this grade in general shows inadequate notch toughness at about -100°F and below.

The ELI grade of Ti-6Al-4V when solution-heat-treated and aged shows no improvement in ductility or notch toughness over the values obtained with the normal-interstitial grade similarly treated. Therefore, it can be eliminated from further consideration.

(3) Weldment Properties

The as-welded properties of sheet material that is tungsten-inert-gas (TIG) welded in the annealed condition are shown in Figures B-26 and B-27. The weld-joint efficiencies of both grades of Ti-6Al-4V are excellent over the entire 75 to -423°F range, being 95% or greater.

With respect to weld-joint ductility as evaluated by percentage of elongation, one set of data on the normal-interstitial grade indicated acceptable ductility at 75°F (10% elongation) with

values below the 10% desired minimum at -320 and -423°F . A second set of values reported by others showed elongation values over the entire temperature range (4% maximum at 75°F to 1.5% minimum at -423°F) to be far below the minimum required.

No information on the elongation obtainable in welds made with mill-annealed ELI-grade Ti-6Al-4V were located. Because it appears that extremely low parent-metal elongation values may be characteristic at -423°F , high elongation cannot be expected in the weld joints fabricated from the ELI grade.

(4) Rating of Material

Because of poor ductility and inadequate notch toughness at -423°F in the parent metal and inconsistent ductility in weld joints at 75 to -423°F , the normal-interstitial and ELI grades of Ti-6Al-4V in the annealed condition were not considered suitable for the application under consideration.

b. Ti-5Al-2.5Sn

This alloy cannot be strengthened by means of heat treatment, and is evaluated below in the mill-annealed condition only.

(1) Normal-Interstitial Grade

The tensile properties for annealed sheet in thicknesses ranging from 0.016 to 0.064 in. are shown in Figures B-28 to B-31. This alloy shows increasing ultimate tensile strength and tensile-yield strength at 75 to -423°F . Mill-annealed sheet with typical values of 125,000 psi for the ultimate tensile strength and 120,000 psi for the tensile-yield strength at 75°F will increase to about 250,000-260,000 and 240,000-250,000 psi, respectively, at -423°F . Ductility as indicated by percentage of elongation is generally in the range from 12 to 16% at 75 to -320°F . When the exposure temperature is lowered to -423°F , however, the elongation decreases to 3 to 8%. The notch toughness as indicated by notched-to-unnotched strength ratio is shown in Figure B-32. A ratio of 0.80 to 0.86 at -423°F with $K_T = 7.2$ is an improvement over the 0.60 to 0.70 reported for Ti-6Al-4V (normal-interstitial grade). However, the notch-toughness rating of normal-interstitial-grade Ti-5Al-2.5Sn at -423°F is still below the desired 0.90 to 1.00. On the basis of notched-strength to unnotched-yield-strength ratio, these values convert to approximately 0.83 to 0.90 (still under the desired minimum of 1.00). With $K_T = 7.2$, the notch toughness of the normal-interstitial grade of Ti-5Al-2.5Sn is adequate to -320°F , as indicated by notched-to-unnotched ratio values of 1.00 and above. In the presence of very sharp notches as represented by $K_T = 21$, however, the notch toughness is inadequate below approximately -100°F .

(2) ELI Grade

By lowering the maximum-allowable limits on iron, oxygen, manganese, carbon, and hydrogen, an ELI grade of the Ti-5Al-2.5Sn is obtained for which remarkably higher ductility and notch toughness at -423°F are claimed. Tensile properties for annealed sheet in thicknesses ranging from 0.014 to 0.040 in. are shown in Figures B-33 and B-34. A sacrifice of about 10,000 to 15,000 psi in both the ultimate-tensile and tensile-yield strengths over the range from 75 to -423°F will be necessary because of the slight decrease in hardening effects resulting from the lower interstitial content. It is compensated, however, by increased ductility and notch toughness. The ductility improvement is evidenced by the 15 to 20% elongation obtained at 75°F , with 12 to 15% retained at -423°F . The notch toughness at -423°F ranges from 0.98 to 1.10 (notched-to-unnotched strength ratio) with $K_T = 7.2$, as indicated in Figure B-35. Even for a very sharp notch as represented by $K_T = 21$, the ELI grade shows superior notch toughness to -300°F as indicated by a notched-to-unnotched strength ratio of 1.00 to 1.04. In the unwelded state, it appears to provide adequate ductility and notch toughness at 75 to -423°F , to make it suitable for the metal shell of GFR metal tanks for cryogenic service.

(3) Weldment Properties

The tensile properties of the mill-annealed normal-interstitial grade of Ti-5Al-2.5Sn welded by the TIG technique are shown in Figures B-36 and B-37 for the as-welded condition. It was assumed the weld bead was not ground flush (not specified in source). The average weld-joint efficiencies ranged from 95 to 100% at 75 to -423°F . The weld-joint ductility was retained at 10% elongation or higher at 75 to -320°F ; at -423°F , however, the weld-joint elongation decreased to 4 to 5%. Thus, at -320 to -423°F , the elongation is below the 10.8% minimum desired.

The tensile properties of as-welded ELI Ti-5Al-2.5Sn similarly fabricated are shown in Figures B-38 and B-39. The weld-joint efficiencies appear to vary from 90 to 100% over the 75 to -320°F range, except for one set of data that showed about 84% at 75°F , rising to 92 to 95% at -320°F . When the temperature is lowered to -423°F , however, the joint efficiency shows a trend toward decreasing to 90 to 95%. The limited amount of elongation values located to date on the weld joints for this material does not permit suitable evaluation over the 75 to -320°F range, and more data are required for ELI-grade weldments. At -423°F , the trend indicates, the ductility may be below the 10.8% minimum elongation desired.

The weldment properties do not appear to show any advantage over those obtainable with the normal-interstitial grade, probably because filler metal was used that had a higher interstitial content than the parent metal. Unless ELI filler metal is used during welding, the increased ductility and notch toughness obtainable in the parent metal can be nullified in the welds. With the use of the proper filler-metal grade, it is assumed that elongation of 12% may be obtained in weld joints

of this material over the entire 75 to -423°F range. With this assumption, together with superior parent-metal ductility and notch toughness to -423°F , Ti-5Al-2.5Sn (ELI grade) is the most suitable of the titanium alloys for use in the present application.

(4) Creep

An unfavorable characteristic reported for titanium alloys is that of room-temperature creep, which appears to be particularly serious in the ELI grades of Ti-6Al-4V and Ti-5Al-2.5Sn (Refs. B-20 and B-21). The room-temperature creep may be significant at stresses above approximately 60% of the tensile-yield value. In tests conducted by AiResearch Manufacturing Company (Ref. B-22), it was demonstrated that appreciable creep will occur in Ti-5Al-2.5Sn (ELI grade) at -320°F when stressed at 95% of its -320°F yield strength. This low-temperature-creep phenomenon may occur in compression as well as in tension. Creep of the metal shell in tension should not be a problem, due to the support provided by the glass filaments, but creep in compression could affect shell performance after a limited number of strain cycles in the metal shell during pressure cycling of the tanks.

c. Fabrication Characteristics

Stiffness permits only a limited amount of cold forming to be performed on titanium alloys. When forming operations are performed at 800 to 1300°F , however, increased ductility, reduced spring-back, and lower forming pressures are obtained. Hot forming is therefore generally preferred, but combinations of cold and hot-forming operations are utilized whenever possible, to minimize the costs of tooling and processing operations in hot forming. The generally applicable operations are hydraulic-press forming, power-brake forming, stretch forming, and drop-hammer forming.

Both grades of Ti-6Al-4V and Ti-5Al-2.5Sn can be successfully fusion-welded, with the TIG process preferred for sheet thicknesses up to about 0.125 in. (Ref. B-23). Titanium at welding temperatures has a high affinity for oxygen and nitrogen, which will embrittle the weld, and extreme care must be exercised to completely shield the material from contact with air during welding. The weld zone must therefore be thoroughly blanketed with an inert atmosphere, such as argon or helium gas.

Residual welding stresses approaching the yield strength of the weld metal are possible in titanium structures. Their magnitudes depend on the rigidity of the structure and the restraint imposed on the weld. With high residual stresses in a structure subjected to stress, the weld may plastically deform at low values of applied stress. If the weld does not have sufficient ductility and toughness to deform in the presence of weld defects, the residual stresses (and/or applied stresses) may cause failure. It has been determined (Refs. B-23 and B-24) for service at cryogenic temperatures that a stress-relief anneal of titanium-alloy weldments is beneficial and desirable because improved tensile-elongation values

are obtainable. For Ti-5Al-2.5Sn the following conditions are recommended:

<u>Stress-Relieving Temperature</u> <u>°F</u>	<u>Time at Temperature</u> <u>hours</u>
900	20
1000	6
1100	2
1200	1

d. Preliminary Rating of Material

The ELI grade of Ti-5Al-2.5Sn is rated as the most suitable of the titanium alloys for fabrication of the metal shell for GFR metal tanks intended for service at 75 to -423°F.

3. Aluminum-Base Alloys

a. Aluminum Alloy 2219

(1) Solution-Treated, Cold-Worked and Aged - T87 Temper

The T87 temper provides the highest strength level for the 2219 aluminum alloy in the unwelded condition. The effect of exposure at 75 to -423°F on the tensile properties of 0.063- to 2.00-in.-thick sheet and plate are shown in Figures B-40 and B-41. Typical properties are a 70,000-psi ultimate tensile strength, 59,000-psi tensile-yield strength, and 12% elongation at 75°F. With cryogenic exposure, all tensile properties increase as the temperature is lowered, reaching the following maximum values: about 100,000-psi ultimate tensile strength, 75,000-psi tensile-yield strength, and 15% elongation at -423°F.

Figure B-42 shows the notch toughness. The notched-to-unnotched strength ratio using $K_T = 7.2$ ranges from 0.98 at 75°F to 0.91 at -423°F, which on a notched-strength to unnotched-yield-strength basis would show values in excess of 1.00. In the presence of a very sharp notch ($K_T = 21.6$), the notch toughness of 2.00-in. plate is low.

These data indicate that 2219-T87 aluminum will provide adequate ductility and notch toughness in the unwelded condition at 75 to -423°F, if there are no defects in excess of that represented by a notch with $K_T = 7.2$ to 8.0. Consideration of weld-joint properties (covered in paragraph IV,B,3,a,(3), below), however, indicated that weldments of this material are unsatisfactory. For this reason, the effect of reheat-treating to the temper after welding was examined, as discussed below.

(2) Solution-Treated and Aged - T62 Temper

The effects of exposure at 75 to -423°F on the tensile properties of 2219-T62 aluminum are shown in Figures B-43 and B-44

for sheet material. In the unwelded condition, this alloy has the following typical 75°F values: 60,000-psi ultimate tensile strength, 44,000-psi tensile-yield strength, and 11% elongation. The tensile properties (except elongation) are somewhat lower than those of the T87 temper because the user applies heat treatment to obtain this temper and no cold work is normally applied after the solution treatment. At cryogenic temperatures, all the tensile properties increase as the temperature is lowered, reaching the following values at -423°F: 93,000-psi ultimate tensile strength, 58,000-psi tensile-yield strength, and 15 to 18% elongation. As indicated in Figure B-45, the notched-to-unnotched strength ratio with $K_T = 8.0$ varies from 0.93 at 75°F to 0.77-0.80 at -423°F. The limited data located indicate that the notch toughness in this temper may be slightly inferior to that in the T87 temper; however, a notched-strength to unnotched-yield-strength ratio in excess of 1.00 is indicated for the entire temperature range.

(3) Weldment Properties

The as-welded ultimate tensile strength and weld-joint efficiency at 75 to -423°F are shown in Figure B-46 for TIG-welded 2219-T87 aluminum for the condition in which the weld bead is left on. The properties have a very marked thickness dependence, with plate (0.500-in. thickness) showing considerable joint-efficiency reduction and the joint efficiency of sheet decreasing from 70-77% at 75°F to a minimum of 60-64% at -100°F. With further exposure-temperature decrease, the joint efficiency increases to about 70% at -320°F and retains a value of 65 to 70% at -423°F.

Because the joint efficiencies for 2219-T87 aluminum welds were so low, the effect of a complete post-welding reheat-treatment or an age treatment only was evaluated. Figure B-47 summarizes the results. The lowest joint-strength and joint-efficiency values are obtained with the T87 temper. Material welded in the T37 temper and then aged to the T87 temper has higher strength and joint-efficiency values than the joint welded in the T87 temper. The maximum joint strengths and efficiencies are obtained when the fabricated component is reheat-treated to the T62 condition, irrespective of the pre-welding temper.

Figure B-48 compares the tensile strengths and elongations of parent metal and welds variously processed after welding. The maximum parent-metal strength with the lowest weld-joint strength is indicated for the T87 temper. Although the parent-metal elongation at 75 to -423°F is satisfactory, the weld-joint elongation never approaches the 12% minimum desired. Components solution-treated and aged to the T62 temper after welding show the lowest parent-metal strength, but the highest weld-joint strength. Both parent-metal elongation and weld-joint elongation are greatest when the component is solution-heat-treated and aged after welding, but the weld-joint values of 7% at -320°F and 4% at -423°F are still under the 10.8% minimum desired. Material welded in the T37 temper and aged to the T87 temper after welding has values for parent-metal strength and elongation, and for weld strength, intermediate between

those reported for the T87 temper and for weld joints solution-treated and aged to the T62 temper after welding. However, the weld-joint elongation is the lowest (approximately 2%) for welding in the T37 temper and aging to the T87 temper after welding.

If it is found advisable to fabricate the metal shells in the T87 temper and utilize weld joints in the as-welded condition, weld-joint reinforcement by means of thick lands will be required. The thickening in the weld-joint area will introduce a thickness effect on the available joint strength. The effect of thickness on the average tensile strength of the weld joint is shown in Figure B-49. Its importance will depend on the increased thickness required in the weld-joint area.

On the basis of this analysis, it appears that solution heat treatment and aging to the T62 temper after welding will provide the optimum weld-joint strength, joint efficiency, and joint ductility with the 2219 aluminum alloy.

b. Aluminum Alloy 7039

Because 2219-T87 aluminum showed weld-joint efficiencies considerably below the 90 to 100% desired, the properties obtainable in the new weldable 7039 aluminum alloy were considered worthy of analysis. This alloy in the T6 temper has the following typical tensile properties: 65,000-psi ultimate tensile strength, 58,000-psi tensile-yield strength, and 13% elongation. It is thus comparable to 2219-T87 aluminum and considerably superior to the 2219-T62 alloy. On cryogenic exposure, the properties increase to maximum values of 95,000 psi for ultimate tensile strength and about 75,000 psi for tensile-yield strength at -423°F . The elongation is retained at levels well above the minimum desired (10.8%) at 75 to -423°F . At 75°F , 7039-T6 aluminum has a notch toughness comparable to that of 2219-T87 and 2219-T62 aluminum, and a notched-to-unnotched strength ratio of 1.00 to 1.10 with $K_T = 6.3$. At -423°F , the notched-to-unnotched strength ratio is 0.83 to 0.85 for $K_T = 6.3$. At -423°F , the notch-toughness rating falls between those of 2219-T87 and 2219-T62 aluminum.

The as-welded tensile properties of 7039-T6 aluminum are shown in Figure B-50. Weld-joint efficiencies of 80 to 88% are obtainable at 75°F with the weld bead left on; this range is superior to that obtained for as-welded 2219-T87 aluminum. At -423°F , however, the as-welded joint efficiency of 7039-T6 aluminum is only 55 to 60%. Weld-joint ductility for sheet gages decreases from 7 to 10% at 75°F to 1% or less at -423°F . Unless the weld-joint efficiency and elongation at -423°F can be significantly improved by means of re-solution heat treatment and aging to the T6 temper after welding, the 7039 aluminum alloy will provide no property improvements over those of 2219-T62 and 2219-T87 aluminum at the lower end of the temperature range (-320 to -423°F). This material was therefore eliminated from further consideration in this analysis.

c. Fabrication Characteristics

The formability of 2219 aluminum alloy is at a maximum in the annealed or -O temper, being possibly slightly superior to that of other common high-strength alloys such as 2024 and 7075 aluminum. As the strength increases in the other available tempers, the formability decreases. Severe forming and drawing operations should be performed with annealed material. Less severe operations may be performed with material in the intermediate T42, T31, and T37 tempers. Only mild forming operations are recommended for material in the artificially aged T62, T81, and T87 tempers.

The 2219 alloy shows superior welding characteristics as compared with the other heat-treatable aluminum alloys of similar strength. Weld cracking is relatively low in 2219-alloy weldments because the filler wire and parent metal are nearly identical in composition. Parent-metal dilution of the weld bead is therefore negligible, resulting in low weld-bead crack sensitivity. Proper joint design and welding techniques must be employed, however, if sound welds are to be produced.

In the heat treatment of 2219 aluminum, the normal quenching from the solution-heat-treat temperature into water at 60°F results in distortion, which is typical for aluminum alloys. Distortion can be minimized by quenching in 150°F water. Quenching at the higher water temperature will reduce the tensile strength about 5000 psi and the yield strength 3000 psi, but will improve the elongation by about 3% in the material after aging to the T62 temper. This treatment is not recommended, however, for applications in which the maximum resistance to stress-corrosion cracking is desired.

d. Preliminary Rating of Material

The following tentative conclusions are indicated for the 2219 aluminum alloy:

(1) Aluminum alloy 2219 welded in the T87 temper and used in the as-welded condition provides (a) the maximum strength, ductility, and notch toughness in parent metal, and (b) the lowest weld-joint strength and weld-joint efficiency.

(2) The 2219 alloy solution-heat-treated and aged to the T62 temper after welding provides (a) the lowest parent-metal strength, and (b) the highest weld-joint strength, joint efficiency, and joint ductility.

(3) The 2219 alloy welded in the T37 temper and aged to the T87 temper after welding provides parent-metal strengths, weld-joint strengths, and weld-joint efficiencies intermediate between those obtained with the other two conditions. The weld-joint ductility, however, is the lowest.

(4) Extensive reinforcement of the weld-joint area will be necessary because of low efficiencies and ductility when welded in the T87 temper, or when welded in T37 temper and aged to the T87 temper after welding. This introduces design problems and costly fabrication problems.

(5) Optimum weld-joint strength, efficiency, and ductility values for 2219 aluminum are obtained by solution heat treatment and aging to the T62 temper after welding. However, the weld-joint stress-strain properties are still inadequate for -320 and -423°F service. Because of the improved weld-joint properties, heat treatment to the T62 temper after welding is recommended for metal shells fabricated from 2219 aluminum alloy.

4. Nickel-Base Alloy, Inconel X-750

a. Annealed Grade

In a further search for material providing suitable weld-joint ductility, it was determined that the nickel-base alloy Inconel X-750 (Huntington Alloy Products Division, International Nickel Company) appears to meet and exceed the requirements for uniaxial ductility and to have adequate yield and tensile strengths for use in GFR metal tanks.

Properties of unwelded material in the solution-treated and aged (STA) condition are shown in Figures B-51, B-52, and B-53. Excellent ductility and notch toughness are indicated for 75 to -423°F.

The increase in strength upon exposure to extremely low temperatures is not of the same magnitude as that indicated for Type 301 SS or the titanium alloys. The yield strength gradually increases from a typical value of 120,000 psi at 75°F to a maximum of 150,000 psi at -423°F. The ultimate tensile strength increases from a typical value of 175,000 psi at 75°F to a maximum of about 230,000 psi at -423°F. The ductility, as indicated by percentage of elongation, increased with decreasing temperature exposure, varying from 25% at 75°F to 30% at -423°F.

The lowest notch-to-unnotched strength ratios indicated for the material at -423°F convert to notched-strength to unnotched-yield-strength ratios in excess of the required value of 1.00. As indicated in Figure B-54, for welding in the solution-treated condition and aging after welding, weld joints with 100% joint efficiency and with uniaxial elongations in excess of 20% are obtainable over the complete temperature range. On the basis of uniaxial properties, Inconel X-750 (STA) thus appears to provide the most satisfactory overall properties of ductility and adequate strength among all the metallic materials that were evaluated. Its disadvantage is its density of 0.300 lb/in.³, which is greater than that of the other candidate materials (0.286 for stainless steel, 0.162 for titanium, and 0.102 for aluminum).

b. Cold-Worked Grade

Inconel X-750 alloy when cold-reduced 20% and double-aged will provide considerably higher parent-metal strength along with acceptable ductility at 75 to -423°F. Higher percentages of cold reduction will result in additional increases in parent-metal strength after double aging. The more severely cold-worked grades show directionality effects, however, and will not provide adequate ductility over the complete temperature range.

The weld-joint strength in the cold-worked grades is approximately the same as that obtained with the annealed grade. Although the weld-joint ductility may be adequate, the strength efficiency for aging after welding will be considerably lower than the 100% obtainable with the annealed material aged after welding.

c. Fabrication Characteristics

In the mill-annealed condition, Inconel X-750 is relatively soft and ductile and therefore is amenable to cold forming. With conventional equipment and techniques, it is readily adaptable to bending, stretch forming, mechanical pressing, hydropressing, rubber-die forming, and spinning. When the hot-forming process is used, slow heating or cooling through the age-hardening temperature range of 1300 to 1550°F must be avoided. When subjected to cold-forming or cold-spinning operations, this material work-hardens fairly rapidly, and cold-forming operations must be performed in several stages to arrive at the desired shape. The material must consequently be subjected to annealing between the various cold-forming operations for recrystallization, to put it in the proper condition for additional cold forming and cold reduction. After the final cold-reduction or cold-forming operation, it must be annealed again before welding. After welding, material in thicknesses of about 0.100 in. or less may be stress-equalized at 1625°F and then aged. Heavy plate thicknesses after welding may require a solution heat treatment at about 2000°F prior to aging.

The only type of fusion welding recommended for Inconel X-750 is the TIG process using Inconel Filler Metal 69. For optimum results the alloy should be in the annealed or solution-treated condition. As indicated above, however, a stress-equalizing heat treatment may be sufficient for thin wall sections. In multiple-pass welds, a tenacious refractory oxide film forms that must be removed from the deposited bead before successive beads are deposited. Because of residual welding stresses present in the weld joint, a stress-relief treatment at 1625°F for 4 hours prior to aging is essential.

5. Cobalt-Base Alloy, Haynes 25

The only cobalt-base alloy readily available in sheet form for which cryogenic-temperature properties could be located was the Haynes 25 alloy (product of Stellite Division, Union Carbide Corporation).

a. Annealed Grade

Figure B-55 summarizes some properties of the alloy. The material has the following typical properties at 75°F: 64,000-psi tensile-yield strength, 136,000-psi ultimate tensile strength, and 44 to 47% elongation in the annealed or solution-heat-treated condition. On cryogenic exposure, the strength increases to maximum values of 140,000 psi in yield strength and 224,000 psi in ultimate strength at -423°F. Although this is accompanied by a ductility decrease as indicated by the lower elongation values of 25 to 29% at -423°F, the elongation over the temperature range is significantly greater than required.

The notch toughness improves with decreasing temperatures, as indicated by notched-to-unnotched strength ratios shown in Figure B-56. For $K_T = 8.0$, the notched-to-unnotched strength ratios range from around 0.80 at 75°F to 0.87 at -423°F. The annealed alloy might therefore be considered marginal with respect to its notch toughness. Since the yield strength is comparatively low with respect to the ultimate strength, however, the notch toughness can be considered very good because the notched-strength to unnotched-yield-strength ratios are considerably greater than 1.00, ranging from 1.76 at 75°F to 1.35 at -423°F.

b. Cold-Worked Grade

This alloy may be strengthened by cold working. When subjected to 20% cold reduction, it will provide typical 75°F values of 120,000 psi in yield strength, 166,000 psi in ultimate tensile strength, and 16 to 17% elongation (see Figure B-55). With decreasing temperature, these values increase to 210,000 psi in yield strength and 270,000 psi in ultimate strength at -423°F. A slight directionality effect on elongation is apparent in the cold-reduced material at low temperatures. Even so, the elongations in the longitudinal and transverse directions appear to be adequate at 75 to -423°F. The directionality effect, however, is more pronounced when the notch toughness is evaluated (see Figure B-56). At $K_T = 7.2$, the notched-to-unnotched strength ratio in the transverse direction varies from about 1.09 at 75°F to 1.03 at -423°F. In the longitudinal direction, however, the value decreases with falling temperature - from 1.03 at 75°F to 0.91 at -275°F. With further temperature decrease, the ratio increases again to 0.98 at -423°F. The 20%-cold-reduced material, although showing this pronounced directionality effect, still appears adequate with respect to notch toughness when rated on the basis of $K_T = 7.2$.

c. Weldment Properties

Figure B-57 shows the tensile properties of weldments. As was true for the parent metal, the strength of welded Haynes 25 alloy increases as the temperature is lowered from 75 to -423°F. The weld-joint efficiency of annealed material is maintained at 95 to 100% from 75 to -423°F. As-welded 20%-cold-reduced material, however, has a weld-joint efficiency of 80% at 75°F, decreasing to 71% at -320°F, and then increasing to 77% at -423°F. No information on the weld-joint ductility was available, other than an elongation value of 37% in 2 in. at 75°F for TIG-welded, annealed material.

d. Fabrication Characteristics

Cold forming is the preferred method for the bending, deep-drawing, and spinning of this alloy because of the excellent ductility. The power requirements for these operations are relatively high because of the high yield strength as compared with annealed stainless steels. The material tends to work harden, and solution heat treatment after each stage of the cold-forming operation may be necessary.

The alloy can be readily welded by metallic-arc, inert-gas-shield arc, and Sigma methods. It is necessary to avoid high heat input to the base metal such as in submerged-arc welding, lest the weld cool slowly and lower the weld-joint ductility.

No low-temperature stress-relief heat treatment is applicable for the relief of internal stresses in weldments. The weldments are generally used as welded. If stresses due to cold working or welding must be relieved, it is necessary to include a solution heat treatment at 2250 to 2265°F followed by a water quench.

e. Rating of Material

On the basis of parent-metal properties, the Haynes 25 alloy would be suitable for the metal shell in both the annealed and 20%-cold-reduced tempers. When the two grades are compared on the basis of weld-joint properties, however, the strength advantages of the 20%-cold-reduced temper are offset by low weld-joint efficiency. Assuming that the weld-joint ductility is adequate, the annealed condition therefore appears to be the most suitable temper of Haynes 25 for the metal shell. The low yield strength and high density (0.330 lb/in.³), however, would not provide the maximum weight savings desired. In addition, the material does not appear to offer advantages over Inconel X-750 for metal-shell fabrication. The alloy was therefore eliminated from further consideration in this analysis.

C. FINAL EVALUATION OF OPTIMUM MATERIAL IN EACH CLASS

The optimum material in each alloy class was established on the basis of the foregoing characterization analysis, and the property data required for the parametric evaluation are summarized below. Values were estimated for unavailable property data, and the basis for estimation is presented. Except for materials hardened by means of cold working during their production, the proportional limits were assumed to be 90% of the yield strength, on the basis of a general trend indicated by typical stress-strain curves for various materials in Ref. B-15.

1. Type 301 SS (1/2 Hard)

Figures B-58 and B-59 present typical uniaxial room-temperature stress-strain curves in tension and compression for the as-rolled and stress-relieved conditions of this material in the longitudinal and transverse

directions, respectively (no stress-strain curves were located for temperatures of -320 and -423°F). As indicated by the broken lines, the tensile stress-strain curves were extrapolated to approximately 6% to facilitate determination of values for the plastic modulus of elasticity. The following typical room-temperature uniaxial proportional limits were established on the basis of these curves:

Material Condition	Proportional Limit, psi			
	Tension		Compression	
	Longitudinal	Transverse	Longitudinal	Transverse
As rolled	30,000	30,000	25,000	35,000
Stress-relieved at 1000°F	50,000	50,000	50,000	60,000

On the assumption that the proportional limit would increase in the same manner indicated for yield strength in Figure B-9, estimated proportional limits of 75,000 and 88,000 psi were established for as-rolled material in the longitudinal direction at -320 and -423°F , respectively. Using these values and the 0.2% offset-yield-strength values from Figure B-9, the estimated tensile-stress-strain curves for as-rolled material at -320 and -423°F were constructed (see Figure B-58). Because cryogenic data were not available, the construction of -320 and -423°F stress-strain curves was not attempted for as-rolled material in the transverse direction and for stress-relieved material in the longitudinal and transverse directions. Estimated uniaxial property values in tension and compression were established, however, assuming that all typical mechanical properties reported in Tables B-4 and B-5 for 301 SS (1/2 hard) in the as-rolled and stress-relieved conditions would follow the trend shown in Figures B-9 and B-10 upon exposure at 75 to -423°F . Table B-6 summarizes these values, together with values for a 1-to-1 biaxial-stress-state condition for use in the parametric evaluation.

Figure B-60 shows the modulus of elasticity at 75 to -423°F for two thicknesses of 60%-cold-rolled material. Because Ref. B-15 provides typical room-temperature values in tension of 26.0×10^6 and 28.0×10^6 psi (longitudinal and transverse, respectively) for all cold-worked tempers of Type 301 SS, the curves designated (1) in Figure B-60 are considered representative for the 1/2-hard temper. Ref. B-15 provides typical room-temperature values in compression of 26.0×10^6 and 27.0×10^6 psi for the modulus in the longitudinal and transverse directions, respectively. It is assumed that the compression-modulus values will follow the same trend as the tension-modulus values over the entire temperature range. The elastic-modulus values for a 1-to-1 biaxial-stress state are in general 10×10^6 psi higher than those for the uniaxial (1-to-0) stress state.

Figure B-61 shows thermal contraction at 75 to -423°F for cold-drawn Type 302 SS, which is considered as representative of Type 301 (1/2 hard).

The low-cycle, high-strain fatigue data presented in Table B-6 are based on predicted values calculated from equations discussed in Appendix C. These data are applicable to unwelded material under uniaxial-

stress conditions. Insufficient data are available for unwelded material subjected to low-cycle fatigue in a multistress field or welded material in both uniaxial and multiaxial stress fields to permit proper evaluation in these regards.

2. Ti-5Al-2.5Sn (Annealed, ELI Grade)

Figure B-62 presents typical uniaxial stress-strain curves in tension at 75, -320, and -423°F for this alloy in sheet form. No compressive stress-strain curves were located. Because Ref. B-15 provides a minimum room-temperature compressive-yield strength for the normal interstitial grade that is 5000 psi higher than the minimum yield strength in tension, a conservative assumption that the compressive-yield strength equals the tensile-yield strength was made for the ELI grade. With this assumption, the curves for compressive stress-strain up to the yield strength should be practically identical to the tensile stress-strain curves. The following typical uniaxial proportional limits were established for both tension and compression on the basis that the limit is 90% of the yield strength:

Direction with Reference to Rolling Direction	Proportional Limit, psi		
	75°F	-320°F	-423°F
Longitudinal	90,000	158,000	180,000
Transverse	95,000	150,000	178,000

Figure B-63 shows the modulus of elasticity for the normal-interstitial grade in tension for 75 to -423°F; it is considered applicable to the ELI grade. Because Ref. B-15 provides identical room-temperature elastic-modulus values in tension and compression (15.5×10^6 psi), it was assumed for the parametric analysis that the same situation exists over the entire range from 75 to -423°F. Elastic-modulus values for a 1-to-1 biaxial-stress-state condition are in general about 8.0×10^6 psi higher than for the uniaxial (1-to-0) stress state.

Table B-7 provides a complete summary of all uniaxial and 1-to-1 biaxial-stress-state values for Ti-5Al-2.5Sn (ELI grade). The low-cycle, high-strain, fatigue data shown there are based on predicted values developed as indicated in Appendix C and are applicable to unwelded material under uniaxial-stress conditions only. The data on welded material or material in any condition under multiaxial stress fields were too limited to permit proper evaluation for use in the parametric analysis.

Figure B-64 shows thermal contraction at 75 to -423°F for the normal-interstitial grade; it is also considered representative of the ELI grade.

3. 2219-T62 Aluminum

Figure B-65 presents typical uniaxial stress-strain curves in tension at 75, -320, and -423°F for this alloy in sheet form; no compressive

stress-strain curves were located. Because Ref. B-15 indicates that the minimum compressive-yield strength is only 2000 psi higher than the minimum yield strength in tension, it was conservatively estimated that the compressive-yield strength equals the tensile-yield strength. With this assumption, the curves for compressive stress-strain up to the yield strength should be practically identical to the tensile stress-strain curves. The following typical uniaxial proportional limits were established for both tension and compression on the basis that the limit is 90% of the yield strength:

Direction with Reference to Rolling Direction	Proportional Limit, psi		
	75°F	-320°F	-423°F
Longitudinal	39,000	50,000	52,000
Transverse	40,000	49,000	53,000

Figure B-66 presents tensile elastic-modulus data for 2219-T87 aluminum at 75 to -423°F and is also considered applicable to 2219-T62 aluminum. Because Ref. B-15 indicates that the room-temperature compressive modulus is only 300,000 psi higher than the tensile modulus, a conservative assumption was made that the compressive modulus equals the tensile modulus for the entire 75 to -423°F range. Elastic-modulus values for a 1-to-1 biaxial-stress state are in general about 6.0×10^6 psi higher than for the uniaxial (1-to-0) stress state.

Table B-8 summarizes the uniaxial and 1-to-1 biaxial-stress-state properties for 2219-T62 aluminum used in the parametric evaluation. The low-cycle, high-strain, fatigue data shown there are based on predicted values developed as indicated in Appendix C and are applicable to unwelded material under uniaxial-stress conditions only. No data were available for welded material or material in any condition under multiaxial stress fields.

Figure B-67 shows thermal contraction at 75 to -423°F for 2219-T87 aluminum and is also considered applicable to 2219-T62 aluminum.

4. Inconel X-750 (STA)

Typical longitudinal tensile stress-strain curves for 0.750-in.-dia bar stock of this material at 75, -320, and -423°F are presented in Figure B-68. Because Ref. B-15 indicates that the room-temperature elongations of sheet and bar under 4.0 in. in diameter are identical, these stress-strain curves are considered as typical for sheet. Figure B-69 presents a typical 75°F stress-strain curve in compression for annealed and aged sheet. Ref. B-15 indicates equal values for tensile and compressive yield strengths. On this basis, the stress-strain curves for sheet should be practically identical in tension and compression. Using this assumption, the following typical uniaxial proportional limits were established for Inconel X-750 (STA) for both tension and compression on the basis that the proportional limit is 90% of the yield strength:

Direction with Reference to Rolling Direction	Proportional Limit, psi		
	75°F	-320°F	-423°F
Longitudinal	108,000	122,000	126,000
Transverse	108,000	124,000	128,000

The tensile modulus of elasticity at 75 to -423°F is shown in Figure B-70. Because Ref. B-15 shows identical room-temperature elastic-modulus values (31.6×10^6 psi) in tension and compression, it was assumed that this situation exists over the entire range from 75 to -423°F. Elastic-modulus values under a 1-to-1 biaxial-stress-state condition are in general about 10×10^6 psi higher than for the uniaxial (1-to-0) stress state.

Table B-9 summarizes the uniaxial and 1-to-1 biaxial-stress-state properties used in the parametric evaluation. The low-cycle, high-strain, fatigue data shown there are based on predicted values developed as indicated in Appendix C and are applicable to unwelded material under uniaxial-stress conditions only. No data were available for welded material or for material in any condition under multiaxial stress fields.

The data on thermal contraction at 75 to -423°F shown in Figure B-71 were developed for a 0.750-in. diameter and are assumed applicable to sheet material.

V. RECOMMENDATIONS

A. Type 301 SS (1/2 hard), when stress-relieved at 800 to 1000°F, shows improved ductility and almost complete elimination of the Bauschinger effect, but no data are available on cryogenic-temperature properties after stress relief for either the parent metal or weldments. A program to determine these properties is recommended, because of the comparatively low cost of this material and the prospect of developing desirable properties by stress relief.

B. The application of cryogenic stretch forming (e.g., the Ardeform process) to vessels fabricated and welded from annealed 301 SS should be thoroughly investigated. This approach will strengthen the parent metal and weldments simultaneously, and will provide practically 100% weld-joint efficiency.

C. Ti-5Al-2.5Sn (ELI grade) appears to satisfy all the property requirements except for the ductility of weldments at -423°F. The limited data available indicate that stress relief and the use of electron-beam welding definitely improve the weld-joint ductility. It is recommended that the effect of stress relief on weld-joint properties be investigated further, particularly when ELI-grade filler wire is used in the TIG process, or without filler wire when the electron-beam technique is used.

D. Practically all the data available on low-cycle, high-strain, fatigue properties are limited to the parent metal at room temperature. It

is recommended that such data on weldments be developed for all apparently acceptable candidate materials at 75 to -423°F , using a compression-tension reverse cycle about zero mean stress. The development of specimen designs and techniques for testing uniaxially and at a 1-to-1 biaxial-stress-state condition is desirable.

E. The application of electron-beam welding to 2219 aluminum alloy in the higher-strength T81 and T87 tempers indicates a possibility that improved joint efficiencies and ductility may be obtainable. A program is desirable for further evaluation of weld joints made with this technique, because of the highly favorable strength-to-density ratio obtainable with 2219 aluminum alloy.

F. It is believed that adequate ductility at -423°F can be obtained in the ELI grade of Ti-5Al-2.5Sn. A program to establish the degree of creep in compression for this alloy at 75 to -423°F is therefore desirable. Although low-temperature creep in tension has been established for Ti-5Al-2.5Sn (ELI grade) at 75°F and -320°F and it is considered serious enough to include a cautionary note in Ref. 15, it is only assumed that such creep could occur in compression. This material has a very good strength-to-weight ratio and is desirable for lightweight GFR pressure vessels; the determination of its low-temperature-creep characteristics in compression therefore appears warranted.

REFERENCES

- B-1. Stainless Steel Fabrication, Allegheny Ludlum Steel Corporation, Pittsburgh, Pennsylvania, 1957.
- B-2. E. L. Terry and S. W. McClaren, Biaxial Stress and Strain Data on High Strength Alloys for Design of Pressurized Components, Technical Documentary Report ASD-TDR-62-401, (Ling-Temco-Vought, Inc. report under Contract AF 33(616)-7720), July 1962.
- B-3. S. W. McClaren and J. H. Best, Low Cycle Fatigue Design Data on Materials Subjected to a Multiaxial Stress Field, Technical Documentary Report RTD-TDR-63-4094 (Ling-Temco-Vought report under Contract AF 33(657)-8525), November 1963.
- B-4. S. W. McClaren and C. R. Foreman, Cryogenic Design Data for Materials Subjected to Uniaxial and Multiaxial Stress Field, Technical Report AFML-TR-64-140 (Ling-Temco-Vought report under Contract AF 33(615)-1329), May 1965.
- B-5. Battelle Memorial Institute, "Biaxial Properties of Metals for Aerospace Applications," Paper No. 2893-63 presented at AIAA Shell Structures Conference, 13 April 1963.
- B-6. Mellon Institute, A Study of the Behavior of Small Pressure Vessels Under Biaxial Stress Conditions and in the Presence of Surface Cracks, Mellon Institute Project 4396 under Contract Nonr-3764 (00)(X), June 1963.
- B-7. R. V. Milligan, R. W. Koo, and J. E. Davidson, The Bauschinger Effect in a High Strength Steel, Watervliet Arsenal (Watervliet, New York) Report WVT-6508 (under DA Project No. I-L-O-13001-A91A), March 1965.
- B-8. J. Dubuc, "Plastic Fatigue Under Cyclic Stress and Cyclic Strain With a Study of the Bauschinger Effect," PhD Thesis submitted to Ecole Polytechnique, Universite de Montreal (Canada), January 1961.
- B-9. J. V. Gluck and J. W. Freeman, Further Investigations of the Effect of Prior Creep on Mechanical Properties of C110M Titanium with Emphasis on the Bauschinger Effect, University of Michigan Research Institute report, March 1960.
- B-10. C. J. Newton, "The Bauschinger Effect and Residual Microstress in Alpha Brass," Journal of Research, National Bureau of Standards, October-December 1961.
- B-11. D. C. Drucker, Graduate Division of Applied Mathematics, Brown University, Stress-Strain Relations in the Plastic Range - A Survey of Theory and Experiment, Technical Report under Office of Naval Research Contract N7onr-358, December 1960.

- B-12. R. W. Smith, M. H. Hirschberg, and S. S. Manson, Fatigue Behavior of Materials Under Strain Cycling in Low and Intermediate Life Range, National Aeronautics and Space Administration TND-1574, April 1963.
- B-13. Low Temperature Creep Characteristics of Ti-5Al-2.5Sn and Ti-6Al-4V Alloys, DMIC Technical Note, Defense Metals Information Center (Battelle Memorial Institute, Columbus, Ohio), 8 June 1964.
- B-14. Cryogenic Materials Data Handbook, Air Force Materials Laboratory Technical Documentary Report ML-TDR-64-280, PB171809 (Revised), August 1964 (with Supplement 1, February 1965 and Supplement 2, July 1965).
- B-15. Metallic Materials and Elements for Flight Vehicle Structures, (Military Handbook) MIL-HDBK-5, August 1962 (with the following change notices: No. 1, 1 May 1963; No. 2, 1 November 1963; No. 3, 1 May 1964; and No. 4, 1 November 1964).
- B-16. R. H. Harrington, Stress-Aging: A New Treatment for Alloys: Part One: Effect on Standard Tensile Properties of Stainless Steels, Watervliet Arsenal Report WVT-RR-6313, November 1963.
- B-17. R. H. Harrington, "Stress-Aging and Its Effects on the Standard Tensile Properties of Some Stainless Steels," American Society for Metals Transactions Quarterly, Vol. 58, No. 2, June 1965.
- B-18. Development of High Strength Alloys by Cryogenic Stretch Forming, Arde-Portland, Inc. (Paramus, New Jersey) Final Report, Part 1, under Contract NOW 63-0387-C, 17 September 1964.
- B-19. Tensile Coupon Tests of Cryoformed AISI 301 Stainless-Steel Pressure Vessels at Cryogenic Temperatures, NASA TN D-2202, October 1964.
- B-20. Low Temperature Creep Characteristics of Ti-5Al-2.5 Sn and Ti-6Al-4V Alloys, DMIC Technical Note, Defense Metals Information Center (Battelle Memorial Institute, Columbus, Ohio) 8 June 1964.
- B-21. DMIC Review of Recent Developments - Titanium and Titanium Alloys, Defense Metals Information Center, 17 September 1965.
- B-22. E. W. Cawthorne, "Trip Report to BMI on Visit to AiResearch Manufacturing Company, Los Angeles, California, May 8, 1964 - Creep at Cryogenic Temperature of Ti-5Al-2.5 Sn Alloy."
- B-23. Titanium Welding Techniques, Titanium Engineering Bulletin No. 6, New York, Titanium Metals Corporation of America, revised September 1964.
- B-24. The Stress Relief of Titanium Welds for Low-Temperature Applications, DMIC Technical Note, Defense Metals Information Center, 26 May 1964.

TABLE B-1

UNIAXIAL AND BIAXIAL PROPERTIES OF MATERIALS AT 75°F*

Average Uniaxial Strength, psi		Speci- men Direc- tion	Elongation, %			Ratio of B to Average A	
			A: Uniaxial (in 2 in.)	B: Biaxial (in 0.5 in.)		1-to-1 Stress Field	2-to-1 Stress Field
				1-to-1	2-to-1		
Yield	Ultimate			Stress Field	Stress Field		
Type 301 SS (3/4 to full hard)							
165,000	196,000	L	21.3	6.3	3.6	0.293	0.167
		L	20.8	3.8	9.8	0.177	0.455
		L	22.5	4.4	9.5	0.204	0.442
		Av	21.5				
149,000	204,000	T	14.3	6.7	6.2	0.470	0.434
		T	12.8	3.8	6.5	0.268	0.455
		T	15.9	4.4	6.0	0.308	0.420
		Av	14.3				
Ti-6Al-4V (Annealed)							
148,000	162,000	L	11.2	4.5	6.5	0.388	0.560
		L	12.0	2.8	3.2	0.241	0.276
		L	11.7	1.4	3.5	0.120	0.302
		Av	11.6				
155,000	169,000	T	12.1	3.4	9.5	0.259	0.725
		T	15.7	1.6	7.2	0.122	0.550
		T	11.5	1.6	-	0.122	-
		Av	13.1				
AM-355 Stainless Steel (SCT)							
197,000	228,000	L	8.2	2.0	7.2	0.251	1.093
		L	7.9	3.8	9.6	0.476	1.200
		L	7.8	-	10.0	-	1.250
		Av	7.9				
201,000	231,000	T	7.7	2.0	8.0	0.254	1.01
		T	7.7	3.8	8.5	0.483	1.08
		T	8.2	-	8.8	-	1.12
		Av	7.8				
18% Nickel Maraging Steel (300 Series)							
295,000	299,000	L	5.0	1.3	1.8	0.325	0.450
		L	2.0	-	2.0	-	0.500
		L	5.0	-	-	-	-
		Av	4.0				
314,000	320,000	T	4.0	1.2	-	0.353	-
		T	2.8	-	-	-	-
		T	3.5	-	-	-	-
		Av	3.4				

*Elongation data derived from Ref. B-3. Specimen thicknesses were 0.036 in. for uniaxial tests and 0.026 in. for biaxial tests. L = longitudinal direction, T = transverse.

Table B-1

TABLE B-2

UNIAXIAL AND BIAXIAL PROPERTIES OF MATERIALS AT VARIOUS TEMPERATURES*

Temp °F	Speci- men Direc- tion	Elongation, %			Ratio of B to Average A	
		A: Uniaxial (in 1 in.)	B: Biaxial (in 0.5 in.)		1-to-1 Stress Field	2-to-1 Stress Field
			1-to-1 Stress Field	2-to-1 Stress Field		
Type 301 Stainless Steel (3/4 Hard)						
75	T	2.1	0.9	-	0.383	-
	T	2.6	0.9	-	0.383	-
	Av	2.35				
	L	1.5	1.1	2.3	0.666	1.39
	L	1.8	0.9	2.6	0.545	1.58
	Av	1.65				
-105	T	4.2	1.7	-	0.350	-
	T	5.5	1.4	-	0.289	-
	Av	4.85				
	L	7.1	2.0	2.8	0.284	0.398
	L	7.0	2.7	3.6	0.383	0.510
	Av	7.05				
-320	T	6.0	2.3	-	0.341	-
	T	7.5	3.3	-	0.490	-
	T	-	1.8	-	0.267	-
	Av	6.75				
	L	8.0	3.0	2.4	0.37	0.296
	L	8.2	2.3	3.7	0.284	0.457
	L	-	2.6	3.8	0.321	0.470
	Av	8.1				
	T	2.5**	1.0	-	0.40	-
	T	2.5**	1.25	-	0.50	-
	T	-	1.0	-	0.40	-
	Av	2.5				
-423	L	2.0**	1.4	2.9	0.70	1.45
	L	2.0**	1.9	2.4	0.95	1.20
	L	-	1.7	2.6	0.85	1.30
	Av	2.0				

*Elongation data derived from Ref. B-4. Specimen thicknesses were 0.036 in. for uniaxial tests and 0.026 in. for biaxial tests. T = transverse direction, L = longitudinal.
 UW = unwelded, W = welded.

**Throughout table, indicates 2-in. gage length.

TABLE B-2 (cont.)

Temp °F	Speci- men Direc- tion	Elongation, %					Ratio of B to Average A		
		A: Uniaxial		B: Biaxial (in. 0.5 in.)			1-to-1		
		(in 1 in.)		1-to-1		2-to-1 Stress Field (UW)	1-to-1		2-to-1 Stress Field (UW)
		Stress Field		Stress Field					
		UW	W	UW	W		UW	W	
5Al-2.5Sn Titanium (Annealed, ELI Grade)									
75	T	5.25	-	4.9	4.9	-	0.910	0.910	-
	T	<u>5.50</u>	-	4.1	3.9	-	0.763	0.725	-
	Av	5.375							
	L	6.0	6.2	4.3	3.5	3.6	0.662	0.540	0.554
	L	<u>7.0</u>	<u>6.1</u>	4.0	4.4	3.0	0.615	0.677	0.461
	Av	6.5	6.15						
-105	T	5.0	-	2.4	1.6	-	0.480	0.320	-
	T	<u>5.0</u>	-	1.1	1.7	-	0.220	0.340	-
	Av	5.0							
	L	7.3	5.2	1.9	3.0	6.0	0.257	0.405	0.810
	L	<u>7.5</u>	<u>4.3</u>	2.4	2.3	6.0	0.324	0.310	0.810
	Av	7.4	4.75						
-320	T	-	-	5.2	1.0	-	0.743	0.143	-
	T	7.0	-	4.4	2.7	-	0.630	0.386	-
	T	<u>-</u>	-	-	4.7	-	-	0.672	-
	Av	7.0							
	L	-	2.0	1.8	1.4	3.4	0.360	0.280	0.680
	L	5.0	2.7	4.3	3.6	6.9	0.860	0.720	1.380
L	<u>-</u>	<u>-</u>	-	4.7	6.6	-	0.940	1.320	
Av	5.0	2.35							
-423	T	2.0**	-	1.7	-	-	0.97	-	-
	T	<u>1.5</u>	-	1.60	-	-	0.914	-	-
	T	<u>-</u>	-	1.80	-	-	1.03	-	-
	Av	1.75							
	L	1.5**	-	1.3	-	1.8	0.650	-	0.90
	L	<u>2.5</u>	-	1.75	-	2.0	0.875	-	1.00
L	<u>-</u>	-	1.80	-	3.0	0.900	-	1.50	
Av	2.0								

TABLE B-2 (cont.)

Temp °F	Speci- men Direc- tion	Elongation, %				Ratio of B to Average A	
		A: Uniaxial (in 1 in.)	B: Biaxial (in 0.5 in.)		1-to-1 Stress Field	2-to-1 Stress Field	
			1-to-1	2-to-1			
			Stress Field	Stress Field			
2219-T81 Aluminum							
75	L	4.5	3.4	2.2	0.653	0.423	
	L	4.2	3.3	5.5	0.635	1.05	
	L	6.9	-	-	-	-	
	Av	5.2					
	T	5.7	2.8	-	0.384	-	
	T	7.3	3.5	-	0.480	-	
	T	8.9	-	-	-	-	
	Av	7.3					
	-105	L	6.1	3.3	4.9	0.560	0.830
L	5.7	3.1	4.6	0.525	0.780		
Av	5.9						
-105	T	11.2	3.6	-	0.394	-	
	T	7.1	2.5	-	0.273	-	
	Av	9.15					
	-320	L	7.0	0.7	4.8	0.103	0.71
L	6.5	2.0	8.0	0.296	1.19		
Av	6.75						
-320	T	6.0	4.3	-	0.44	-	
	T	13.5	1.9	-	0.195	-	
	Av	9.75					
	-423	L	5.0**	2.3	6.0	0.384	1.00
L	7.0	2.5	4.5	0.417	0.75		
L	-	3.0	4.0	0.500	0.67		
Av	6.0						
-423	T	6.0**	2.5	-	0.417	-	
	T	-	2.9	-	0.484	-	
	T	-	2.0	-	0.33	-	
	Av	6.0					

Table B-2, Sheet 3

TABLE B-3

PROPERTIES USED IN EVALUATION OF CANDIDATE METAL-SHELL MATERIALS

Uniaxial properties in tension (parent metal and welded joints)	Proportional limit Yield strength Ultimate strength Elongation Stress-strain curves Modulus of elasticity Weld-joint efficiency and ductility Fracture toughness (notched-unnotched tensile- strength ratio; notched-strength, unnotched- yield-strength ratio; critical crack-extension force, G_C ; and critical crack toughness, K_C)
Uniaxial properties in compression (parent metal and welded joints)	Proportional limit Yield strength Stress-strain curves Modulus
Low-cycle, high- strain fatigue char- acteristics (parent metal and welded joints)	--
Biaxial properties in 1-to-1 and 2-to-1 stress fields (parent metal and welded joints)	Proportional limit Yield strength Ultimate strength Elongation Stress-strain curves Modulus of elasticity Weld-joint efficiency and ductility
Other properties	Poisson's ratio Coefficient of thermal contraction Creep Buckling strength Thickness effect Directionality effect
Fabrication characteristics	Formability Spinning Weldability Heat treatment and stress relief Distortion

Table B-3

TABLE B-4

TYPICAL ROOM-TEMPERATURE STRENGTHS OF TYPE 301 SS, VARIOUS TEMPER

<u>Direction*</u>	<u>Annealed</u>	<u>1/4 Hard</u>	<u>1/2 Hard</u>	<u>3/4 Hard</u>	<u>Full Hard</u>	<u>Extra Full Hard**</u>
Tensile Strength, psi						
L	95,000	135,000	155,000	175,000	185,000	220,000+
T	95,000	140,000	160,000	185,000	200,000	230,000+
Yield Strength, psi						
L	36,000	80,000	120,000	140,000	160,000	180,000+
T	36,000	85,000	125,000	150,000	170,000	190,000+
Elongation, % in 2 in.						
L	60	42	23	17	15	9
T	60	40	20	13	11	4
Compressive Yield Strength, psi						
L	38,000	50,000	90,000	100,000	115,000	175,000
T	38,000	90,000	140,000	170,000	190,000	275,000

* L = longitudinal, T = transverse.

** Specific values for properties depend on amount of cold reduction used to obtain extra-full-hard temper. Cold reduction for this temper may vary from 60 to 80%. Values given are for 60% reduction.

Table B-5

TABLE B-5

EFFECT OF STRESS RELIEF ON PROPERTIES OF COLD-WORKED TEMPER, TYPE 301 SS

Direction*	Stress Relief as Indicated														
	1/4 Hard			1/2 Hard			3/4 Hard			Full Hard			Extra Full Hard		
	2 Hours at			2 Hours at			2 Hours at			2 Hours at			2 Hours at		
	None	800°F	1000°F	None	800°F	1000°F	None	800°F	1000°F	None	800°F	1000°F	None	800°F	1000°F
Tensile Strength, psi															
L	139,000	132,000	134,000	157,000	155,000	152,000	176,000	181,000	176,000	186,000	199,000	168,000	260,000	275,000	235,000
T	139,000	133,000	136,000	160,000	157,000	151,000	180,000	188,000	184,000	204,000	213,000	170,000	279,000	294,000	263,000
Yield Strength, psi															
L	80,000	77,000	73,000	122,000	128,000	120,000	142,000	155,000	151,000	160,000	175,000	148,000	217,000	249,000	210,000
T	84,000	79,000	76,000	123,000	130,000	122,000	145,000	155,000	154,000	163,000	181,000	151,000	241,000	270,000	239,000
Elongation, % in 2 in.															
L	42	47	47	23	24	29	17	11	11	15	7	8	3	1.5	2
T	40	48	47	19	18	26	13	10	10	11	5	11	4.5	1.0	1.5
Compressive Yield Strength, psi															
L	50,000	73,000	74,000	90,000	111,000	113,000	100,000	133,000	133,000	115,000	169,000	145,000	181,000	237,000	221,000
T	91,000	84,000	79,000	142,000	144,000	132,000	170,000	176,000	175,000	191,000	209,000	179,000	286,000	318,000	274,000

* L = longitudinal, T = transverse.

TABLE B-6

TYPE 301 SS (1/2 HARD), TYPICAL PROPERTIES FOR USE IN PARAMETRIC EVALUATION

Con- di- tion	Speci- men Direc- tion	Uniaxial			1-to-1 Biaxial-Stress State			
		75°F	-320°F	-423°F	75°F	-320°F	-423°F	
Proportional Limit, psi								
Tension	AR	L	30,000	75,000*	88,000*	Same as uniaxial		
	AR	T	30,000	75,000*	88,000*			
	SR	L	50,000	95,000*	108,000*			
	SR	T	50,000	95,000*	108,000*			
Compression	AR	L	25,000	70,000*	83,000*	Same as uniaxial		
	AR	T	35,000	80,000*	93,000*			
	SR	L	50,000	95,000*	108,000*			
	SR	T	60,000	105,000	118,000			
Ratio of Proportional Limit to Density (0.286 lb/in. ³), in. x 10 ³								
Compression	AR	L	87	245*	290*	Same as uniaxial		
	AR	T	122	281*	325*			
	SR	L	175	332*	378*			
	SR	T	210	367	413			
Yield Strength, psi								
Tension	AR	L	122,000	168,000*	180,000*	Same as uniaxial		
	AR	T	125,000	171,000*	185,000*			
	SR	L	120,000	166,000*	178,000*			
	SR	T	122,000	168,000*	180,000*			
Compression	AR	L	90,000	136,000*	148,000*			
	AR	T	140,000	186,000*	200,000*			
	SR	L	113,000	159,000*	141,000*			
	SR	T	132,000	178,000	192,000			
Tensile Strength, psi								
Tension	AR	L	157,000	288,000*	270,000*	Same as uniaxial		
	AR	T	160,000	291,000*	273,000*			
	SR	L	152,000	283,000*	265,000*			
	SR	T	151,000	282,000	264,000			
Elongation, % in 2 in.**								
Tension	AR	L	23	29	20	5.75	7.25	5.0
	AR	T	20	-	-	5.0	-	-
	SR	L	29	-	-	7.25	-	-
	SR	T	26	-	-	6.5	-	-

*Throughout table: One asterisk indicates an estimated value. AR = as rolled, SR = stress-relieved. L = longitudinal direction, T = transverse. Dashes in last six columns indicate no data available.

**Biaxial elongation assumed to be 25% of uniaxial value.

TABLE B-6 (cont.)

Con- di- tion	Speci- men Direc- tion	Uniaxial			1-to-1 Biaxial-Stress State			
		75°F	-320°F	-423°F	75°F	-320°F	-423°F	
Modulus of Elasticity, psi								
Tension	AR	L	26,000,000	28,500,000	30,000,000	36,000,000	38,500,000	40,000,000
	AR	T	28,000,000*	30,000,000*	31,000,000*	38,000,000*	40,000,000*	41,000,000*
	SR	L	26,000,000*	28,500,000*	30,000,000*	36,000,000*	38,500,000*	40,000,000*
	SR	T	28,000,000	30,000,000*	31,000,000*	38,000,000*	40,000,000*	41,000,000*
Compression	AR	L	26,000,000	28,500,000*	30,000,000*	36,000,000	38,500,000*	40,000,000*
	AR	T	27,000,000*	29,000,000*	30,000,000*	37,000,000*	39,000,000*	40,000,000*
	SR	L	26,000,000*	28,500,000*	30,000,000*	36,000,000*	38,500,000*	40,000,000*
	SR	T	27,000,000	29,000,000	30,000,000	37,000,000	39,000,000	40,000,000
Fracture Toughness, Notch-to-Unnotch Strength Ratio								
Parent Metal								
0.015-in. sheet, $K_T=7.2$	AR**	L	1.10	0.85	0.82	-	-	-
0.020-in. sheet	AR**	L	1.05	0.90	0.92	-	-	-
0.063-in. sheet	AR**	L	0.92	0.655	0.64	-	-	-
0.015-in. sheet	AR**	T	1.08	0.80	0.72	-	-	-
0.063-in. sheet, $K_T=7.2$	AR	T	0.85	0.48	0.33	-	-	-
$K_T=7.2$	SR	-***	-	-	-	-	-	-
$K_T = 21$	AR	L	0.83	0.56	0.44	-	-	-
$K_T = 21$	SR	-	-	-	-	-	-	-
Welded	-	-	-	-	-	-	-	-
Fracture Toughness, Notched-Strength to Unnotched-Yield-Strength Ratio								
Parent Metal								
0.015-in. sheet, $K_T=7.2$	AR**	L	1.21	1.20	1.01	-	-	-
0.020-in. sheet	AR**	L	1.21	1.52	1.38	-	-	-
0.063-in. sheet	AR**	L	1.19	1.155	0.91	-	-	-
0.015-in. sheet, $K_T=7.2$	AR	T	1.36	1.23	0.98	-	-	-
$K_T = 7.2$	SR	-	-	-	-	-	-	-
$K_T = 21$	AR	L***	1.07	0.77	0.72	-	-	-
$K_T = 21$	SR	-	-	-	-	-	-	-
Welded	-	-	-	-	-	-	-	-
Weld-Joint Properties								
Joint efficiency, %	AR**	-	70	96	89	Same as uniaxial		
Elongation, % in 2 in.	AR	-	21	14	3	5.25	3.5	0.75
Fracture toughness	AR	-	-	-	-	-	-	-
-	SR	-	-	-	-	-	-	-
Poisson's Ratio								
-	-	-	0.29	0.29	0.29	Same as uniaxial		

** Throughout table: Applicable to 3/4 hard temper; assumed that 1/2 hard will be equivalent or better.

*** Throughout table: Assumed.

TABLE B-6 (cont.)

Con- di- tion	Speci- men Direc- tion	Uniaxial			1-to-1 Biaxial-Stress State			
		75°F	-320°F	-423°F	75°F	-320°F	-423°F	
		Low-Cycle, High-Strain Fatigue - Reversed Cycle ****						
Parent Metal								
No. of cycles to failure at max operating strain range	AR	-	900	9000	3000	-	-	-
Magnitude of cyclic elastic-strain range for failure at 100 cycles (max $\Delta \epsilon_e$), in./in.	AR	-	0.0110	0.0190	0.0180	-	-	-
Factor of safety based on 100-cycle requirement	AR	-	9.00	90.0	30.0	-	-	-
Factor of safety based on max $\Delta \epsilon_e$	AR	-	1.28	1.71	1.50	-	-	-
-	SR	-	-	-	-	-	-	-
Welded	-	-	-	-	-	-	-	-

Predicted values from Appendix C.

TABLE B-7

Ti-5Al-2.5Sn (ANNEALED, ELI GRADE), TYPICAL PROPERTIES FOR USE IN PARAMETRIC EVALUATION*

	Specimen Direction	Uniaxial			1-to-1 Biaxial-Stress State		
		75°F	-320°F	-423°F	75°F	-320°F	-423°F
Proportional Limit, ** psi							
Tension	L	90,000	158,000	180,000	Same as uniaxial	↓	
	T	95,000	150,000	178,000			
Compression	L	90,000	158,000	180,000	Same as uniaxial		
	T	95,000	150,000	178,000			
Ratio of Proportional Limit to Density (0.162 lb/in. ³), in. x 10 ³							
Compression	L	556	975	1111	Same as uniaxial	↓	
	T	586	926	1099			
Yield Strength, psi							
Tension	L	100,000	175,000	200,000			
	T	105,000	167,000	198,000			
Compression	L	100,000	175,000	200,000			
	T	105,000	167,000	198,000			
Tensile Strength, psi							
Tension	L	116,000	190,000	220,000	Same as uniaxial	↓	
	T	120,000	187,000	226,000			
Elongation, % in 2 in. ***							
Tension	L	17	12	12.5	4.25	3	3.1
	T	14	11	11	3.5	2.75	2.75
Modulus of Elasticity, psi							
Tension	L	15,600,000	17,100,000	17,000,000	23,600,000	25,100,000	25,000,000
	T	15,100,000	18,300,000	19,400,000	23,100,000	26,300,000	27,400,000
Compression	L	15,600,000	17,100,000	17,000,000	23,600,000	25,100,000	25,000,000
	T	15,100,000	18,300,000	19,400,000	23,100,000	26,300,000	27,400,000
Fracture Toughness, Notch-to-Unnotch Strength Ratio							
Parent Metal							
0.014-in. sheet, K _T =7.2	L	1.32	1.22	1.08	-	-	-
0.034-in. sheet, ↓	L	1.33	1.20	1.12	-	-	-
0.040-in. sheet	L	1.35	1.13	0.97	-	-	-
0.014-in. sheet	T	1.34	1.27	1.04	-	-	-
0.034-in. sheet	T	1.33	1.20	1.12	-	-	-
0.040-in. sheet, K _T =7.2	T	1.33	1.11	0.85	-	-	-
0.020-in. sheet, K _T =8	L	1.30	1.13	0.82	-	-	-
0.020-in. sheet, K _T =8	T	1.28	1.03	0.74	-	-	-
0.025-in.-sheet, K _T =21	L	1.02	0.94	0.58	-	-	-
Welded	-	-	-	-	-	-	-

* L = longitudinal direction, T = transverse. Dashes in last six columns indicate data not available.

*** Biaxial elongation assumed to be 25% of uniaxial value.

** Adjusted to correlate with stress-strain curves of Figure B-62.

TABLE B-7 (cont.)

Specimen Direction	Uniaxial			1-to-1 Biaxial-Stress State		
	75°F	-320°F	-423°F	75°F	-320°F	-423°F
Fracture Toughness, Notched-Strength to Unnotched-Yield-Strength Ratio						
Parent Metal						
0.014-in. sheet, $K_T=7.2$	L	1.55	1.29	1.10	-	-
0.034-in. sheet	L	1.47	1.33	1.23	-	-
0.040-in. sheet	L	1.37	1.22	1.04	-	-
0.014-in. sheet	T	1.78	1.45	1.20	-	-
0.034-in. sheet	T	1.47	1.33	1.23	-	-
0.040-in. sheet, $K_T=7.2$	T	1.43	1.19	0.91	-	-
0.020-in. sheet, $K_T=8$	L	1.45	1.20	-	-	-
0.020-in. sheet, $K_T=8$	T	1.37	1.16	-	-	-
0.025-in. sheet, $K_T=21$	L	1.21	1.03	0.585	-	-
Welded	-	-	-	-	-	-
Weld-Joint Properties						
Joint efficiency, %	L	95	97	95	Same as uniaxial	
	T	93	94	92	Same as uniaxial	
Elongation, % in 2 in.	L	12	8	4	3	2
Fracture toughness	-	-	-	-	-	-
Poisson's Ratio						
-	-	0.295	0.28	0.305	Same as uniaxial	
Low-Cycle, High-Strain Fatigue - Reversed Cycle*						
Parent Metal						
No. of cycles to failure at max operating strain range	-	400	180	130	Insufficient data available	
Magnitude of cyclic elastic-strain range for failure at 100 cycles ($\max \Delta \epsilon_e$), in./in.	-	0.015	0.0220	0.0300	Insufficient data available	
Factor of safety based on 100 cycle requirement	-	4.00	1.80	1.30		
Factor of safety based on $\max \Delta \epsilon_e$	-	1.20	1.07	1.04	Insufficient data available	
Welded	-	-	-	-	-	-

* Predicted values from Appendix C.

TABLE B-8

2219-T62 ALUMINUM, TYPICAL PROPERTIES FOR USE IN PARAMETRIC EVALUATION*

Speci- men Direc- tion		Uniaxial			1-to-1 Biaxial-Stress State					
		75°F	-320°F	-423°F	75°F	-320°F	-423°F			
Proportional Limit, psi										
Tension	L	39,000	50,000	52,000	Same as uniaxial					
	T	40,000	49,500	53,000						
Compression	L	39,000	50,000	52,000	Same as uniaxial					
	T	40,000	49,500	53,000						
Ratio of Proportional Limit to Density (0.102 lb/in. ³), in. x 10 ³										
Compression	L	379	490	510	Same as uniaxial					
	T	392	485	520						
Yield Strength, psi										
Tension	L	43,000	56,000	58,000	Same as uniaxial					
	T	44,500	55,000	59,000						
Compression	L	43,000	56,000	58,000						
	T	44,500	55,000	59,000						
Tensile Strength, psi										
Tension	L	59,000	78,000	92,000						
	T	63,000	79,000	92,000						
Elongation, % in 2 in. **										
Tension	L	10.5	12	14	2.6	3	3.5			
	T	10	14.5	14	2.5	3.6	3.5			
Modulus of Elasticity, psi										
Tension	L	10,300,000	11,500,000	11,600,000	16,300,000	17,500,000	17,600,000			
	T	10,300,000	11,200,000	12,000,000	16,300,000	17,200,000	18,000,000			
Compression	L	10,300,000	11,500,000	11,600,000	16,300,000	17,500,000	17,600,000			
	T	10,300,000	11,200,000	12,000,000	16,300,000	17,200,000	18,000,000			
Fracture Toughness, Notch-to-Unnotch Strength Ratio										
Parent Metal										
0.090-in. sheet, K _T =8	L	0.93	0.86	0.77	-	-	-			
0.100-in. sheet, K _T =8	L	0.94	0.865	0.79	-	-	-			
0.125-in. sheet, K _T =21	L	0.82	0.78	0.73	-	-	-			
0.090-in. sheet, K _T =8	T	0.93	0.865	0.79	-	-	-			
0.100-in. sheet, K _T =8	T	0.93	0.84	0.79	-	-	-			
0.125-in. sheet, K _T =21	T	0.80	0.75	0.64	-	-	-			
Welded	-	-	-	-	-	-	-			

* L = longitudinal direction, T = transverse. Dashes in last six columns indicate data not available.

** Biaxial elongation assumed to be 25% of uniaxial value.

TABLE B-8 (cont.)

Specimen Direction	Uniaxial			1-to-1 Biaxial-Stress State		
	75°F	-320°F	-423°F	75°F	-320°F	-423°F
Fracture Toughness, Notched-Strength to Unnotched-Yield-Strength Ratio						
Parent Metal						
0.090-in. sheet, $K_T=8$	L	1.28	1.22	1.24	-	-
0.100-in. sheet, $K_T=8$	L	1.29	1.205	1.22	-	-
0.125-in. sheet, $K_T=21$	L	1.215	1.148	1.24	-	-
0.090-in. sheet, $K_T=8$	T	1.27	1.227	1.235	-	-
0.100-in. sheet, $K_T=8$	T	1.258	1.19	1.29	-	-
0.125-in. sheet, $K_T=21$	T	1.17	1.13	1.137	-	-
Welded	-	-	-	-	-	-
Weld-Joint Properties						
Joint Efficiency, %	L*	114	96	87.5	Same as uniaxial	
	T**	103.5	98	87.5	Same as uniaxial	
	L**	100	99	87.5	Same as uniaxial	
Elongation, % in 2 in.	L	9.0	7	4	2.25	1.75
Fracture toughness	-	-	-	-	-	1.0
Poisson's Ratio						
-	-	0.325	0.335	0.335	Same as uniaxial	
Low-Cycle, High-Strain Fatigue - Reversed Cycle ***						
Parent Metal						
No. of cycles to failure at max operating strain range	-	1500	1500	3500	Insufficient data available	
Magnitude of elastic-strain range for failure at 100 cycles ($\max \Delta \epsilon_e$), in./in.	-	0.0120	0.0140	0.0155	Insufficient data available	
Factor of safety based on 100-cycle requirement	-	15	15	35		
Factor of safety based on $\max \Delta \epsilon_e$	-	1.42	1.43	1.55		
Welded	-	-	-	-	-	-

* Welded in T62 temper and then reheat-treated to T62 temper.

** Welded in T31 temper and then reheat-treated to T62 temper.

*** Predicted values from Appendix C.

TABLE B-9

INCONEL X-750 (SOLUTION-TREATED AND AGED), TYPICAL PROPERTIES FOR USE IN PARAMETRIC EVALUATION*

Specimen Direction		Uniaxial			1-to-1 Biaxial-Stress State					
		75°F	-320°F	-423°F	75°F	-320°F	-423°F			
Proportional Limit, psi										
Tension	L	108,000	122,000	126,000	Same as uniaxial					
	T	108,000	124,000	128,000						
Compression	L	108,000	122,000	126,000	Same as uniaxial					
	T	108,000	124,000	128,000						
Ratio of Proportional Limit to Density (0.300 lb/in. ³), in. x 10 ³										
Compression	L	360	407	420	Same as uniaxial					
	T	360	413	427						
Yield Strength, psi										
Tension	L	120,000	136,000	140,000	Same as uniaxial					
	T	120,000	138,000	142,000						
Compression	L	120,000	136,000	140,000						
	T	120,000	138,000	142,000						
Tensile Strength, psi										
Tension	L	174,000	214,000	234,000						
	T	174,000	216,000	234,000						
Elongation, % in 2 in.**										
Tension	L	25	31	28	6.25	7.75	7.0			
	T	25.5	30	31	6.4	7.5	7.75			
Modulus of Elasticity, psi										
Tension	L	31	31.5	32	41	41.5	42			
	T	31	31.5	32	41	41.5	42			
Compression	L	31	31.5	32	41	41.5	42			
	T	31	31.5	32	41	41.5	42			
Fracture Toughness, Notch-to-Unnotch Strength Ratio										
Parent Metal										
K _T =6.3	L	0.97	0.86	0.85	-	-	-			
K _T =6.3	T	0.97	0.87	0.86	-	-	-			
K _T =7.2	L	0.99	0.88	0.80	-	-	-			
K _T =8	L	1.00	0.86	0.86	-	-	-			
K _T =8	T	0.97	0.86	0.85	-	-	-			
K _T =10	L	0.90	0.79	0.82	-	-	-			
Welded	-	-	-	-	-	-	-			

* L = longitudinal direction, T = transverse. Dashes in last six columns indicate data not available.

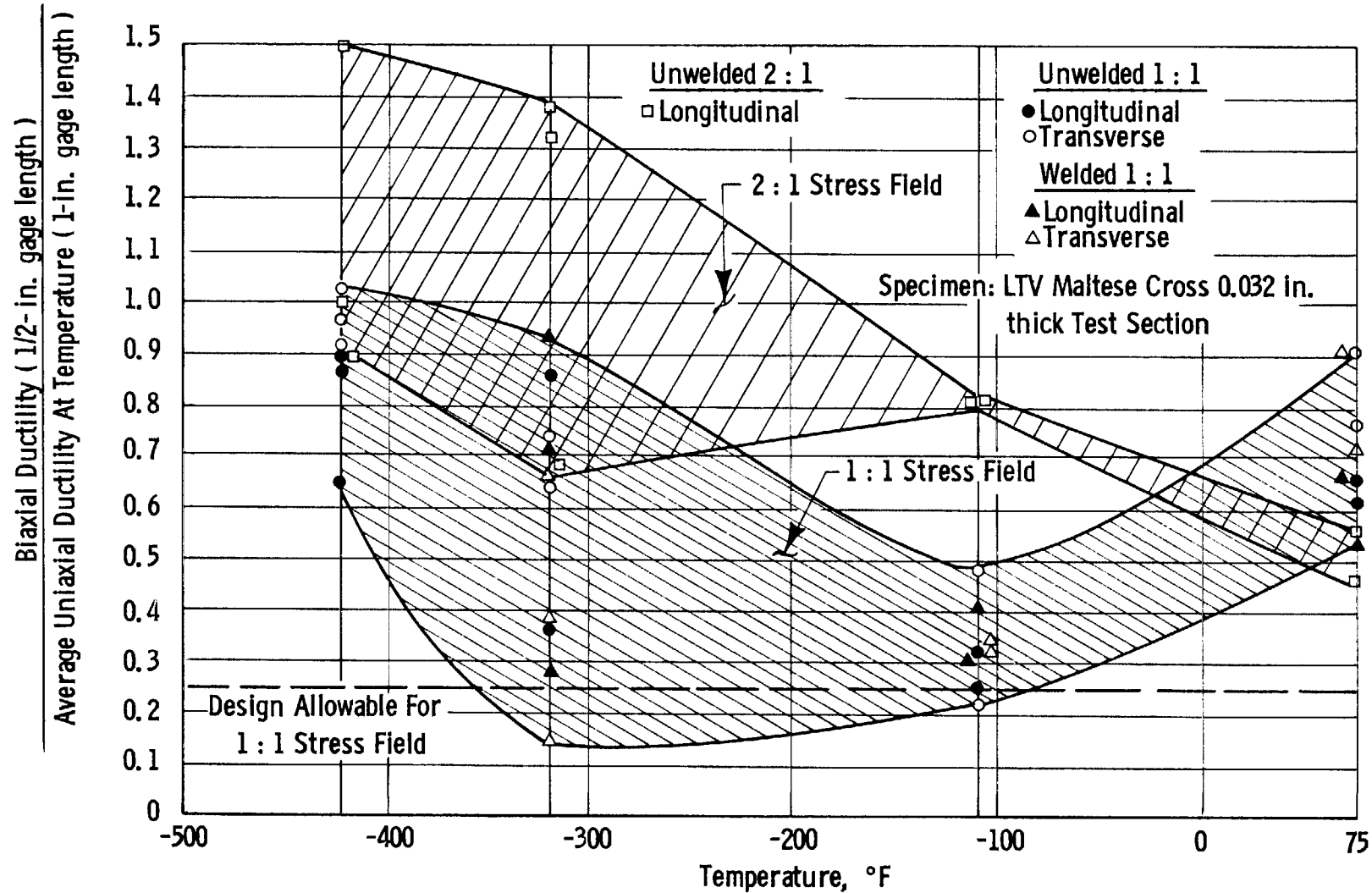
** Biaxial elongation assumed to be 25% of uniaxial value.

TABLE B-9 (cont.)

Specimen Direction	Uniaxial			1-to-1 Biaxial-Stress State		
	75°F	-320°F	-423°F	75°F	-320°F	-423°F
Fracture Toughness, Notched-Strength to Unnotched-Yield-Strength Ratio						
Parent Metal						
K _T =6.3	L	1.42	1.41	1.48	-	-
K _T =6.3	T	1.42	1.41	1.44	-	-
K _T =7.2	L	1.44	1.42	1.50	-	-
K _T =8	L	1.40	1.32	1.41	-	-
K _T =8	T	1.40	1.38	1.36	-	-
K _T =10	L	1.28	1.25	1.33	-	-
Welded	-	-	-	-	-	-
Weld-Joint Properties						
Joint efficiency, %	-	105	119	116	Same as uniaxial	
Elongation, % in 2-in.	-	20.5	21	24	5.1	5.25 6.0
Poisson's Ratio						
-	-	0.29	0.29	0.29	Same as uniaxial	
Low-Cycle, High-Strain Fatigue - Reversed Cycle*						
Parent Metal						
No. of cycles to failure at max operating strain range	-	3500	7000	10,000	Insufficient data available	
Magnitude of elastic-strain range for failure at 100 cycles (max $\Delta\epsilon_e$), in./in.	-	0.0120	0.0145	0.0150	↓ Insufficient data available	
Factor of safety based on 100-cycle requirement	-	35	70	100		
Factor of safety based on max $\Delta\epsilon_e$	-	1.50	1.67	1.74		
Welded	-	-	-	-	-	-

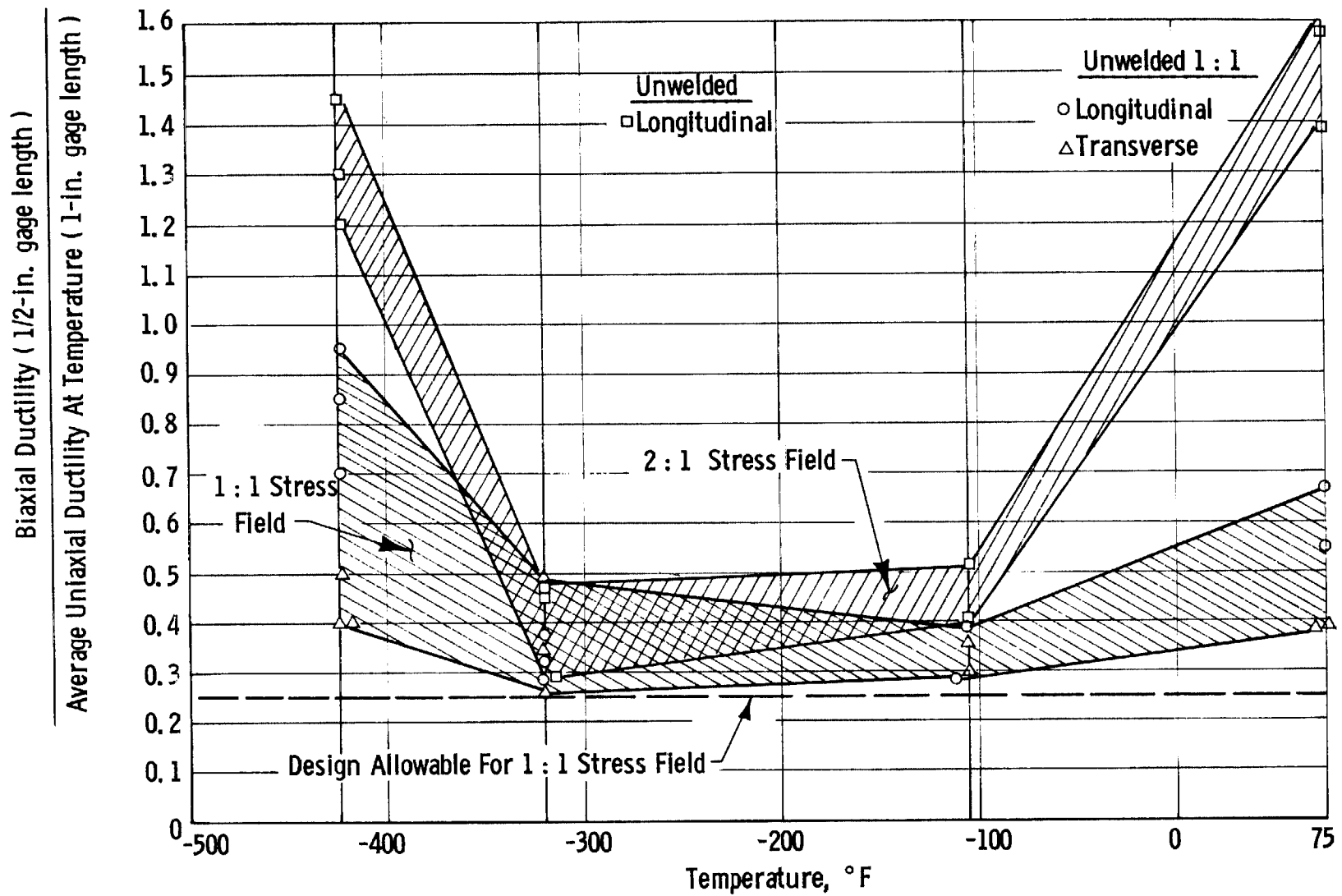
*Predicted values from Appendix C.

Figure B-1



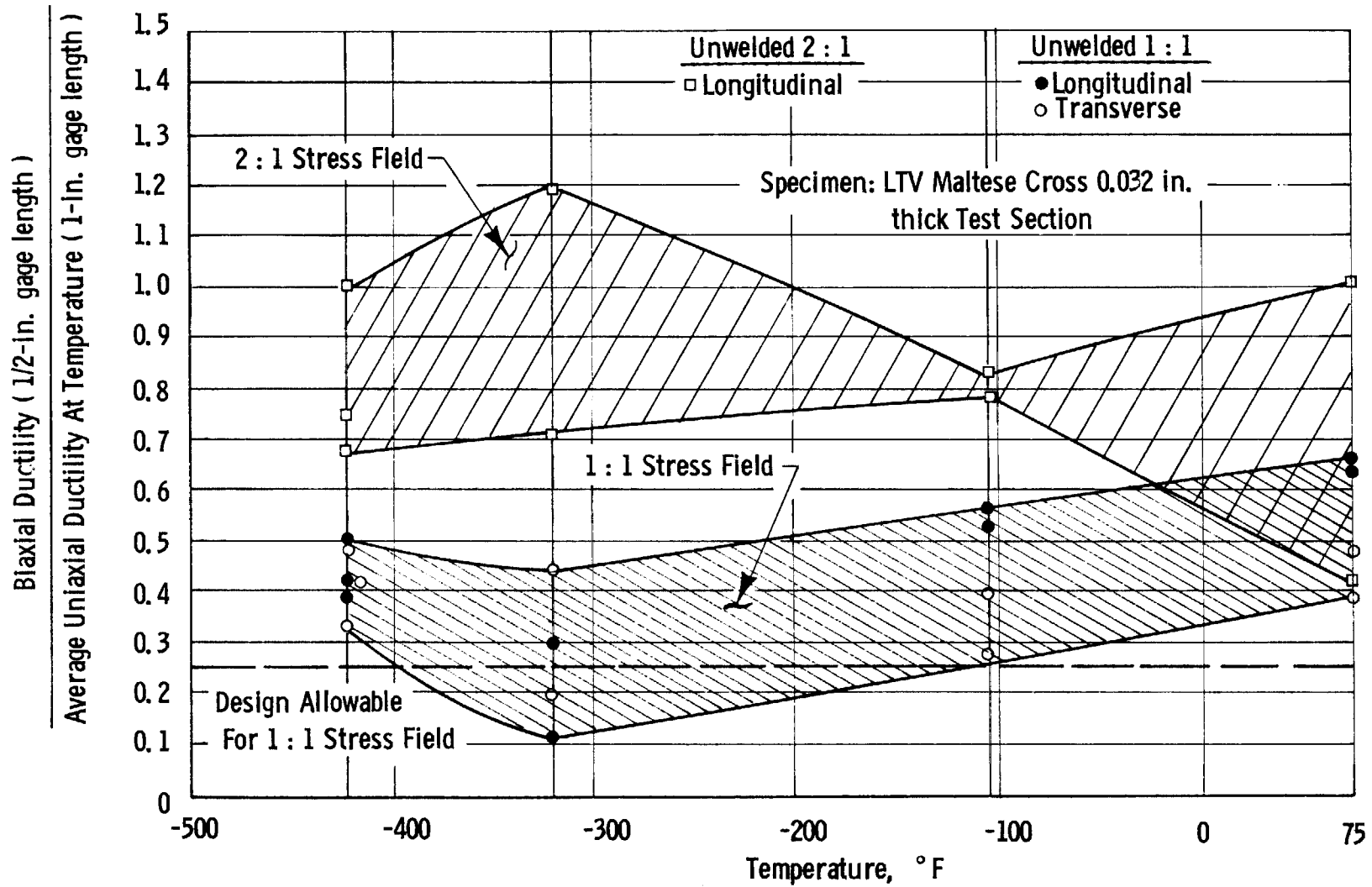
BIAXIAL - TO - UNIAXIAL DUCTILITY RATIOS FOR 5 Al - 2.5 Sn TITANIUM (ANNEALED, ELI), WELDED AND UNWELDED

Figure B-2

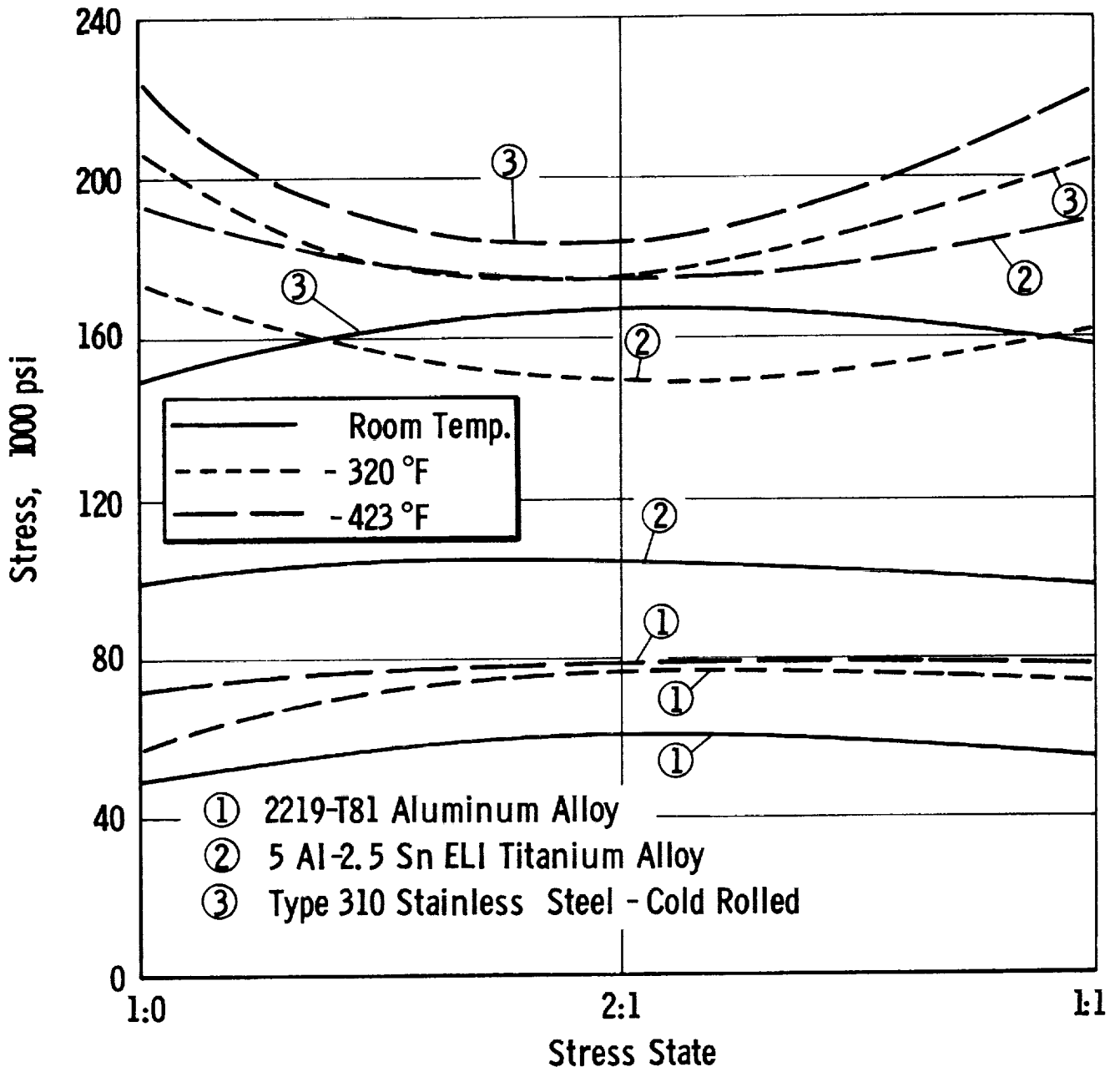


BIAXIAL-TO-UNIAXIAL DUCTILITY RATIOS FOR 310 STAINLESS STEEL (3/4 HARD)

Figure B-3

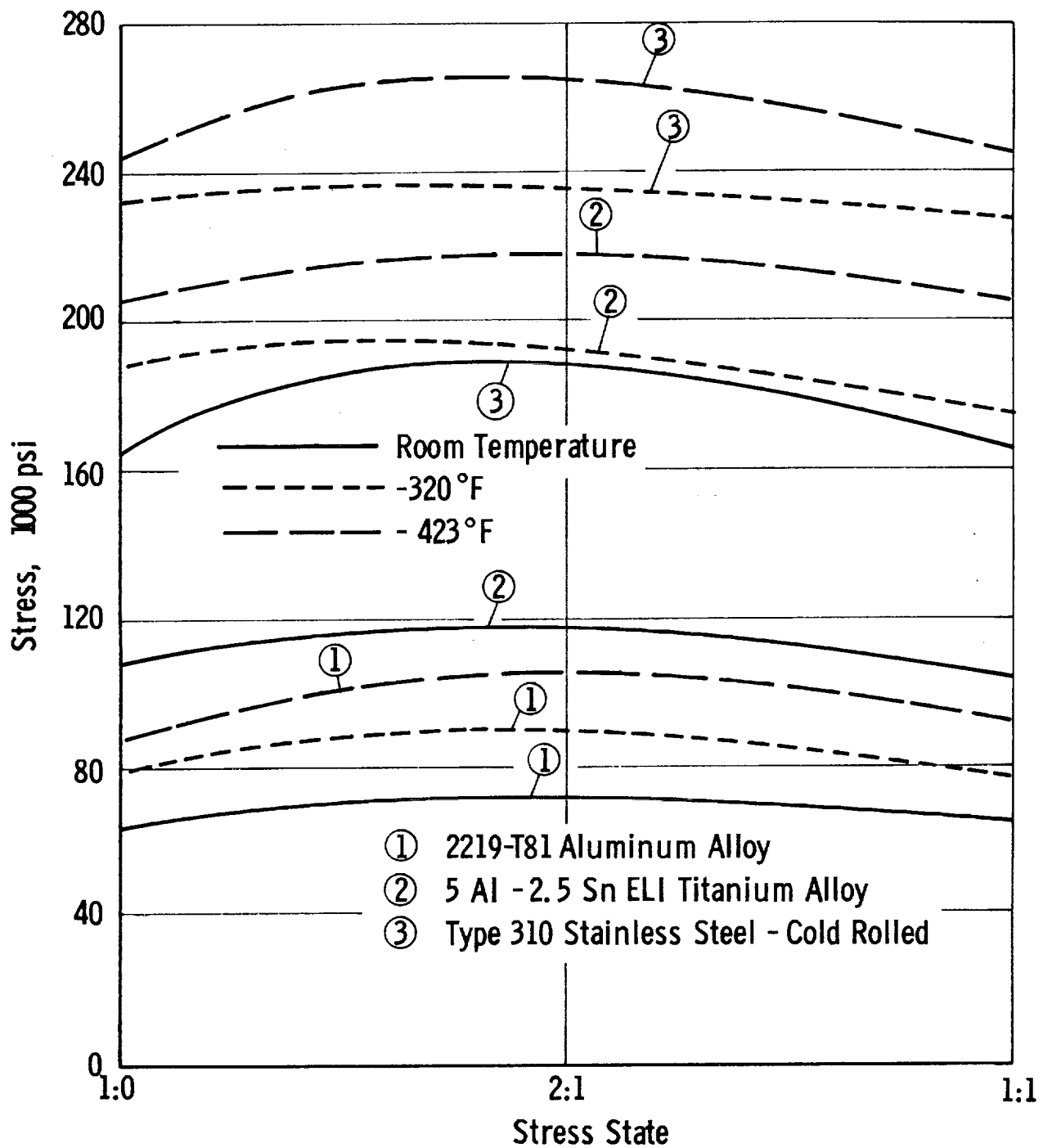


BIAXIAL-TO-UNIAXIAL DUCTILITY RATIOS FOR 2219-T81 ALUMINUM ALLOY



EFFECT OF BIAXIAL STRESS STATE ON TENSILE YIELD STRENGTH

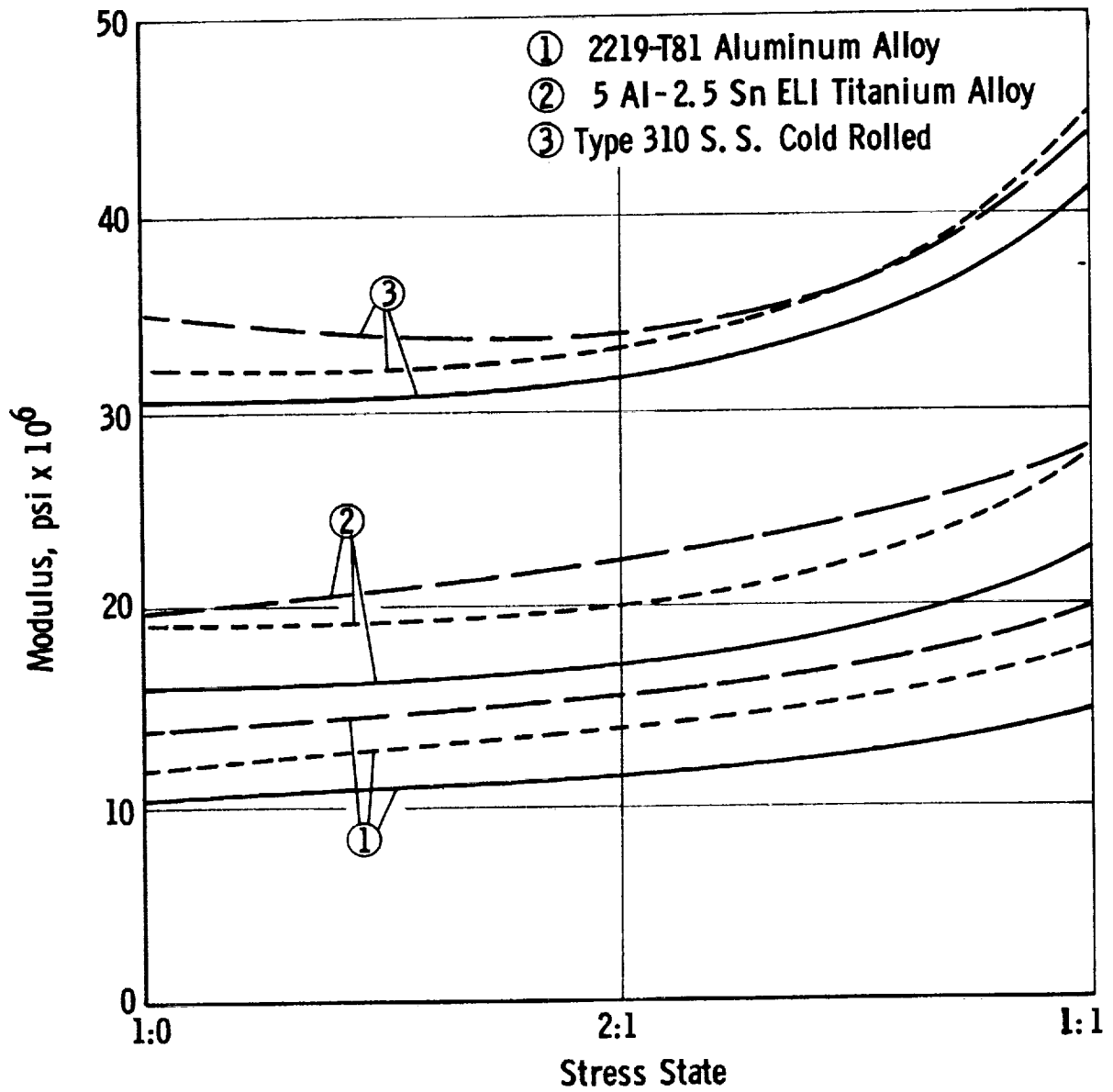
Figure B-4



EFFECT OF BIAXIAL STRESS STATE ON TENSILE STRENGTH

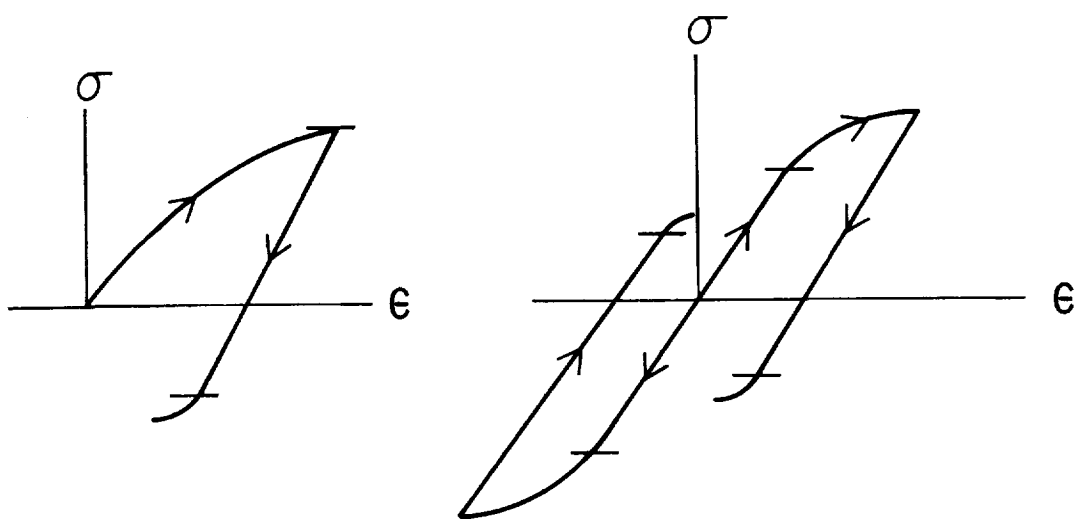
Figure B-5

— Room Temperature
 - - - 320°F
 — — — 423°F



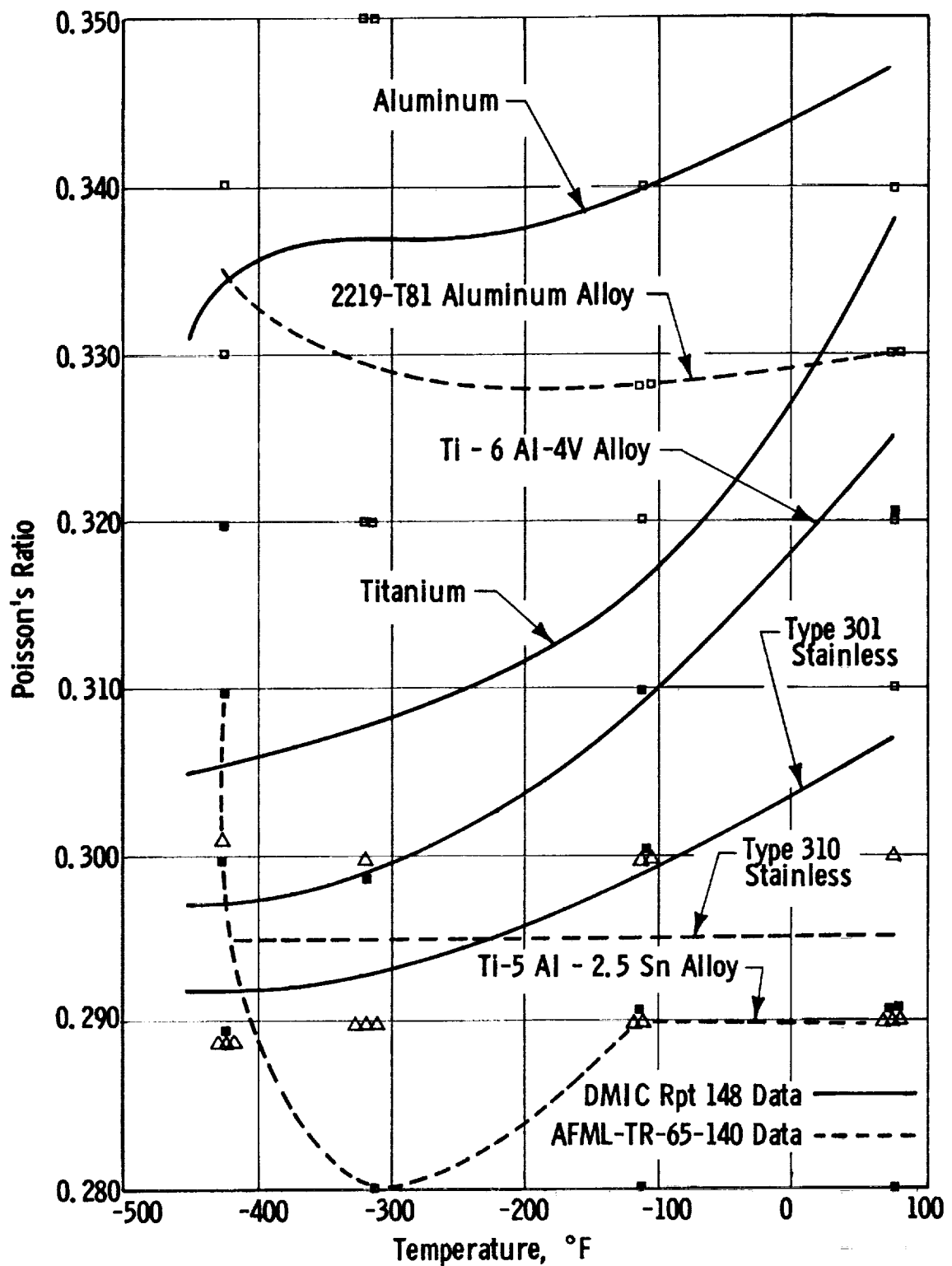
EFFECT OF BIAXIAL STRESS STATE ON MODULUS OF ELASTICITY

Figure B-6



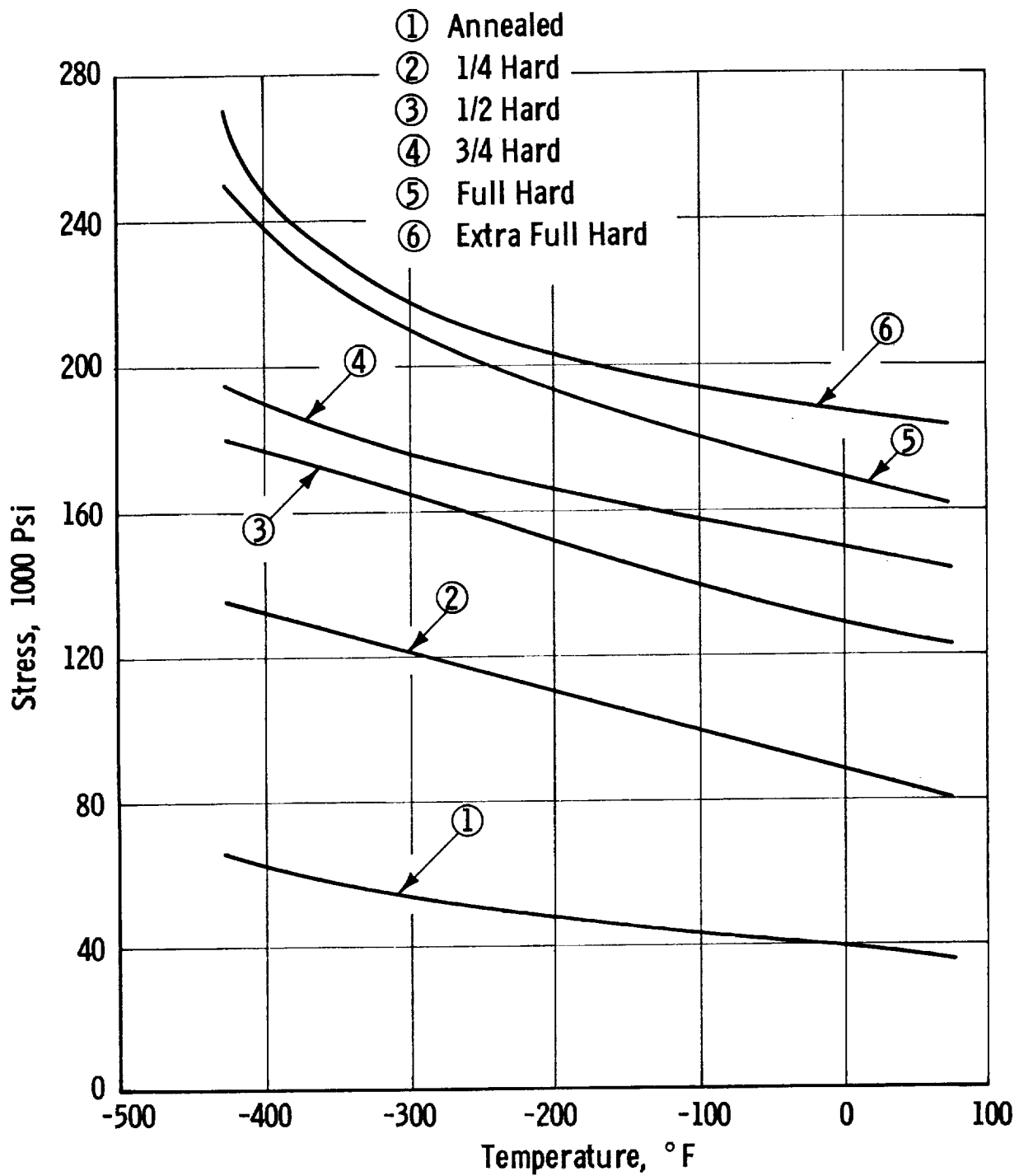
BAUSCHINGER EFFECT

Figure B-7



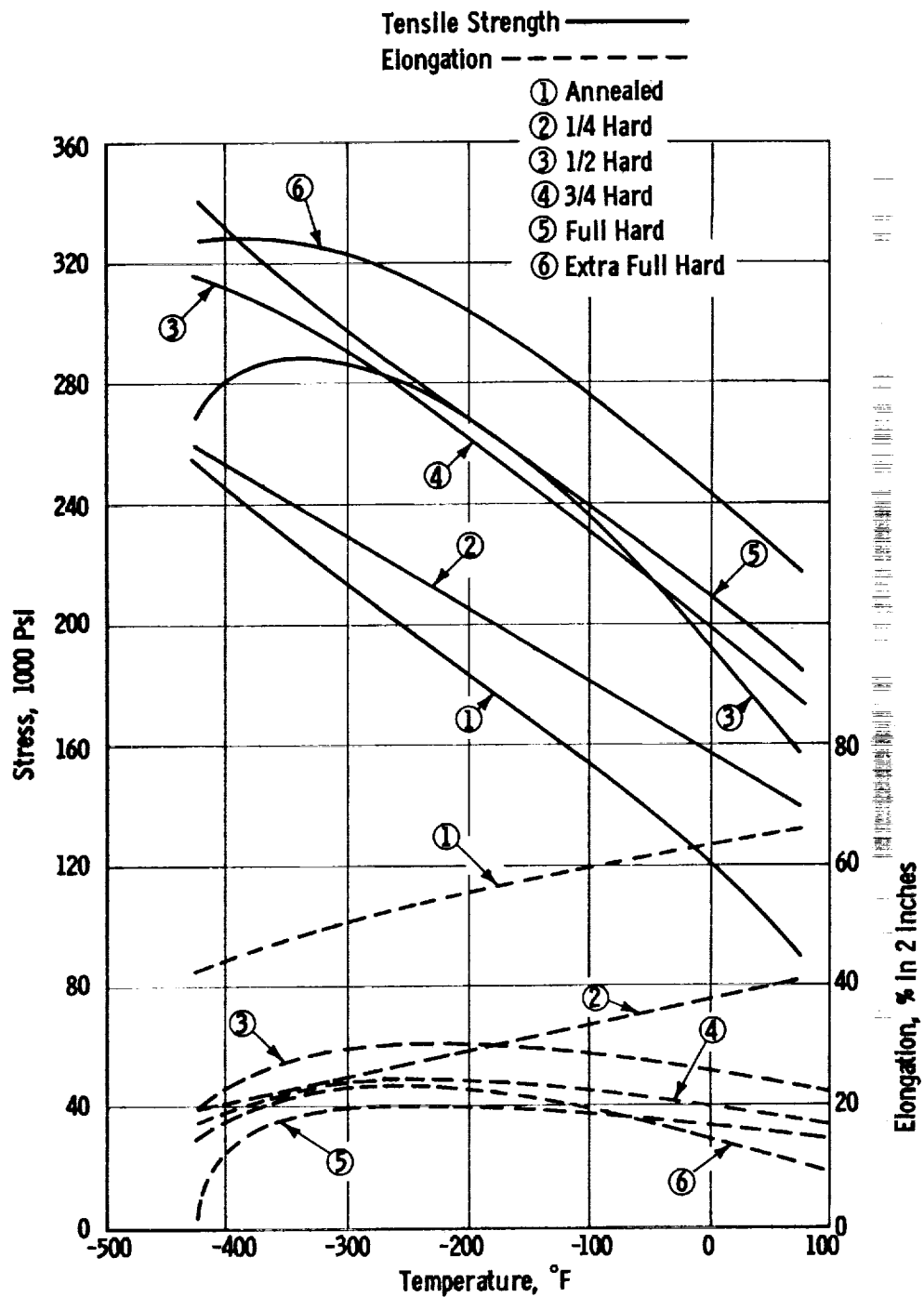
POISSON'S RATIO AS A FUNCTION OF TEMPERATURE

Figure B-8



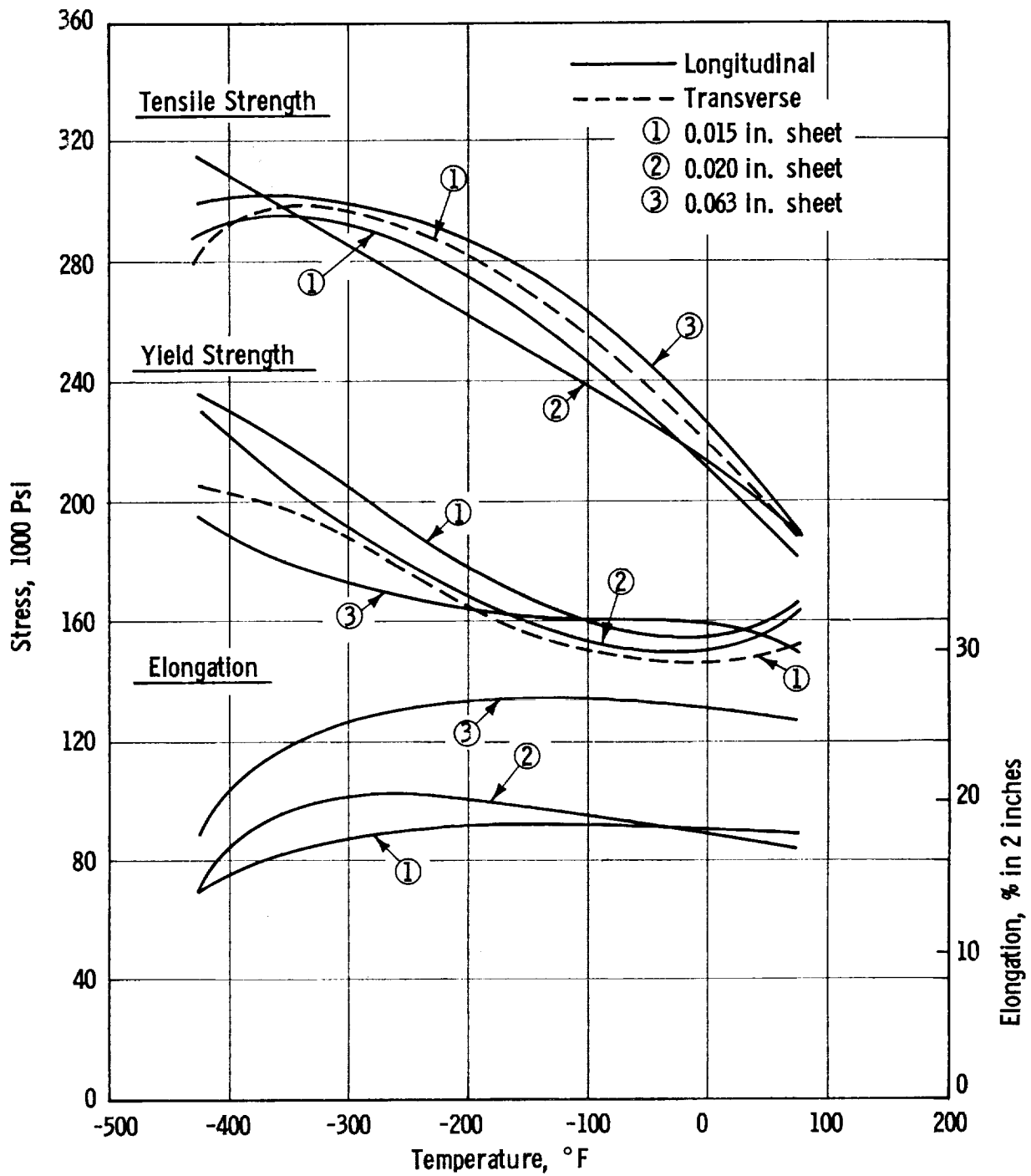
TYPE 301 STAINLESS STEEL-TYPICAL YIELD STRENGTH - LONGITUDINAL

Figure B-9



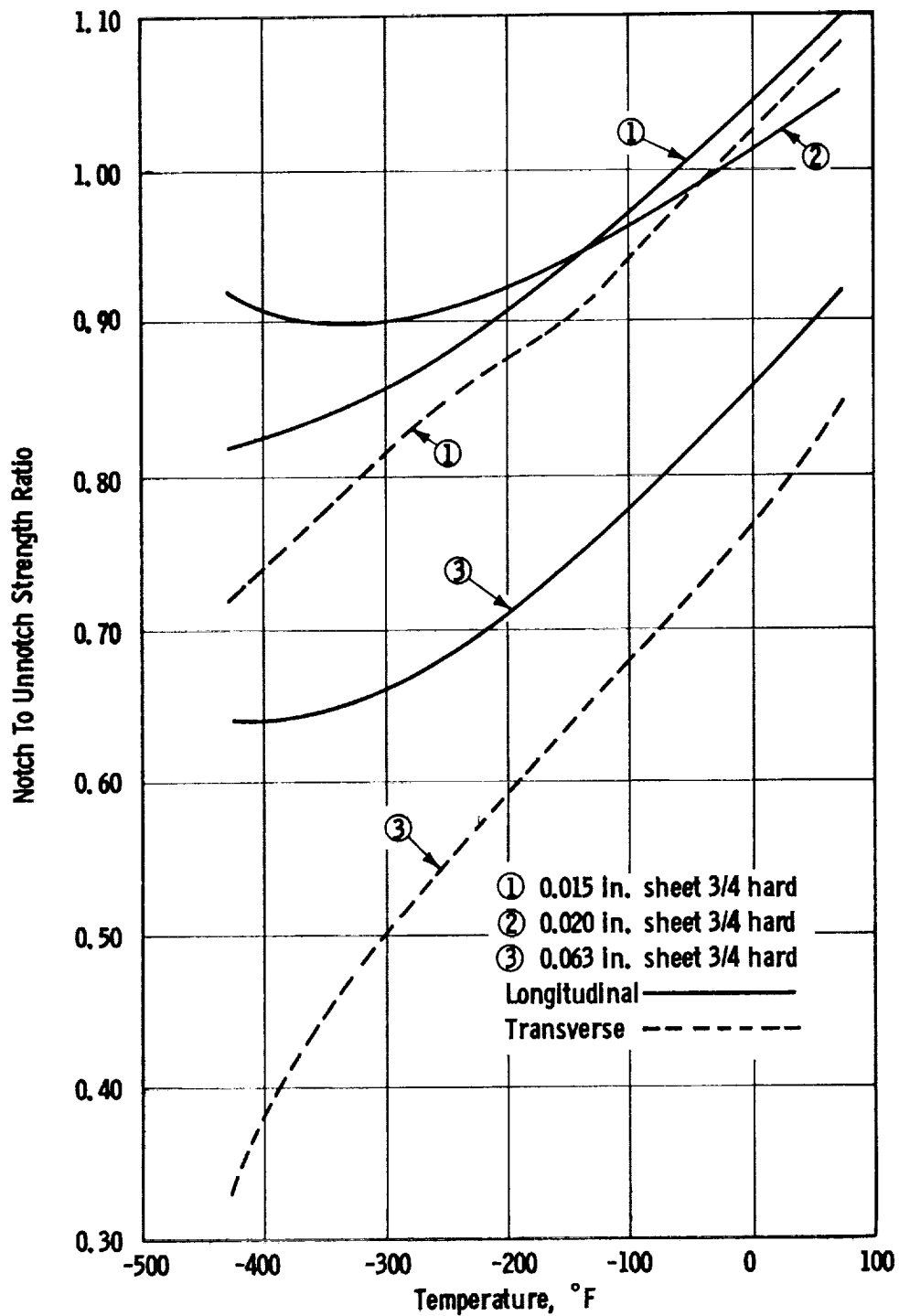
TYPE 301 STAINLESS STEEL-TYPICAL TENSILE STRENGTH AND ELONGATION-LONGITUDINAL

Figure B-10



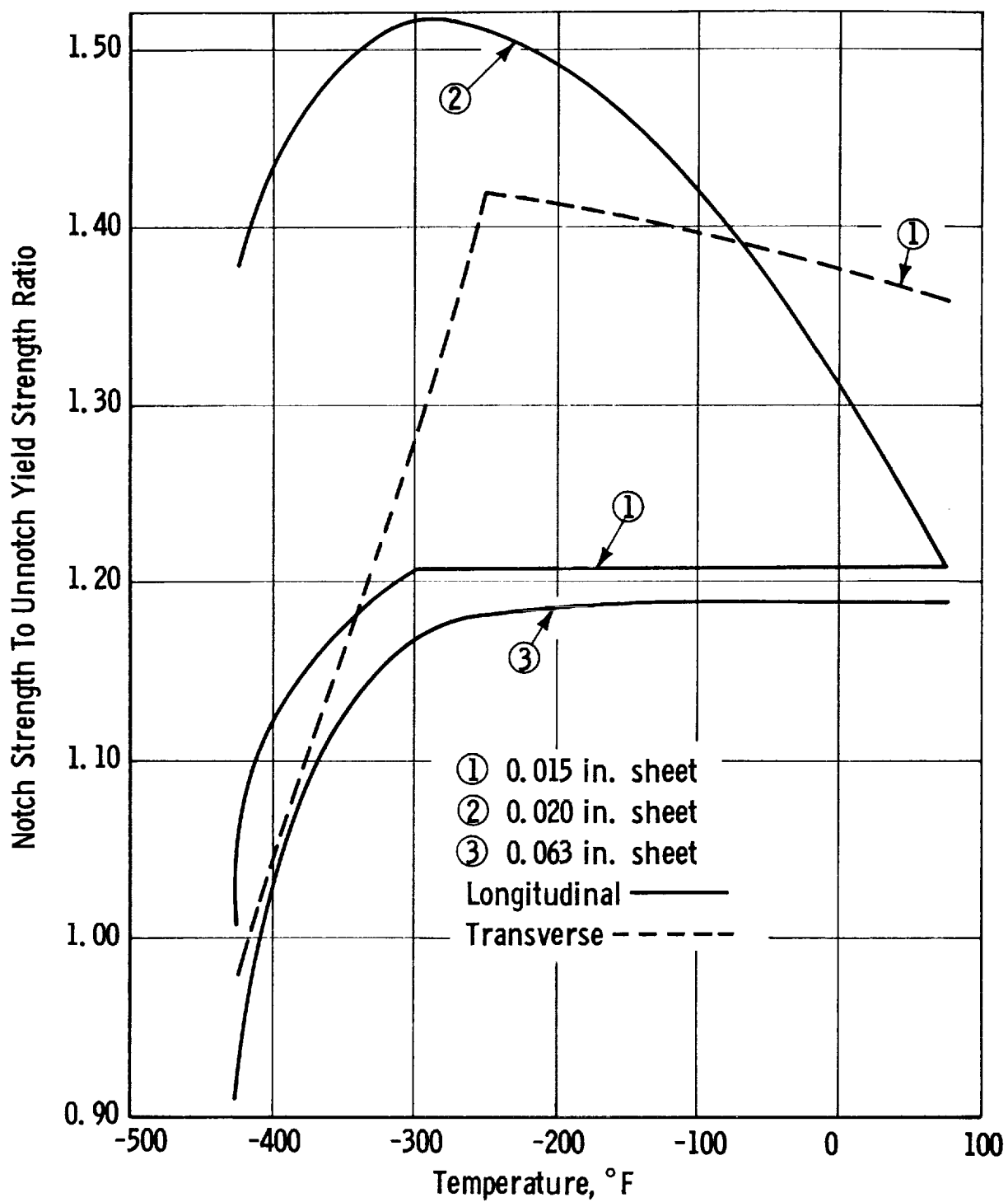
TYPE 301 STAINLESS STEEL - 3/4 HARD (40% CR), TENSILE PROPERTIES

Figure B-11



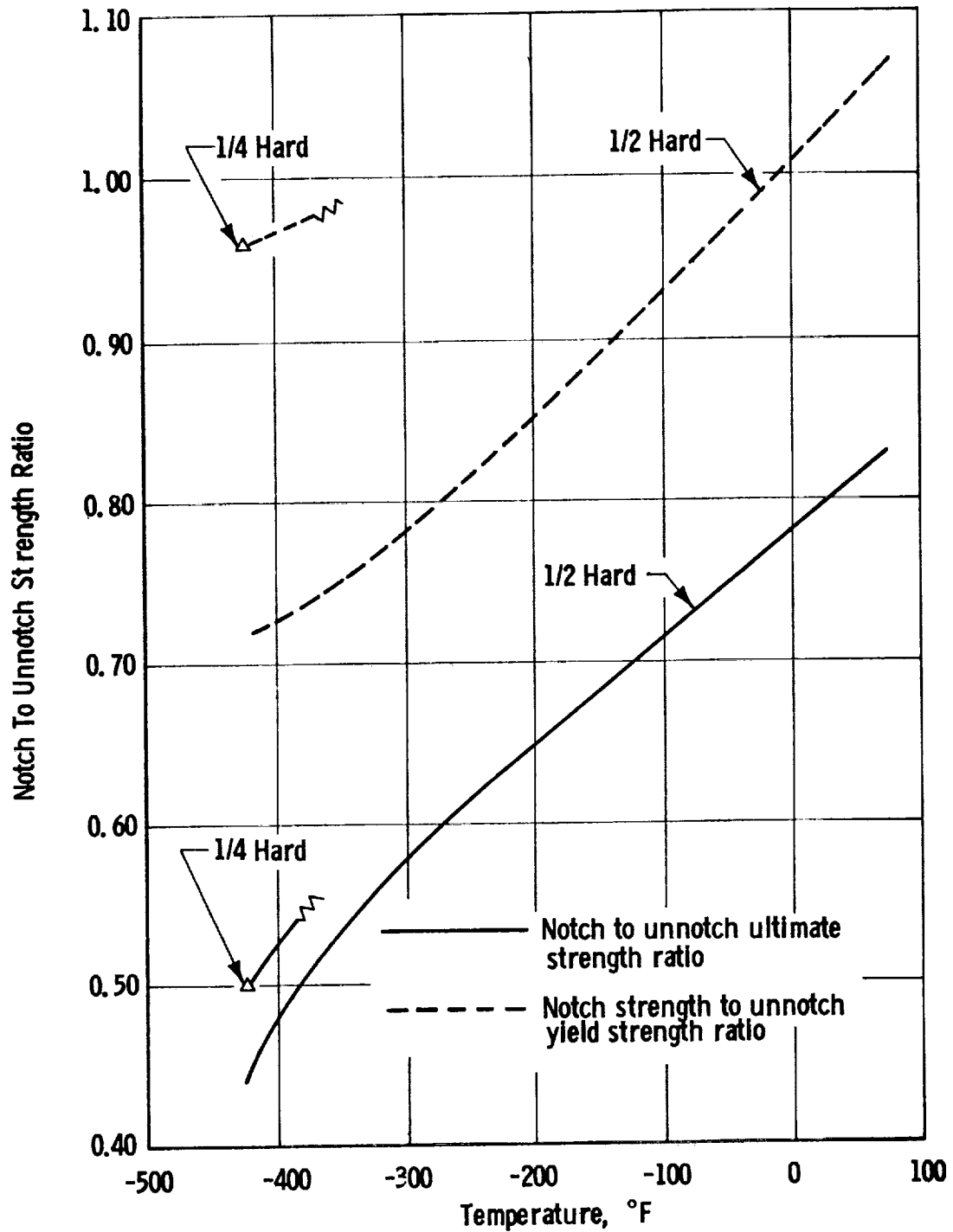
TYPE 301 STAINLESS STEEL - 3/4 HARD NOTCH TO UNNOTCH STRENGTH RATIO ($K_T = 7.2$)

Figure B-12



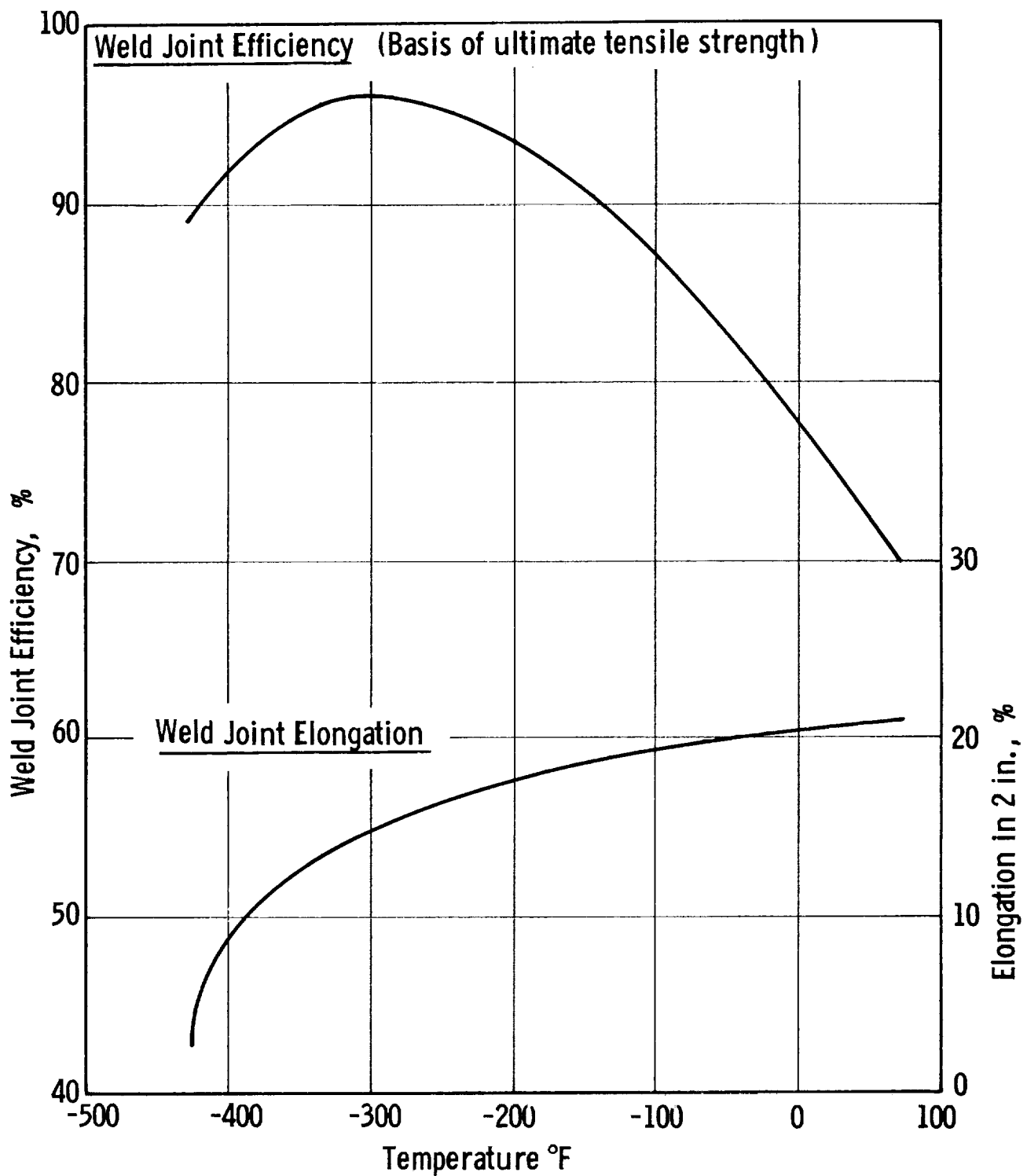
TYPE 301 STAINLESS STEEL (3/4 HARD TEMPER)
 NOTCH STRENGTH TO UNNOTCH YIELD STRENGTH RATIO ($K_T = 7.2$)

Figure B-13



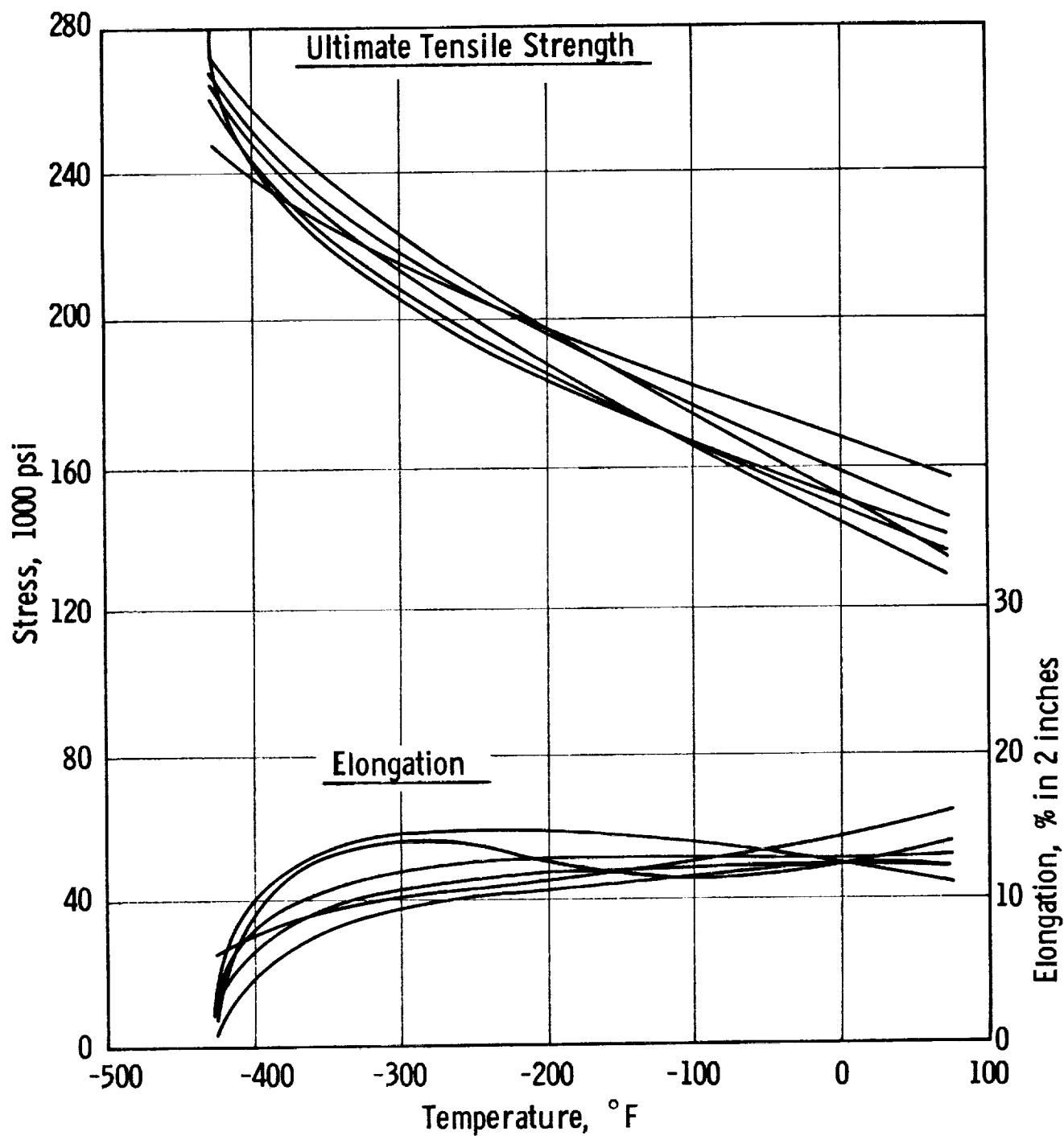
TYPE 301 STAINLESS STEEL - 1/4 HARD AND 1/2 HARD TEMPERS
NOTCH TO UNNOTCH STRENGTH RATIOS ($K_T = 21$)

Figure B-14



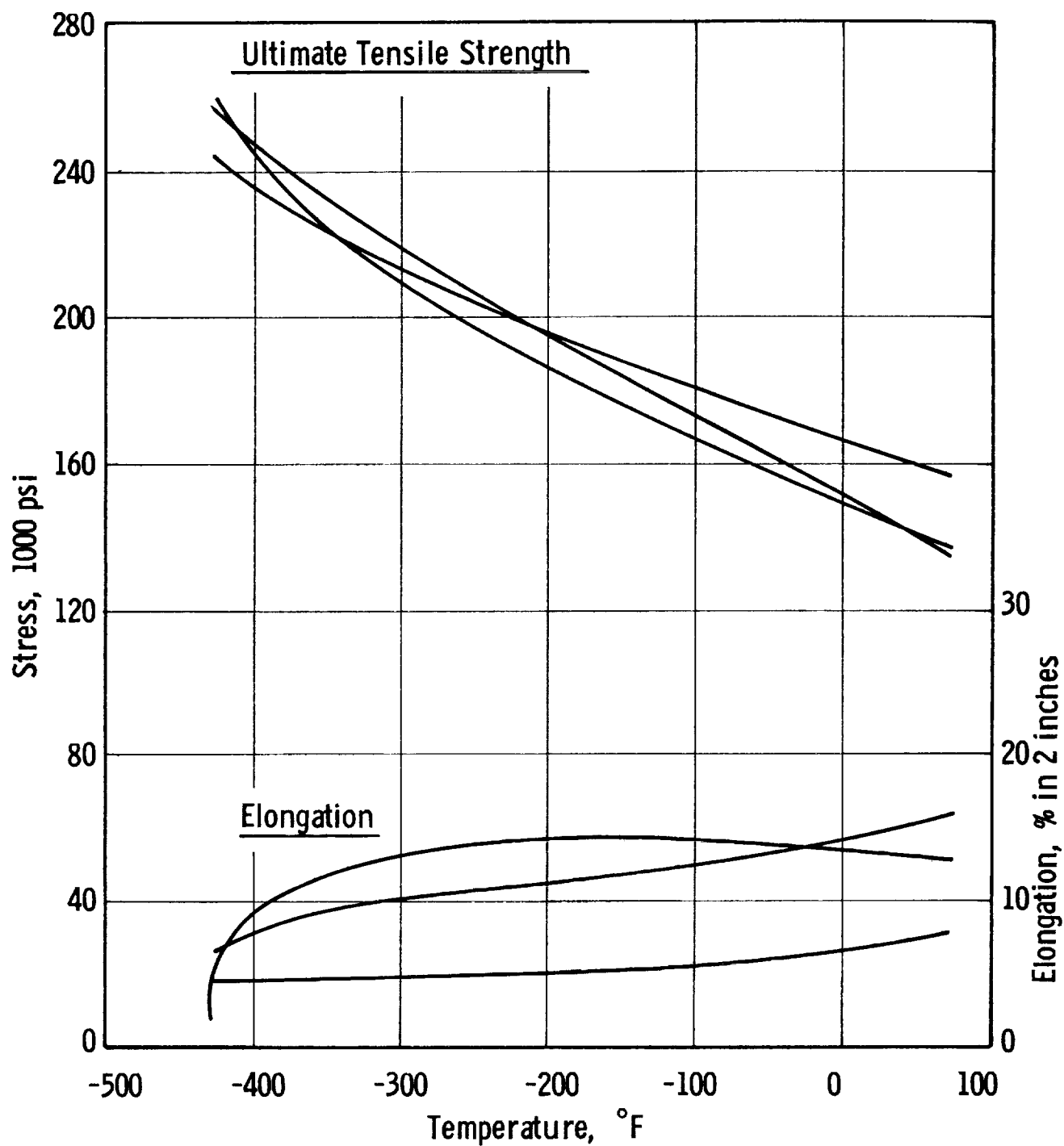
TYPE 301 STAINLESS STEEL-3/4 HARD TEMPER, WELDED JOINT PROPERTIES

Figure B-15



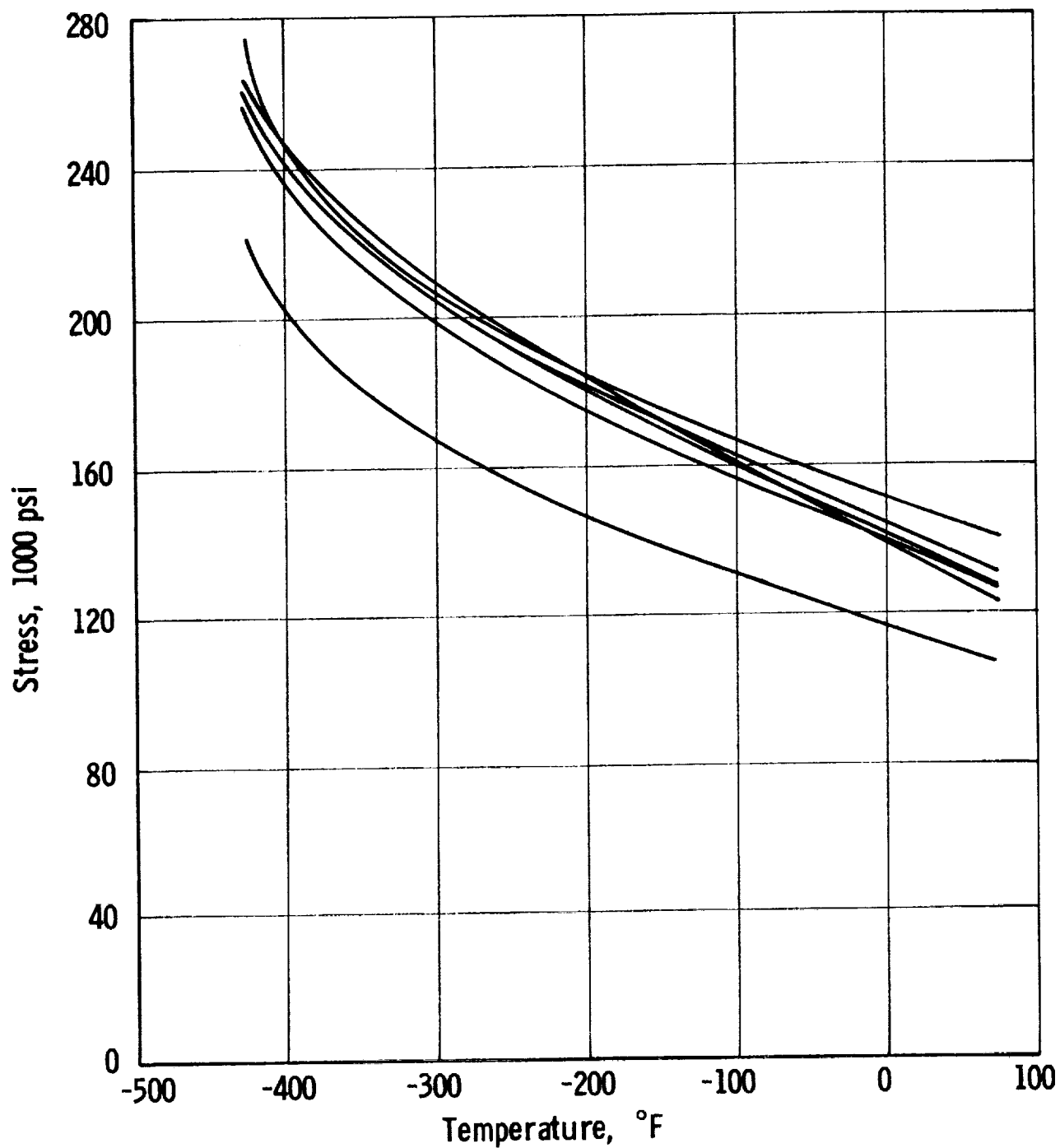
Ti-6Al-4V-NORMAL INTERSTITIAL-ULTIMATE TENSILE STRENGTH
AND ELONGATION - SHEET, LONGITUDINAL - ANNEALED.
(THICKNESS RANGE - 0.040 IN. TO 0.090 IN.)

Figure B-16



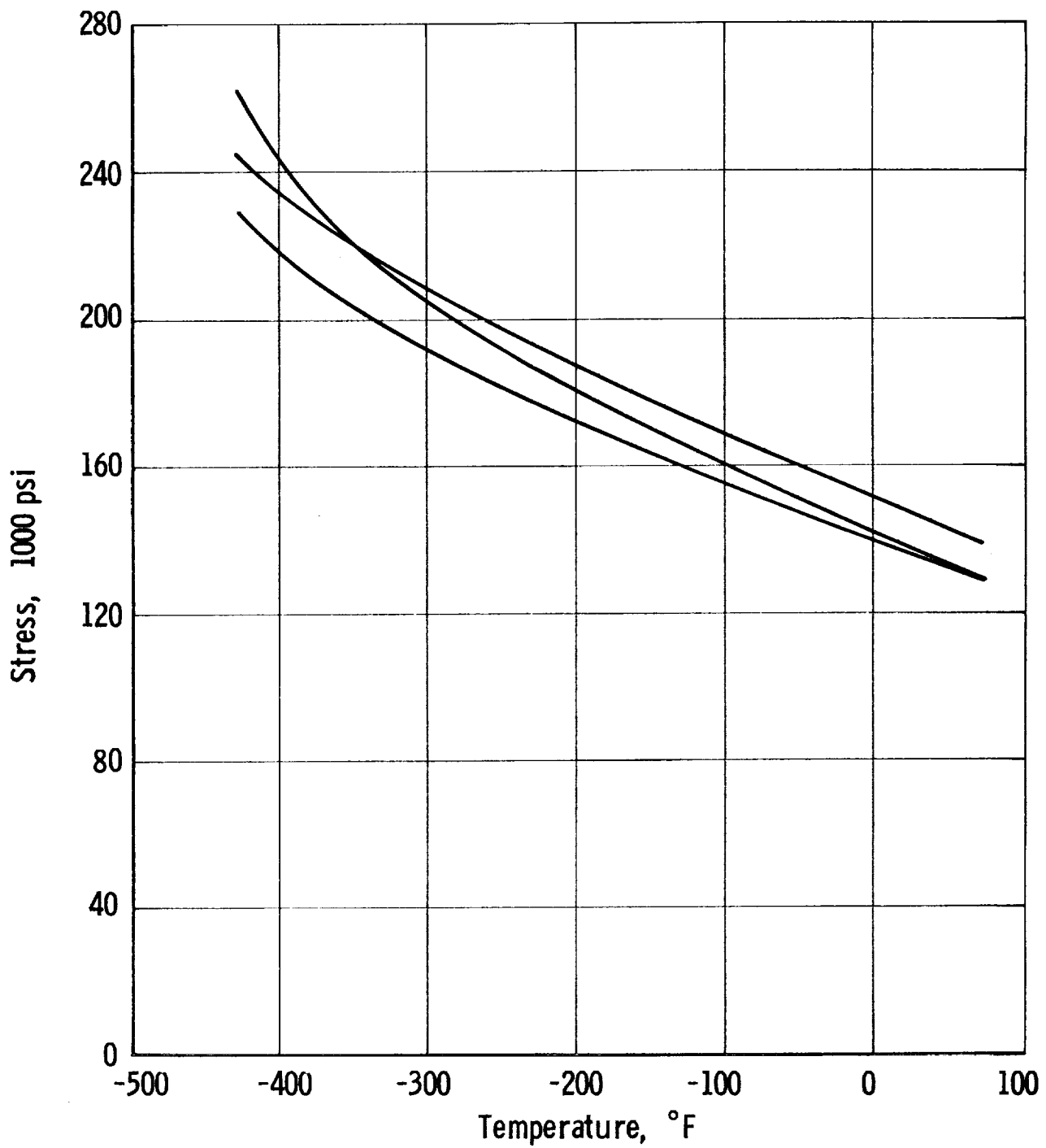
Ti-6Al-4V-NORMAL INTERSTITIAL-ULTIMATE TENSILE STRENGTH
AND ELONGATION - SHEET, TRANSVERSE - ANNEALED.
(THICKNESS RANGE 0.040 IN. TO 0.090 IN.)

Figure B-17



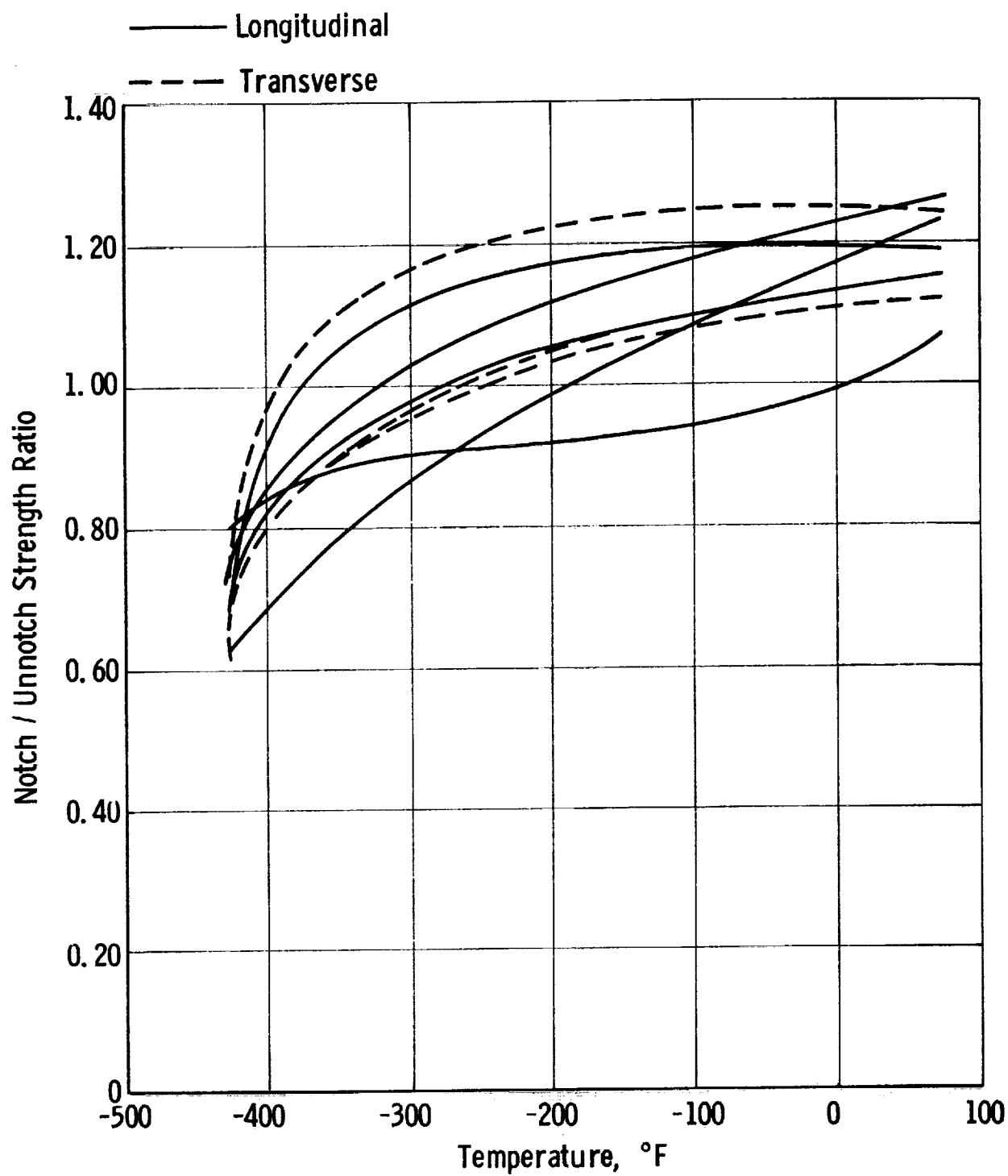
Ti-6 Al-4V-NORMAL INTERSTITIAL-YIELD STRENGTH-SHEET,
ANNEALED-LONGITUDINAL (THICKNESS RANGE 0.040 IN. TO 0.090 IN.)

Figure B-18



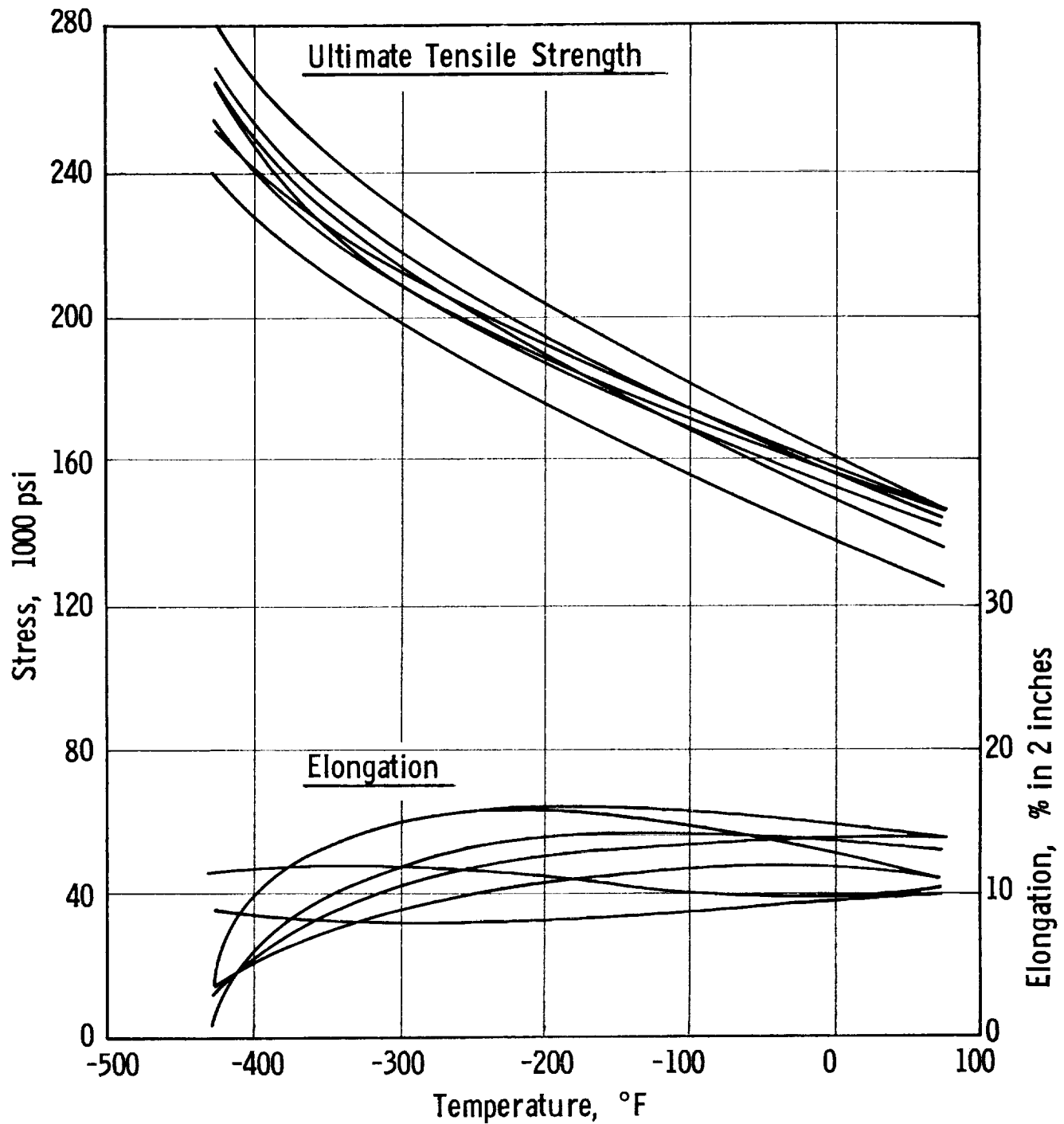
Ti-6 Al-4V-NORMAL INTERSTITIAL-YIELD STRENGTH-SHEET,
ANNEALED-TRANSVERSE. (THICKNESS RANGE 0.040 IN. TO 0.090 IN.)

Figure B-19



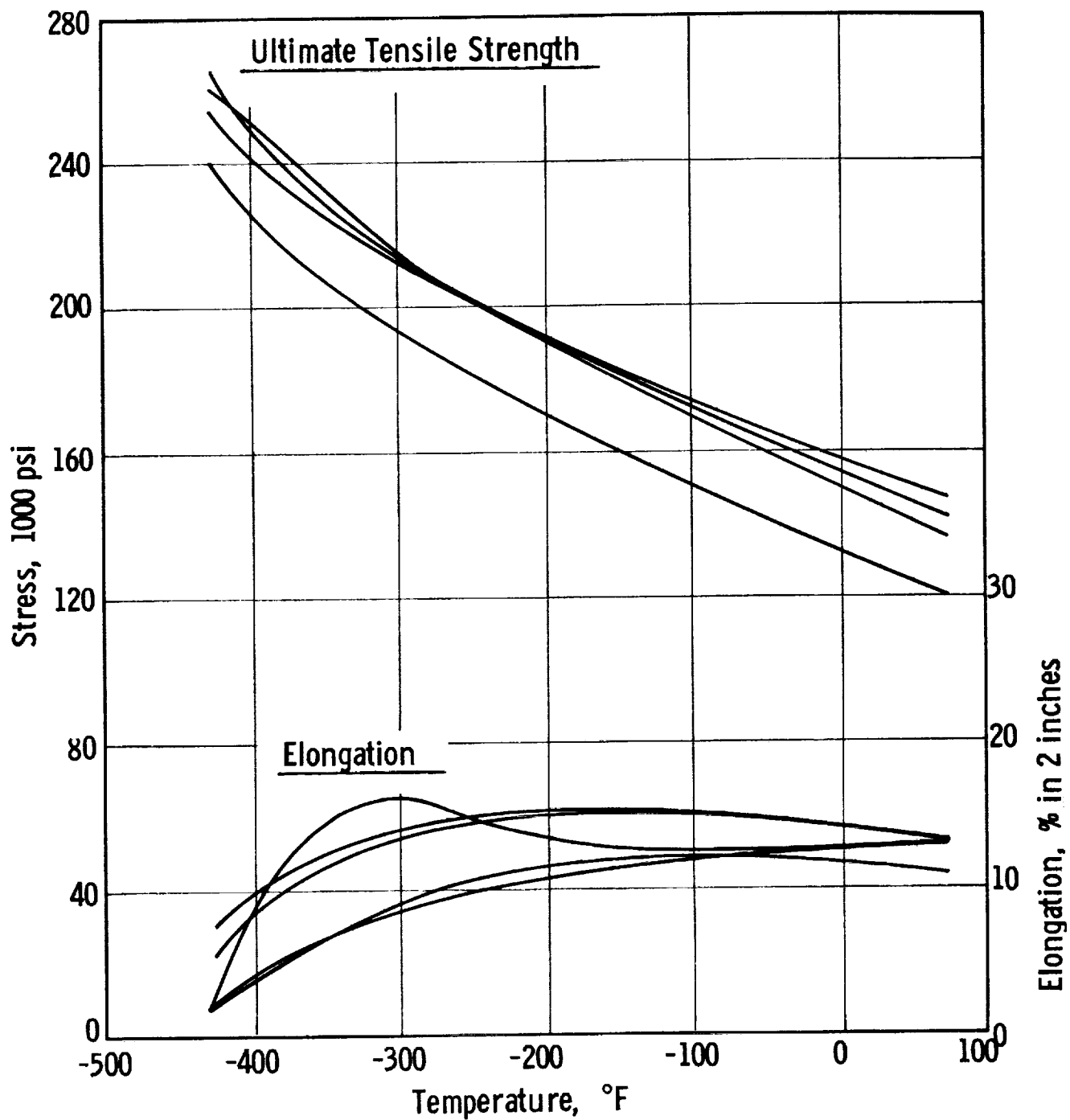
Ti-6 Al-4V-NORMAL INTERSTITIAL-NOTCH / UNNOTCH STRENGTH RATIO
SHEET, ANNEALED (THICKNESS RANGE 0.040 IN. TO 0.090 IN.)

Figure B-20



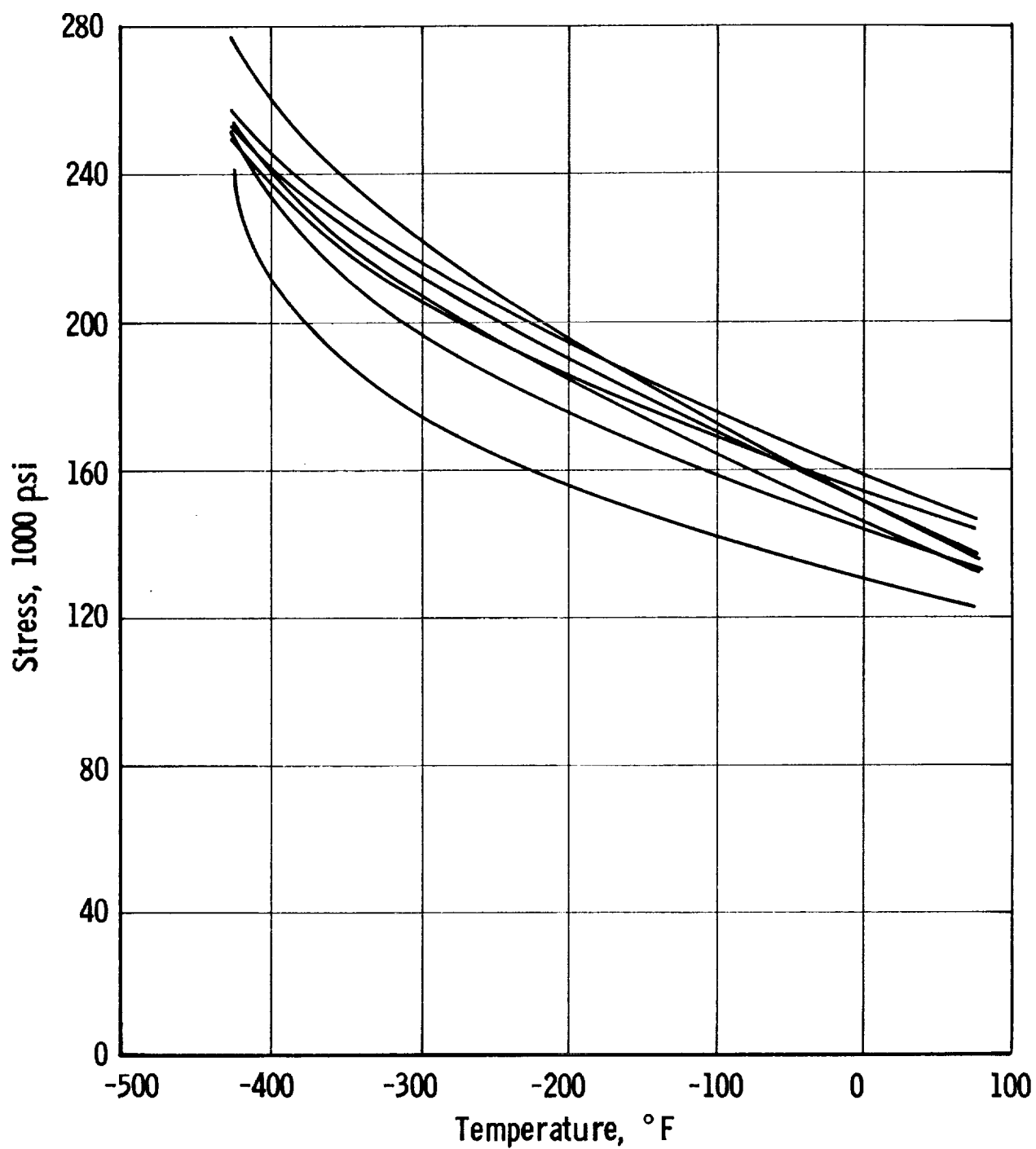
Ti-6 Al-4V-ELI GRADE-ULTIMATE TENSILE STRENGTH AND ELONGATION-SHEET, LONGITUDINAL-ANNEALED
(THICKNESS RANGE 0.025 IN. TO 0.063 IN.)

Figure B-21



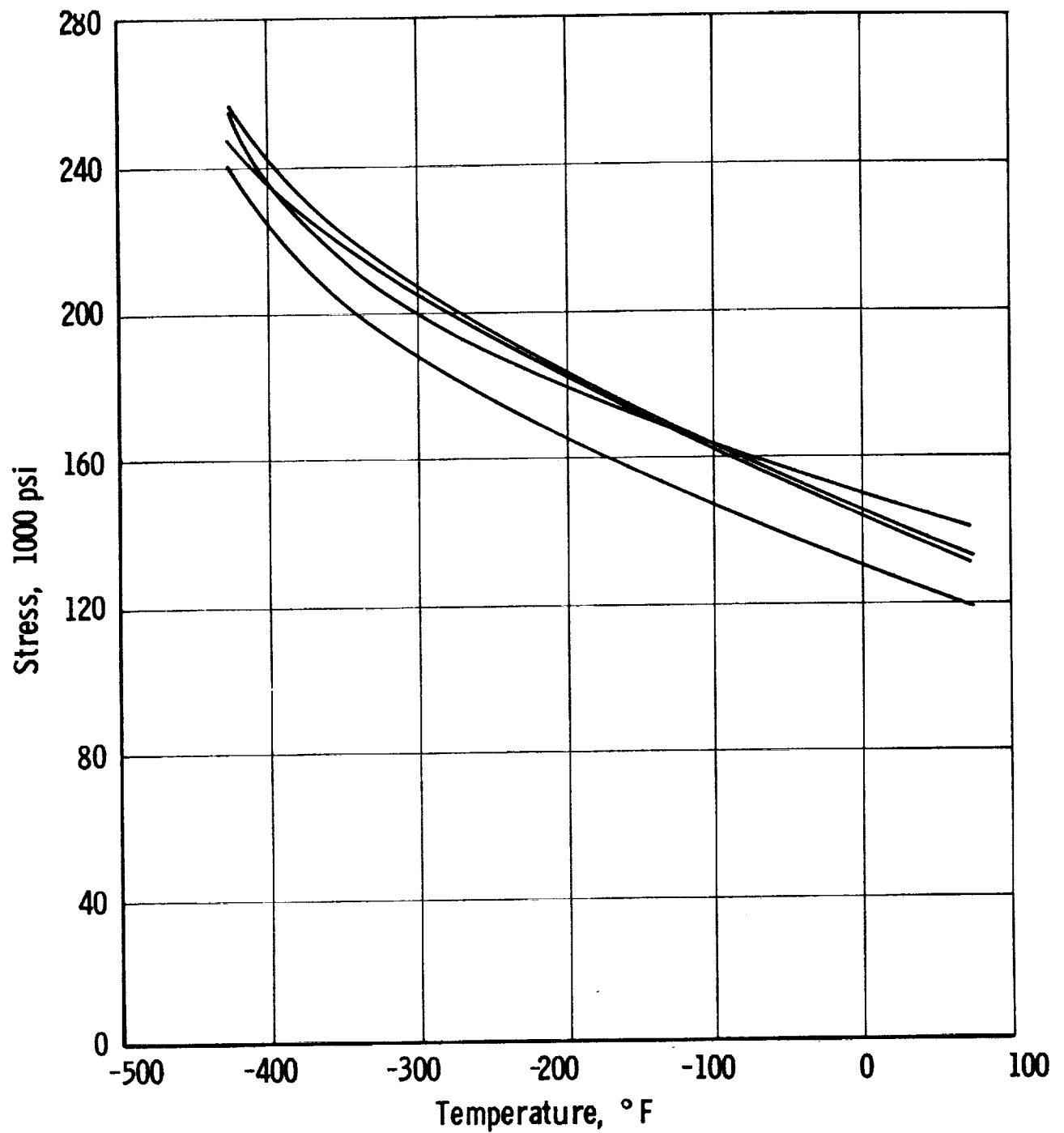
Ti-6Al-4V-ELI GRADE-ULTIMATE TENSILE STRENGTH AND ELONGATION SHEET, TRANSVERSE, -ANNEALED (THICKNESS RANGE 0.025 IN. TO 0.063 IN.)

Figure B-22



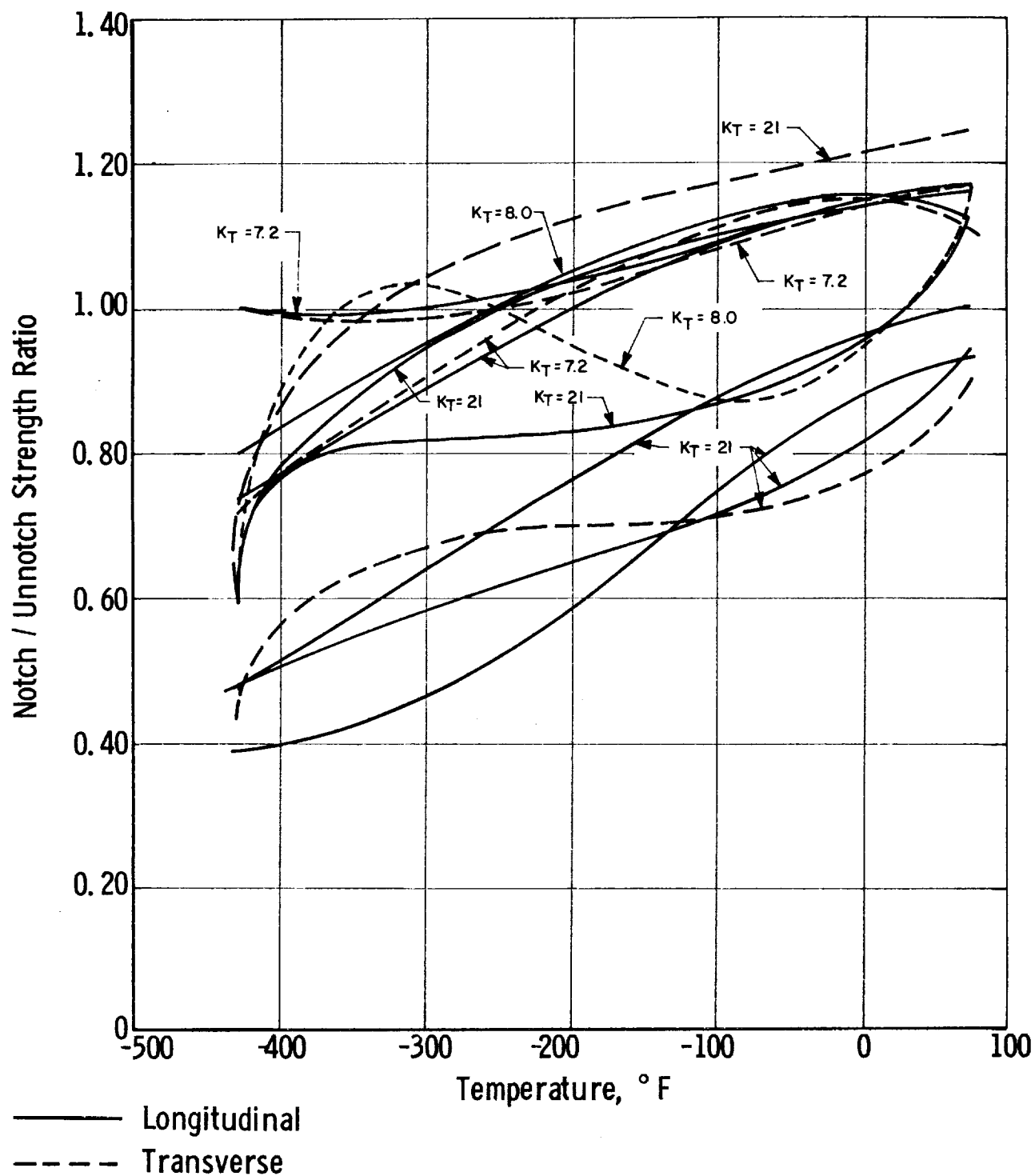
Ti-6 Al-4V-ELI GRADE-YIELD STRENGTH-SHEET, ANNEALED-LONGITUDINAL
(THICKNESS RANGE 0.025 IN. TO 0.063 IN.)

Figure B-23



Ti-6 Al-4V-ELI GRADE-YIELD STRENGTH-SHEET, ANNEALED-TRANSVERSE
(THICKNESS RANGE 0.025 IN. TO 0.063 IN.)

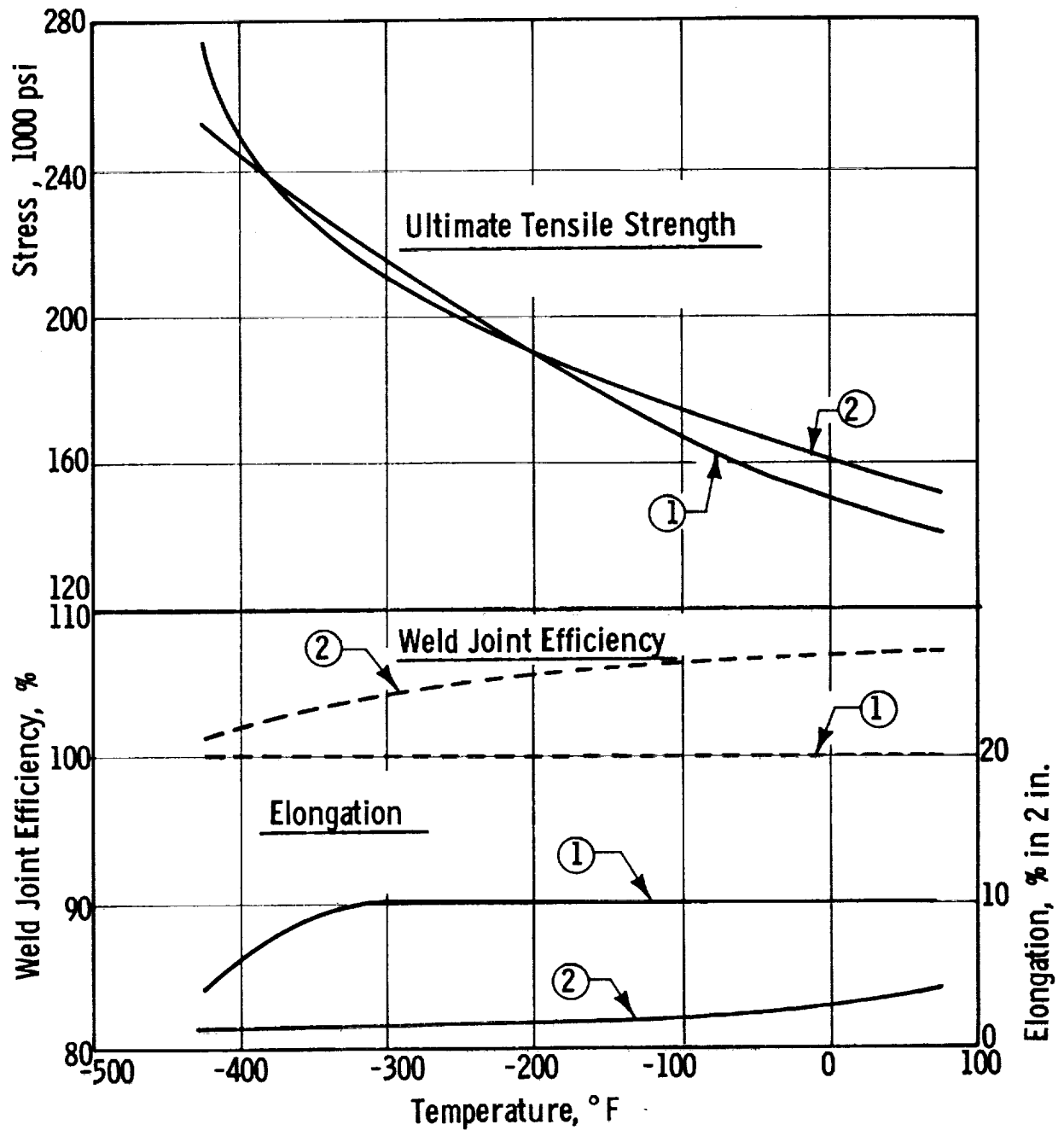
Figure B-24



Ti-6 Al-4V ELI GRADE-NOTCH / UNNOTCH STRENGTH RATIO
 SHEET, ANNEALED. (THICKNESS RANGE 0.025 IN. TO 0.063 IN.)

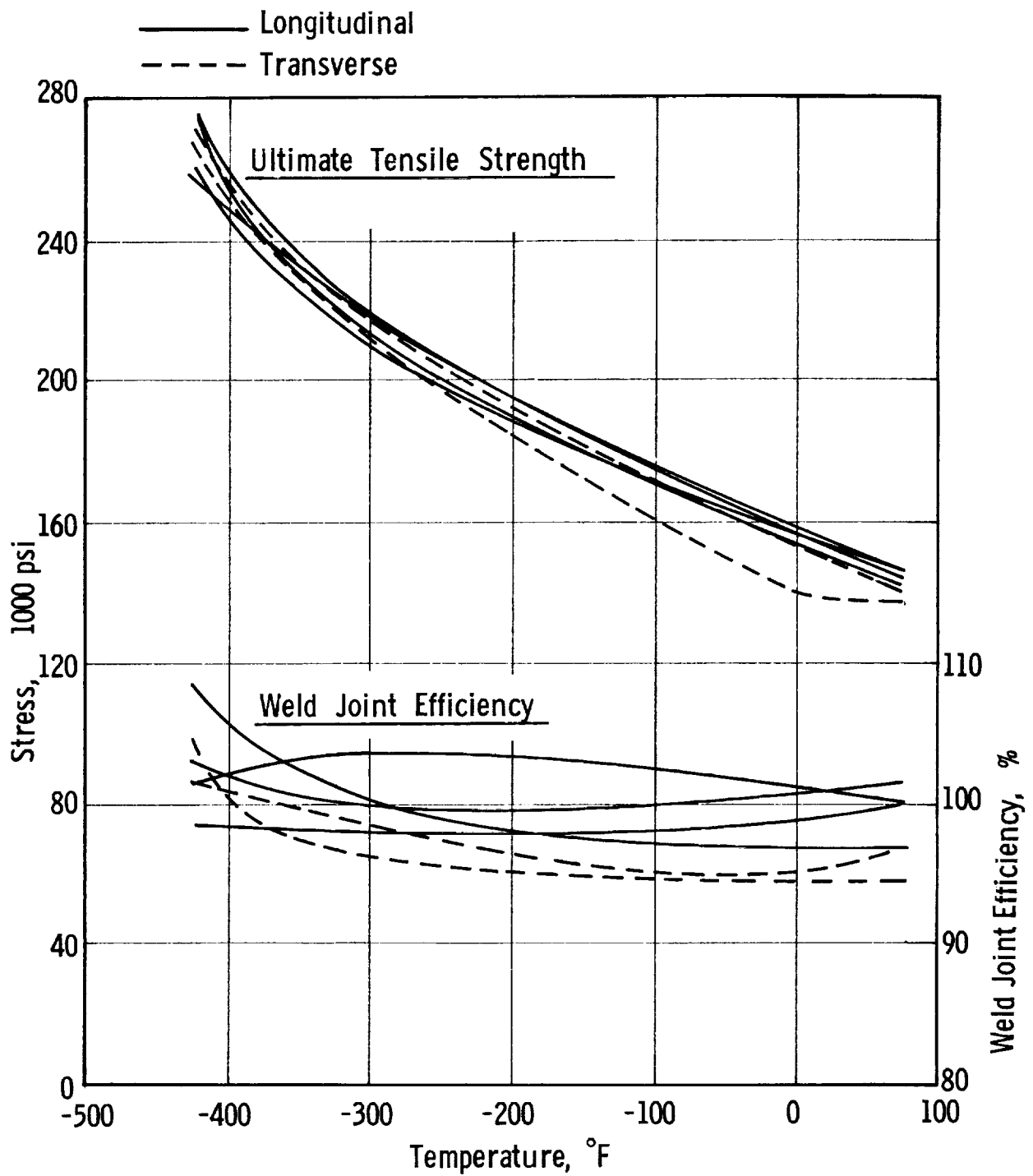
Figure B-25

- ① 0.063 in. sheet
- ② 0.062 in. sheet



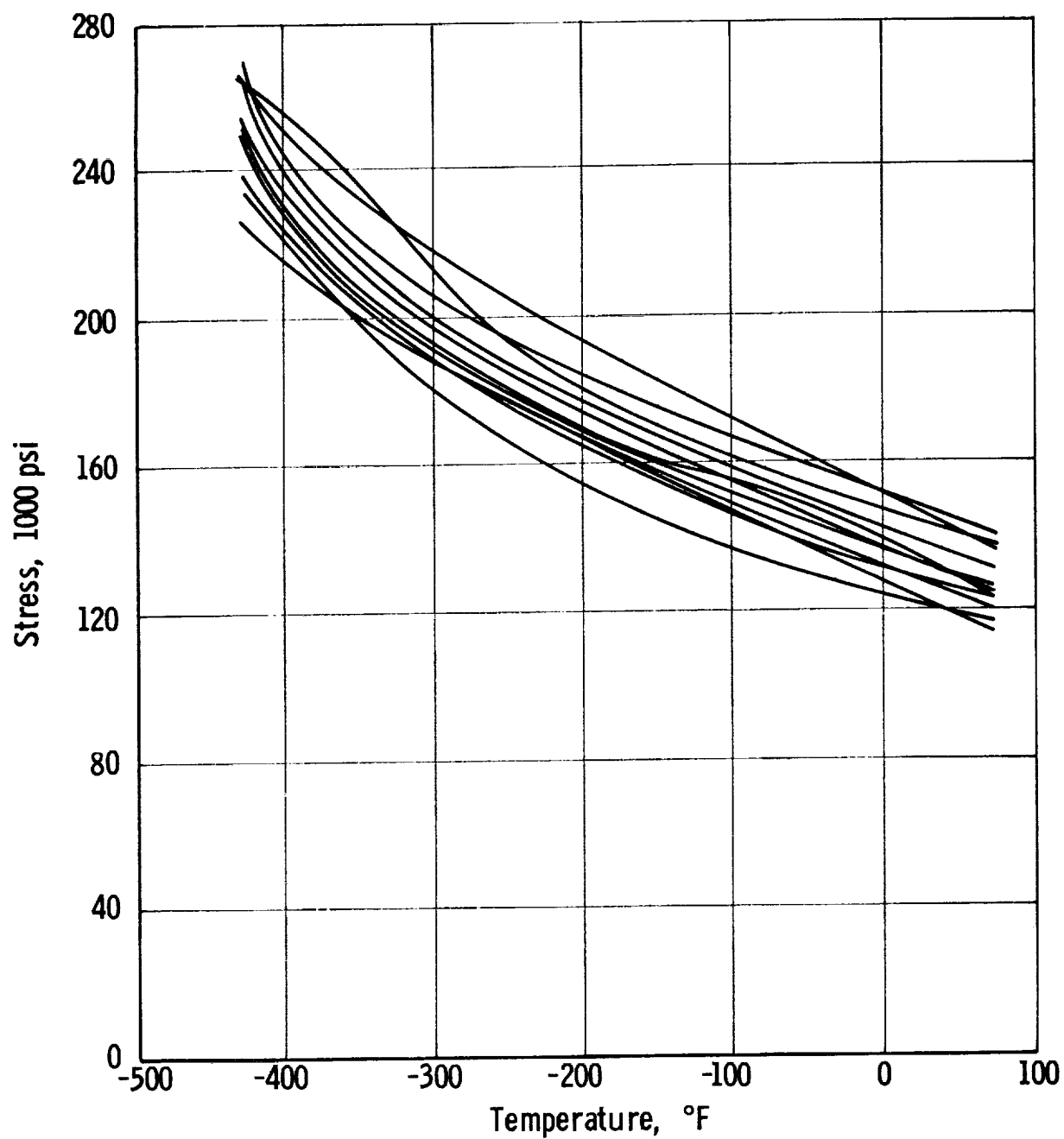
Ti-6Al-4V-NORMAL INTERSTITIAL - WELD PROPERTIES
ANNEALED, AS WELDED

Figure B-26



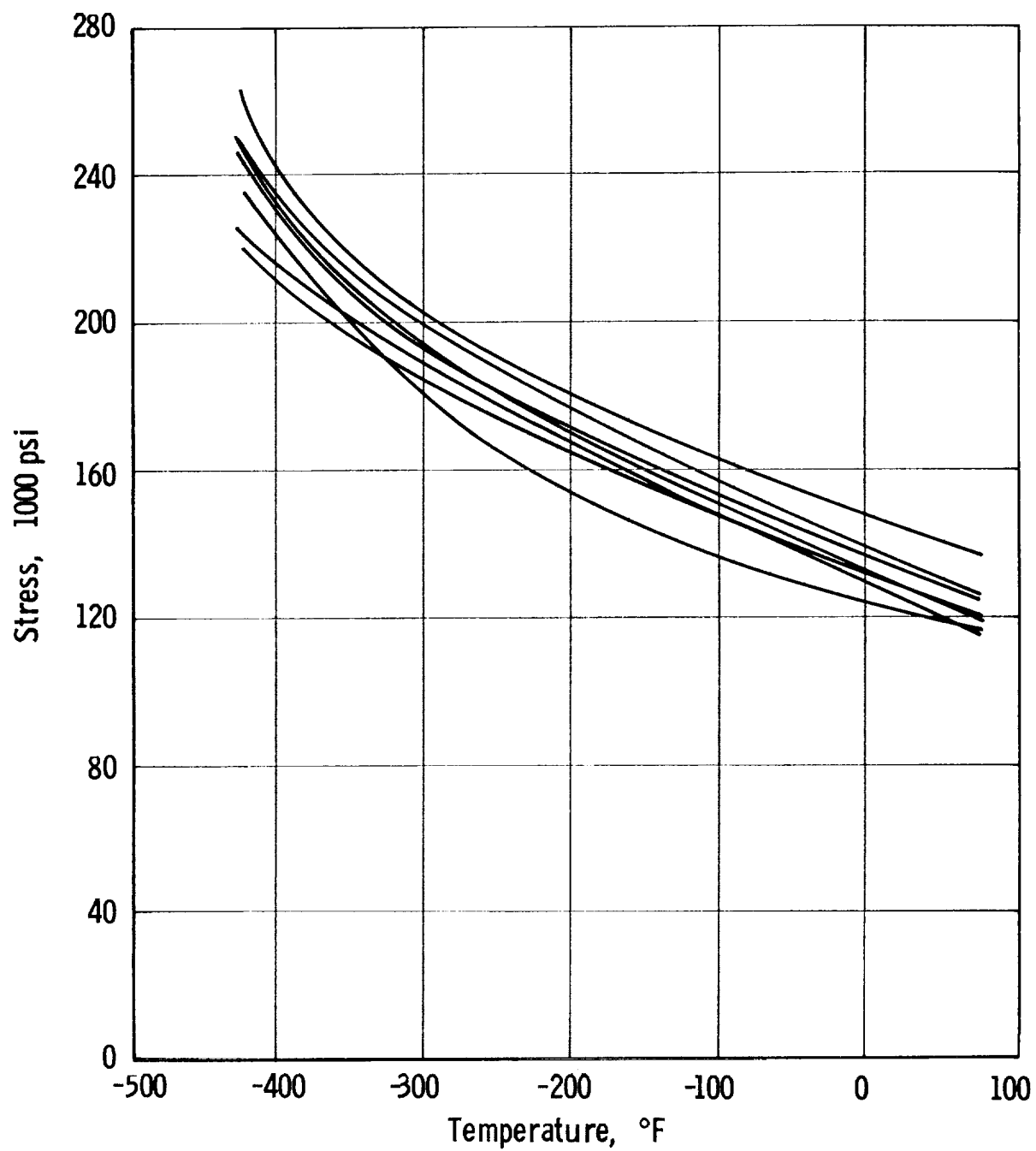
Ti-6Al-4V-ELI GRADE - WELDED - ULTIMATE TENSILE STRENGTH AND
JOINT EFFICIENCY - ANNEALED, AS WELDED
(THICKNESS RANGE - 0.025 IN. TO 0.063 IN.)

Figure B-27



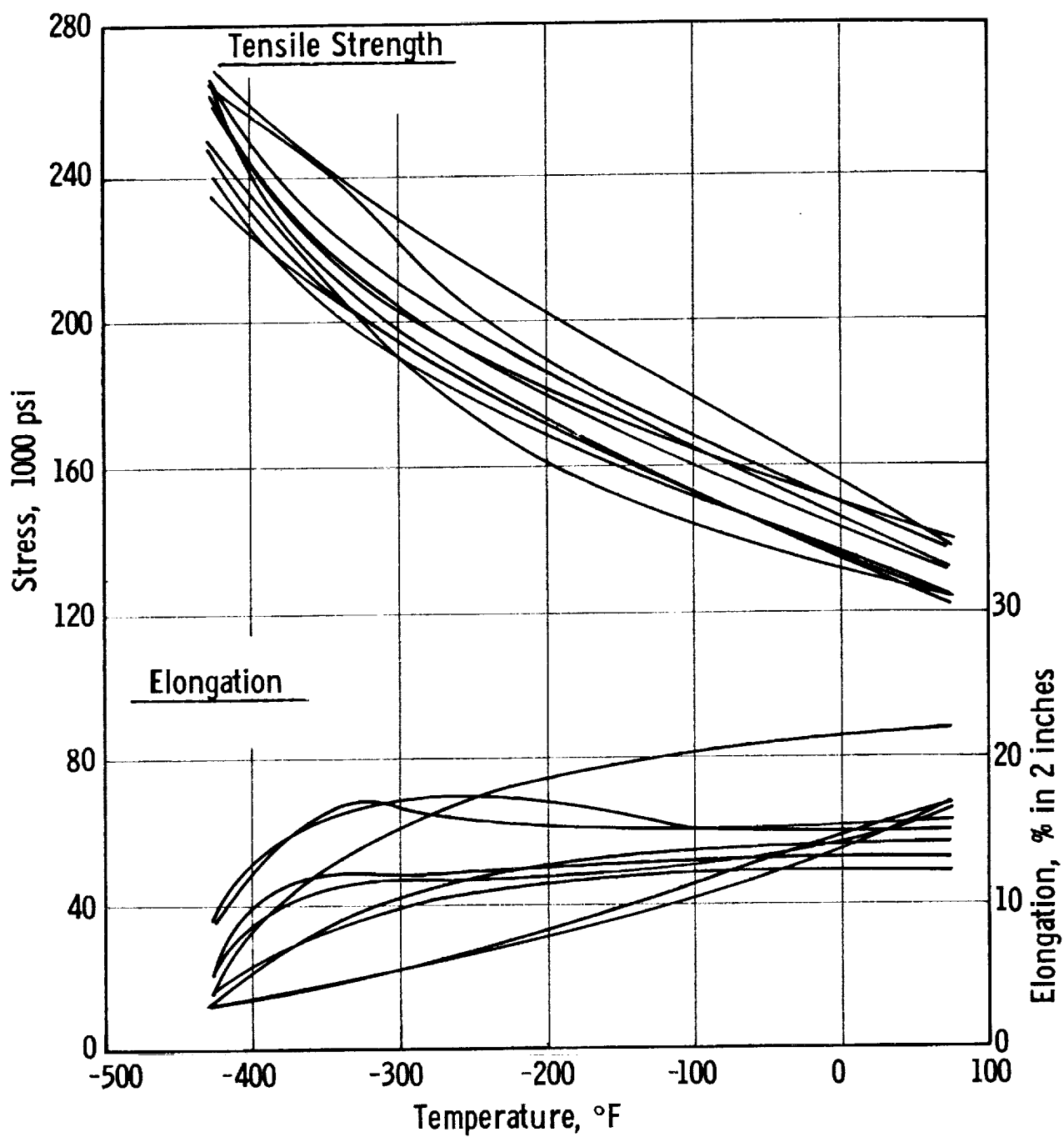
Ti-5Al-2.5 Sn-NORMAL INTERSTITIAL-YIELD STRENGTH-SHEET,
ANNEALED-LONGITUDINAL (THICKNESS RANGE 0.016 IN. TO 0.064 IN.)

Figure B-28



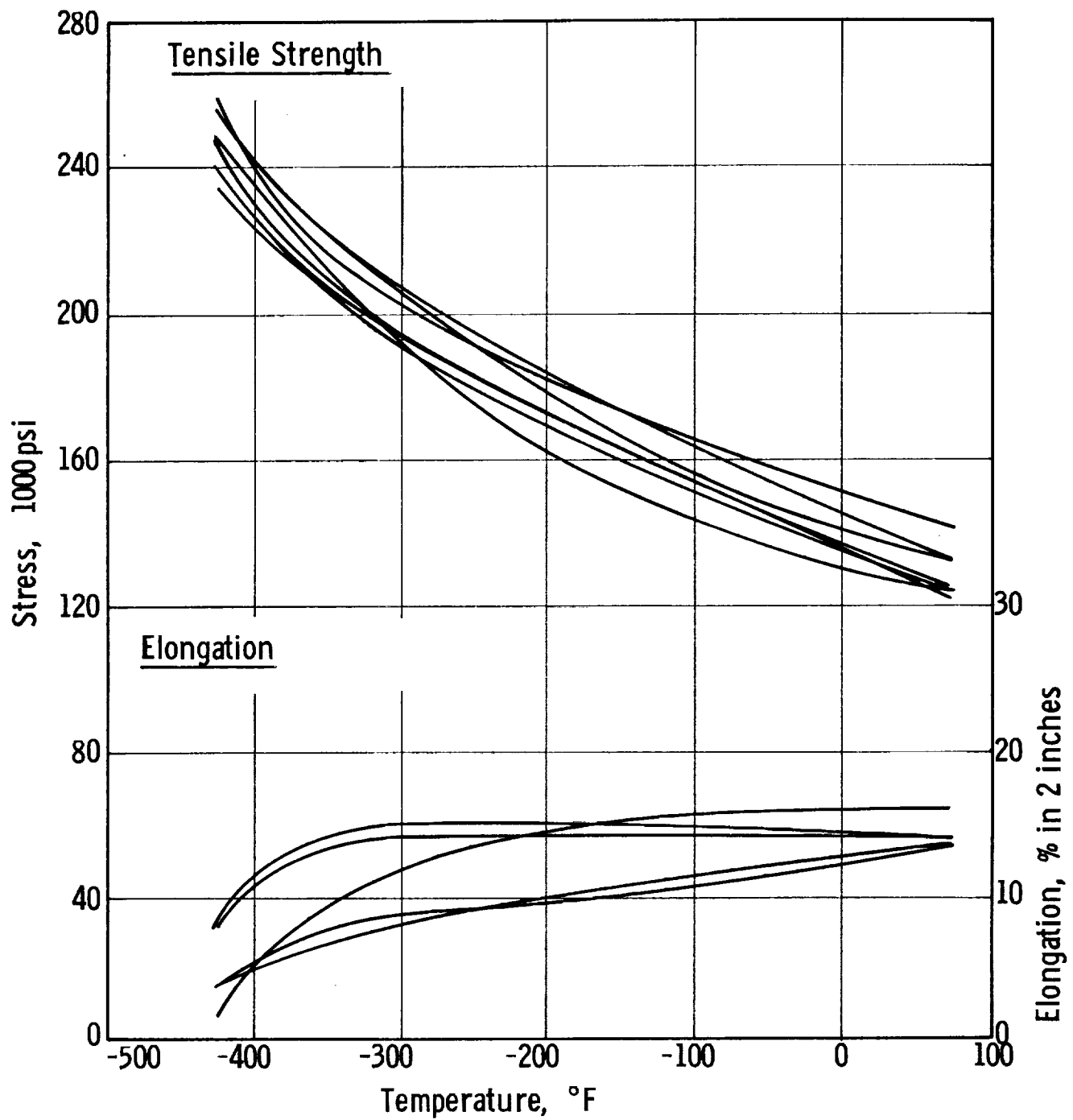
Ti-5Al-2.5 Sn-NORMAL INTERSTITIAL-YIELD STRENGTH-SHEET,
ANNEALED-TRANSVERSE (THICKNESS RANGE 0.016 IN. TO 0.064 IN.)

Figure B-29



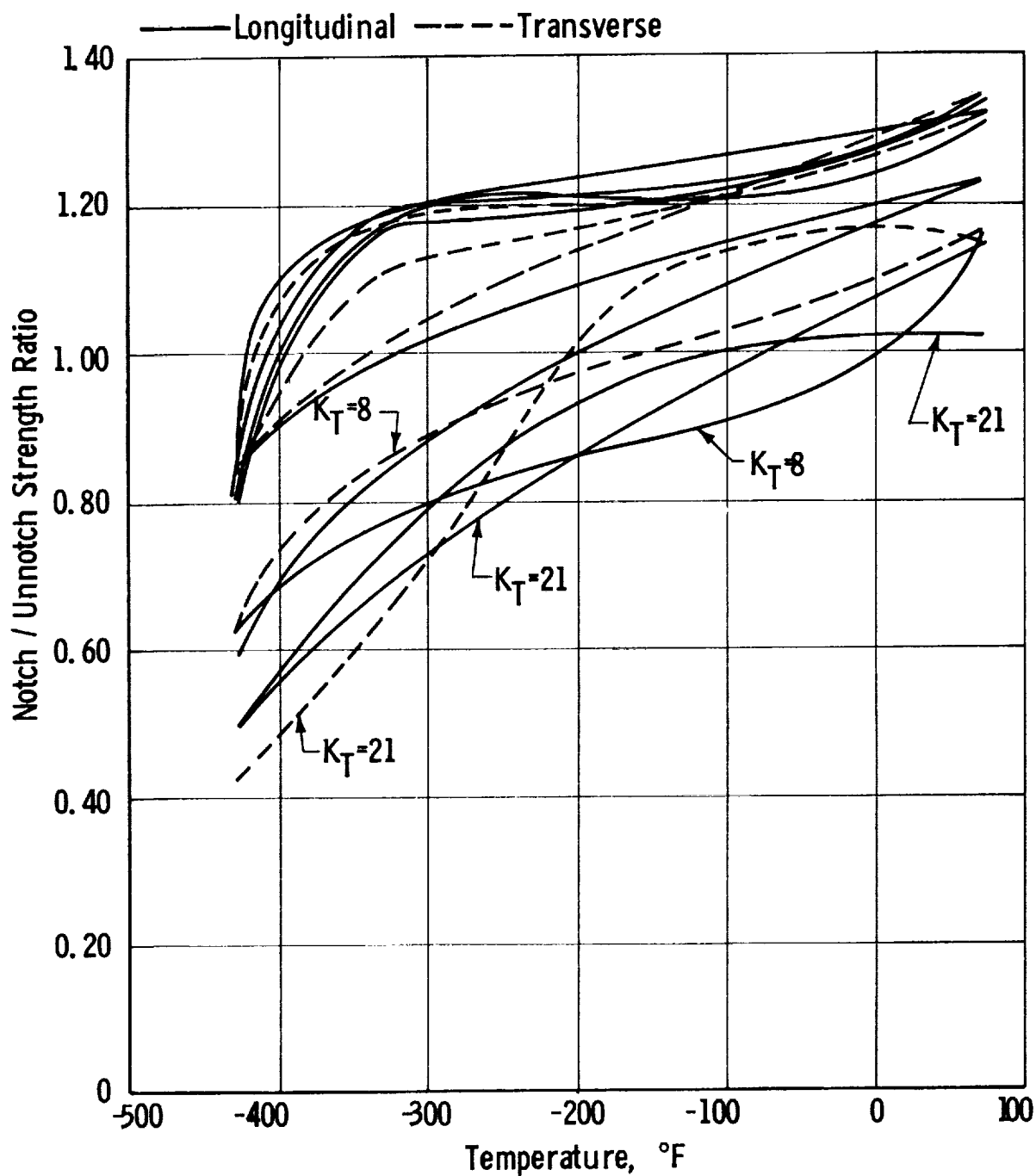
Ti-5Al-2.5 Sn-NORMAL INTERSTITIAL-TENSILE STRENGTH AND
 ELONGATION-SHEET, ANNEALED-LONGITUDINAL
 (THICKNESS RANGE 0.016 IN. TO 0.064 IN.)

Figure B-30



Ti-5 Al-2.5 Sn-NORMAL INTERSTITIAL-TENSILE STRENGTH AND
ELONGATION-SHEET, ANNEALED-TRANSVERSE
(THICKNESS RANGE 0.016 IN. TO 0.064 IN.)

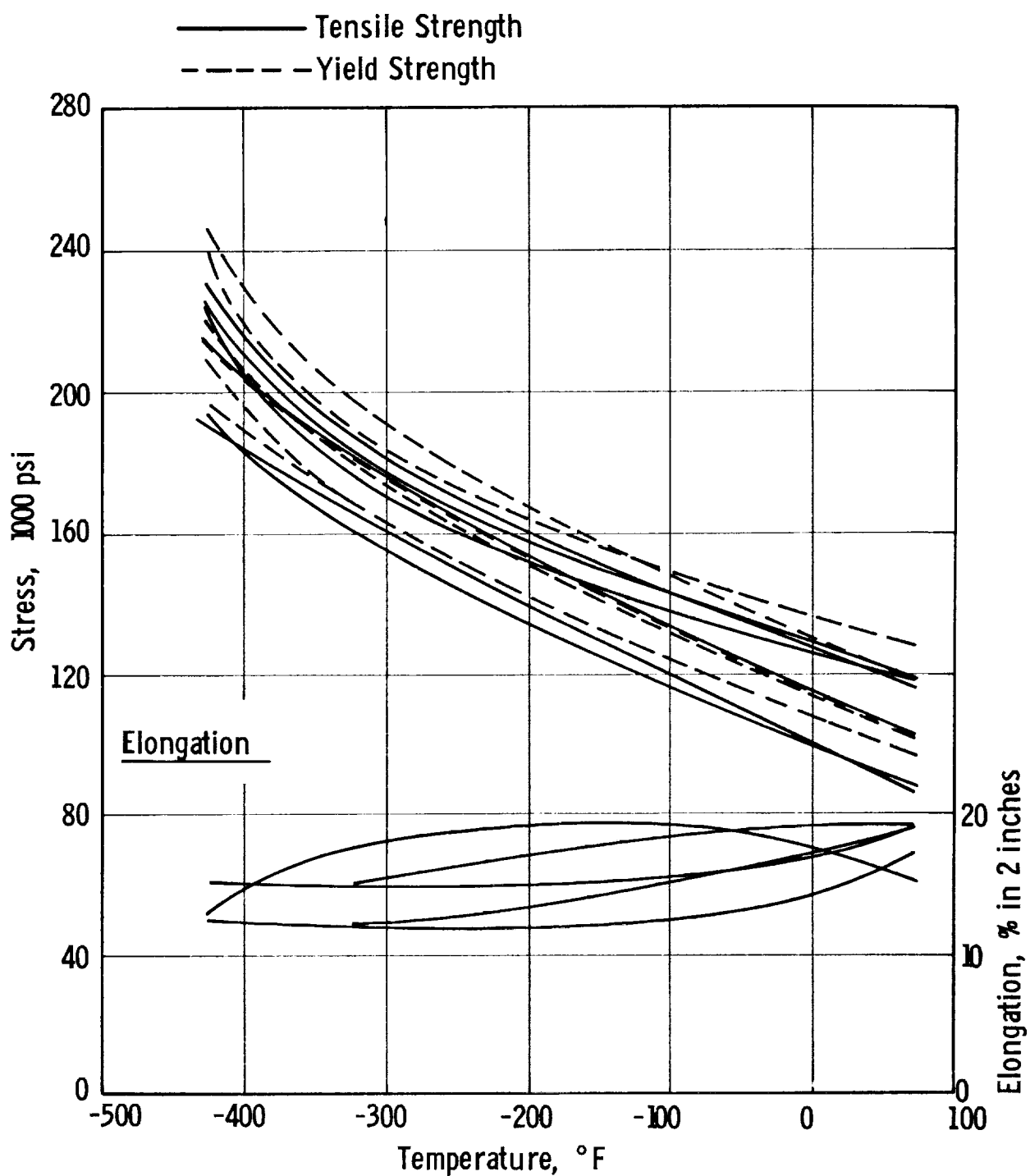
Figure B-31



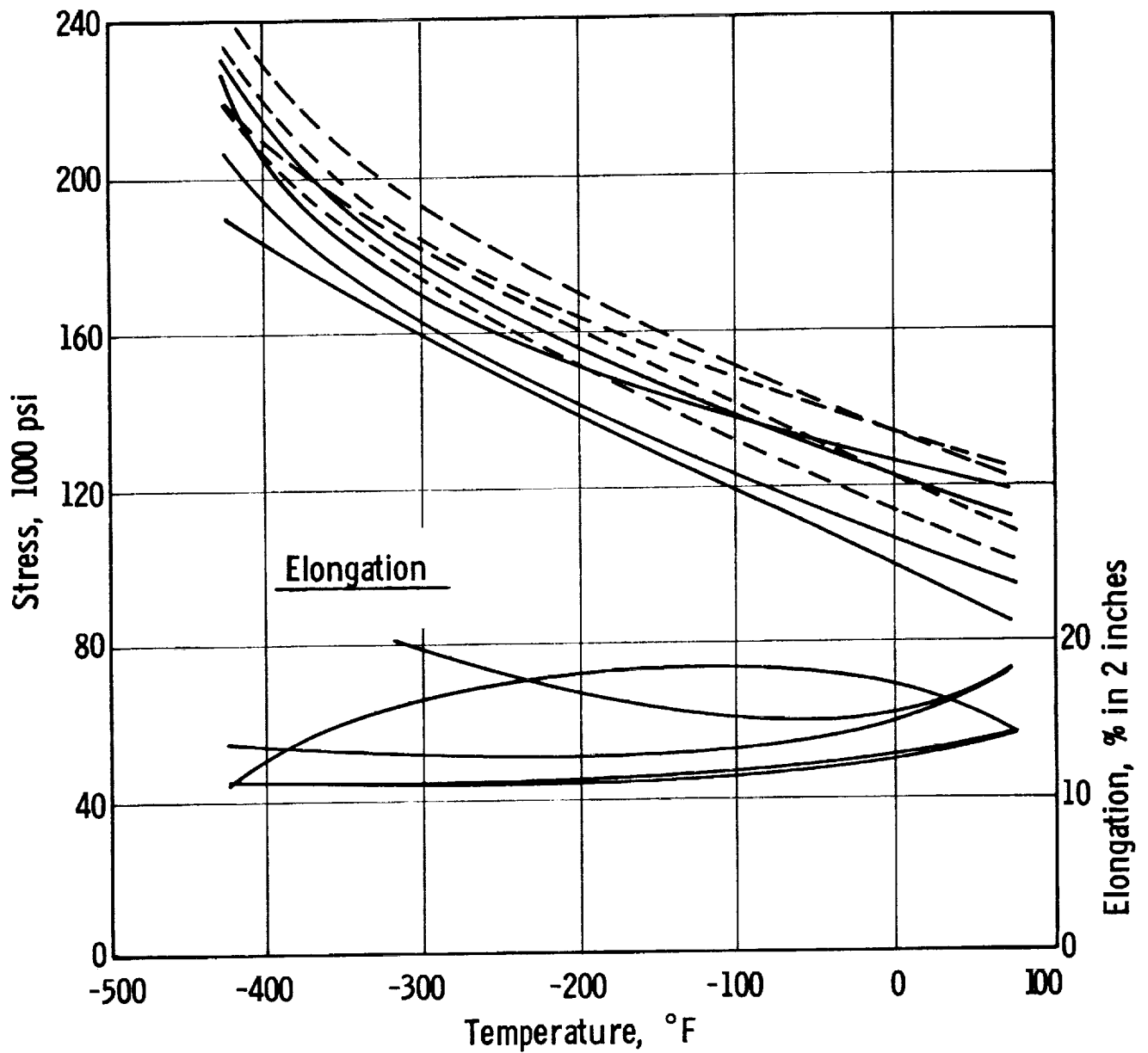
Note:
 $K_T = 7.2$ Except As Indicated

Ti-5 Al-2.5 Sn-NORMAL INTERSTITIAL-NOTCH / UNNOTCH STRENGTH RATIO
 SHEET, ANNEALED. (THICKNESS RANGE 0.016 IN. TO 0.064 IN.)

Figure B-32



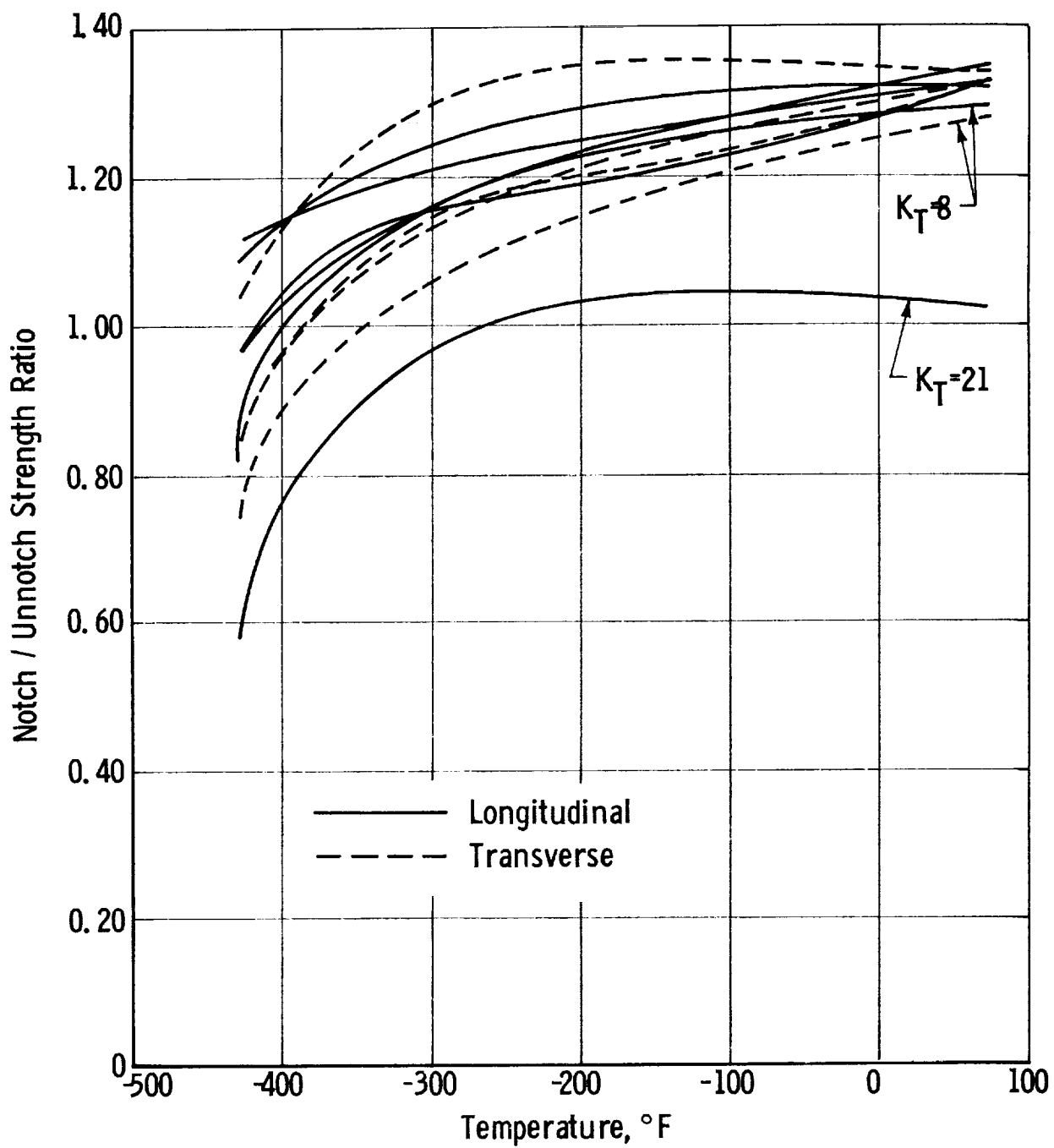
Ti-5 Al-2.5 Sn-ELI GRADE-TENSILE PROPERTIES-SHEET,
 ANNEALED-LONGITUDINAL (THICKNESS RANGE 0.014 IN. TO 0.040 IN.)



--- Tensile Strength
 — Yield Strength

Ti-5 Al-2.5 Sn-ELI GRADE-TENSILE PROPERTIES-SHEET,
 ANNEALED-TRANSVERSE (THICKNESS RANGE 0.014 IN. TO 0.040 IN.)

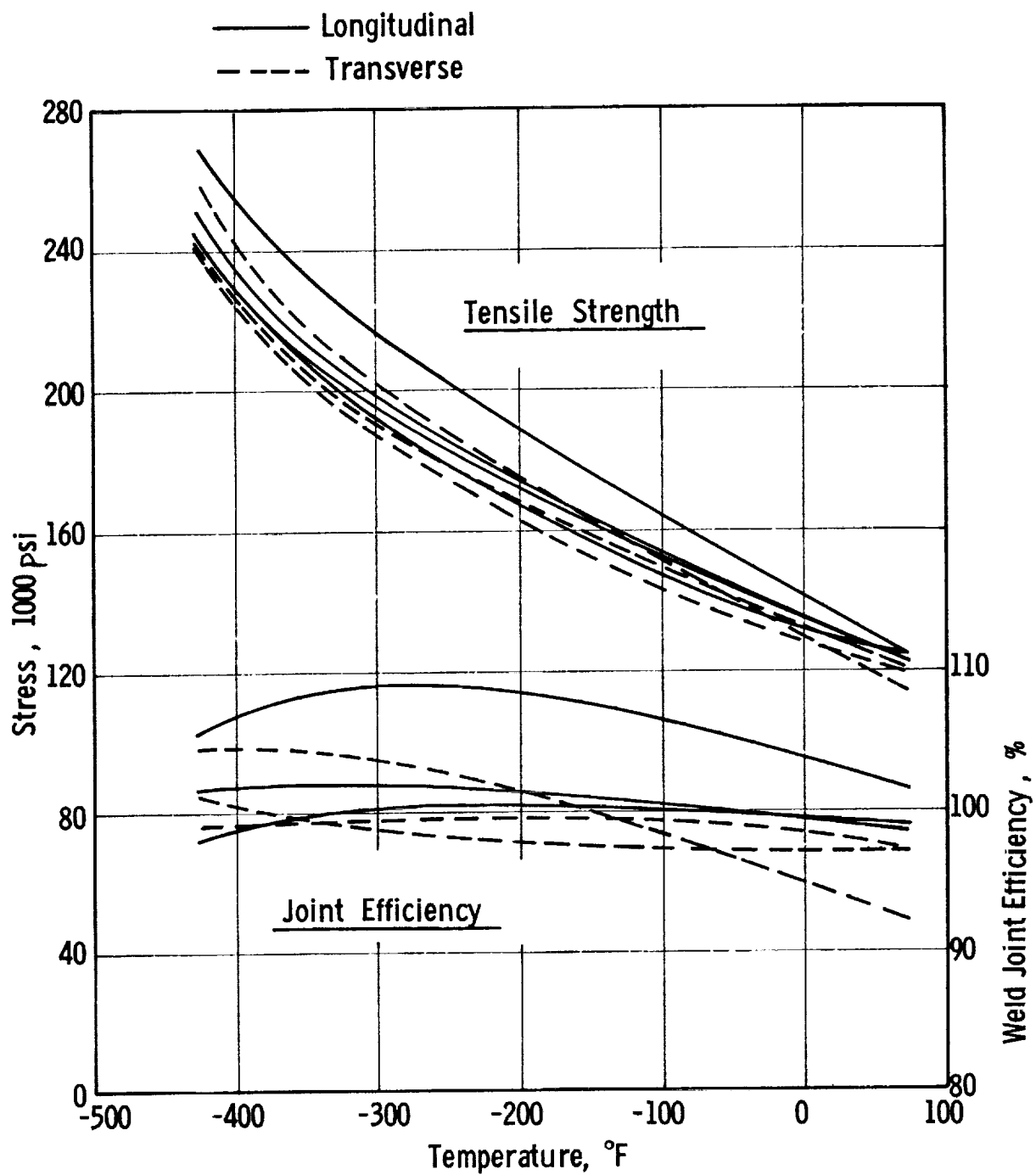
Figure B-34



$K_T = 7.2$ Except as indicated

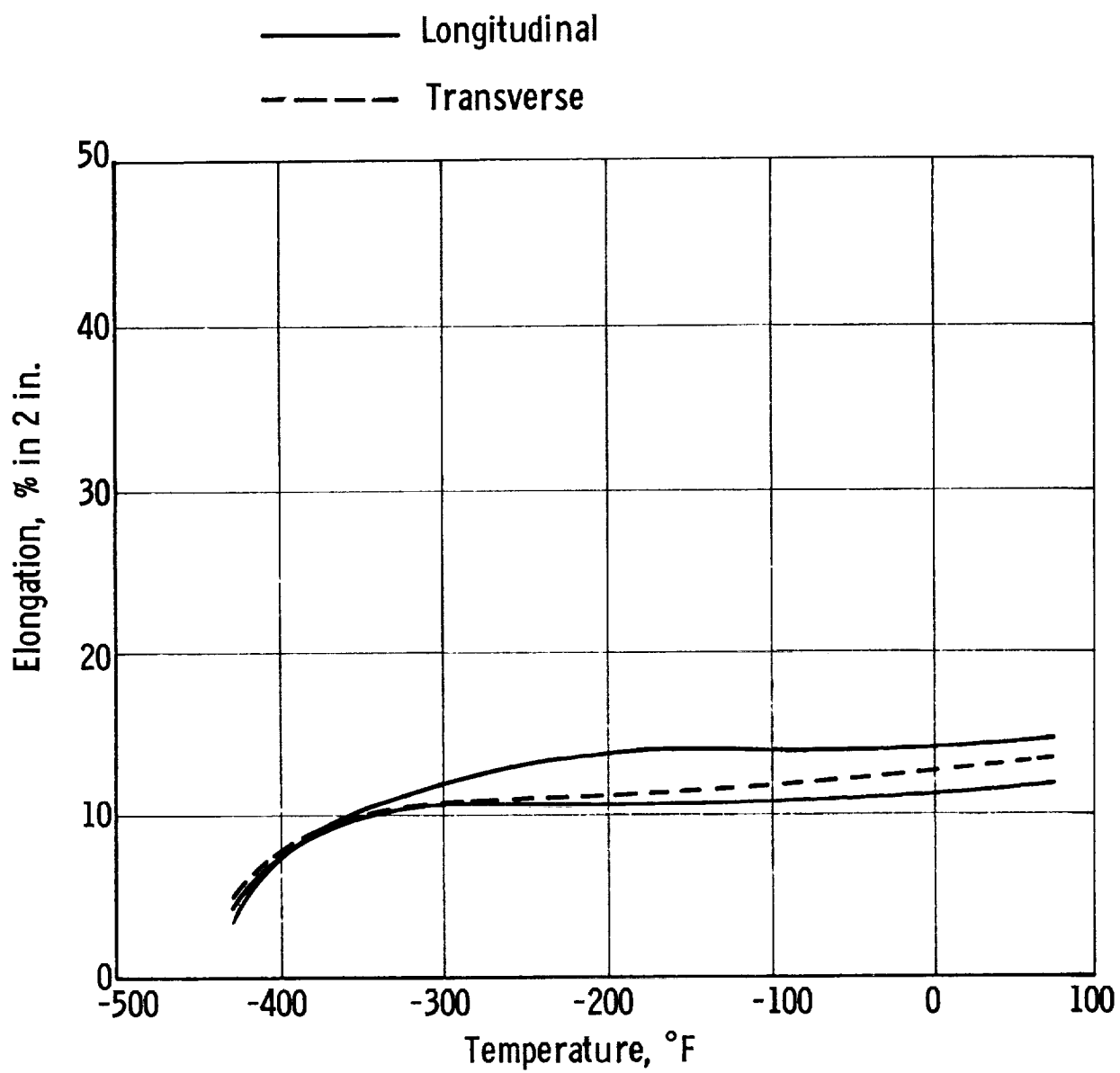
Ti-5 Al-2.5 Sn-ELI GRADE-NOTCH / UNNOTCH STRENGTH RATIO
SHEET, ANNEALED (THICKNESS RANGE 0.014 IN. TO 0.040 IN.)

Figure B-35



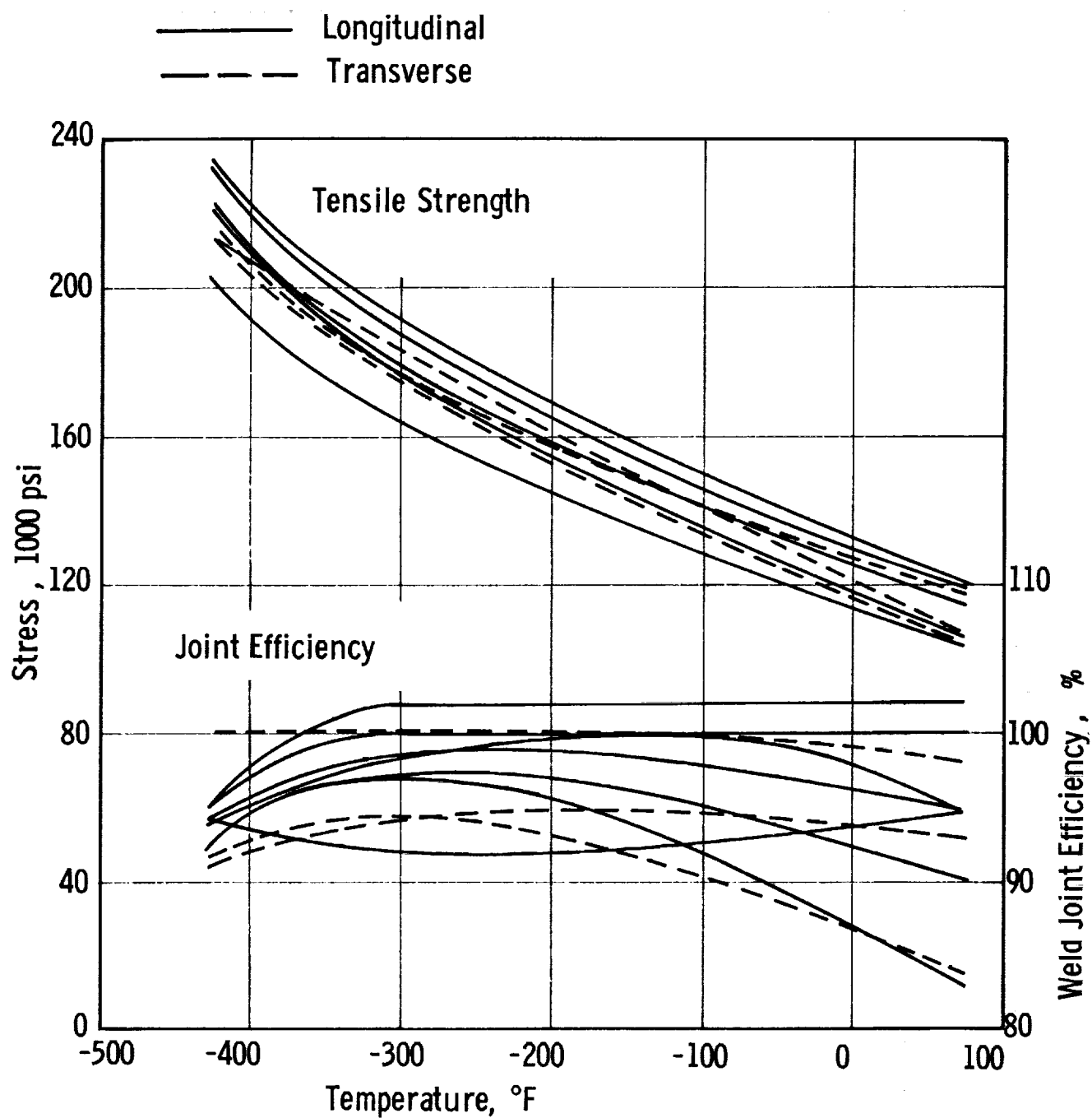
Ti-5Al-2.5 Sn - NORMAL INTERSTITIAL - WELDED TENSILE STRENGTH
AND WELD JOINT EFFICIENCY - SHEET, ANNEALED
(THICKNESS RANGE - 0.020 IN. TO 0.032 IN.)

Figure B-36



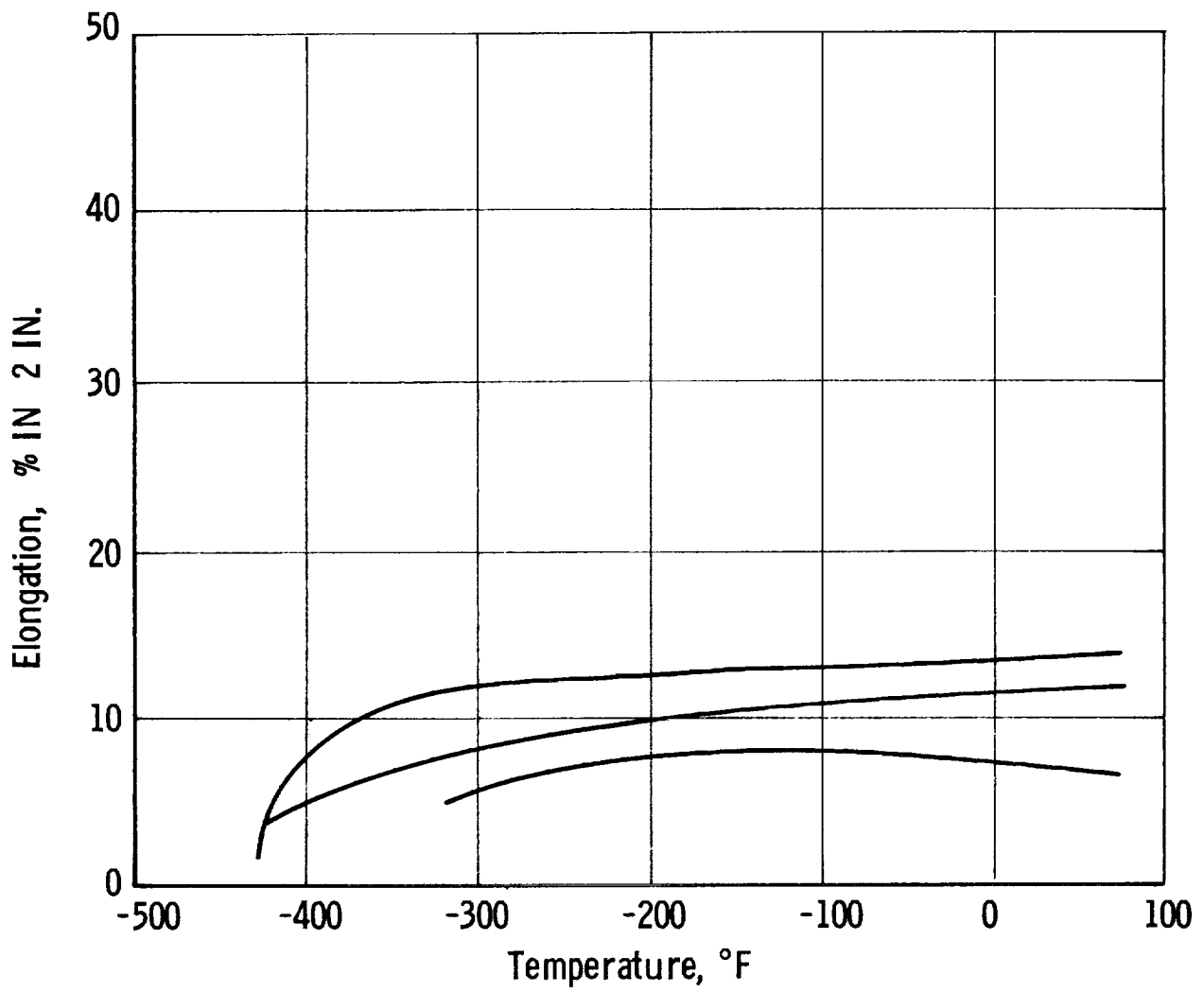
Ti-5Al-2.5 Sn - NORMAL INTERSTITIAL - WELDED - AS WELDED ELONGATION

Figure B-37



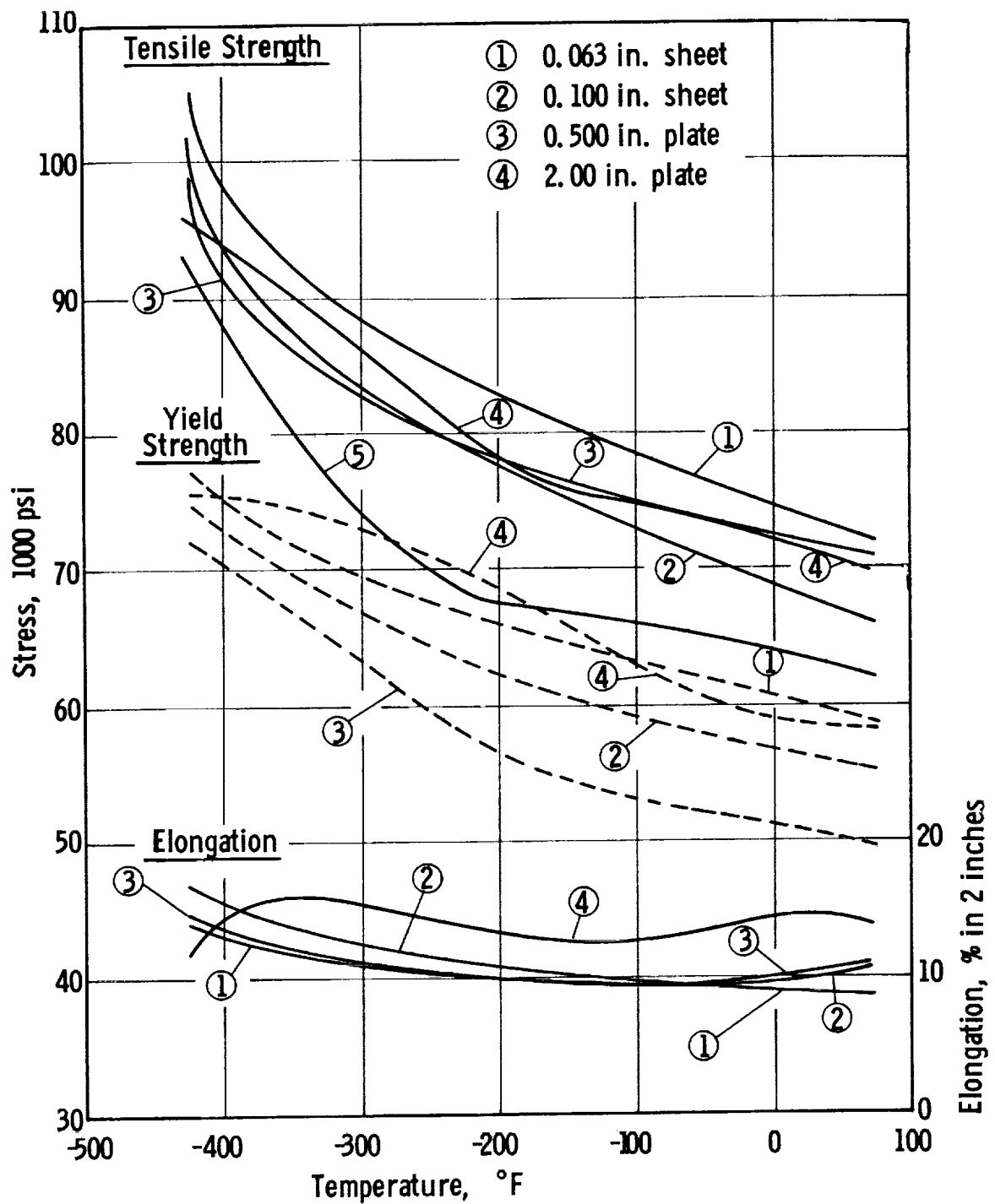
Ti-5Al-2.5 Sn-ELI GRADE-WELDED TENSILE STRENGTH AND WELDED
JOINT EFFICIENCY - SHEET, ANNEALED
(THICKNESS RANGE -0.014 IN. TO 0.040 IN.)

Figure B-38

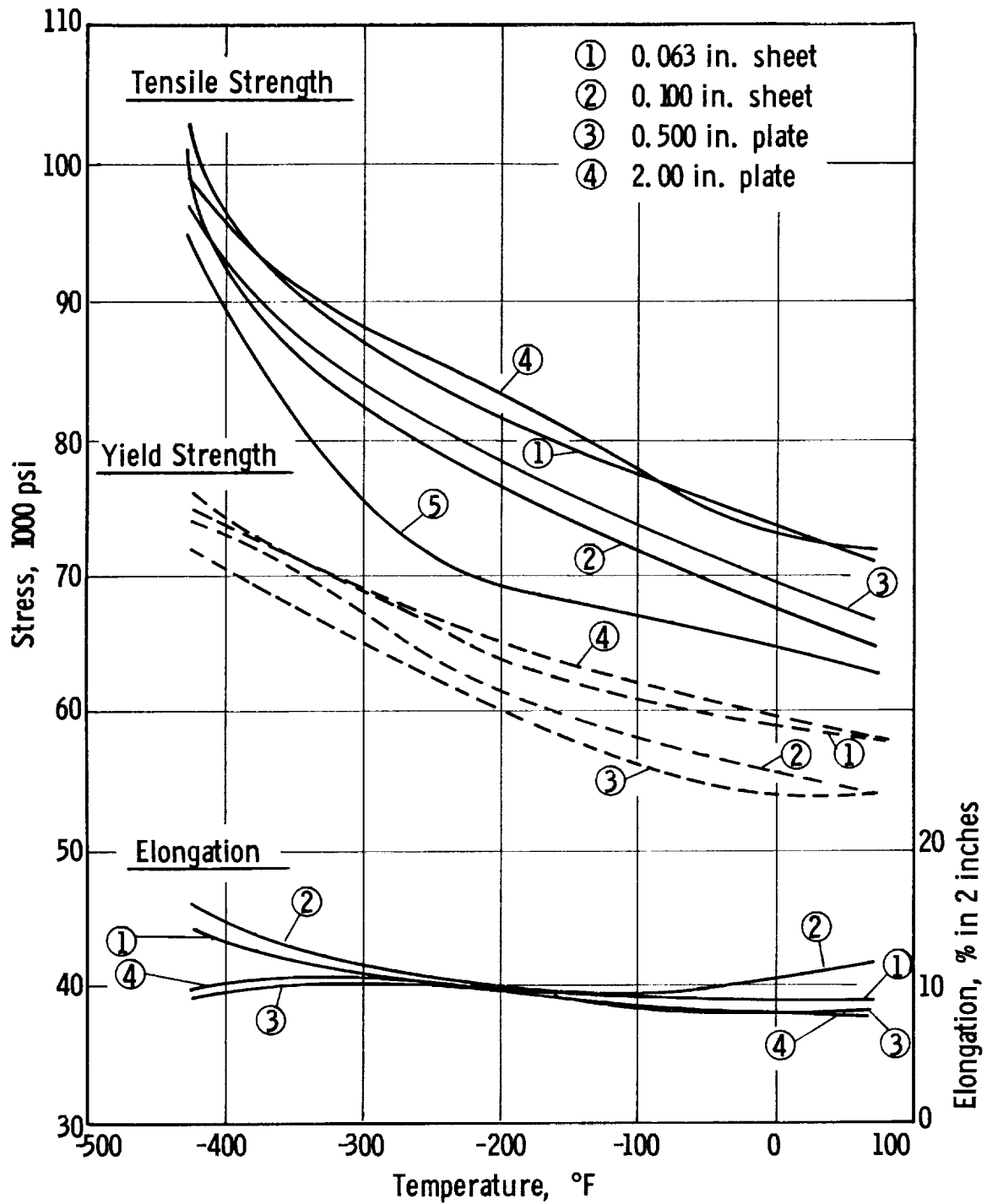


Ti-5Al-2.5 Sn - ELI GRADE - WELDED - AS WELDED ELONGATION

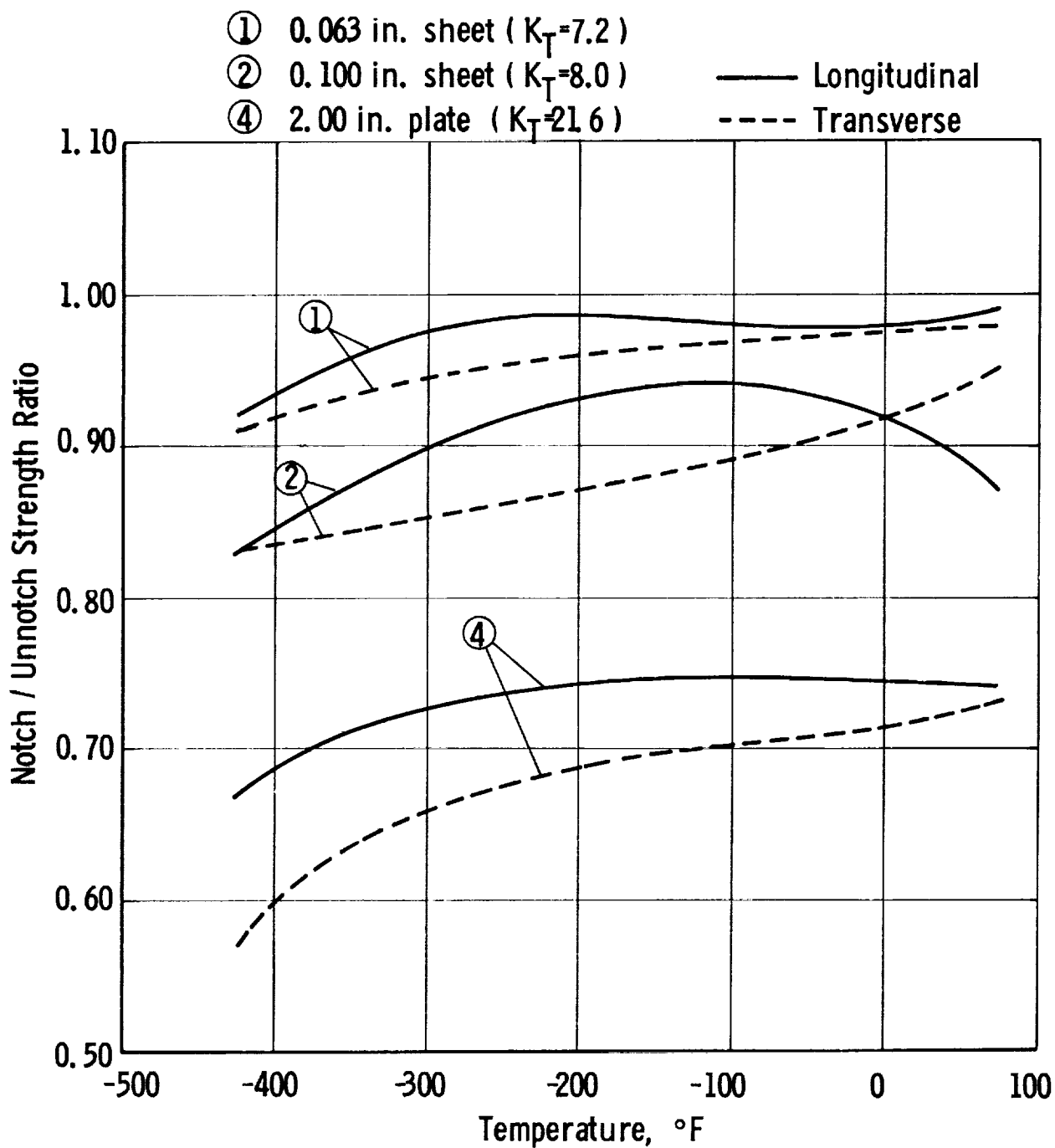
Figure B-39



ALUMINUM ALLOY 2219-T87 TENSILE PROPERTIES - LONGITUDINAL

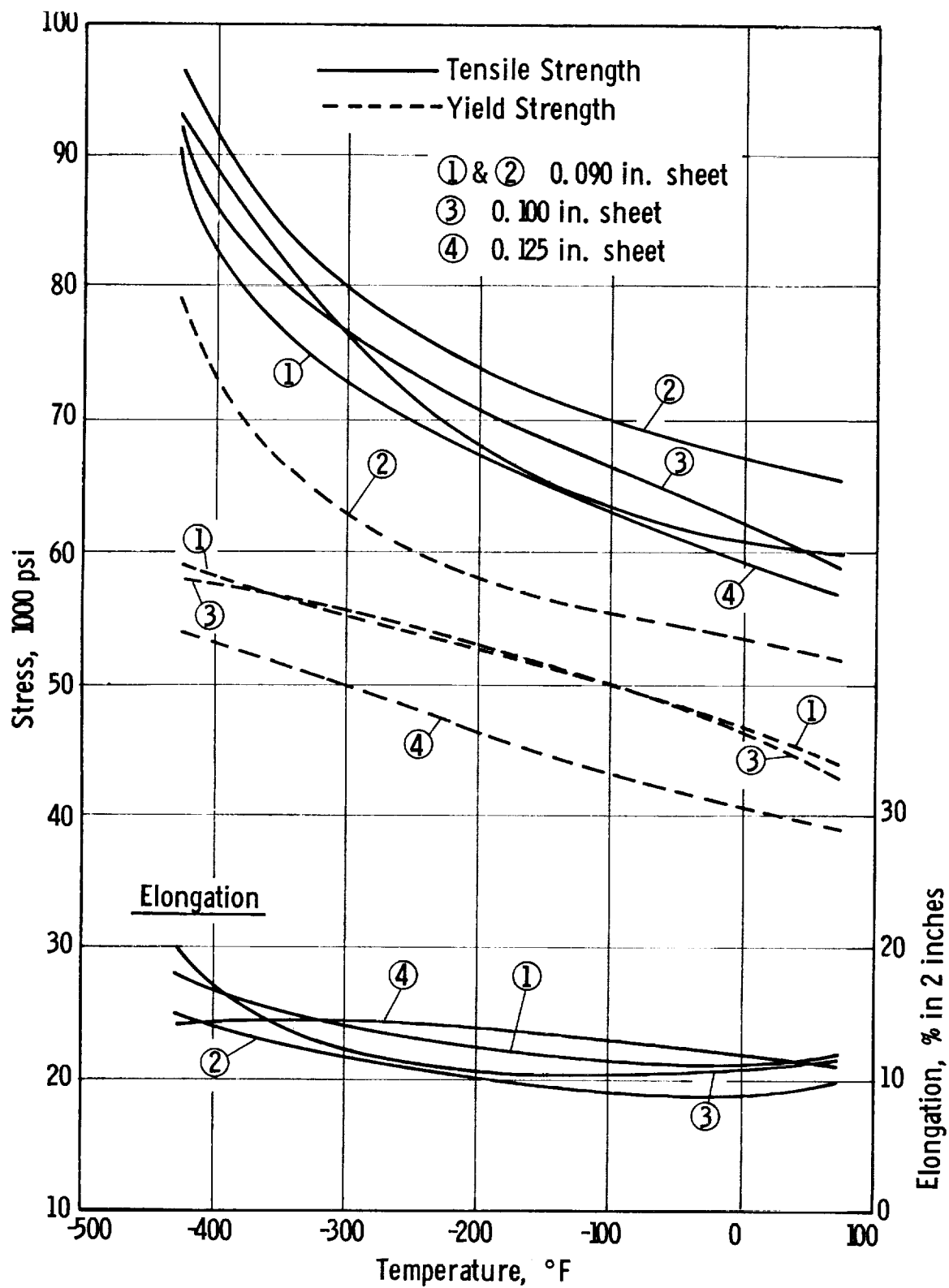


ALUMINUM ALLOY 2219-T87 TENSILE PROPERTIES - TRANSVERSE

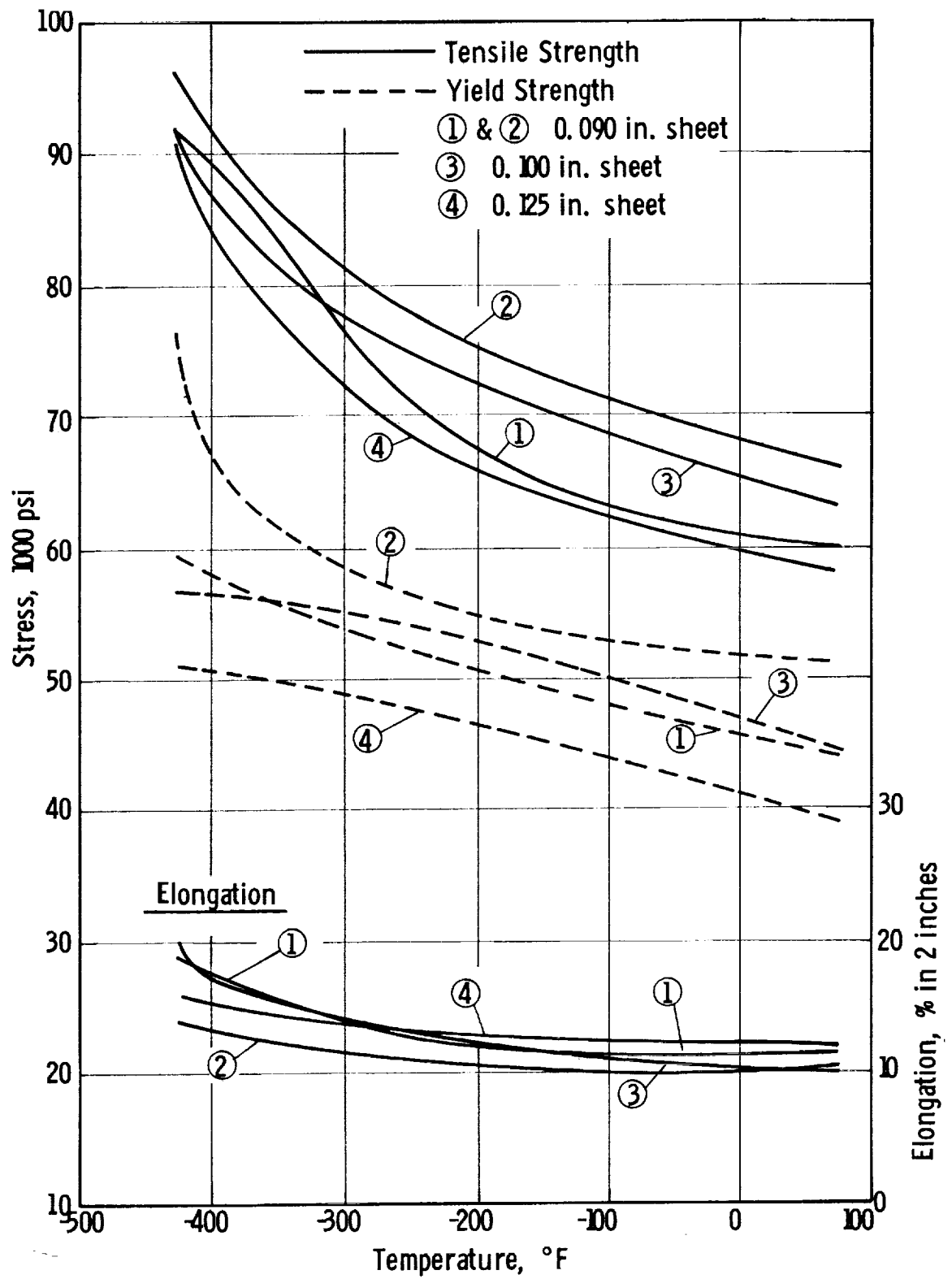


ALUMINUM ALLOY 2219-T87 - NOTCH / UNNOTCH STRENGTH RATIO

Figure B-42

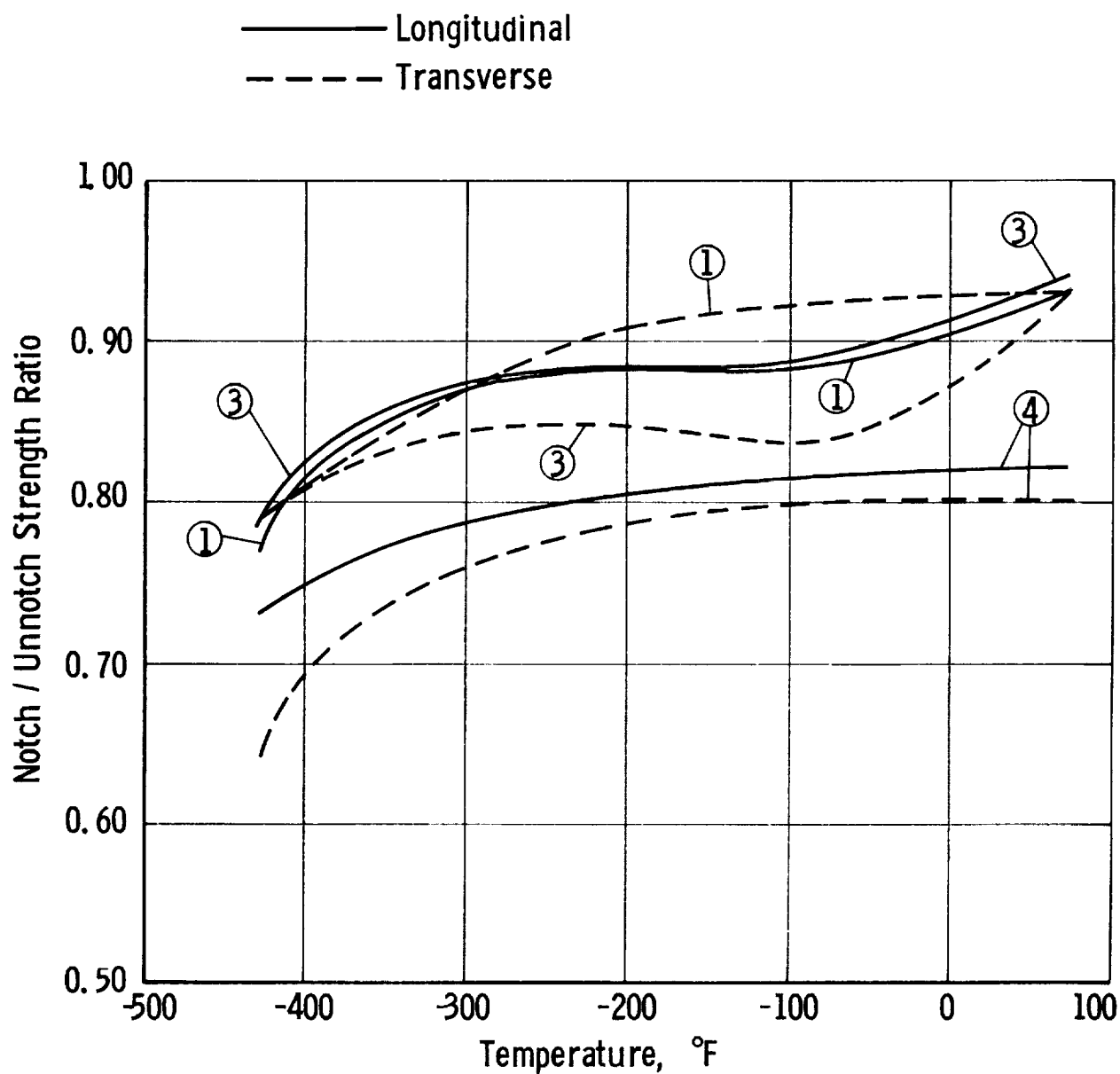


ALUMINUM ALLOY 2219-T62 - TENSILE PROPERTIES - LONGITUDINAL



ALUMINUM ALLOY 2219-T62 - TENSILE PROPERTIES - TRANSVERSE

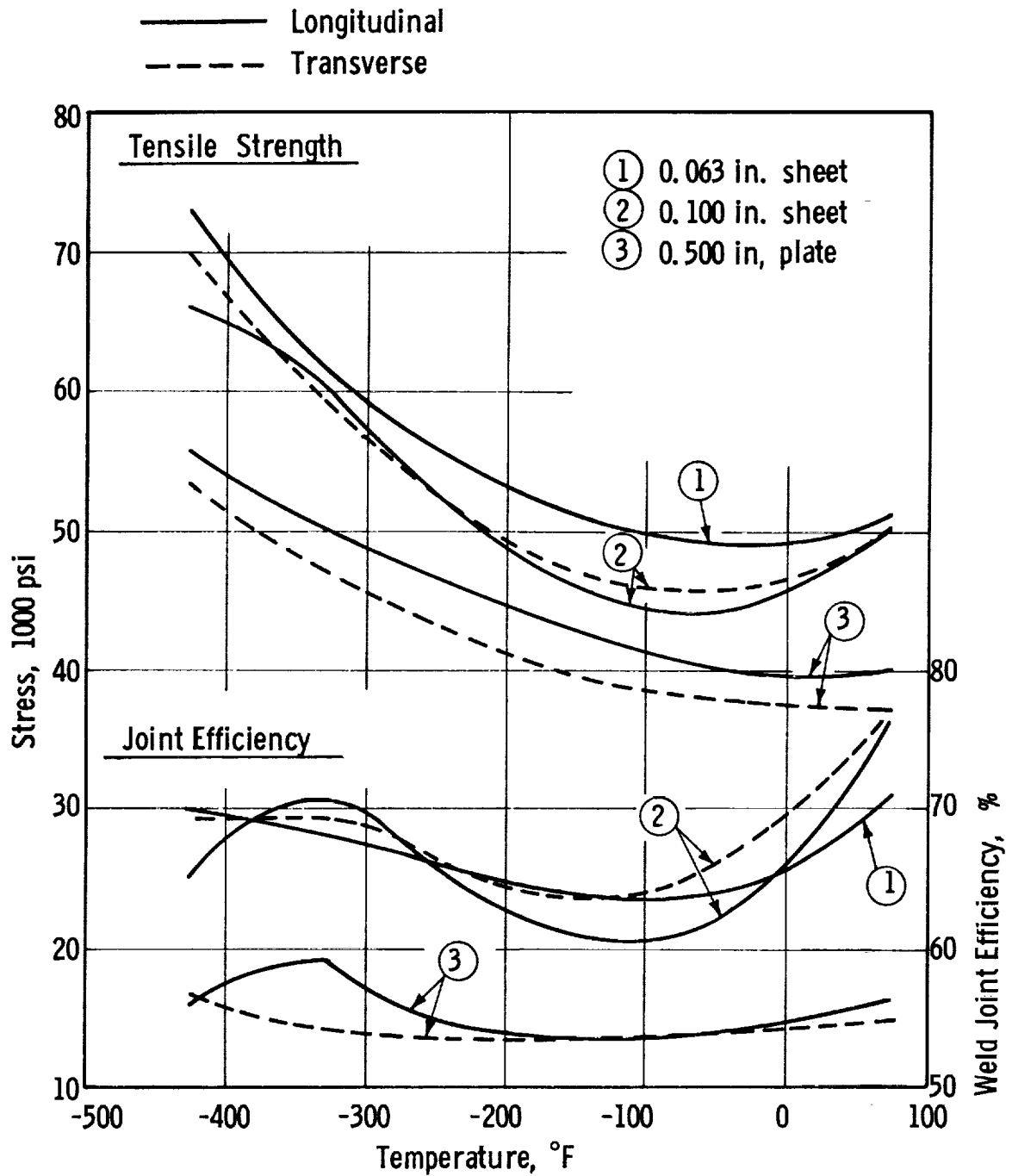
Figure B-44



- ① 0.090 in. sheet - $K_T=8.0$
- ③ 0.100 in. sheet - $K_T=8.0$
- ④ 0.125 in. sheet - $K_T=21.0$

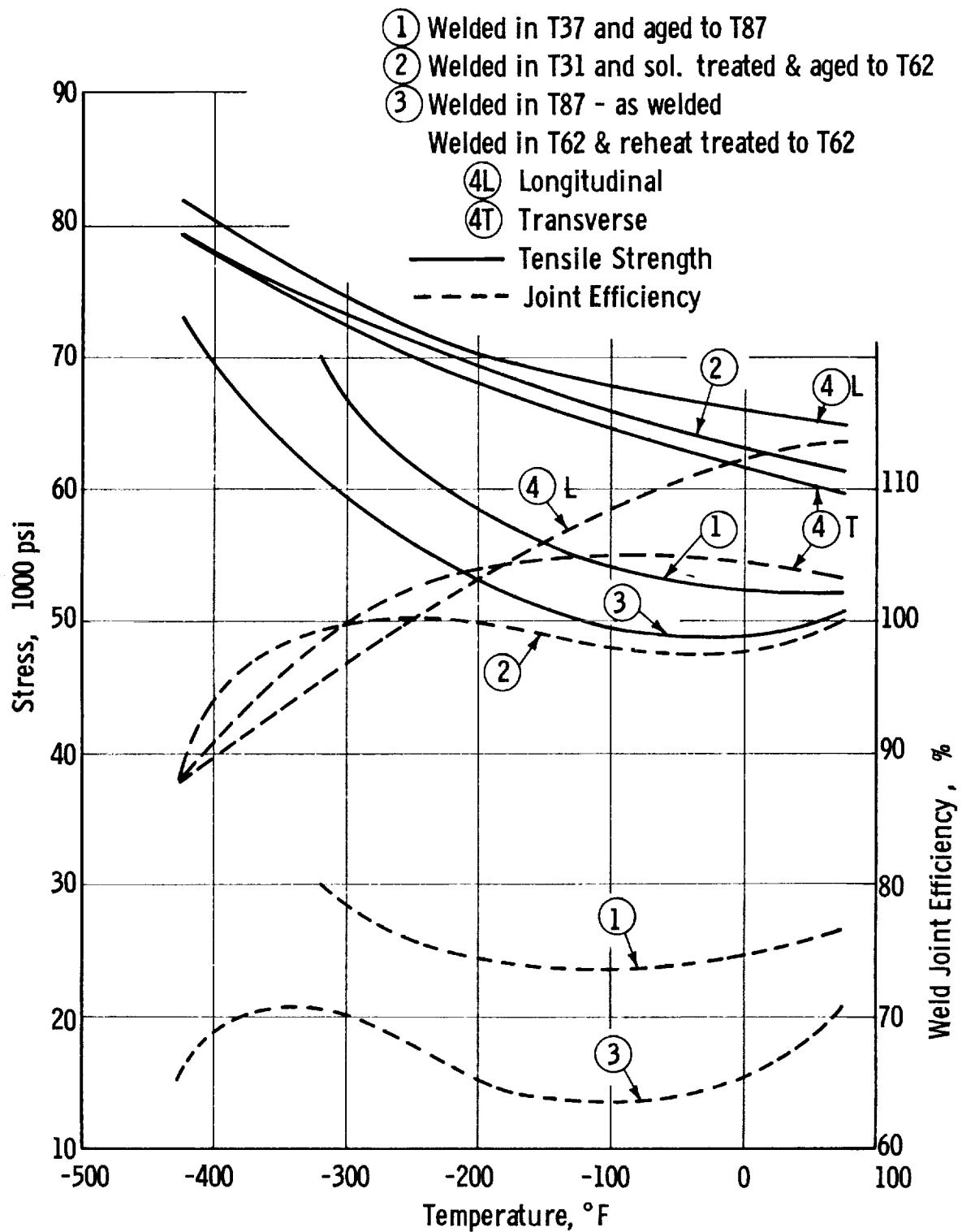
ALUMINUM ALLOY 2219-T62 - NOTCH / UNNOTCH STRENGTH RATIO

Figure B-45

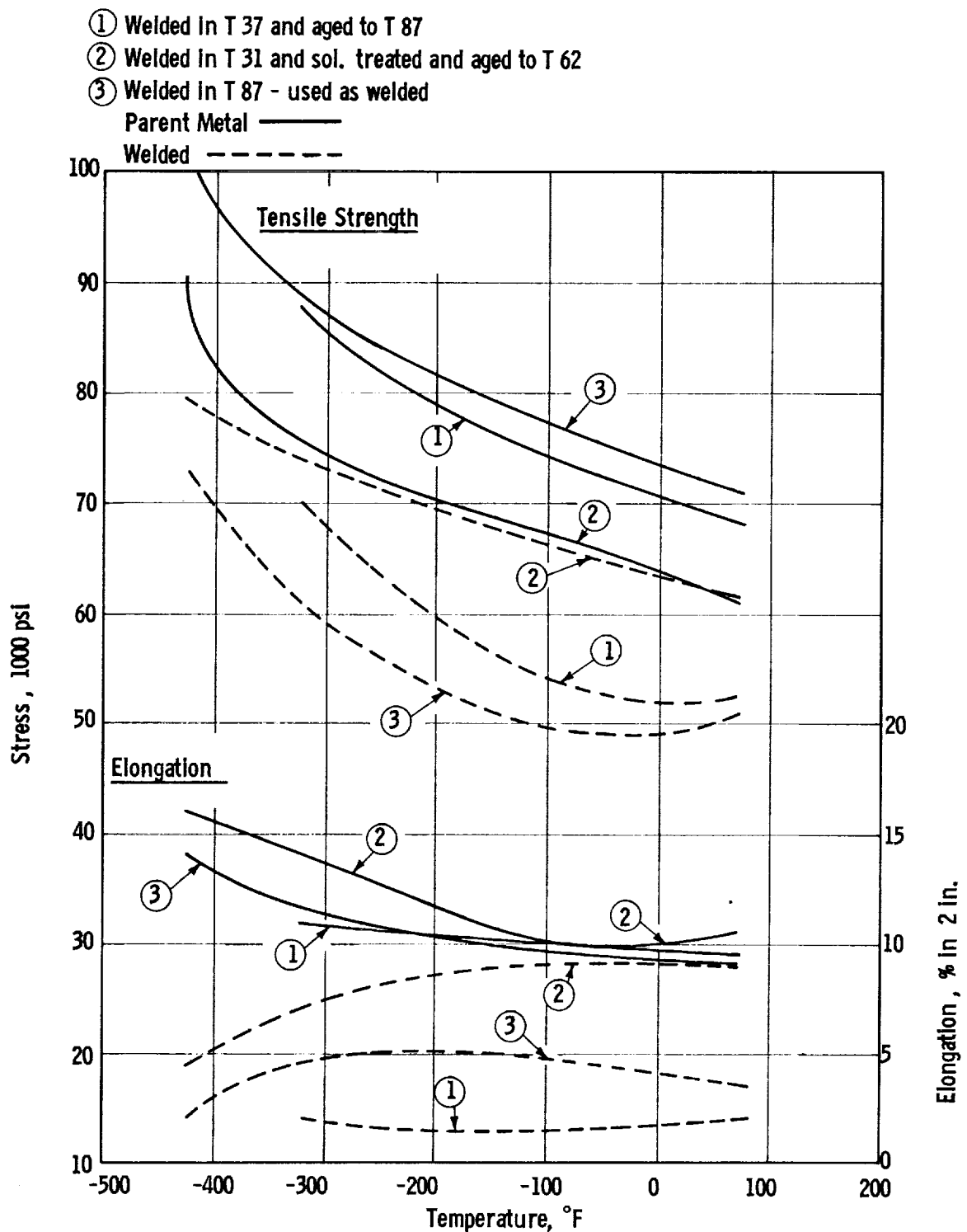


ALUMINUM ALLOY 2219-T87-AS WELDED TENSILE STRENGTH
AND WELD-JOINT EFFICIENCY

Figure B-46



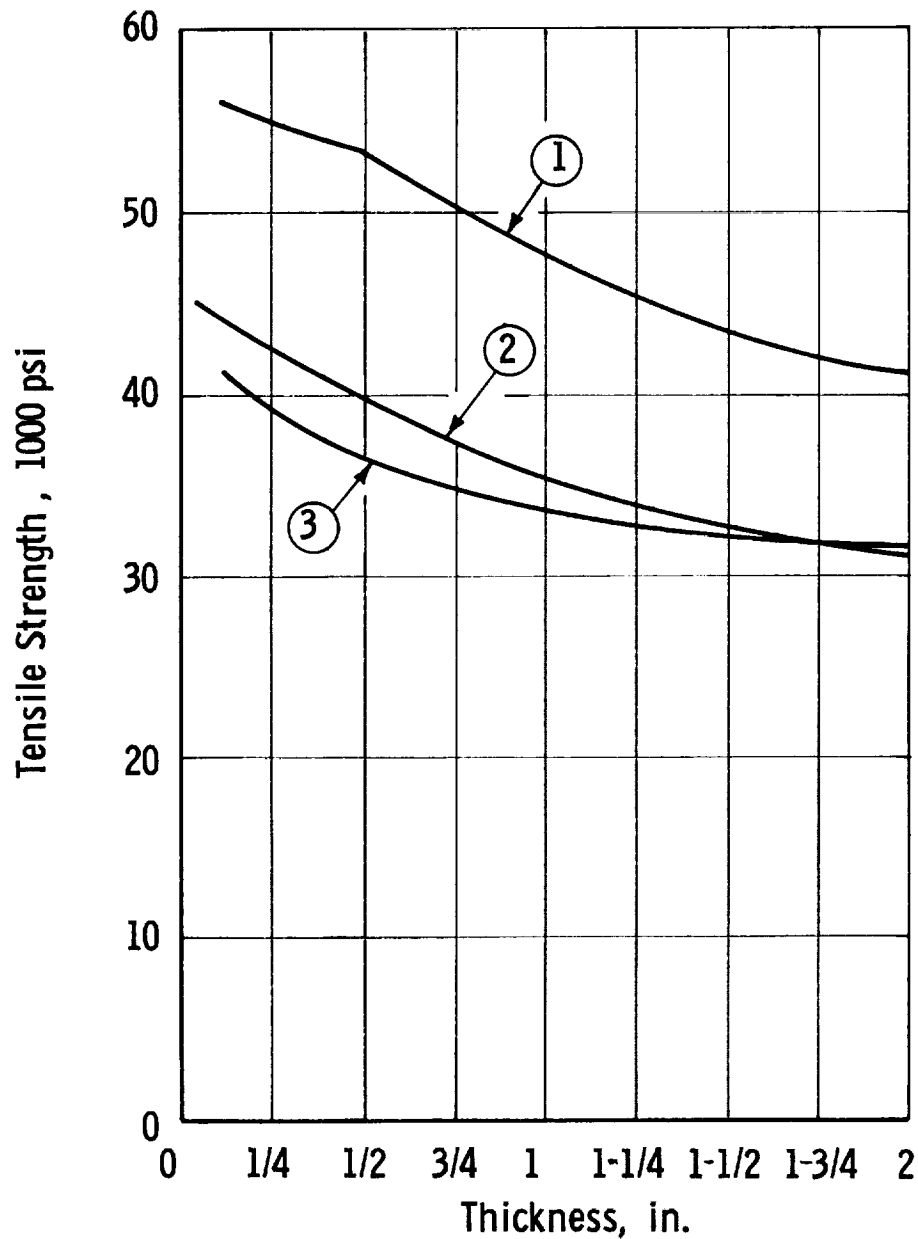
ALUMINUM ALLOY 2219 - WELDED - TENSILE STRENGTH & JOINT EFFICIENCY



ALUMINUM ALLOY 2219 - COMPARISON OF PARENT METAL AND WELDED PROPERTIES
 (0.063 IN. SHEET)

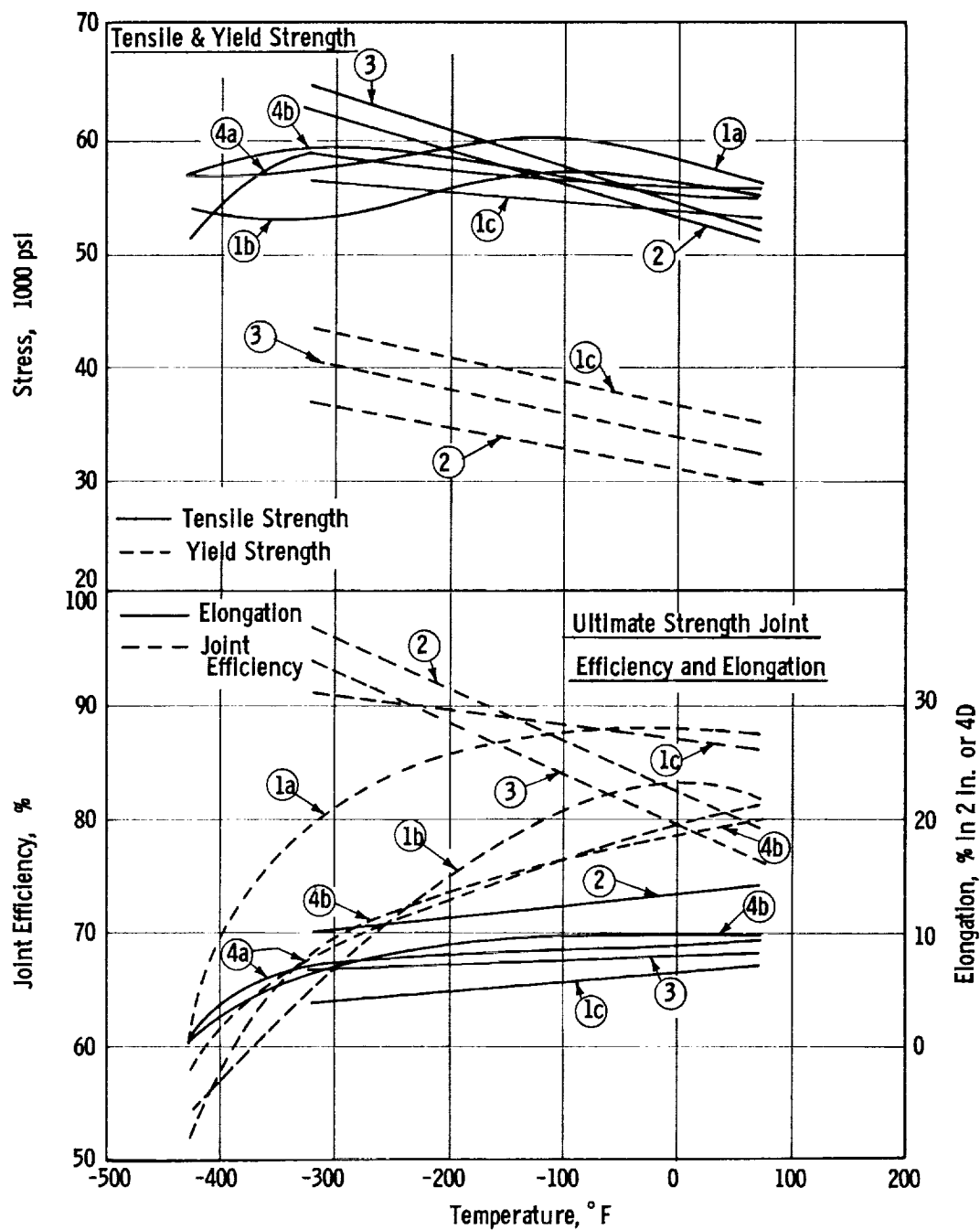
Figure B-48

- ① Solution treated and aged to T 62 temper after welding
- ② Welded in T 31 or T 37 temper. Aged to T 81 or T 87 temper after welding
- ③ T 81 or T 87 tempers - as welded



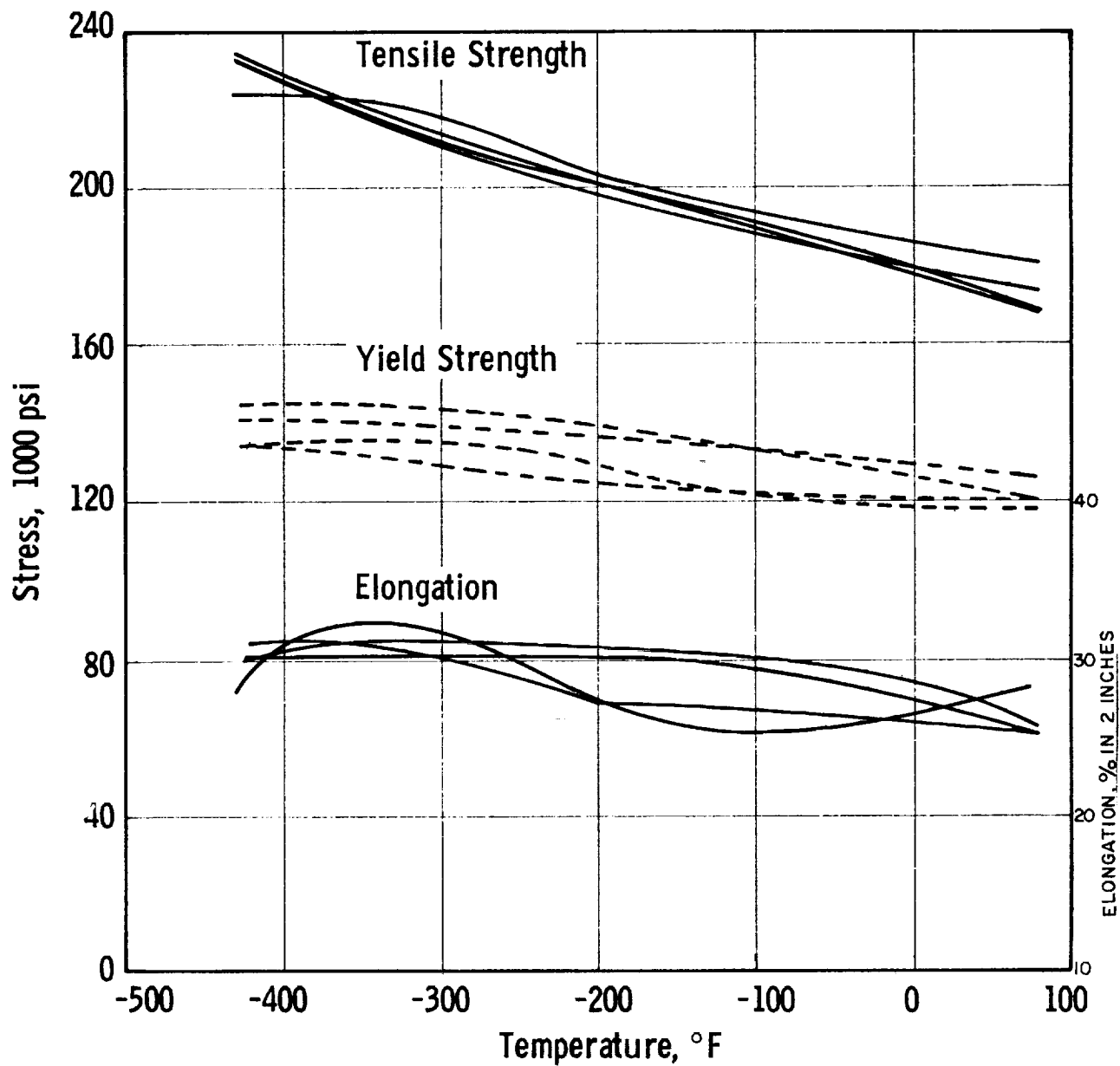
ALUMINUM ALLOY 2219 - EFFECT OF THICKNESS ON AVERAGE
TENSILE STRENGTH OF WELDS

- ①a 0.125 in. sheet-longitudinal
- ①b 0.125 in. sheet-transverse
- ①c 0.125 in. sheet-weld bead on
- ② 0.375 in. plate-weld bead off
- ③ 0.75 in. plate-weld bead off
- ④a 0.063 in. sheet-longitudinal
- ④b 0.063 in. sheet-transverse

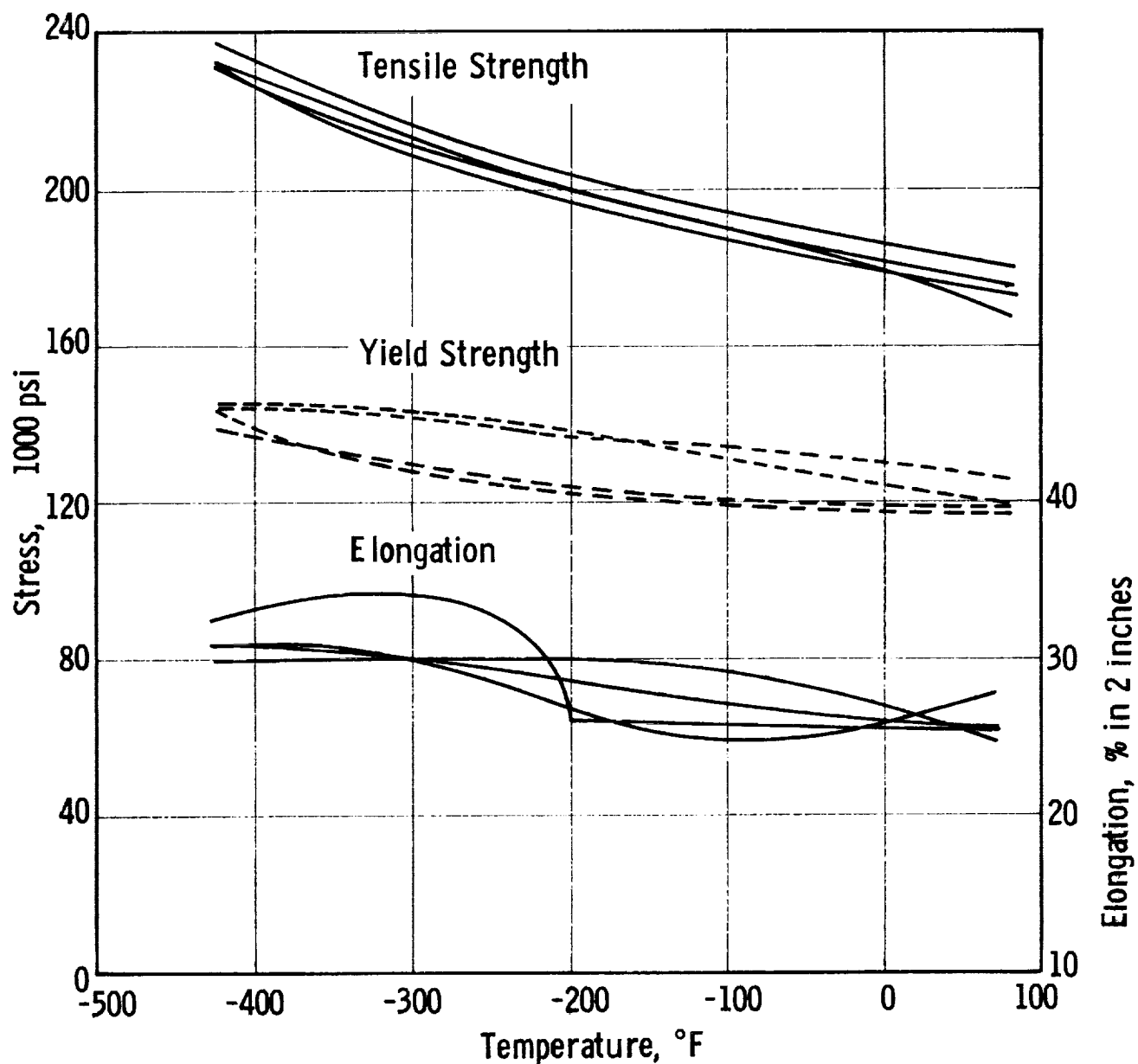


ALUMINUM ALLOY 7039-T6-AS WELDED PROPERTIES

Figure B-50

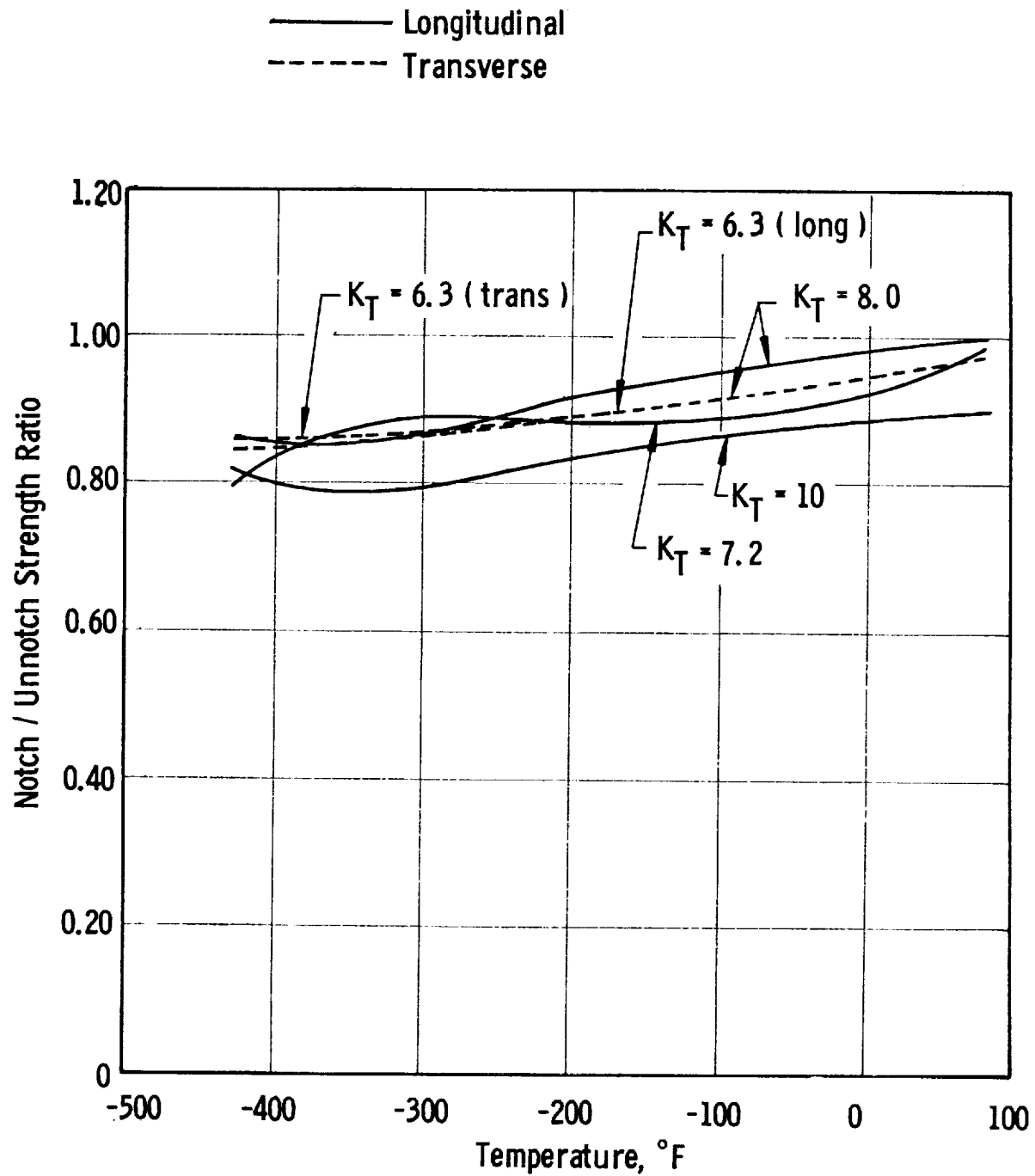


INCONEL ALLOY X-750 (INCONEL X) - TENSILE PROPERTIES
OF SHEET-SOLUTION TREATED & AGED - LONGITUDINAL

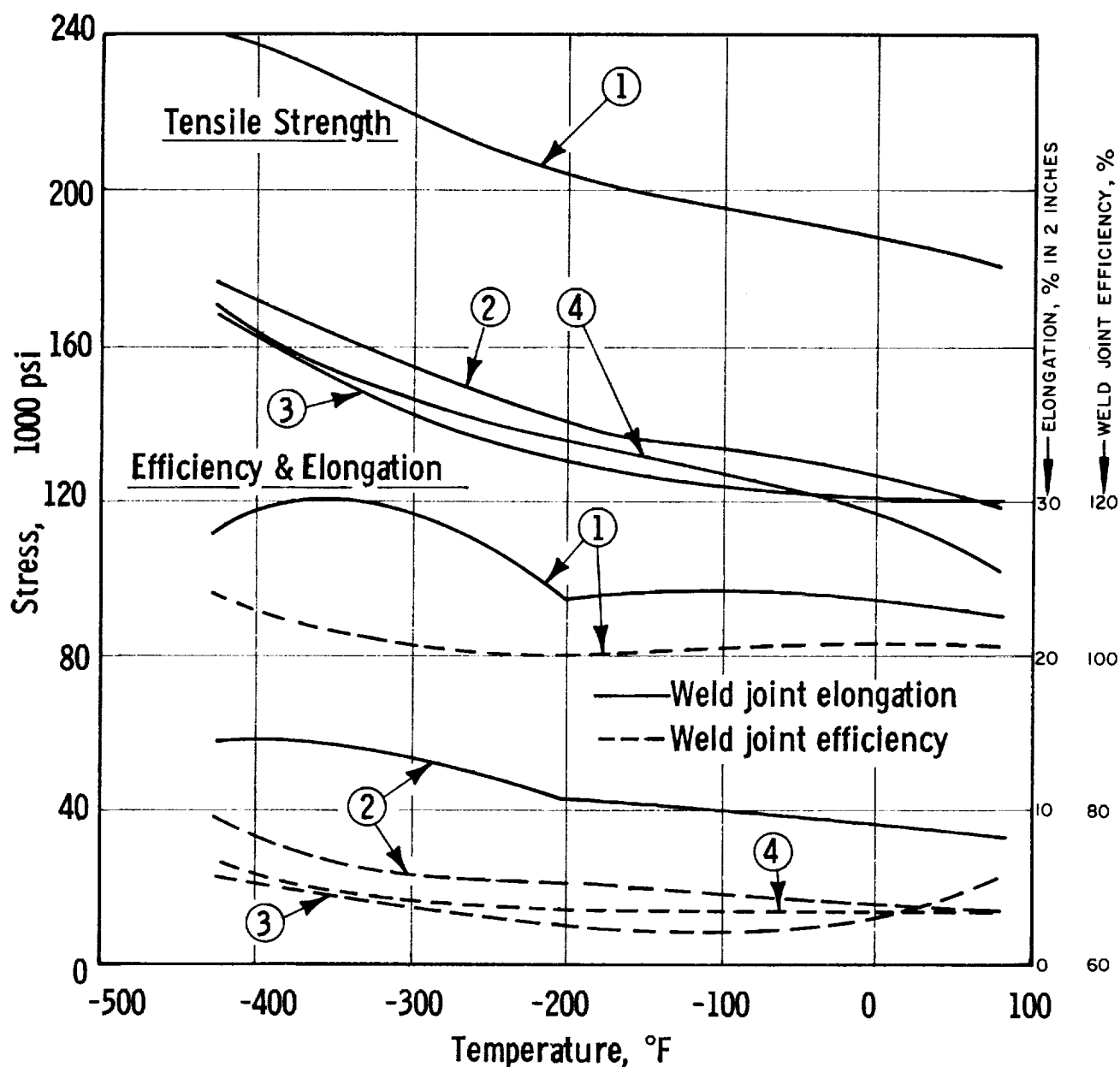


INCONEL ALLOY X - 750 (INCONEL X) - TENSILE PROPERTIES OF SHEET - SOLUTION TREATED AND AGED - TRANSVERSE

Figure B-52



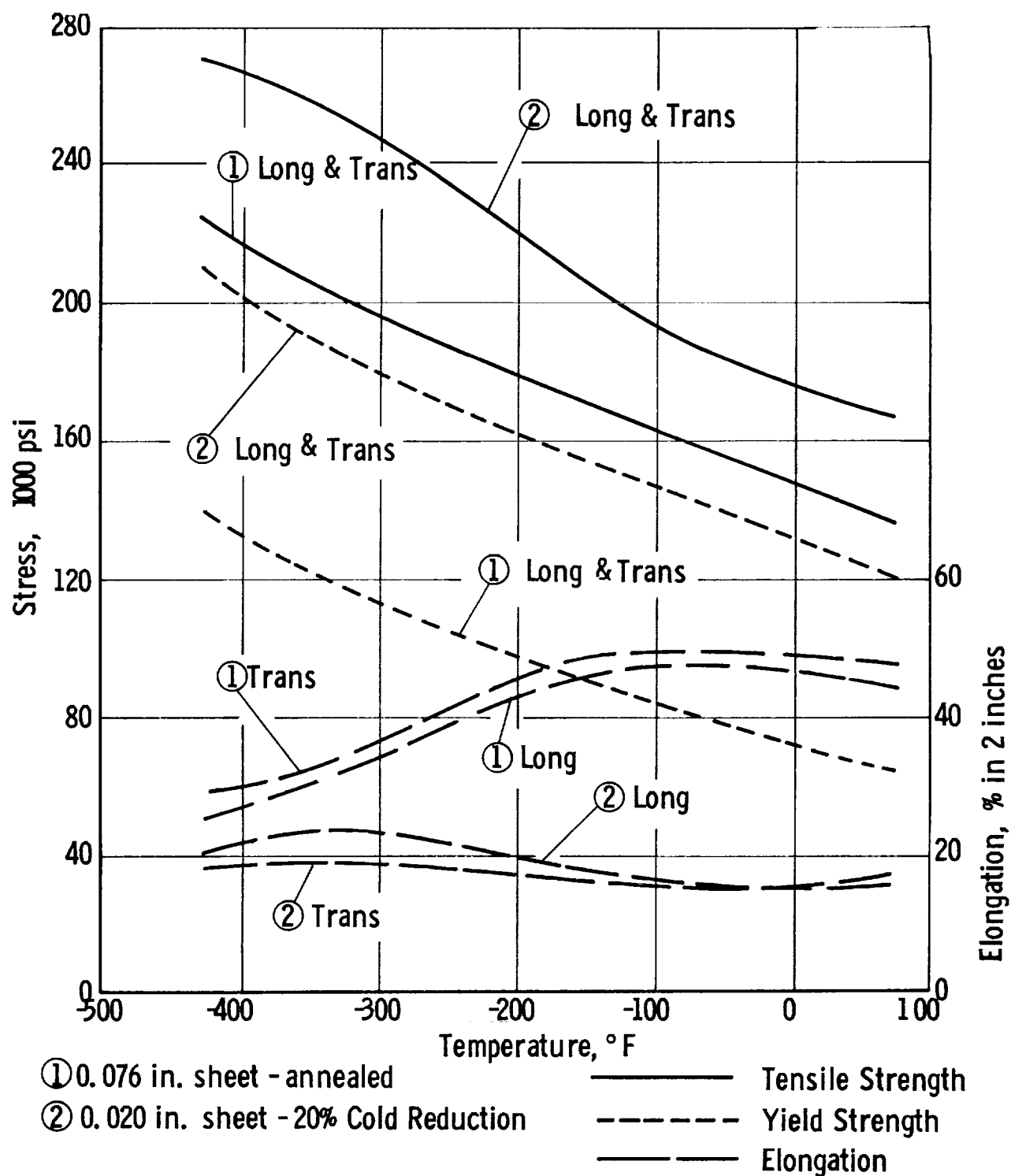
INCONEL ALLOY ALLOY X-750 (INCONEL X) - NOTCH / UNNOTCH
STRENGTH RATIO OF SHEET - SOLUTION TREATED & AGED



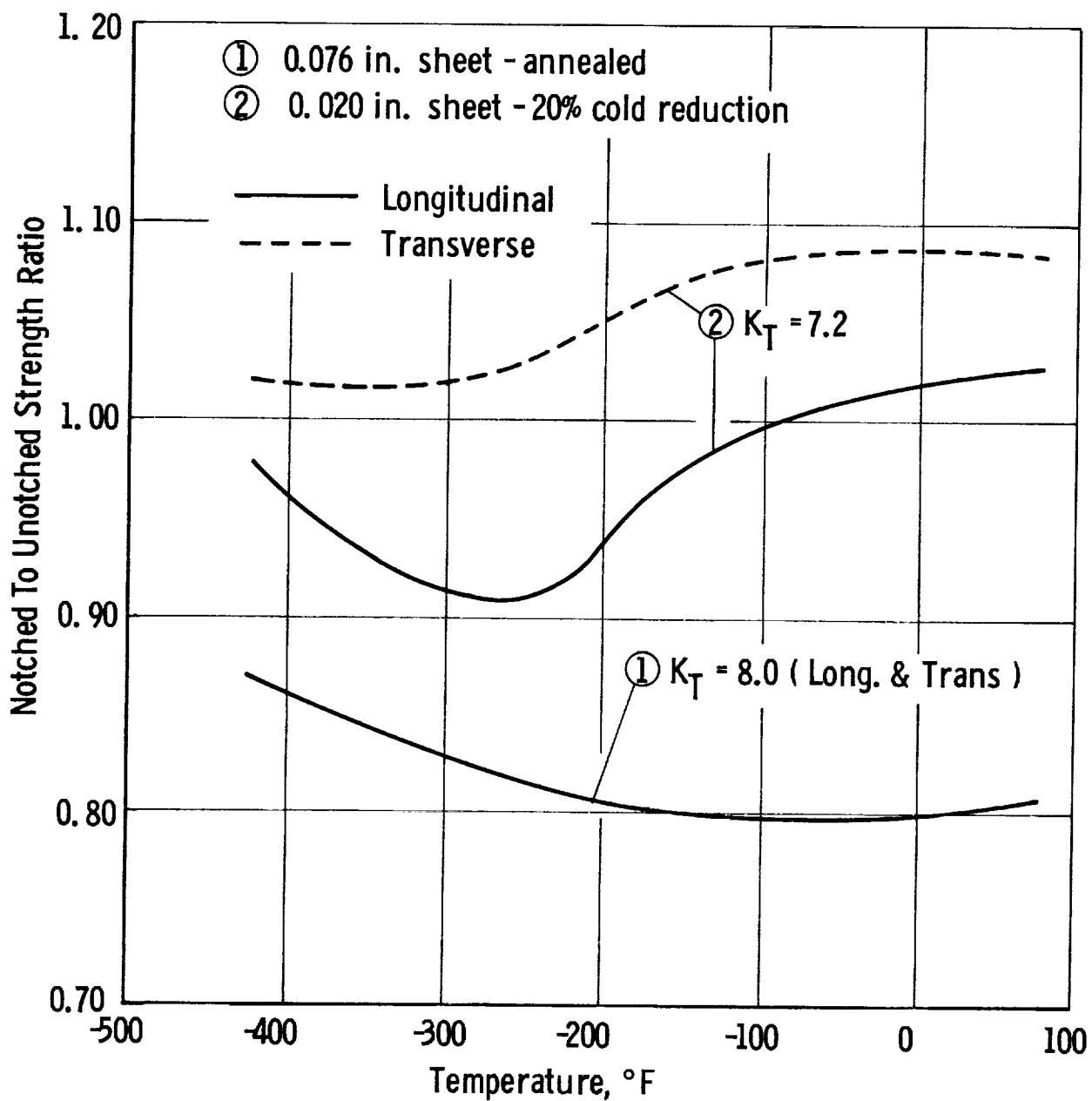
- ① Welded in solution treated condition-aged after welding-longitudinal
- ②&③ Welded in solution treated and aged condition-as welded-longitudinal
- ④ Welded in solution treated and aged condition-as welded-transverse

INCONEL ALLOY X-750 (INCONEL X) - WELDED PROPERTIES

Figure B-54

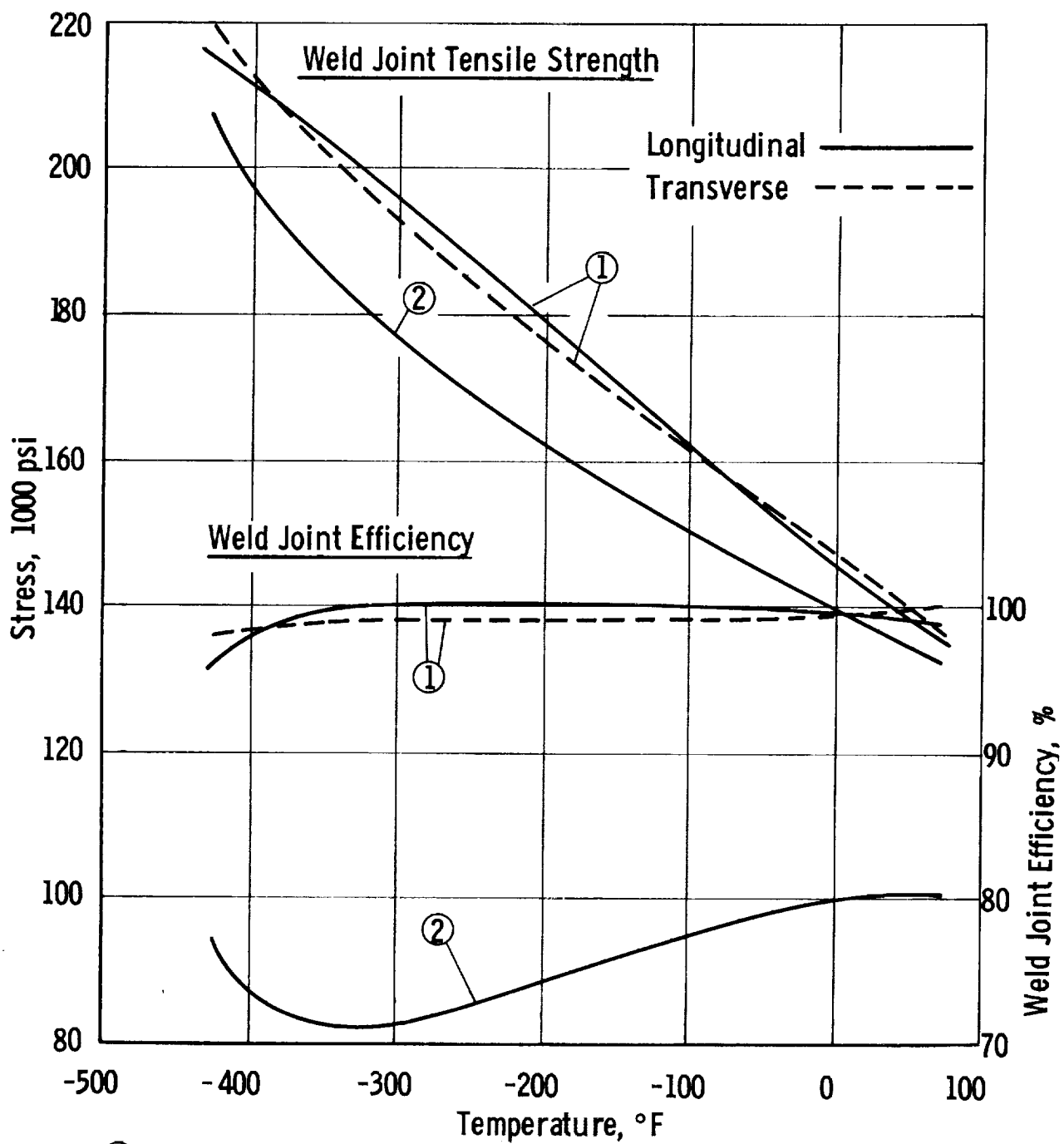


HAYNES 25 COBALT BASE ALLOY - TENSILE PROPERTIES



HAYNES 25 COBALT BASE ALLOY - NOTCH STRENGTH RATIO

Figure B-56

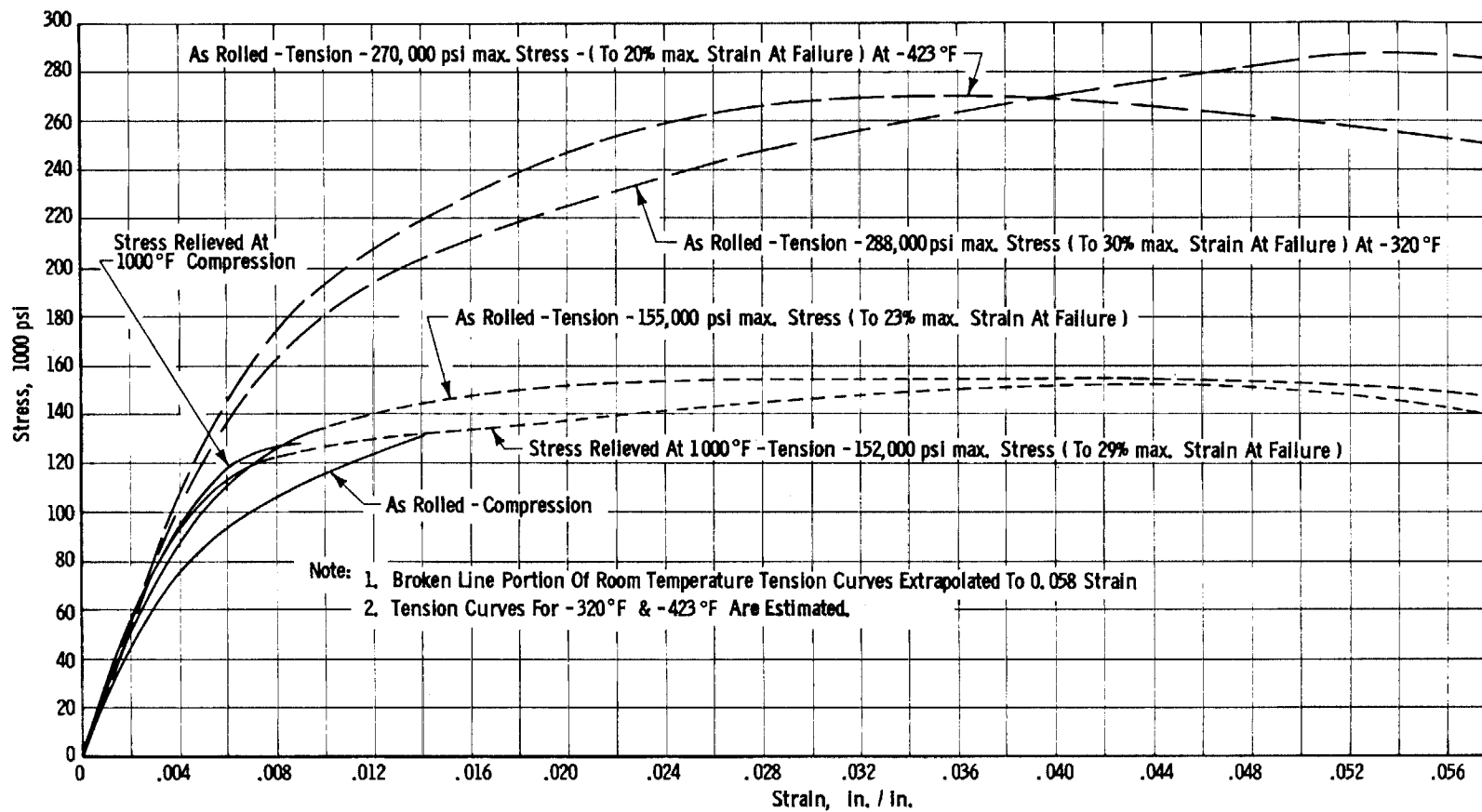


- ① 0.076 in. sheet - annealed
② 0.020 in. sheet - 20% cold reduction

HAYNES 25 COBALT BASE ALLOY - TENSILE PROPERTIES - AS WELDED

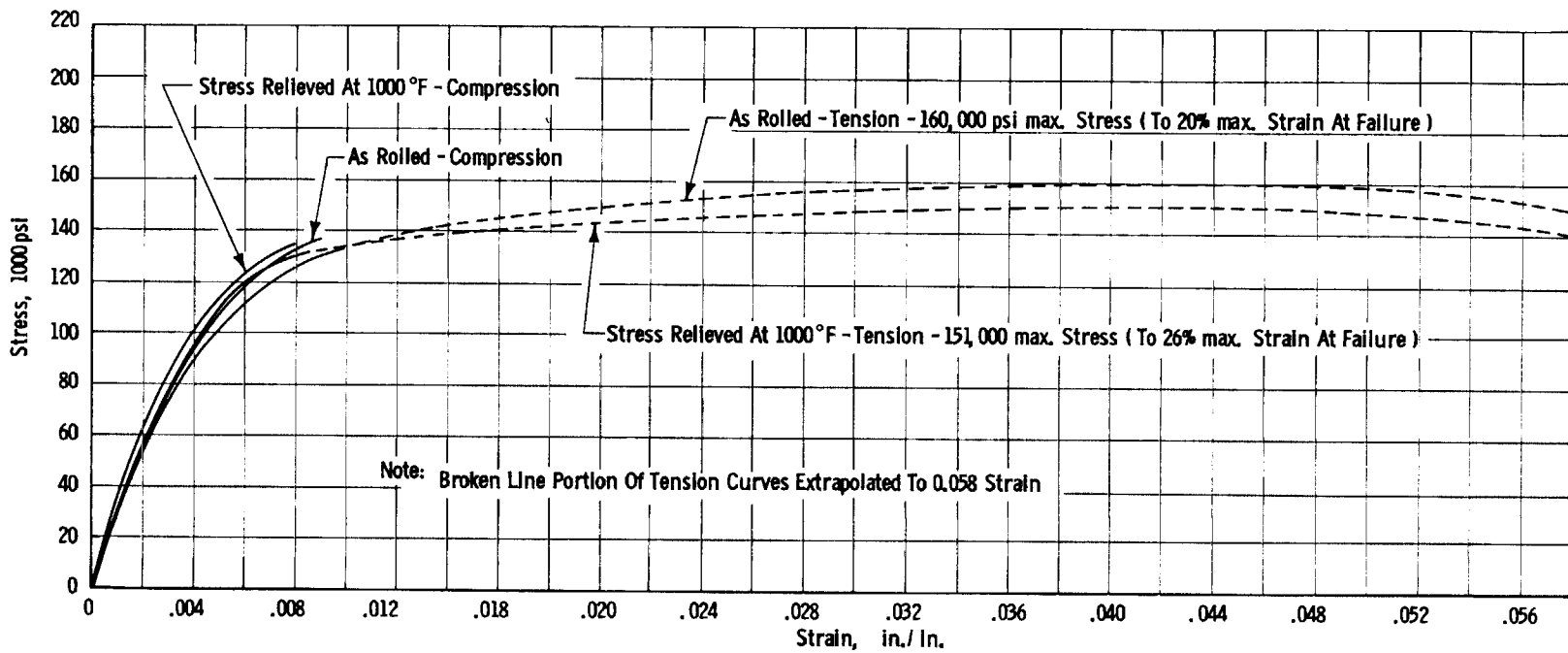
Figure B-57

Figure B-58

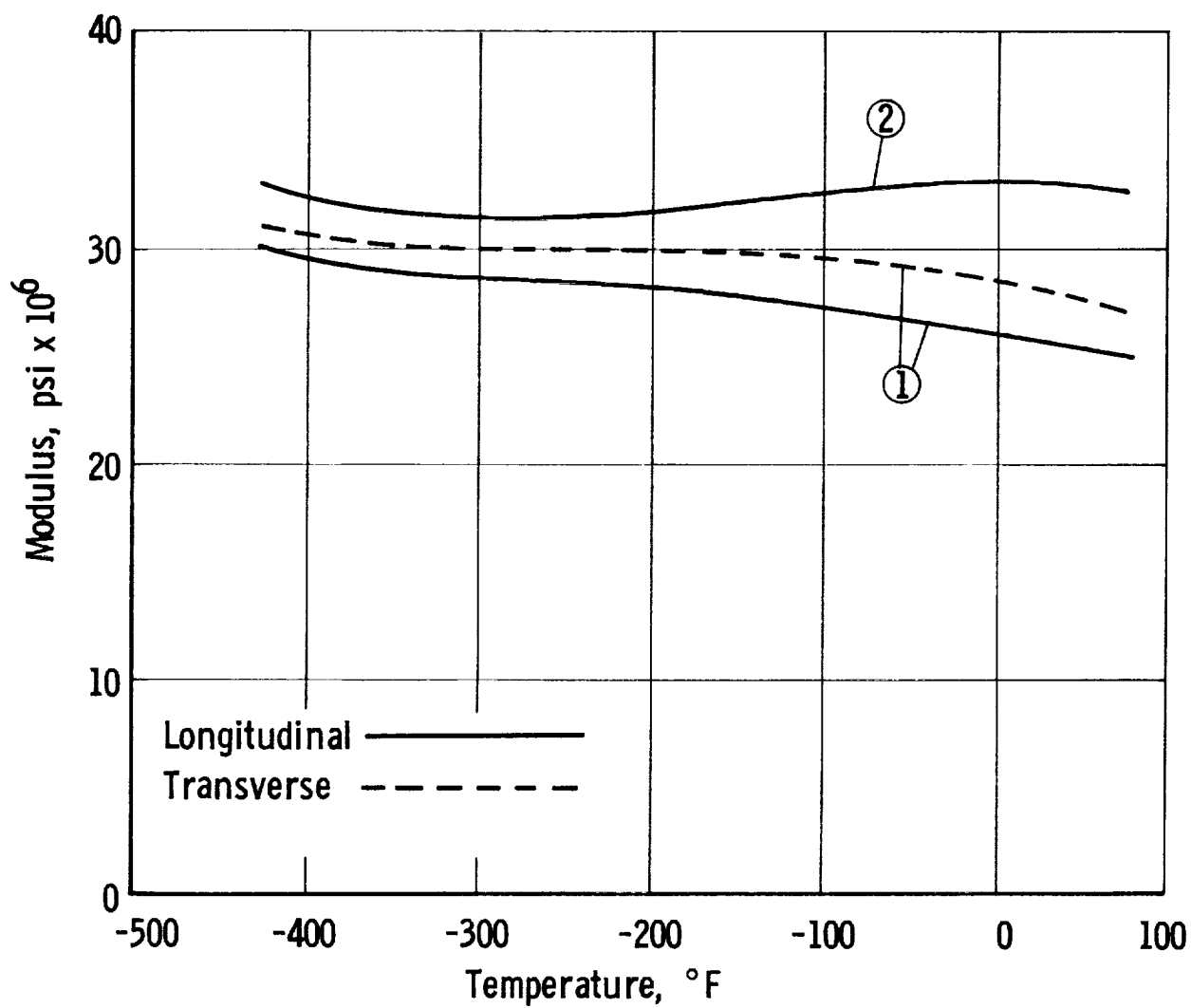


TYPICAL STRESS-STRAIN CURVES -TYPE 301 STAINLESS STEEL -1/2 HARD -LONGITUDINAL -ROOM TEMPERATURE EXCEPT AS NOTED

Figure B-59



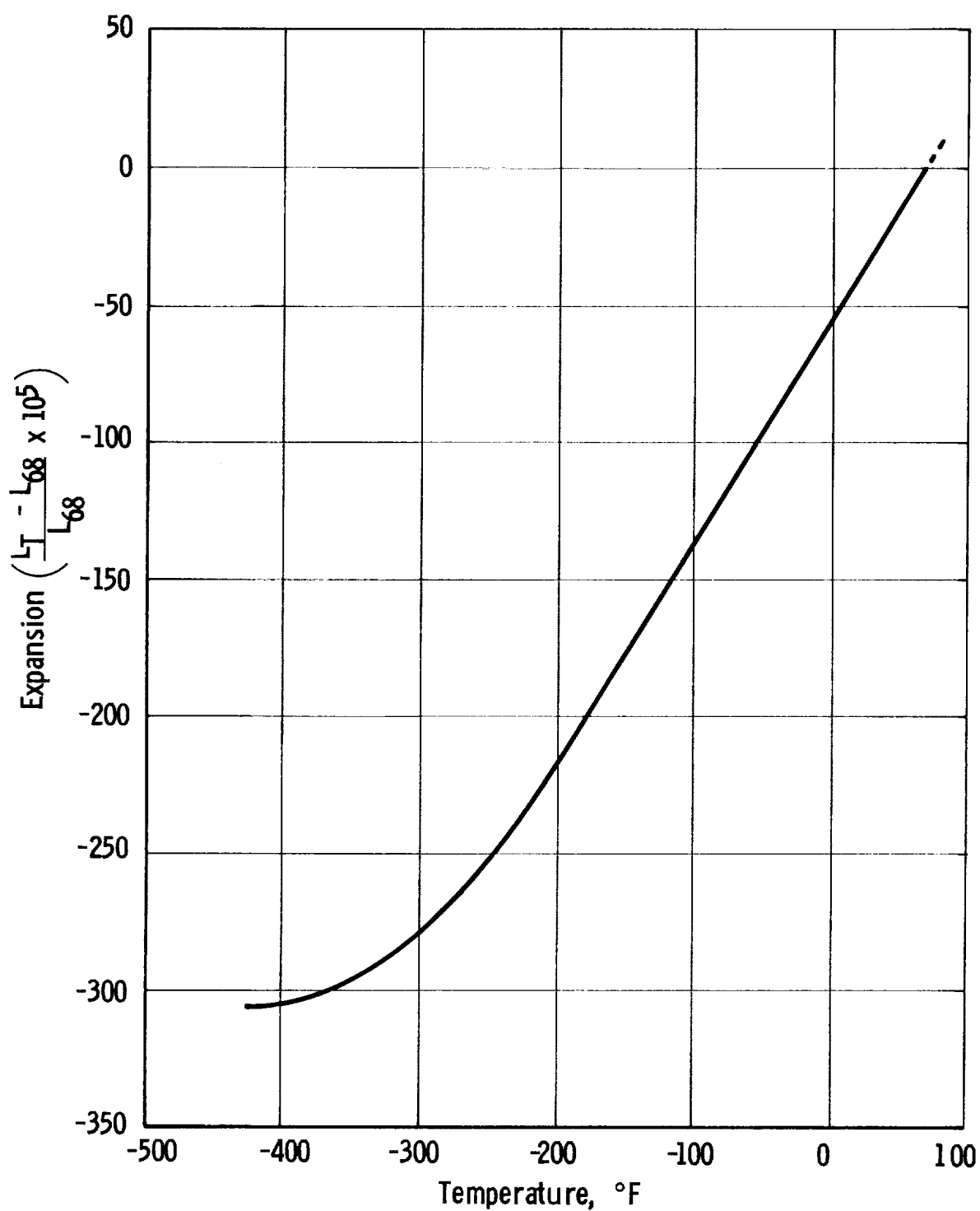
TYPICAL STRESS-STRAIN CURVES - TYPE 301 STAINLESS STEEL - 1/2 HARD - TRANSVERSE - ROOM TEMPERATURE



- ① 0.025 in. sheet - 60% Cold Rolled
- ② 0.060 in. sheet - 60% Cold Rolled

MODULUS OF ELASTICITY OF TYPE 301 STAINLESS STEEL

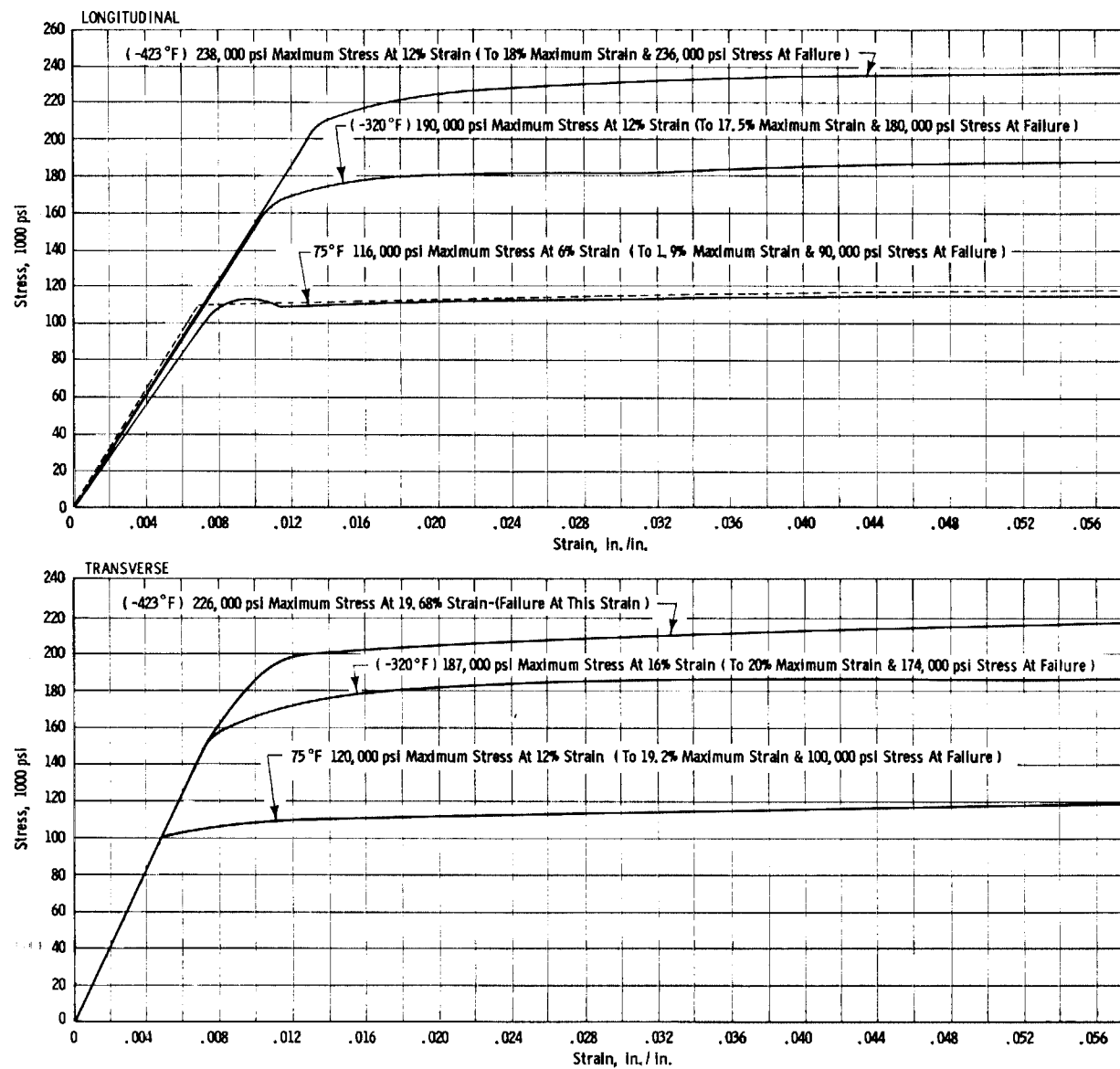
Figure B-60



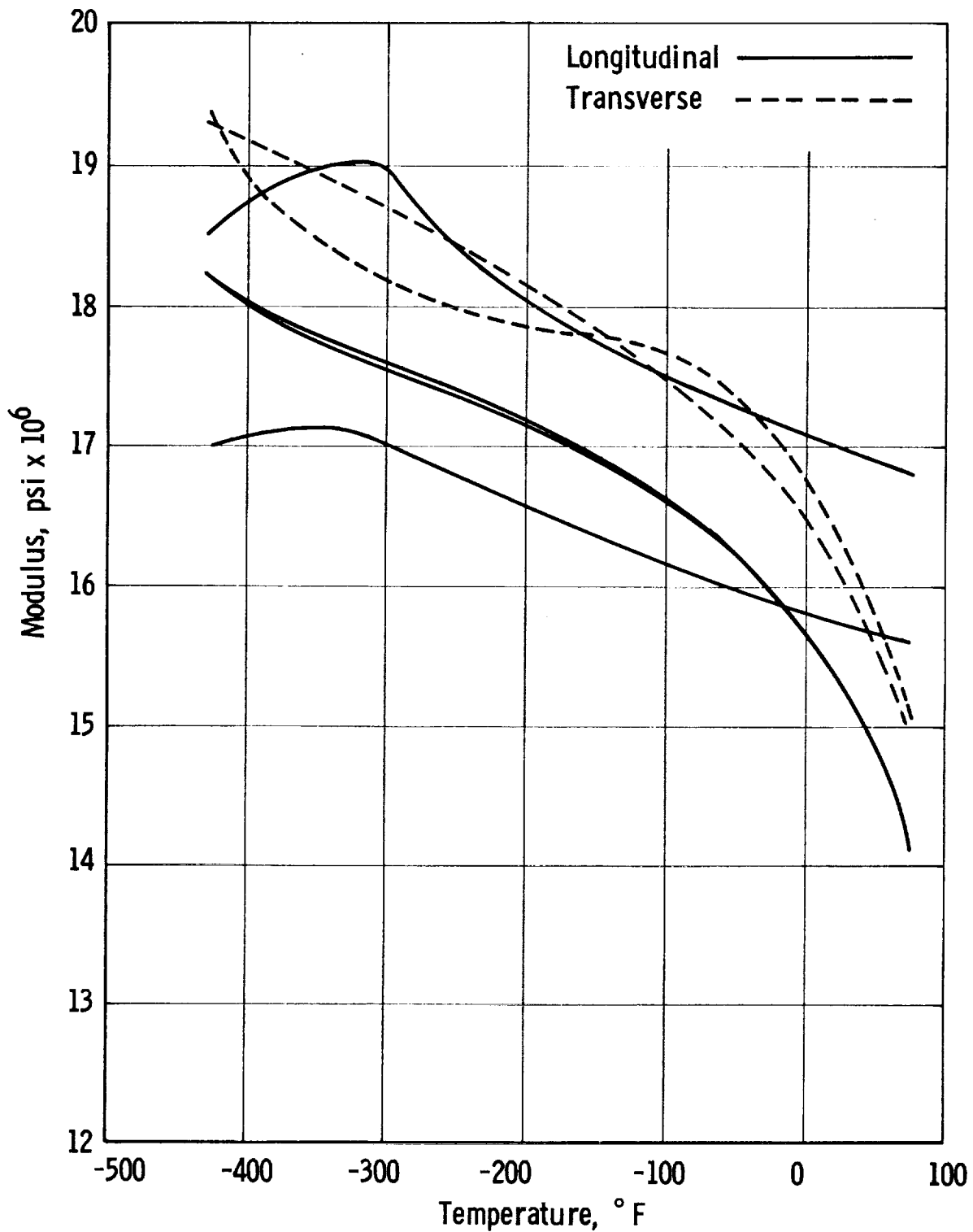
TYPE 302 STAINLESS STEEL -COLD DRAWN,
125,000 PSI. -THERMAL CONTRACTION

Figure B-61

Figure B-62

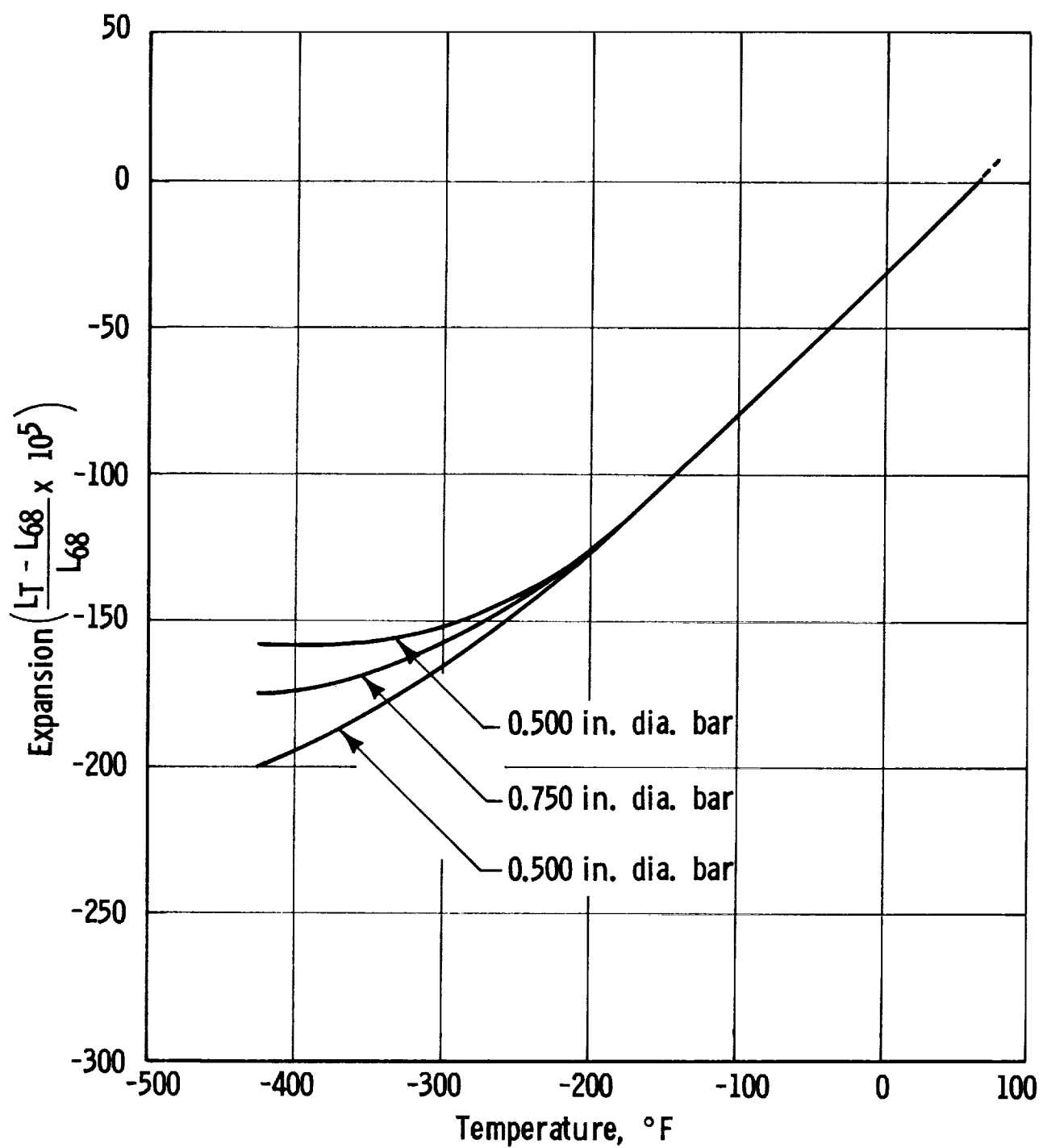


TYPICAL STRESS-STRAIN CURVES FOR Ti-5Al-2.5Sn ELI - LONGITUDINAL AND TRANSVERSE - 0.100 INCH SHEET - TENSION



Ti-5Al-2.5 Sn - NORMAL INTERSTITIAL - MODULUS OF ELASTICITY - SHEET, ANNEALED

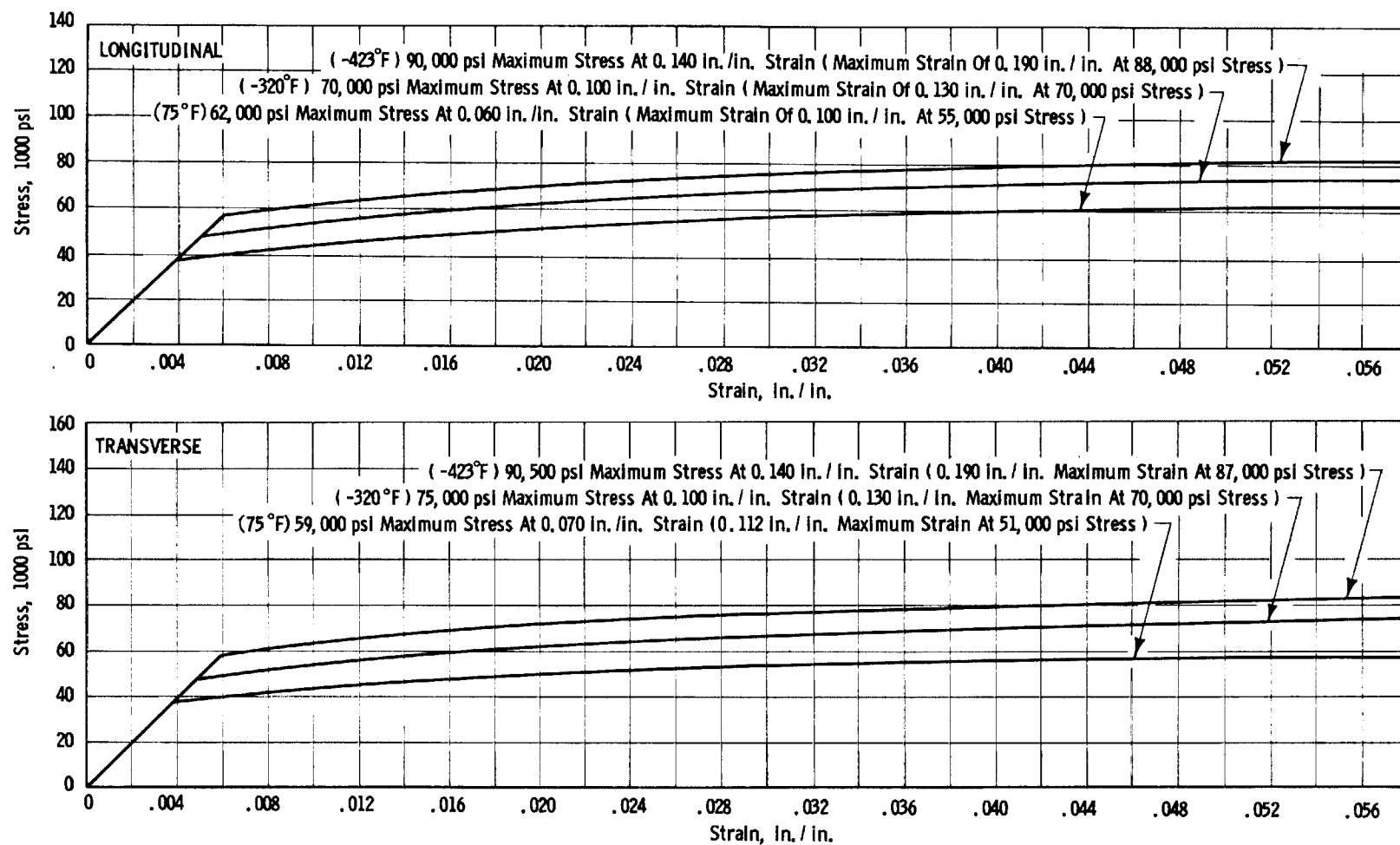
Figure B-63



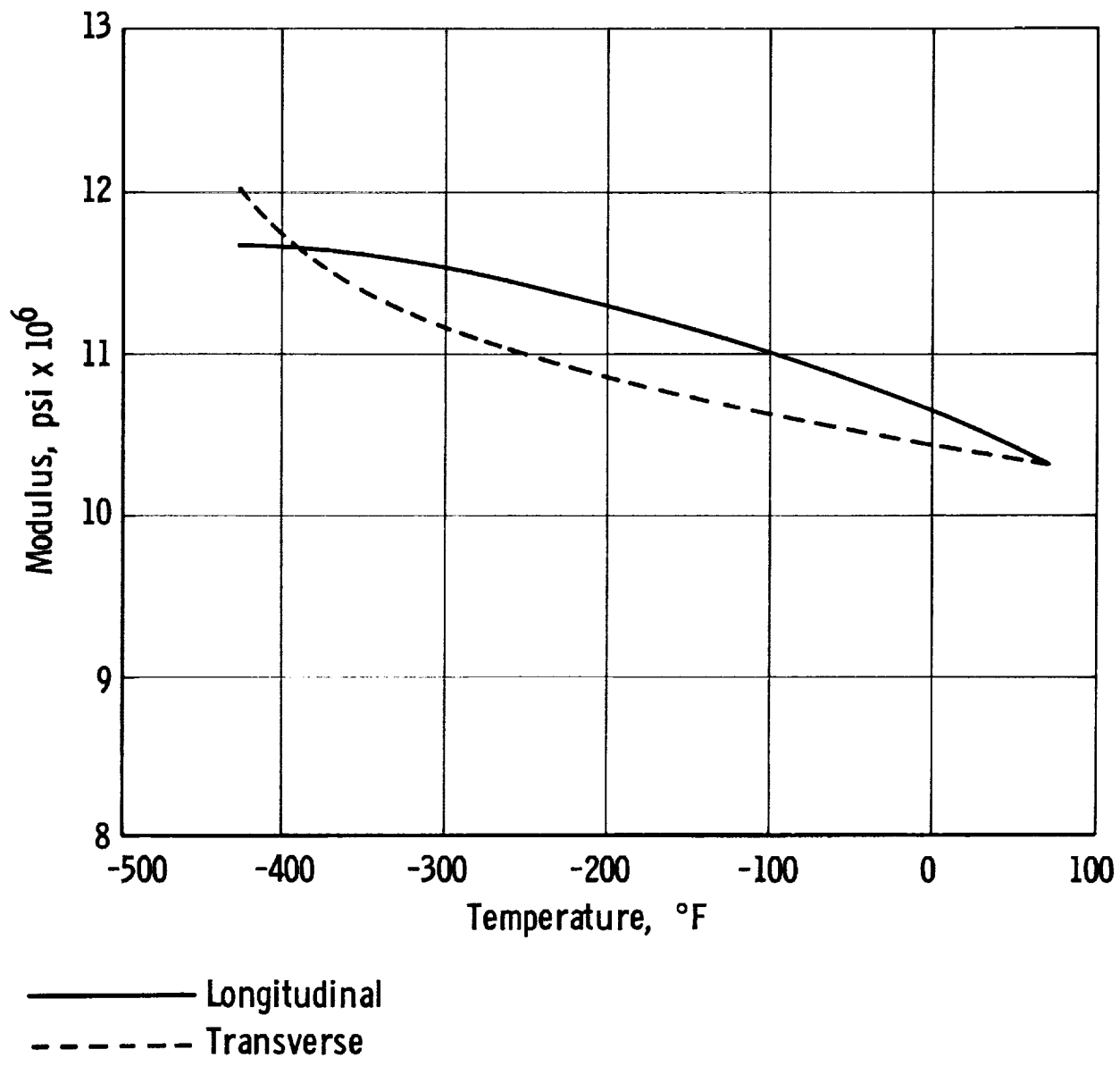
Ti-5Al-2.5 Sn ALLOY - NORMAL INTERSTITIAL GRADE
THERMAL CONTRACTION

Figure B-64

Figure B-65

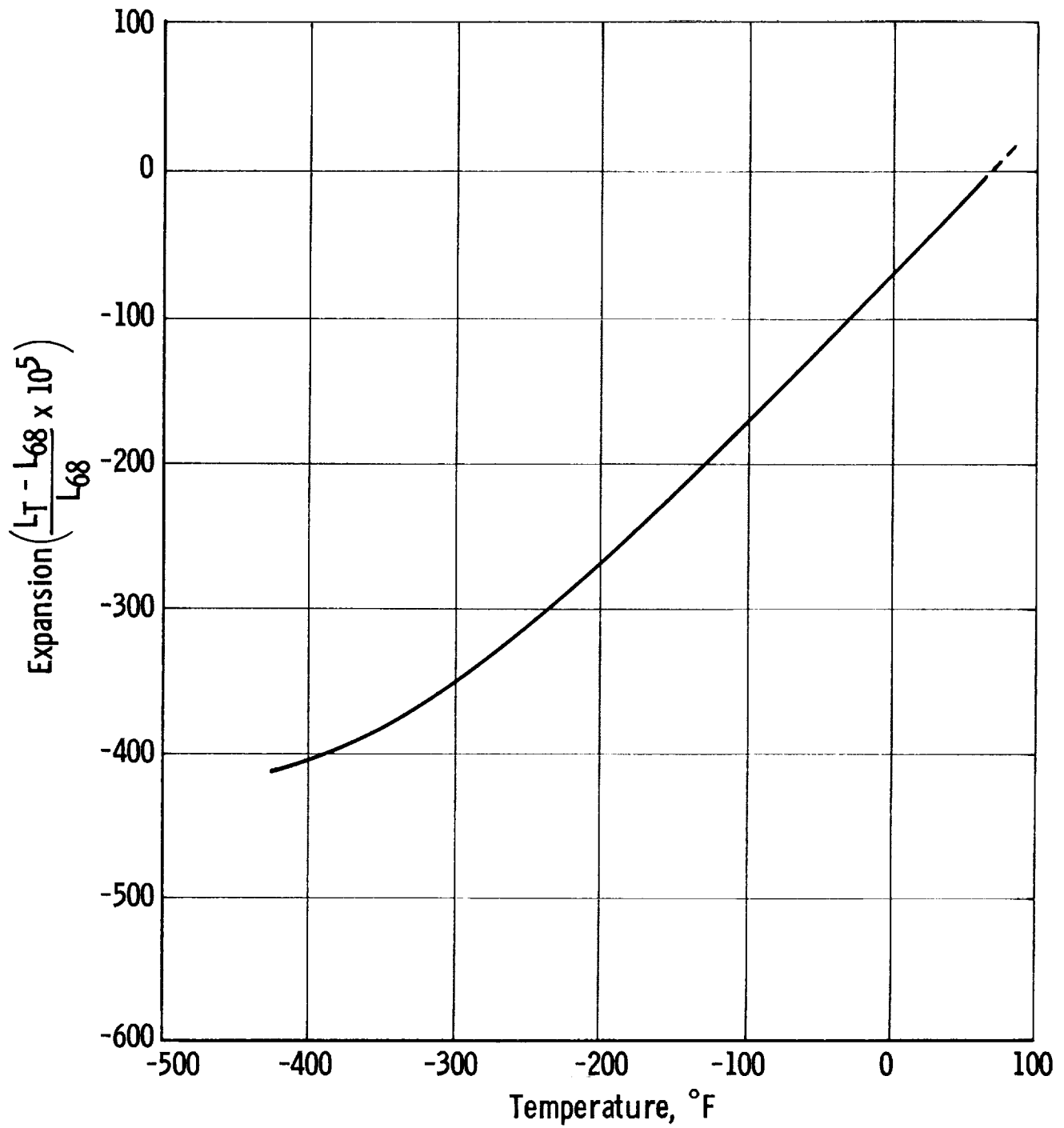


TYPICAL STRESS-STRAIN CURVES FOR ALUMINUM ALLOY 2219-T62 - TENSION - LONGITUDINAL AND TRANSVERSE (0.100 INCH SHEET)



ALUMINUM ALLOY 2219-T87 - MODULUS OF ELASTICITY
TENSION (0.100 IN. SHEET)

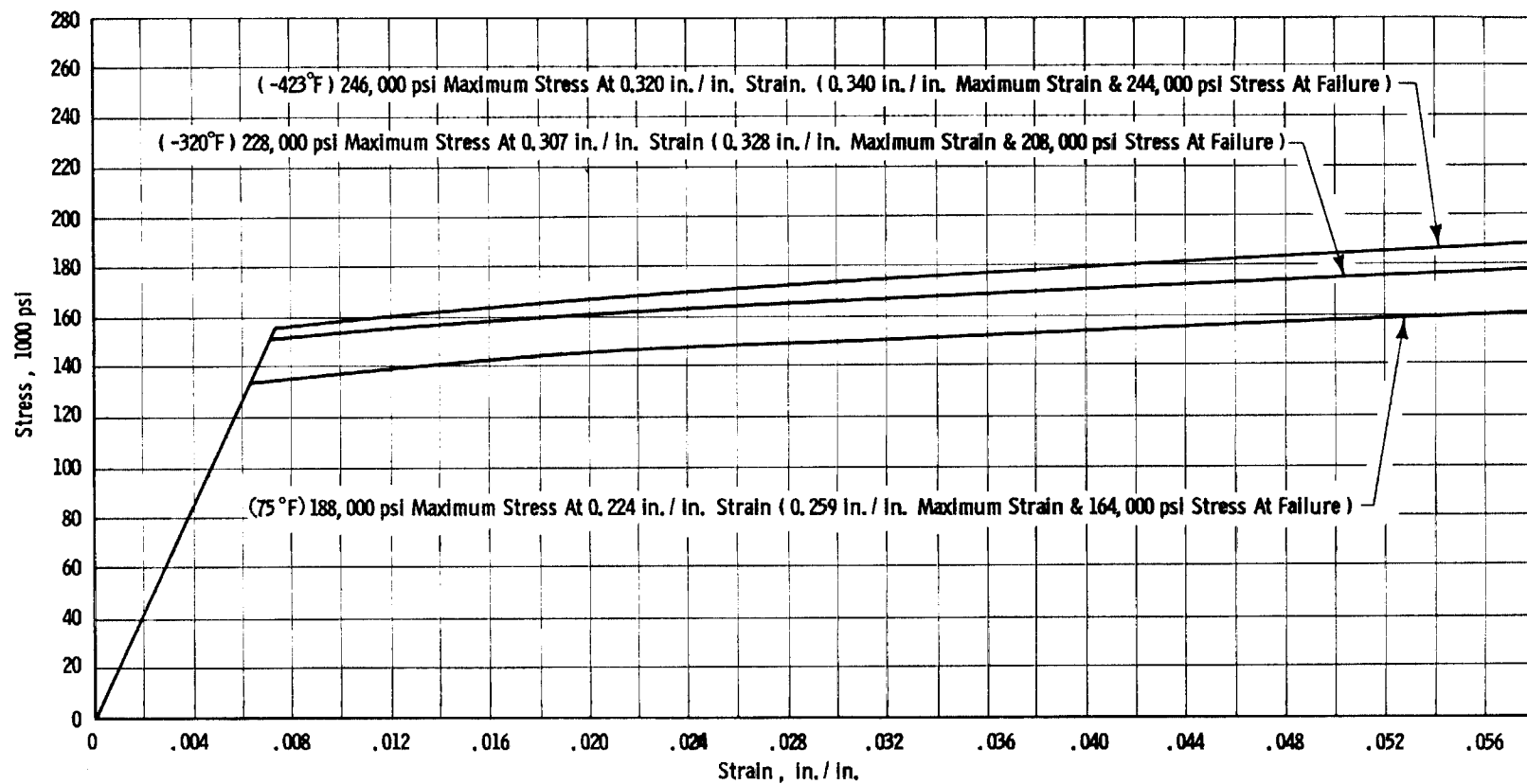
Figure B-66



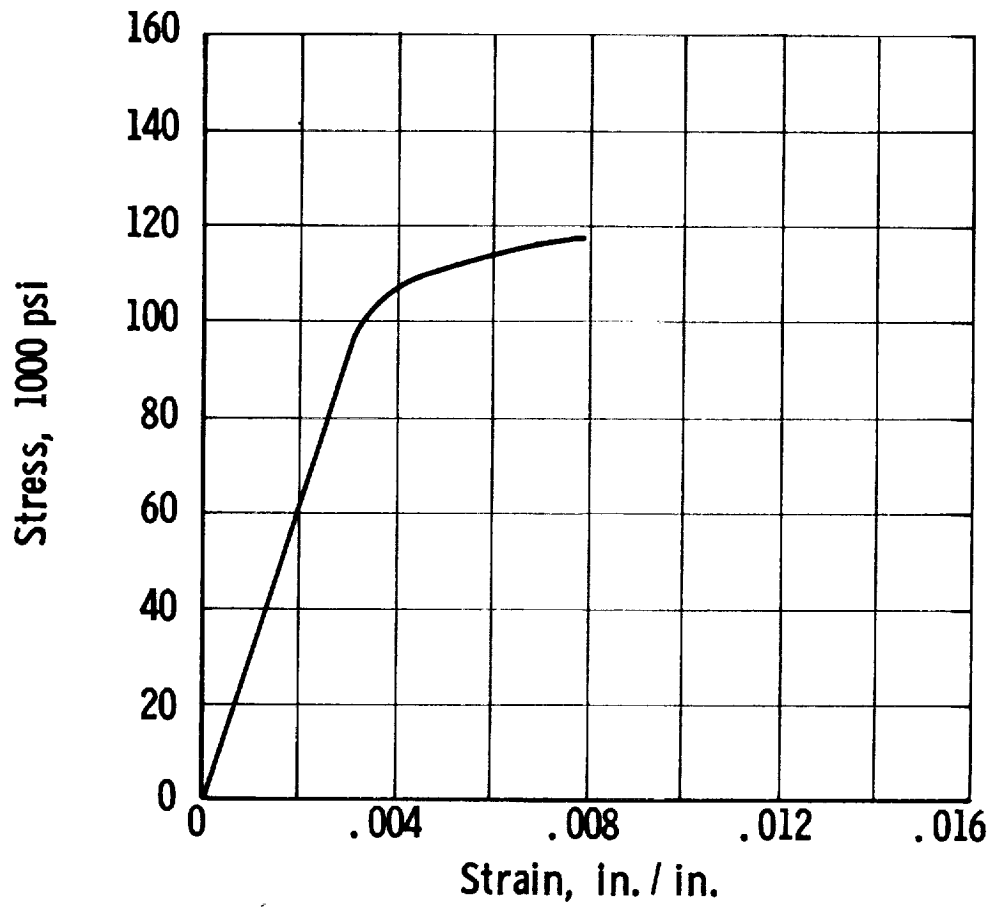
2219 - T87 ALUMINUM ALLOY PLATE - THERMAL CONTRACTION

Figure B-67

Figure B-68

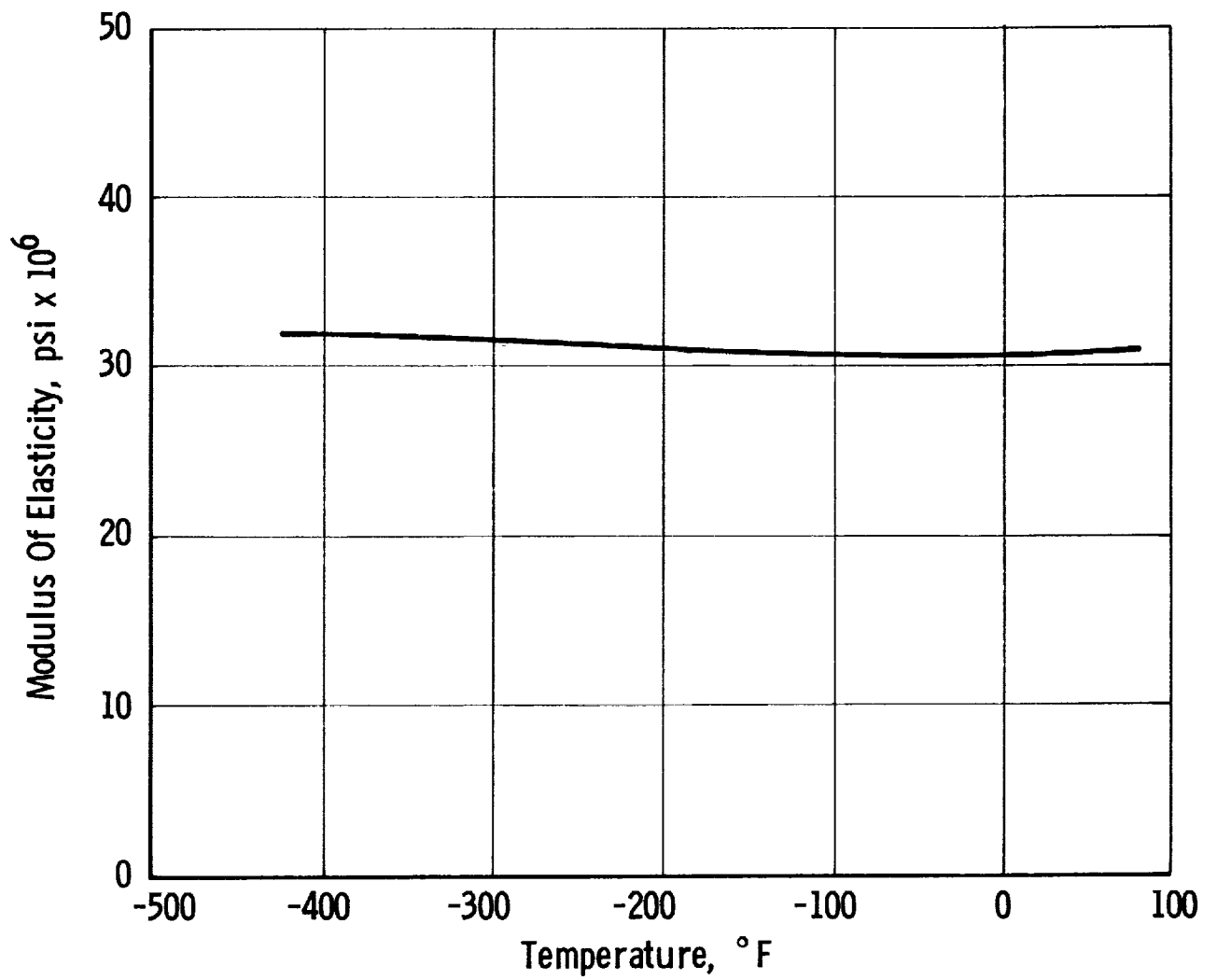


TYPICAL STRESS - STRAIN CURVES - INCONEL X-750 ALLOY - SOLUTION TREATED AND AGED - 0.750 INCH DIAMETER BAR - TENSION



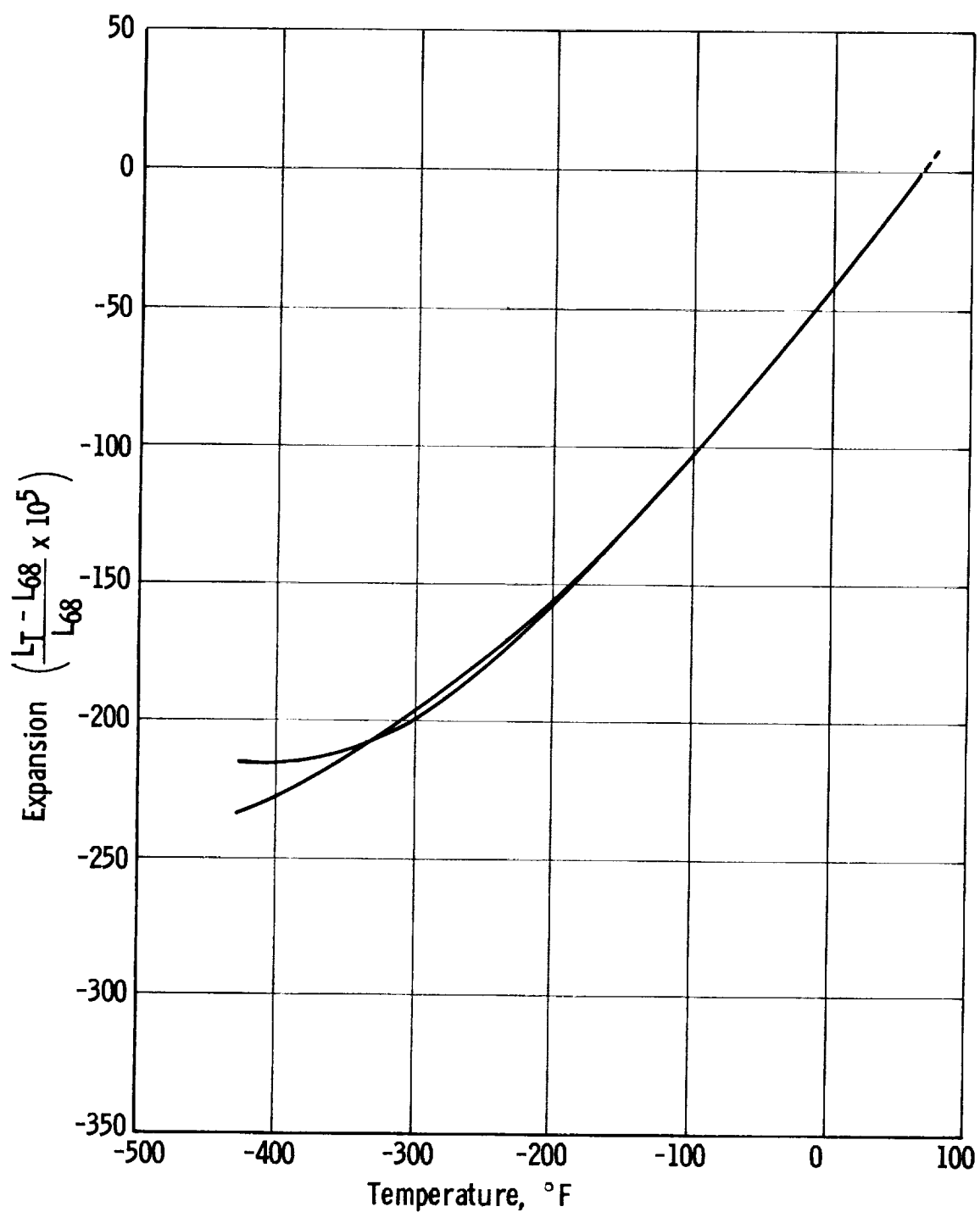
TYPICAL STRESS-STRAIN CURVE - INCONEL ALLOY X-750 -
COMPRESSION - SHEET (0.064 IN.) - ANNEALED & AGED -
ROOM TEMPERATURE

Figure B-69



INCONEL ALLOY X-750 - MODULUS OF ELASTICITY

Figure B-70



INCONEL X-750 ALLOY - SOLUTION TREATED AND AGED
0.750 IN. DIA. BAR - THERMAL CONTRACTION

Figure B-71

APPENDIX C

LOW-CYCLE, HIGH-STRAIN FATIGUE RESISTANCE OF CANDIDATE MATERIALS

I. SUMMARY

An investigation was undertaken to determine the low-cycle, high-strain-range fatigue resistance of candidate stainless steel, and titanium-, nickel-, and aluminum-alloy shell materials* in the unwelded condition for use in GFR metal tanks over the temperature range from +75 to -423°F. Fatigue-performance predictions in this range were compared with the fatigue-loading conditions in GFR metal tanks, and the candidates were ranked for the imposed service conditions.

For factors of safety associated with aerospace tankage and the materials under consideration, application of prestress pressure to the composite tankage results in considerable plastic deformation of the metal shell under 1-to-1 biaxial-stress-field conditions. When the prestress pressure is relieved, the metal shell springs back along its offset stress-strain curve and is pushed into compression by the overwrapped glass-filament shell. When the tankage is pressure-cycled between zero and the operating level (100 cycles assumed), the metal shell operates up and down the offset stress-strain curve because the operating pressure will be less than the prestress pressure. No additional plastic deformation of the liner occurs until the pressure applied is greater than the prestress value, when the tankage is burst-tested. Maximum values for the biaxial (1-to-1 stress field), elastic-strain ranges imposed on the metal shell during cycling between zero and the operating pressures were calculated for each material at +75, -320, and -423°F. For comparison with uniaxial low-cycle fatigue-test results and predictions of uniaxial fatigue life, the biaxial-elastic-strain ranges were converted into equivalent uniaxial-elastic-strain ranges.

Data on fatigue characteristics of metals subjected to uniaxial and biaxial cyclic loading in the high strain range were compiled from References C-1 through C-39 and were evaluated. Almost all the available data were for unwelded materials tested at 75°F.

Uniaxial-test results and interpretations of uniaxial-test data were analyzed. They indicate that the maximum compressive and tensile stresses during any one cycle of zero-mean-strain fatigue testing remain approximately unchanged throughout the test. The hardening or softening of a material due to cyclic straining thus affected the peak tensile or compressive stresses equally, and the mean stress remained essentially constant at zero. This result provides a basis for ignoring the Bauschinger effect** in analyzing metal-shell-material properties.

* Chosen in the analysis described in Appendix B.

** Reduced deformation resistance in one loading direction following initial prestraining in the opposite direction (Refs. 35-39).

Tests of a large number of materials indicate that metals can resist approximately the same uniaxial-cyclic-strain range about zero mean strain ($\pm 1.0\%$ strain) when the fatigue life approximates 10^3 cycles. When the strain range is increased or decreased from $\pm 1.0\%$, however, significant fatigue-life variations occur.

Several investigators have found that uniaxial-strain-cycling fatigue behavior at 75°F in the low-cycle, high-strain range can be accurately related to the elastic, plastic, and/or total strain ranges by power laws. These laws require the definition of only a few basic mechanical properties of a material in order to predict the low-cycle fatigue life up to 10^6 cycles. One of the power laws (Manson's, Ref. C-7) was used to predict low-cycle fatigue life vs cyclic-elastic-strain range about zero mean strain for the candidate materials at 75 , -320 , and -423°F . The power law

$$\Delta\epsilon_e = 3.5 \frac{\sigma_u}{E} N_f^{-0.12} \quad (\text{C-1})$$

where

$\Delta\epsilon_e$ = elastic-strain range about zero mean strain, in./in.

N_f = number of cycles to failure

E = elastic modulus, psi

σ_u = ultimate tensile strength, psi

was assumed to describe behavior at 75°F and in the cryogenic-temperature range on the basis that the correlations of mechanical-property data with room-temperature fatigue characteristics may be expected to be maintained qualitatively at cryogenic temperatures. A limitation may be that this assumption cannot provide for the effect of metallurgical brittle-ductile transition conditions at low temperatures.

Actual uniaxial-fatigue data and fatigue-life predictions based on Equation (C-1) led to the following ranking of candidate metal-shell materials in the 75 to -423°F range (in the order of their ability to sustain cyclic elastic strains of the magnitude imposed during the service life of GFR metal tanks):

Inconel X-750 nickel-base alloy (solution-treated and aged)

Type 301 stainless steel (SS) (3/4 hard)

Type 301 SS (1/2 hard)

2219-T62 aluminum alloy

Ti-5Al-2.5Sn (annealed, ELI grade)

Ti-6Al-4V (annealed, ELI grade)

In fatigue characteristics, Inconel X-750 significantly outranked all others over the entire temperature range. Equation (C-1) indicates all these materials in the unwelded condition appear to be able to sustain the strain-cycling conditions of GFR metal tanks.

The limited data at 75°F for 1-to-1 and 2-to-1, biaxial-stress-field, low-cycle fatigue indicate that 301 SS (full hard) outranks Ti-6Al-4V (annealed). Both materials, however, have excellent fatigue-resistance capabilities at 75°F for the design conditions of GFR metal tanks. Data on biaxial-fatigue characteristics at cryogenic temperatures could not be found, and the materials could not be ranked on the basis of biaxial-fatigue performance at such temperatures.

The investigation is reported in detail below.

II. STRESS-STRAIN CONDITIONS IN METAL SHELL

Significantly different stress-strain conditions are imposed on GFR metal tanks during application of the internal pressures associated with tank fabrication, proof testing, burst testing, and operation. These stress-strain states for the metal and glass-fiber components during fabrication, after mandrel removal, at the proof pressure, at zero pressure, at the operating pressure, and at the burst pressure are depicted in Figure C-1, to which the remainder of this discussion refers. As indicated there, the metal may be held in a stress-free (or strain-free) state by a rigid mandrel while being overwrapped with filaments [point (M), Figure C-1]. Upon mandrel removal, however, the metal shell will spring back into a compressive state because of the filament-overwrapping pressure [point (O)]. The magnitude of the compression at zero internal-pressure equilibrium depends on the relative thicknesses and moduli of the overwrapped filaments and metal shell, as well as the biaxial stress-strain characteristics of the metal shell and the filament-winding tension used during fabrication.

When the first pressure load, p_1 , is applied to the GFR metal tank, the structure is strained to point (A), which is fixed by the component-material properties and thicknesses and by the pressure load. For factors of safety associated with aerospace tankage, and glass-filament and metallic materials being considered in this study, point (A) will be beyond the metal-shell yield point and considerable plastic deformation will occur. In general, the metal-shell biaxial tensile strain produced by p_1 will exceed 1% (safety factor of 2.0 at 75°F) and may be greater than 2.5% (safety factor of 1.25 at -320 or -423°F).

When the initial pressure load is removed, the metal shell will spring back along the offset biaxial elastic stress-strain curve (A)-(E), and will be pushed into high compression by external pressure from the overwrapped glass-filament shell until load equilibrium is reached at some point (E)

[strain (G)]. The GFR metal tanks being studied in this program are designed so that point (E) does not exceed the critical buckling-stress level of the metal shell in the absence of a bond between the metal and glass-filament composite, or the compressive elastic limit of the metal shell. If the design is based on the second condition, the maximum compressive stress in the metal shell during operation may be fixed for each material and operating temperature.

The operating-pressure level, p_o , will always be less than or equal to p_i . Therefore, during the application of cyclic operating-pressure loads to the GFR metal tank (100 cycles assumed), the metal-shell strain range is between points (G) and (K), and the value of (K) may be as large as that of (B).

Specific stress and strain values fixing the range between (G) and (K) depend on tank-design details, but maximum values can be estimated on the basis of material properties by assuming that the minimum value of (G) occurs at the biaxial compressive-yield stress of the metal-shell material, and that the maximum value of (K) occurs when $p_o = p_i$ and is equal to strain (B). Associated with the minimum value of strain (G) is the stress σ_E , and with the maximum value of strain (K) the stress σ_J . As an approximation, and in the absence of the Bauschinger effect, it may be considered that $-\sigma_E = \sigma_J$ = material tensile-yield point, in accordance with the foregoing assumptions. The strain range between σ_E and σ_J is the maximum-permissible operating-strain range for GFR metal tanks.

Table C-1 summarizes the mechanical properties of candidate metal-shell materials at 75, -320, and -423°F, and presents calculations for the maximum 1-to-1 biaxial-stress-field elastic-strain ranges between points (G) and (K), and the equivalent maximum uniaxial-elastic-strain ranges. Figure C-2 shows the calculated strain ranges for 301 SS (1/2 and 3/4 hard), 2219-T62 aluminum, annealed Ti-6Al-4V and Ti-5Al-2.5Sn, and Inconel X-750 associated with the compressive-to-tensile yield points (the maximum total operational-pressure-cycling strain ranges) at 75, -320, and -423°F.

III. CYCLIC-FATIGUE CONDITIONS IN METAL SHELL

The number of operational-pressure-load applications over the strain ranges indicated in Figure C-2 is assumed to be 100. The biaxial and equivalent uniaxial cyclic-loading strain ranges of the metal shell during tank operation for 100 cycles may be summarized as follows:

Material	Temp °F	Maximum Operational Pressure- Cycling Elastic-Strain Range About Zero Mean Strain, in./in.	
		Biaxial (1-to-1 Stress Field)	Equivalent Uniaxial
301 SS (3/4 hard)	75	0.0072	0.0103
	-320	0.0082	0.0117
	-423	0.0091	0.0130
301 SS (1/2 hard)	75	0.0060	0.0086
	-320	0.0078	0.0111
	-423	0.0084	0.0120
2219-T62 aluminum	75	0.0057	0.0085
	-320	0.0066	0.0098
	-423	0.0067	0.0100
Ti-5Al-2.5Sn (annealed, ELI grade)	75	0.0088	0.0125
	-320	0.0144	0.0205
	-423	0.0168	0.0240
Ti-6Al-4V (annealed, ELI grade)	75	0.0114	0.0163
	-320	0.0183	0.0259
	-423	0.0200	0.0286
Inconel X-750 (solution-treated and aged)	75	0.0057	0.0080
	-320	0.0062	0.0087
	-423	0.0061	0.0086

IV. METAL-FATIGUE CHARACTERISTICS UNDER CYCLIC LOADING IN HIGH STRAIN RANGE

An extensive literature survey on low-cycle fatigue of metals was made to identify the suitability of each candidate material under the biaxial-cyclic-loading conditions existing in GFR metal tanks (Refs. 1-34), and pertinent data were abstracted. Nearly all the data were for unwelded materials tested at 75°F. Data were practically nonexistent for low-cycle, high-strain-range fatigue of weldments or parent metal and weldments at cryogenic temperatures.

A. RESPONSE TO UNIAXIAL LOADING

1. Loading Conditions

Many uniaxial-strain-cycling fatigue tests have been conducted on metals in which the mean strain is zero and equal magnitudes of tensile and compressive strain are imposed during each cycle. To produce fatigue failure of metal specimens under this completely reversed strain-loading condition within 10^5 to 10^4 cycles, it has usually been necessary to impose

very large strains that include significant plastic components. Figure C-3a shows the characteristic situation in which the specimen is forced to deform cyclically between points 1 and 2; the response is described by a hysteresis loop. The first loading involves both elastic and plastic deformation to reach the strain corresponding to position 2'. Upon unloading, elastic and plastic action is again produced; in some cases, the plastic behavior occurs well before the stress is fully reversed, because of the Bauschinger effect. At 1' the strain has returned to zero, but a compression stress is required to bring this about. Subsequent cycling soon results in a characteristic hysteresis loop in which further changes occur rather slowly.

Figure C-3b shows a typical hysteresis loop, the dimensions of which can be described by the width, $\Delta\epsilon$ (called the strain range), and height, $\Delta\sigma$ (defined as the stress range). The strain range may be divided into elastic and plastic components. Because there is always an elastic response for any change in stress, there are an elastic-strain range

$$\Delta\epsilon_e = \frac{\Delta\sigma}{E} \quad (C-2)$$

where E is the elastic modulus of the material, and a plastic-strain range

$$\Delta\epsilon_p = \Delta\epsilon - \Delta\epsilon_e \quad (C-3)$$

Because the hysteresis loop changes slowly with cycling, $\Delta\epsilon_e$ and $\Delta\epsilon_p$ likewise change, even though the total-strain range is kept constant during the test. These changes are small and are sometimes ignored; when $\Delta\epsilon$ is small (e.g., 1% or less), the stress range often stays nearly constant for thousands of cycles and $\Delta\epsilon_p$ remains constant. When $\Delta\epsilon$ is larger (e.g., 10%), $\Delta\sigma$ can increase or decrease significantly, but because $\Delta\epsilon_e$ is now very much smaller than $\Delta\epsilon_p$, $\Delta\epsilon_p \approx \Delta\epsilon$ and $\Delta\epsilon_p$ again remains nearly constant.

2. Property Changes During Strain Cycling

When metals are subjected to cycling between fixed strain limits near or above the proportional limits, the stress range generally changes during the test. If the range increases with the number of cycles, the material is said to be cyclic-strain hardening; if the range decreases, the material is considered cyclic-strain softening. The most significant changes in the stress range for many materials occur within the first 20% of specimen life, after which the range remains relatively constant. This value, $\Delta\sigma$, is then considered a characteristic value corresponding to the applied strain range.

The 75°F data presented in Ref. C-6 and reproduced in Figures C-4 and C-5 show that Inconel X and the 300-series stainless steels (annealed and hardened) are strain hardening, and Ti-6Al-4V (solution-treated and aged) is strain softening. No data were found for Ti-5Al-2.5Sn and the 2219-series aluminum alloy, or for cryogenic-temperature tests of any of the materials. The 75°F data in Figures C-4 and C-5 indicate that, under

uniaxial-loading conditions, strain hardening at the cyclic-strain amplitude and number of cycles of interest (Table C-1) would amount to strength increases of about 10% for 300-series SS in the hard condition, and of less than 20% for Inconel X. For Ti-6Al-4V, a strength decrease of about 10 to 20% could occur during strain cycling.

3. General Response to Strain Cycling

Several investigators have noted that a variety of metals can resist approximately the same uniaxial cyclic strain about zero mean strain when the fatigue life approximates 10^3 to 10^4 cycles of completely reversed strain cycling. This characteristic is shown in Figure C-6 (from Ref. C-6) for 15 different materials as a plot of diametral strain range* of circular test specimens used in the uniaxial strain cycling vs the number of cycles to failure.

Low strength, high-ductility metals derive their cyclic-strain resistance from their capacity to be plastically deformed (ductility). The cyclic-strain resistance of high-strength, low-ductility metals results from their ability to resist large elastic strains. The cyclic-strain resistance of intermediate-strength metals results from a combination of strength and ductility (toughness). The three types of resistance are illustrated schematically in Figure C-7 for a ductile, a strong, and a tough metal. The fatigue lives of the three metals would be nominally the same (about 10^3 cycles) for the cyclic strain shown ($\Delta\epsilon = 0.02$ in./in.).

Analyses of representative fatigue lives for 48 metals (including 21 steels, two cast nickel-base alloys, and hot-pressed beryllium) resulted in the following conclusions (Ref. C-3):

a. If the total-strain range is less than the ultimate tensile strength divided by the elastic modulus, fatigue is seldom a problem for reasonably ductile metals, unless the strain is applied millions of times.

*The diametral strain range measured was transverse to the direction of loading; the strain in the direction of loading is given by (Ref. C-6)

$$\Delta\epsilon_a^l = \left(\frac{1}{2} - 2\nu \right) \frac{\Delta P}{AE} + 2\Delta\epsilon_d$$

where $\Delta\epsilon_a^l$ is the applied longitudinal strain amplitude, in./in.; ν is Poisson's ratio; ΔP the applied load range, lb; A the cross-sectional area, in.²; E the elastic modulus, psi; and $\Delta\epsilon_d$ the applied diametral strain range, in./in. The strain range in the direction of loading is thus about 2 times the indicated value of diametral strain range from Figure C-6.

b. If the total-strain range is greater than 2% (amplitude of $\pm 1\%$), fatigue failure will probably occur in less than 1000 cycles.

c. Attempts to evaluate the relative fatigue performance of several metals on the basis of fatigue lives obtained by subjecting them to repeated strains in the neighborhood of $\pm 1\%$ may be pointless, because all will have nominally the same fatigue lives.

d. High cyclic strains should be avoided in low-ductility metals.

4. Analysis of Response to Strain Cycling

a. Plastic-Strain Range

In the low-cycle fatigue range ($1/4$ to 1000 cycles), where $\Delta\epsilon_p \approx \Delta\epsilon$, a logarithmic plot of the plastic-strain range vs the number of cycles to failure, N_f , yields very nearly a straight line for a large number of materials. In this fatigue range, the cyclic life is thus related to the cyclic-strain range by a power law in the following form:

$$\Delta\epsilon_p = MN_f^Z \approx \Delta\epsilon \quad (C-4)$$

where M and Z are material constants. Coffin has suggested that Z is a universal constant with a value of -0.5 (Refs. C-1, -11, -15, -16, and -24). Manson, on the other hand, has shown that Z is a material constant rather than a universal constant, with values generally ranging from -0.4 to -0.8 (Refs. C-5 and -9).

Coffin has proposed that the constant M is related to the true fracture ductility, ϵ_f , in a uniaxial tensile test. Assuming that $N_f = 1/4$ for a uniaxial tensile test and $Z = -0.5$, from Equation (C-4),

$$\Delta\epsilon_p = MN_f^Z = M (1/4)^{-0.5} = \epsilon_f \quad (C-5)$$

whence

$$\Delta\epsilon_p = \frac{\epsilon_f}{2} N_f^{-0.5} \quad (C-6)$$

Using this equation, it is possible to predict the cyclic-strain fatigue characteristics of a material in the low-cycle fatigue range knowing only the true fracture ductility. This is accomplished by plotting the fracture ductility at $N_f = 1/4$ on logarithmic coordinates and extending the relationship of $\Delta\epsilon_p$ vs N_f as a line of slope -0.5 , as shown in Figure C-8.

Manson's analysis of available data resulted in a recommendation that the relationship between the plastic-strain range and the number of cycles to failure be approximated by

$$\Delta \epsilon_p = \epsilon_f^{0.6} N_f^{-0.6} \quad (C-7)$$

Using this equation, $\epsilon_f^{0.6}$ is plotted at $N_f = 1$ (rather than ϵ_f at $N_f = 1/4$) to obtain the best correlation with test results. The relationship $\Delta \epsilon_p$ vs N_f is established by extending from this point a line of slope = -0.6. This method is compared with the method of Coffin in Figure C-8.

b. Elastic-Strain Range

It has been found for a large number of materials that a plot of the stress range ($\Delta \sigma$) vs N_f on logarithmic coordinates results in reasonably straight lines. The cyclic life may thus be assumed to be related to the elastic-strain range by a power law of the following form:

$$\Delta \epsilon_e = \frac{\Delta \sigma}{E} = \frac{G}{E} N_f^\gamma = 3.5 \frac{\sigma_u}{E} N_f^{-0.12} \quad (C-8)$$

where $\Delta \epsilon$ is the cyclic elastic-strain range corresponding to N_f , E the elastic modulus, σ_u the ultimate tensile strength, and G and γ other material properties found by Manson to equal $3.5 \sigma_u$ and -0.12, respectively (Refs. C-5 and -9). The relationship has been shown to characterize many materials to 10^6 cycles.

c. Total-Strain Range

Manson has further proposed (Refs. C-5 and -9) that low-cycle fatigue life in the range from 10 to 10^6 cycles can be described by

$$\Delta \epsilon = \Delta \epsilon_e + \Delta \epsilon_p = \frac{G}{E} N_f^\gamma + M N_f^Z \quad (C-9)$$

where

$\Delta \epsilon$ = total-strain range about zero mean strain corresponding to N_f

$\Delta \epsilon_e$ = cyclic elastic-strain portion of the strain range corresponding to N_f

$\Delta \epsilon_p$ = cyclic plastic-strain portion of the strain range corresponding to N_f

N_f = number of cycles to failure

E = elastic modulus of material

G, γ, M, Z = other material constants

Figure C-9a shows the characteristic behavior as a function of strain range and cycles to failure. There is a notable similarity

between the model of Figure C-9 and the cyclic-fatigue data for 15 materials shown in Figure C-6.

After considerable detailed study of the data, Manson has suggested the use of a method of universal slopes for predicting the fatigue life of metals under strain cycling. With this approach, it is assumed that the slopes of the elastic and plastic lines shown in Figure C-9a are the same for all materials. Analysis of the empirical data from 29 materials (Refs. C-5 and -9) showed that the following transformation of Equation (C-9) closely described the test data:

$$\Delta\epsilon = \Delta\epsilon_e + \Delta\epsilon_p = 3.5 \frac{\sigma_u}{E} N_f^{-0.12} + \epsilon_f^{0.6} N_f^{-0.6} \quad (C-10)$$

where

σ_u = ultimate tensile strength, psi

ϵ_f = fracture ductility, $\ln \frac{1}{1-RA}$

RA = reduction in area, %

N_f = number of cycles to failure

Letting $N_f = 1$, the intercept of the plastic line at $N_f = 1$ is $D^{0.6}$, and the intercept of the elastic line is $3.5 \sigma_u/E$, as shown in Figure C-9b.

5. Predicted Response to Required Strain-Cycling Conditions

Figure C-10 from Refs. C-5 and -6 reproduces representative data on the uniaxial elastic and plastic components of the total-strain range (cycling about zero mean strain) vs cycles to failure for solution-treated and aged Ti-6Al-4V, annealed Ti-5Al-2.5Sn, 304 SS in the annealed and hard conditions, Inconel X-750, and 2014-T6, 2024-T4, and 7075-T6 aluminum at 75°F.

It was stated in the preceding section that Equation (C-8) closely describes the 75°F uniaxial-elastic-strain-cycling range capability of a material as a function of cycles to failure. Even though considerable changes occur in the mechanical properties of metals in going to cryogenic temperatures, correlations of mechanical-property data with fatigue characteristics established at room temperature may be expected to be maintained qualitatively at the low temperatures. Using the assumption that Equation (C-8) is valid in the 75 to -423°F range, relationships were established between the uniaxial-elastic-strain-cycling range and cycles to failure at 75, -320, and -423°F for annealed ELI grade Ti-6Al-4V and Ti-5Al-2.5Sn, 1/2 and 3/4 hard 301 SS, solution-treated and aged Inconel X-750, and the 2219-T62 aluminum alloy. The design values for σ_u and E at each temperature used in Equation (C-8), with calculations, are given in Table C-2. The resulting relationships for $\Delta\epsilon_e$ vs N_f from Equation (C-8) for each candidate metal-shell material are shown in Figures C-11 to -16. Also shown are the maximum equivalent uniaxial-elastic-strain-cycling ranges previously given in Section III for each candidate

material at each temperature. Table C-2 summarizes the estimated performance of each candidate material under the imposed strain-cycling conditions.

6. Ranking of Materials

Factor-of-safety comparisons (Table C-2) provided the basis for the following ranking of materials for the strain-cycling requirements of GFR metal tanks:

<u>Service Temp, °F</u>	<u>Rating</u>	<u>Material</u>
75	1	Inconel X-750
	2	2219-T62 aluminum
	3	Type 301 SS (1/2 hard)
	4	Type 301 SS (3/4 hard)
	5	Ti-5Al-2.5Sn
	6	Ti-6Al-4V
-320	1	Type 301 SS (3/4 hard)
	2	Type 301 SS (1/2 hard)
	3	Inconel X-750
	4	2219-T62 aluminum
	5	Ti-5Al-2.5Sn
	6	Ti-6Al-4V
-423	1	Inconel X-750
	2	Type 301 (3/4 hard)
	3	2219-T62 aluminum
	4	Type 301 SS (1/2 hard)
	5	Ti-5Al-2.5Sn
	6	Ti-6Al-4V

B. RESPONSE TO BIAXIAL LOADING

Limited but valuable, low-cycle, high-strain, fatigue testing has been conducted at 75°F under biaxial-loading conditions (Ref. C-34). Uniaxial and biaxial fatigue data were obtained for full-hard 301 SS and annealed Ti-6Al-4V. For biaxial testing, both cross-shaped specimens and cylindrical pressure vessels were employed. The tests encompassed 1-to-1 and 2-to-1 states of stress, and "R" factors (minimum stress/maximum stress) of 0.10 and 0.50. Biaxial and uniaxial fatigue characteristics are presented in Figures C-17 to -22. The materials sustained appreciable amounts of biaxial plastic strain under fatigue conditions. Both the 301 SS and Ti-6Al-4V displayed excellent resistance to uniaxial and biaxial load applications.

The data for these materials were analyzed to compare the cyclic life for a given stress level in each of three states of stress (1-to-0, 1-to-1, and 2-to-1 biaxial-stress ratios) on the basis of life vs state of stress for a given stress-level condition and R factor. Figures C-23 and -24 show the results; the stress levels indicated in the curves represent the

percentages of ultimate strength for the given state of stress. In 301 SS the degree of severity between 1-to-0, 1-to-1, and 2-to-1 stress states tends to change at a different rate with a decrease in the operating stress level. This is observed in the fact that the uniaxial (1-to-0) life at 99% of the ultimate strength is the lowest life obtained for the three stress states. In successive lower percentages of ultimate strength, however, the 1-to-1 and 2-to-1 stress states exhibit a shorter life. When this type of comparison was made for Ti-6Al-4V, it was observed that the uniaxial state of stress resulted in the shortest life of the three states considered. In this material and for these stress states down to 85% and $R = 0.10$, it appears that the use of uniaxial-fatigue data would result in a conservative design.

V. CONCLUSIONS

The conclusions presented below are based on analysis of the stress-strain conditions imposed on the metal shell of a GFR metal tank, and compilation and evaluation of data on the uniaxial and biaxial, low-cycle, high-strain fatigue of unwelded metallic materials.

A. The maximum cyclic-loading conditions to be imposed on the metal shell of a GFR metal tank include 100 strain cycles between the tensile and compressive yield points of the shell under approximately 1-to-1 stress-field conditions. It is expected that GFR metal tanks will usually be designed to operate at a slightly reduced strain range.

B. Data from Ref. C-6 indicate that, in general, the maximum compressive and tensile stresses during any one cycle of zero-mean-strain fatigue testing remain approximately equal to each other throughout the test. Cyclic-strain hardening or softening affects the peak tensile or compressive stresses equally. This result provides a basis for ignoring the Bauschinger effect in analysis of the mechanical properties of candidate metal-shell materials.

C. Inconel X (solution-treated and aged) and the 300-series stainless steels (annealed and hardened) are cyclic-strain hardening; solution-treated and aged Ti-6Al-4V is cyclic-strain softening. Although data are not available, it is believed that annealed Ti-6Al-4V and Ti-5Al-2.5Sn are cyclic-strain-hardening materials.

D. Actual uniaxial-test data or predictions of high-strain-cycling fatigue life from accurate relationships yielded the following ranking of the six candidate metal-shell materials in order of their ability to sustain the high-strain-cycling conditions in a GFR metal tank at 75°F:

1. Inconel X-750 (solution-treated and aged)
2. 2219-T62 aluminum
3. Type 301 SS (1/2 hard)
4. Type 301 SS (3/4 hard)
5. Ti-5Al-2.5Sn (annealed, ELI grade)

6. Ti-6Al-4V (annealed, ELI grade)

E. Predicted uniaxial-strain-cycling performance at -320°F led to the following ranking of materials:

1. Type 301 SS (3/4 hard)
2. Type 301 SS (1/2 hard)
3. Inconel X-750 (solution-treated and aged)
4. 2219-T62 aluminum
5. Ti-5Al-2.5Sn (annealed, ELI grade)
6. Ti-6Al-4V (annealed, ELI grade)

F. Predicted uniaxial-strain-cycling performance at -423°F resulted in the following ranking of materials:

1. Inconel X-750 (solution-treated and aged)
2. Type 301 SS (3/4 hard)
3. 2219-T62 aluminum
4. Type 301 SS (1/2 hard)
5. Ti-5Al-2.5Sn (annealed, ELI grade)
6. Ti-6Al-4V (annealed, ELI grade).

G. In predicted uniaxial-fatigue characteristics, Inconel X-750 outranked all other candidate materials by a large percentage at 75 and -423°F , and the material was excellent in this regard at -320°F . Analysis indicated that all six candidate materials in the unwelded condition are capable of sustaining the strain-cycling requirements established for GFR metal tanks without fatigue failure.

H. Type 301 SS (full hard) outranked Ti-6Al-4V (annealed) on the basis of biaxial-test data at 75°F . Both materials, however, appear to display excellent fatigue resistance at 75°F for GFR metal tanks.

I. Because data on the biaxial-fatigue characteristics of materials at cryogenic temperatures could not be found, the materials could not be ranked at these temperatures on the basis of biaxial-fatigue performance.

VI. RECOMMENDATIONS

The efforts expended to acquire data on cryogenic-temperature fatigue characteristics of candidate materials and the limited information located

indicate that the data listed below are needed to ensure more reliable designs of GFR metal tanks for cryogenic service.

A. Uniaxial, high-strain, low-cycle, fatigue data for specimens subjected to completely reversed strain cycling about zero mean strain should be developed for parent-metal and welded specimens of candidate metals in the 75 to -423⁰F range.

B. Similarly, biaxial testing in 1-to-1 strain fields should be conducted on parent-metal and welded specimens to obtain high-strain, low-cycle, fatigue data in the 75 to -423⁰F range for candidate metals subjected to completely reversed strain cycling about zero mean strain.

REFERENCES

LOW-CYCLE, HIGH-STRAIN FATIGUE

- C-1. J. F. Tavernelli and L. F. Coffin, "Experimental Support for Generalized Equations Predicting Low Cycle Fatigue," ASME Paper 61-WA-199, November 1961 (in Journal of Basic Engineering, Series D, December 1962).
- C-2. C. H. Wells and C. P. Sullivan, "Low Cycle Fatigue Characteristics of a Nickel Base Super Alloy at Room Temperature," Transactions Quarterly, American Society for Metals, December 1964.
- C-3. Jo Dean Morrow, "Correlation Between Cyclic Strain Range and Low Cycle Fatigue Life of Metals," Materials Research and Standards, January 1965.
- C-4. J. T. P. Jao and W. H. Munse, "Low Cycle Fatigue of Metals - A Literature Review," Welding Journal, p. 41, 1962.
- C-5. S. S. Manson and M. H. Hirschberg, "Fatigue Behavior in Strain Cycling in the Low and Intermediate-Cycle Range," in Fatigue-An Interdisciplinary Approach; Proceedings of the Sagamore Army Materials Research Conference, Raquette Lake, N.Y., August 1963, Syracuse University Press, 1964.
- C-6. R. W. Smith, M. H. Hirschberg, and S. S. Manson, Fatigue Behavior of Materials Under Strain Cycling in Low and Intermediate Life Range, NASA TND-1574, April 1963.
- C-7. S. S. Manson, A. J. Nachtigall, C. R. Ensign, and J. C. Freche, "Further Investigation of a Relation for Cumulative Damage in Bending," Paper presented at Society of Automotive Engineers and American Society of Mechanical Engineers, National Air Transport and Space Meeting, New York, April 1964.
- C-8. J. G. Sessler and V. Weiss, "Low Cycle Fatigue Damage in Pressure Vessel Materials," Journal of Basic Engineering, Vol. 85, Series D, December 1963.
- C-9. S. S. Manson, "Fatigue: A Complex Subject - Some Simple Approximations," (presented to Society for Experimental Stress Analysis, Cleveland, 30 October 1964), NASA-TM-X-52084, 1965.
- C-10. V. Weiss, "Analysis of Crack Propagation in Strain Cycling Fatigue," in Fatigue - An Interdisciplinary Approach, ed by J. J. Burke, N. L. Reed, and V. Weiss, Syracuse University Press, 1964.
- C-11. L. F. Coffin, "Low Cycle Fatigue," Metals Engineering Quarterly, American Society for Metals, November 1963.

- C-12. M. Gross, "Low Cycle Fatigue of Materials for Submarine Construction," Naval Engineers Journal, Vol. 75, No. 4, October 1963.
- C-13. R. E. Peterson, "Fatigue of Metals-Engineering and Design Aspects," Materials and Research Standards, February 1963.
- C-14. B. F. Langer, "Design of Pressure Vessels for Low-Cycle Fatigue," Journal of Basic Engineering, September 1962.
- C-15. L. F. Coffin and J. F. Tavernelli, "The Cyclic Straining and Fatigue of Metals," Transactions of the Metallurgical Society of the AIME, October 1959.
- C-16. J. F. Tavernelli and L. F. Coffin, "A Compilation and Interpretation of Cyclic Strain Fatigue Tests on Metals," Transactions of the American Society for Metals, Vol. LI, 1959.
- C-17. P. D. Schweikert and G. J. Moyer, An Application of Linear Hardening Plasticity Theory to Cycle and Path Dependent Strain Accumulation, University of Illinois T. & A.M. Report No. 212 (ASD-TDR-62-730), January 1962.
- C-18. D. E. Güçer, "Cumulative Fatigue at High Plastic Strains," Transactions Quarterly, American Society for Metals, June 1961.
- C-19. C. T. Mackenzie and P. Benham, "Cyclic Strain Softening of a Heat Treated Steel," The Engineer, 214 (1962), 1104, 28 December 1960.
- C-20. L. F. Coffin, "The Stability of Metals Under Cyclic Plastic Strain," Journal of Basic Engineering, Vol. 82, Series D, September 1960.
- C-21. E. E. Baldwin, G. J. Sokol, and C. F. Coffin, "Cyclic Strain Fatigue Studies on AISI Type 347 Stainless Steel," Proceedings of the ASTM, Vol. 57, 1957.
- C-22. S. S. Gill and J. Parker, "Plastic Stress-Strain Relationships - Some Experiments on the Effect of Loading Path and Loading History," Journal of Applied Mechanics, Vol. 26, 1959.
- C-23. D. Dugdale, "Stress-Strain Cycles of Large Amplitude," Journal of the Mechanics and Physics of Solids, 1959.
- C-24. L. F. Coffin, "Low Cycle Fatigue - A Review," Applied Materials Research, Vol. 1, No. 3, October 1962.
- C-25. C. E. Feltner and J. D. Morrow, "Microplastic Strain Hysteresis Energy as a Criterion for Fatigue Fracture," Journal of Basic Engineering, March 1961.
- C-26. L. F. Kooistra, "Effect of Plastic Fatigue on Pressure Vessel Materials and Design," Welding Research Supplement, March 1957.

- C-27. R. W. Swindeman and D. A. Douglas, "The Failure of Structural Metals Subjected to Strain Cycling Conditions," Journal of Basic Engineering, June 1959.
- C-28. J. H. Gross, D. E. Gücer, and R. D. Strout, "The Plastic Fatigue Strength of Pressure Vessel Steels," Welding Research Supplement, August 1964.
- C-29. S. S. Manson, "Interpretive Report on Cumulative Fatigue Damage in the Low Cycle Range," Welding Research Supplement, August 1964.
- C-30. P. P. Benham and H. Ford, "Low Endurance Fatigue of a Mild Steel and an Aluminum Alloy," Journal of Mechanical Engineering Science, Vol. 3, No. 2, 1961.
- C-31. M. R. Gross, "Low Cycle Fatigue of Materials," Marine Engineering Laboratory (Annapolis, Maryland) Technical Memorandum MEL-TM-37/64, 31 May 1964.
- C-32. G. W. Brown and C. E. Work, "An Evaluation of the Influence of Cyclic Prestressing on Fatigue Limit," Proceedings of the ASTM, Vol. 163, 1963.
- C-33. A. M. Willner and F. A. McClintock, "Cracking in Low Cycle Torsional Fatigue with Increasing Strain Amplitudes," ASME Paper No. 61-WA-273, 1961.
- C-34. S. W. McClaren, Low Cycle Fatigue Design Data on Materials in a Multi-axial Stress Field, RTD-TDR-63-4094 (prepared by Ling-Temco-Vought, Dallas, under Contract AF 33(657)-8525), November 1963.

BAUSCHINGER EFFECT

- C-35. R. V. Milligan, W. H. Koo, and J. E. Davidson, The Bauschinger Effect in a High Strength Steel, Report No. WVT-6508, DA Project No. 1-L-O-13001-A91A, Watervliet Arsenal, Watervliet, New York, March 1965.
- C-36. J. Dubuc, "Plastic Fatigue Under Cyclic Stress and Cyclic Strain with a Study of the Bauschinger Effect," Ph.D. thesis submitted to Ecole Polytechnique, Universite de Montreal, Montreal, Canada, January 1961.
- C-37. J. V. Gluck and J. W. Freeman, Further Investigations of the Effect of Prior Creep on Mechanical Properties of C110M Titanium with Emphasis on the Bauschinger Effect, University of Michigan Research Institute report, March 1960.
- C-38. C. J. Newton, "The Bauschinger Effect and Residual Microstress in Alpha Brass," Journal of Research of the National Bureau of Standards, October-December 1961.
- C-39. D. C. Drucker, Stress-Strain Relations in the Plastic Range - A Survey of Theory and Experiment, Office of Naval Research Technical Report prepared under Contract N7-ONR-358 by Graduate Division of Applied Mathematics, Brown University, December 1960.

TABLE C-1

ESTIMATED MAXIMUM OPERATIONAL PRESSURE CYCLING STRAIN RANGE

Material	Temp °F	Yield Stress σ_y psi	$2\sigma_y$ psi	Elastic Modulus E, psi	Poisson's Ratio, ν	$1-\nu$	Magnitude of Elastic- Strain Range, in./in.	
							Biaxial	Equivalent
							$\frac{2\sigma_y}{E/(1-\nu)}$	Uniaxial $\Delta\epsilon_e = 2\sigma_y/E$
Type 301 SS (3/4 Hard)	75	145,000	290,000	28.0×10^6	0.30	0.70	0.0072	0.0103
	-320	175,000	350,000	30.0			0.0082	0.0117
	-423	195,000	390,000	30.0			0.0091	0.0130
Type 301 SS (1/2 Hard)	75	120,000	240,000	28.0	0.30	0.70	0.0060	0.0086
	-320	167,000	334,000	30.0			0.0078	0.0111
	-423	180,000	360,000	30.0			0.0084	0.0120
2219-T62 Aluminum	75	44,000	88,000	10.4	0.33	0.67	0.0057	0.0085
	-320	55,000	110,000	11.2			0.0066	0.0098
	-423	58,000	116,000	11.6			0.0067	0.0100
Ti-5Al-2.5Sn (Annealed, ELI Grade)	75	100,000	200,000	16.0	0.30	0.70	0.0088	0.0125
	-320	175,000	350,000	17.0			0.0144	0.0206
	-423	210,000	420,000	17.5			0.0168	0.0240
Ti-6Al-4V (Annealed, ELI Grade)	75	130,000	260,000	16.0	0.30	0.70	0.0114	0.0163
	-320	220,000	440,000	17.0			0.0183	0.0259
	-423	250,000	500,000	17.5			0.0200	0.0286
Inconel X-750 (Solution- Treated and Aged)	75	120,000	240,000	30.0	0.29	0.71	0.0057	0.0080
	-320	135,000	270,000	31.0			0.0062	0.0087
	-423	138,000	276,000	32.0×10^6			0.0061	0.0086

Table C-1

TABLE C-2

PREDICTED ELASTIC-STRAIN RANGES, CYCLES TO FAILURE,
AND FACTORS OF SAFETY ON STRAIN CYCLING FOR CANDIDATE METALS

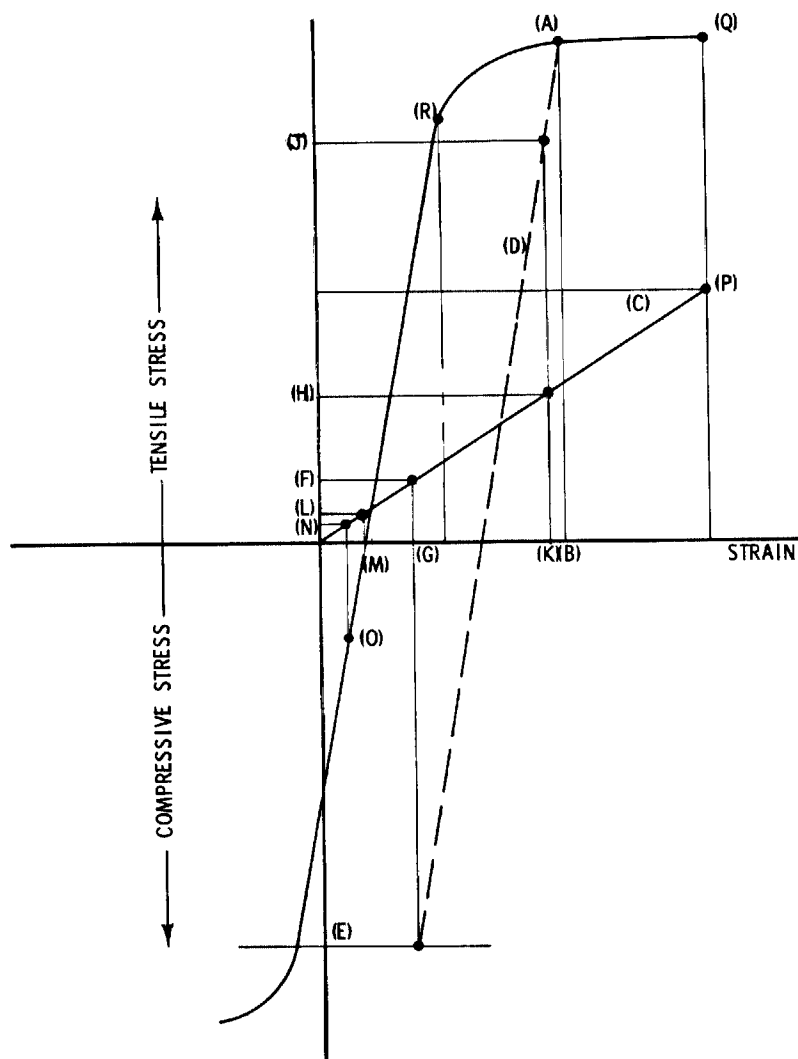
Temp °F	Ultimate Tensile Strength σ_u , psi	Elastic Modulus E, psi	σ_u/E	$3.5 \sigma_u/E$	Magnitude of Equiv Uniaxial Elastic-Strain Range, $\Delta\epsilon$ in./in.* ^e	No. of Cycles to Failure for $\Delta\epsilon_e^{**}$	Maximum $\Delta\epsilon_e$ for Failure in 100 Cycles in./in.	Factor of Safety Based on	
								100-Cycle Requirement	Maximum $\Delta\epsilon_e$
Ti-6Al-4V (Annealed, ELI Grade)									
75	140,000	16.0 x 10 ⁶	0.0088	0.0306	0.0163	200	0.0175	2.00	1.07
-320	220,000	17.0	0.0130	0.0454	0.0259	110	0.0260	1.10	1.01
-423	260,000	17.5	0.0149	0.0520	0.0286	120	0.0300	1.20	1.05
Ti-5Al-2.5Sn (Annealed, ELI Grade)									
75	120,000	16.0	0.0075	0.0262	0.0125	400	0.0150	4.00	1.20
-320	190,000	17.0	0.0112	0.0392	0.0206	180	0.0220	1.80	1.07
-423	220,000	17.5	0.0126	0.0440	0.0240	130	0.0250	1.30	1.04
Type 301 SS (3/4 Hard)									
75	180,000	28.0	0.0064	0.0225	0.0103	550	0.0130	5.50	1.26
-320	300,000	30.0	0.0100	0.0350	0.0117	10,000	0.0201	100.0	1.72
-423	315,000	30.0	0.0105	0.0368	0.0130	6,000	0.0201	60.0	1.55
Type 301 SS (1/2 Hard)									
75	160,000	28.0	0.0057	0.0200	0.0086	900	0.0110	9.00	1.28
-320	290,000	30.0	0.0097	0.0340	0.0111	9,000	0.0190	90.0	1.71
-423	270,000	30.0	0.0090	0.0315	0.0120	3,000	0.0180	30.0	1.50
Inconel X-750 (Solution-Treated and Aged)									
75	180,000	30.0	0.0060	0.0210	0.0080	3,500	0.0120	35.0	1.50
-320	220,000	31.0	0.0071	0.0248	0.0087	7,000	0.0145	70.0	1.67
-423	230,000	32.0	0.0072	0.0251	0.0086	10,000	0.0150	100.0	1.74
2219-T62 Aluminum									
75	61,000	10.4	0.0059	0.0206	0.0085	1,500	0.0120	15.0	1.42
-320	75,000	11.2	0.0067	0.0234	0.0098	1,500	0.0140	15.0	1.43
-423	90,000	11.6 x 10 ⁶	0.0078	0.0271	0.0100	3,500	0.0155	35.0	1.55

* From Table C-1.

** From Figures C-11 through C-16.

Table C-2

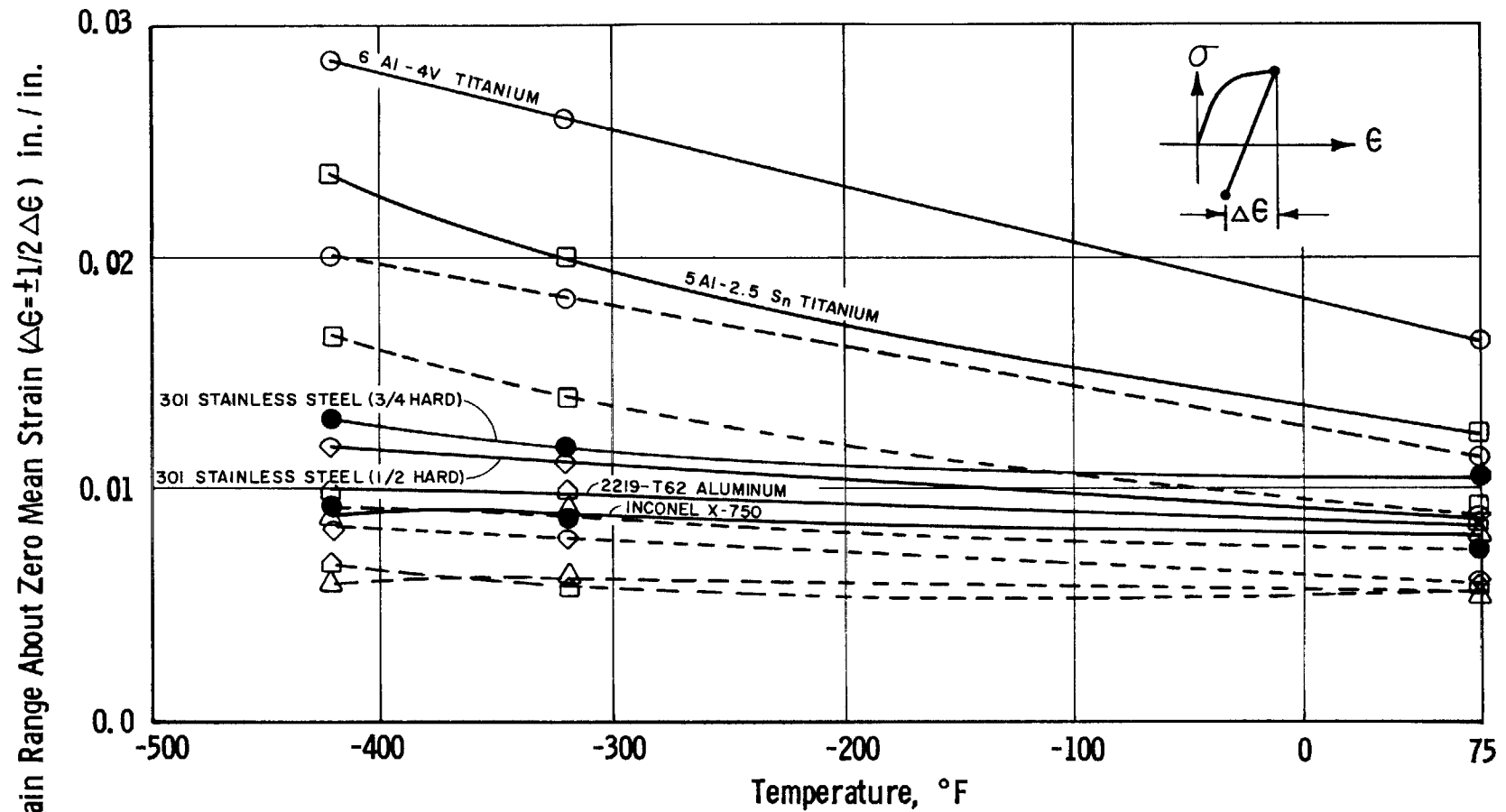
Figure C-1



STRESS-STRAIN DIAGRAM FOR GLASS FILAMENT REINFORCED METALLIC SHELL

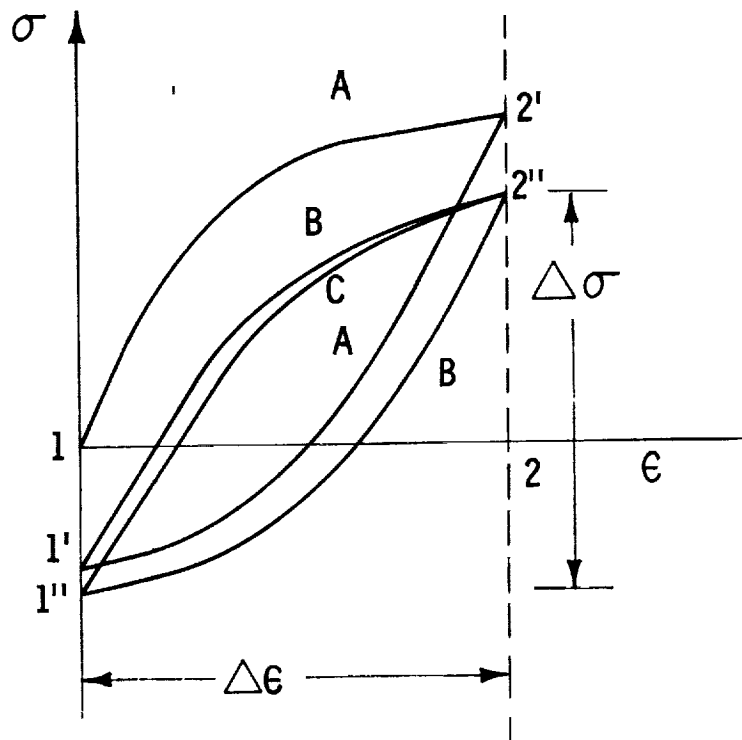
- (A) STRESS-STRAIN CURVE FOR METAL SHELL - FIRST CYCLE
- (B) MAXIMUM STRAIN REQUIRED OF COMPLETE SHELL - FIRST CYCLE
- (C) STRESS-STRAIN CURVE FOR GLASS-FIBER SHELL - ALL CYCLES
- (D) STRESS-STRAIN CURVE FOR METAL SHELL-UNLOADING FROM FIRST CYCLE
- (E) COMPRESSIVE STRESS ACHIEVED IN METAL SHELL WHEN VESSEL PRESSURE IS ZERO AFTER STRAIN TO (A)
- (F) TENSION STRESS IN GLASS FIBER SHELL THAT BALANCES COMPRESSION STRESS (E) IN METAL SHELL
- (G) RESIDUAL STRAIN IN GLASS FIBER AND METAL SHELLS WHEN VESSEL PRESSURE IS ZERO AFTER STRAIN TO (A)
- (H) OPERATING STRESS IN GLASS FIBER SHELL - ALL CYCLES SUBSEQUENT TO THE FIRST
- (I) OPERATING STRESS IN METAL SHELL - ALL CYCLES SUBSEQUENT TO FIRST
- (K) OPERATING STRAIN IN GLASS-FIBER AND METAL SHELLS - ALL CYCLES SUBSEQUENT TO FIRST
- (L) STRESS IN GLASS FIBER SHELL FROM WINDING ON RIGID MANDREL
- (M) STRAIN IN GLASS FIBER SHELL FROM WINDING ON A RIGID MANDREL; ZERO STRAIN POINT OF METAL SHELL BEFORE WINDING
- (N) STRESS IN GLASS FIBER SHELL AFTER MANDREL REMOVAL WHEN VESSEL PRESSURE IS ZERO
- (O) STRAIN IN METAL AND GLASS FIBER SHELLS AFTER MANDREL REMOVAL WHEN VESSEL PRESSURE IS ZERO
- (P) ULTIMATE STRESS OR STRAIN OF GLASS FIBER SHELL
- (Q) ULTIMATE STRESS OR STRAIN OF METAL SHELL WHEN FILAMENTS FRACTURE
- (R) ARBITRARY STRAIN POINT IN METAL SHELL AND GLASS FIBER SHELL BELOW METAL SHELL PROPORTIONAL LIMIT

- 301 Stainless Steel (3/4 hard) ○ 6Al-4V Titanium Alloy (annealed) - - - Biaxial 1:1
- △ 2219-T62 Aluminum Alloy △ Inconel X-750 ——— Equivalent Uniaxial
- 5Al-2.55 Sn Titanium ◇ 301 Stainless Steel (1/2 hard)



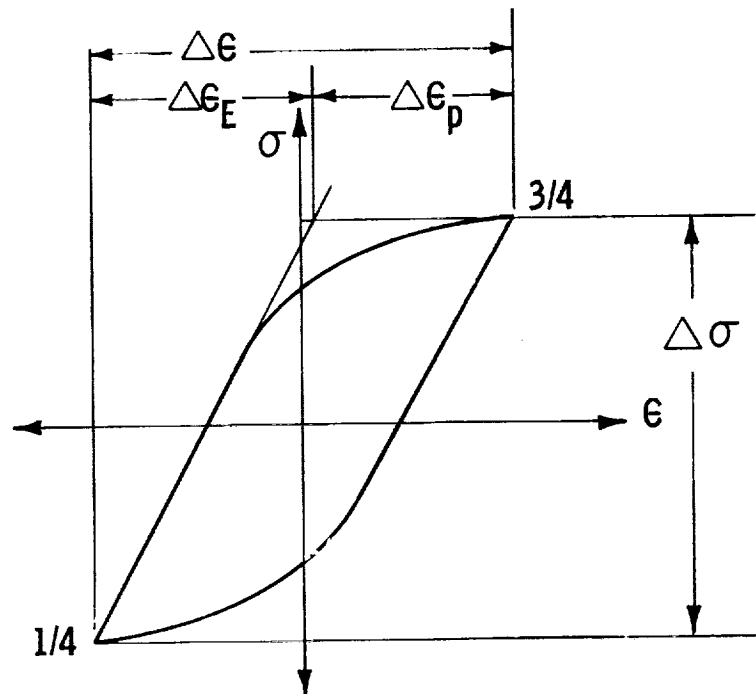
MAXIMUM OPERATIONAL PRESSURE CYCLING STRAIN RANGE FOR
METAL SHELL OF GFR METALLIC TANK

Figure C-2

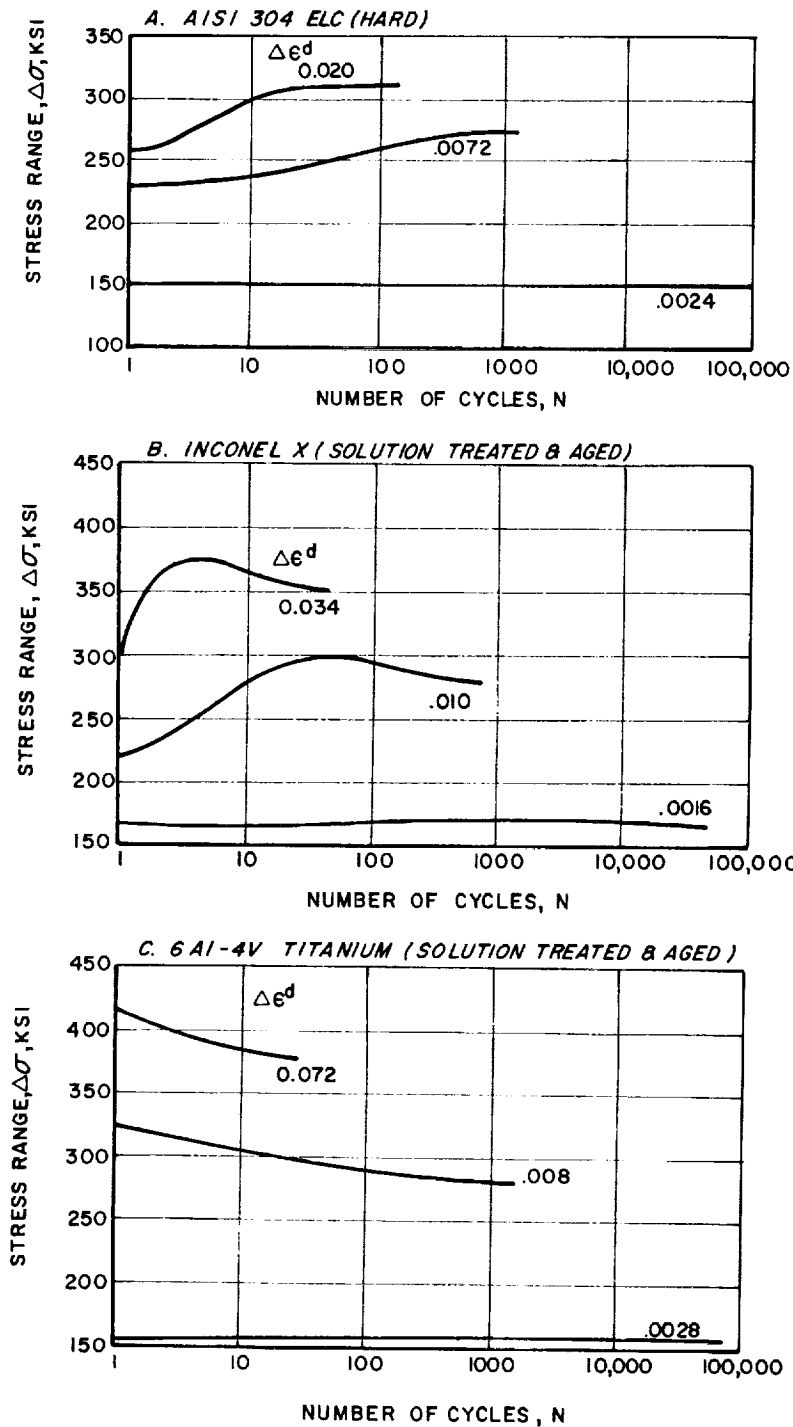


a. STRESS-STRAIN RELATIONS FOR UNIAXIAL CYCLIC LOADING

Key:
 σ = Stress
 ϵ = Strain
 ϵ_E = Elastic Strain
 ϵ_p = Plastic Strain
 $\Delta\epsilon_p = \Delta\epsilon - \frac{\Delta\sigma}{E}$
 Δ = Range
 E = Modulus of Elasticity

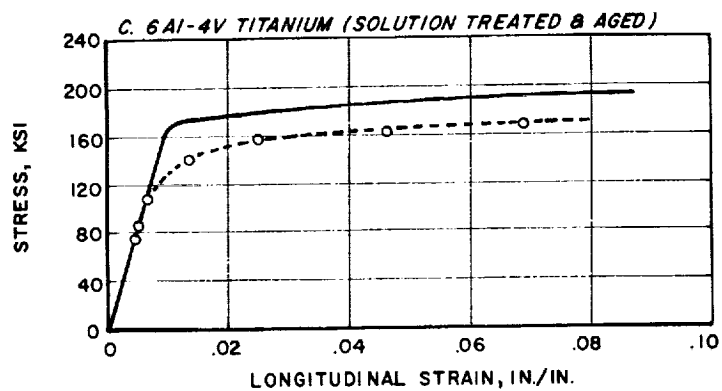
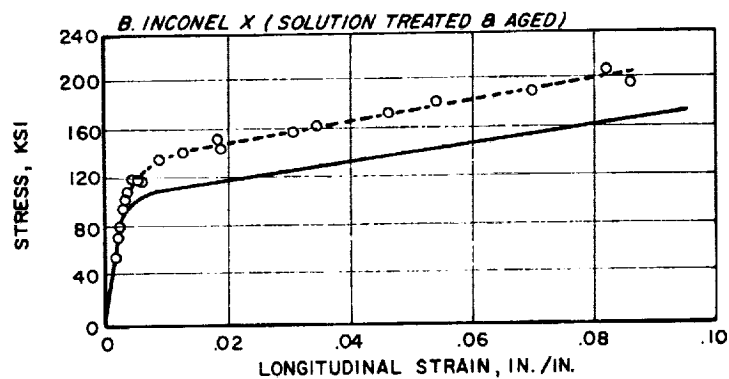
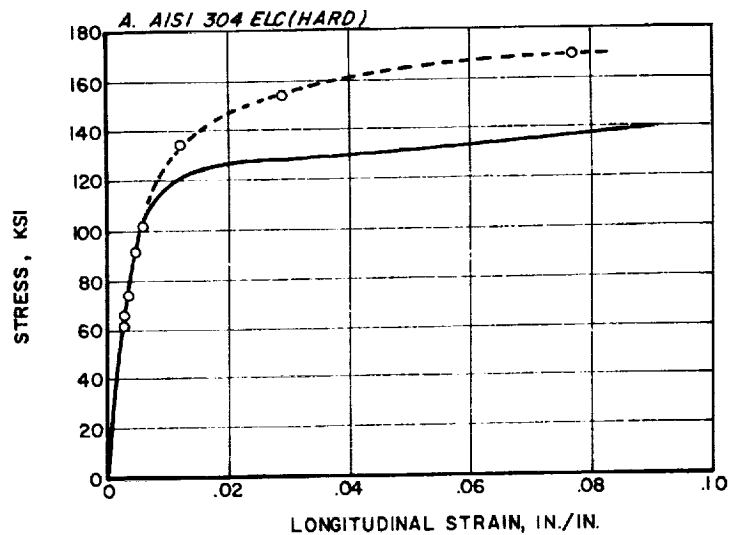


b. HYSTERESIS LOOP OF A STRAIN-CYCLE FATIGUE SPECIMEN



VARIATION OF STRESS RANGE WITH CYCLES FOR
 STRAIN CYCLING ABOUT ZERO MEAN STRAIN
 ($\Delta \epsilon^d$, IN IN./IN. IS MAGNITUDE OF DIAMETRICAL
 STRAIN RANGE USED IN CYCLIC TESTS) (Ref. C-6)

Figure C-4

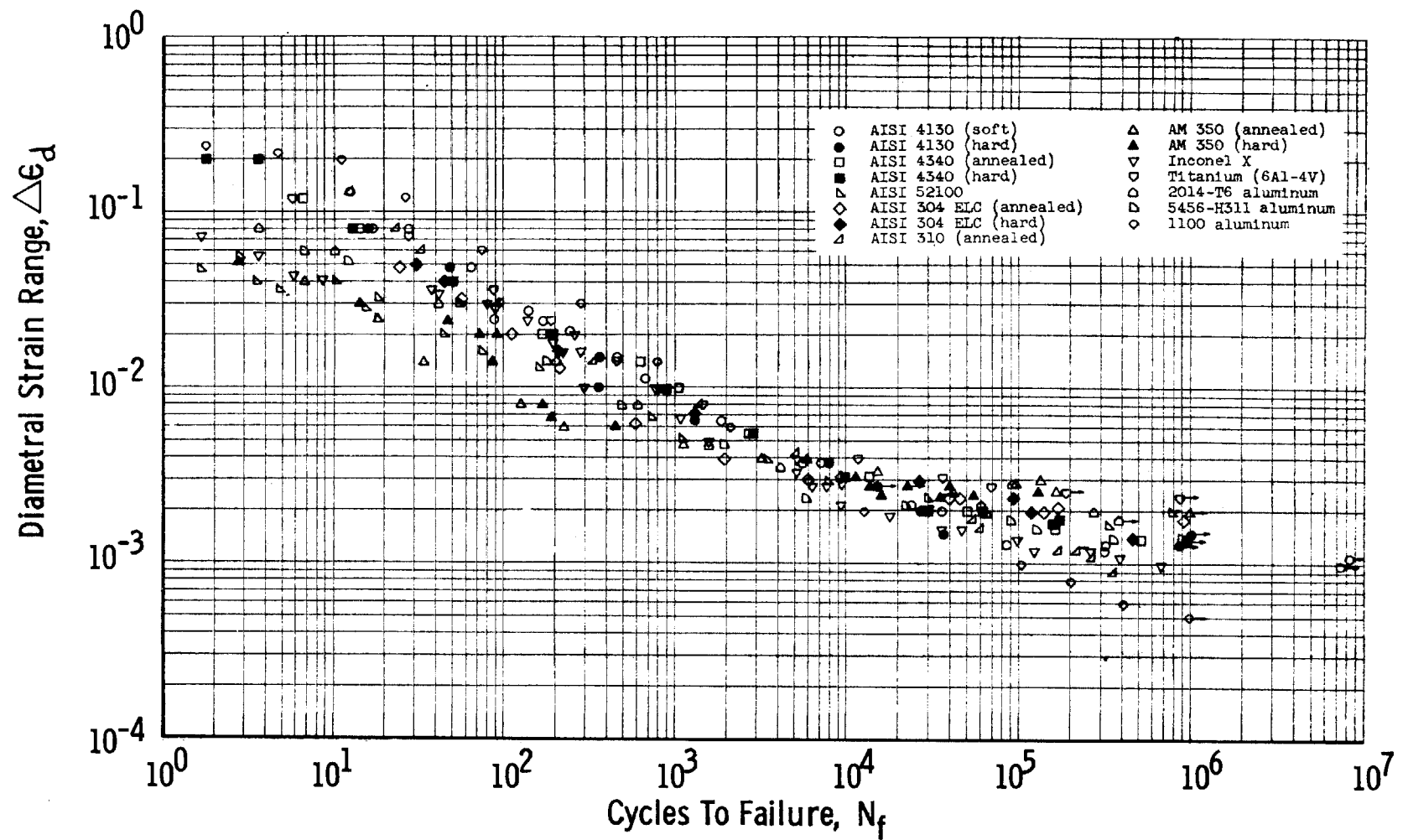


— Virgin Tensile Tests
 - - - - - Strain Cycling Tests About Zero Mean Strain At Longitudinal Strain Value Indicated.

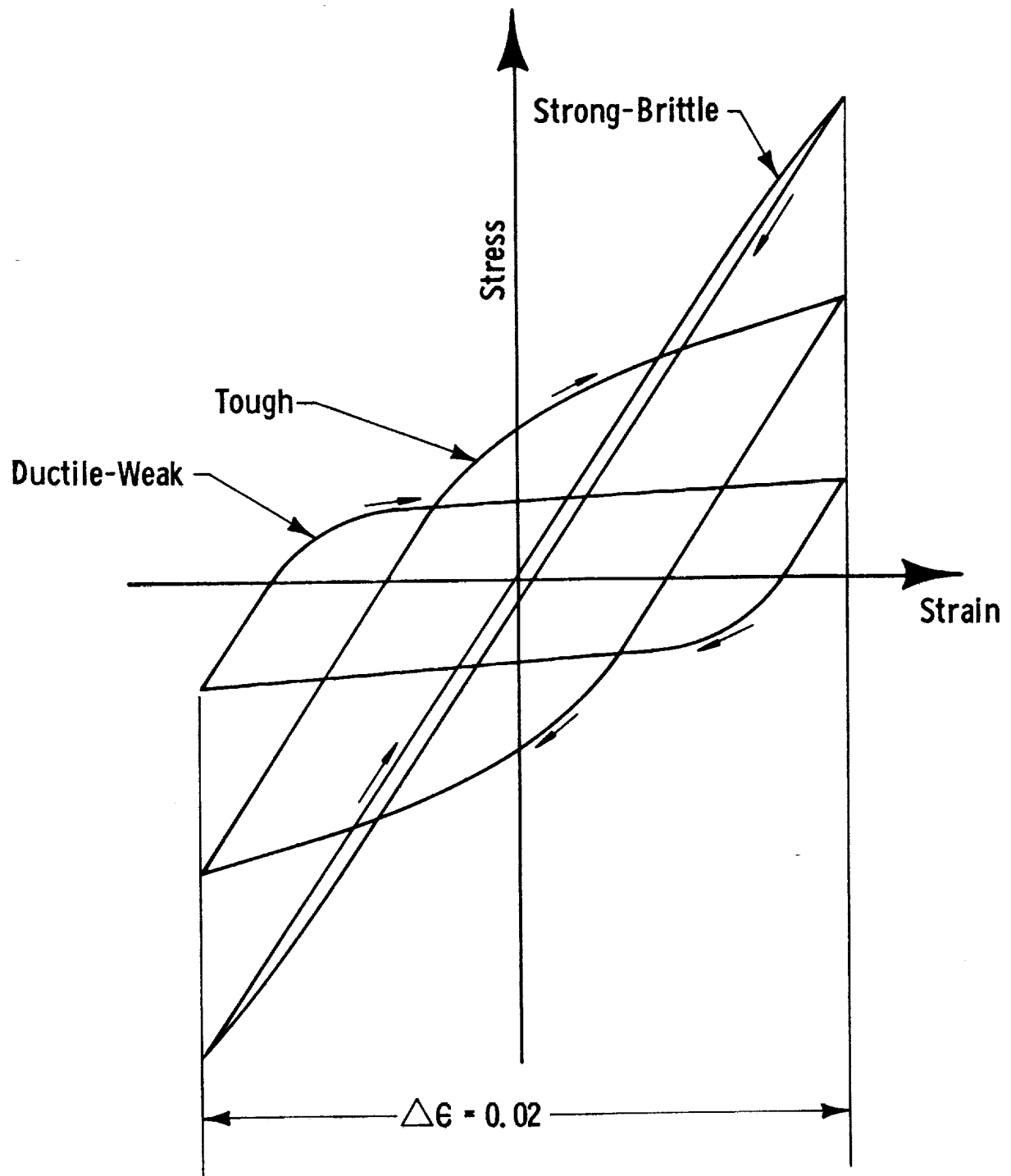
COMPARISON OF CYCLIC & VIRGIN TENSILE STRESS - STRAIN CURVES
 (Ref. C-6)

Figure C-5

Figure C-6



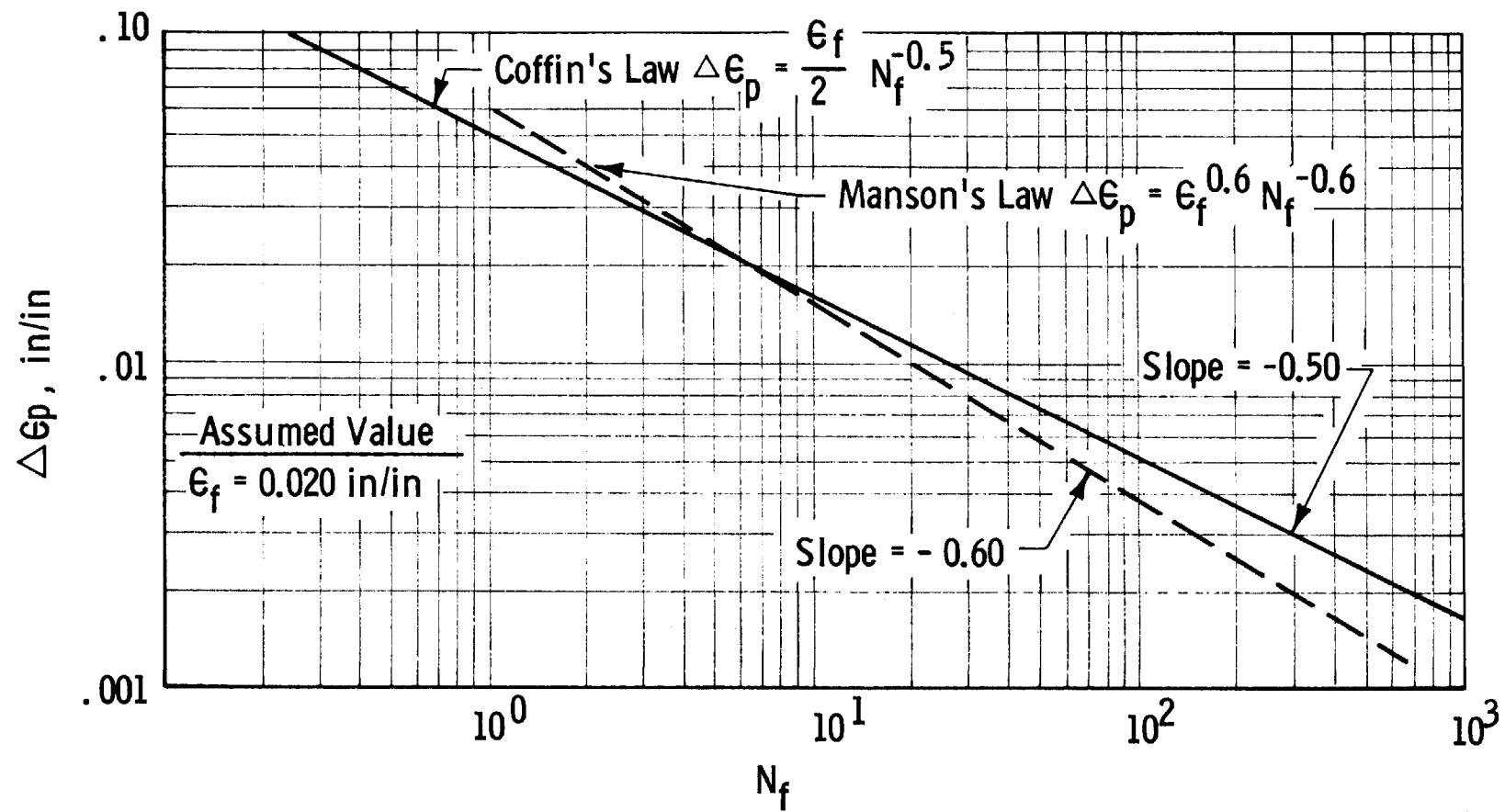
EFFECT OF DIAMETRAL STRAIN RANGE ON FATIGUE LIFE (Ref. C-6)



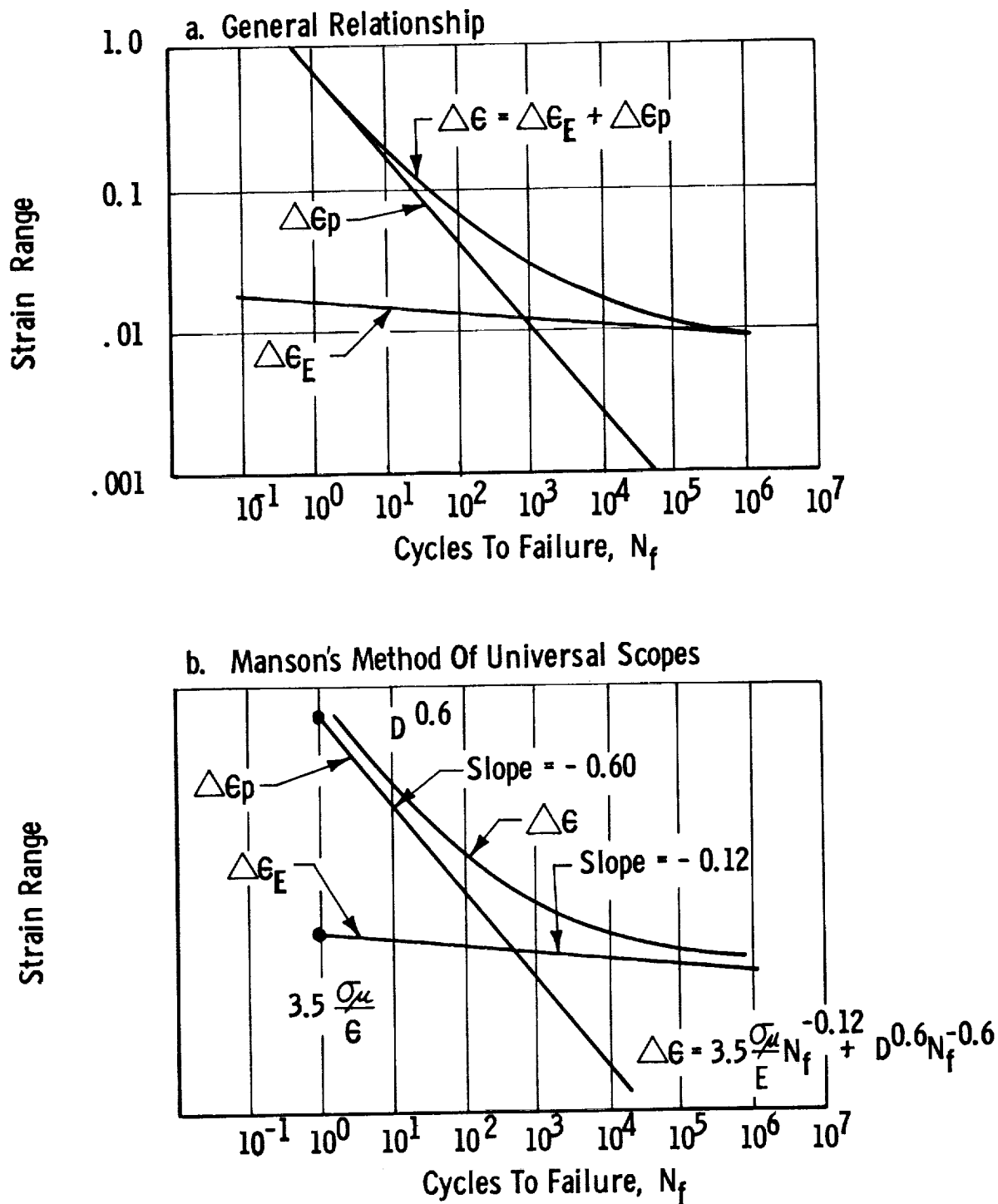
SCHEMATIC REPRESENTATION OF THE WAY THAT DUCTILE, STRONG,
AND TOUGH METALS RESIST CYCLIC STRAIN (Ref. C-3)

Figure C-7

Figure C-8

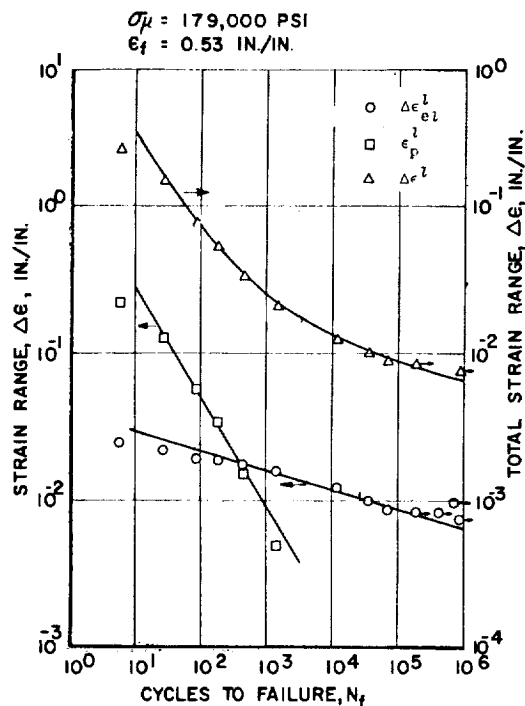


COMPARISON OF THE METHODS OF MANSON AND COFFIN



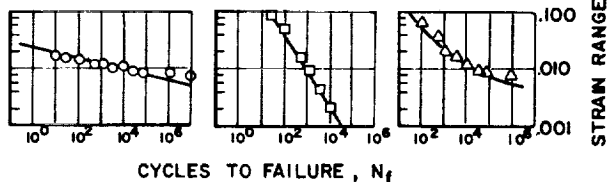
RELATIONSHIP OF PLASTIC STRAIN RANGE ($\Delta\epsilon_p$), ELASTIC STRAIN RANGE ($\Delta\epsilon_E$), AND TOTAL STRAIN RANGE ($\Delta\epsilon$) TO CYCLES TO FAILURE

Figure C-9



○ - $\Delta \epsilon_E$, Elastic Strain Range
□ - $\Delta \epsilon_P$, Plastic Strain Range
△ - $\Delta \epsilon$, Total Strain Range

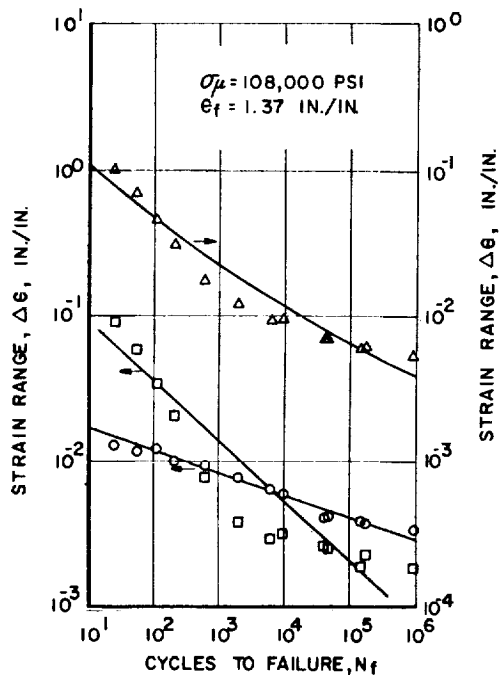
$\sigma_{\mu} = 130,400$ PSI
 $\epsilon_f = 0.566$ IN./IN.



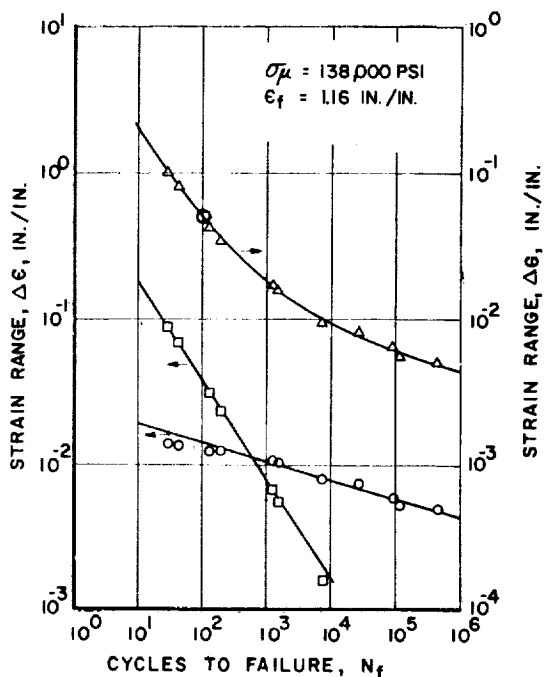
Note: Strain cycling about zero mean strain.

b. 5 Al - 2.5 Sn Titanium

a. 6 Al-4V Titanium (Solution treated & aged)

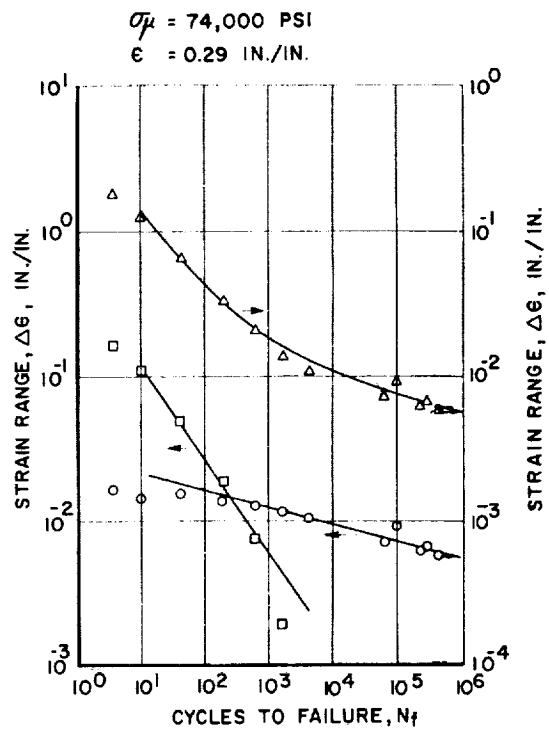
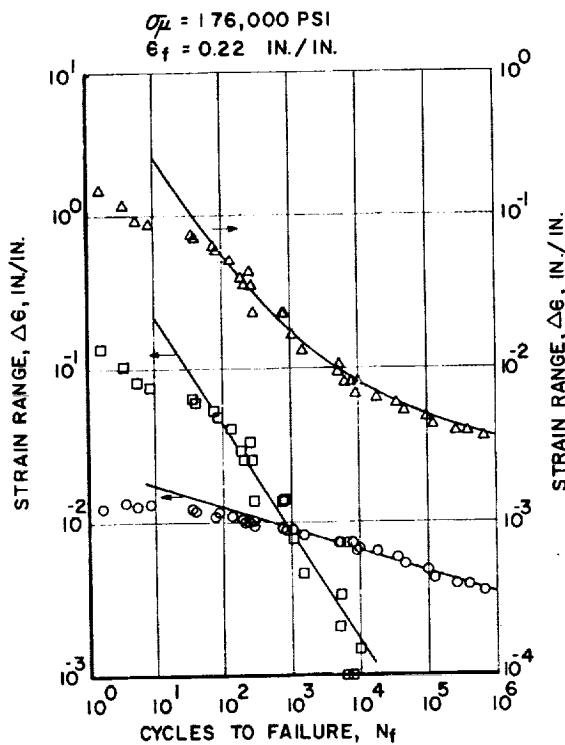


c. AISI 304 ELC (Annealed)



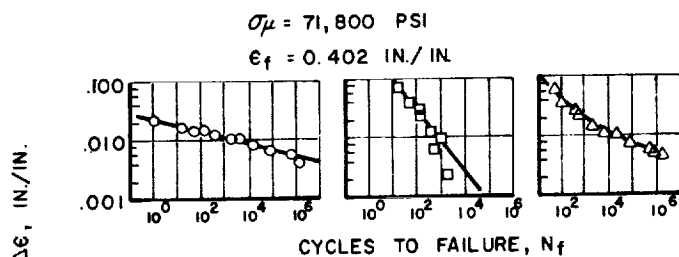
d. AISI 304 ELC (Hard)

ELASTIC, PLASTIC & TOTAL STRAIN RANGE VARIATIONS WITH
CYCLIC LIFE AT 75°F (Refs. 5 and 6)

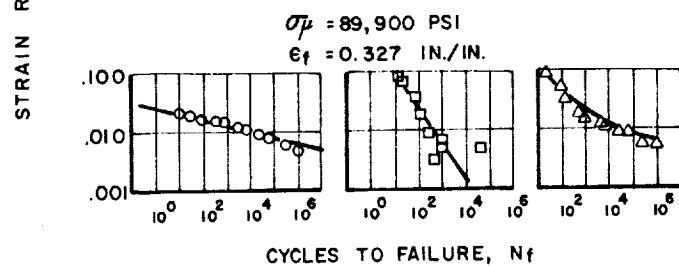


e. Inconel X

f. 2014-T6 Aluminum



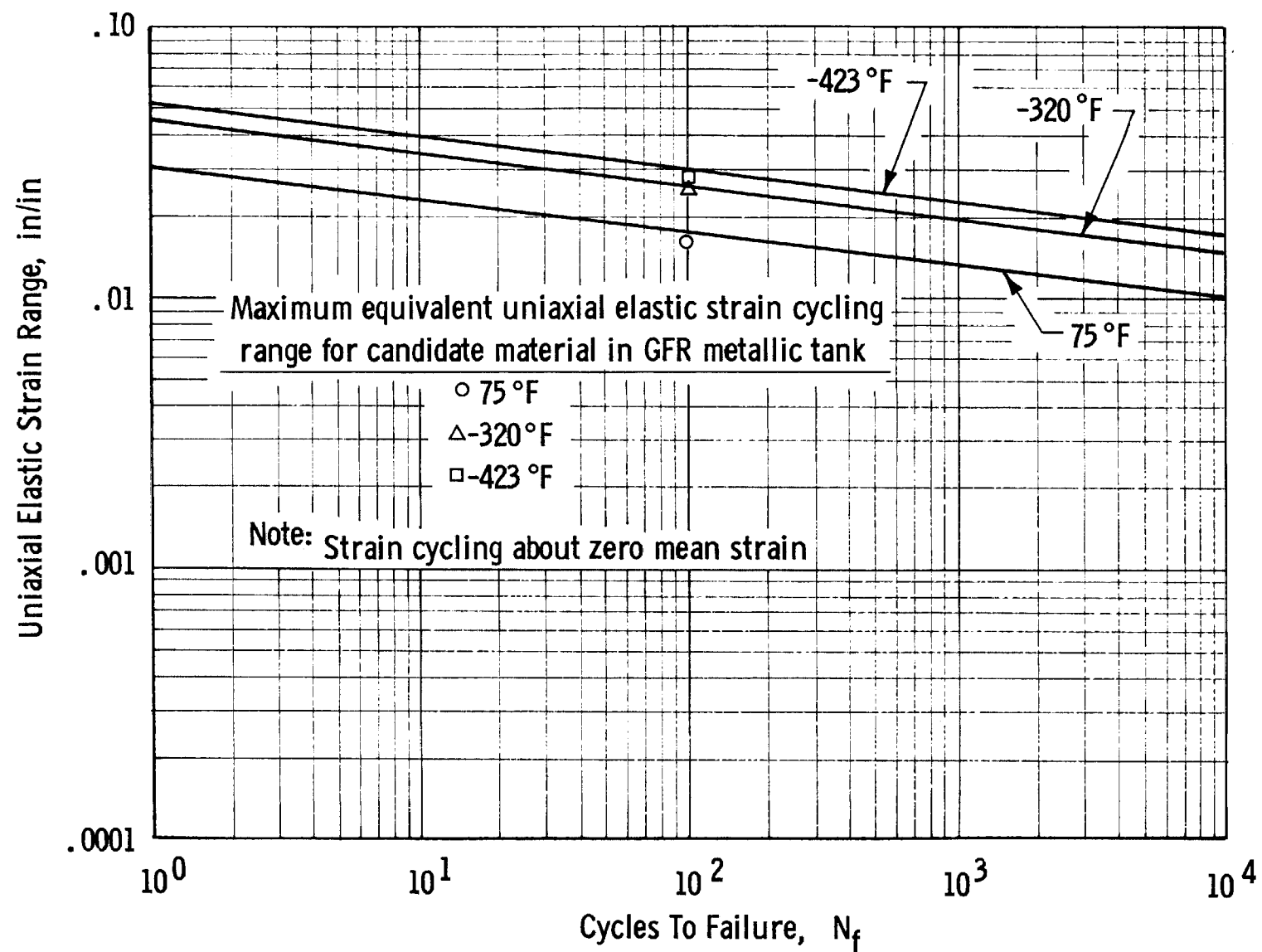
g. 2024-T4 Aluminum



h. 7075-T6 Aluminum

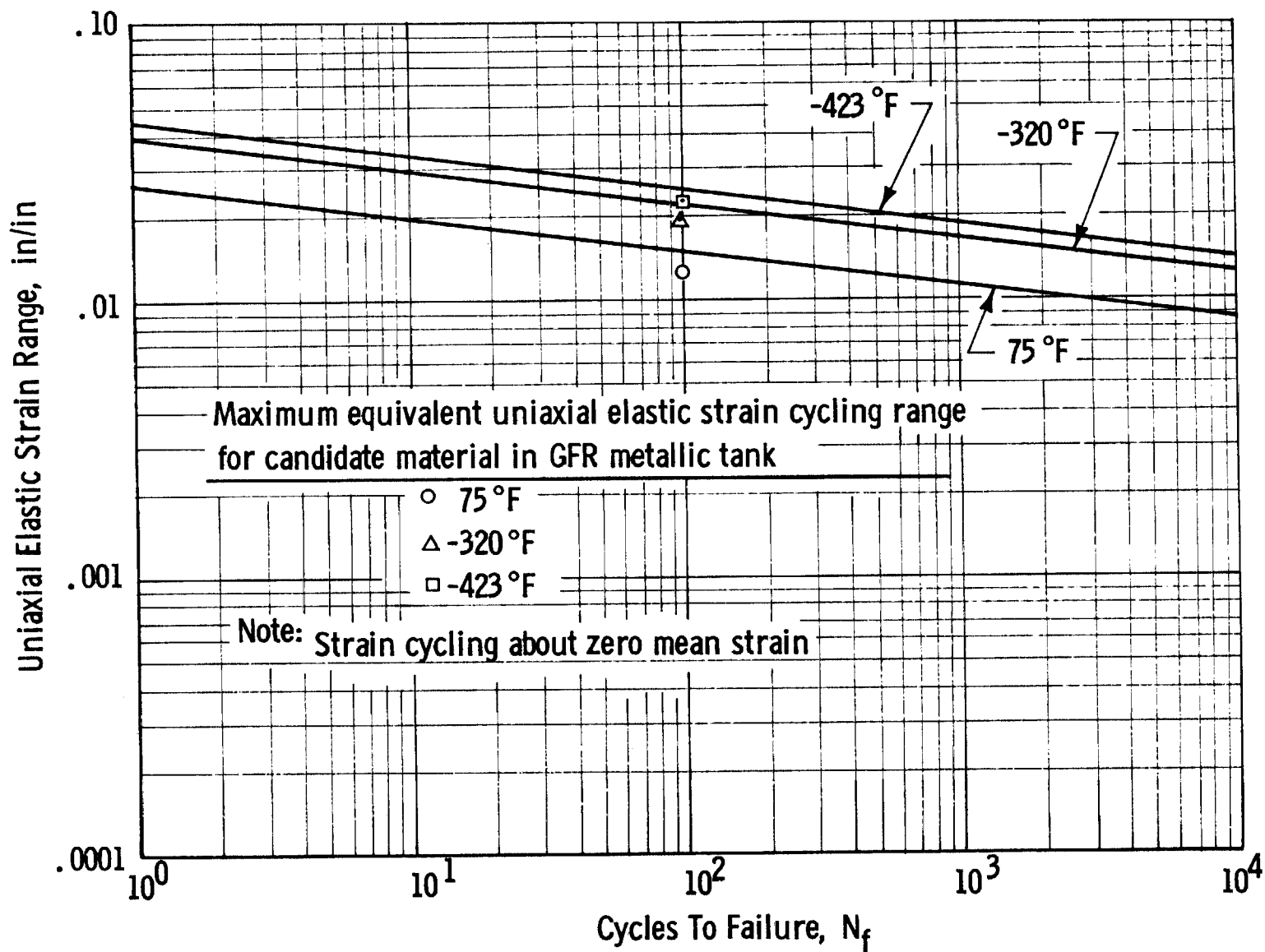
ELASTIC, PLASTIC & TOTAL STRAIN RANGE VARIATIONS WITH
CYCLIC LIFE AT 75°F (Refs. 5 and 6)

Figure C-11



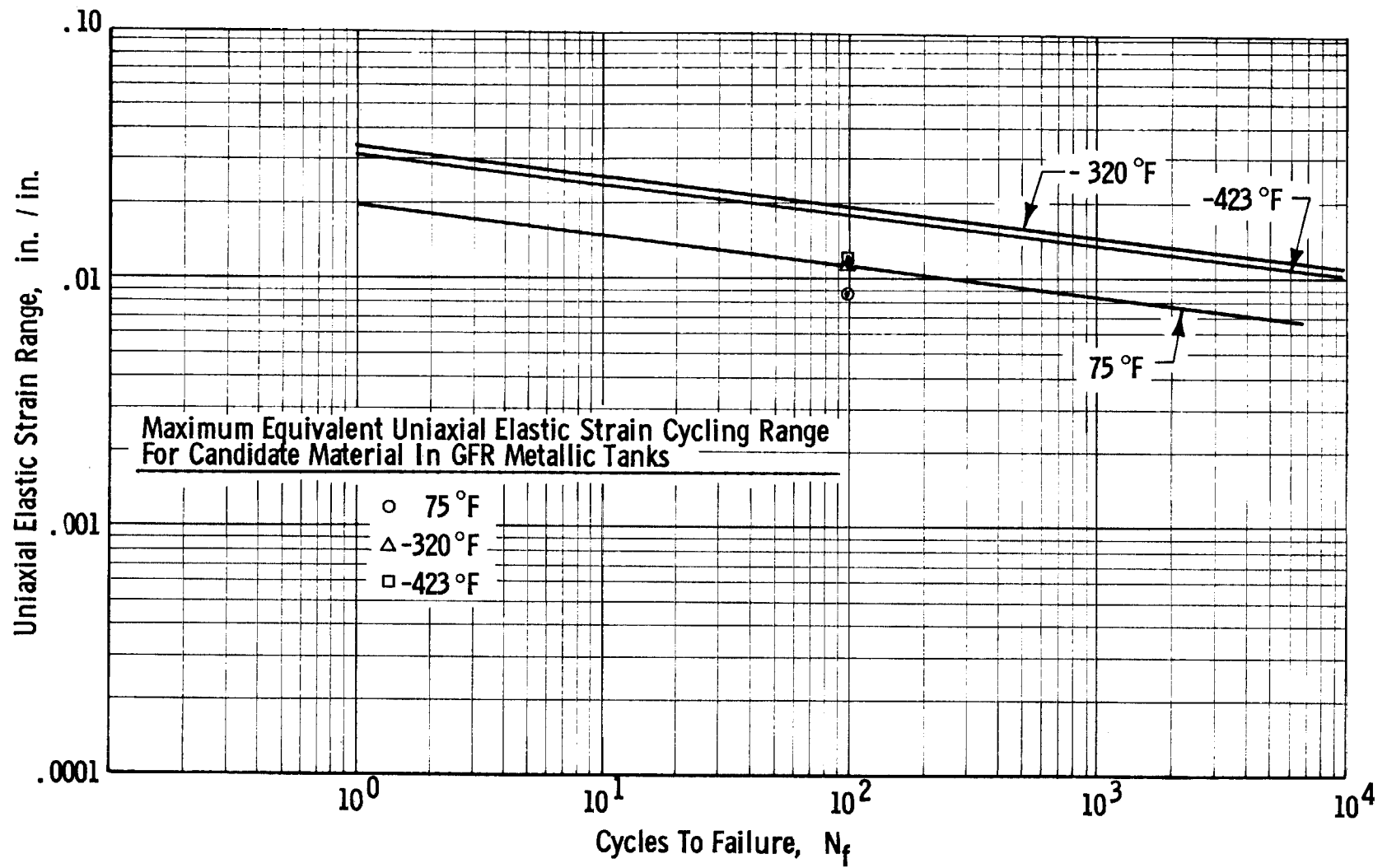
PREDICTED ELASTIC STRAIN RANGE VS CYCLES TO FAILURE FOR 6Al-4V TITANIUM (ANNEALED)

Figure C-12



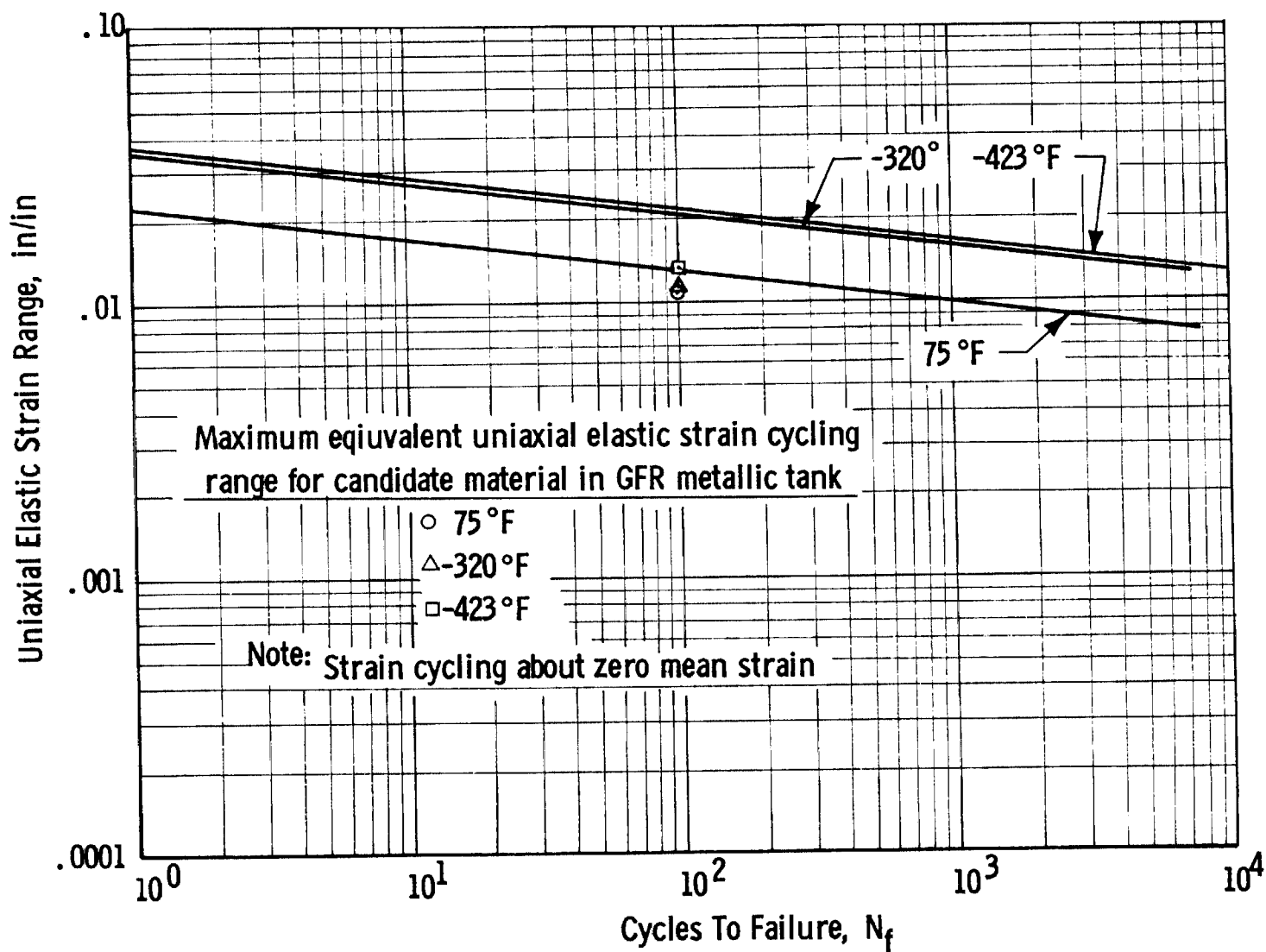
PREDICTED ELASTIC STRAIN RANGE VS CYCLES TO FAILURE FOR 5 Al - 2.5 Sn TITANIUM

Figure C-15



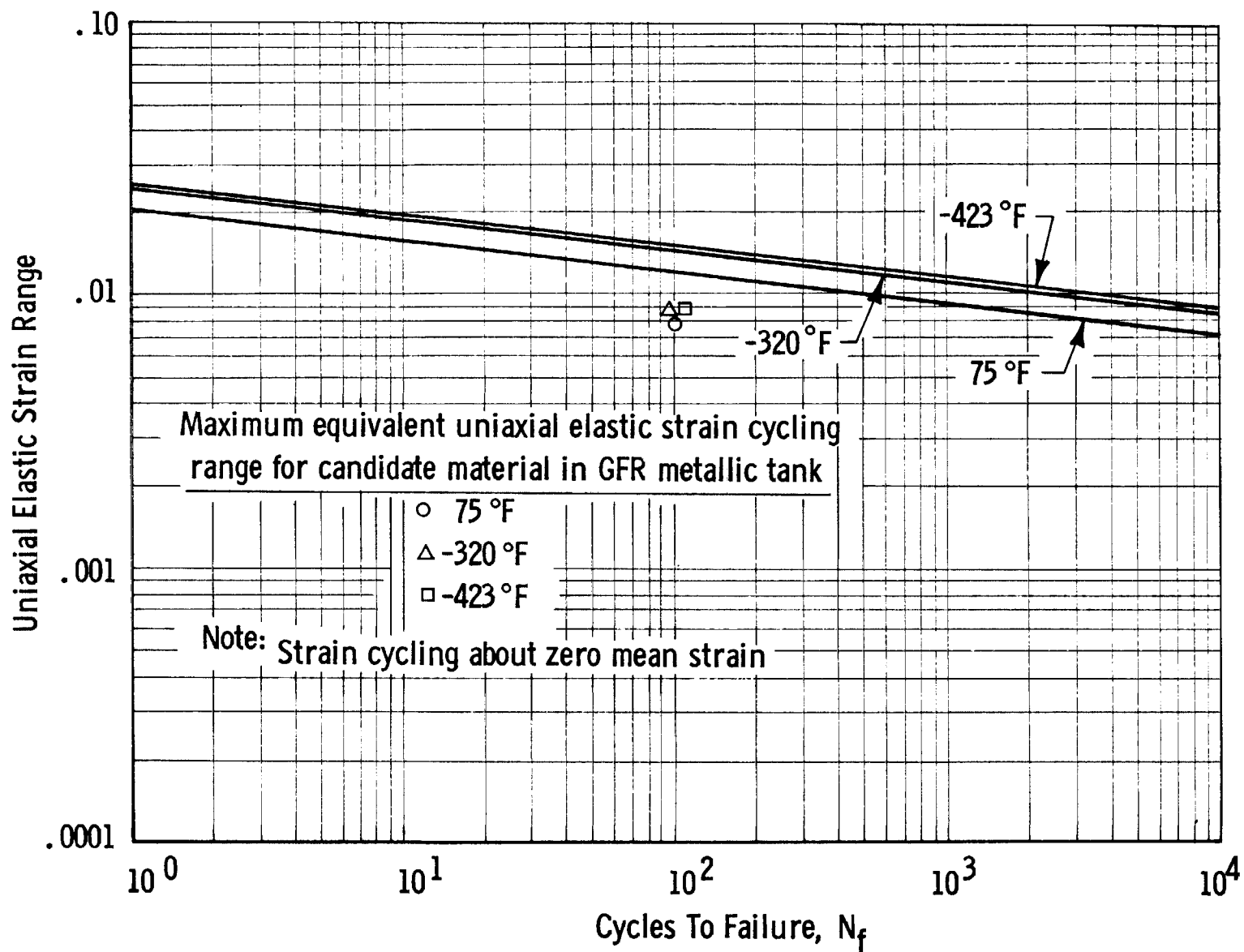
PREDICTED ELASTIC STRAIN RANGE VS CYCLES TO FAILURE FOR 301 STAINLESS STEEL (1/2 HARD)

Figure C-14



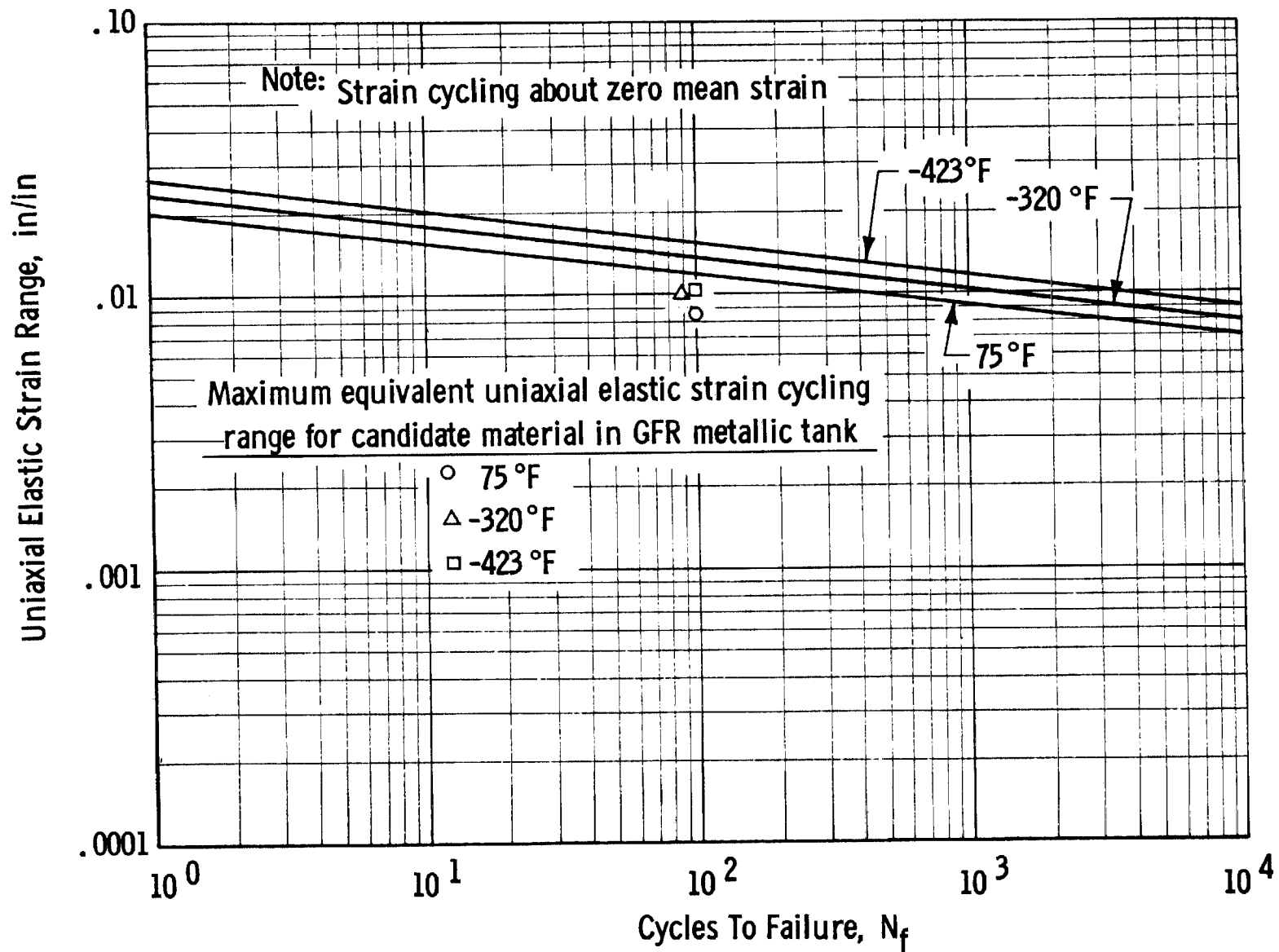
PREDICTED ELASTIC STRAIN RANGE VS CYCLES TO FAILURE FOR 301 STAINLESS STEEL (3/4 HARD)

Figure C-15



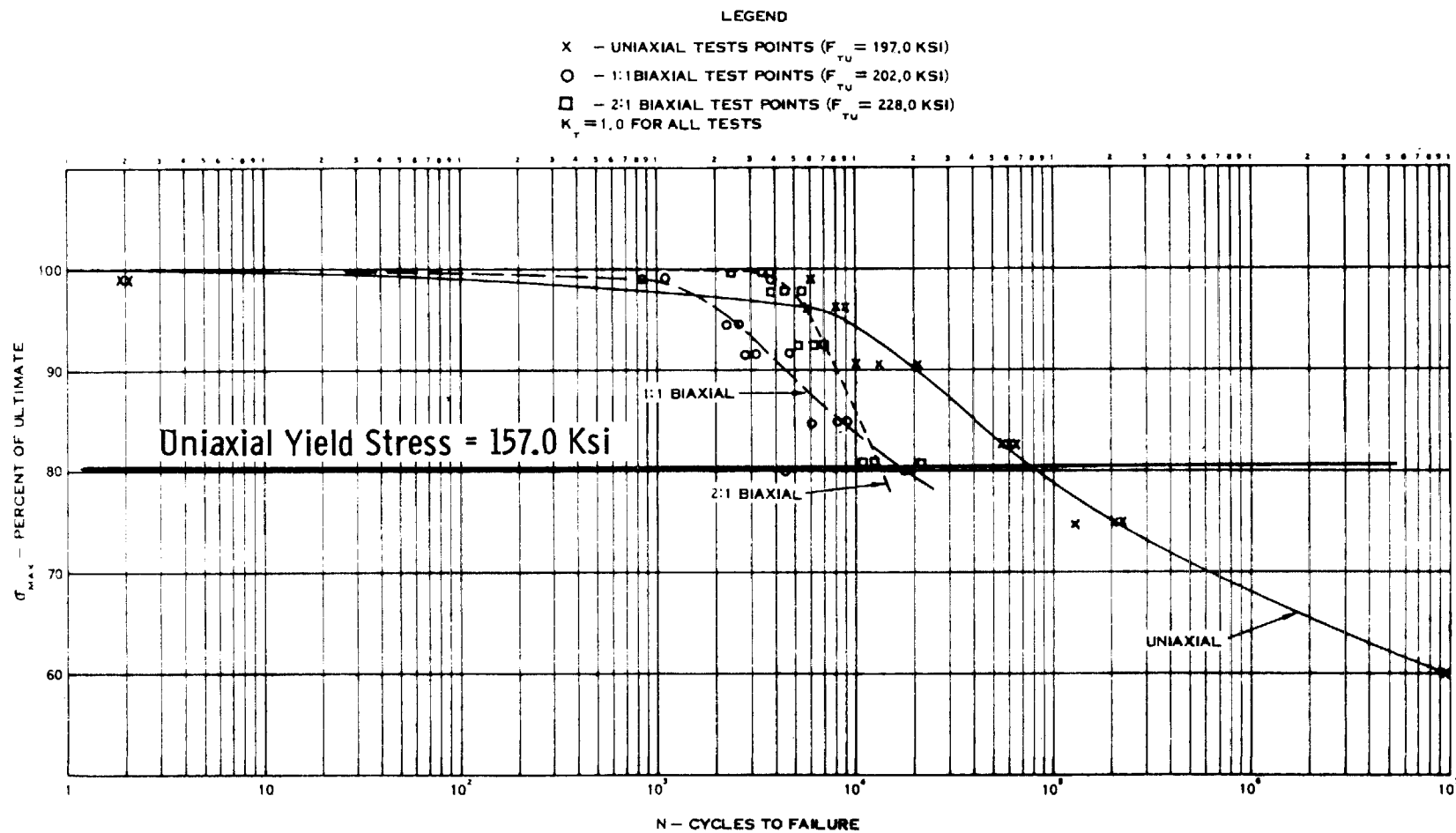
PREDICTED ELASTIC STRAIN RANGE VS CYCLES TO FAILURE FOR INCONEL X-750

Figure C-16



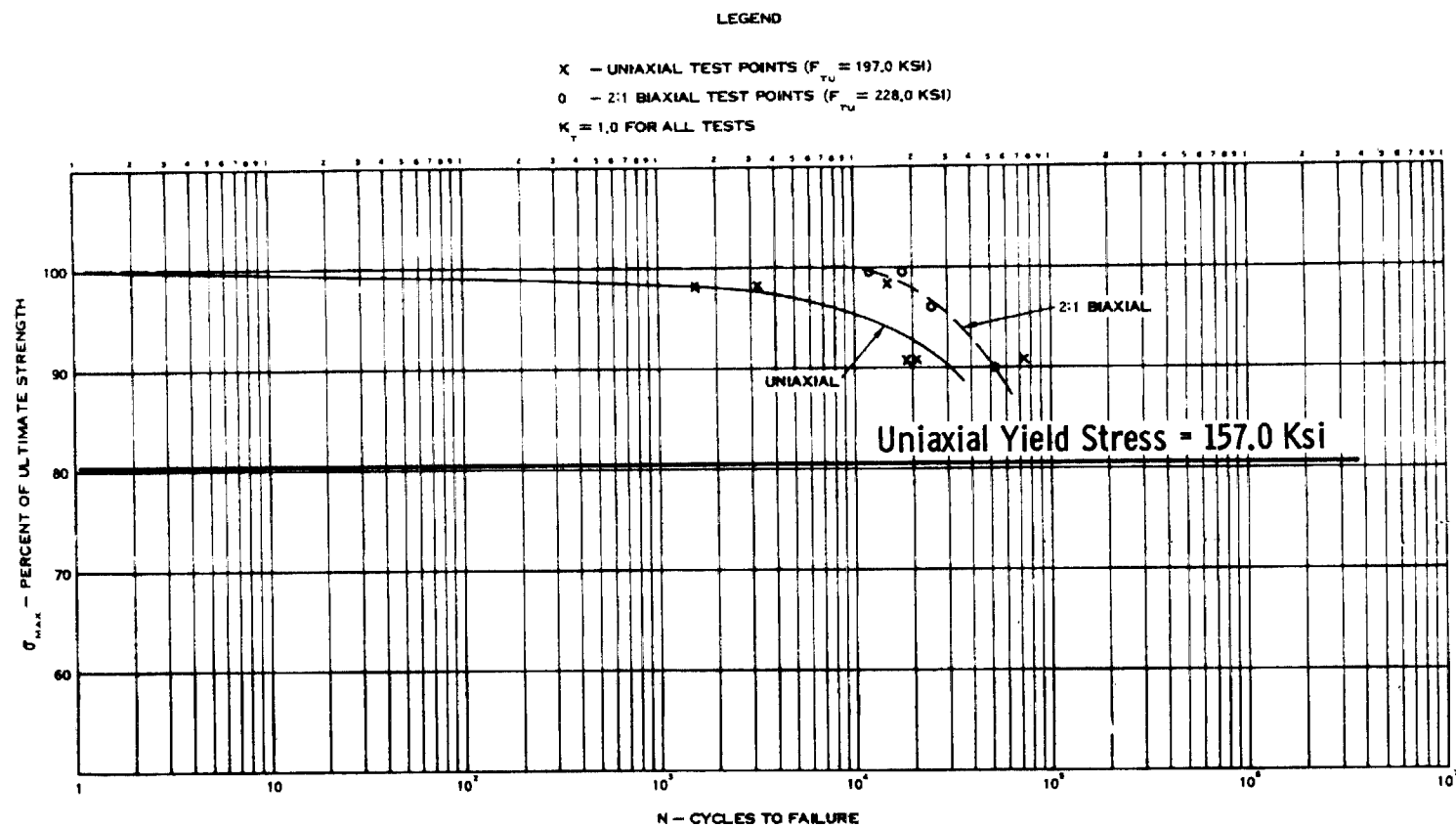
PREDICTED ELASTIC STRAIN RANGE VS CYCLES TO FAILURE FOR 2219-T62 ALUMINUM

Figure C-17



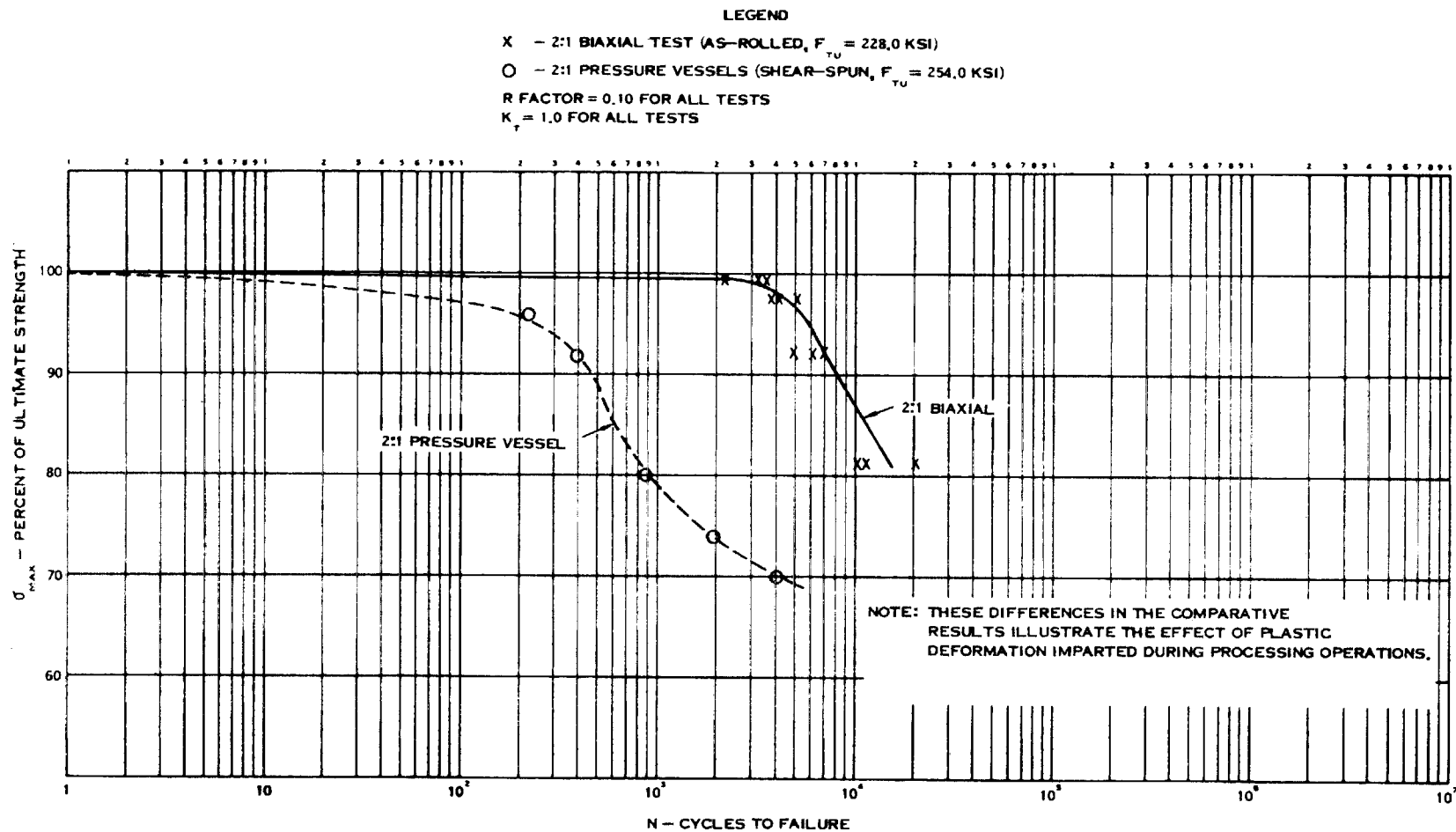
COMPARISON OF UNIAXIAL AND BIAXIAL S-N CURVES FOR 301
 STAINLESS STEEL (AS-ROLLED), $R = 0.10$ (Ref. C-34)

Figure C-18



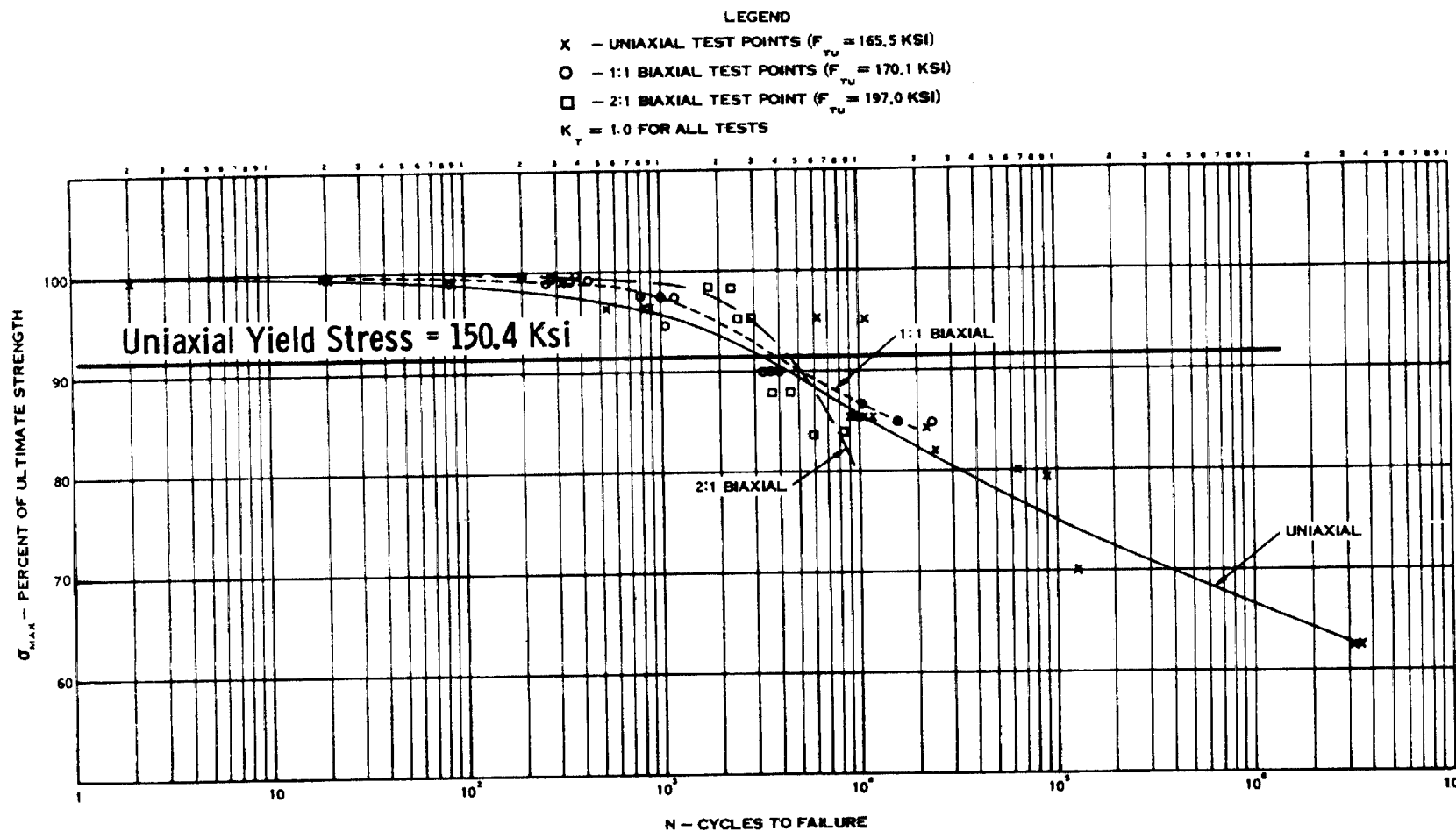
COMPARISON OF UNIAXIAL AND BIAXIAL S-N CURVES FOR 301 STAINLESS STEEL (AS-ROLLED) R=0.50
(Ref. C-34)

Figure C-19



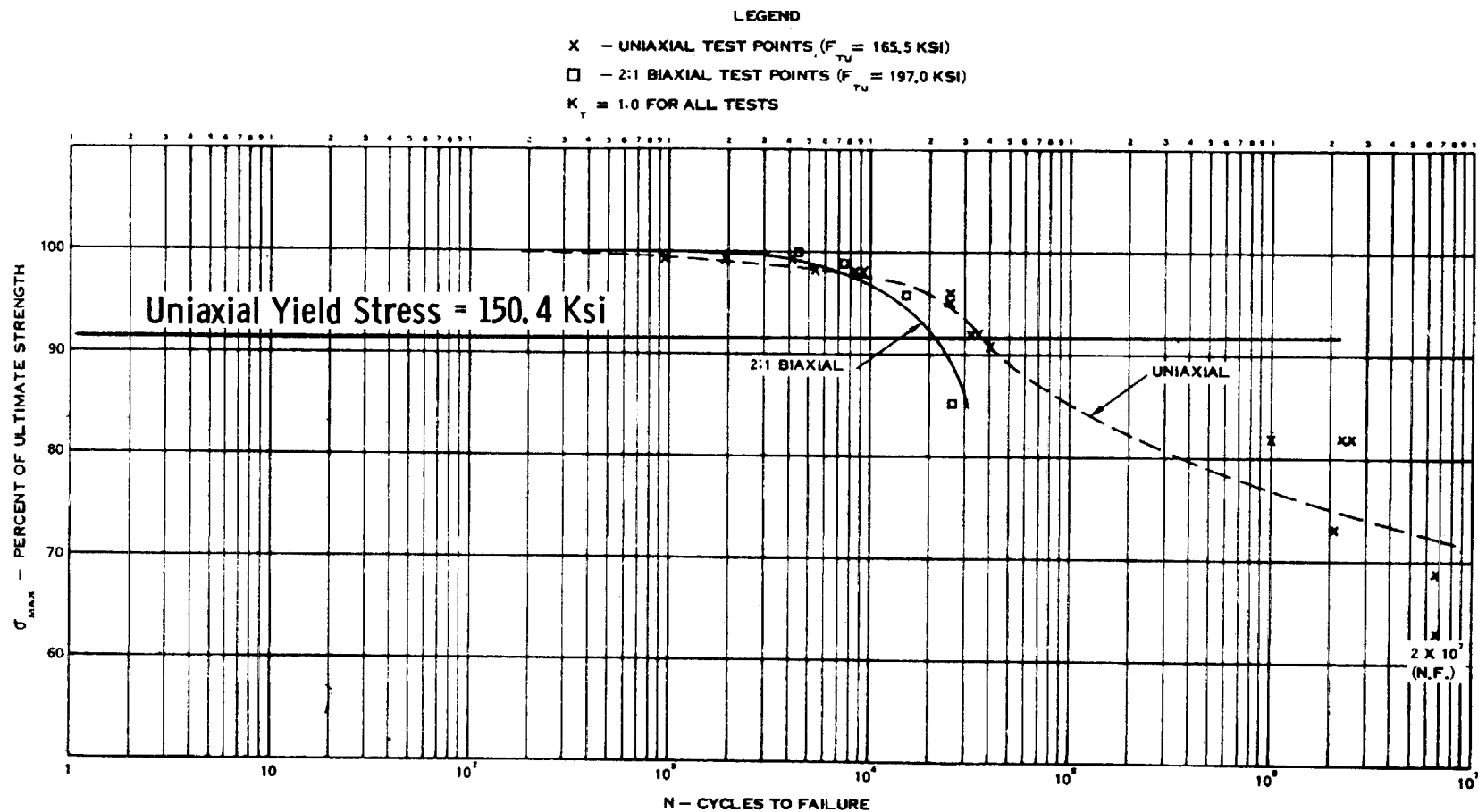
COMPARISON OF S-N CURVES FOR 301 STAINLESS STEEL FROM THE 2:1 BIAXIAL SPECIMENS (AS ROLLED) AND THE CYLINDRICAL PRESSURE VESSELS (SHEAR - SPUN) (Ref. C-34)

Figure C-20



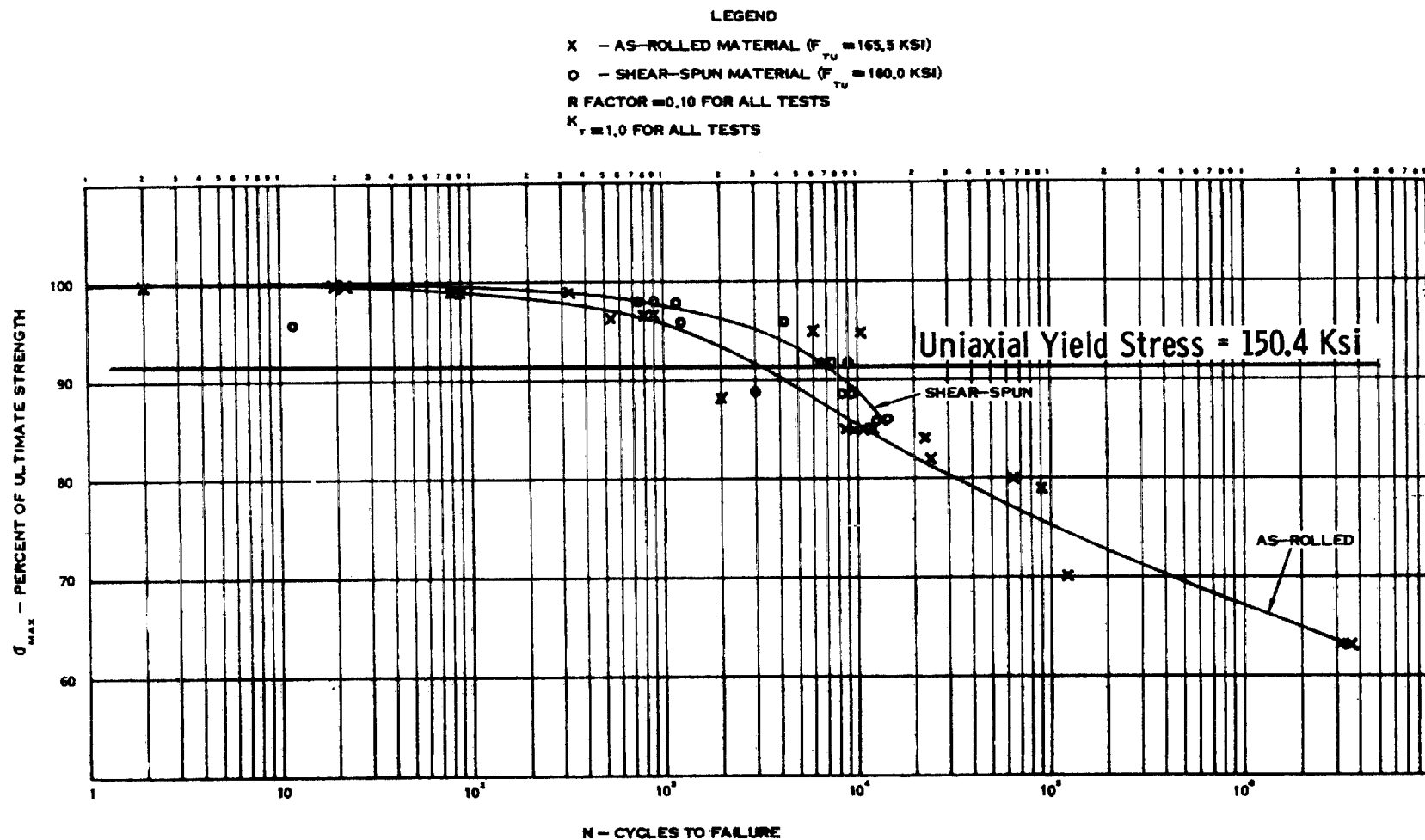
COMPARISON OF UNIAXIAL AND BIAXIAL S-N CURVES FOR
6Al-4V TITANIUM ALLOY (AS-ROLLED), $R = 0.10$ (Ref. C-34)

Figure C-21

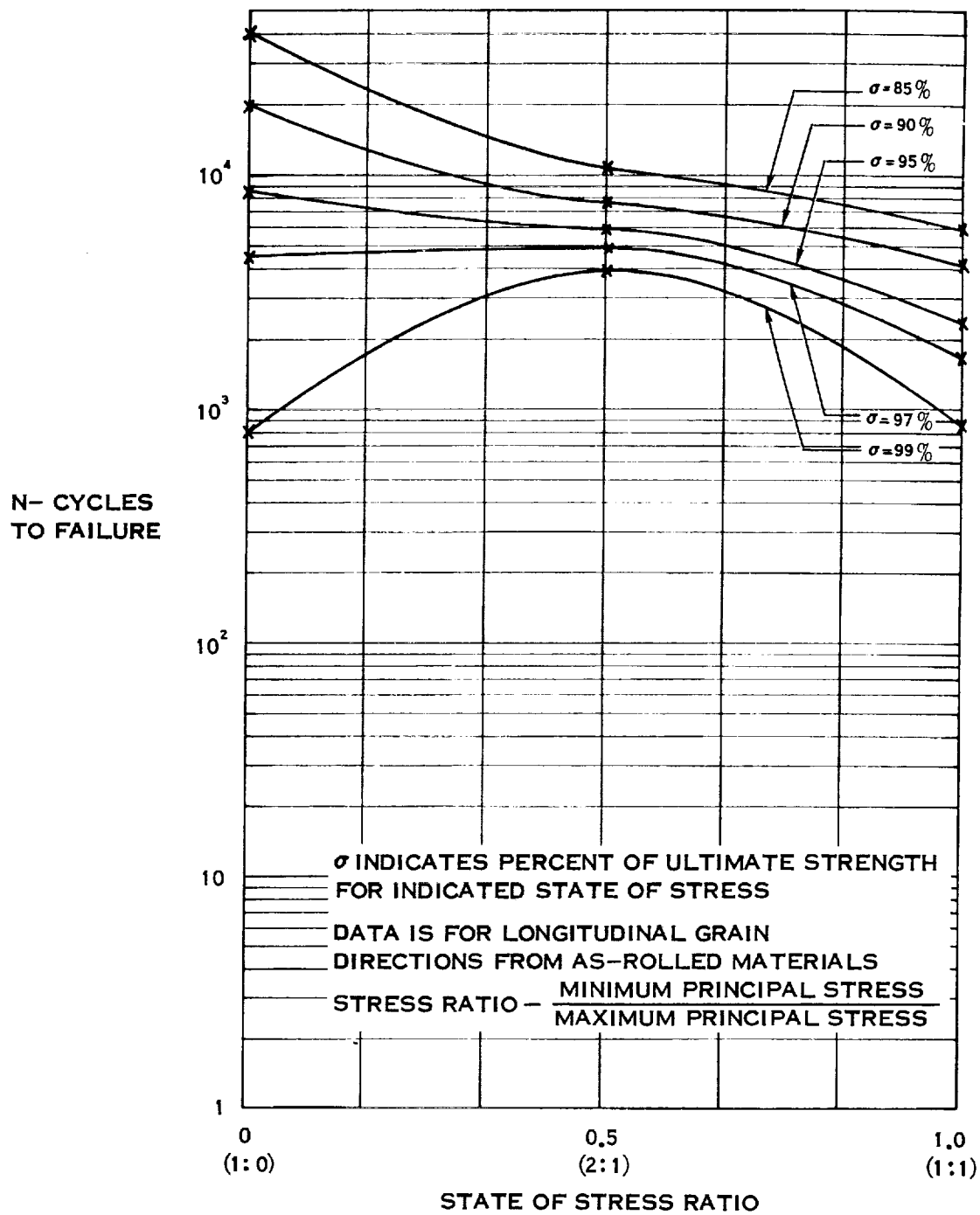


COMPARISON OF UNIAXIAL AND BIAxIAL S-N CURVES FOR
6 Al-4V TITANIUM ALLOY (AS-ROLLED), $R = 0.50$ (Ref. C-34)

Figure C-22

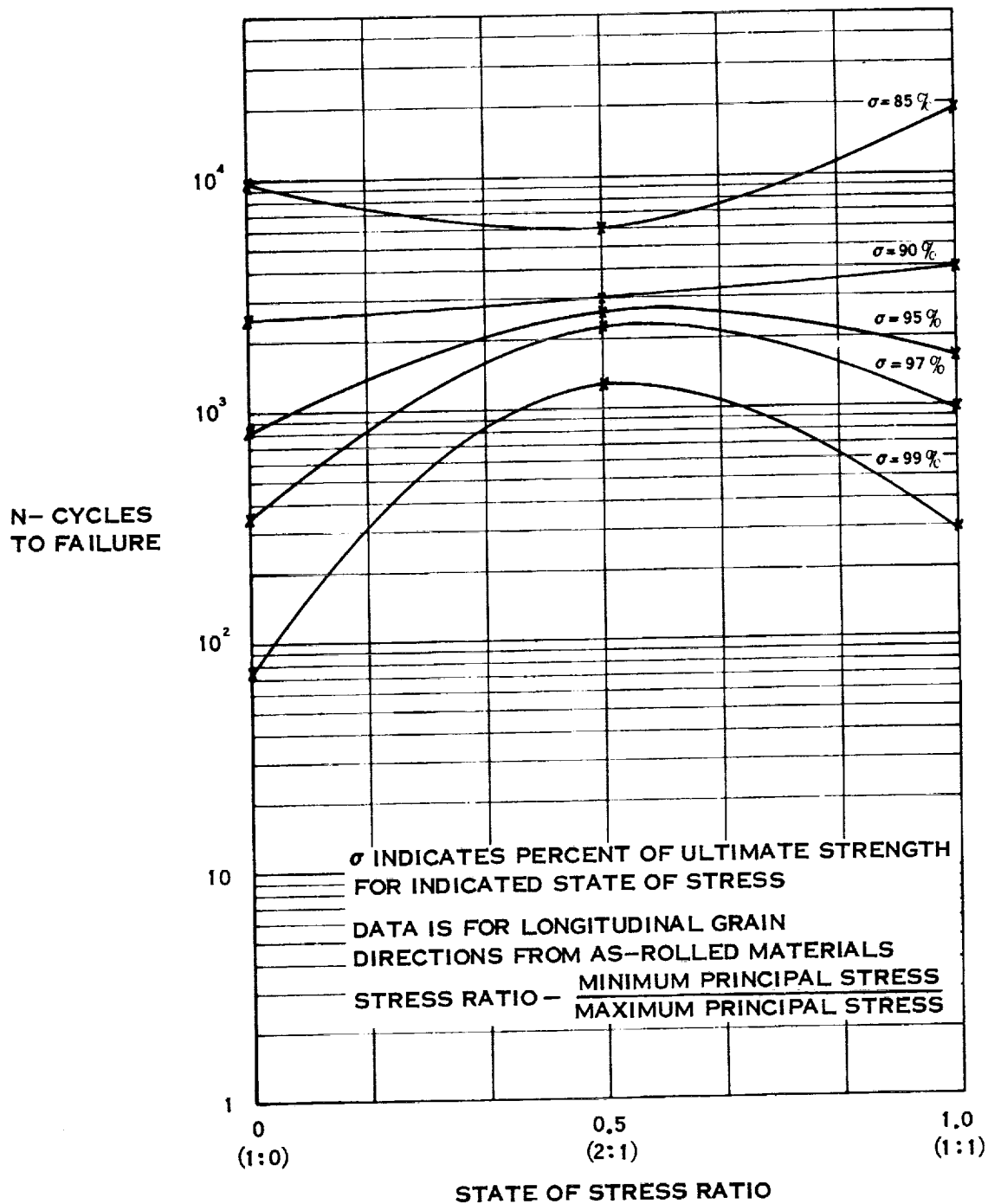


COMPARISON OF UNIAXIAL S-N CURVES FOR 6 AL-4V TITANIUM
ALLOY WITH DIFFERENT MATERIAL CONDITIONS (Ref. C-34)



COMPARISON OF FATIGUE LIFE OF 301 STAINLESS STEEL FOR
 VARIOUS STATES OF STRESS - $R = 0.1$, $K_T = 1.0$ (Ref. C-34)

Figure C-23



COMPARISON OF FATIGUE LIFE OF 6 AL-4V TITANIUM ALLOY
FOR VARIOUS STATES OF STRESS - $R = 0.10$, $K_T = 1.0$ (Ref. C-34)

Figure C-24

APPENDIX D

ANALYSIS OF FILAMENT-WOUND-COMPOSITE PRESSURE VESSELS WITH LOAD-CARRYING LINERS

I. INTRODUCTION

The optimum pressure vessel may be described as one having equal margins of safety in all directions at all locations on the shell. This requires that the filament stresses be constant along their length and that the liner be subjected to a 1-to-1 stress field.

The analysis described in this appendix was established to comply with these requirements at a specified design pressure. Compliance with the requirement for a balanced stress field in the liner is not maintained for all conditions, however, because the physical responses of the liner and composite vary with the magnitude of the load and the direction of the fiber. The vessel design is therefore contingent on the design pressure as well as the dimensional and physical characteristics of the liner and composite.

The design of the optimum-performance pressure vessel must also meet criteria for efficient filament-reinforced composites: minimum resin stresses and continuity of fiber direction. Minimum resin stresses are achieved by fiber orientation and the equations of differential strains in principal directions (minimized change of fiber orientation with pressure). Continuity of fiber direction is obtained by equations in the analysis that establish the filament path.

Based on these criteria, the following design assumptions were made:

The filament stresses are constant along their length at the winding and design conditions.

The liner stresses are constant in the meridional direction at the design condition.

The changes in strains in the meridional and hoop directions are equal from the winding condition to the design condition.

Filament rotation is negligible as the pressure is increased or decreased from the winding pressure.

The resin-matrix effect is negligible (a netting analysis can be used).

Poisson's ratio for the composite is negligible.

Single temperature values can be used for the composite and liner for any given condition.

Additional assumptions required to reduce the complexity of the design included the following:

The thickness of the liner is constant for all points.

The differences in radii of curvature for the pressurized and unpressurized conditions are negligible.

The stress-strain relationship of the liner can be represented by two straight lines (i.e., primary and secondary moduli).

The stress-strain relationship of the filaments can be represented by a straight line.

Poisson's ratio for the metal is $1/2$ in the plastic range.

The stress field in the liner approaches 1 to 1 when yield occurs and the biaxial yield point can be approximated by the uniaxial yield point.

II. ANALYSIS

The design and analysis of optimum filament-reinforced pressure vessels with load-carrying liners has been divided into five sections representing basic analytical operations: analysis of parameters, head design, cylinder design, structural analysis, and vessel characteristics.

The analysis of parameters was established to complete the dimensional and conditional parameters of the composite and liner structure at the equator of the head on the basis of known parameters and equilibrium and compatibility equations. Two primary methods of vessel fabrication are covered: fabrication on a rigid mandrel and fabrication on a pressure-stabilized liner.

The design of the head is based on the solution of a differential equation that describes both the balance of force field in the head and the path of the filaments on the surface of the vessel (i.e., planar path or helical path). Special solutions of the location of the surface of the head at a point nearest the axis are given, depending on the wrap pattern and the location of the inflection point in the differential equation.

The design of the cylindrical portion of the vessel provides the method of defining the thickness and wrap tension of the hoop filaments on the basis of design and wrapping conditions.

The structural analysis establishes equilibrium and compatibility equations for the analysis of the vessel designed by the foregoing procedures. Both stresses and strains are calculated on the basis of prior conditions in order to provide for the analysis of sequential conditions and permanent set of the vessel.

The vessel-characteristics section provides a method of establishing dimensional and performance parameters for the vessel, including (a) the arc length of the filament, (b) the surface area, (c) the weight of the composite, liner, and total vessel, (d) the internal volume, and (e) the performance factor of the vessel, pV/W .*

* Symbols are defined in a list at the end of this appendix.

A. ANALYSIS OF PARAMETERS

1. Compatibility and Equilibrium Equations at Equator

In order that the optimum shape of a filament-wound pressure vessel with a load-carrying liner may be defined, it is necessary to establish the equations of compatibility and equilibrium for the liner and the composite. This may be accomplished by equating the strains and defining the load distribution in both components.

For the analysis presented in this appendix, the following assumptions were used: (a) The winding always occurs at room temperature, T_R , and (b) the physical properties of both liner and composite vary in a straight-line relationship with temperature. For example,

$$E_{LT} = E_L + \frac{dE_L}{dT} \Delta T_L$$

where

$$\Delta T_L = T_{dL} - T_R$$

It was assumed that the liner, which may either be held rigid (zero stress and strain) or be under some internal pressure, is over-wrapped with filaments, which are under a constant tension. It is desired to establish the thicknesses of liner and filaments in addition to their initial stresses so that the complete vessel will support a specified design pressure. At the design pressure, the filaments should be at a design stress (which may contain a safety factor) and the liner may be stressed past its yield point. Furthermore, the design conditions may include significant temperature changes, and the filaments and liners may be at different temperatures themselves.

When plastic flow is involved, the order of temperature or pressure application affects the final stress condition. It is therefore necessary to assume that the change from the winding temperature to the design temperature occurs at a condition below the yield stress of the liner.

The structural responses of the combined composite and liner vary with the direction (i.e., the vessel expands at different rates in the hoop and meridional directions). This variation demands that the change in strains in the hoop and meridional directions can only be equated between two conditions. Because the orientation and efficiency of the filaments are most critical at the design condition, this condition was chosen to complement the winding condition by maintaining equal strains and thus maintaining a zero net rotation of the fibers. The compatibility of the composite and liner strains at other design conditions was assumed to be governed by equal meridional strains, because the fiber direction at the equator will approach this direction for pressure-vessel designs considered in this study, where the diameter of the bosses and the wrap angles are small.

With the foregoing assumptions, the equations that follow govern the design at the equator of the head.

a. Equilibrium of Forces at Design Conditions

Meridional Direction

$$\sigma_{fd} t_e + \sigma_{bLT} t_L = \frac{p_d a}{2} \quad (1)$$

Hoop Direction

$$\sigma_{fd} t_e \tan^2 \alpha_o + \sigma_{bLHT} t_L = \frac{p_d a}{2} \left(2 - \frac{a}{r_{1,o}} \right) \quad (1a)$$

where

$$t_e = K t_o \cos^2 \alpha_o$$

b. Compatibility of Strains from Winding to Design Condition

Meridional Direction

$$\frac{\sigma_{fd}}{E_{fT}} - \frac{\sigma_{of}}{E_f} + \alpha_f \Delta T_f = e_{tL} - \frac{1}{E_L} (\sigma_{oL} - \nu_L \sigma_{oLH}) + \alpha_L \Delta T_L \quad (2)$$

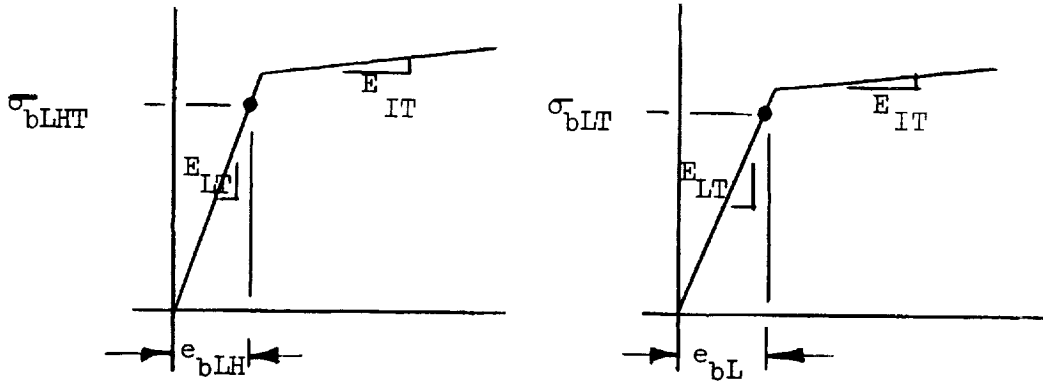
Hoop Direction

$$\frac{\sigma_{fd}}{E_{fT}} - \frac{\sigma_{of}}{E_f} + \alpha_f \Delta T_f = e_{tLH} - \frac{1}{E_L} (\sigma_{oLH} - \nu_L \sigma_{oL}) + \alpha_L \Delta T_L \quad (2a)$$

where

e_{tL} and e_{tLH} are computed as follows:

Condition 1: $e_{bL} \leq \frac{\sigma_{yLT}}{E_{LT}}$ and $e_{bLH} \leq \frac{\sigma_{yLT}}{E_{LT}}$



In the meridional direction,

$$e_{tL} = e_E + e_p$$

$$e_E = \frac{\sigma_{bLT}}{E_{LT}} - \nu_{LT} \frac{\sigma_{bLHT}}{E_{LT}}$$

$$e_p = 0$$

$$\therefore e_{tL} = \frac{1}{E_{LT}} (\sigma_{bLT} - \nu_{LT} \sigma_{bLHT})$$

Since

$$e_{bL} = \frac{\sigma_{bLT}}{E_{LT}} \quad \text{and} \quad e_{bLH} = \frac{\sigma_{bLHT}}{E_{LT}}$$

then

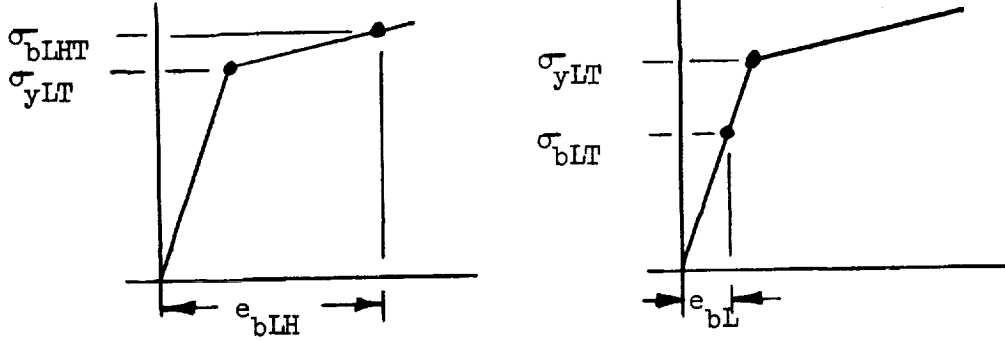
$$e_{tL} = e_{bL} - \nu_{LT} e_{bLH}$$

Similarly, for the hoop direction,

$$e_{tLH} = \frac{1}{E_{LT}} (\sigma_{bLHT} - \nu_{LT} \sigma_{bLT})$$

$$e_{tLH} = e_{bLH} - \nu_{LT} e_{bL}$$

Condition 2: $e_{bL} < \frac{\sigma_{yLT}}{E_{LT}}$ and $e_{bLH} \geq \frac{\sigma_{yLT}}{E_{LT}}$



In the meridional direction,

$$e_{tL} = e_E + e_p$$

$$e_E = \frac{\sigma_{bLT}}{E_{LT}} - \nu_{LT} \frac{\sigma_{yLT}}{E_{LT}}$$

$$e_p = -\frac{1}{2} \frac{(\sigma_{bLHT} - \sigma_{yLT})}{E_{IT}}$$

$$\therefore e_{tL} = \frac{\sigma_{bLT}}{E_{LT}} - \nu_{LT} \frac{\sigma_{yLT}}{E_{LT}} - \frac{1}{2} \frac{(\sigma_{bLHT} - \sigma_{yLT})}{E_{IT}}$$

$$= \frac{\sigma_{bLT}}{E_{LT}} - \frac{1}{2} \frac{(\sigma_{bLHT} - \sigma_{yLT})}{E_{IT}} - \frac{1}{2} \frac{\sigma_{yLT}}{E_{LT}} + \frac{1}{2} \frac{\sigma_{yLT}}{E_{LT}} - \nu_{LT} \frac{\sigma_{yLT}}{E_{LT}}$$

Since

$$e_{bL} = \frac{\sigma_{bLT}}{E_{LT}} \quad \text{and} \quad e_{bLH} = \frac{\sigma_{bLHT} - \sigma_{yLT}}{E_{IT}} + \frac{\sigma_{yLT}}{E_{LT}}$$

then

$$e_{tL} = e_{bL} - \frac{1}{2} e_{bLH} + \left(\frac{1}{2} - \nu_{LT} \right) \frac{\sigma_{yLT}}{E_{LT}}$$

For the hoop direction,

$$e_{tLH} = e_E + e_p$$

$$e_E = \frac{\sigma_{yLT}}{E_{LT}} - \nu_{LT} \frac{\sigma_{bLT}}{E_{LT}}$$

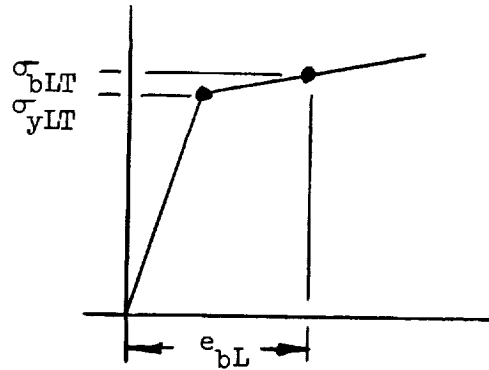
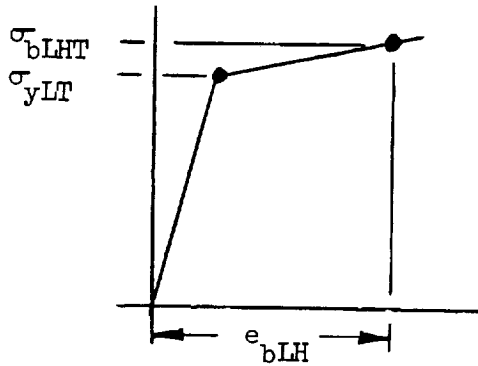
$$e_p = \frac{\sigma_{bLHT} - \sigma_{yLT}}{E_{IT}}$$

$$\therefore e_{tLH} = \frac{\sigma_{bLHT} - \sigma_{yLT}}{E_{IT}} + \frac{\sigma_{yLT}}{E_{LT}} - \nu_{LT} \frac{\sigma_{bLT}}{E_{LT}}$$

and

$$e_{tLH} = e_{bLH} - \nu_{LT} e_{bL}$$

Condition 3: $e_{bL} > \frac{\sigma_{yLT}}{E_{LT}}$ and $e_{bLH} > \frac{\sigma_{yLT}}{E_{LT}}$



In the meridional direction,

$$e_{tL} = e_E + e_p$$

$$e_E = \frac{\sigma_{yLT}}{E_{LT}} - \nu_{LT} \frac{\sigma_{yLT}}{E_{LT}}$$

$$e_p = \frac{\sigma_{bLT} - \sigma_{yLT}}{E_{IT}} - \frac{1}{2} \frac{(\sigma_{bLHT} - \sigma_{yLT})}{E_{IT}}$$

$$\therefore e_{tL} = \frac{\sigma_{yLT}}{E_{LT}} - \nu_{LT} \frac{\sigma_{yLT}}{E_{LT}} + \frac{\sigma_{bLT} - \sigma_{yLT}}{E_{IT}} - \frac{1}{2} \frac{(\sigma_{bLHT} - \sigma_{yLT})}{E_{IT}}$$

Since

$$e_{bL} = \frac{\sigma_{bLT} - \sigma_{yLT}}{E_{IT}} + \frac{\sigma_{yLT}}{E_{LT}}$$

and

$$e_{bLH} = \frac{\sigma_{bLHT} - \sigma_{yLT}}{E_{IT}} + \frac{\sigma_{yLT}}{E_{LT}}$$

then

$$e_{tL} = \frac{\sigma_{bLT} - \sigma_{yLT}}{E_{IT}} + \frac{\sigma_{yLT}}{E_{LT}} - \frac{1}{2} \frac{(\sigma_{bLHT} - \sigma_{yLT})}{E_{IT}} - \frac{1}{2} \frac{\sigma_{yLT}}{E_{LT}} + \frac{1}{2} \frac{\sigma_{yLT}}{E_{LT}} - \nu_{LT} \frac{\sigma_{yLT}}{E_{LT}}$$

and

$$e_{tL} = e_{bL} - \frac{1}{2} e_{bLH} + \left(\frac{1}{2} - \nu_{LT} \right) \frac{\sigma_{yLT}}{E_{LT}}$$

Similarly, for the hoop direction,

$$e_{tLH} = \frac{\sigma_{bLHT}}{E_{IT}} - \frac{\sigma_{bLT}}{2E_{IT}} + \left(\frac{1}{E_{LT}} - \frac{1}{2E_{IT}} - \frac{LT}{E_{LT}} \right) \sigma_{yLT}$$

$$= e_{bLH} - \frac{1}{2} e_{bL} + \left(\frac{1}{2} - LT \right) \frac{\sigma_{yLT}}{E_{LT}}$$

Condition 4: $e_{bL} \geq \frac{\sigma_{yLT}}{E_{LT}}$ and $e_{bLH} < \frac{\sigma_{yLT}}{E_{LT}}$

The fourth condition, which assumes that the liner has yielded in the meridional direction and not yielded in the hoop direction, has been eliminated from consideration in the design of the vessel by the assumption that the hoop stress will always lead or be equal to the meridional stress at the design conditions.

c. Equilibrium at Zero Pressure and Design Temperature

Meridional Direction

$$\sigma_{ofT} t_e + \sigma_{oLT} t_L = 0 \quad (3)$$

Hoop Direction

$$\sigma_{ofT} t_e \tan^2 \alpha_o + \sigma_{oLHT} t_L = 0 \quad (3a)$$

d. Compatibility of Strains During Temperature Change at Zero Pressure

Meridional Direction

$$\frac{\sigma_{ofT}}{E_{fT}} - \frac{\sigma_{of}}{E_f} + \alpha_f \Delta T_f = \frac{(\sigma_{oLT} - \nu_{LT} \sigma_{oLHT})}{E_{LT}}$$

$$- \frac{(\sigma_{oL} - \nu_L \sigma_{oLH})}{E_L} + \alpha_L \Delta T_L \quad (4)$$

- e. Equilibrium at Zero Pressure and Room Temperature

Meridional Direction

$$\sigma'_{of} t_e + \sigma'_{oL} t_L = 0 \quad (5)$$

Hoop Direction

$$\sigma'_{of} t_e \tan^2 \alpha_o + \sigma'_{oLH} t_L = 0 \quad (5a)$$

- f. Compatibility of Strains When Relaxing from Winding Pressure

Meridional Direction

$$\frac{\sigma'_{of} - \sigma_{of}}{E_f} = \frac{\sigma'_{oL} - \nu_L \sigma'_{oLH}}{E_L} - \frac{\sigma_{oL} - \nu_L \sigma_{oLH}}{E_L} \quad (6)$$

- g. Equilibrium of Forces at Winding Conditions

Meridional Direction

$$\sigma_{of} t_e + \sigma_{oL} t_L = \frac{p_w a}{2} \quad (7)$$

Hoop Direction

$$\sigma_{of} t_e \tan^2 \alpha_o + \sigma_{oLH} t_L = \frac{p_w a}{2} \left(2 - \frac{a}{r_{l,o}} \right) \quad (7a)$$

2. Solution of Equations

Eight force-equilibrium equations and four strain-compatibility equations are available for the determination of the 19 unknown variables shown in Table D-1. The wrap angle at the equator (α_o) can be approximated, and later verified, to eliminate one unknown, and the vessel radius (a), initial filament-winding stress (σ_{of}), and meridional stress in the liner at the wrap condition (σ_{oL}) are fixed to eliminate another three unknowns. Because strain compatibility from the wrap condition to the design condition is assumed, the four applicable equations [(1), (1a), (2), (2a)] involving eight of the remaining 15 unknowns may be satisfied first. The following cases, involving the nine remaining unknowns, are considered representative of conditions that may be expected in practice:

Case No.	Unknown Variables*							
	σ_{oLH}	σ_{fd}	$e_{bLH}(\sigma_{bLH})$	$e_{bL}(\sigma_{bL})$	t_L	t_o	p_d	$r_{1,o}$
1	X	X	-	-	(Two X, one -)	-	-	-
2	X	-	X	-	(Two X, one -)	-	-	-
3	-	X	X	-	(Two X, one -)	-	-	-
4	-	-	X	X	(Two X, one -)	-	-	-
5**	-	X	-	-	X	-	X	-

Two conditions can exist during winding: A rigid mandrel can be used to control the strains within the liner, or the liner can be stabilized by internal pressure. The first two cases in the tabulation above deal with the condition of fixed liner strain during winding (e.g., liner supported by rigid mandrel). In both rigid-mandrel cases, the hoop stress in the liner at the wrap condition (σ_{oLH}) is fixed.

For Case 1, σ_{fd} and two of the three variables t_L , t_o , and p_d are also fixed. The simultaneous solution of Equations (2) and (2a), subject to the fixed variables, results in the following equation for σ_{bLH} :***

$$\sigma_{bLH} = \frac{1}{M_{54}} \left[\frac{\sigma_{fd}}{E_{fT}} - \frac{\sigma_{of}}{E_f} + \frac{1}{E_L} (\sigma_{oL} - \nu_L \sigma_{oLH}) - \alpha_L \Delta T_L + \alpha_f \Delta T_f - \frac{M_{53}}{E_{LT}} + M_{55} \right] \quad (8)$$

For Case 2, $e_{bLH}(\sigma_{bLH})$ and two of the three variables t_L , t_o , and p_d are fixed in addition to σ_{oLH} . The solution of Equations (2) and (2a) is used to calculate σ_{fd} as follows:

* X denotes fixed, - denotes unfixed.

** Equations (7) and (7a) are used in the solution of this case in addition to Equations (1), (1a), (2), and (2a).

*** All constants (M) are evaluated subsequently throughout this section.

$$\sigma_{fd} = E_{fT} \left[M_{54} \sigma_{bLH} + \frac{\sigma_{of}}{E_f} - \frac{1}{E_L} (\sigma_{oL} - \nu_L \sigma_{oLH}) + \alpha_L \Delta T_L - \alpha_f \Delta T_f + \frac{M_{53}}{E_{LT}} - M_{55} \right] \quad (9)$$

For both rigid-mandrel cases,

$$\sigma_{bL} = M_{52} \sigma_{bLH} + M_{53} \quad (10)$$

If t_L is given, Equation (1) reduces to

$$t_e = \frac{p_d a}{2\sigma_{fd}} - \frac{\sigma_{bL} t_L}{\sigma_{fd}} \quad (11)$$

If t_e is given, Equation (1) becomes

$$t_L = \frac{p_d a}{2\sigma_{bL}} - \frac{\sigma_{fd} t_e}{\sigma_{bL}} \quad (12)$$

From Equation (1a),

$$\frac{a}{r_{1,o}} = 2 \left[1 - \frac{\sigma_{fd} t_e \tan^2 \alpha_o}{p_d a} - \frac{t_L \sigma_{bLH}}{p_d a} \right] \quad (13)$$

Although the wrap pressure is fictitious for the rigid mandrel, it can be calculated from Equation (7) as

$$p_w = \frac{2}{a} [\sigma_{of} t_e + \sigma_{oL} t_L] \quad (14)$$

Unknown variables at other than the winding and design conditions are computed as follows:

$$\sigma'_{of} = \frac{\frac{\sigma_{of}}{E_f} - \left(\frac{\sigma_{oL} - \nu_L \sigma_{oLH}}{E_L} \right)}{\frac{1}{E_f} + \frac{1}{E_L} \left(\frac{t_e}{t_L} \right) (1 - \nu_L \tan^2 \alpha_o)} \quad (15)$$

$$\sigma'_{oL} = - \frac{t_e}{t_L} \sigma'_{of} \quad (16)$$

$$\sigma'_{oLH} = - \frac{t_e}{t_L} \sigma'_{of} \tan^2 \alpha_o \quad (17)$$

$$\sigma_{ofT} = \frac{\frac{\sigma_{of}}{E_f} - \left(\frac{\sigma_{oL} - \nu_L \sigma_{oLH}}{E_L} \right) + \alpha_L \Delta T_L - \alpha_f \Delta T_f}{\frac{1}{E_{fT}} + \frac{1}{E_{LT}} \left(\frac{t_e}{t_L} \right) (1 - \nu_{LT} \tan^2 \alpha_o)} \quad (18)$$

$$\sigma_{oLT} = - \frac{t_e}{t_L} \sigma_{ofT} \quad (19)$$

$$\sigma_{oLHT} = - \frac{t_e}{t_L} \sigma_{ofT} \tan^2 \alpha_o \quad (20)$$

The M constants depend upon whether the liner stresses exceed the yield or not:

Condition 1: σ_{bL} and $\sigma_{bLH} < \sigma_{yLT}$

$$M_{52} = 1.0$$

$$M_{53} = \frac{E_{LT}}{E_L} \left(\frac{1 + \nu_L}{1 + \nu_{LT}} \right) (\sigma_{oL} - \sigma_{oLH})$$

$$M_{54} = \frac{1 - \nu_{LT}}{E_{LT}}$$

$$M_{55} = 0.0$$

Condition 2: $\sigma_{bL} < \sigma_{yLT}$ and $\sigma_{bLH} \geq \sigma_{yLT}$

$$M_{52} = \frac{3 E_{LT}}{2 E_{IT} (1 + \nu_{LT})}$$

$$M_{53} = M_{52} \left\{ \frac{2 E_{IT} (\sigma_{oL} - \sigma_{oLH}) (1 + \nu_L)}{3 E_L} - \sigma_{yLT} \left[1 - \frac{2 E_{IT} (1 + \nu_{LT})}{3 E_{LT}} \right] \right\}$$

$$M_{54} = \frac{M_{52}}{E_{LT}} - \frac{1}{2 E_{IT}}$$

$$M_{55} = -\sigma_{yLT} \left[\frac{1}{2E_{IT}} - \nu_{LT} \left(\frac{1}{E_{LT}} \right) \right]$$

Condition 3: σ_{bL} and $\sigma_{bLH} \geq \sigma_{yLT}$

$$M_{52} = 1.0$$

$$M_{53} = \frac{2}{3} \left(\frac{E_{LT}}{E_L} \right) (1 + \nu_L) (\sigma_{oL} - \sigma_{oLH})$$

$$M_{54} = \frac{1}{2E_{IT}}$$

$$M_{55} = \sigma_{yLT} \left[\frac{1}{2E_{IT}} - \frac{(1 - \nu_{LT})}{E_{LT}} \right]$$

The remaining three cases deal with a pressure-stabilized mandrel. For Case 3, σ_{fd} , e_{bLH} (σ_{bLH}), and two of the three variables t_L , t_o , and p_d are fixed. As in Cases 1 and 2, the strain-compatibility equations between the wrap condition and the design condition [Equations (2) and (2a)] are solved simultaneously, subject to the position of the liner stress relative to the yield stress.

Condition 1: σ_{bL} and $\sigma_{bLH} < \sigma_{yLT}$

$$\sigma_{oLH} = \frac{E_L}{1 - \nu_L \nu_{LT}} \left[\frac{\sigma_{oL}}{E_L} (\nu_L - \nu_{LT}) + e_{bLH} (1 - \nu_{LT}^2) - M_{60} (1 + \nu_{LT}) \right] \quad (21)$$

$$\sigma_{bL} = \sigma_{bLH} + \frac{E_{LT} (1 + \nu_L)}{E_L (1 + \nu_{LT})} (\sigma_{oL} - \sigma_{oLH}) \quad (22)$$

Condition 2: $\sigma_{bL} < \sigma_{yLT}$ and $\sigma_{bLH} \geq \sigma_{yLT}$

$$\begin{aligned} \sigma_{oLH} = \frac{E_L}{1 - \nu_L \nu_{LT}} \left[\frac{\sigma_{oL}}{E_L} (\nu_L - \nu_{LT}) + e_{bLH} \left(1 - \frac{\nu_{LT}}{2} \right) - M_{60} (1 + \nu_{LT}) \right. \\ \left. + \nu_{LT} \left(\frac{1}{2} - \nu_{LT} \right) \frac{\sigma_{yLT}}{E_{LT}} \right] \quad (21a) \end{aligned}$$

$$\sigma_{bL} = \frac{E_{LT}}{1 + \nu_{LT}} \left[\frac{3(\sigma_{bLH} - \sigma_{yLT})}{2E_{IT}} + (1 + \nu_{LT}) \frac{\sigma_{yLT}}{E_{LT}} + \frac{(1 + \nu_L)(\sigma_{oL} - \sigma_{oLH})}{E_L} \right] \quad (22a)$$

Condition 3: σ_{bL} and $\sigma_{bLH} \geq \sigma_{yLT}$

$$\sigma_{oLH} = \frac{E_L}{1 - \frac{\nu_L}{2}} \left[\frac{\sigma_{oL}}{E_L} (\nu_L - \frac{1}{2}) + \frac{3}{4} e_{bLH} - \frac{3}{2} M_{60} + \frac{3}{2} (\frac{1}{2} - \nu_{LT}) \frac{\sigma_{yLT}}{E_{LT}} \right] \quad (21b)$$

$$\sigma_{bL} = \sigma_{bLH} + \frac{2E_{IT} (1 + \nu_L)}{3 E_L} (\sigma_{oL} - \sigma_{oLH}) \quad (22b)$$

For the three conditions of liner stress, the constant M_{60} is evaluated as follows:

$$M_{60} = \frac{\sigma_{fd}}{E_{ft}} - \frac{\sigma_{of}}{E_f} + \alpha_f \Delta T_f - \alpha_L \Delta T_L$$

The remainder of the unknown variables are calculated from the same equations used for Cases 1 and 2 [see Equations (11) through (20)].

For Case 4, e_{bLH} (σ_{bLH}), e_{bL} (σ_{bL}), and two of the three variables t_L , t_o , and p_d are fixed.

Condition 1: σ_{bL} and $\sigma_{bLH} < \sigma_{yLT}$

$$\sigma_{oLH} = \sigma_{oL} + \frac{E_L (1 + \nu_{LT})}{1 + \nu_L} (e_{bLH} - e_{bL}) \quad (23)$$

$$\sigma_{fd} = E_{ft} \left[M_{70} + \frac{1}{E_{LT}} (\sigma_{bL} - \nu_{LT} \sigma_{bLH}) \right] \quad (24)$$

Condition 2: $\sigma_{bL} < \sigma_{yLT}$ and $\sigma_{bLH} \geq \sigma_{yLT}$

$$\sigma_{oLH} = \sigma_{oL} + \frac{E_L}{1 + \nu_L} \left[\frac{3}{2} e_{bLH} - (1 + \nu_{LT}) e_{bL} - (\frac{1}{2} - \nu_{LT}) \frac{\sigma_{yLT}}{E_{LT}} \right] \quad (23a)$$

$$\sigma_{fd} = E_{fT} \left[M_{70} + \frac{\sigma_{bL}}{E_{LT}} - \frac{\sigma_{bLH}}{2E_{IT}} + \left(\frac{1}{2E_{IT}} - \frac{\nu_{LT}}{E_{LT}} \right) \sigma_{yLT} \right] \quad (24a)$$

Condition 3: σ_{bL} and $\sigma_{bLH} \geq \sigma_{yLT}$

$$\sigma_{oLH} = \sigma_{oL} + \frac{3E_L}{2(1 + \nu_L)} (e_{bLH} - e_{bL}) \quad (23b)$$

$$\sigma_{fd} = E_{fT} \left[M_{70} + \frac{\sigma_{bL}}{E_{IT}} - \frac{\sigma_{bLH}}{2E_{IT}} + \left(\frac{1}{E_{LT}} - \frac{1}{2E_{IT}} - \frac{\nu_{LT}}{E_{LT}} \right) \sigma_{yLT} \right] \quad (24b)$$

The constant M_{70} is determined from

$$M_{70} = \frac{\sigma_{of}}{E_f} + \alpha_L \Delta T_L - \alpha_f \Delta T_f - \frac{1}{E_L} (\sigma_{oL} - \nu_L \sigma_{oLH})$$

and all other unknown variables are calculated as in Cases 1 through 3 [see Equations (11) through (20)].

In Case 5, σ_{fd} , t_L , and p_d are fixed. Six equations [(1), (1a), (2), (2a), (7), and (7a)] are solved simultaneously to provide equations for pressure-mandrel solutions with minimum variable fixation. These equations introduce an additional variable, p_w , which must be determined in addition to other unknown variables related to the winding and design conditions. The longitudinal stress in the liner at the design condition (σ_{bL}) is calculated from the general quadratic equation:

$$\sigma_{bL} = \frac{M_{77} \pm \sqrt{M_{77}^2 - 4M_{78}}}{2} \quad (25)$$

and the initial hoop stress in the liner at the wrap condition (σ_{oLH}) is

$$\begin{aligned} \sigma_{oLH} = & M_{70} - M_{71} \sigma_{bL} + M_{72} \tan^2 \alpha_o \sigma_{bL}^2 \\ & - M_{72} \sigma_{bL} \sigma_{bLH} + M_{73} \sigma_{bLH} \end{aligned} \quad (26)$$

where the constants M , which do not depend on liner stress, are as follows:

$$\begin{aligned} M_{70} &= \sigma_{oL} \tan^2 \alpha_o \\ M_{71} &= \frac{\sigma_{of}}{\sigma_{fd}} \tan^2 \alpha_o + \frac{2t_L \sigma_{oL}}{p_d a} \tan^2 \alpha_o \\ M_{72} &= \frac{\sigma_{of}}{\sigma_{fd}} \left(\frac{2 t_L}{p_d a} \right) \end{aligned}$$

$$M_{73} = \frac{\sigma_{of}}{\sigma_{fd}} + \frac{2 t_L \sigma_{oL}}{p_d a}$$

$$M_{74} = \frac{\sigma_{fd}}{E_{ft}} - \frac{\sigma_{of}}{E_f} - \alpha_L \Delta T_L + \alpha_f \Delta T_f$$

All other M values in Equations (25) and (26) and the hoop stress in the liner at the design condition (σ_{bL}) depend on the design condition of liner stress relative to the yield stress:

Condition 1: σ_{bL} and $\sigma_{bLH} < \sigma_{yLT}$

$$M_{75} = M_{74} - \frac{\nu_L \sigma_{oL}}{E_L} + \frac{M_{70}}{E_L} - \frac{1}{(1 - \nu_{LT})} \left\{ (1 + \nu_L) M_{74} + \frac{\sigma_{oL}}{E_L} (1 - \nu_L^2) + \frac{M_{73}}{E_L} \left[(1 + \nu_{LT}) E_{LT} M_{74} + \frac{E_{LT}}{E_L} \sigma_{oL} (1 - \nu_L^2) \right] \right\}$$

$$M_{76} = \frac{E_{LT} (1 + \nu_L) M_{74} M_{72}}{E_L (1 - \nu_{LT})} - \frac{(1 + \nu_{LT})}{E_{LT}} + \frac{M_{71}}{E_L} + \frac{E_{LT} \sigma_{oL} (1 - \nu_L^2) M_{72}}{E_L^2 (1 - \nu_{LT})} + \frac{M_{73}}{E_L}$$

$$M_{77} = \frac{E_L M_{76}}{M_{72} (1 + \tan^2 \alpha_o)}$$

$$M_{78} = \frac{E_L M_{75}}{M_{72} (1 + \tan^2 \alpha_o)}$$

$$\sigma_{bLH} = \frac{1}{1 - \nu_{LT}} \left[(1 + \nu_L) E_{LT} M_{74} + \frac{E_{LT} \sigma_{oL} (1 - \nu_L^2)}{E_L} - \sigma_{bL} (1 - \nu_{LT}) \right] \quad (27)$$

Condition 2: $\sigma_{bL} < \sigma_{yLT}$ and $\sigma_{bLH} \geq \sigma_{yLT}$

$$\begin{aligned}
 M_{75} &= M_{74} - \frac{\nu_L \sigma_{oL}}{E_L} + \frac{M_{70}}{E_L} - \frac{(M_{73} E_I - E_L)}{E_L (\frac{1}{2} + \nu_L)} \left[(1 + \nu_L) M_{74} + \frac{\sigma_{oL} (1 - \nu_L^2)}{E_L} \right. \\
 &\quad \left. + \sigma_{yLT} \left(\frac{\nu_{LT}}{E_{LT}} + \frac{1}{2E_I} - \frac{\nu_L}{E_{LT}} + \frac{\nu_L}{E_I} \right) \right] - \sigma_{yLT} \left(\frac{1}{E_{LT}} - \frac{1}{E_I} \right) \\
 M_{76} &= \frac{M_{72} E_I}{E_L (\frac{1}{2} + \nu_L)} \left\{ (1 + \nu_L) M_{74} + \frac{\sigma_{oL} (1 - \nu_L^2)}{E_L} \right. \\
 &\quad \left. + \sigma_{yLT} \left(\frac{\nu_{LT}}{E_{LT}} + \frac{1}{2E_I} - \frac{\nu_L}{E_{LT}} + \frac{\nu_L}{E_I} \right) \right\} + \frac{M_{71}}{E_L} - \frac{\nu_{LT}}{E_{LT}} \\
 &\quad + (M_{73} E_I - E_L) \left[\frac{(1 - \nu_L \nu_{LT})}{E_L E_{LT} (\frac{1}{2} + \nu_L)} \right] \\
 M_{77} &= \frac{E_L E_{LT} (\frac{1}{2} + \nu_L) M_{76}}{M_{72} \left[E_{LT} \tan^2 \alpha_o (\frac{1}{2} + \nu_L) + E_I (1 - \nu_L \nu_{LT}) \right]} \\
 M_{78} &= \frac{E_L E_{LT} (\frac{1}{2} + \nu_L) M_{75}}{M_{72} \left[E_{LT} \tan^2 \alpha_o (\frac{1}{2} + \nu_L) + E_I (1 - \nu_L \nu_{LT}) \right]} \\
 \sigma_{bLH} &= \frac{E_I}{(\frac{1}{2} + \nu_L)} \left[(1 + \nu_L) M_{74} + \frac{\sigma_{oL} (1 - \nu_L^2)}{E_L} \right. \\
 &\quad \left. + \sigma_{yLT} \left(\frac{\nu_{LT}}{E_{LT}} + \frac{1}{2E_I} - \frac{\nu_L}{E_{LT}} + \frac{\nu_L}{E_I} \right) - \frac{\sigma_{bL}}{E_L} (1 - \nu_L \nu_{LT}) \right] \quad (27a)
 \end{aligned}$$

Condition 3: σ_{bL} and $\sigma_{bLH} \geq \sigma_{yLT}$

$$M_{75} = M_{74} - \frac{\nu_L \sigma_{oL}}{E_L} + \frac{M_{70}}{E_L} + \frac{(M_{73} E_I - E_L)}{E_L (\nu_L - \frac{1}{2})} \left\{ (1 + \nu_L) M_{74} + \frac{\sigma_{oL} (1 - \nu_L^2)}{E_L} \right\}$$

$$\begin{aligned}
& - \sigma_{yLT} (1 + \nu_L) \left[\frac{(1 - \nu_{LT})}{E_{LT}} - \frac{1}{2E_I} \right] \left\{ - \sigma_{yLT} \left[\frac{(1 - \nu_{LT})}{E_{LT}} - \frac{1}{2E_I} \right] \right. \\
M_{76} = & \frac{M_{72} E_I}{E_L (\nu_L - \frac{1}{2})} \left\{ (1 + \nu_L) M_{74} + \frac{\sigma_{oL} (1 - \nu_L^2)}{E_L} \right. \\
& - \sigma_{yLT} (1 + \nu_L) \left[\frac{(1 - \nu_{LT})}{E_{LT}} - \frac{1}{2E_I} \right] \left\{ + \frac{M_{71}}{E_L} - \frac{1}{2E_I} \right. \\
& + (M_{73} E_I - E_L) \left[\frac{(1 - \frac{\nu_L}{2})}{E_L E_I (\nu_L - \frac{1}{2})} \right] \\
M_{77} = & \frac{E_L (2 \nu_L - 1) M_{76}}{M_{72} [(2 - \nu_L) + (2 \nu_L - 1) \tan^2 \alpha_o]} \\
M_{78} = & \frac{E_L (2 \nu_L - 1) M_{75}}{M_{72} [(2 - \nu_L) + (2 \nu_L - 1) \tan^2 \alpha_o]} \\
\sigma_{bLH} = & \frac{E_I}{\nu_L - \frac{1}{2}} \left\{ (1 + \nu_L) M_{74} + \frac{\sigma_{oL} (1 - \nu_L^2)}{E_L} \right. \\
& - \sigma_{yLT} (1 + \nu_L) \left[\frac{(1 - \nu_{LT})}{E_{LT}} - \frac{1}{2E_I} \right] - \frac{\sigma_{bL} (1 - \frac{\nu_L}{2})}{E_I} \left. \right\} \quad (27b)
\end{aligned}$$

The remaining variables are again calculated from the remaining equations used in Cases 1 through 4.

B. HEAD DESIGN

The load carried by the filaments at the design pressure is the internal-pressure load minus the load carried by the liner. The liner's meridional load at the design pressure will be constant because of the assumption of constant thickness and constant meridional liner stress. The liner load in

the hoop direction will differ from the load in the meridional direction and will vary along the surface of the head because of differences in load proportionment in the filaments and liner caused by winding-angle variation and components of filament stress.

Using the geometric notation of Figure D-1, the equilibrium equations are

$$N_{\phi} = N_{\phi L} + N_{\phi F} = \frac{pr_2}{2} \quad (28)$$

and

$$N_{\theta} = N_{\theta L} + N_{\theta F} = \frac{pr_2}{2} \left(2 - \frac{r_2}{r_1} \right) \quad (29)$$

The netting analysis, which assumes that the composite loads are all carried by tension in the filaments, requires that

$$\frac{N_{\theta F}}{N_{\phi F}} = \tan^2 \alpha \quad (30)$$

Because the meridional stress in the liner is constant at all points on the contour at the design pressure

$$N_{\phi L} = \sigma_{bLT} t_L = k_1 \frac{p_d a}{2} \quad (31)$$

the liner hoop loads can be expressed as

$$N_{\theta L} = \sigma_{bLHT} t_L = N_{\phi L} + \Delta N_L (1 - \tan^2 \alpha) \quad (31a)$$

where

$$\Delta N_L = \left(\frac{\sigma_{bLH} - \sigma_{bL}}{1 - \tan^2 \alpha_o} \right) t_L \quad (31b)$$

Thus,

$$\tan^2 \alpha = \frac{\frac{r_2}{a} \left(2 - \frac{r_2}{r_1} \right) - k}{\frac{r_2}{a} - k} \quad (32)$$

where

$$k = k_1 + \frac{2\Delta N_L}{p_d a} \quad (32a)$$

The radii of curvature can be expressed in geometric coordinates as*

$$\frac{r_1}{a} = \frac{- \left[1 + (u')^2 \right]^{3/2}}{u''} \quad (33)$$

and

$$\frac{r_2}{a} = \frac{- Z \left[1 + (u')^2 \right]^{1/2}}{u'} \quad (34)$$

where

$$u = \frac{y}{a} \quad (35)$$

and

$$Z = \frac{x}{a} \quad (36)$$

For a geodesic isotenoid** of $D = \frac{x_0}{a}$,

$$\sin \alpha = \frac{x_0}{x} = \frac{D}{Z} \quad (37)$$

*Improved Filament-Wound Construction for Cylindrical Pressure Vessels, Technical Documentary Report ML-TDR-64-43, Vol. I (prepared by Aerojet-General under Contract AF 33(616)-8442), March 1964, p. 13.
 **Ibid., p. 14.

$$\tan^2 \alpha = \frac{\sin^2 \alpha}{\cos^2 \alpha} = \frac{\sin^2 \alpha}{1 - \sin^2 \alpha} = \frac{D^2}{Z^2 - D^2} \quad (38)$$

For in-plane patterns,*

$$\tan \alpha = \frac{\tan \gamma \sin \phi + \cos \phi \cos \theta}{\sin \theta} \quad (39)$$

From Equation (14),

$$r_2 = \frac{-Za}{u'} \left[1 + (u')^2 \right]^{1/2} \quad (34a)$$

From Figure D-1,

$$\sin \phi = -\frac{x}{r_2} = \frac{x u'}{Z a \left[1 + (u')^2 \right]^{1/2}} = \frac{u'}{\left[1 + (u')^2 \right]^{1/2}} \quad (40)$$

$$\tan \phi = \frac{dy}{dx} = \frac{du}{dZ} = u' \quad (41)$$

$$\cos \phi = \frac{\sin \phi}{\tan \phi} = \frac{1}{\left[1 + (u')^2 \right]^{1/2}} \quad (42)$$

Thus Equation (39) becomes

$$\tan \alpha = \frac{\tan \gamma (u') + \cos \theta}{\sin \theta \left[1 + (u')^2 \right]^{1/2}} \quad (39a)$$

$$\tan^2 \alpha = \frac{\left[\tan \gamma (u') + \cos \theta \right]^2}{\sin^2 \theta \left[1 + (u')^2 \right]} \quad (43)$$

* Ibid., p. 16.

From Figure D-2,

$$\cos \theta = \frac{y \tan \gamma + Ca}{x} = \frac{u \tan \gamma + C}{Z} \quad (44)$$

$$\sin \theta = \frac{\left[x^2 - (y \tan \gamma + Ca)^2 \right]^{1/2}}{x} = \frac{\left[Z^2 - (u \tan \gamma + C)^2 \right]^{1/2}}{Z} \quad (45)$$

With

$$u' = \frac{1}{Q}$$

$$\tan^2 \alpha = \frac{\left[\frac{Z}{Q} \tan \gamma + u \tan \gamma + C \right]^2}{\left[Z^2 - (u \tan \gamma + C)^2 \right] \left[1 + \left(\frac{1}{Q} \right)^2 \right]} = \frac{\left[Z \tan \gamma + (u \tan \gamma + C) Q \right]^2}{(1 + Q^2) \left[Z^2 - (u \tan \gamma + C)^2 \right]} \quad (46)$$

Substituting Equations (33) and (34) into Equation (32), the differential equation becomes

$$\tan^2 \alpha = \frac{\frac{-Z \left[1 + (u')^2 \right]^{1/2}}{u'} \left[2 - \frac{Z u''}{u' \left[1 + (u')^2 \right]} \right] - k}{\frac{-Z \left[1 + (u')^2 \right]^{1/2}}{u'} - k} \quad (32a)$$

Setting

$$Q = \frac{1}{u'}$$

then

$$u' = \frac{du}{dZ} = \left(\frac{1}{Q} \right)$$

and

$$u'' = \frac{d(u')}{dZ} = \frac{d}{du} \left(\frac{1}{Q} \right) \frac{du}{dZ} = - \frac{1}{Q^3} \frac{dQ}{du}$$

Thus

$$\tan^2 \alpha = \frac{-ZQ \left[1 + \left(\frac{1}{Q} \right)^2 \right]^{1/2} \left\{ 2 - \frac{\frac{-Z}{Q^3} \frac{dQ}{du}}{\frac{1}{Q} \left[1 + \left(\frac{1}{Q} \right)^2 \right]} \right\} - k}{-ZQ \left[1 + \left(\frac{1}{Q} \right)^2 \right]^{1/2} - k}$$

$$= \frac{Z (Q^2 + 1)^{1/2} \left[2 + \frac{Z \frac{dQ}{du}}{Q^2 + 1} \right] - k}{Z (Q^2 + 1)^{1/2} - k} \quad (32b)$$

Solving for $\frac{dQ}{du}$,

$$\frac{dQ}{du} = \frac{2 (Q^2 + 1)}{Z} \left\{ \frac{\tan^2 \alpha \left[Z (Q^2 + 1)^{1/2} - k \right] + k}{2Z (Q^2 + 1)^{1/2}} - 1 \right\}$$

$$= \frac{2 (Q^2 + 1)}{Z} \left[\frac{-k (\tan^2 \alpha - 1) + Z (Q^2 + 1)^{1/2} (\tan^2 \alpha - 2)}{2Z (Q^2 + 1)^{1/2}} \right]$$

$$= \frac{2 (Q^2 + 1)^{1/2}}{Z} \left[\frac{-k}{2Z} (\tan^2 \alpha - 1) + (Q^2 + 1)^{1/2} (1/2 \tan^2 \alpha - 1) \right] \quad (47)$$

where $\tan^2 \alpha$ is defined by Equations (38) and (46) for the geodesic-isotenoid and in-plane patterns, respectively.

Equation (47) is solved by Runge-Kutta integration using a high-speed digital computer, noting the following boundary conditions at the equator of the head: $Z = 1$, $u = 0$, and $Q = 0$.

Filament-wound pressure vessels contain an inflection point that, for vessels without a load-carrying liner ($k = 0$), occurs at $\alpha = \tan^{-1} \sqrt{2}$.

This inflection, which occurs when Equation (47) changes sign, is also present in the vessel configurations derived for filament-wound vessels with load-carrying liners. As seen in Equation (47), the change in sign occurs at $\alpha = 45^\circ$. Because there is a discontinuity when Equation (47) changes sign and because Equation (47) $\rightarrow \infty$ when $\alpha \rightarrow \pi/2$ or $\theta \rightarrow 0^\circ$, special equations must be written for the last point on the contour ($\alpha = \pi/2$). There are four areas of concern:

1. The in-plane wrap where the next-to-last point is on a sphere (i.e., the point is past the inflection point).
2. The next-to-last point of an in-plane wrap is on the true contour (i.e., the inflection point has not occurred).
3. Equivalent of first area for geodesic isotenoid.
4. Equivalent of second area for geodesic isotenoid.

For cases where $\alpha \rightarrow \pi/2$ as the last point is approached, and since $\alpha \rightarrow \pi/2$, Equation (12) $\rightarrow 0$ and $k = r_2/a$. For this end condition, Equation (12) (substituting $u' = 1/Q$) becomes

$$\frac{r_2}{a} = k = \frac{-Z \left[1 + \left(\frac{1}{Q} \right)^2 \right]^{1/2}}{\left(\frac{1}{Q} \right)} \quad (32c)$$

$$Q = \pm \left(\frac{k^2}{Z^2} - 1 \right)^{1/2} \quad (48)$$

The negative of the square root should be used because Q is negative.

For the first area of concern, Z of the last point equals Z_L , and u of the last point equals u_L :

$$Z_L = u_L \tan \gamma + C \quad (49)$$

If Z_p and u_p are the coordinates of the next-to-last point, the infinite-difference form is

$$\frac{Z_L - Z_p}{u_L - u_p} = Q = \left[\frac{k^2}{\left(\frac{Z_L + Z_p}{2} \right)^2} - 1 \right]^{1/2} \quad (50)$$

Equations (49) and (50) are solved to define Z_L and u_L .

For the condition of an in-plane pattern on a sphere, z_L and u_L are obtained as indicated below. The circular arc is

$$z^2 + (u - s)^2 = \left(\frac{r}{2}\right)^2 \quad (51)$$

where

$$r = r_1 = r_2$$

Thus, at the next-to-last point,

$$s = u_p - \sqrt{\left(\frac{r}{a}\right)^2 - (z_p)^2} \quad (52)$$

The derivative of Equation (51) is

$$2Z \, dZ + 2(u - s) \, dy = 0 \quad (53)$$

Since

$$Q = \frac{dZ}{du}$$

$$Q = - \frac{u - s}{Z} \quad (54)$$

and

$$Q_L = \frac{s - u_L}{Z_L} \quad (54a)$$

where

$$Z_L = u_L \tan \gamma + C \quad (49)$$

For the third area of concern,

$$Z_L = D$$

Thus

$$\frac{D - Z_p}{u_L - u_p} = - \sqrt{\frac{k^2}{\left(\frac{D - Z_p}{2}\right)^2} - 1} \quad (55)$$

where

$$u_L \tan \gamma + C = D \quad (49a)$$

For the final area of concern,

$$Z_L = D$$

Thus

$$u_L \tan \gamma + C = D \quad (49a)$$

and

$$Q_L = \frac{s - u_L}{D}$$

where

$$s = u_p - \left[\left(\frac{r}{a} \right)^2 - (Z_p)^2 \right]^{1/2} \quad (52)$$

The actual solution of the head contour and stresses in a filament-wound pressure vessel with a load-carrying liner is accomplished by the application of the previously derived equations in an order defined by the specific input to a computer.

C. CYLINDER DESIGN

In order for the cylindrical portion of the vessel to complement the head design, stress continuity must be maintained at the junction of the head and cylinder. At the design pressure, Equation (1) defines the equilibrium of forces in the meridional direction of the head at the equator and must also be valid for the longitudinal direction of the cylinder:

$$\sigma_{fd} t_e + \sigma_{bLL} t_L = \frac{p_d a}{2} \quad (1)$$

The load-carrying capability of the hoop composite must be incorporated into the force-equilibrium equation in the hoop direction:

$$\sigma_{fHd} t_H + \sigma_{bLHT} t_L + \sigma_{fd} t_e \tan^2 \alpha_o = p_d a \quad (56)$$

At the design pressure, the hoop filaments are assumed to be at the same stress level as the longitudinal filaments. With this assumption and the previously established liner and composite thicknesses, Equation (56) is used to determine the thickness of the hoop composite:

$$t_H = \frac{1}{\sigma_{fd}} (p_d a - \sigma_{fd} t_e \tan^2 \alpha_o - \sigma_{bLHT} t_L) \quad (57)$$

Equilibrium of forces must also be maintained in the cylinder at the wrapping condition. Continuity requires the same equilibrium of forces in the longitudinal direction of the cylinder as exists in the meridional direction of the head at the equator:

$$\sigma_{of} t_e + \sigma_{oL} t_L = \frac{p_w a}{2} \quad (7)$$

In the hoop direction of the cylinder, the force-equilibrium equation includes the hoop-filament contribution and can be expressed as

$$\sigma_{ofH} t_H + \sigma_{oLHC} t_L + \sigma_{of} t_e \tan^2 \alpha_o = p_w a \quad (58)$$

Liner hoop stress and filament hoop stress are both unknowns in this equation. Because stress continuity in the liner at the junction of the heads with the cylinder is desirable, the hoop stress in the cylindrical portion of the liner is assumed equal to the liner hoop stress at the equator of the head. Equation (58) may now be rewritten so that the hoop-wrap filament stress is expressed as

$$\sigma_{ofH} = \frac{1}{t_H} (p_w a - \sigma_{of} t_e \tan^2 \alpha_o - \sigma_{oLH} t_L) \quad (59)$$

D. STRUCTURAL ANALYSIS

For the structural analysis of filament-reinforced pressure vessels with load-carrying liners, compatibility is controlled in the meridional direction only in the head and in the hoop and longitudinal directions in the cylinder.

1. Equilibrium of Forces at p_N , T_{NL} , and T_{NF}

Meridional Direction

$$\sigma_{Nf_x} t_{e_x} + \sigma_{NL_x} t_L = \frac{p_N r_2}{2} \quad (60)$$

Hoop Direction

$$\sigma_{Nf_x} t_{e_x} \tan^2 \alpha + \sigma_{NLH_x} t_L + \sigma_{NfH} t_H = \frac{P_N r_2}{2} \left(2 - \frac{r_2}{r_1} \right) \quad (61)$$

2. Compatibility of Strains from Condition "OLD" to Condition "N"

Longitudinal or Meridional Direction

$$\begin{aligned} \frac{\sigma_{Nf_x}}{E_{Nf}} - \frac{\sigma_{OLDf}}{E_{OLDf}} + \alpha_f \Delta T_f &= e_{tL_x} - \frac{1}{E_{OLDL}} (\sigma_{OLDL_H} - \nu_{oL} \sigma_{OLDH_x}) \\ &+ \alpha_L \Delta T_L \end{aligned} \quad (62)$$

Hoop Direction (Cylinder Only)

$$\begin{aligned} \frac{\sigma_{NfH_x}}{E_{Nf}} - \frac{\sigma_{OLDfH_x}}{E_{OLDf}} + \alpha_f \Delta T_f &= e_{tLH_x} \\ &- \frac{1}{E_{OLDL}} (\sigma_{OLDL_x} - \nu_{oL} \sigma_{OLDH_x}) \end{aligned} \quad (63)$$

where

e_{tL_x} and e_{tLH_x} are computed as follows:

Condition 1: $\sigma_{NL_x} < \sigma_{NyL_x}$ and $\sigma_{NLH_x} < \sigma_{NyLH_x}$

$$e_{tL_x} = \frac{1}{E_{NL}} (\sigma_{NL_x} - \nu_{NL} \sigma_{NLH_x})$$

$$e_{tLH_x} = \frac{1}{E_{NL}} (\sigma_{NLH_x} - \nu_{NL} \sigma_{NL_x})$$

Condition 2: $\sigma_{NL_x} < \sigma_{NyL_x}$ and $\sigma_{NLH_x} \geq \sigma_{NyLH_x}$

$$e_{tL_x} = \frac{\sigma_{NL_x}}{E_{NL}} - \frac{\sigma_{NLH_x}}{2E_{N1}} + \sigma_{NyLH_x} \left[\frac{1}{2E_{N1}} - \frac{\nu_{NL}}{E_{NL}} \right]$$

$$e_{tLH_x} = \frac{\sigma_{NLH_x}}{E_{N1}} - \frac{\nu_{NL} \sigma_{NL_x}}{E_{NL}} + \sigma_{NyLH_x} \left[\frac{1}{E_{N1}} - \frac{1}{E_{NL}} \right]$$

Condition 3: $\sigma_{NL_x} \geq \sigma_{NyL_x}$ and $\sigma_{NLH_x} \geq \sigma_{NyLH_x}$

$$e_{tL_x} = \frac{\sigma_{NL_x}}{E_{N1}} - \frac{\sigma_{NLH_x}}{2E_{N1}} + \sigma_{NyLH_x} \left[\frac{1}{2E_{N1}} - \frac{\nu_{NL}}{E_{NL}} \right]$$

$$- \sigma_{NyL_x} \left[\frac{1}{E_{N1}} - \frac{1}{E_{NL}} \right]$$

$$e_{tLH_x} = \frac{\sigma_{NLH_x}}{E_{N1}} - \frac{\sigma_{NL_x}}{2E_{N1}} + \sigma_{NyL_x} \left[\frac{1}{2E_{N1}} - \frac{\nu_{NL}}{E_{NL}} \right]$$

$$- \sigma_{NyLH_x} \left[\frac{1}{E_{N1}} - \frac{1}{E_{NL}} \right]$$

Condition 4: $\sigma_{NL_x} \geq \sigma_{NyL_x}$ and $\sigma_{NLH_x} < \sigma_{NyLH_x}$

$$e_{tL_x} = \frac{\sigma_{NL_x}}{E_{N1}} - \frac{\nu_{NL} \sigma_{NLH_x}}{E_{NL}} - \sigma_{NyL_x} \left[\frac{1}{E_{N1}} - \frac{1}{E_{NL}} \right]$$

$$e_{tLH_x} = \frac{\sigma_{NLH_x}}{E_{NL}} - \frac{\sigma_{NL_x}}{2E_{N1}} + \sigma_{NyL_x} \left[\frac{1}{2E_{N1}} - \frac{\nu_{NL}}{E_{NL}} \right]$$

3. Solution of Equations

Simultaneous solution of Equations (62) and (63), subject to each condition, produces the required N filament stresses in terms of material and geometry constants. Generally, the equations can be written as follows:

$$\sigma_{Nf_x} = \frac{M_{32} + \frac{M_{36}}{M_{34}} M_{33}}{M_{31} - \frac{M_{36}}{M_{34}} M_{35}} \quad (64)$$

$$\sigma_{NfH_x} = \frac{M_{33} + M_{35} \sigma_{Nf_x}}{M_{34}} \quad (65)$$

*The constants (M_n) are evaluated differently, depending on the state of elasticity (i.e., which condition prevails).

Special considerations for heads and cylinders are as follows:
 For heads, $M_{33} = M_{35} = M_{36} = 0$, and $M_{34} = 1.0$, $t_H = 0$; and for cylinders,
 $r_2/r_1 = 0$.

All other constants depend upon whether the liner stresses exceed the yield or not:

Condition 1: $\sigma_{NL_x} < \sigma_{NyL_x}$ and $\sigma_{NLH_x} < \sigma_{NyLH_x}$

$$M_{31} = 1 + \frac{E_{Nf}}{E_{NL}} \left(\frac{t_e}{t_L} \right) - \frac{E_{Nf}}{E_{NL}} \nu_{NL} \left(\frac{t_e}{t_L} \right) \tan^2 \alpha$$

$$M_{32} = \frac{E_{Nf}}{E_{NL}} \left(\frac{p_N r_2}{2 t_L} \right) \left[1 - \nu_{NL} \left(2 - \frac{r_2}{r_1} \right) \right]$$

$$- \frac{E_{Nf}}{E_{OLDL}} \left[\sigma_{OLDL_x} - \nu_{OL} \sigma_{OLDH_x} \right] + E_{Nf} \left[\alpha_L \Delta T_L - \alpha_f \Delta T_f \right]$$

$$+ \frac{E_{Nf}}{E_{OLDf}} \sigma_{OLDf_x}$$

For cylinder only,

$$M_{33} = \frac{E_{Nf}}{E_{NL}} \left(\frac{p_N r_2}{t_L} \right) \left(1 - \frac{\nu_{NL}}{2} \right) - \frac{E_{Nf}}{E_{OLDL}} \left[\sigma_{OLDH} - \nu_{OL} \sigma_{OLDL} \right]$$

$$+ E_{Nf} \left[\alpha_L \Delta T_L - \alpha_f \Delta T_f \right] + \frac{E_{Nf}}{E_{OLDf}} \sigma_{OLDfH}$$

$$M_{34} = 1 + \frac{E_{Nf}}{E_{NL}} \left(\frac{t_H}{t_L} \right)$$

$$M_{35} = \left(\frac{t_e}{t_L} \right) \frac{E_{Nf}}{E_{NL}} \left[\nu_{NL} - \tan^2 \alpha \right]$$

$$M_{36} = \nu_{NL} \left(\frac{t_H}{t_L} \right) \frac{E_{Nf}}{E_{NL}}$$

Condition 2: $\sigma_{NL_x} < \sigma_{NyL_x}$ and $\sigma_{NLH_x} \geq \sigma_{NyLH_x}$

$$M_{31} = 1 + \frac{E_{Nf}}{E_{NL}} \left(\frac{t_{ex}}{t_L} \right) - \frac{E_{Nf}}{2E_{N1}} \left(\frac{t_{ex}}{t_L} \right) \tan^2 \alpha$$

$$M_{32} = \frac{E_{Nf}}{E_{NL}} \left(\frac{p_N r_2}{2t_L} \right) - \frac{E_{Nf}}{2E_{N1}} \left(\frac{p_N r_2}{2t_L} \right) \left(2 - \frac{r_2}{r_1} \right)$$

$$\begin{aligned} & - \frac{E_{Nf}}{E_{OLDL}} \left[\sigma_{OLDL_x} - \nu_{oL} \sigma_{OLDH_x} \right] + \sigma_{NyLH_x} \left[\frac{E_{Nf}}{2E_{N1}} - \frac{\nu_{NL} E_{Nf}}{E_{NL}} \right] \\ & + E_{Nf} \left[\alpha_L \Delta T_L - \alpha_f \Delta T_f \right] + \frac{E_{Nf}}{E_{OLDf}} \sigma_{OLDf_x} \end{aligned}$$

For cylinder only,

$$M_{33} = \frac{E_{Nf}}{E_{N1}} \left(\frac{p_N r_2}{t_L} \right) - \frac{\nu_{NL} E_{Nf}}{E_{NL}} \left(\frac{p_N r_2}{2t_L} \right)$$

$$\begin{aligned} & - \sigma_{NyLH} \left[\frac{E_{Nf}}{E_{N1}} - \frac{E_{Nf}}{E_{NL}} \right] - \frac{E_{Nf}}{E_{OLDL}} \left[\sigma_{OLDH} - \nu_{oL} \sigma_{OLDL} \right] + E_{Nf} \left[\alpha_L \Delta T_L - \alpha_f \Delta T_f \right] \\ & + \frac{E_{Nf}}{E_{OLDf}} \sigma_{OLDfH} \end{aligned}$$

$$M_{34} = 1 + \frac{E_{Nf}}{E_{N1}} \left(\frac{t_H}{t_L} \right)$$

$$M_{35} = \left(\frac{t_e}{t_L} \right) \left[\frac{\nu_{NL} E_{Nf}}{E_{NL}} - \frac{E_{Nf} \tan^2 \alpha}{E_{N1}} \right]$$

$$M_{36} = \frac{E_{Nf}}{2E_{N1}} \left(\frac{t_H}{t_L} \right)$$

Condition 3: $\sigma_{NL_x} \geq \sigma_{NyL_x}$ and $\sigma_{NLH_x} \geq \sigma_{NyLH_x}$

$$M_{31} = 1 + \frac{E_{Nf}}{E_{N1}} \left(\frac{t_{ex}}{t_L} \right) - \frac{E_{Nf}}{2E_{N1}} \left(\frac{t_{ex}}{t_L} \right) \tan^2 \alpha$$

$$\begin{aligned}
M_{32} = & \frac{E_{Nf}}{E_{N1}} \left(\frac{p_N r_2}{2t_L} \right) \left(\frac{r_2}{2r_1} \right) + \sigma_{NyLH_x} \left[\frac{E_{Nf}}{2E_{N1}} - \frac{E_{Nf}}{E_{NL}} \nu_{NL} \right] + \sigma_{NyL_x} \\
& \left[\frac{E_{Nf}}{E_{NL}} - \frac{E_{Nf}}{E_{N1}} \right] + E_{Nf} \left[\alpha_L \Delta T_L - \alpha_f \Delta T_f \right] - \frac{E_{Nf}}{E_{OLDL}} \left[\sigma_{OLDL_x} - \nu_{oL} \sigma_{OLDH_x} \right] \\
& + \frac{E_{Nf}}{E_{OLDf}} \sigma_{OLDf_x}
\end{aligned}$$

For cylinder only,

$$\begin{aligned}
M_{33} = & \frac{3E_{Nf}}{4E_{N1}} \left(\frac{p_N r_2}{t_L} \right) - \sigma_{NyLH} \left[\frac{E_{Nf}}{E_{N1}} - \frac{E_{Nf}}{E_{NL}} \right] \\
& + \sigma_{NyL} \left[\frac{E_{Nf}}{2E_{N1}} - \frac{\nu_{NL} E_{Nf}}{E_{NL}} \right] - \frac{E_{Nf}}{E_{OLDL}} \left[\sigma_{OLDH} - \nu_{oL} \sigma_{OLDL} \right] + E_{Nf} \\
& \left[\alpha_L \Delta T_L - \alpha_f \Delta T_f \right] + \frac{E_{Nf}}{E_{OLDf}} \sigma_{OLDfH} \\
M_{34} = & 1 + \frac{E_{Nf}}{E_{N1}} \left(\frac{t_H}{t_L} \right) \\
M_{35} = & \left(\frac{t_e}{t_L} \right) \frac{E_{Nf}}{E_{N1}} \left[\frac{1}{2} - \tan^2 \alpha \right] \\
M_{36} = & \frac{E_{Nf}}{2E_{N1}} \left(\frac{t_H}{t_L} \right)
\end{aligned}$$

Condition 4: $\sigma_{NL_x} \geq \sigma_{NyL_x}$ and $\sigma_{NLH_x} < \sigma_{NyLH_x}$

$$M_{31} = 1 + \frac{E_{Nf}}{E_{N1}} \left(\frac{t_e}{t_L} \right) - \frac{\nu_{NL} E_{Nf}}{E_{NL}} \left(\frac{t_e}{t_L} \right) \tan^2 \alpha$$

$$\begin{aligned}
M_{32} &= \frac{E_{Nf}}{E_{N1}} \left(\frac{p_N r_2}{2t_L} \right) - \frac{E_{Nf} \nu_{NL}}{E_{NL}} \left(\frac{p_N r_2}{2t_L} \right) \left(2 - \frac{r_2}{r_1} \right) \\
&+ \sigma_{NyL_x} \left[\frac{E_{Nf}}{E_{NL}} - \frac{E_{Nf}}{E_{N1}} \right] - \frac{E_{Nf}}{E_{OLDL}} \left[\sigma_{OLDL_x} - \nu_{oL} \sigma_{OLDH_x} \right] \\
&+ E_{Nf} \left[\alpha_L \Delta T_L - \alpha_f \Delta T_f \right] + \frac{E_{Nf}}{E_{OLDf}} \sigma_{OLDf_x}
\end{aligned}$$

For cylinder only,

$$\begin{aligned}
M_{33} &= \frac{E_{Nf}}{E_{NL}} \left(\frac{p_N r_2}{2t_L} \right) \left(2 - \frac{r_2}{r_1} \right) - \frac{E_{Nf}}{2E_{N1}} \left(\frac{p_N r_2}{2t_L} \right) + \sigma_{NyL} \left[\frac{E_{Nf}}{2E_{N1}} - \frac{E_{Nf} \nu_{NL}}{E_{NL}} \right] \\
&- \frac{E_{Nf}}{E_{OLDL}} \left[\sigma_{OLDH} - \nu_{oL} \sigma_{OLDL} \right] + E_{Nf} \left[\alpha_L \Delta T_L - \alpha_f \Delta T_f \right] \\
&+ \frac{E_{Nf}}{E_{OLDf}} \sigma_{OLDfH}
\end{aligned}$$

$$M_{34} = 1 + \frac{E_{Nf}}{E_{NL}} \left(\frac{t_H}{t_L} \right)$$

$$M_{35} = \left(\frac{t_e}{t_L} \right) \left[\frac{E_{Nf}}{2E_{N1}} - \frac{E_{Nf} \tan^2 \alpha}{E_{NL}} \right]$$

$$M_{36} = \frac{E_{Nf} \nu_{NL}}{E_{NL}} \left(\frac{t_H}{t_L} \right)$$

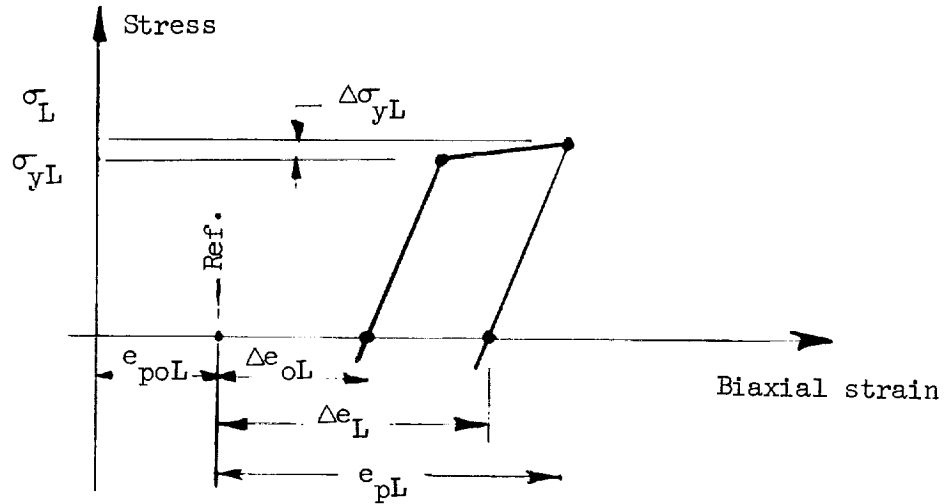
Once the filament stresses are known, the liner stresses can be determined from Equations (60) and (61):

$$\sigma_{NL_x} = \frac{p_N r_2}{2t_L} - \frac{t_e \sigma_{Nf_x}}{t_L} \quad (60a)$$

$$\sigma_{NLH_x} = \frac{p_N r_2}{2t_L} \left(2 - \frac{r_2}{r_1}\right) - \frac{t_e \sigma_{Nf_x} \tan^2 \alpha}{t_L} + \frac{t_H \sigma_{NfH_x}}{t_L} \quad (61a)$$

4. Strains

The total biaxial strain of the metal shell in either direction has three components: elastic, plastic, and thermal strains. The elastic and plastic portions are further complicated by the influence of Poisson's effect. When these considerations are combined, four stress-field-dependent conditions may exist for the calculation of total strain. A generalization of the method presented in Section II,A,1 will be used to provide equations for the calculation of metal-shell biaxial strains for any stress field. All metal-shell strains are referred to the initial zero-strain condition as shown in the simplified sketch below.



Condition 1: $\sigma_L < \sigma_{yL}$ and $\sigma_{LH} < \sigma_{yLH}$

The total biaxial strains in the meridional and hoop directions are

$$e_{pL} = \frac{\sigma_L}{E_L} - \nu_L \frac{\sigma_{LH}}{E_L} + \alpha_L \Delta T_L - e_{poL} + \Delta e_{oL} \quad (66)$$

$$e_{pLH} = \frac{\sigma_{LH}}{E_L} - \nu_L \frac{\sigma_L}{E_L} + \alpha_L \Delta T_L - e_{poLH} + \Delta e_{oLH} \quad (67)$$

The changes in yield stresses are

$$\Delta\sigma_{yL} = 0.0 \quad (68)$$

$$\Delta\sigma_{yLH} = 0.0 \quad (69)$$

The plastic sets are

$$\Delta e_L = \Delta e_{oL} \quad (70)$$

$$\Delta e_{LH} = \Delta e_{oLH} \quad (71)$$

Condition 2: $\sigma_{LH} > \sigma_{yLH}$ and $\sigma_L \leq \sigma_{yL}$

The total biaxial strains in the meridional and hoop directions are

$$e_{pL} = \frac{\sigma_L}{E_L} - \left(\frac{1}{2}\right) \frac{\sigma_{LH}}{E_I} + \sigma_{yLH} \left(\frac{1}{2E_I} - \frac{\nu_L}{E_L} \right) + \alpha_L \Delta T_L - e_{poL} + \Delta e_{oL} \quad (66a)$$

$$e_{pLH} = \frac{\sigma_{LH}}{E_I} - \frac{\nu_L}{E_L} \sigma_L + \sigma_{yLH} \left(\frac{1}{E_L} - \frac{1}{E_I} \right) + \alpha_L \Delta T_L - e_{poLH} + \Delta e_{oLH} \quad (67a)$$

The changes in yield stresses are

$$\Delta\sigma_{yL} = 0.0 \quad (68a)$$

$$\Delta\sigma_{yLH} = \sigma_{LH} - \sigma_{yLH} \quad (69a)$$

The plastic sets are

$$\Delta e_L = \left(\frac{\nu_L}{E_L} - \frac{1}{2E_I} \right) \Delta\sigma_{yLH} + \Delta e_{oL} \quad (70a)$$

$$\Delta e_{LH} = \left(\frac{1}{E_I} - \frac{1}{E_L} \right) \Delta\sigma_{yLH} + \Delta e_{oL} \quad (71a)$$

Condition 3: $\sigma_L > \sigma_{yL}$ and $\sigma_{LH} > \sigma_{yLH}$

The total biaxial strains in the meridional and hoop directions are

$$e_{pL} = \frac{\sigma_L}{E_I} - \frac{\sigma_{LH}}{2E_I} + \sigma_{yL} \left(\frac{1}{E_L} - \frac{1}{E_I} \right) - \sigma_{yLH} \left(\frac{\nu_L}{E_L} - \frac{1}{2E_I} \right) + \alpha_L \Delta T_L - e_{poL} + \Delta e_{oL} \quad (66b)$$

$$e_{pLH} = \frac{\sigma_{LH}}{E_I} - \frac{\sigma_L}{2E_I} + \sigma_{yLH} \left(\frac{1}{E_L} - \frac{1}{E_I} \right) - \sigma_{yL} \left(\frac{\nu_L}{E_L} - \frac{1}{2E_I} \right) + \alpha_L \Delta T_L - e_{poLH} + \Delta e_{oLH} \quad (67b)$$

The changes in yield stresses are

$$\Delta \sigma_{yL} = \sigma_L - \sigma_{yL} \quad (68b)$$

$$\Delta \sigma_{yLH} = \sigma_{LH} - \sigma_{yLH} \quad (69b)$$

The plastic sets are

$$\Delta e_L = \Delta \sigma_{yL} \left(\frac{1}{E_I} - \frac{1}{E_L} \right) + \Delta \sigma_{yLH} \left(\frac{\nu_L}{E_L} - \frac{1}{2E_I} \right) + \Delta e_{oL} \quad (70b)$$

$$\Delta e_{LH} = \Delta \sigma_{yLH} \left(\frac{1}{E_I} - \frac{1}{E_L} \right) + \Delta \sigma_{yL} \left(\frac{\nu_L}{E_L} - \frac{1}{2E_I} \right) + \Delta e_{oLH} \quad (71b)$$

Condition 4: $\sigma_L > \sigma_{yL}$ and $\sigma_{LH} \leq \sigma_{yLH}$

The total biaxial strains in the meridional and hoop directions are

$$e_{pL} = \frac{\sigma_L}{E_I} - \frac{\nu_L}{E_L} \sigma_{LH} + \sigma_{yL} \left(\frac{1}{E_L} - \frac{1}{E_I} \right) + \alpha_L \Delta T_L - e_{poL} + \Delta e_{oL} \quad (66c)$$

$$e_{pLH} = \frac{\sigma_{LH}}{E_L} - \left(\frac{1}{2} \right) \frac{\sigma_L}{E_I} + \sigma_{yL} \left(\frac{1}{2E_I} - \frac{\nu_L}{E_L} \right) + \alpha_L \Delta T_L - e_{poLH} + \Delta e_{oLH} \quad (67c)$$

The changes in yield stresses are

$$\Delta \sigma_{yL} = \sigma_L - \sigma_{yL} \quad (68c)$$

$$\Delta \sigma_{yLH} = 0.0 \quad (69c)$$

The plastic sets are

$$\Delta e_L = \left(\frac{1}{E_I} - \frac{1}{E_L} \right) \Delta \sigma_{yL} + \Delta e_{oL} \quad (70c)$$

$$\Delta e_{LH} = \left(\frac{\nu_L}{E_L} - \frac{1}{2E_I} \right) \Delta \sigma_{yL} + \Delta e_{oLH} \quad (71c)$$

E. VESSEL CHARACTERISTICS

1. Arc Length

The length of the filament path over each head is

$$S_H = \sum^n \Delta S_H \quad (72)$$

where

$$\Delta S_H = \frac{\Delta y}{\sin \phi_n \cos \alpha_n} \quad \text{for } \phi > 45^\circ$$

$$\Delta S_H = \frac{x_{n-1} \Delta \theta}{\sin \alpha_n} \quad \text{for } \phi \leq 45^\circ$$

For one pass along the cylinder,

$$S_c = \frac{(CYL)}{\cos \alpha_o} \quad (73)$$

The total arc length for the vessel is

$$S_T = S_c + S_{H_1} + S_{H_2} \quad (74)$$

2. Surface Area

The middle surface of the longitudinal composite is used to represent the head surface area. The total surface area for each head, including the port area, is

$$A_H = \pi x_o^2 + 2\pi \sum^n \bar{x}_n \sqrt{\Delta x^2 + \Delta y^2} \quad (75)$$

The surface area of the cylinder, referenced to the midplane of the longitudinal composite, is

$$A_c = 2\pi a (CYL) \quad (76)$$

and the total surface area of the vessel is

$$A_T = A_c + A_{H_1} + A_{H_2} \quad (77)$$

3. Weight

The total weight of the vessel is found by summation of the volume-density products of the materials of construction. The weight of hardware has been neglected so that total weight is given by

$$W_T = \rho_L V_L + \rho_g V_c \quad (78)$$

For each head, the filament-composite volume is

$$V_C = 2\pi a t_o \cos \alpha_o S_H \quad (79)$$

where S_H was found from previous calculations. The volume of liner for each head is approximately equal to the product of surface area and thickness. The surface area, however, is calculated at the middle surface of the longitudinal wrap. A second-order approximation would correct this area by the factor

$$\left[\frac{a - \left(\frac{t_o + t_L}{2} \right)}{a} \right]^2$$

Because the wrap thickness varies and is always $\geq t_o$, this factor will still overestimate the volume of the liner. An "exact" (numerical) calculation produces difficulties near the port, where the filament-composite thickness becomes extremely large. The following approximation is therefore used:

$$V_{LH} = t_L (A_H - \pi x_o^2) \left[\frac{a - \left(\frac{t_o}{2} + t_L \right)}{a} \right]^2 \quad (80)$$

The cylinder-liner volume is calculated as follows:

$$V_{LC} = 2\pi(CYL)t_L \left(a - \frac{t_o + t_L}{2} \right) \quad (81)$$

and similarly, the filament-composite volume, which includes the hoop and longitudinal wraps, is

$$V_{CC} = 2\pi(CYL) (t_o + t_{HC}) (a + \frac{t_{HC}}{2}) \quad (82)$$

Thus, the total weight of the vessel is

$$W_T = \rho_L (V_{LH_1} + V_{LH_2} + V_{LC}) + \rho_g (V_{C_1} + V_{C_2} + V_{CC}) \quad (78a)$$

4. Internal Volume

The internal volume of each head referenced to the middle surface is

$$V_{oL} = \pi x_o^2 y_o + \sum^n 2\pi \bar{x} \bar{y} \Delta x \quad (83)$$

This volume is corrected by subtracting half the filament-composite volume and the liner volume to give the volume available for fluid storage:

$$V_H = V_{oL} - (\frac{1}{2} V_C + V_{LH}) \quad (84)$$

The contained volume of the cylinder is

$$V_{CYL} = \pi(CYL)(a - \frac{t_o}{2} - t_L)^2 \quad (85)$$

and the total available volume is

$$V_T = V_{H_1} + V_{H_2} + V_{CYL} \quad (86)$$

5. Performance Factor

The efficiency of the complete pressure vessel is represented by the performance factor

$$\frac{p_d V_T}{W_T} \quad (87)$$

where p_d is the pressure at which the vessel was designed.

III. CONCLUSIONS

A. LIMITATIONS OF ANALYSIS

The analysis presented in this appendix can be applied to any filament-reinforced, lined pressure vessel with the following restrictions:

1. The only applied load is a constant internal pressure.
2. The liner has a constant, finite thickness.
3. The stress-strain curve of the filaments can be described by a straight line.
4. The stress-strain curve of the liner can be described by one or two straight lines with slopes representing primary and secondary moduli.
5. The winding pattern is on either a geodesic path or a planar path.
6. The tensile modulus of the resin must be small in comparison with the filament tensile modulus.
7. The maximum strains in the vessel are small; it is suggested that they be less than 5%.
8. The wrap angle must be greater than zero; this requires that the bosses have finite diameters.
9. No temperature gradient exists in either the composite or liner.
10. Changes in temperature and pressure must be analyzed separately if the liner is not in the elastic range.

The analysis assumes that the liner and composite react to membrane loads only. Discontinuities in the vicinity of bosses are not considered. This assumption is consistent with previous composite-pressure-vessel data indicating that the composite in the vicinity of the small bosses (less than 20% of the case diameter) has a higher margin of safety than other areas of the head.

B. FUTURE EXTENSIONS OF ANALYSIS

Advanced design analyses of filament-reinforced pressure vessels with load-carrying liners can be based on the approach presented, with the following possible variations:

1. The liner thickness varies in some set pattern (e.g., thickness is a function of radial position or of the wrap angle at a point).

2. The stress-strain curve of the liner is expressed as an equation rather than two straight lines.

3. Attachment and acceleration loads can be included as well as pressure.

SYMBOLS

	Definition	Units
A_c	Surface area of cylindrical section	in. ²
A_H	Surface area of head	in. ²
A_T	Total surface area of vessel	in. ²
a	Radius of vessel at equator	in.
C	Distance from vessel axis to intersection of wrap plane with equator divided by radius a	-
CYL	Length of cylindrical section	in.
D	Boss radius divided by radius a	-
E_f	Elastic modulus of filaments at room temperature	lb/in. ²
E_{fT}	Elastic modulus of filaments at design temperature	lb/in. ²
E_I	Plastic modulus of liner at room temperature	lb/in. ²
E_{IT}	Plastic modulus of liner at design temperature	lb/in. ²
E_L	Elastic modulus of liner at room temperature	lb/in. ²
E_{LT}	Elastic modulus of liner at design temperature	lb/in. ²
E_{Nf}	Elastic modulus of filaments at condition "N"	lb/in. ²
E_{NL}	Elastic modulus of liner at condition "N"	lb/in. ²
E_{OLDf}	Elastic modulus of filaments at condition "OLD"	lb/in. ²
E_{OLDL}	Elastic modulus of liner at condition "OLD"	lb/in. ²
e_{bL}	Design strain of liner (uniaxial) in longitudinal direction	in./in.
e_{bLH}	Design strain of liner (uniaxial) in hoop direction	in./in.
e_E	Elastic strain	in./in.
e_p	Plastic strain	in./in.
e_{pL}	Liner biaxial strain in longitudinal direction	in./in.
e_{pLH}	Liner biaxial strain in hoop direction	in./in.
e_{poL}	Zero strain base for liner, relative to filaments, in longitudinal direction	in./in.
e_{poLH}	Zero strain base for liner, relative to filaments, in hoop direction	in./in.
e_{tL}	Total positive liner strain including Poisson's effect in meridional direction	in./in.
e_{tLH}	Total positive liner strain including Poisson's effect in hoop direction	in./in.

SYMBOLS (cont.)

	Definition	Units
K	Filament fraction in composite	-
k	Defined by Equation (32a)	-
k_l	Fraction of load taken by liner	-
N_θ	Circumferential force per unit of width	lb/in.
$N_{\theta f}$	Circumferential force per unit of width in filaments	lb/in.
$N_{\theta L}$	Circumferential force per unit of width in liner	lb/in.
N_ϕ	Meridional force per unit of width	lb/in.
$N_{\phi f}$	Meridional force per unit of width in filaments	lb/in.
$N_{\phi L}$	Meridional force per unit of width in liner	lb/in.
n	As subscript, evaluated at nth point	-
p	Pressure	lb/in. ²
p_d	Design pressure	lb/in. ²
p_N	Condition "N" pressure	lb/in. ²
p_w	Winding pressure	lb/in. ²
Q	Inverse derivative of u with respect to Z	-
Q_L	Inverse derivative of u with respect to Z at $x = x_0$	-
r	Radius	in.
r_l	Meridional radius of curvature	in.
$r_{l,0}$	Meridional radius of curvature at equator	in.
r_2	Circumferential radius of curvature	in.
S_c	Filament arc length over cylindrical section	in.
S_H	Filament arc length over head	in.
S_T	Total filament arc length	in.
s	Normalized distance to center of spherical close-off dome	-
T_d	Design temperature	°F
T_{df}	Design temperature of filaments	°F
T_{dL}	Design temperature of liner	°F
T_R	Room temperature, RT	°F
t_e	Equivalent filament thickness in meridional direction	in.
t_H	Equivalent hoop-filament thickness	in.

SYMBOLS (cont.)

	Definition	Units
t_{HC}	Hoop-composite thickness	in.
t_L	Liner thickness	in.
t_o	Composite thickness at equator	in.
u	Axial coordinate, y/a	-
u_L	Axial coordinate at $x = x_o$	-
u_p	Axial coordinate of next-to-last point on head contour	-
u'	First derivative of u with respect to Z	-
u''	Second derivative of u with respect to Z	-
V_C	Volume of filament-composite material in head	in. ³
V_{CC}	Total volume of filament-composite material in cylindrical section	in. ³
V_{CYL}	Contained volume of cylindrical section	in. ³
V_H	Contained volume of head	in. ³
V_L	Total volume of liner material	in. ³
V_{LC}	Volume of liner material in cylindrical section	in. ³
V_{LH}	Volume of liner material in head	in. ³
V_{oL}	Internal volume of head referred to middle surface	in. ³
V_T	Total contained volume of vessel	in. ³
W_T	Total vessel weight	lb
x	Radial coordinate (used as subscript, indicates evaluated at point x)	in.
x_o	Boss radius	in.
\bar{x}	Average radial distance	in.
y	Axial coordinate	in.
y_o	Axial coordinate at $x = x_o$	in.
\bar{y}	Average axial distance	in.
Z	Radial coordinate, x/a	-
Z_L	Radial coordinate at $x = x_o$	-
Z_p	Radial coordinate of next-to-last point on head contour	-
1	As subscript, refers to Head No. 1	-
2	As subscript, refers to Head No. 2	-

SYMBOLS (cont.)

	Definition	Units
α	Angle between meridian and filament	degrees
α_f	Coefficient of thermal expansion, composite	in./in.-°F
α_L	Coefficient of thermal expansion, liner	in./in.-°F
α_o	Angle between meridian and filament at equator of head	degrees
γ	Angle between wrap plane and axis of vessel	degrees
Δ	Finite change	-
Δe_L	Increment of liner plastic set in longitudinal direction	in./in.
Δe_{LH}	Increment of liner plastic set in hoop direction	in./in.
Δe_{oL}	Change in liner zero strain base in longitudinal direction	in./in.
Δe_{oLH}	Change in liner zero strain base in hoop direction	in./in.
θ	Polar angle	degrees
ν_L	Poisson's ratio of liner at room temperature	-
ν_{LT}	Poisson's ratio of liner at given temperature	-
ν_{NL}	Poisson's ratio of liner at condition "N"	-
ν_{oL}	Poisson's ratio of liner at condition "OLD"	-
ρ_g	Density of filament composite	lb/in. ³
ρ_L	Density of liner	lb/in. ³
σ_{bLHT}	Design stress in liner (hoop)	lb/in. ²
σ_{bLT}	Design stress in liner (meridian)	lb/in. ²
σ_{fd}	Design stress in longitudinal filament	lb/in. ²
σ_{fHd}	Design stress in hoop filament	lb/in. ²
σ_L	Longitudinal stress in liner	lb/in. ²
σ_{LH}	Hoop stress in liner	lb/in. ²
σ_{Nf}	Longitudinal-filament stress at condition "N"	lb/in. ²
σ_{NfH}	Hoop-filament stress at condition "N"	lb/in. ²
σ_{NL}	Liner stress in longitudinal direction at condition "N"	lb/in. ²
σ_{NLH}	Liner stress in hoop direction at condition "N"	lb/in. ²
σ_{NyL}	Liner yield stress in longitudinal direction at condition "N"	lb/in. ²
σ_{NyLH}	Liner yield stress in hoop direction at Condition "N"	lb/in. ²

SYMBOLS (cont.)

	Definition	Units
σ_{of}	Longitudinal-filament stress due to winding pressure at room temperature	lb/in. ²
σ_{ofH}	Hoop-filament stress due to winding pressure at room temperature	lb/in. ²
σ_{ofT}	Filament stress at zero pressure and design temperature	lb/in. ²
σ_{oL}	Liner stress due to winding pressure at room temperature (meridian)	lb/in. ²
σ_{OLDf}	Longitudinal-filament stress at condition "OLD"	lb/in. ²
σ_{OLDfH}	Hoop-filament stress at condition "OLD"	lb/in. ²
σ_{OLDH}	Liner stress in hoop direction at condition "OLD"	lb/in. ²
σ_{OLDL}	Liner stress in longitudinal direction at condition "OLD"	lb/in. ²
σ_{oLH}	Liner stress due to winding pressure at room temperature (hoop)	lb/in. ²
σ_{oLHC}	Liner hoop stress in cylinder due to winding pressure at room temperature	lb/in. ²
σ_{oLHT}	Liner stress at zero pressure and design temperature (hoop)	lb/in. ²
σ_{oLT}	Liner stress at zero pressure and design temperature (meridian)	lb/in. ²
σ_{yL}	General liner yield stress in longitudinal direction	lb/in. ²
σ_{yLH}	General liner yield stress in hoop direction	lb/in. ²
σ_{yLT}	Yield stress of liner in tension at design temperature	lb/in. ²
σ'_{of}	Filament stress at zero pressure and room temperature	lb/in. ²
σ'_{oL}	Liner stress at zero pressure and room temperature (meridian)	lb/in. ²
σ_{oLH}	Liner stress at zero pressure and room temperature (hoop)	lb/in. ²
ϕ	Angle between normal to surface and axis of vessel	degrees

TABLE D-1

UNKNOWN S AT EQUATOR OF HEAD

Winding pressure, p_w Liner thickness, t_L Wrap angle, α_o
 Design pressure, p_d Composite thickness, t_o (t_e) Radius in meridional direction, $r_{1.0}$
 Radius of vessel, a

	Stress Unknowns			
	<u>At Design Pressure</u>	<u>At Zero Pressure and Temperature</u>	<u>At Zero Pressure and Room Temperature</u>	<u>At Winding Pressure</u>
Fiber	σ_{fd}	σ_{ofT}	σ'_{of}	σ_{of}
Liner, meridian	$\sigma_{bL} (e_{bL})$	σ_{oLT}	σ'_{oL}	σ_{oL}
Liner, hoop	$\sigma_{bLH} (e_{bLH})$	σ_{oLHT}	σ'_{oLH}	σ_{oLH}

Table D-1

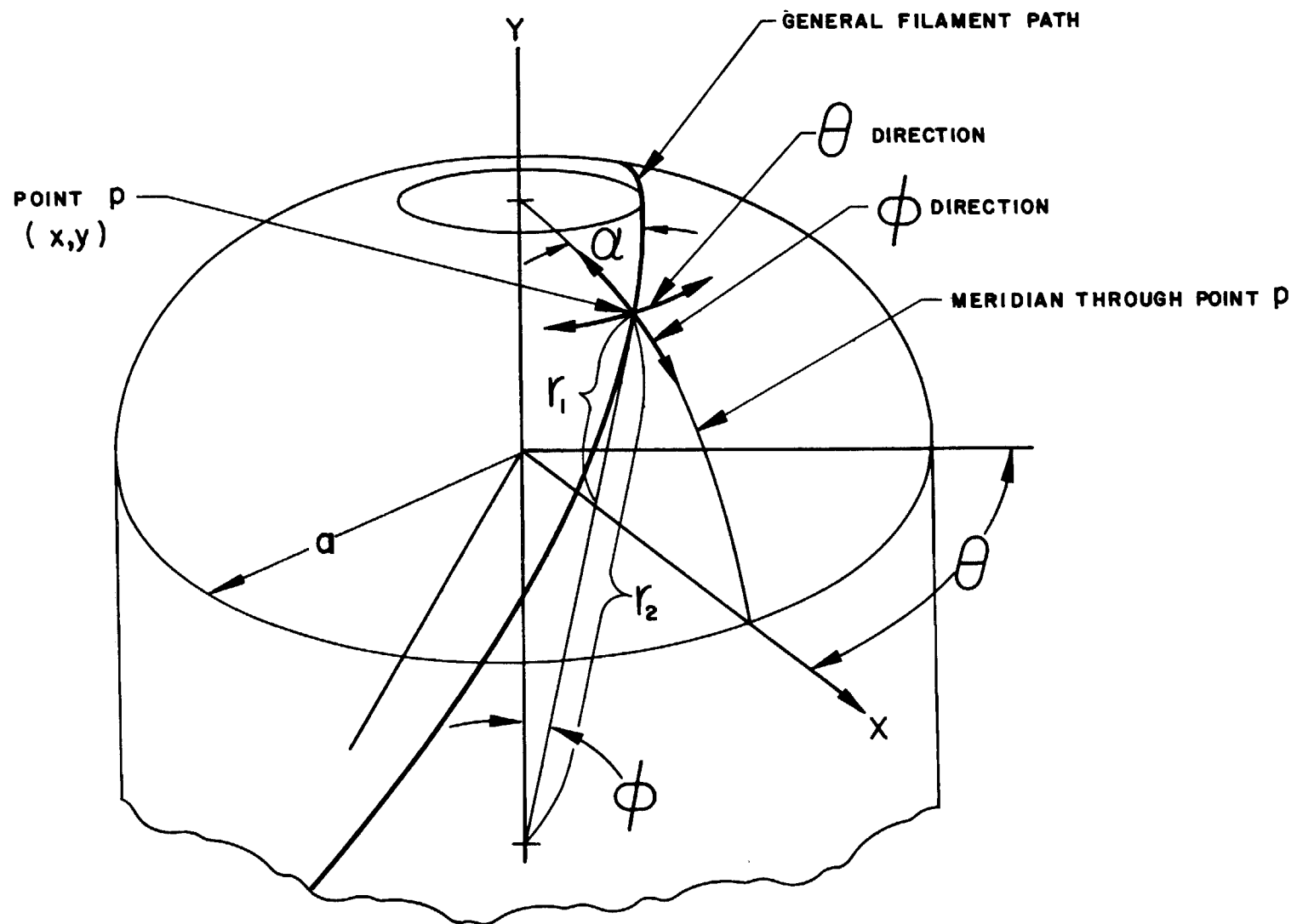
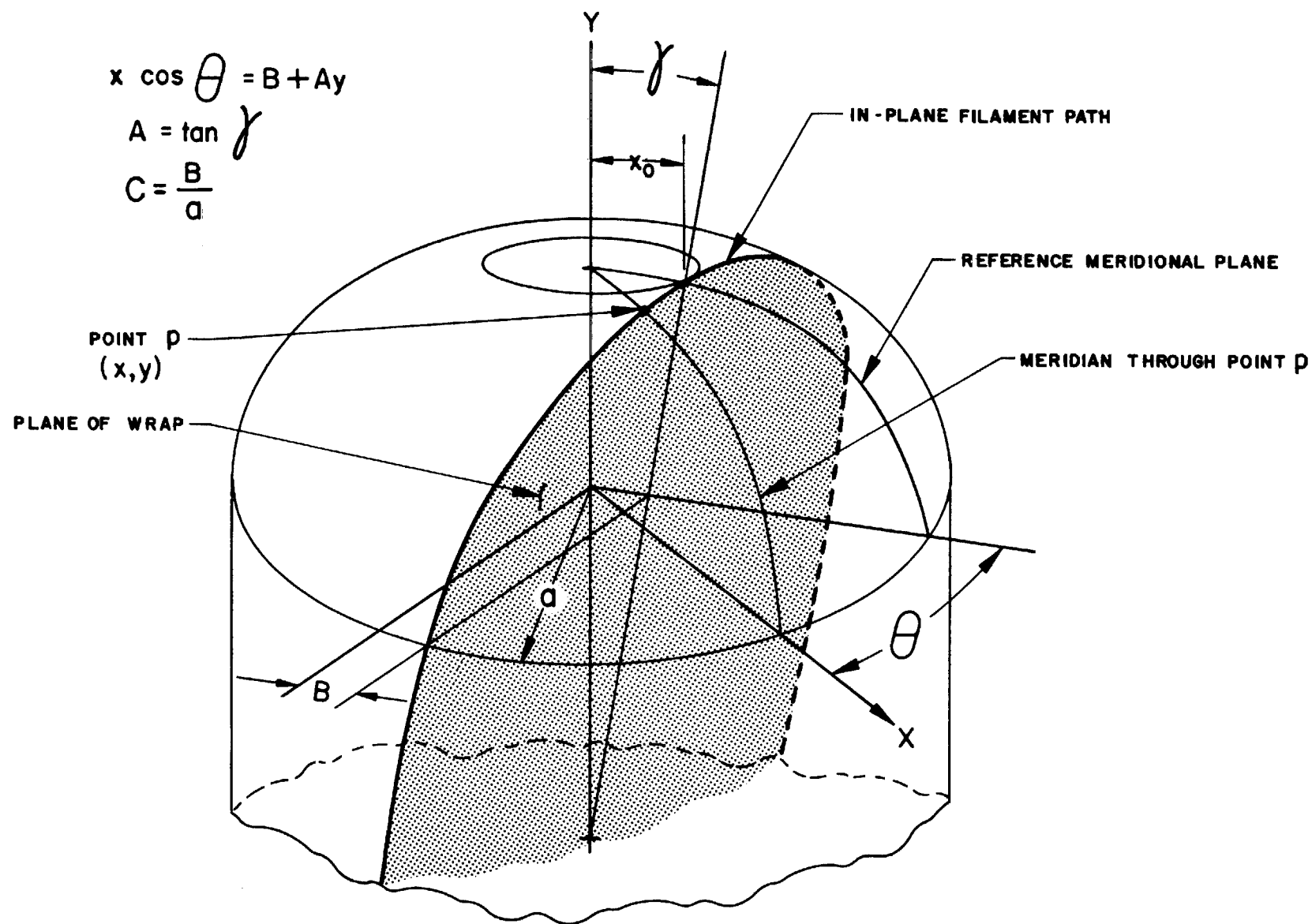


Figure D-1

GEOMETRY OF GENERAL WINDING PATTERN



GEOMETRY OF IN-PLANE WINDING PATTERN

APPENDIX E

FACTORS OF SAFETY FOR GFR METAL TANKS

The goal of component-development programs is to determine well designed and economically manufactured configurations that will perform satisfactorily under the expected service conditions. The requirements for pressure-vessel components include ability to withstand maximum internal-pressure levels, cycles, and load durations in combination with the external forces and environmental conditions that may be imposed. Appropriate structural materials, design-allowable properties, and vessel configurations for the evolution of a design are selected on the basis of analysis of other design factors, such as weight limitations, in addition to the loads and environments the vessel must successfully resist during its life. A factor of safety is applied to the design to further ensure that the performance requirements will be met.

Specifications for the performance capability of a pressure vessel may be stated in terms of the original strength, strength retention, and required service-cycle loading conditions, using the following three factors of safety:

<u>Basis</u>	<u>Ratio</u>
Original strength	$\frac{\text{single-cycle failure pressure}}{\text{service-cycle pressure load}}$
Strength retention	$\frac{\text{failure pressure after service cycle}}{\text{service-cycle pressure load}}$
Service-cycle requirement	$\frac{\text{service-cycle life capability}}{\text{service-cycle life requirement}}$

Factor-of-safety selections can be rather arbitrary and difficult to justify except on the basis of experience in use. The specific values used have depended on the intended service, quality-control levels for materials and processes, and the quality-assurance testing program. For commercial pressure vessels, the ASME Unfired Pressure Vessel Code required an initial design factor of safety of 5 prior to World War II. During the war, this requirement was dropped to 4, and there is current interest in reducing the value even more. For aerospace pressure vessels, initial safety-factor values have generally ranged from 2.22 (for manned systems, or systems imposing severe service-life requirements) down to as low as 1.25 (based on allowable ultimate strength) or 1.10 (based on allowable yield strength).

I. CONSIDERATIONS

A. VALUE BASED ON OPERATING PRESSURE

In GFR metal tanks five factors of safety can be identified at any given design pressure, due to the large difference in elastic and strength

properties of the component materials. These are σ_{ult}/σ_o for the metal and filament shells in the hoop and longitudinal directions, and p_b/p_o for the complete vessel (where σ_{ult} is the ultimate strength, σ_o the stress at operating pressure, p_b the design ultimate pressure, and p_o the operating pressure). In general, at the operating pressure, metal-shell factors of safety will be less than p_b/p_o factors of safety, and glass-filament-shell factors of safety will be higher.

B. VALUE BASED ON PRESTRESS PRESSURE

After plastic deformation of the metal-shell component by application of the initial pressure load (prestress pressure), the shell operates up and down its offset stress-strain curve during cycling between zero pressure and the operating pressures. If a metal is loaded so that plastic deformation occurs and is then unloaded, stress increase to a level that will again cause plastic strain will make plastic flow occur more easily than if unloading had not taken place (i.e., more easily than if the prior deformation had been continued without interruption). The difference in behavior with and without the interruption may be very large or very small, depending on the temperature, the amount of strain prior to interruption, and the direction of the post-interruption strain relative to the direction of prior strain. The difference is particularly large when the strain direction is reversed (the condition existing in GFR metal tanks). To preclude this "rounding of the corner of the re-loading stress-strain curve" (a manifestation of the Bauschinger effect) and to minimize the magnitude of the hysteresis loop in the metal shell during pressure cycling, it is desirable to keep the operating-stress level below the initial prestress level. This may be accomplished by requiring that the operating-stress level be less than the prestress level by a fixed amount, or that the operating pressure be a fixed percentage of the prestress pressure.

Because it is more desirable to maintain a fixed ratio between the prestress and operating stresses and to let the ratio between the prestress and operating pressures become the variable, the former design criterion is used in the parametric study.

The operating-stress level is held below the prestress level by implementation of the design condition that

$$\sigma_p = 1.10 \sigma_o$$

where σ_p is the metal-shell tensile stress at prestress pressure.

C. VALUE BASED ON SERVICE-CYCLE REQUIREMENT

This factor of safety was set at 1.00 because the service cycle defined for GFR metal tanks in this program is based on the required fatigue and creep-strength values. The minimum-weight tanks that can meet this service-life requirement are the optimum configurations. This safety factor is therefore used in the parametric analysis.

II. RELIABILITY ANALYSIS COMPARED WITH FACTOR-OF-SAFETY CRITERIA FOR DESIGN AND QUALIFICATION TESTING

The application of reliability-analysis techniques provides a more realistic statement of burst-strength requirements or service-life capability than the factor-of-safety concept. This fact assumes great significance in the definition of design and qualification-test procedures for GFR metal tanks in a specific application. (In the absence of the GFR-metal-tank data required for this type of analysis, however, the factor-of-safety approach to design and evaluation is employed in the parametric study and for comparisons of GFR metal tanks with all-metal pressure vessels. Meaningful results will be obtained, because factors of safety are universally used in fixing strength requirements for a structural design.)

All factors of safety are somewhat arbitrary, both in magnitude and definition. A question can therefore be raised about the necessity for adhering to a certain factor-of-safety magnitude as a requirement to ensure design adequacy. It can only be answered by judging the structure in terms of a different measure of adequacy, such as reliability.

Considerable interest now exists in the use of rational probability analysis and statistical methods for structural design. Such methods are inherently attractive, because the material properties and structural performance are probabilistic rather than deterministic, while the applied loads may be either. Both the applied loads and the allowable strengths of a structural element can be described by two Gaussian-type distribution curves, and the reliability can then be calculated from the tail overlap. This concept is shown in Figure E-1. It is also possible to relate the effect of strength degradation after manufacture to the resulting reliability of the structure. Such methods have been applied to missile structures; e.g., the Polaris A3 filament-wound motor case (Refs. E-1 and E-2).

Structural reliability is the probability that a structure will function properly in its environment. It is more difficult to estimate than the factor of safety because it depends on the probability distributions for structural strength and applied loads (Ref. E-1). These distributions cannot both be defined in terms of a single parameter, but the reliability and factor of safety can be related by fixing all load and strength parameters. If the load and strength are assumed to be independent and normally distributed random variables, the parameters needed (in addition to mean strength) to define reliability and to relate the burst-strength reliability to the factor of safety are (a) the standard deviation of strength, (b) the mean operating pressure, (c) the standard deviation of the operating pressure, (d) the proof-test pressure, and (e) the strength degradation that occurs after the proof test.

Parameters of the Polaris A3, first-stage, filament-wound, motor case are used here to exemplify the reliability relationship. The results (from Refs. E-1 and E-3) are shown in Figure E-2. The curve for zero degradation after proof testing shows high reliability for all factors of safety because proof testing ensures that the pressure-vessel strength lies above all but the most extreme possible loads. For the Polaris-motor case, the most important

feature of Figure E-2 is the sharp drop in reliability for factors of safety less than 1.2 if the strength degradation is greater than 2%. If strength degradation of the composite structure occurs during or after proof testing (e.g., during pressure cycling), the pressure-vessel strength may fall into the region of the more probable loads, and the reliability level for the vessel is rapidly decreased. This analytical method is applicable to GFR metal pressure vessels once the parameters needed for reliability calculations are fixed by means of a structural-evaluation-test program.

When internal-pressure loading is the principal design criterion, the following test and analysis plan is suggested as an efficient method to demonstrate pressure-vessel design adequacy and satisfactory performance under the expected service conditions (Ref. E-3):

- A. Determination of the single-cycle burst-strength level, and the standard deviation of the strength
- B. Generation of strength-degradation characteristics, standard deviations, and reliability levels for the specific service-cycle requirements
- C. If required, readjustment of the burst-strength level to provide initial strength and degradation characteristics compatible with the required service-life reliability level
- D. Assurance that all vessels are fabricated to the established design
- E. Implementation of a periodic quality-assurance testing program.

REFERENCES

- E-1. D. M. Aspinwall, Lockheed Missiles and Space Company, "Relationship Between Burst-Strength, Reliability, and Factor of Safety Requirements," presented at Third Semiannual Polaris Glass Reinforced Plastic Research and Development Conference, Wilmington, Delaware, 17-18 July 1962.
- E-2. H. D. Anderson and D. M. Aspinwall, Lockheed Missiles and Space Company, "Structural Reliability Considerations in Establishing Burst-Strength Test Requirements," presented at Fourth Semiannual Polaris Glass Reinforced Plastic Research and Development Conference, Sacramento, California, 22-23 January 1963.
- E-3. E. E. Morris, "Design and Qualification Test Procedures for Filament-Wound Pressure Vessels," presented at U.S. Air Force Aeronautical Systems Division Conference on Structural Plastics, Adhesive, and Filament-Wound Composites, Dayton, Ohio, 11-13 December 1962.

OVERLAPPING STRENGTH AND LOAD DISTRIBUTIONS

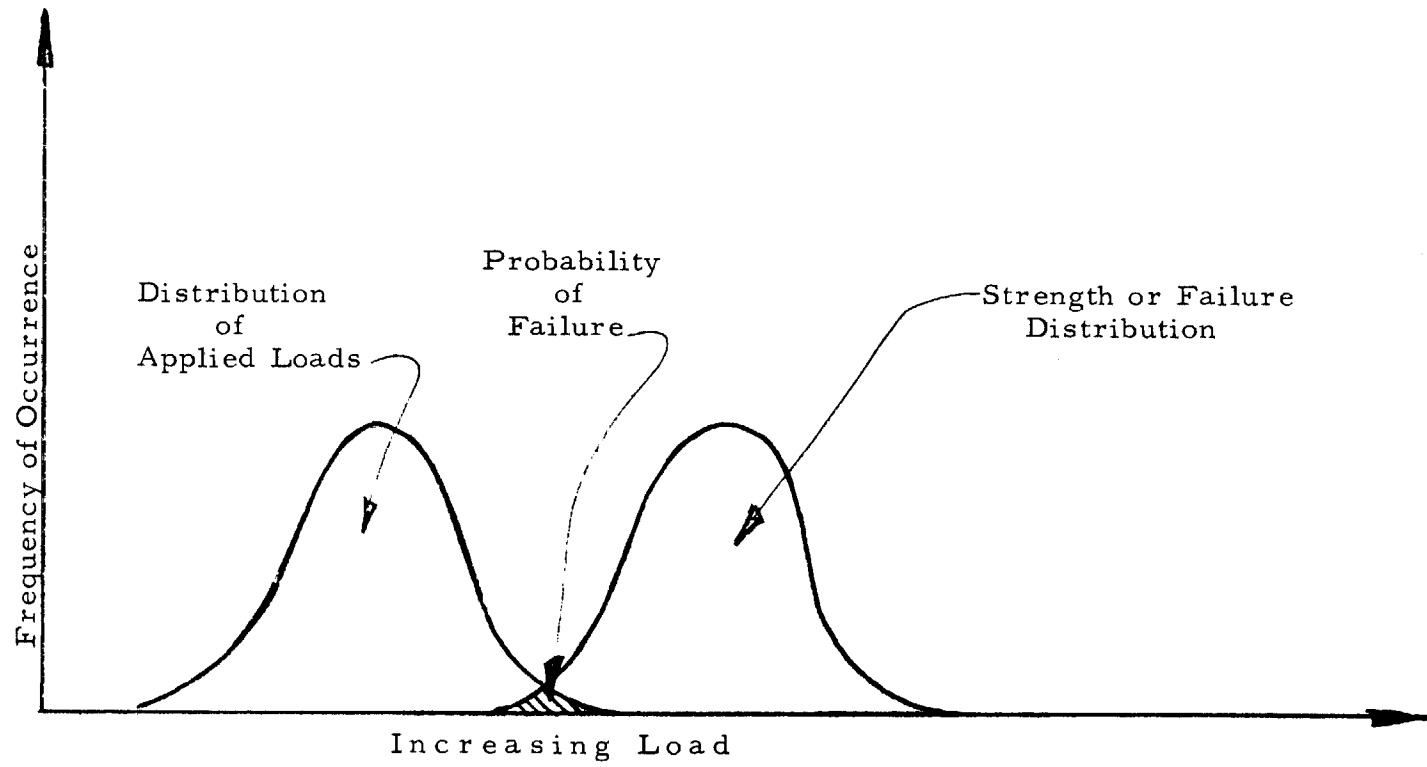
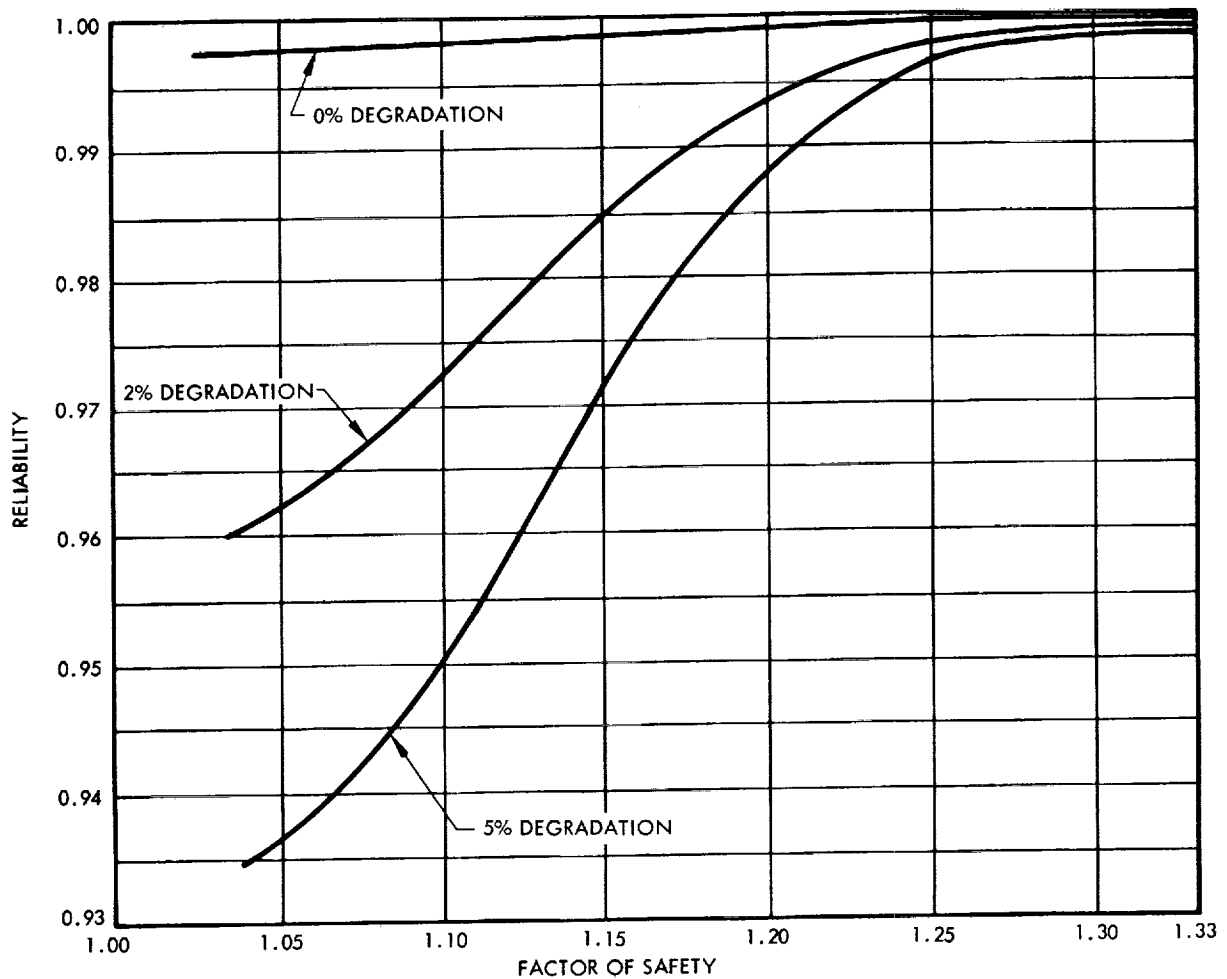


Figure E-1



$$\text{FACTOR OF SAFETY} = \frac{\text{ORIGINAL MEAN STRENGTH}}{\text{PROOF PRESSURE LEVEL}} = \frac{\text{ORIGINAL MEAN STRENGTH}}{945 \text{ psig}}$$

$$\text{RELIABILITY} = 1 - \int_{K_1}^{\infty} \frac{e^{-\frac{1}{2} \left(\frac{L - \mu_L}{\sigma_L} \right)^2}}{\sqrt{2\pi} \sigma_L} dL \int_{K_1}^L \frac{e^{-\frac{1}{2} \left[\frac{S - \mu_S (100-D)/100}{\sigma_S} \right]^2}}{\sqrt{2\pi} \sigma_S N} dS$$

WHERE

L = PRESSURE LOAD

S = CHAMBER STRENGTH

D = PERCENT DEGRADATION OF MEAN STRENGTH

K = PROOF TEST PRESSURE MINUS $\mu_S D/100$

N = NORMALIZING FACTOR WHICH ACCOUNTS FOR THE MOTOR CASES LOST IN PROOF TEST

μ_S = MEAN STRENGTH OF THE MOTOR CASE

σ_S = STANDARD DEVIATION OF THE MOTOR CASE STRENGTH, SELECTED AS 80 psi

μ_L = MEAN LOAD, SELECTED AS 900 psi

σ_L = STANDARD DEVIATION OF THE LOAD, SELECTED AS 30 psi

RELIABILITY VS FACTOR OF SAFETY FOR VARIOUS STRENGTH DEGRADATIONS

Figure E-2

DISTRIBUTION LIST

	<u>No. of Copies</u>
National Aeronautics and Space Administration	
Lewis Research Center	
21000 Brookpark Road	
Cleveland, Ohio 44135	
Attention: Contracting Officer, MS 500-210	1
Liquid Rocket Technology Branch, MS 500-209	8
Technical Report Control Office, MS 5-5	1
Technology Utilization Office, MS 3-16	1
AFSC Liaison Office, MS 4-1	2
Library	2
Office of Reliability & Quality Assurance, MS 500-203	1
R. H. Kemp, MS 49-1	1
National Aeronautics and Space Administration	
Washington, D.C. 20546	
Attention: Code RV-2	2
NASA Scientific and Technical Information Facility	
P. O. Box 33	
College Park, Maryland 20740	
Attention: NASA Representative	6
National Aeronautics and Space Administration	
Ames Research Center	
Moffett Field, California 94035	
Attention: Library	1
National Aeronautics and Space Administration	
Flight Research Center	
P.O. Box 273	
Edwards, California 93523	
Attention: Library	1
National Aeronautics and Space Administration	
Goddard Space Flight Center	
Greenbelt, Maryland 20771	
Attention: Library	1

DISTRIBUTION LIST (cont.)

No. of Copies

National Aeronautics and Space Administration Langley Research Center Langley Station Hampton, Virginia 23365 Attention: Library	1
National Aeronautics and Space Administration Manned Spacecraft Center Houston, Texas 77001 Attention: Library	1
National Aeronautics and Space Administration George C. Marshall Space Flight Center Huntsville, Alabama 35812 Attention: Library	1
Mr. Robert E. Shannon, Code R-P&VE-MN	1
Mr. J. Blumrich, Code R-P&VE-SA	1
National Aeronautics and Space Administration Western Operations 150 Pico Boulevard Santa Monica, California 90406 Attention: Library	1
National Aeronautics and Space Administration John F. Kennedy Space Center Cocoa Beach, Florida 32931 Attention: Library	1
Jet Propulsion Laboratory 4800 Oak Grove Drive Pasadena, California 91103 Attention: Library	1
U.S. Department of the Interior Bureau of Mines 4800 Forbes Avenue Pittsburgh, Pennsylvania 15213 Attention: M. M. Dolinar, Repts Librarian Explosives Research Center	1

DISTRIBUTION LIST (cont.)

No. of Copies

Office of the Director of Defense Research & Engineering Washington, D.C. 20301 Attention: Dr. H. W. Schulz, Office of Asst. Dir. (Chem. Technology)	1
RTD(RTNP) Bolling Air Force Base Washington, D.C. 20332	1
Arnold Engineering Development Center Attention: AEOIM Air Force Systems Command Tullahoma, Tennessee 37389	1
AFSC(SCTR/Captain S. W. Bowen) Andrews Air Force Base Washington, D.C. 20332	1
AFRPL(RPR) Edwards, California 93523	1
AFRPL(RPM) Edwards, California 93523	1
AFTTC(FTBPP-2) Edwards AFB, California 93523	1
Office of Research Analyses (OAR) Attention: RRRT Holloman Air Force Base, New Mexico 88330	1
Air Force Office of Scientific Research Washington, D.C. 20333 Attention: SREP, Dr. J. F. Masi	1
AFRPL(RPC) Edwards, California 93523	1
Wright-Patterson Air Force Base, Ohio 45433 Attention: AFML(MAAE)	1
Mr. T. J. Reinhart, Jr.	1
Wright-Patterson Air Force Base, Ohio 45433 Attention: AFML(MAAM)	1

DISTRIBUTION LIST (cont.)

No. of Copies

Commanding Officer
Ballistic Research Laboratories
Aberdeen Proving Ground, Maryland 21005
Attention: AMXBR-1

1

Department of the Army
U.S. Army Materiel Command
Washington, D.C. 20315
Attention: AMCRD-RC

1

Commanding Officer
U.S. Army Research Office (Durham)
Box CM, Duke Station
Durham, North Carolina 27706

1

U.S. Army Missile Command
Redstone Scientific Information Center
Redstone Arsenal, Alabama 35808
Attention: Chief, Document Section

1

Bureau of Naval Weapons
Department of the Navy
Washington, D.C. 20360
Attention: DLI-3

1

Bureau of Naval Weapons
Department of the Navy
Washington, D.C. 20360
Attention: RMMP-2

1

Bureau of Naval Weapons
Department of the Navy
Washington, D.C. 20360
Attention: RMMP-4

1

Bureau of Naval Weapons
Department of the Navy
Washington, D.C. 20360
Attention: RRRE-6

1

Bureau of Ships
Department of the Navy
Washington, D.C. 20306
Attention: Polymer & Fiber Packaging Section
Ser. 634C3-228

1

DISTRIBUTION LIST (cont.)

No. of Copies

Commander U.S. Naval Missile Center Point Mugu, California 93041 Attention: Technical Library	1
Commander U.S. Naval Ordnance Laboratory White Oak Silver Spring, Maryland 20910 Attention: Library	1
Commander (Code 753) U.S. Naval Ordnance Test Station China Lake, California 93557 Attention: Technical Library	1
Superintendent U.S. Naval Postgraduate School Naval Academy Monterey, California 93900	1
Commanding Officer Office of Naval Research 1030 E. Green Street Pasadena, California 91101	1
Director (Code 6180) U.S. Naval Research Laboratory Washington, D.C. 20390 Attention: H. W. Carhart	1
Director Special Projects Office Department of the Navy Washington, D.C. 20360	1
Commanding Officer U.S. Naval Underwater Ordnance Station Newport, Rhode Island 02844 Attention: W. W. Bartlett	1
Commander U.S. Naval Weapons Laboratory Dahlgren, Virginia 22448 Attention: Technical Library	1

DISTRIBUTION LIST (cont.)

No. of Copies

Aerojet-General Corporation 11711 South Woodruff Avenue Downey, California 90241 Attention: F. M. West, Chief Librarian	1
W. L. Arter	1
Aerojet-General Corporation P.O. Box 1947 Sacramento, California 95809 Attention: Technical Library 2484-2015A	3
Aeronutronic Division Philco Corporation Ford Road Newport Beach, California Attention: Dr. L. H. Linder, Manager Technical Information Department	1
Aerospace Corporation P.O. Box 95085 Los Angeles, California 90045 Attention: Library-Documents	1
Air Products and Chemicals Company Allentown, Pennsylvania Attention: P. J. DeRea	1
Arde Portland, Incorporated 100 Century Road Paramus, New Jersey	1
ARO, Incorporated Arnold Engrg. Dev. Center Arnold Air Force Station, Tennessee 37389 Attention: Dr. B. H. Goethert Chief Scientist	1
Atlantic Research Corporation Shirley Highway & Edsall Road Alexandria, Virginia 22314 Attention: Security Office for Library	1
Battelle Memorial Institute 505 King Avenue Columbus, Ohio 43201 Attention: Defense Metals Information Center	1

DISTRIBUTION LIST (cont.)

	<u>No. of Copies</u>
Bell Aerosystems Box 1 Buffalo, New York 14205 Attention: T. Reinhardt	1
The Boeing Company Aero Space Division P.O. Box 3707 Seattle, Washington 98124 Attention: Ruth E. Peerenboom (1190)	1
Chemical Propulsion Information Agency Applied Physics Laboratory 8621 Georgia Avenue Silver Spring, Maryland 20910	1
Douglas Aircraft Company, Inc. Santa Monica Division 3000 Ocean Park Blvd. Santa Monica, California 90405 Attention: Mr. J. L. Waisman	1
Mr. J. M. Toth, Jr.	1
The Garrett Corporation 20545 Center Ridge Road Cleveland, Ohio 44116	1
General Dynamics/Convair P.O. Box 1128 San Diego, California 92112 Attention: Library and Information Services (128-00)	1
B. F. Goodrich Company Aerospace & Defense Products 500 South Main Street Akron, Ohio	1
Goodyear Aerospace Corporation 1210 Massillon Road Akron, Ohio	1
Hercules Powder Company Chemical Propulsion Division 910 Market Street Wilmington, Delaware	1

DISTRIBUTION LIST (cont.)

No. of Copies

IIT Research Institute Technology Center Chicago, Illinois 60616 Attention: C. K. Hersh, Chemistry Division	1
Narmco Research and Development Company Wittaker Corporation 131 N. Ludlow Street Dayton, Ohio 45402	1
North American Aviation, Inc. Space and Information Systems Division 12214 Lakewood Blvd. Downey, California 90242 Attention: Technical Information Center D/096-722 (AJ01)	1
Plastics Technical Evaluation Center Picatinny Arsenal Dover, New Jersey 07801	1
Rocketdyne 6633 Canoga Avenue Canoga Park, California 91304 Attention: Library, Department 596-306	1
Rohr Corporation Department 145 Chula Vista, California	1
TRW Systems 1 Space Park Redondo Beach, California 90200 Attention: Tech. Lib. Doc. Acquisitions	1
Sandia Corporation Sandia Base Albuquerque, New Mexico Attention: H. E. Montgomery B. R. Allen	1 1
Swedlow, Incorporated 6986 Bandini Blvd. Los Angeles, California	1

DISTRIBUTION LIST (cont.)

No. of Copies

Thiokol Chemical Corporation Wasatch Division P.O. Box 524 Brigham City, Utah 84302 Attention: Library Section	1
United Aircraft Corporation United Technology Center P.O. Box 358 Sunnyvale, California 94088 Attention: Librarian	1
U.S. Rubber Company Mishawaka, Indiana	1
General Electric Company Apollo Support Department P.O. Box 2500 Daytona Beach, Florida 32015 Attention: C. Day	1
Brunswick Corporation Defense Products Division 1700 Messler Street Muskegon, Michigan	1
Grumman Aircraft Engineering Corp. Bethpage Long Island, New York	1
Defense Documentation Center Cameron Station Alexandria, Virginia 22314	1
Internal	50